28TH Annual Conference Proceedings

Nickel-Cobalt-Copper

Sponsored by

SEDGMAN

ALTA Metallurgical Services, Melbourne, Australia

www.altamet.com.au

PROCEEDINGS OF
ALTA 2024 Nickel-Cobalt-Copper SESSIONS

27 May 2024
Perth, Australia

978-0-6458390-0-5

ALTA Metallurgical Services Publications

Monday 27 May 2024

Sponsored by SEDGMAN

Tuesday 28 May 2024

Sponsored by SEDGMAN

Wednesday 29 May 2024

Sponsored by SEDGMAN

Keynote Address

RECENT GROWTH OF NICKEL LATERITE PROCESSING IN INDONESIA

By

Taufiq Hidayat, Zulfiadi Zulhan, Mohammad Zaki Mubarok, Edy Sanwani

Metallurgy Engineering Research Group,
Institut Teknologi Bandung, Indonesia

SUMMARY

Indonesia is one of the countries with significant nickel reserves contributing to approximately 20% of the total world nickel reserves. In 2022, Indonesia nickel mining production reached almost half of the total world nickel mining production. Nickel in Indonesia is predominantly found as laterite deposit with layers having different characteristics. The layer under the top soil contains limonite ore with relatively low nickel and low MgO contents, while the layer located deeper but above the bedrock contains saprolite ore with relatively high nickel and high MgO contents. The Indonesian government has introduced a set of strategic regulations aimed to harness its nickel resources and strengthening its domestic industrial capacities. One of the prominent regulations is regarding the nickel ore export ban that was implemented to encourage domestic nickel processing. The export ban on ore has been a catalyst for the recent surge in nickel laterite processing in indonesia. The law shifted Indonesia's role from initially being one of the major exporters of nickel ore to the leading exporter of nickel-containing intermediate and semi-finished products. The High Pressure Acid Leaching (HPAL) is implemented for processing the limonite ore, while the Rotary Kiln Electric Furnace (RKEF) is dominantly applied for processing the saprolite ore. The development of HPAL and RKEF plants in Indonesia will be presented. In addition, the possible directions or strategies of Indonesian nickel industry will be discussed.

BIO

Education

Taufiq completed his undergraduate education from the Department of Metallurgical Engineering from ITB in 2005. Taufiq then obtained a Master's degree in 2008 and Doctoral's degree in 2013 both in Pyrometallurgy field at the University of Queensland, Australia.

Current Position

Taufiq is currently lecturer and researcher in the Metallurgical Engineering Research Group at the Faculty of Mining and Petroleum Engineering, Institut Teknologi Bandung, Indonesia since 2019. He is also actively involved in discussion and preparation of documents related to mineral sector development policies in indonesia, such as Indonesian Grand Strategies of Nickel, Copper, Bauxite, Tin, Gold-Silver, Coal, and Dolomite.

Previous Experience

Prior to Metallurgical Engineering Research Group, Taufiq served as Research Fellow at Pyrometallurgy Innovation Centre at the University of Queensland, Australia from 2014 until 2018. Some of the research areas he covered during his research fellow position include slag chemistry, non-ferrous high temperature processing, kinetics of heterogeneous reaction, and computer coupling of phase diagrams and thermochemistry (CALPHAD). Recognition of Taufiq's research experience is demonstrated by the publication of 80 technical papers in metalurgy area and several awards, such as Extraction & Processing Division Science Award by TMS in 2018, Extraction & Processing Division Pyrometallurgy Best Paper Award by TMS in 2018, and Editor Choice Award for 2017 by the Journal of Phase Equilibria and Diffusion.

RECENT GROWTH OF NICKEL LATERITE PROCESSING IN INDONESIA

Taufiq Hidayat, Zela Tanlega, Zulfiadi Zulhan, Mohammad Zaki Mubarok, Edy Sanwani

Metallurgical Engineering Research Group
Institut Teknologi Bandung
Indonesia

Content

- Indonesia Nickel Laterite Resources and Reserves
- Indonesia Nickel Laterite Mineralogy
- Nickel Laterite Mining in Indonesia
- Nickel Laterite Processing in Indonesia
- Directions / Strategies of Indonesian Nickel Industry
- Concluding Remarks

Background

- Nickel is vital element in electric mobility, renewable energy, and other strategic technologies.
- Indonesia has emerged as a major nickel producer in recent years due to the implementation of a nickel ore export ban policy, supported by massive foreign investment.
- Indonesia currently dominates nickel mining production representing more than half of the global supply.
- More than 50 nickel processing plants are in operation in Indonesia producing nickel intermediate products.

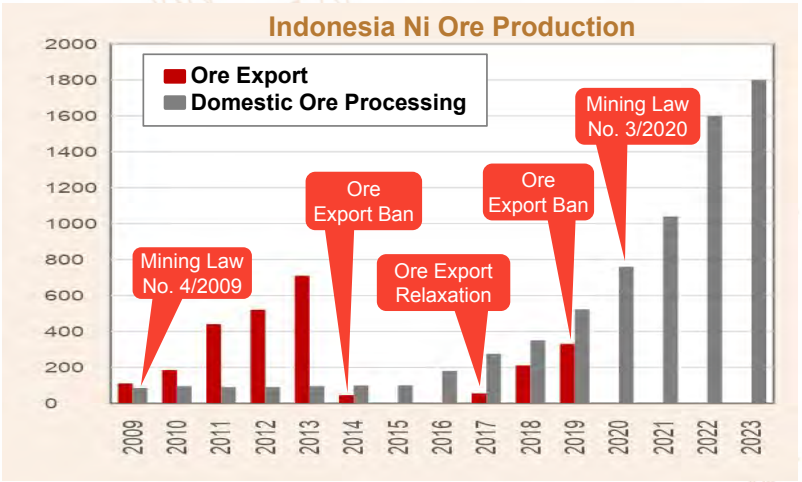

Sources: 1) https://www.climatechange.ie/iea-mineral-supplies-for-electric-cars-must-increase-30-fold-to-meet-climate-goals/ (with further data processing)
2) U.S. Geological Survey, 2024, Mineral commodity summaries 2024: U.S. Geological Survey, p 12., https://pubs.usgs.gov/periodicals/mcs2024/mcs2024.pdf

Indonesia Nickel Laterite Resources and Reserves

World Nickel Laterite Resources 2023: >180 Million Ton Nickel

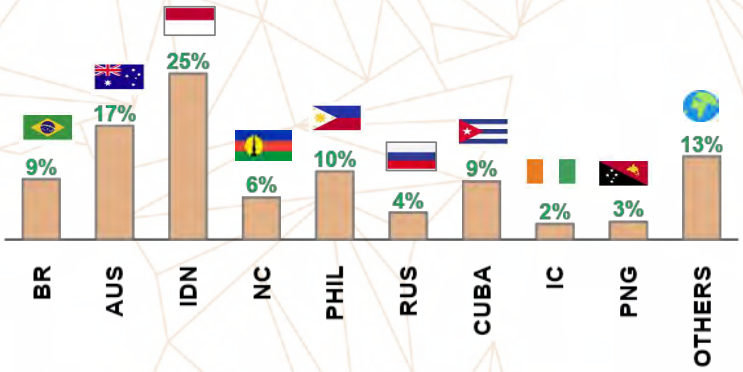

World Nickel Reserves 2023: >130 Million Ton Nickel

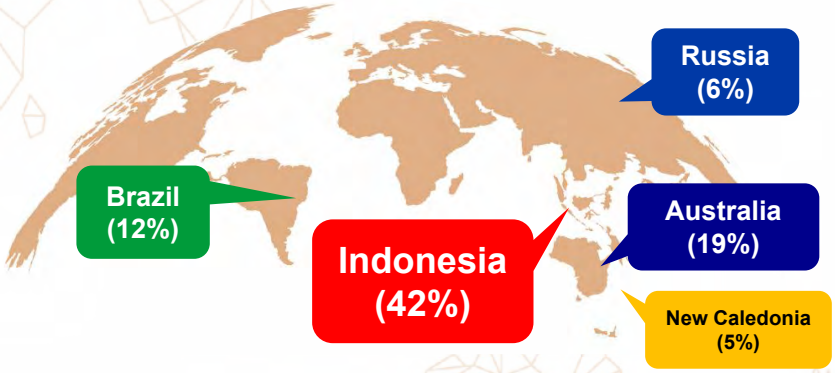

- Indonesia is placed number one rank in nickel laterite resources and reserves.
- Indonesia is reported to hold 25% of global nickel laterite resources which equates to ~45 Million tons Ni.
- According to the latest report by the Indonesia Geology Agency, verified nickel laterite resources reach ~73 Million ton Ni.
- Indonesia owns around 42% of world's nickel reserves which equates to ~55 Million ton Ni.

Sources: 1) https://nickelinstitute.org/en/about-nickel-and-its-applications/
2) U.S. Geological Survey, 2024, Mineral commodity summaries 2024: U.S. Geological Survey, p 12., https://pubs.usgs.gov/periodicals/mcs2024/mcs2024.pdf
3) Indonesia Geology Agency, Centre for Mineral Resources, Coal & Geothermal, Updating the potential, resources and reserves of nickel greenfield in Indonesia - May 2024

Indonesia Nickel Laterite Resources and Reserves

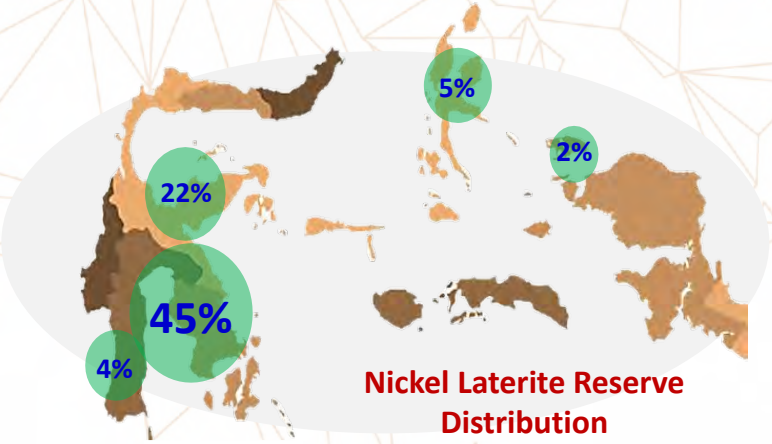

Nickel Laterite Reserve Distribution in Indonesia 2023

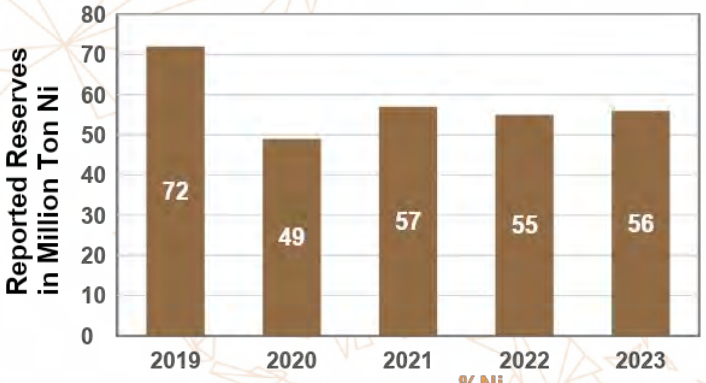

- The nickel deposits are concentrated in Sulawesi, Maluku, and West Papua Islands.
- Indonesia historical data shows steady reported metal reserves at around 50 Million ton Ni for the last 4 years.
- The Indonesia nickel laterite reported reserves is dominated with ore containing more than 1.2% Ni.

Ni grade (Amount relative to reserve)

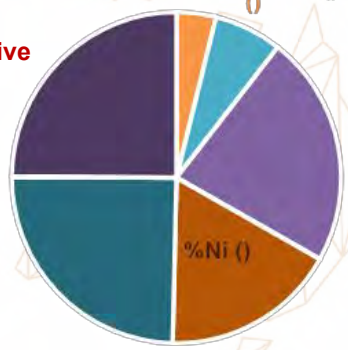

Sources: 1) Centre for Mineral Resources, Coal & Geothermal – December 2023
2) Indonesia Geology Agency, Centre for Mineral Resources, Coal & Geothermal, Updating the potential, resources and reserves and nickel greenfield in Indonesia – May 2024

Indonesia Nickel Laterite Mineralogy

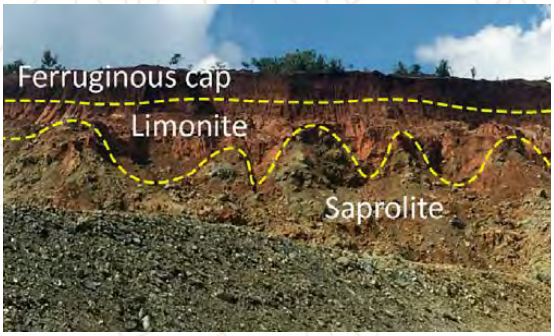

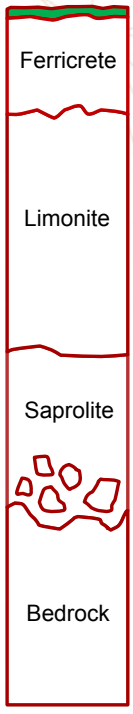

- Nickel laterite consists of different layers with different mineralogy.
- Limonite and Saprolite are valuable feedstocks for nickel industries.
- Due to the different ore characteristics, different processing routes are required.

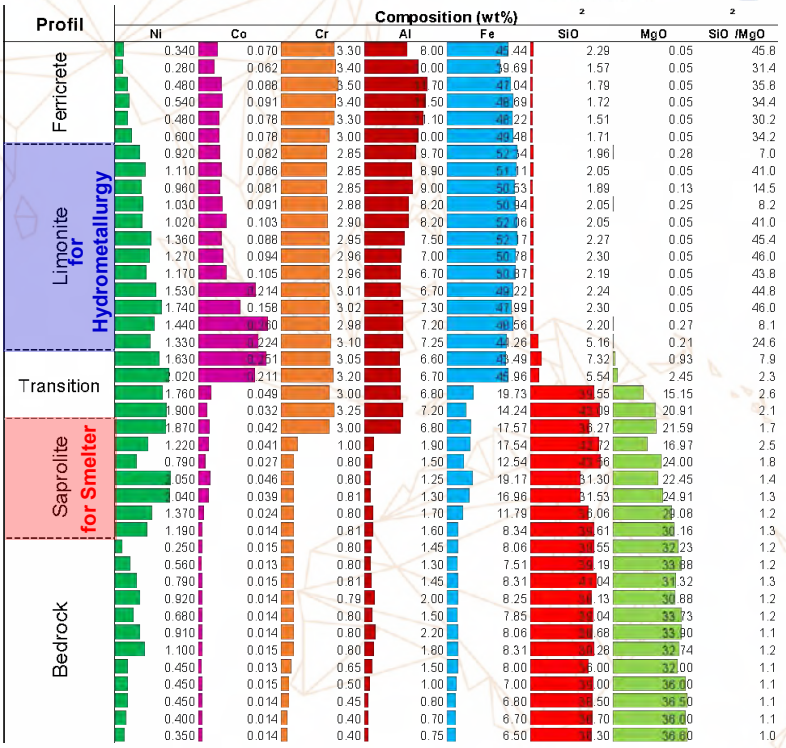

Sources: 1) Choi Y, Lee I and Moon I (2021) Geochemical and Mineralogical Characteristics of Garnierite From the Morowali Ni-Laterite Deposit in Sulawesi, Indonesia. Front. Earth Sci. 9:761748. doi: 10.3389/feart.2021.761748.
2) M.F. Azim et al., Geochemical and Physical Characteristics of Nickel-Cobalt Laterite Deposits on Maniang Island, Kolaka, Southeast Sulawesi: Proceedings PIT IAGI 51st, 2022.

Indonesia Nickel Laterite Mineralogy

Chemical Compositions of Saprolite Ore

	Obi Island %	North Morowali-1 %	North Morowali-2 %	East Luwu %
Ni	1.70	1.79	1.99	1.68
Co	0.08	0.03	0.04	0.07
Fe	16.08	12.9	17.55	19.86
SiO_2	32.9	47.3	35.39	36.46
Al_2O_3		3.12	3.21	3.11
MgO	26.5	20.1	17.93	15.50
Mn		0.22	0.35	0.48
Cr		0.62	0.77	0.93
Ca	0.12	0.42	0.20	0.36
Moisture	35%	27%		

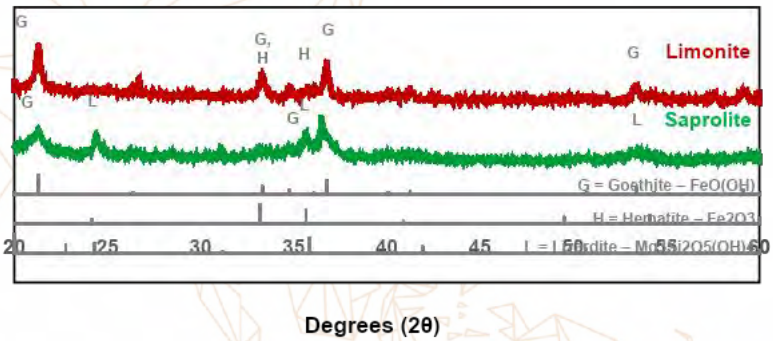

Chemical Compositions of Limonite Ore

	Obi Island %	North Morowali %	Bulong %	Cawse %	Murrin Murrin %	Moa Bay %	Taganito %
Ni	1.35	1.13	1.11	1.0	1.24	1.35	0.98
Co	0.17	0.11	0.08	0.07	0.089	0.12	
Fe	41.2	32.3	20.8	18.0	21.7	45	
SiO_2	15.2	20.7	42.9	42.5	42.1	8.3	
Al	3.0	4.23	2.75	1.71	2.51	4.8	1.87
Mg	1.60	2.76	4.62	1.58	4.02	0.55	1.16
Mn	0.97	0.83	0.36	0.17	0.40		
Cr	1.0	1.69	0.6	0.92	0.88	2.0	
Ca	0.02	0.11	0.03	0.03	0.53		
Moisture		40%	<35%	<10%	~30%	>20%	

- Saprolite is dominantly composed of magnesium silicate minerals, such as serpentine – $Mg_3Si_2O_5(OH)_4$. Limonite is dominantly composed of iron oxide minerals, such as goethite – FeO(OH).
- The Cut-off Grade (COG) of the saprolite ore is 1.3%Ni and the average ore grade in pyromet plants feed is 1.6%Ni.
- The COG of limonite ore is 0.7%Ni with average Ni content in hydromet plants feed around 1.1%Ni.

Sources: 1) T. Gultom and A. Sianipar, High pressure acid leaching: a newly introduced technology in Indonesia. IOP Conf. Series: Earth and Environmental Science 413 (2020) 012015 IOP Publishing. doi:10.1088/1755-1315/413/1/012015.
2) Zhang, Y., Qie, J., Wang, X.F. et al., Mineralogical Characteristics of the Nickel Laterite, Southeast Ophiolite Belt, Sulawesi Island, Indonesia. Mining, Metallurgy & Exploration 37, 79–91 (2020). https://doi.org/10.1007/s42461-019-00147-y
3) J.H. Kyle, Pressure Acid Leaching of Australian Nickel/Cobalt Laterites. Nickel '96. Kalgoorlie, 27-29 Nov 1996; 4) https://news.metal.com; 5) https://www.mysteel.net/news/5046573-china-nickel-ore-market-2023-review-and-2024-prospect

Nickel Laterite Mining in Indonesia

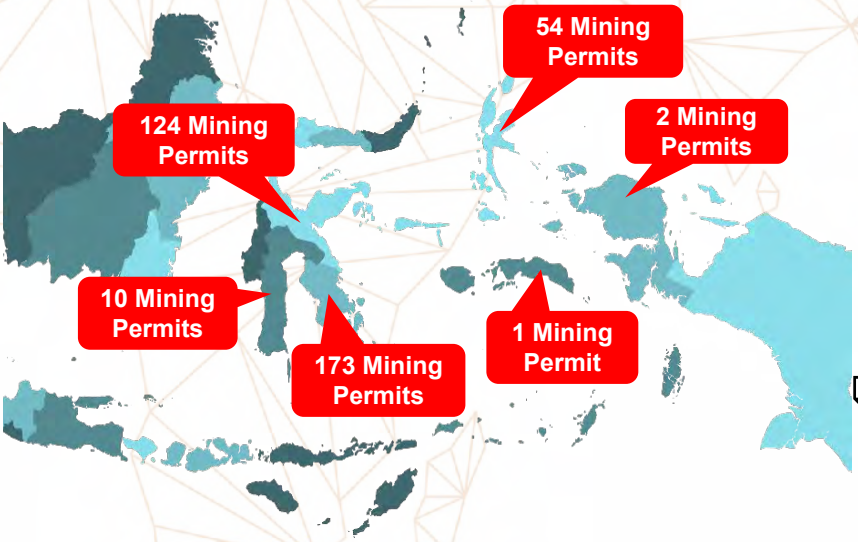

Top 3 Companies with Largest Mining Area*

VALE antam weda bay nickel

Mining Production 2023: ~3.6 Million Ton Nickel

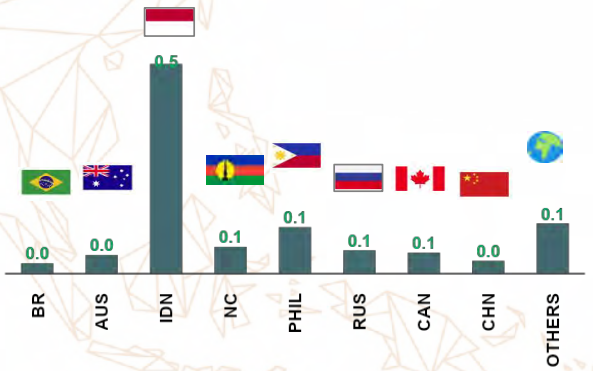

- Mining and exploration areas are spread in Central Sulawesi, South Sulawesi, South-East Sulawesi, Maluku, North Maluku, Papua, and West Papua Islands.
- Total mining permits reaches 364.
- Total mining area covers ~900,000 hectares.

Sources: 1) U.S. Geological Survey, 2024, Mineral commodity summaries 2024: U.S. Geological Survey, p 12., https://pubs.usgs.gov/periodicals/mcs2024/mcs2024.pdf
2) Ministry of Energy and Mineral Resources of Republic of Indonesia, 2024

Nickel Laterite Mining in Indonesia

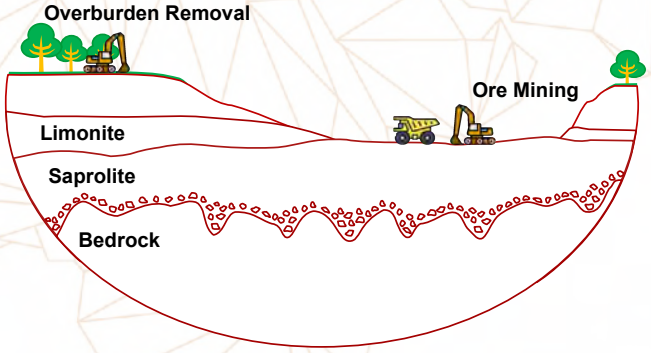

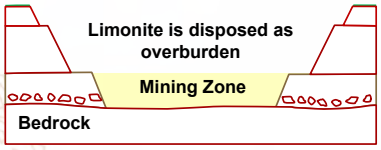

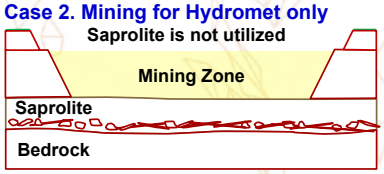

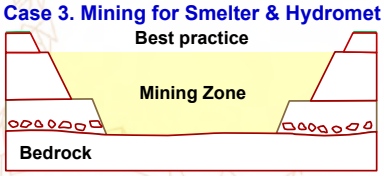

Top 3 Mining Permits with Largest Production in 2023

weda bay nickel

PT SULAWESI CAHAYA MINERAL (SCM)

TBP
Trimegah Bangun Persada

- Prior to the availability of High-Pressure Acid Leaching (HPAL), limonite ore was disposed as overburden.
- The mining operation was mainly focusing on the saprolite ore for the Rotary Kiln-Electric Furnace plants.
- With the availability of HPAL, total mining of saprolite and limonite ores is encouraged.
- This optimized mining method lowers the production cost of limonite ore.

Sources: 1) A. Matano, Nickel laterite mining, 2019

Nickel Laterite Processing in Indonesia

Processing Routes of Laterite Ores

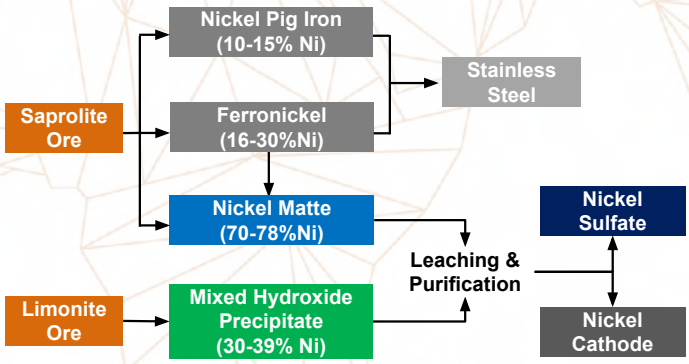

- Dominant utilization of Saprolite Ore is for the production of Nickel Class 2 (NPI and FeNi).
- Indonesia contributed more than 75% of global NPI production in 2023.
- The utilization of Limonite Ore is for the production of Nickel Class 1 (MHP).
- Production of Nickel Class 1* in Indonesia reached more than 20% of total nickel products in 2023.

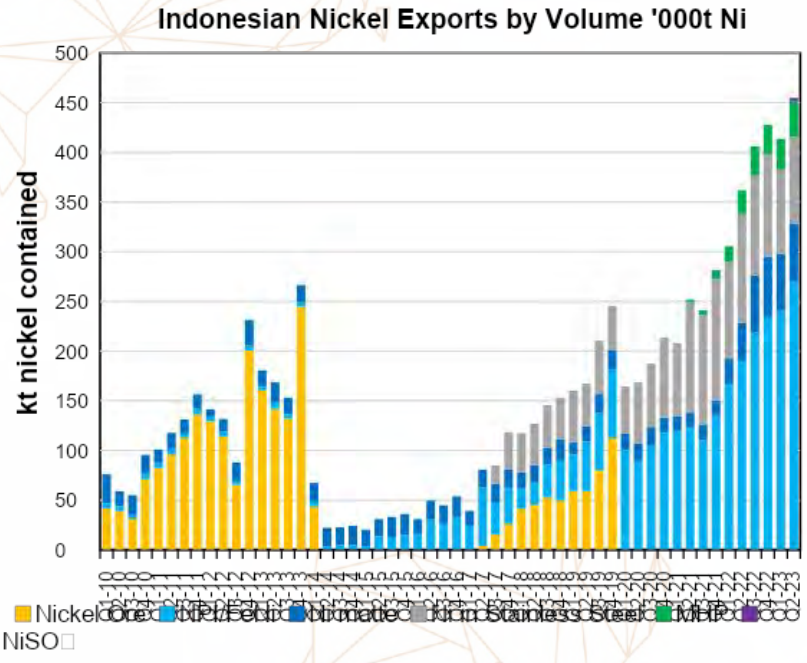

Nickel Class I = Ni matte, Ni hydroxide, Ni sulphate, electrolytic Ni, Ni powder, Ni briquettes, Ni carbonyl.
Nickel Class 2 = NPI and FeNi. The product is used mainly in stainless steel production.

Sources: 1) TDM, INSG, Macquarie Commodities Strategy, October 2023

Nickel Laterite Processing in Indonesia - Products

Element	Example of Composition				
	Nickel Pig Iron	Ferronickel	Nickel Matte	Mixed Hydroxide Precipitate	$NiSO_4 \cdot 6H_2O$
Ni	10-15 %	16-30 %	70–78 %	30–39 %	> 22 %
Fe	remaining	Remaining	< 4%	< 0.5 %	< 5 ppm
S	0.40 %	< 0.05 %	~20 %	3–5 %	
Mn				4–9 %	< 5 ppm
Mg				3–5 %	< 10 ppm
Co	0.29 %	0.36 %	< 1 %	2–5 %	< 50 ppm
Cu				1–4 %	< 5 ppm
Zn				1–4 %	< 5 ppm
Cr	0.55 %	0.08 %			< 5 ppm
C	0.25 %	< 1.2 %			
Si	0.45 %	0.4 %			< 10 ppm
P	0.02 %	< 0.02 %			
Al				< 0.5 %	< 5 ppm
Na					< 20 ppm
Ca					< 10 ppm
Cd					< 5 ppm
Pb					< 5 ppm
H_2O				35–45 %	


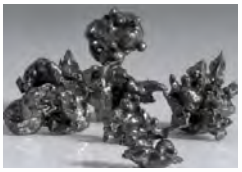


Sources: 1) Taken from various data

Nickel Laterite Processing in Indonesia - Pyromet Plants

Indonesia Ni Pyromet Plants in 2023

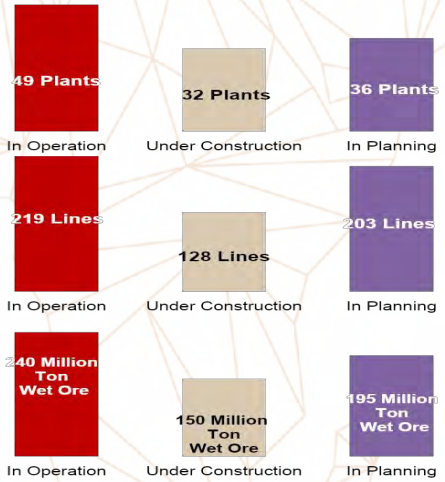

- **Previous fiscal incentives (Tax Holiday, Tax Allowance) led to exponential growth of smelters.**
- **Despite Indonesian authorities had previously ban new pyrometallurgical facilities in 2022, the construction of pre-approved capacities is still allowed.**
- **Recent trend is shifting NPI/FeNi (Ni Class 2) to Ni matte (Ni Class 1).**

Top 3 Smelters with Largest Capacities in 2023

OSS
PT OBSIDIAN STAINLESS STEEL

PT. GUNBUSTER NICKEL INDUSTRY

INDONESIA TSINGSHAN STAINLESS STEEL

Key Locations

IMIP = Indonesia Morowali Industrial Park
IWIP = Indonesia Weda Bay Industrial Park

Sources: 1) Coordinating Ministry for Maritime Affairs and Investment - Republic of Indonesia, Industrialization of minerals in Indonesia now and in the future, 2023

Pyromet Plants – Rotary Kiln-Electric Furnace (RKEF)

- Rotary Kiln – Electric Furnace technology dominates the pyro processing of saprolite ore.
- There is a wide range of furnace capacities from as small as 18 to 80 Mega Watts.
- Feed ore must be strictly controlled in terms of Ni content, SiO_2/MgO ratio, and Fe/Ni ratio.
- Most plants have dedicated power plants, while few procure electricity from the national grid.

Pyromet Plants – RKEF : Process Flow

- **Rotary Dryer**
  - Partial elimination of moisture from ~40% to ~20%

$$H_2O_{(moisture)} \rightarrow H_2O_{(gas)}$$

- **Rotary Kiln**
  - Elimination surface & crystalline water

$$2\,(Mg_{1-x-y},Fe_x,Ni_y)_3Si_2O_5(OH)_{4\,(serpentine)} \rightarrow 3\,(Mg_{1-x-y},Fe_x,Ni_y)_2SiO_{4\,(olivine)} + SiO_{2\,(quartz)} + 4H_2O_{(gas)}$$

  - decomposition of minerals & partial reduction of oxides

$$\tfrac{1}{2}\,(Mg_{1-x-y},Fe_x,Ni_y)_2SiO_{4\,(olivine)} + (x+y)\,C_{(coal)} \rightarrow \tfrac{1}{2}(1-x-y)\,Mg_2SiO_{4\,(olivine)} + \tfrac{1}{2}(x+y)\,SiO_{2\,(quartz)} + Fe_xNi_{y\,(metal)} + (x+y)\,CO_{(gas)}$$

- **Electric Furnace**
  - Reduction of oxides to metal & slag-metal separation

$$Mg_2SiO_{4\,(olivine)} + y\,SiO_{2\,(quartz)} + Fe_xNi_{y\,(metal)} \rightarrow 2MgO\text{-}(1+y)SiO_{2\,(slag)} + Fe_xNi_{y\,(molten)}$$

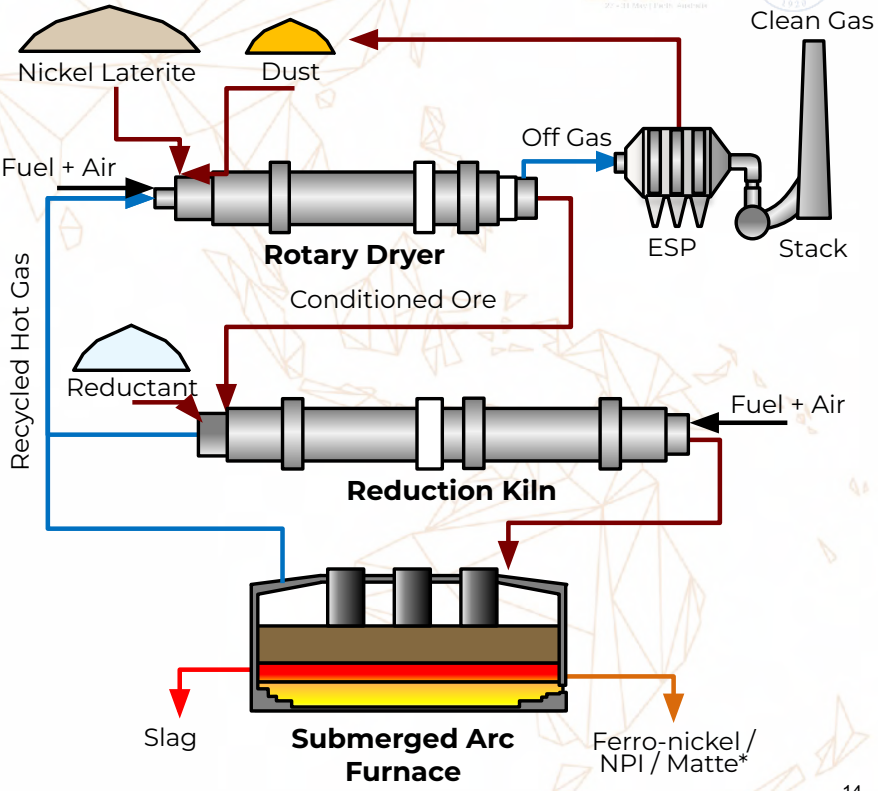

*Matte is produced via sulfur

Pyromet Plants – RKEF : Rotary Dryer

- Rotary Dryer (RD) uses hot gas to dry wet ore.
- Hot gas enters around 800°C and exits around 120°C.
- Different types of fuel (pulverized coal, natural gas, HSFO, etc) can be used to generate hot gas in boiler / stove / hot gas generator.
- Some NPI smelters reuse off-gas from Rotary Kiln and Electric Furnace as sources of hot gas.
- RD approximate dimension φ=5 m, L=50 m

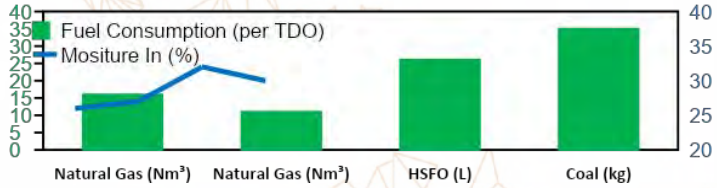

Sources: 1) A.E.M. Warner, C.M. Díaz, A.D. Dalvi, P.J. Mackey, and A.V. Tarasov. JOM World Nonferrous Smelter Survey, Part III: Nickel: Laterite. JOM, 2006

Pyromet Plants – RKEF : Rotary Kiln

- Rotary Kiln (RK) is cylindrical steel structure lined with Al_2O_3-rich castable heated by a burner.
- Solid material temperature in RK reached 700-900°C.
- Different types of fuel can be used, such pulverized coal, coal gasification, natural gas, HSFO, etc.
- NPI smelters utilize semi-coke as reductant.
- RK approximate dimension φ=5 m, L=100 m

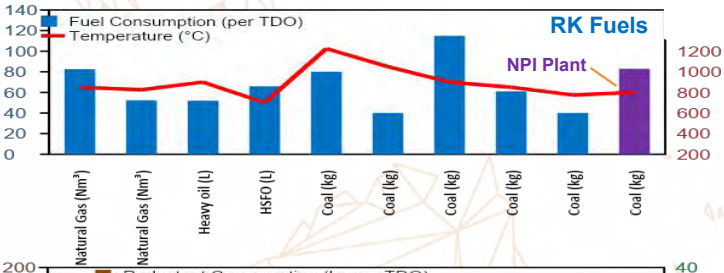

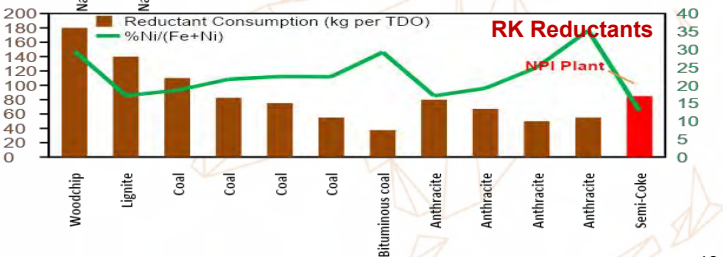

Sources: 1) A.E.M. Warner, C.M. Díaz, A.D. Dalvi, P.J. Mackey, and A.V. Tarasov. JOM World Nonferrous Smelter Survey, Part III: Nickel: Laterite. JOM, 2006

Pyromet Plants – RKEF : Electric Furnace

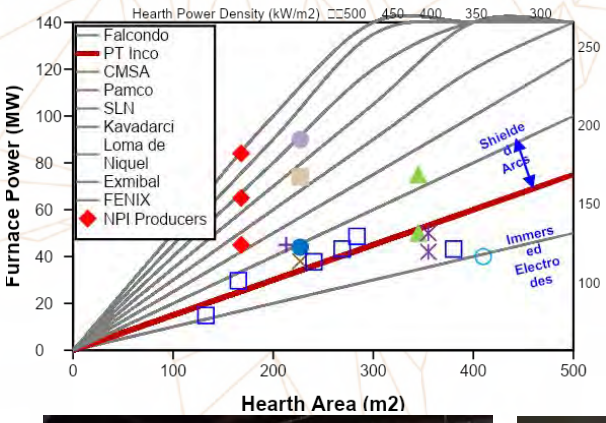

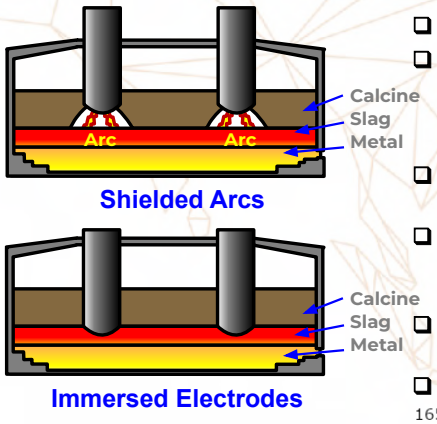

- Furnace operating temperature around 1500°C.
- Most NPI smelters operates in immersed electrodes to have a lesser power fluctuation and has simplified shell configuration without plate or finger copper coolers.
- In 2023, the Indonesia total NPI production reached ~1.4 Million t-Ni/yr.
- Part of the molten NPI is delivered to a stainless-steel plant within the industrial complex.
- Other part of the NPI is shipped overseas in the form of ingots.
- Some NPI has been converted to Ni matte.

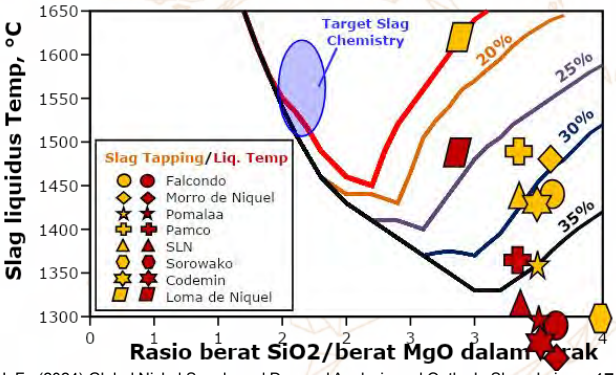

Sources: 1) https://www.sec.gov/Archives/edgar/data/1322422/000119312509009939/dex99106.htm 2) J. Fu (2024) Global Nickel Supply and Demand Analysis and Outlook. Shanghai Metals Market Webinar

Pyromet Plants – RKEF : FeNi to Matte

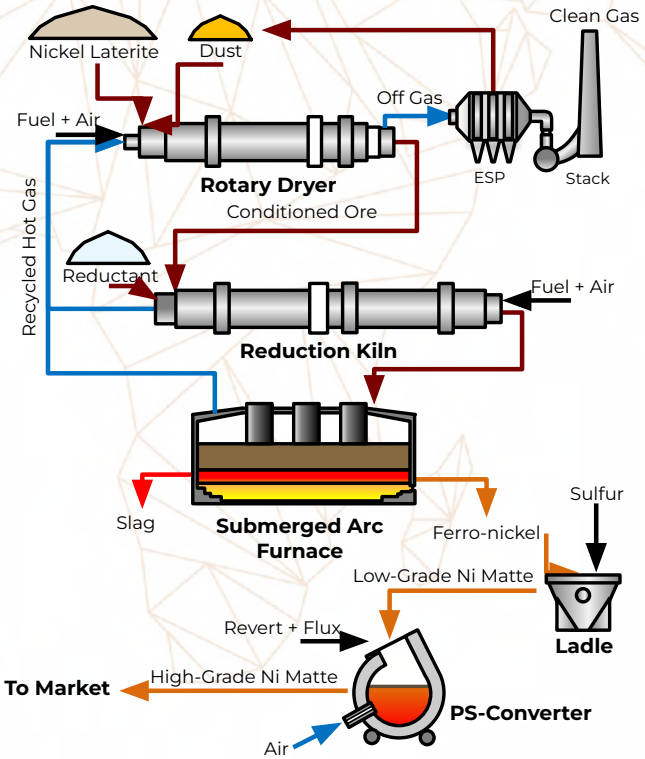

- Prior to 2022, matte was only produced by PT Vale Indonesia at Sorowako site.
- Due to high nickel matte profit margin, several companies has shifted from initially producing NPI (Ni Class 2) to producing Ni matte (Ni Class 1).
- The shift has been done through the addition of sulfur into the alloy and performing converting process in PS-converters.
- In 2023, the total nameplate capacity of the matte conversion facilities reached ~285 kt-Ni/yr with utilization rate at ~55%.

Sources: 1) J. Fu (2024) Global Nickel Supply and Demand Analysis and Outlook. Shanghai Metals Market Webinar

Pyromet Plants – RKEF : Waste Management

- **Significant waste generated at a smelter plant is slag. In case of NPI production, around 5 tons of slag is generated for every ton of metal product.**
- **Nickel slag is not considered as toxic and hazardous waste based on Indonesia Gov. Reg. No 22 Year 2021. This is confirmed by its TLCP* result which is below safe limit.**
- **The slag is commonly transported by trucks to an assigned dumping location where it is used as construction base for new plant area.**

* Toxicity Characteristic Leaching

RKEF Project Data

Plant Name	Location	Capacity, t Ni/yr	Year	Capex USD, millions	Unit Capex USD/t Ni/yr, thousands	Product
Onca Puma	Brazil	52,000	2011	3,200	62	FeNi
Barro Alto	Brazil	40,000	2011	1,900	48	FeNi
Koniambo	New Caledonia	30,000	2013	7,000	116	FeNi
Hengjaya Ni (TS/NIC)	Indonesia	16,500	2017	200*	12	NPI
Ranger Ni (TS/NIC)	Indonesia	16,500	2017	286*	17	NPI
Bahodopi (Vale/Tisco/Xinhai)	Indonesia	73,000	2025	2,200	30	FeNi

* Not including power plant

Sources: 1) https://nickelindustries.com/carbon/wp-content/uploads/2021/04/3-10-2019-Presentation-to-Investors.pdf
2) https://vale.com/in/w/financial-results-3q22#:~:text=The%20project%20estimated%20CAPEX%20is,400%20million%20for%20the%20mine

Pyromet Plants – Other Technologies

Blast Furnace (BF)

- BF is a conventional technology that has been utilized in Indonesia since the implementation of the export ban.
- Two BF plants are still in operation and four plants had been shutdown.
- Existing plants have total capacity between 100 and 500 kton Nickel Pig Iron / yr.

Oxygen-Rich Side-Blown Furnace (OESBF)

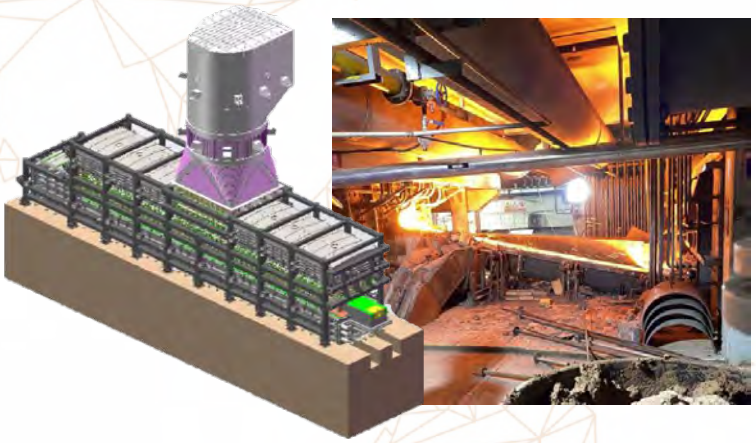

- OESBF is a new technology in Indonesia.
- One OESBF facility is already in operation and five OESBF facilities are under construction.
- Existing OESBF plant produces nickel matte product.
- Capital intensity of OESBF is claimed to be 9,000 USD/ton Ni/yr

Sources: 1) https://www.centralomega.com/id/release/news/progres-pembangunan-smelter
2) W. Yang (2023). Development and application of oxygen rich side blown bath melting technology for smelting high grade nickel matte in laterite nickel ore. Nickel and Cobalt Industry Chain Summit

Nickel Laterite Processing in Indonesia - Hydromet Plants

Indonesia Ni Hydromet Plants in 2023

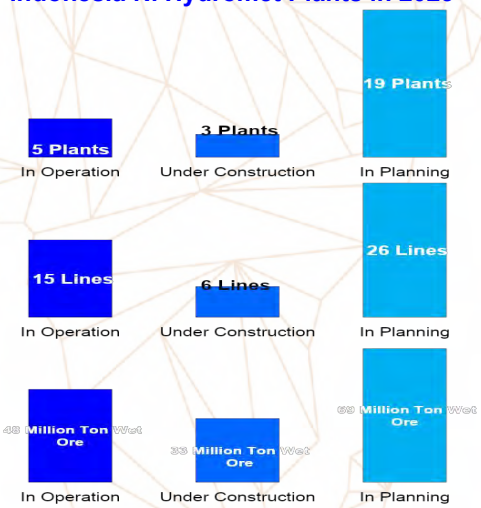

HPAL Companies in Operation in 2023

PT Halmahera Persada Lygend

QMB New Energy Materials

HUAYUE

HUAFEI

- Attractive pricing and royalty has boosted limonite processing.
- Fiscal incentives are available to accelerate HPAL development.
- The HPAL technology has enabled the total processing of all laterite layers.
- One company has advanced to further processing of MHP to $NiSO_4$ and $CoSO_4$.
- Indonesia government has strict rules on the disposal of HPAL tailing.

Key Locations

IMIP = Indonesia Morowali Industrial Park
IWIP = Indonesia Weda Bay Industrial Park

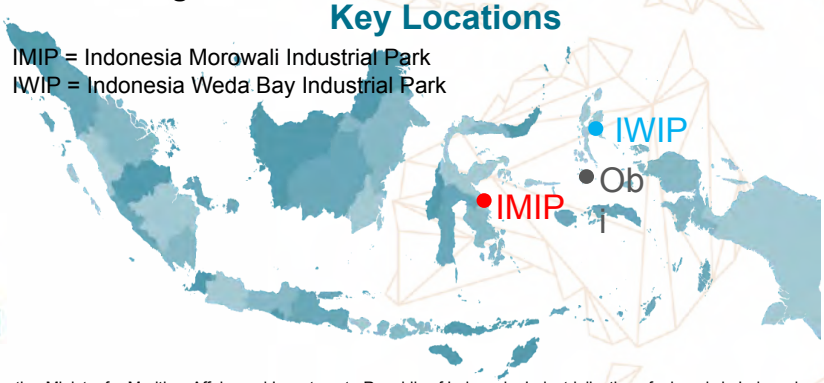

Sources: 1) Coordinating Ministry for Maritime Affairs and Investment - Republic of Indonesia, Industrialization of minerals in Indonesia now and in the future, 2023

Hydromet Plants – High Pressure Acid Leaching (HPAL)

- High Pressure Acid Leaching technology dominates the hydro processing of limonite ore.
- It is only suitable for processing limonite (mainly goethite mineral) because of its low Mg content and high Fe content.
- It can extract Ni and Co with a higher dissolution rate in a shorter time and lower acid consumption.

Hydromet Plants– HPAL : Process Flow

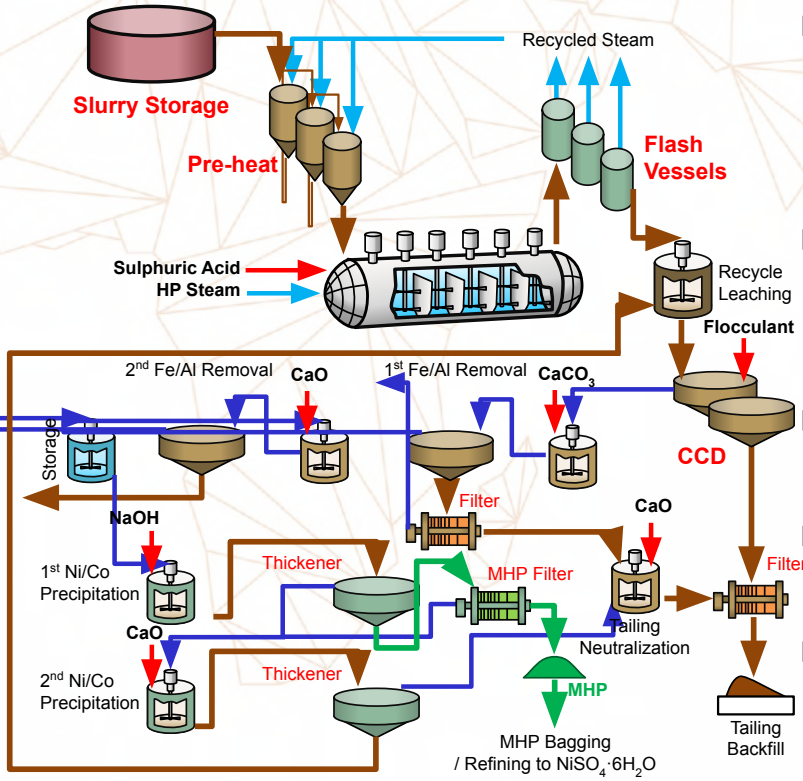

- **Pressure Acid Leaching**
  - Dissolution of Ni-Co, and precipitation of Fe

$$NiO_{(s)} + 2H^+_{(aq)} \rightarrow Ni^{2+}_{(aq)} + H_2O_{(aq)}$$
$$CoO_{(s)} + 2H^+_{(aq)} \rightarrow Co^{2+}_{(aq)} + H_2O_{(aq)}$$
$$2FeOOH_{(s)} + 6H^+_{(aq)} \rightarrow 2Fe^{3+}_{(aq)} + 4H_2O_{(aq)}$$
$$2Fe^{3+}_{(aq)} + 3H_2O_{(aq)} \rightarrow Fe_2O_{3(s)} + 6H^+_{(aq)}$$

- **Fe, Al, Cr Neutralization**
  - Elimination of Fe, Al and Cr impurities

$$Fe^{3+}_{(aq)} + 3OH^-_{(aq)} \rightarrow Fe(OH)_{3(s)}$$
$$Al^{3+}_{(aq)} + 3OH^-_{(aq)} \rightarrow Al(OH)_{3(s)}$$
$$Cr^{3+}_{(aq)} + 3OH^-_{(aq)} \rightarrow Cr(OH)_{3(s)}$$

- **MHP Precipitation**
  - Precipitation of Ni and Co hydroxide

$$xNi^{2+}_{(aq)} + (1\text{-}x)Co^{2+}_{(aq)} + 2OH^-_{(aq)} \rightarrow (Ni_x,Co_{(1-x)})(OH)_{2\,(s)}$$

- **Re-Leaching**
  - Dissolution of MHP

$$(Ni_x,Co_{(1-x)})(OH)_{2\,(s)} + 2H^+_{(aq)} \rightarrow xNi^{2+}_{(aq)} + (1\text{-}x)Co^{2+}_{(aq)} + 2H_2O_{(aq)}$$

- **Production of Ni-sulfate and Co-sulfate**
  - Separation and Recovery of Ni-Co as sulfates

$$Ni^{2+}_{(aq)} + SO_4^{2-}{}_{(aq)} + 6H_2O_{(aq)} \rightarrow NiSO_4\cdot6H_2O_{(s)}$$
$$Co^{2+}_{(aq)} + SO_4^{2-}{}_{(aq)} + 7H_2O_{(aq)} \rightarrow CoSO_4\cdot7H_2O_{(s)}$$

Hydromet Plants– HPAL : Autoclave

- Leaching at a temperature of 240-270 ºC (by steam injection), pressure 33-55 bar.
- The main leaching reagent is sulfuric acid.
- Performed in a titanium-lined autoclave (φ=~5 m, L=~40 m).
- Ni and Co recovery up to 95-96% can be achieved in just ±1 hour.
- Existing plants have 3-4 HPAL lines with capacity per line around 15,000 to 20,000 t-Ni/yr.
- Most plant is equipped with a dedicated sulfuric acid plant.
- The sulfuric acid plant produces residual steam which can be utilized for heating other process units and power generation.
- Indonesia total MHP production reached around 186 kt-Ni/yr in 2023.

Sources: 1) Indonesia Nickel Miners Association (2024) Indonesia's Nickel Strategy: Navigating Price Challenges And Sustaining Industry Growth.
2) https://www.kompas.id/baca/nusantara/2023/04/16/babak-baru-hilirisasi-nikel-di-pulau-obi

Hydromet Plants– HPAL : Waste Management

- Around 1.3 ton of tailing (dry basis) is generated for every ton of limonite processed.
- Three common tailing management methods for leaching waste:
  - Dry tailing storage
  - Storage in tailing ponds / dams
  - Deep sea tailing placement
- In Indonesia, deep sea tailing placement of HPAL tailing is not permitted by the Ministry of Environment and Forestry.
- The current practice for HPAL tailing handling in Indonesia is through dry tailing storage.

HPAL Project Data

Plant Name	Location	Capacity, t Ni/yr	Year	Capex USD, millions	Unit Capex USD/t Ni/yr, thousands	Product	Ramp-Up
Coral Bay Line 1	Philippines	10,000	2004	180	18	MSP	Fast
Coral Bay Line 2	Philippines	12,000	2008	370	31	MSP	Fast
Ravensthorpe	Australia	50,000	2008	3,900	78	MHP	Slow
Ramu	PNG	31,150	2011	2,100	67	MHP	Slow
Goro	New Caledonia	60,000	2012	6,000	100	MHP	Very Slow
Ambatovy	Madagaskar	60,000	2012	7,200	120	Metal	Slow
Taganito	Philippines	36,000	2013	1,700	47	MSP	Fast
Gördes	Turkey	10,000	2014	360	36	MHP	Slow
PT HPL Phase 1	Indonesia	35,574	2021	684	19	MHP	Very Fast
PT HPL Full Phase	Indonesia	55,875	2023	1,061	19	Sulfate	Very Fast
PT QMB	Indonesia	50,000	2022	998	20	MHP	Very Fast
PT Huayue Nickel Cobalt	Indonesia	55,655	2022	1,230	22	MHP	Very Fast
PT Huafei Nickel Cobalt	Indonesia	120,000	2023	2,080	17	MHP	In-Progress
PT Obi Nickel Cobalt	Indonesia	65,000	2024	1,100	17	MHP	In-Progress

Sources: 1) https://nickelindustries.com/carbon/wp-content/uploads/2021/04/3-10-2019-Presentation-to-Investors.pdf
2) Macquarie Research, CLSA 3) Global Mining Research, 2018

Hydromet Plants – Other Technology

Step Temperature Acid Leach (STAL) Technology

- **Process concept by PT Hydrotech Metal Indonesia**
  1. **Sulphation Roasting (In Rotary Kiln)**

     $NiO_{(s)} + H_2SO_{4(aq)} \rightarrow NiSO_{4(s)} + H_2O_{(g)}$

     $Fe_2O_{3(s)} + 3H_2SO_{4(aq)} \rightarrow Fe_2(SO_4)_{3(s)} + 3H_2O_{(g)}$

     At T > 600 °C : $Fe_2(SO_4)_{3(s)} \rightarrow 3SO_{3(g)} + Fe_2O_{3(s)}$

     $NiO_{(s)} + SO_{3(g)} \rightarrow NiSO_{4(s)}$
  2. **Water Leaching (In Leaching Tank)**

     $NiSO_{4(s)} + H_2O_{(l)} \rightarrow NiSO_{4(aq)} + H_2O_{(aq)}$
- **A similar concept has already been applied commercially for processing REE concentrates.**
- **The advantage of this process is that it operates at atmospheric pressure and its efficiency is not affected by the profile of the laterite ore.**
- **The application of this concept is already in pilot plant stage and is seeking opportunities to move to the commercial stage.**

STAL Technology's Pilot Plant

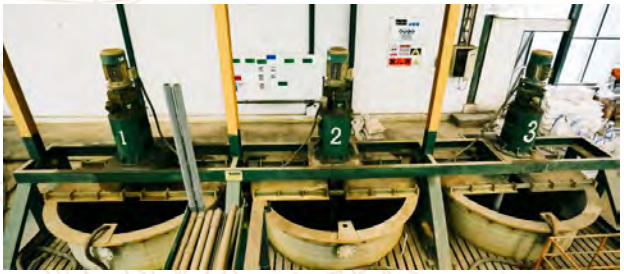

Sources: 1) https://hydrotechmetals.com/
2) https://stalt[illegible].com/stal_technology

Ni Payability, Selling Price and Cash Cost of Various Products

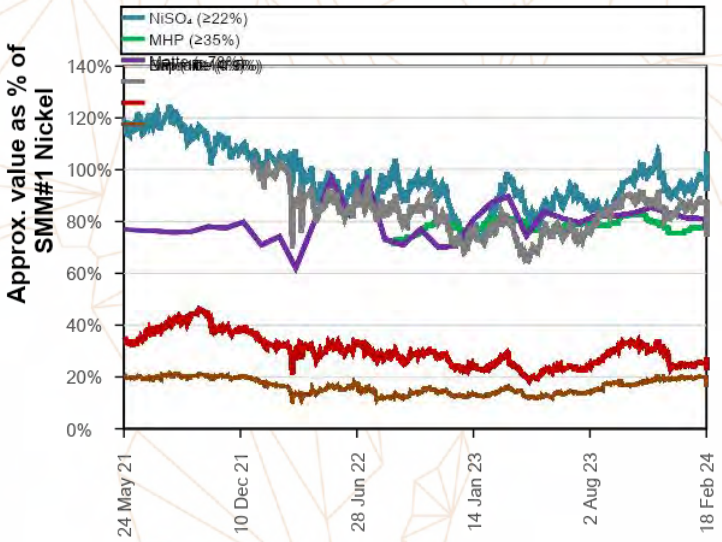

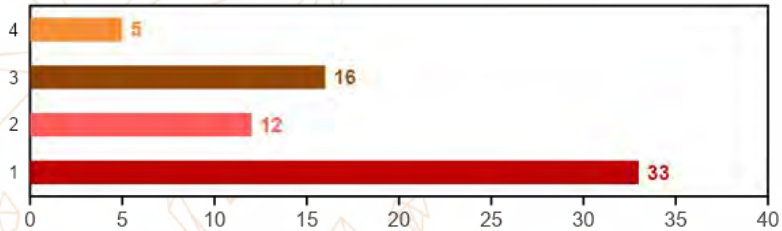

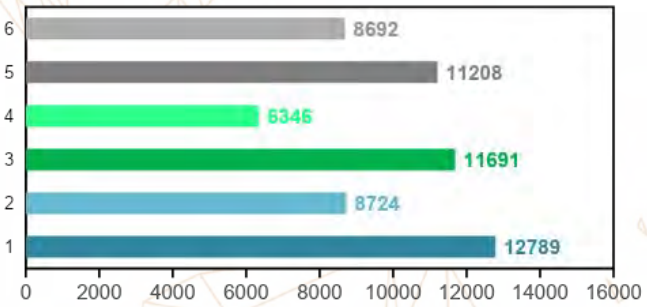

- Between 2021-2024, the Ni payability in ore is between 10-40%.
- The Ni payability in NPI dropped to 69% in December 2022 and rose back to around 70% in June 2023.
- The Ni payabilities in Nickel matte and MHP have been steady at around 80%.
- $NiSO_4$ is always highly priced with Ni payability fluctuates around 80 and 120%.
- Some of miners and processors in Indonesia maintain positive margins amidst drops in nickel prices.

Sources: 1) https://www.metal.com/Nickel 2) Indonesian Central Statistics Agency. Accessed 2024

Directions / Strategies of Indonesian Nickel industry

- Several strategies are already implemented / being tested to reduce emissions in nickel industry in Indonesia including:
  - Implementing heat recovery solutions to reduce coal consumption;
  - Use of biomass and biocarbon as a coal replacement;
  - Use of biofuels to reduce the emissions of vehicles and stationary equipment;
  - Use of conveyor belts or slurry pipeline for material transport to minimize vehicle emissions and dust pollution from material transportation;
  - Minimizing dependency on coal-fired power plant through substitution of energy source / power plant fuel;
  - Reducing the use of limestone;
  - Using electrification for transport vehicles;
  - Increasing efficiency of processes, machinery, and equipment.
- In addition, it is worth noting that the ore export ban policy also contributes to minimizing the carbon footprint associated with the transport of the low-grade ore materials.

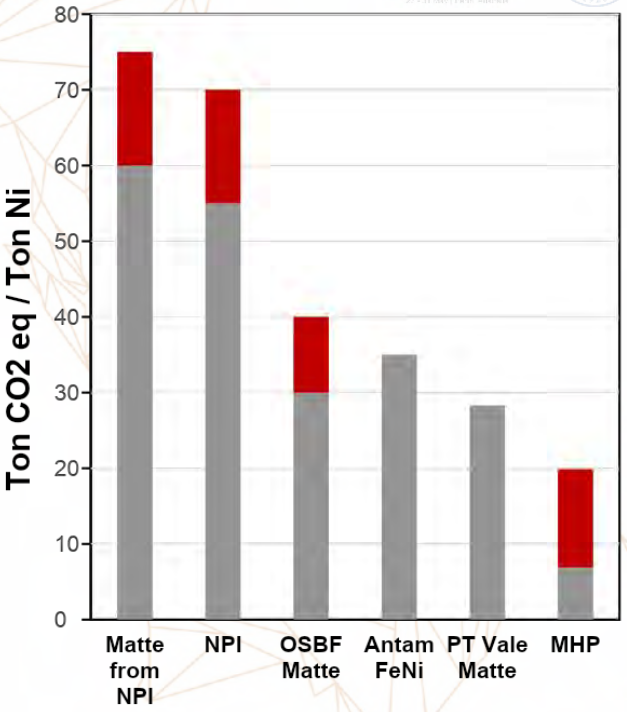

Sources: 1) McKinsey cite in T. Nugraha (2024) Evaluation of the Implementation and Development Direction of Nickel Downstreaming. Coordinating Ministry for Maritime Affairs and Investment of the Republic of Indonesia
2) https://wwwcdn.imo.org/localresources/en/OurWork/Environment/Documents/SecondIMOGHGStudy2009.pdf; 3) https://tbpnickel.com/sustainability/climate-change/greenhouse-gas-emissions;

Concluding Remarks

- **Indonesia has experienced significant growth in nickel laterite processing, driven by strategic initiatives.**
- **The government's policies, such as the nickel ore export ban, have attracted substantial foreign investment.**
- **The policies lead to the establishment of numerous nickel processing facilities. As a result, Indonesia has become a dominant player in global nickel production.**
- **Future government's supportive policies, coupled with innovative practices and research, will aim to ensure the sustainable operation and development in Indonesia nickel industry.**

THANK YOU FOR YOUR ATTENTION

Metallurgy Engineering Research Group
Faculty of Mining and Petroleum Engineering
Institut Teknologi Bandung
Jalan Ganesha No. 10, Bandung - 40132, Indonesia
Phone : +62 22 2502239
Fax : +62 22 2504209

t.hidayat@itb.ac.id
www.metallurgy.itb.ac.id

NICKEL LATERITES — GRADE DEFINITION AND PROCESS OPTIMIZATION BY MINERALOGICAL MONITORING USING X-RAY DIFFRACTION XRD

By

Uwe König

Malvern Panalytical B.V., The Netherlands

Presenter and Corresponding Author

Uwe König
uwe.koenig@malvernpanalytical.com

ABSTRACT

Nickel laterite production is on the rise, surpassing conventional sulfide deposits, to ensure global supply in the future. Nickel laterite ore is used to produce nickel metal, predominantly to manufacture stainless steel as well as nickel sulfate, a key ingredient in the batteries that drive electric vehicles.

The efficiency of mining and processing nickel laterites is defined by their mineralogical composition. Typical profiles of nickel laterites are divided into a saprolite and a laterite horizon. Nickel is mainly concentrated and hosted in a variety of secondary oxides, hydrous Mg silicates and clay minerals like smectite or lizardite in the saprolite horizon, whereas the laterite horizon can host cobalt that can be extracted as a side product.

A case study from both saprolite and laterite horizons was performed using X-ray diffraction (XRD) in combination with statistical methods such as cluster analysis. Besides the identification of the different mineral phases, the quantitative composition of the samples was also determined with the Rietveld method. Data clustering of the samples was tested and allows a fast and easy separation of the different lithologies and ore grades.

Mineralogy also plays a key role during further processing of nickel laterites to nickel metal. XRD was used to monitor the mineralogy of calcine, matte and slag. The value of mineralogical monitoring for grade definition, ore sorting, and processing will be explained in the presentation.

Keywords: nickel laterite; ore sorting; XRD; Rietveld; cluster analysis

Nickel laterites

Grade definition and process optimization by mineralogical monitoring using XRD

Uwe König, The Netherlands, uwe.koenig@malvernpanalytical.com

Malvern Panalytical
a spectris company

Types of nicke

Lateritic vs sulfidic

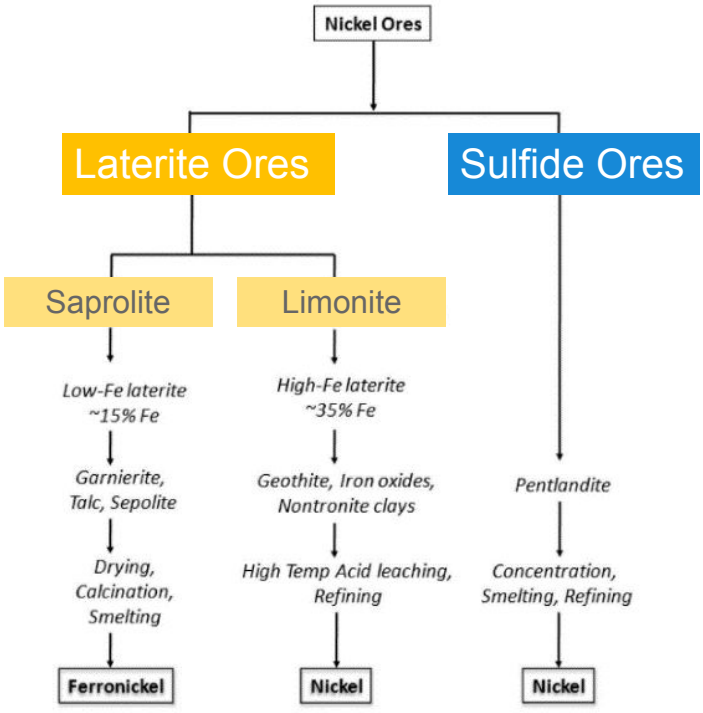

2011)

Nickel laterite processing

Mining

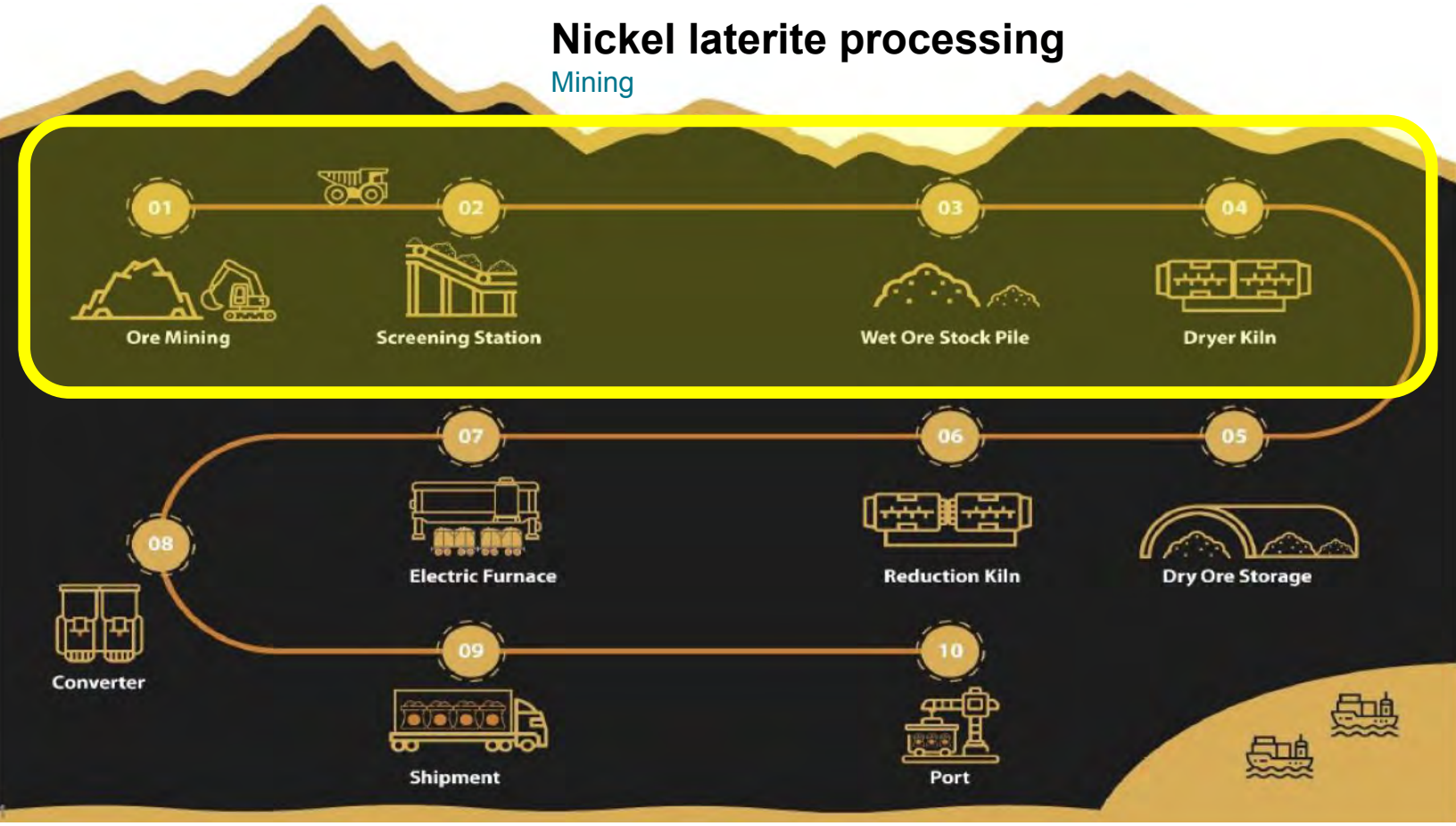

Nickel laterites

Schematic hydrous Mg-Si-silicate laterite profile

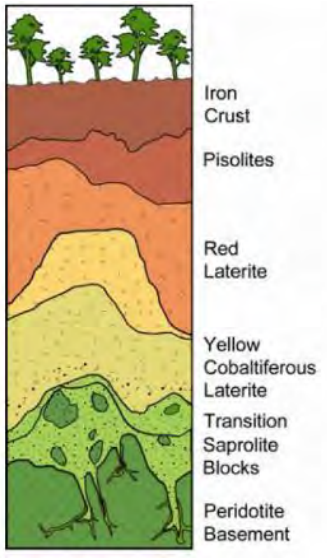

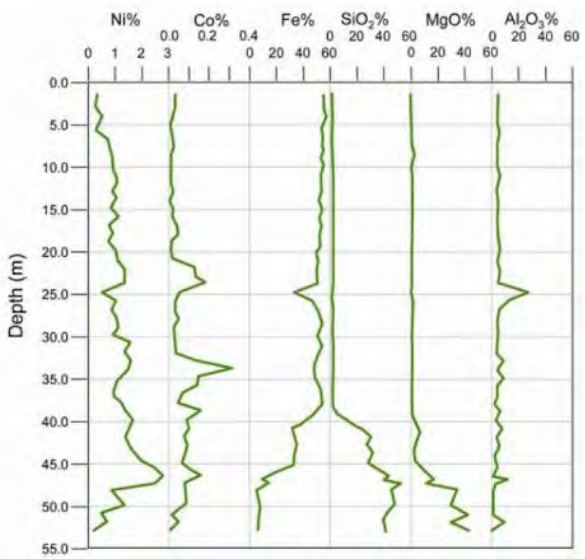

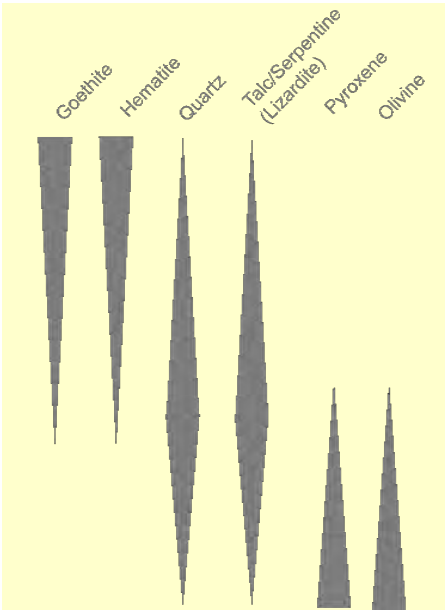

(Goro Nickel, 2006)

Nickel laterites

Samples

40 nickel laterite samples prepared for XRD measurements representing five main groups in the nickel laterite profile, left = high goethite, right = high lizardite

X-ray diffraction (XRD)

How does it work ?

- Identification and quantification of crystalline phases and amorphous content
- Monitoring of process parameters

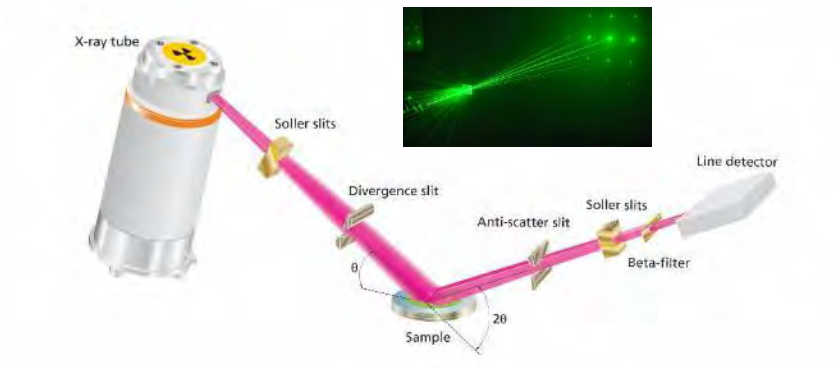

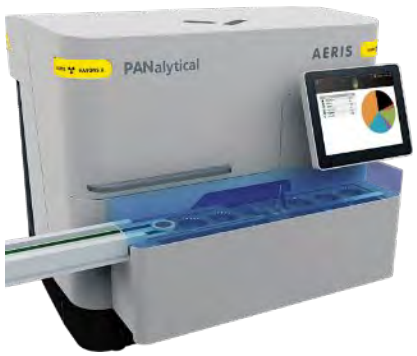

X-ray diffraction (XRD)

Mineralogy and more ….

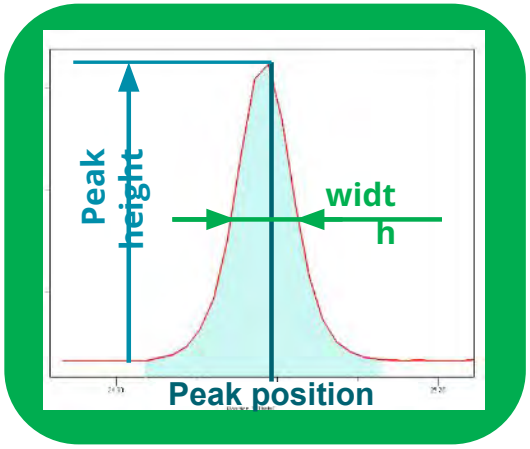

- Phase composition
- Amorphous content
- Crystallite size/microstrain
- Structural information
- Process parameters

Nickel laterites

Cluster analysis for ore sorting

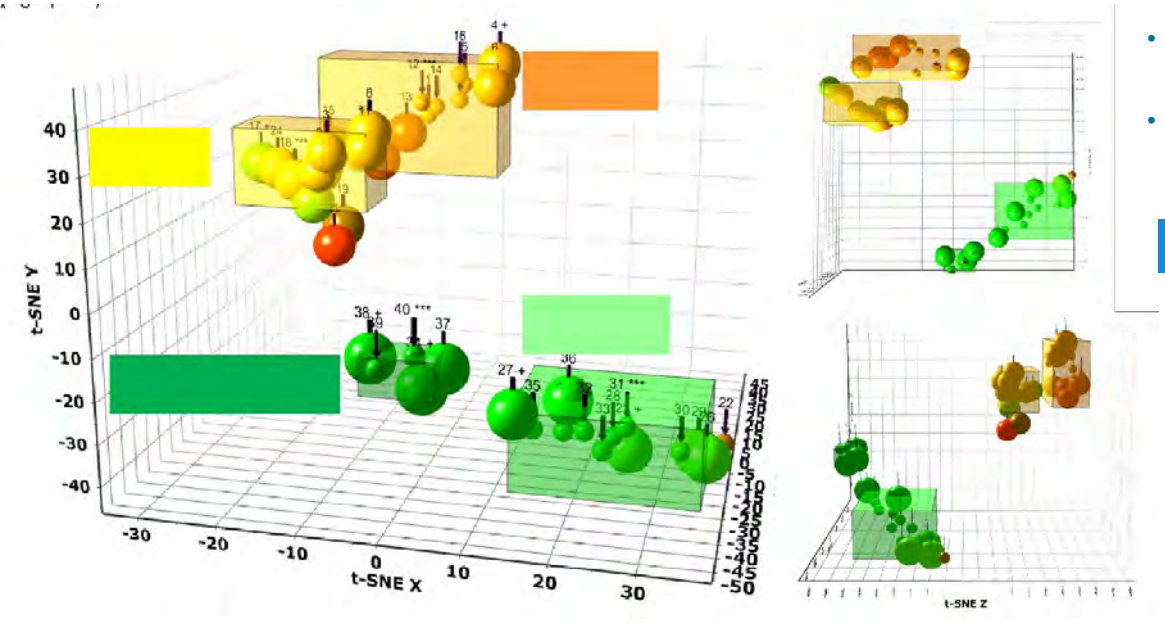

- 40 powder samples
- Clear separation between laterite and saprolite ores

Measurement time 5 min

Nickel laterites

Mineral identification / quantification

Mineral	Formula
Goethite	FeOOH
Hematite	Fe_2O_3
Gibbsite	$Al(OH)_3$
Quartz	SiO_2
Lizardite	$(Mg,Ni)_3(Si_2O_5)(OH)_4$
Talc	$Mg_3[(OH)_2Si_4O_{10}]$
Enstatite (Pyroxene)	$Mg_{15.44}Ca_{0.56}Si_{16}O_{48}$
Forsterite (Olivine)	$Mg_{7.17}Fe_{0.8}Ni_{0.02}Mn_{0.01}Si_4O_{16}$

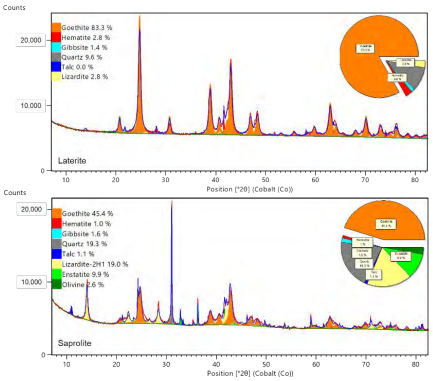

Nickel laterites

Mineral identification / quantification

Mineral	Formula
Goethite	FeOOH
Hematite	Fe_2O_3
Gibbsite	$Al(OH)_3$
Quartz	SiO_2
Lizardite	$(Mg,Ni)_3(Si_2O_5)(OH)_4$
Talc	$Mg_3[(OH)_2Si_4O_{10}]$
Enstatite (Pyroxene)	$Mg_{15.44}Ca_{0.56}Si_{16}O_{48}$
Forsterite (Olivine)	$Mg_{7.17}Fe_{0.8}Ni_{0.02}Mn_{0.01}Si_4O_{16}$

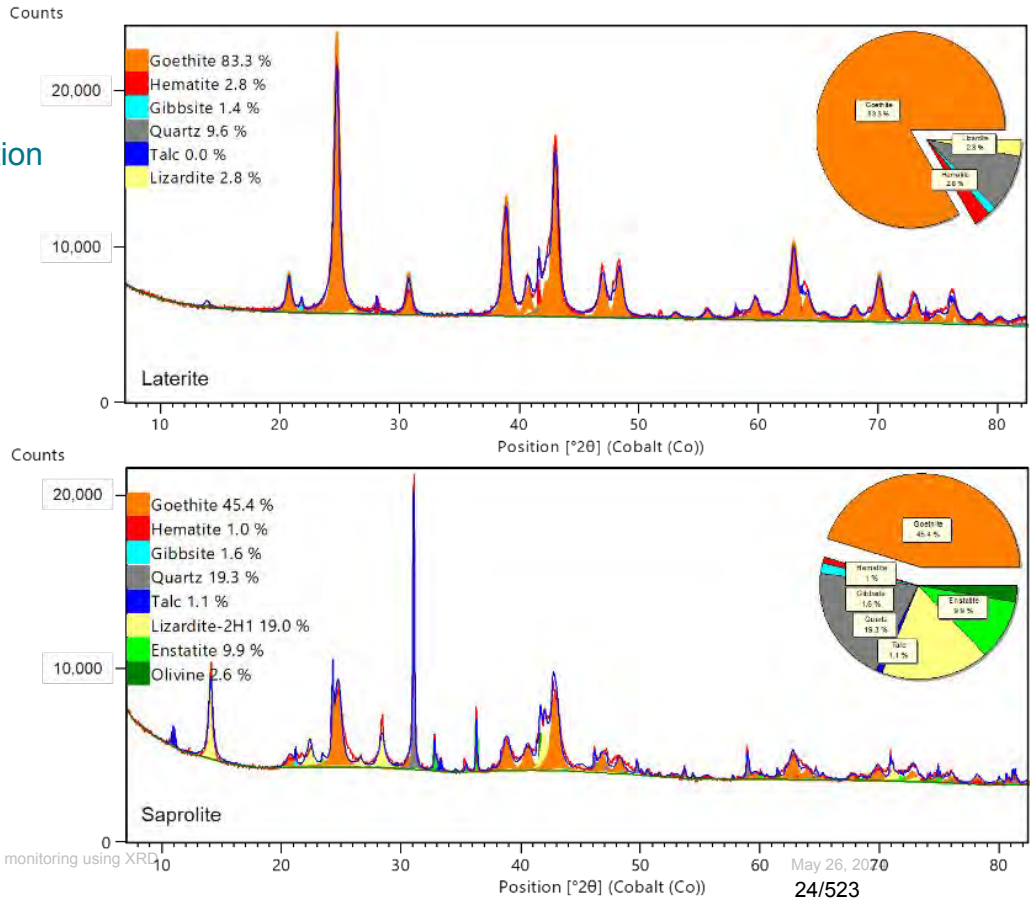

Nickel laterites

Mineral quantification

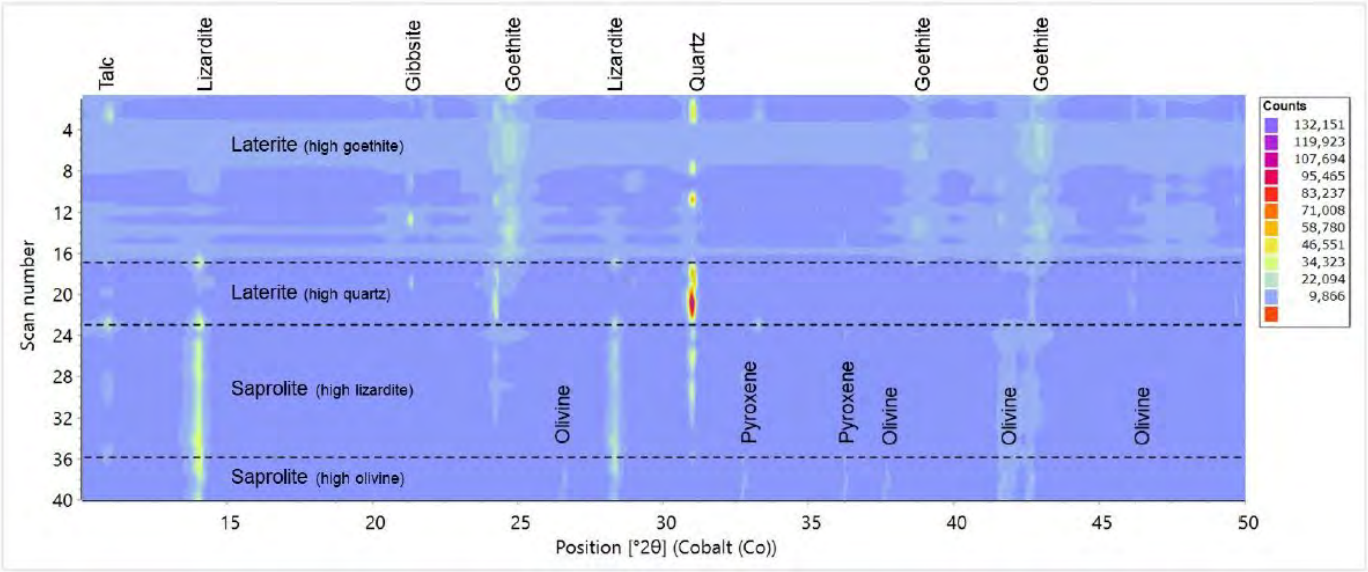

Figure 8. XRD scan surface plot of the region between 10° 2θ and 50° 2θ showing intensities of the main mineral phases.

May 26, 2024

Nickel laterites

Mineral quantification

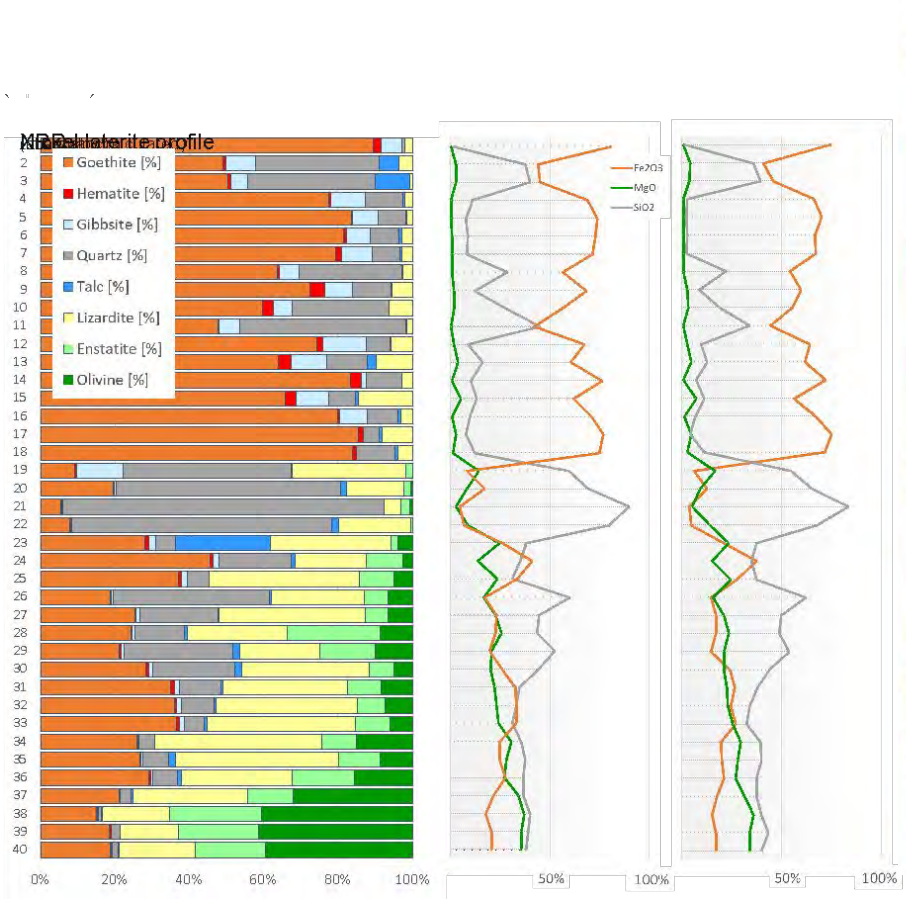

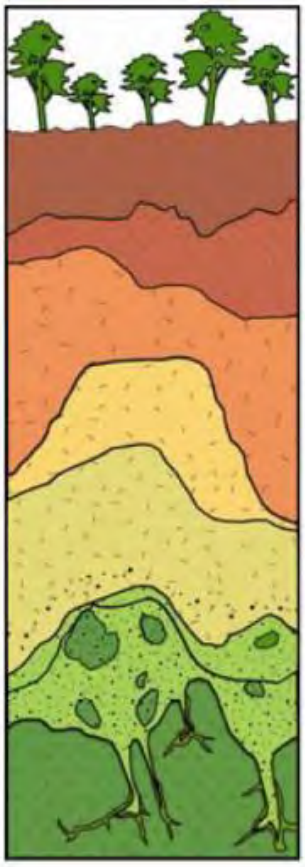

Mineralogical and elemental composition of 40 samples from a hydrous Mg-Si-silicate laterite profile

Nickel laterites

Lizardite and nickel content

- Comparison of the amount of lizardite (XRD) and the nickel content (XRF) in the saprolitic samples of the profile

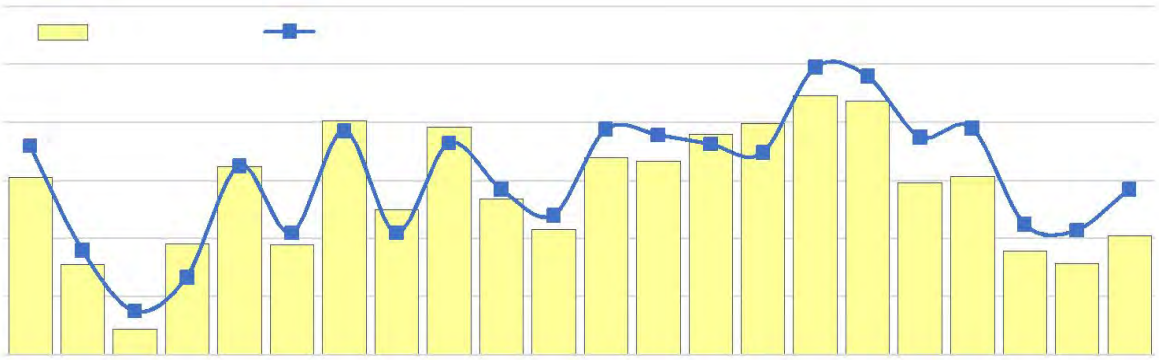

Nickel laterite processing

Smelting

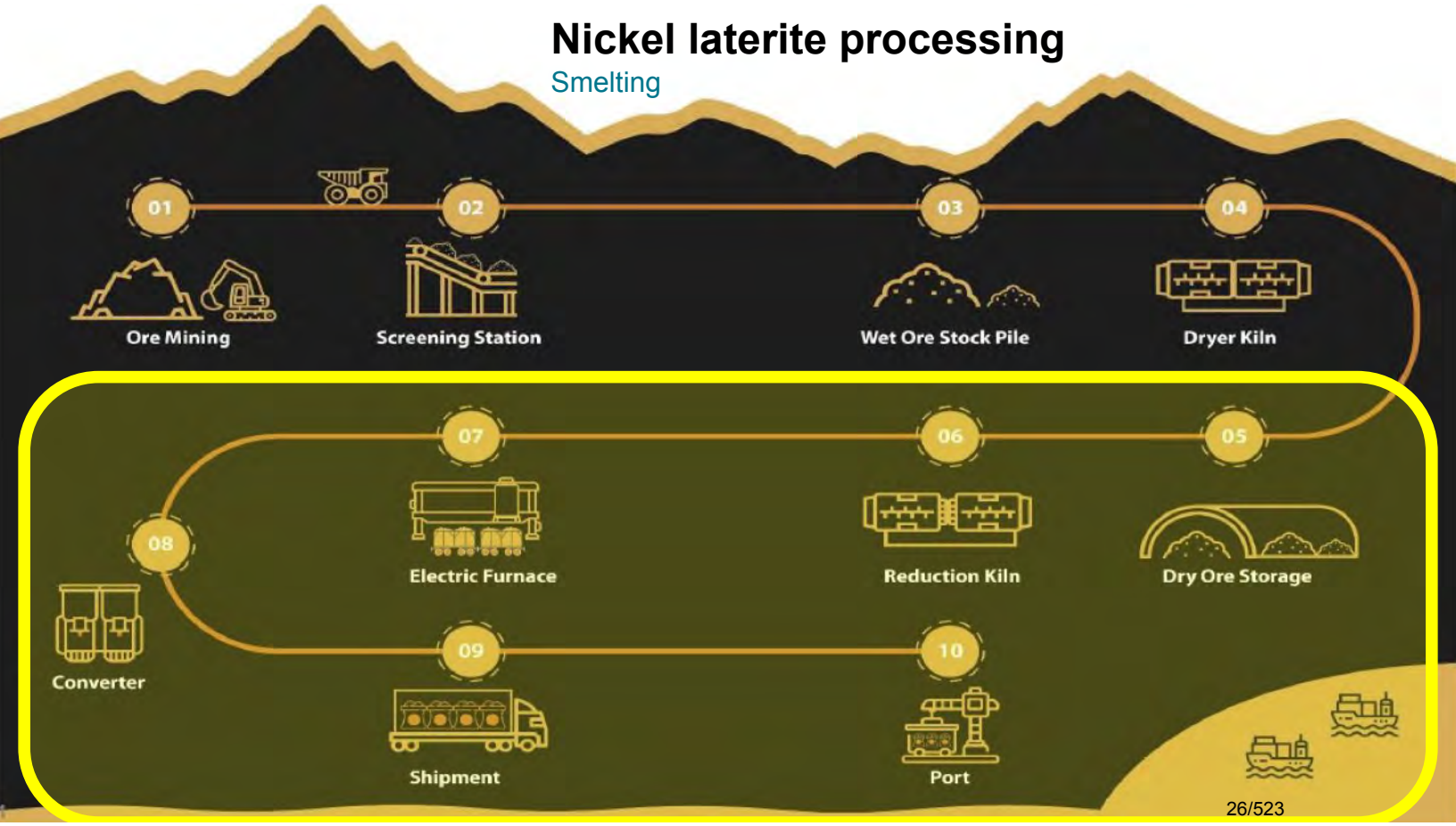

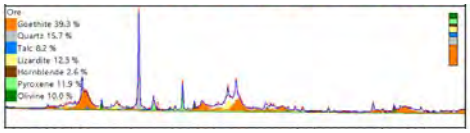

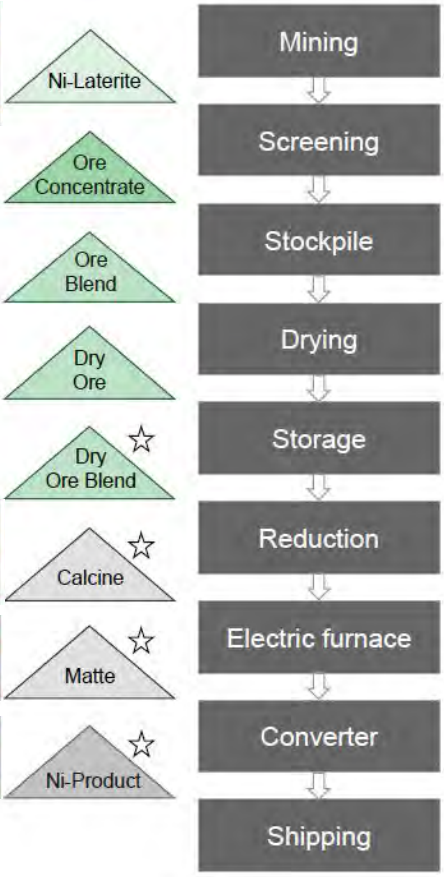

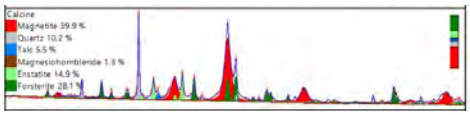

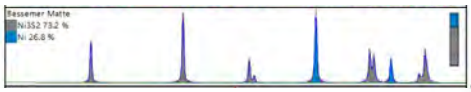

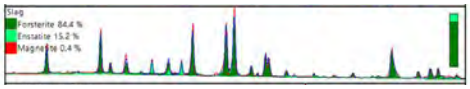

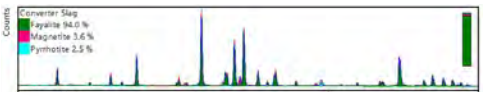

Table 4. Identified minerals in the process samples.

Mineral	Formula
Magnetite	Fe_3O_4
Hornblende	$(Ca,Na)_{2-3}(Mg,Fe,Al)_5(Al,Si)_8O_{22}(OH,F)_2$
Pyrrhotite	$Fe_{(1-x)}S$
Fayalite (Olivine)	Fe_2SiO_4
Nickel	Ni
Heazlewoodite	Ni_3S_2
Iron	Fe
Troilite	FeS

Nickel laterite processing

Ore

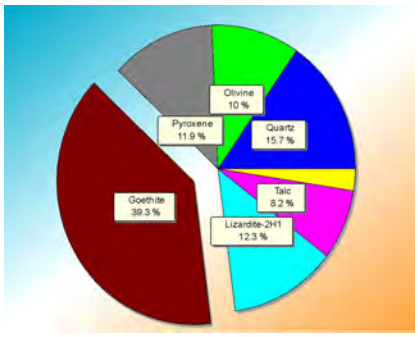

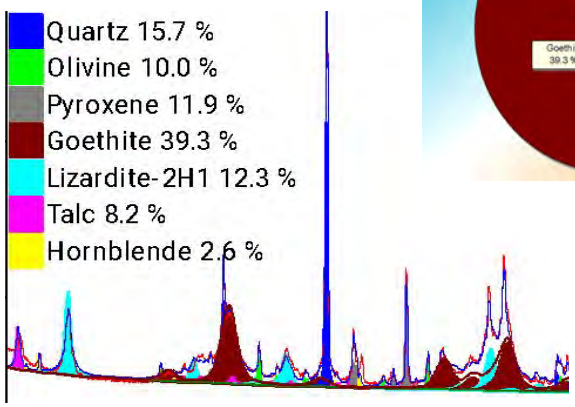

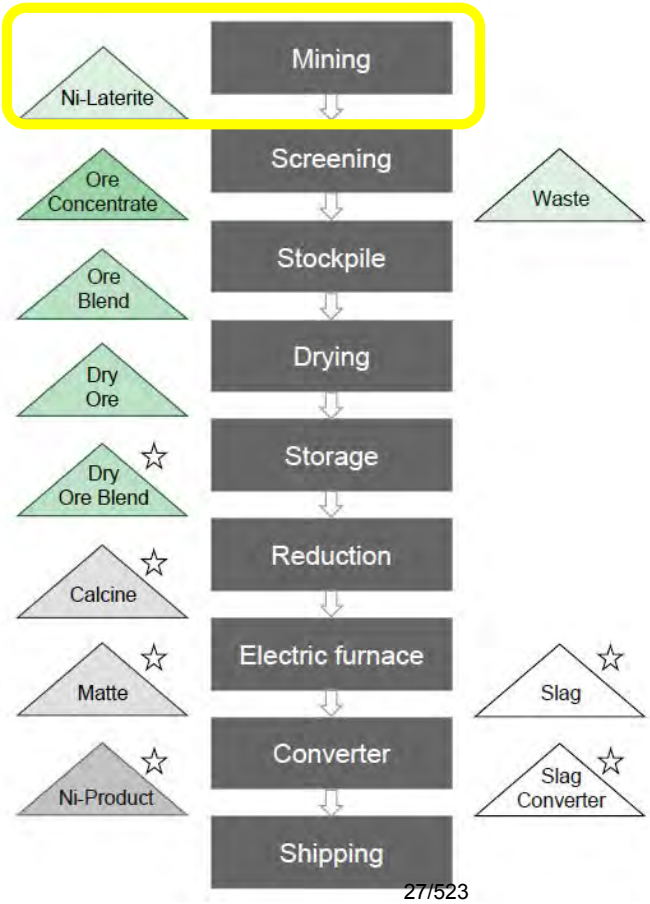

Nickel laterite processing

Blending

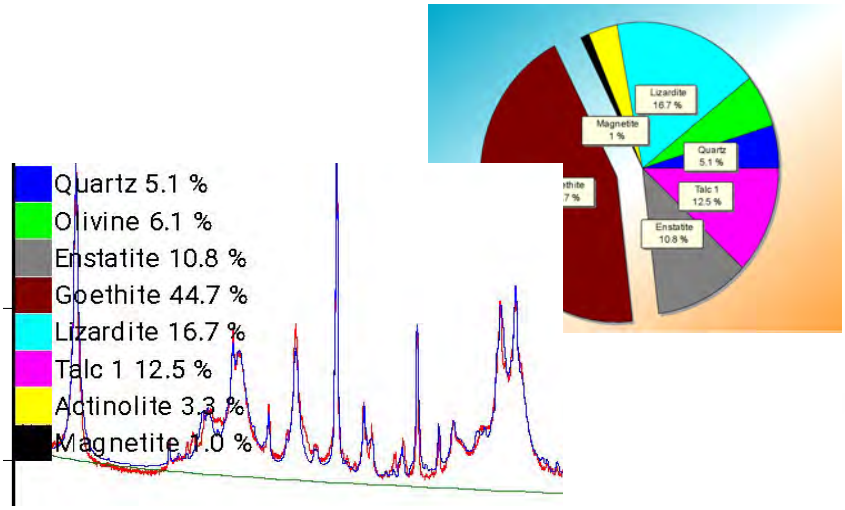

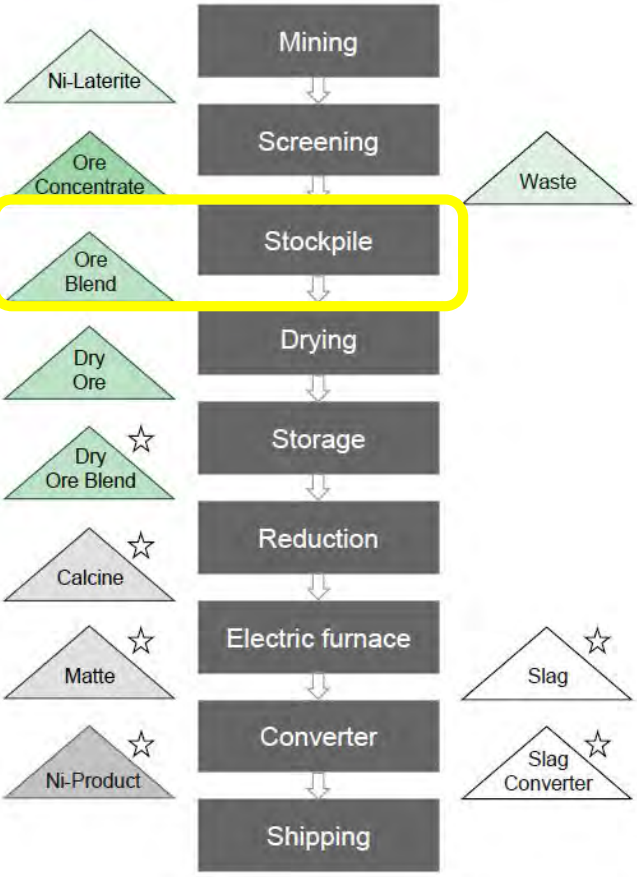

Nickel laterite processing

Roasting, Dehydration (Pre-reduction)

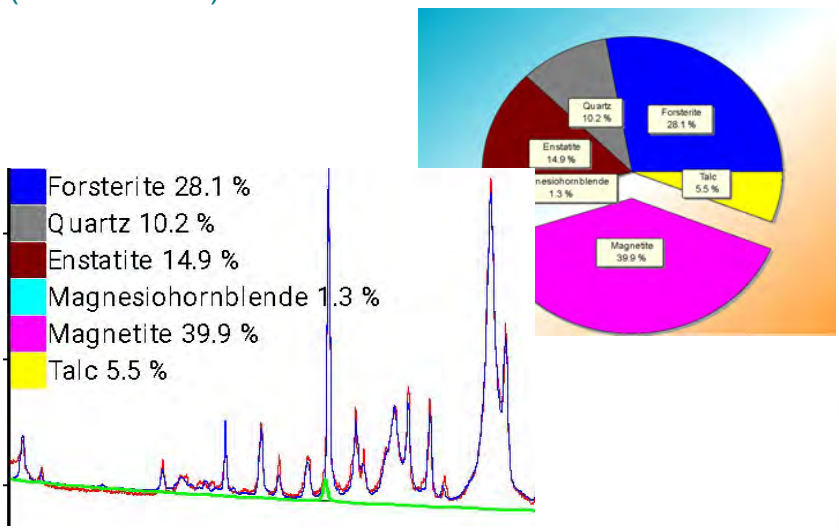

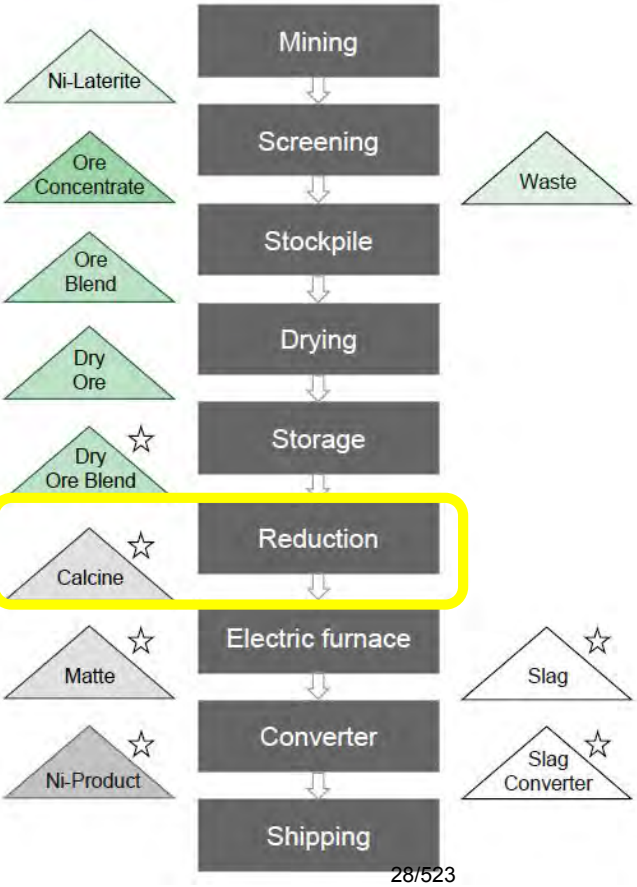

Nickel laterite processing

Matte (Sulphur addition)

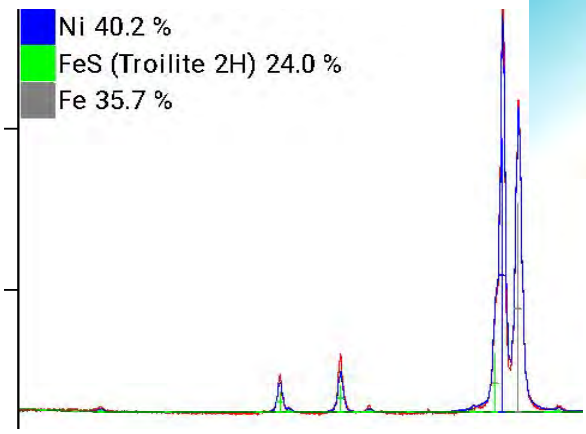

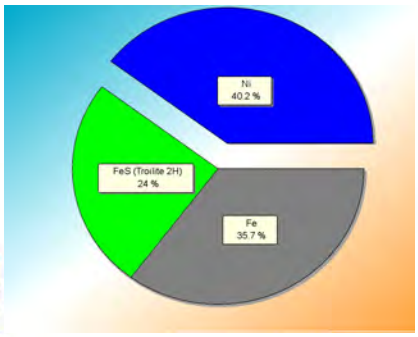

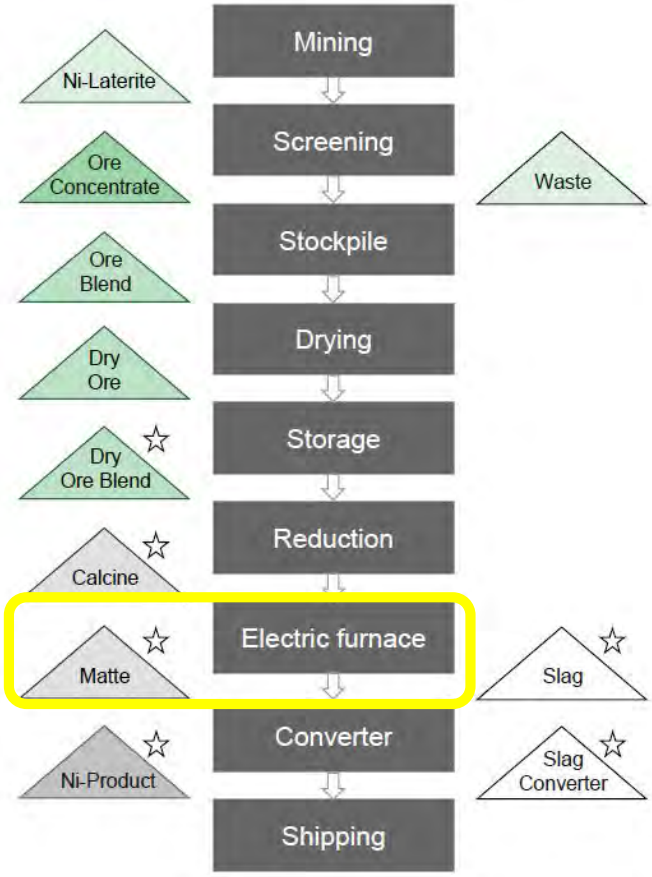

Nickel laterite processing

Product

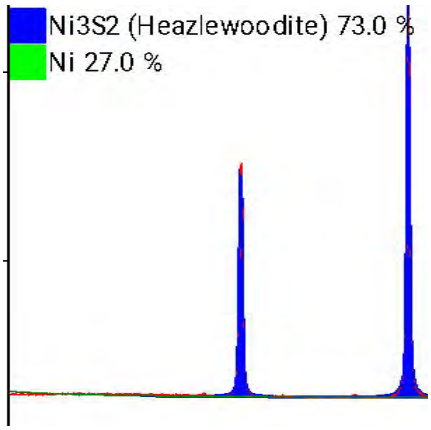

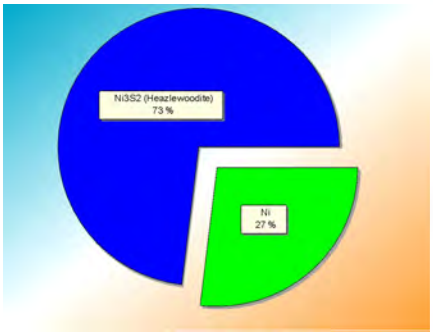

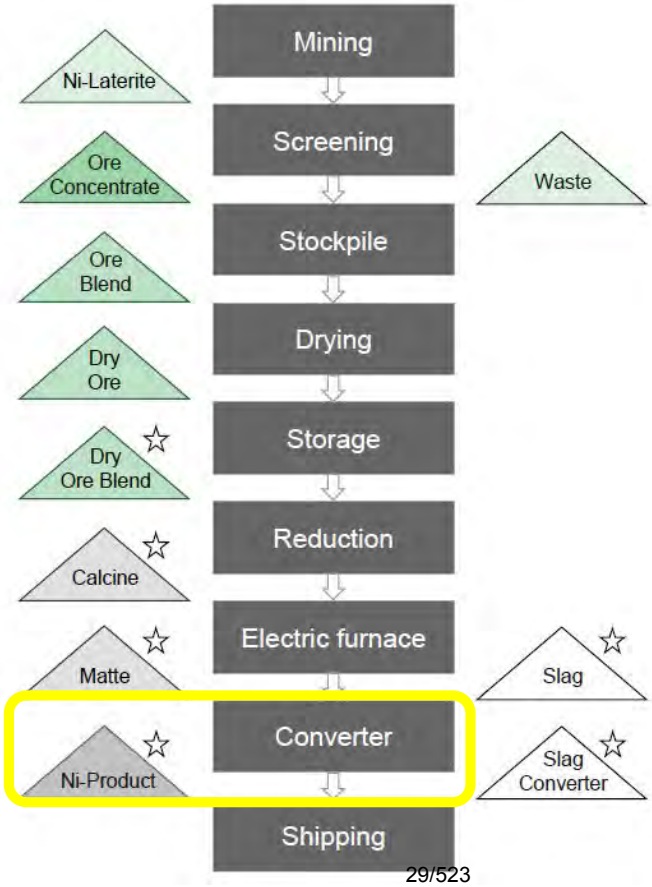

Nickel laterite processing

Converter slag

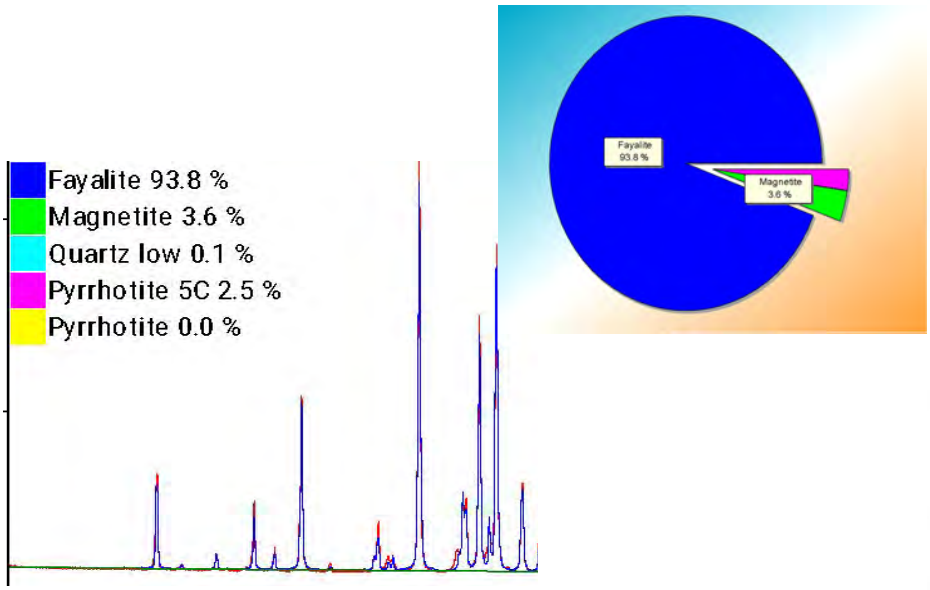

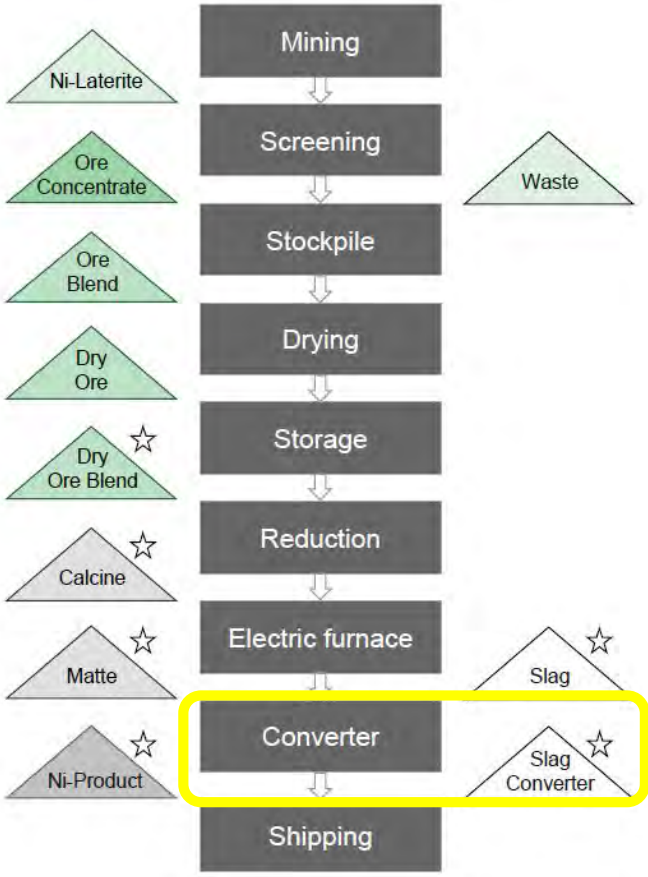

Value of mineralogical monitoring

Nickel laterites

Value	XRD - Tool
Optimization of ore blends from various nickel laterite deposits	Cluster analysis
Adjustment of superheat in the feed and optimization of energy costs	Mineralogy of ore blend
Control of mineralization acidity	Silicate composition
Prevention of highly corrosive slag causing erosion of the refractories	Silicate composition
Better reducibility in the furnace	Olivine content
Boost nickel recovery rates and reduction of metal loss in slag	Slag composition
Increase of cobalt recoveries	Co-bearing minerals

Suited for industrial environments

Aeris Benchtop diffractometer

- No need to access optical path for routine operation
  - No tampering
  - Good dust protection
- External sample loading makes automation very easy

Open Access Article

Nickel Laterites—Mineralogical Monitoring for Grade Definition and Process Optimization

by Uwe König

Malvern Panalytical B.V., Lelyweg 1, 7602 EA Almelo, The Netherlands

Academic Editor: Fang Xia

Minerals **2021**, *11*(11), 1178; https://doi.org/10.3390/min11111178

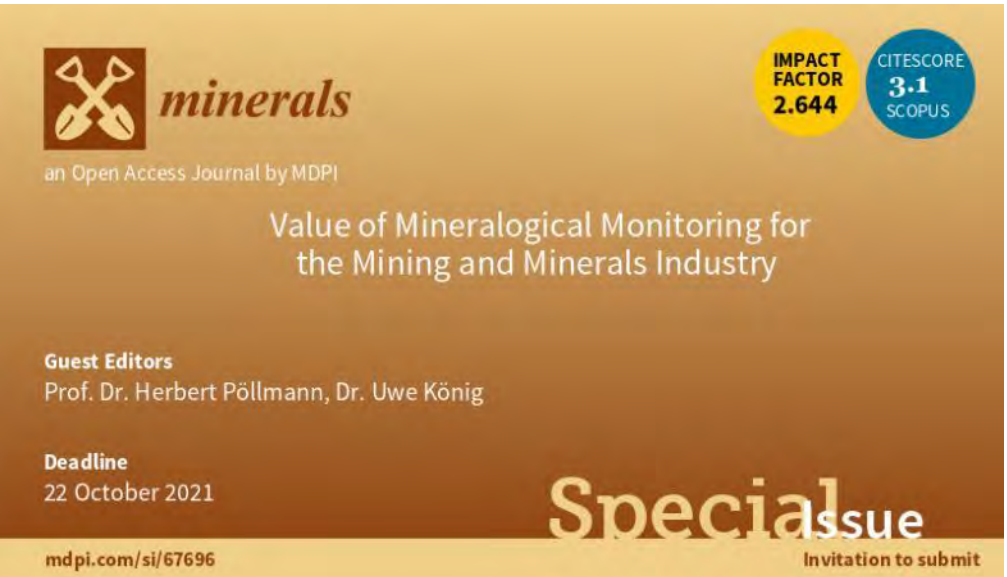

https://www.mdpi.com/1327496

NIR chemometric modelling

Nickel Laterites

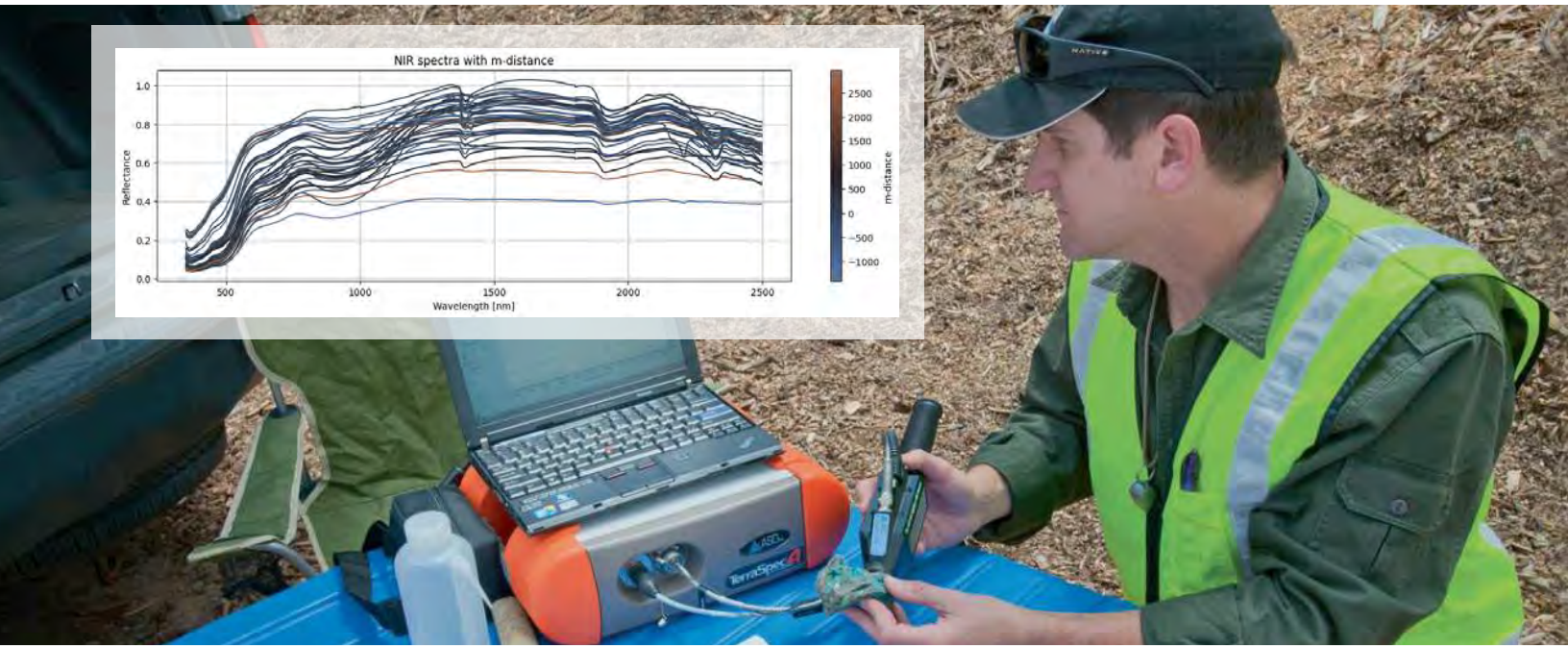

NIR chemometric modelling

XRD mineral composition comparison.

XRD

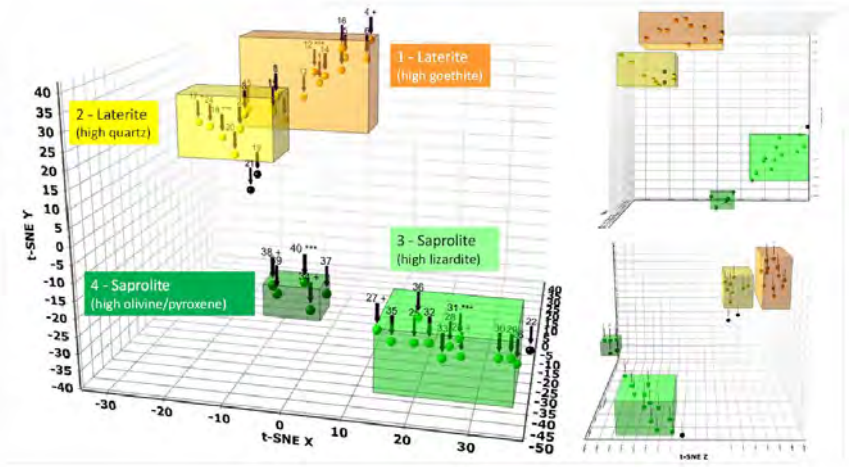

NIR

NIR chemometric modelling

Nickel Laterites – Single Assay Models

Lizardite

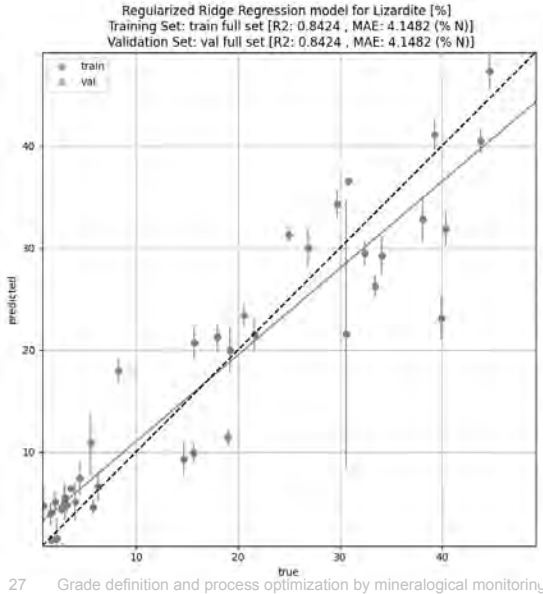

Goethite

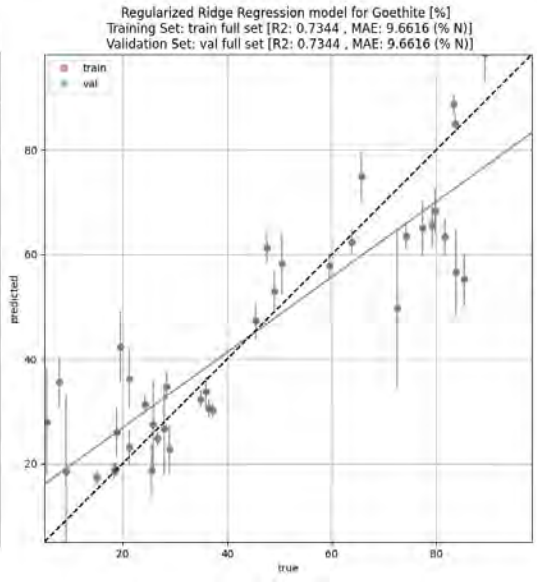

4 fold models trained on 30 samples and 10 test samples.
No data was held out for testing, performance on whole training set.

Acknowledgement:
Ed Morris, Malvern Panalytical
Evelien Rost, Malvern Panalytical

THE ATLAS MATERIALS PROCESS FOR LOW CARBON NICKEL

By

David Dreisinger, Jeremy Ley, Alexander Burns, Ken Baxter, [2]Mike Johnson, [2]Sridevi Thomas, [2]Niels Verbaan

Atlas Materials, USA
[2]SGS, Canada

Presenter and Corresponding Author

David Dreisinger
david.dreisinger@atlasmaterials.com

ABSTRACT

Atlas Materials is a climate technology startup with the objective of producing low carbon materials and contributing significantly to atmospheric decarbonization. The Atlas Materials Process treats nickel laterite ore using hydrochloric acid leaching to produce a silica residue for addition to cement making, a mixed hydroxide product containing nickel and cobalt for battery material processing, a small amount of manganese dioxide and magnesium hydroxide for the chemical market and, in the longer term, for carbon sequestration. Natural olivine mineral and sodium hydroxide are used to neutralize and precipitate the various products. Hydrochloric acid and sodium hydroxide are regenerated using the chlor-alkali process.

Atlas Materials has MOUs in place with two mining groups in New Caledonia (Société Minière Georges Montagnat (SMGM) and Société des Mines de la Tontouta (SMT)) for the supply of nickel saprolite ore. This ore will be processed in North America to create a domestic supply of nickel and cobalt for electrification of the transport sector while contributing to decarbonization of cement making and supply of the magnesium chemicals market.

The results of the Atlas Materials Demonstration Pilot Plant program conducted at SGS Canada (Lakefield, Ontario) will be presented and discussed. The program has been conducted in separate campaigns around (1) saprolite milling, (2) hydrochloric acid leaching and olivine neutralization for iron, aluminum and chromium removal, (3) two stage mixed hydroxide recovery and, (4) manganese removal and magnesium hydroxide precipitation. Finally, the entire process has been operated in continuous fashion over an extended period to supply engineering data for the first commercial facility, products for commercial evaluation and all necessary process environmental testing to facilitate permitting.

Keywords: Saprolite, hydrochloric acid, sodium hydroxide, chlor-alkali, supplemental cementitious materials, mixed hydroxide precipitate, manganese dioxide, magnesium hydroxide, decarbonization

The Atlas Materials Process for Low Carbon Nickel

David Dreisinger
ALTA 2024

Summary

- Nickel is critical to **the energy transition**
- Unique technology for producing low carbon, onshore, **fully traceable and clean battery grade nickel**
- **Well funded following US$27M Series A** in summer 2023
- **Plans for first commercial plant** well advanced

We are not on track to meet the Paris goals

- Electrification is the key

> The path to 1.5 °C has narrowed, but **clean energy growth is keeping it open.**
>
> **IEA**

https://www.iea.org/reports/net-zero-roadmap-a-global-pathway-to-keep-the-15-0c-goal-in-reach/executive-summary

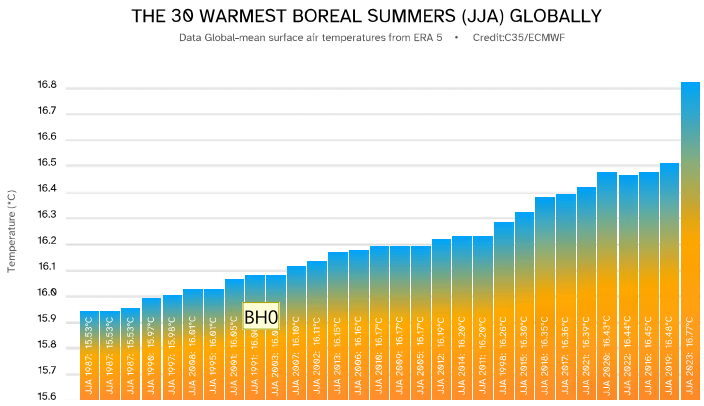

Nickel is critical but comes at an unsustainable cost

Nickel industry CO_2e curve (Scope 1 and 2 only) for 2020

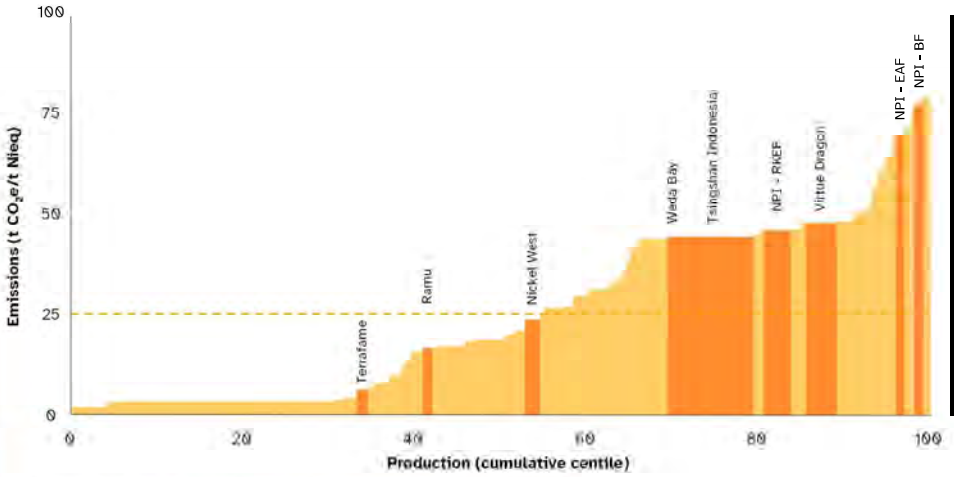

Nickel demand forecast to increase by up to 350% by 2050*

To reach net zero by 2050, **nickel value chains need to cut absolute emissions by ~90%** from 2020 levels**

But... **GHG emissions from primary nickel production could increase by up to 164% by 2050** reaching 232 MtCO2e/y**

Source: Wood Mackenzie

* https://www.sciencedirect.com/science/article/abs/pii/S0921344917301617

** https://ccsi.columbia.edu/sites/default/files/content/docs/publications/ccsi-net-zero-roadmap-copper-nickel.pdf

Huge demand growth from the EV sector

- Demand for battery grade nickel rising rapidly and beyond current capacity forecasts
- Supply chain standards are critical for major OEMs
- Currently very limited sources of sustainably produced nickel

> “Electric vehicles are the key technology to decarbonise road transport, a sector that accounts for around one-sixth of global emissions.”
>
> **IEA**

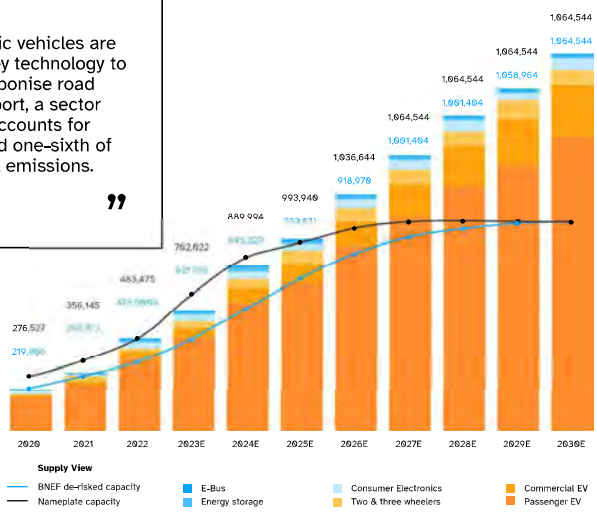

Source: BNEF

Atlas unlocks saprolite ore for batteries

Providing new sources of clean nickel

	Type of ore, % of global reserves	BH5 Countries	Processing Route	End Use
	Sulfide **(33%)**	Russia, Canada, Australia	Smelting	
Laterites	Limonite **(33%)**	Indonesia, Philippines, New Caledonia	HPAL	
Laterites	Saprolite **(33%)**	Indonesia, Philippines, New Caledonia	Smelting / Atlas	

How Atlas compares

	HYDROMETALLURGICAL ROUTES		PYROMETALLURGICAL ROUTES	
	Atlas Process	**High Pressure Acid Leach (HPAL)**	**Laterite Matte**	**Flash Smelting**
CO_2 Emissions (scope 1 and 2) t CO_2 per t Ni equivalent	0.1t[1,2]	19t	44t[3]	13t[4]
Gaseous Emissions	None	CO_2	CO_2	CO_2 and fugitive SO_2
Solid Emissions per t contained Ni	None	39t residue (dry basis)	50t slag	50 – 200t flotation tails 5.5 smelter slag

1. Determined by a third party engineering company as a part of a study commissioned by Atlas. Reference: Perrenin, A, & Benotmane, A. (2023). Atlas Saprolite Process Comparison: Final Report (No. H376678-0000-109-066-0001). Hatch.
2. Production in USA using renewable energy. The stated value is for the primary production step within Atlas. Operational control, from mined ore to MHP.
3. Production in SE Asia. The stated value is for the primary production step, from mined ore to MHP or matte.
4. Production I Australia. The stated value is the average of BHP's Australian operations, and includes all emissions within BHP's operational control. Reference: BHP ESG Standards and Databook 2022. (2022). BHP.

Atlas clean nickel

Less than 0.1 ton of CO_2 per ton of nickel when powered by renewables

Zero waste - all ore is utilized

No SOx or NOx

Pilot Plant Operations Continuing and FEL-3 Engineering Studies Nearing Completion

Proven, low risk technology

Works at **atmospheric pressure***

Works at **atmospheric temperature***

Combines existing proven processing technologies

Proven on ores from **major nickel mines**

* Perrenin, A, & Benotmane, A. (2023). Atlas Saprolite Process Comparison: Final Report- Hatch

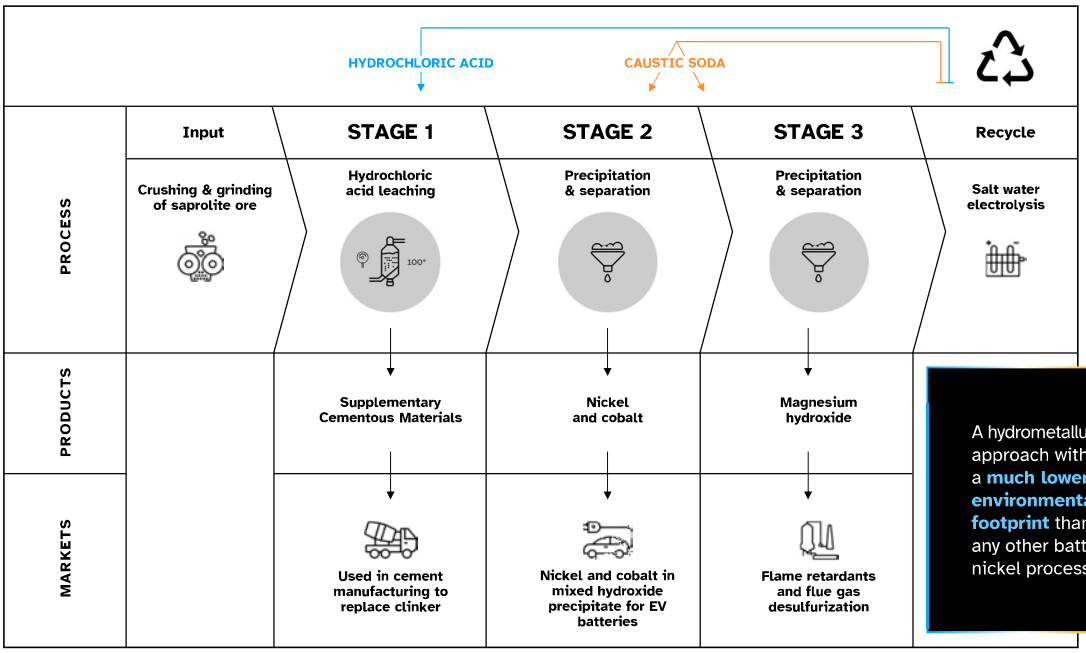

Process chart

A hydrometallurgical approach with a **much lower environmental footprint** than any other battery nickel processes.

Process Chemistry

Original Concept (Simplified)

- Hydrochloric Acid Extraction of Magnesium from Magnesium Silicate Materials
- Precipitation of Magnesium Hydroxide Using Caustic
- Regeneration of Hydrochloric Acid and Caustic Using Renewable Electricity
  - $Mg_2SiO_4 + 4HCl(a) = 2MgCl_2 + SiO_2 + 2H_2O$ (1)
  - $2MgCl_2 + 4NaOH = 2Mg(OH)_2 + 4NaCl$ (2)
  - $4NaCl + 4H_2O = 4NaOH + 2Cl_2(g) + 2H_2(g)$ (3)
  - $2Cl_2(g) + 2H_2(g) = 4HCl(g)$ (4)
  - $4HCl(g) = 4HCl(aq)$ (5)

What about other elements?

Process Chemistry

Other Elements

- Fe, Al, Cr, Ni, Co, Zn, Mn etc are extracted by the strong HCl leach
- Original approach
  - Caustic to remove Fe/Al/Cr as hydroxide
  - Caustic to precipitate Ni/Co + (Zn/Cu) as MHP
  - Caustic/Bleach to precipitate Mn as MnO_2
  - Caustic to precipitate $Mg(OH)_2$
- Fe/Al/Cr precipitate very fine and difficult to separate from solution.
- New idea – use olivine as a base for precipitation

Process Chemistry

Ferrous Oxidation and Olivine Precipitation

$$2FeCl_2 + NaOCl + 2HCl = 2FeCl_3 + NaCl + H_2O \quad (6)$$

$$4FeCl_3 + 3Mg_2SiO_4 + 2H_2O = 4FeO.OH + 6MgCl_2 + 3SiO_2 \quad (7)$$

$$4AlCl_3 + 3Mg_2SiO_4 + 2H_2O = 4AlO.OH + 6MgCl_2 + 3SiO_2 \quad (8)$$

Nickel Precipitation

$$NiCl_2 + 2NaOH = Ni(OH)_2 + 2NaCl \quad (9)$$

Manganese Oxidation and Precipitation

$$MnCl_2 + NaOCl + 2NaOH = MnO_2 + 3NaCl + H_2O \quad (10)$$

Magnesium Hydroxide Precipitation

$$MgCl_2 + 2NaOH = Mg(OH)_2 + 2NaCl \quad (11)$$

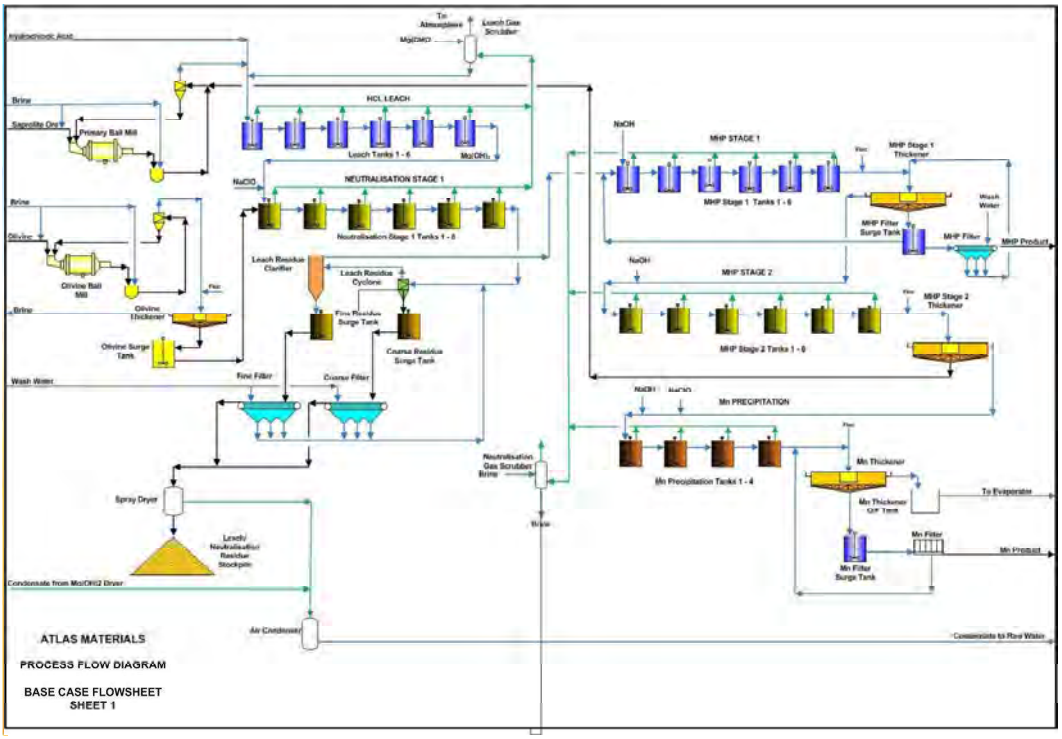

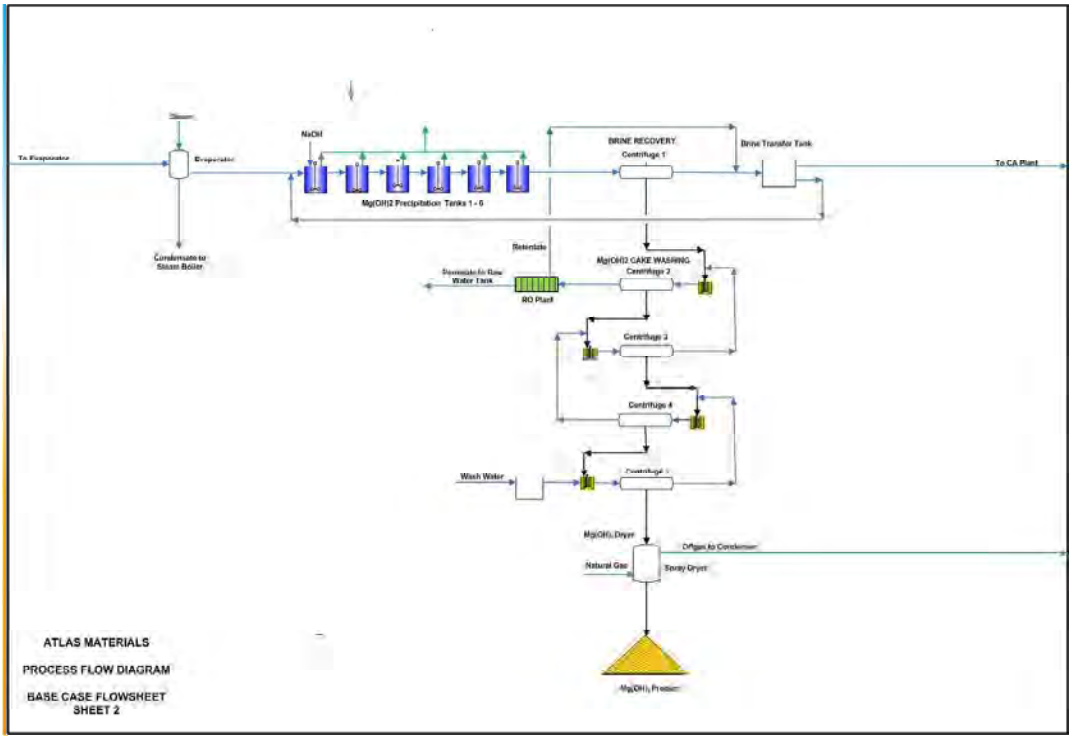

Demonstration Pilot Plant Results

Pilot Plant Program

- Pilot plant 1 (PP1) - acid leach and olivine neutralization process
- Pilot plant 2 (PP2) - precipitation of MHP and scavenger MHP
- Pilot plant 3 (PP3) manganese removal + $Mg(OH)_2$ pptn
- Saprolite ore from Societé des Mines de la Tontouta (SMT) and Société Minière Georges Montagnat (SMGM). Olivine from Sibelco

Chemical Analysis

Element	Analysis (%)	
	Saprolite (SMT)	Olivine
Ni	1.75	0.28
Co	0.07	0.01
Fe	8.67	5.27
Mg	16.1	28.7
Al	0.18	0.33
Cr	0.42	0.25
Mn	0.16	0.08
Ca	0.04	0.20
Si	21.7	19.4
LOI	14.7	2.19

Pilot Plant 1 (Leach and Olivine Neutralization)

Continuous testing for 5 days (24/7)

The ground ore (34% solids) added at a rate of 2 kg/h (dry basis) to a series of four stirred leaching reactors that overflowed in a cascade fashion.

32% HCl was added to the first reactor at dosage of 640 kg HCl/t ore (dry basis).

Temperature of 102 °C.

The leach residence time was 4 hours.

Five olivine neutralization reactors. The olivine slurry (60% solids) addition rate of 0.28 g/g ore feed.

Bleach (11% NaOCl) added to the third reactor to oxidize ferrous ion.

ORP control

Pilot Plant 1 (Leach and Olivine Neutralization)

Leach Extractions (Average): 98% Ni, 95% Fe, 95% Mg, 46% Al, 14% Cr, 97% Mn, 84% Ca were achieved with residual free acid at 1-6 g/L HCl.

Final solution after olivine neutralization: 5.1 g/L Ni, 0.197 g/L Co, 7.9 mg/L Fe, 60.4 g/L Mg, 0.9 mg/L Al, <0.3 mg/L Cr, 0.37 g/L Mn, 0.34 g/L Ca, 23 mg/L Si.

High extraction and effective purification

Residue analysis: 30.9% Si (66.1% SiO_2), 11.4% Fe, 4.24% Mg, 0.31% Al, 0.51% Cr, 0.13% Ni, 0.01% Co.

This material is under evaluation as a fly ash replacement for cement making.

The solutions were recovered by filtration and wash water addition.

Pilot Plant 1 (Leach and Olivine Neutralization)

Leach Solution Analysis

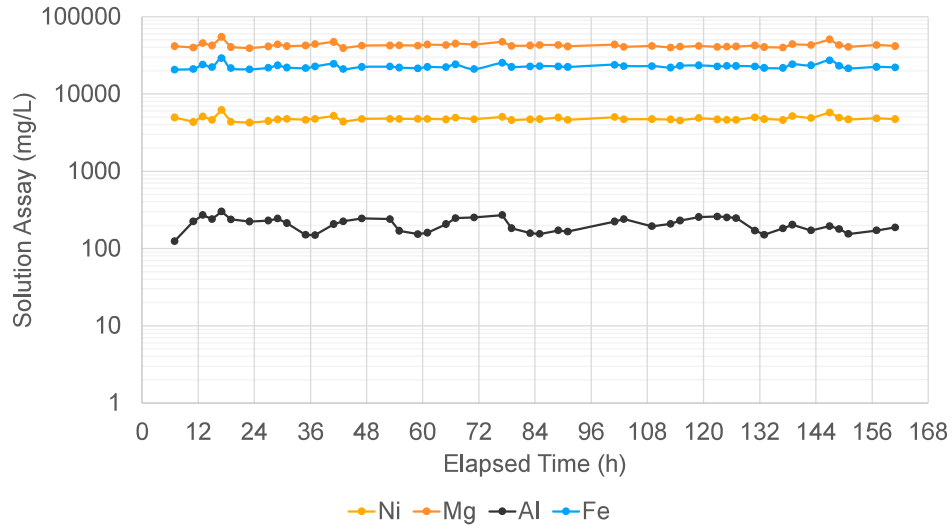

Pilot Plant 1 (Leach and Olivine Neutralization)

Solution assays from Olivine Neutralization Reactor 5

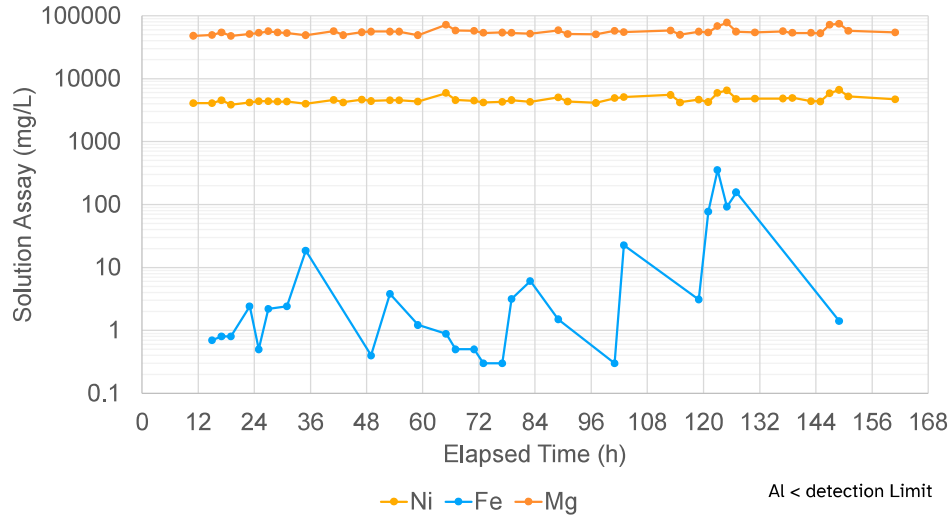

Pilot Plant 2 (MHP Stages 1 and 2)

10% NaOH in brine solution to precipitate Ni/Co at 75 °C with three reactors for each of MHP and SHP.

The circuit was gradually fine-tuned to precipitate approximately 90% of the Ni in the incoming solution.

The average grade of the MHP product was 45% Ni, 1.79% Co, 4.5% Mg, 0.01% Fe, 0.02% Al, <0.01% Cr and 0.3% Si.

The SHP circuit was quickly tuned to achieve <10 mg/L Ni in solution.

The SHP solids averaged 29.1% Ni, 0.64% Co, 15.3% Mg, 0.02% Fe, 0.01% Al, 4.97% Mn, <0.01% Cr, 0.06% Si.

This material recycles to the leach circuit discharge to ensure high recovery of nickel and cobalt to the primary MHP product.

Pilot Plant 2 (MHP Stages 1 and 2)

Solution assays from MHP 1 Precipitation

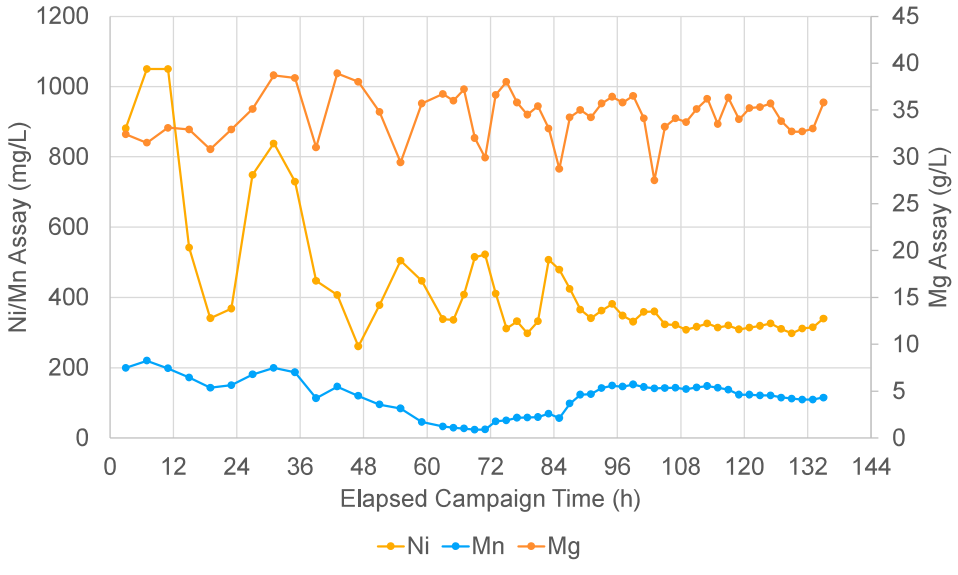

Pilot Plant 2 (MHP Stages 1 and 2)

Solution assays from MHP 2 Precipitation

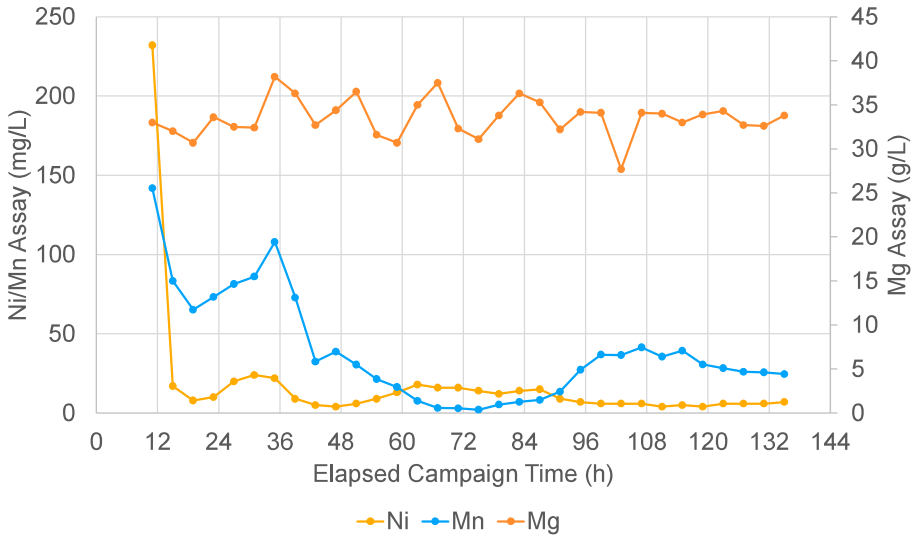

Pilot Plant 3 (Mn Removal and $Mg(OH)_2$ Production)

Mn Removal: three stages at 75 °C with addition of 11% NaOCl to oxidize manganese followed by 10% NaOH solution in brine to pH ~6 to precipitate manganese.

Manganese and nickel levels less than 1 mg/L in the final solution.

The average solid assays were 22.4% Mn, 11.7% Mg.

The magnesium hydroxide precipitation by direct addition of 50% NaOH.

three stages of precipitation were used with caustic addition to stage 1 and all reactors maintained at 80 °C.

Magnesium was reduced from ~ 30 g/L to ~1 g/L toward the end of the pilot plant.

Calcium was not precipitated.

The residual magnesium and calcium would be removed in the chlor-alkali pre-treatment circuit (conventional technology).

Pilot Plant 3 (Mn Removal and $Mg(OH)_2$ Production)

Solution assays for the Mn precipitation process

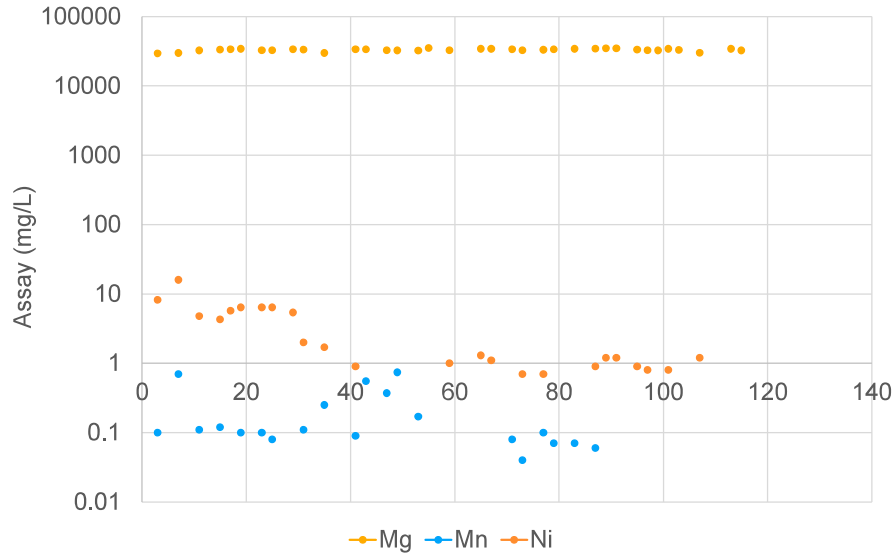

Pilot Plant 3 (Mn Removal and $Mg(OH)_2$ Production)

Solution assays for the Mg precipitation process

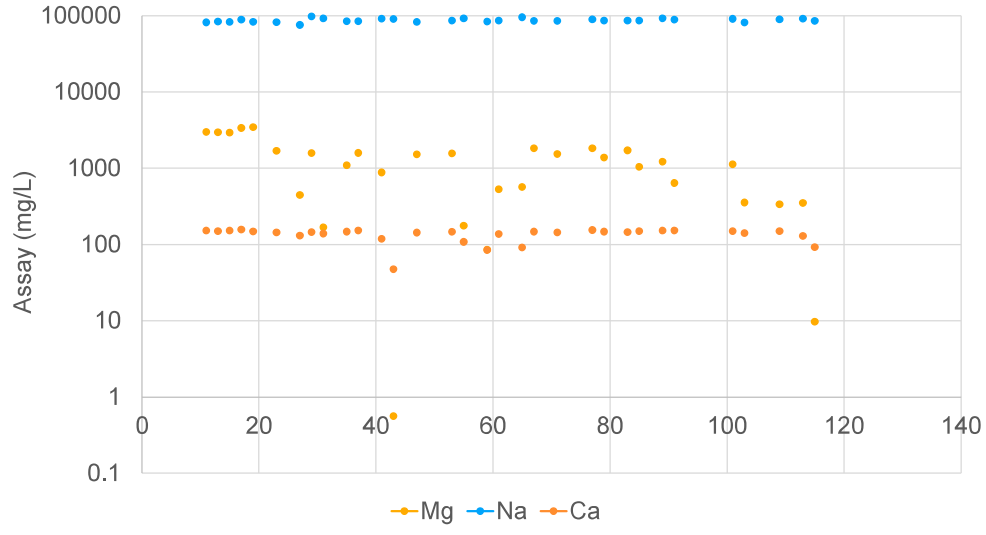

$Mg(OH)_2$ Product Analysis

Element	Analysis (% or g/t)
Ni	11 g/t
Co	<3 g/t
Fe	11 g/t
Mg	39.9 %
Al	4 g/t
Cr	<1 g/t
Mn	<0.4 g/t
Ca	388 g/t
Cl	357 g/t

Conclusions and Next Steps

The Atlas Materials base case process has advanced significantly from the early proof of concept pilot plant.

The challenges that were apparent in the 2022 proof of principle pilot plant have been addressed through further bench work and are now being confirmed in the demonstration pilot plant at SGS Canada.

The development of the olivine neutralization process for iron/aluminum and chromium removal has been a breakthrough in development.

The leach solution purification can be achieved in one step to produce solutions with < 1 mg/L Fe, Al, Cr content.

In addition, the production of high purity magnesium hydroxide has been demonstrated in the pilot plant program.

The development of our first commercial plant is well advanced.

SULPHURIC ACID PLANT INTEGRATION IN NICKEL HYDROMETALLURGICAL FACILITIES

By

Matthew King, Benjamin Senyard[1], [2]Herbert Lee

Worley Chemetics, Australia
[2]Worley Chemetics, Canada

Presenter and Corresponding Author

Matthew King
Matthew.J.King@Worley.com

ABSTRACT

Nearly all base metals hydrometallurgical processes require sulphuric acid. This acid is often produced on-site in one or more conventional double contact double absorption (DCDA) type sulphuric acid plants. On-site production has the key benefit of providing steam and electricity as co-products. This paper provides an overview of sulphuric acid plants used at nickel leaching operations and insight into the challenges faced when balancing acid, steam and electricity demand - especially during transient and turndown operation. CORE-SO2™ technology is presented which has been tailored to specifically meet the industry's need for lower capital cost, decreased tail gas emissions (without effluent generation), maximized energy recovery along with reliable turndown capability and zero CO_2 emissions. CORE-SO2™ plants can produce from 100 t/d up to 13,000 t/d of acid in a single train.

Keywords: Sulphuric acid plants, base metal and nickel hydrometallurgy, emissions

INTRODUCTION

Sulphuric acid is used to leach valuable metals such as nickel, copper, cobalt and rare earth elements. This acid is supplied from an external source or by on-site production from sulphur. A key benefit to on-site production is the acid plant's heat recovery process that generates steam that can be used in the hydrometallurgical plant or for electricity generation. Acid plants can also provide low grade heat as hot water that can be used for process heating or for desalination. Most hydrometallurgical plants are in remote locations where the acid plant's electricity generating capability plays a critical role in maintaining efficient, low-cost operations.

REFERENCE PLANTS

Table 1 shows several nickel and copper hydrometallurgical facilities and their on-site acid plant production capacity along with their associated power generating equipment and its capacity. All the acid plants burn sulphur to produce sulphuric acid and raise high pressure superheated steam. The superheated steam is most often used to generate electricity, but in some cases it is sent to the hydrometallurgical facility for heating purposes.

Some of the world's largest single train acid plants are found at nickel hydrometallurgical facilities which is the focus of this paper. Acid plants are also used at copper leaching operations. The NorAcid plant in Chile is located on the coast and produces acid for use at several copper leaching operations in the region.

Table 1: Operating Acid Plants and Their Power Generating Capacity

Owner	Operation	Metal	Location	Acid Production	Generating Capacity
First Quantum Minerals	Ravensthorpe	Ni	Western Australia	1 x 4400 t/d	3 x 18 MWe STG[1]
Glencore	Minara	Ni	Western Australia	1 x 4500 t/d	2 x 28 MWe STG[2] 1 x 31.5 MWe GT[2]
MCC-JJJ Mining	Ramu	Ni	Papua New Guinea	2 x 1700 t/d	No co-gen[3]
Sumitomo/Komir	Ambatovy	Ni	Madagascar	2 x 2750 t/d	3 x 45 MWe STG[4]
CMOC	Tenke Fungurume	Cu	DR Congo, Africa	1 x 825 t/d 1 x 1400 t/d	1 x 6 MWe STG 1 x 20 MWe STG[5]
Freeport McMoRan	Safford	Cu	Arizona, USA	1 x 1550 t/d	1 x 17 MWe STG[6]
NorAcid S.A.	Mejillones	Cu	Chile	1 x 2060 t/d	1 x 26 MWe STG[7]

*GT = Gas Turbine Generator, STG = Steam Turbine Generator

HYDROMETALLURGICAL PLANT UTILITY CONFIGURATIONS

Overview

Many options are available to the designer when integrating a sulphuric acid plant into a remote hydrometallurgical facility. The term remote in this case means that the facility is located where a connection to an electrical grid is not available. Electricity cannot be imported or exported and must be generated on-site. The remoteness of the site also prevents sulphuric acid from being exported to external customers.

The demand for acid, steam and electricity at steady state and at turndown conditions must be considered and appropriate supplemental systems installed to manage varying operating conditions. Start-up electrical and steam generating systems often consist of fuel fired diesel generators and fuel fired package boilers. These systems must be installed to ensure the acid plant can be preheated and commence operation after construction and after subsequent cold shutdowns.

The next few sections provide example configurations for hydrometallurgical facilities based on their acid, steam and electricity requirements. In the figures that follow:

- Medium pressure (MP) steam (7 bar(g), saturated) is used to indirectly melt sulphur and is also supplied to the acid plant for use in the deaerator. The deaerator conditions the boiler feed water prior to it being pumped to the acid plant economizers and steam generating system. Additional steam pressure let down to 3 - 5 bar(g) occurs prior to some users

(filters, tanks, jacketing, etc.) in the sulphur melting area. It should be noted that MP steam can also be 20 bar(g) steam that is sometimes required for the hydrometallurgical plant.

- High pressure (HP) steam is usually specified as 40 bar(g) or 60 bar(g) steam. Superheated steam is supplied to the steam turbine generator (STG) and is typically 400°C for 40 bar(g) systems and 500°C for 60 bar(g) systems. Conventional double contact double absorption (DCDA) type sulphur burning acid plants produce 1.2 – 1.4 t superheated HP steam (60 bar(g) / 500°C) per t acid (100% H_2SO_4 basis).

- The hydrometallurgical plant may need HP steam for its process (usually high-pressure acid leach (HPAL) autoclaves) or MP steam for process heating. Both are often supplied at saturated or slightly superheated temperatures (i.e., 5 - 10°C above saturation temperature).

- STG MP steam is produced in an extraction port located on the turbine. This is a common design feature that enhances power generation while meeting the acid plant demand for MP steam.

- Unless otherwise noted, the STG's are condensing which maximizes power generating capacity.

High Electricity Consumption

The block flow diagram shown in Figure 1 is for a facility with electricity demand that exceeds what can be produced from acid plant steam. In this example, a gas turbine generator with a HRSG (heat recovery steam generator) provides additional steam to the STG(s). Dashed lines represent intermittent operation. This applies to this figure and all subsequent figures in this paper.

Fuel fired package boilers can be used to increase steam production. This steam is used to generate electricity if the gas turbine generator or acid plant are not supplying sufficent steam. Fuel fired generators (not shown) are used to provide start-up and back-up electricity.

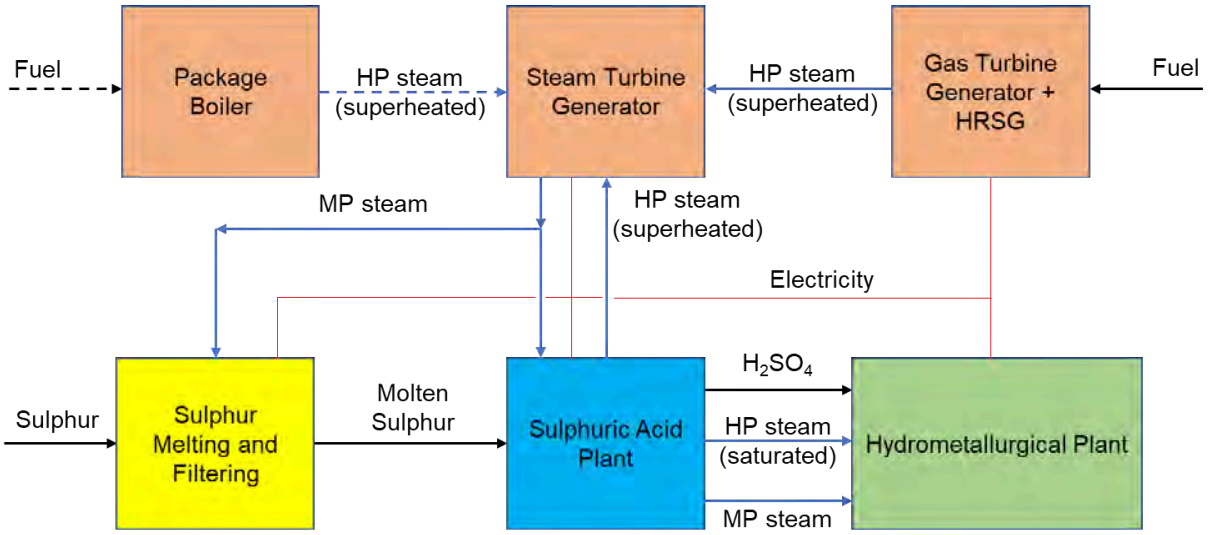

Figure 1: Utility Block Flow Diagram, High Electricity Consumption

In Figure 1, MP steam from the acid plant can be produced by installing an Acid Low Pressure Heat Absorption (ALPHA™) system in the acid plant that generates steam (5-10 bar(g), 0.55 t steam per t acid (100% H_2SO_4 basis)) from hot, approximately 200°C, concentrated, 99 wt.% H_2SO_4 acid (Figure 2). This system decreases the amount of cooling water required for the acid plant which decreases water consumption if evaporative cooling is used and decreases electricity consumption if indirect air cooling ("fin-fan") is used.

A feature of ALPHA™ is its ability to be turned on and off while maintaining design sulphuric acid production rates from the acid plant. This flexibility allows the MP steam system operation to be optimized to meet hydrometallurgical plant requirements.

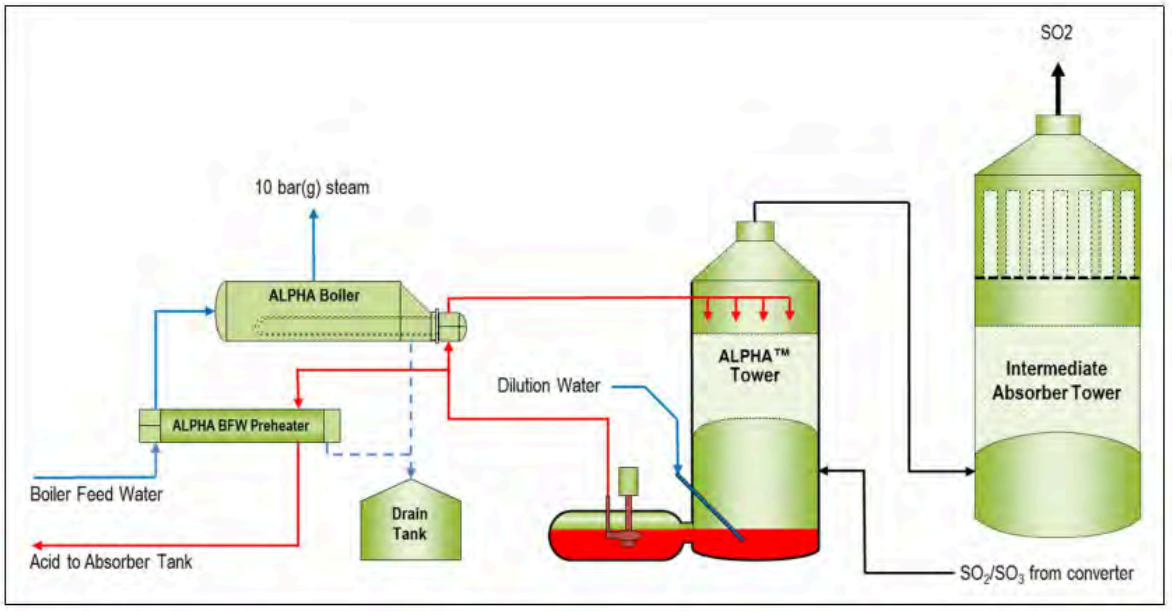

Figure 2: ALPHA™ System for Producing 10 bar(g) MP Steam from Hot Sulphuric Acid

High Steam Consumption

This configuration is used when MP steam demand in the hydrometallurgical plant is high and the electricity demand is low. A back-pressure steam turbine generator is used to produce electricity and MP steam (typically 20 bar(g)). Less electricity is produced in a back-pressure turbine because the steam is not condensed. MP steam can also be produced in the acid plant by installing a steam turbine driven blower instead of an electric driven blower. Steam turbine driven blowers are commonly used in phosphate fertilizer acid plants where MP steam demand from the fertilizer plant is high.

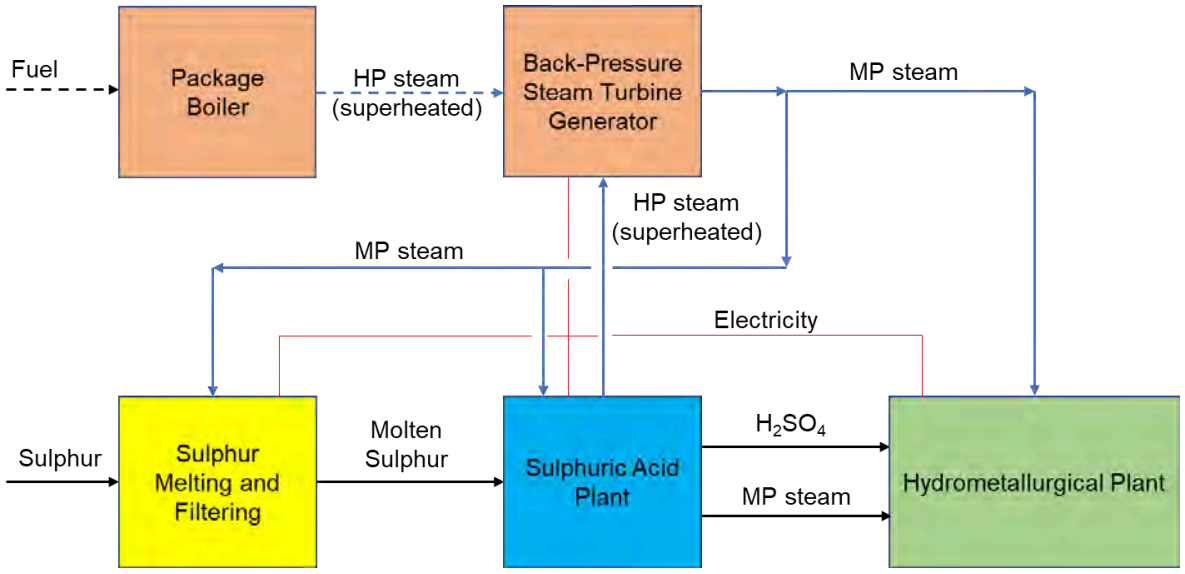

Figure 2: Utility Block Flow Diagram, High Steam Consumption

Hot Water for Desalination

Many metallurgical sites are located where water quality is poor or where seawater is available and can be used for the process. Desalination plants are often installed to produce higher quality water. Low grade heat generated in the acid plant's acid circuit can be recovered as 90°C hot water and

sent to the desalination plant where the water is cooled and returned to the acid plant in a closed loop. Figure 3 shows this configuration. Hot water production is maximised and no MP steam is produced in the acid plant.

The acid cooling circuit design should account for possible fluctuations in demand for hot water from the desalination plant. Additional cooling water system capacity should be designed into the circuit to effectively decouple the acid plant from the desalination plant. This is shown in Figure 4 where the absorbing acid cooler and cooling water tower are sized so that the acid plant design production rate can be maintained with the desalination water heater off-line.

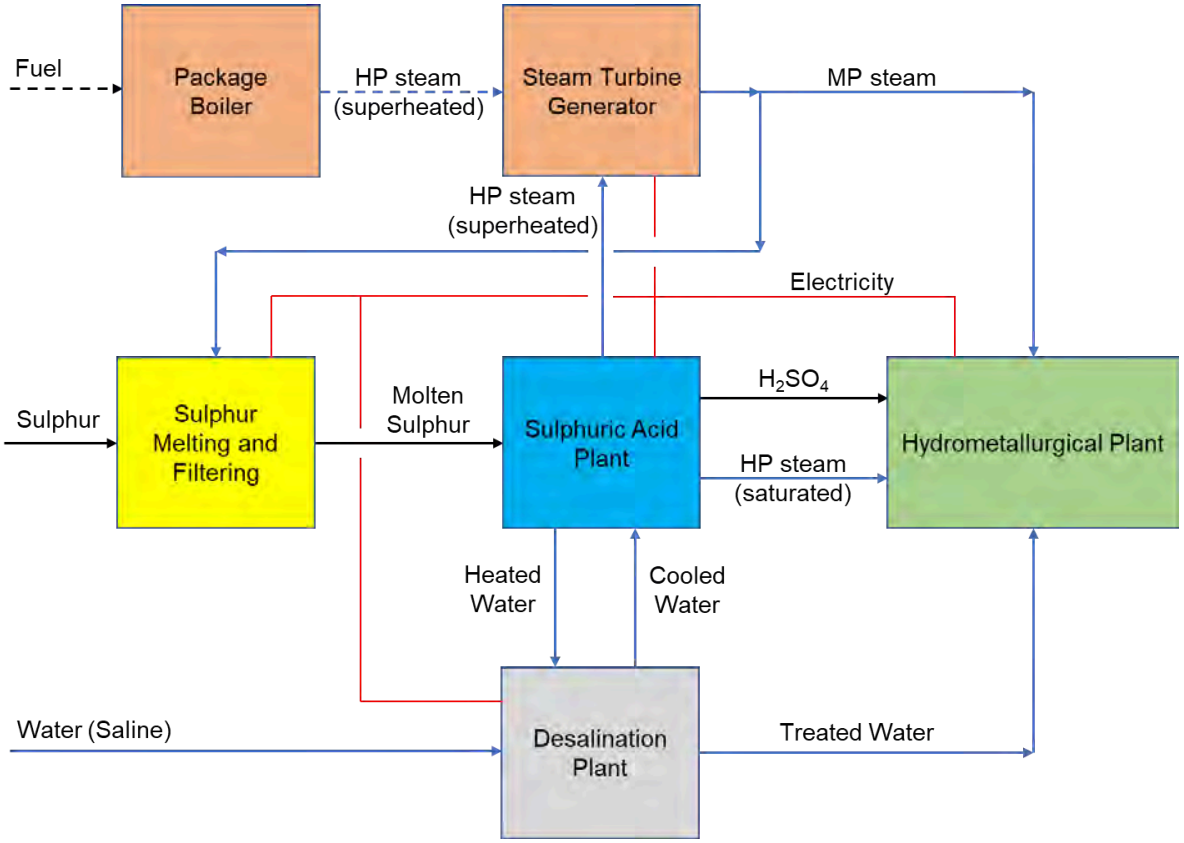

Figure 3: Utility Block Flow Diagram with Desalination Plant

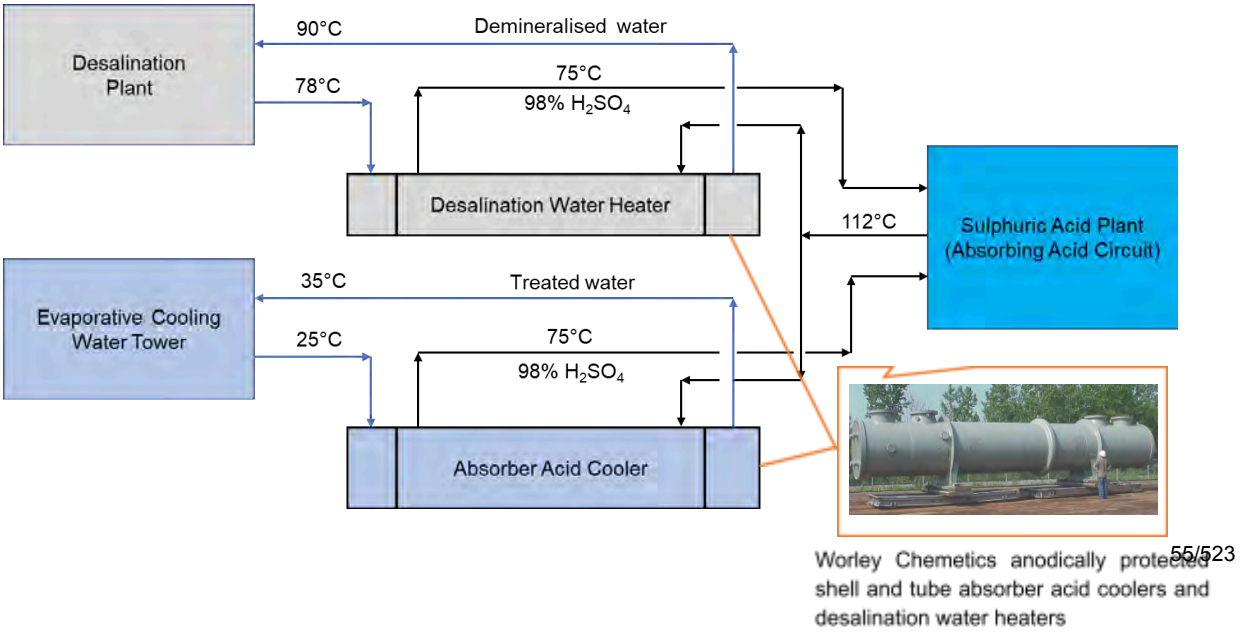

Worley Chemetics anodically protected shell and tube absorber acid coolers and desalination water heaters

Figure 4: Desalination Plant Hot Water Supply Circuit

ACID, STEAM AND ELECTRICITY BALANCES

Acid

Sulphuric acid is stored at site in large, unlined carbon steel tanks sometimes with anodic protection. Storage quantities are equivalent to between 5 and 10 days of acid production. More acid storage capacity gives the site the ability to operate for longer periods of time with the acid plant off-line. Fortunately, most sulphur burning acid plants have a high availability, often between 98% and 99% and in some cases, approaching 100% outside of major turnarounds.

Major turnarounds are required every 3 to 5 years for catalyst screening and typically last anywhere from 12 to 20 days depending on the scope of repairs required. During this period, the acid plant is cooled to ambient temperature and the vessels opened for inspection and repair. The acid plant is restarted by burning fuel in the sulphur furnace to heat the furnace which is then followed by a series of “dry blows” where dry air is sent through the furnace with the fuel burner turned off to heat the catalyst beds to a temperature above the dew point to prevent catalyst damage during subsequent direct firing. Once all the catalyst bed temperatures are above the dew point temperature, direct firing of the furnace is started and the catalyst beds are heated to around 400°C. The fuel burner is removed and sulphur firing commences.

Most hydrometallurgical facilities will also schedule major maintenance to coincide with the acid plant shutdown because the acid storage capacity is insufficient to provide enough acid to operate at full rates during the outage. In addition, fuel must be burned to generate steam for electricity generation that would normally be provided by the acid plant which increases operating costs for this period.

During periods with the acid plant on-line, hydrometallurgical plant maintenance must also occur. A good example is at nickel HPAL operations where one of the autoclaves will be taken off-line and descaled while the other(s) remain on-line. Acid, steam and electricity demand all decrease which needs to be included in the overall facility design.

Steam

Package boilers are used to generate supplemental steam when the acid plant is off-line to ensure electricity generation in the steam turbine generator(s) is maintained. These systems often require the burning of hydrocarbon fuels such as natural gas, LPG, coal, distillate or fuel oil. These fuels can be expensive, especially at remote sites. CO_2 emissions increase.

Excess steam can be sent to a dump condenser to recover valuable boiler feed water. Dump condensers are usually shell and tube exchangers that use cooling water to condense steam. Some sites have dump condensers installed in parallel with their STG’s to ensure acid production remains available even when the STG is off-line. Operating scenarios that require the use of the dump condenser should be minimised to minimise water and/or energy that is required to condense the steam via evaporative cooling towers or fin-fan air coolers.

Electricity

The acid plant produces more electricity than it consumes. The excess electricity is used in the hydrometallurgical plant and other plant wide systems. Fuel fired generators (often diesel) are used to provide acid plant start-up electricity and emergency power when the acid plant is off-line for short durations (a few hours). Electricity demand varies with the demand from the hydrometallurgical plant and the acid plant.

Based on the previous discussion, it is clear that acid, steam and electricity supply and demand are all interrelated. The next section further illustrates this point.

Operating Scenarios

Table 2 provides a qualitative summary of the effect of varying acid, steam and electricity demand on the operation. “High” represents operation at the design capacity for the plant and “Low”

represents operating at the turndown capacity of the plant. In these scenarios, the assumption is that acid cannot be exported to an external customer and electricity cannot be stored in batteries. In addition, fuel is not required to produce steam or electricity when the acid plant operates at its design rate.

Table 2: Operating Scenario Impact on Acid, Electricity and Steam Balance

Demand			Supply		Outcome
Acid	Electricity	Steam	SAP Rate	Fuel	
High	High	High	Design	None	Supply = Demand
High	High	Low	Design	None	Excess steam condensed in dump condenser to recover water
High	Low	Low	Design	None	STG steam by-pass, excess steam to dump condenser
High	Low	High	Design	None	STG steam by-pass, remaining steam to process plant
Low	Low	Low	Turndown	None	Supply = Demand
Low	Low	High	Turndown	Low	Package boiler steam for process plant
Low	High	High	Turndown	High	Package boiler steam for process plant and power generation
Low	High	Low	Turndown	Medium	Package boiler steam for power generation, not process plant

TECHNOLOGICAL ADVANCES IN SULPHURIC ACID MANUFACTURE

Conventional DCDA Plants

The modern contact process has been used for more than 100 years to make concentrated, 98% H_2SO_4, acid. The process reactions are as follows:

(1) $S + O_2 \xrightarrow{\text{in air}} SO_2$ $\quad \Delta H°_{25°C} = -300$ kJ/mol

(2) $SO_2 + 0.5O_2 \xrightarrow{\text{in catalyst}} SO_3$ $\quad \Delta H°_{25°C} = -99$ kJ/mol

(3) $SO_3 + H_2O \rightarrow H_2SO_4$ (in 98.5% H_2SO_4) $\quad \Delta H°_{25°C} = -130$ kJ/mol

Each reaction generates heat which is recovered as steam or rejected to the atmosphere via cooling systems. Figure 5 shows the flowsheet for a modern conventional double contact double absorption (DCDA) type sulphuric acid plant. Reaction (1) takes place in the sulphur furnace where molten sulphur at 140°C is sprayed into a hot, (1150°C) refractory lined furnace where it burns in dry air to generate sulphur dioxide (SO_2). The SO_2 is then sent through three catalyst beds where it oxidises to sulphur trioxide (SO_3) (Reaction (2)).

Heat exchangers and a superheater are located between the catalyst beds to cool and heat the process gas and superheat steam that is sent to the STG. The hot gases leaving the third catalyst bed are cooled in an economizer and superheater prior to entry into the ALPHA™ system and cold absorption system where the SO_3 reacts with H_2O in 98.5% H_2SO_4 to produce H_2SO_4 (Reaction (3)). Dilution water is added to maintain the desired product acid concentration, typically 98.5% H_2SO_4.

The cold gases are then reheated in gas/gas heat exchangers prior to entering the fourth catalyst bed for final SO_2 conversion to SO_3. The gases are then cooled in an economizer prior to entering the final absorption system where SO_3 is reacted with 98.5% H_2SO_4. The gases then leave the final absorption system and are exhausted to the atmosphere via a stack.

Significant improvements to the conventional DCDA design have been made in the past fifty years (nearly all by Worley Chemetics!). These improvements focused on better materials of construction, more efficient heat exchanger designs and improved heat recovery resulting in safer, more reliable and more efficient acid plants. These plants recover more than 99.8% of the feed sulphur to sulphuric acid and can recover more than 93% of the energy generated by the process reactions. However, opportunities exist to further improve the design to address its inherent limitations:

1) Single train capacity: DCDA plants are limited in size to approximately 5,000 t/d for economic reasons (costs increase rapidly at higher capacities) – although technically they can be designed for higher capacities. This capacity limitation requires some sites to install two or more acid plants to meet demand increasing complexity and cost.
2) Emissions: lower tail gas SO_2 concentrations are difficult to achieve without costly scrubbers that use water and expensive reagents (amine, caustic or hydrogen peroxide) and, in some cases, generate waste streams that require disposal
3) Turndown capability is limited to approximately 40% of the design rate
4) Hydrocarbon fuels are required for cold start-up resulting in CO_2 emissions
5) Large equipment, mostly stainless steel, resulting in high capital costs and significant on-site fabrication.

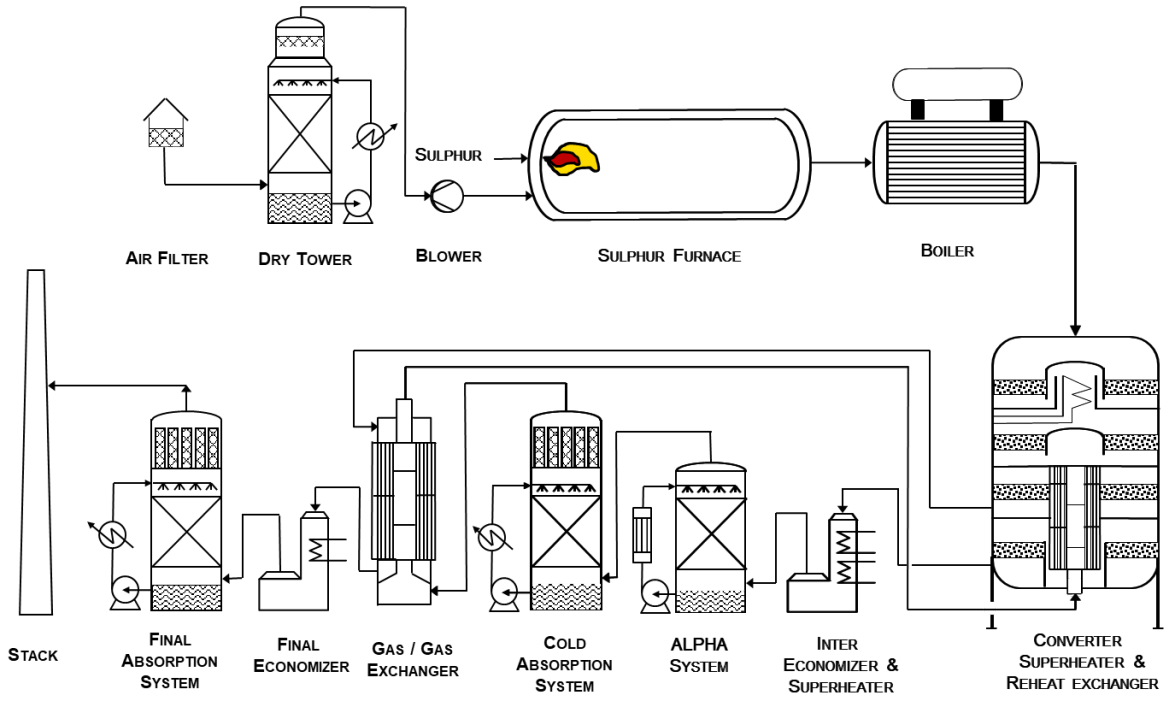

Figure 5: Conventional DCDA Flowsheet with ALPHA™

Worley Chemetics' CORE-SO2™ overcomes these limitations by using industrial oxygen instead of air as shown in Figure 6. The process is discussed further in the next section.

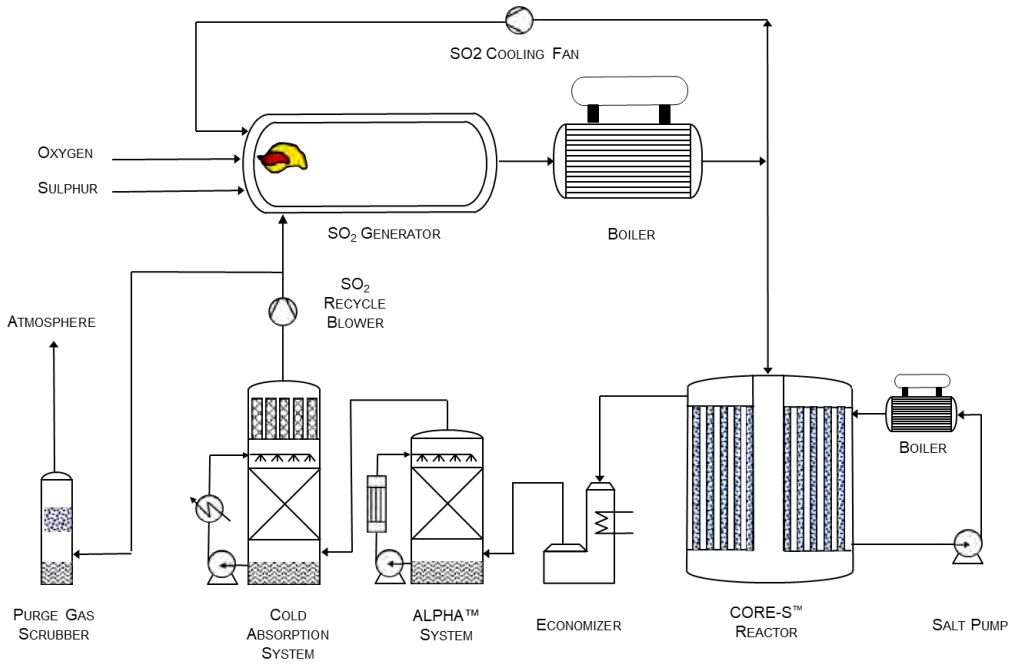

Figure 6: CORE-SO2™ Flowsheet

CORE-SO2™

Process Description

Ambient air is drawn into the oxygen plant (VPSA or cryogenic type depending on capacity) where it is dried and the oxygen and nitrogen are separated to produce a stream of 95 – 98 vol% oxygen which is sent to the SO_2 Generator. In the SO_2 Generator, molten sulphur is reacted with oxygen to form concentrated SO_2 gas (40 vol.% or 60 vol.%). The SO_2 Generator is a proprietary design which allows complete combustion of the sulphur at modest temperature due to recycle of cool SO_2 gas and recycle of gas from the Cold Absorption System. Hot SO_2 gas leaves the SO_2 Generator and is cooled in a boiler where the heat is recovered as high pressure (40 bar(g) or 60 bar(g)) steam. The strong SO_2 gas then flows to the CORE-S™ Reactor.

In the CORE-S™ Reactor, the exothermic conversion of SO_2 to SO_3 takes place as the process gas passes through the catalyst filled tubes. The energy released inside the tubes is transferred to the molten salt coolant flowing on the shell side, resulting in a nearly constant temperature of the process gas enabling high SO_2 conversion rates. The gas leaving the converter is cooled to about 170°C in an Economizer. The cooled gas then enters the (optional) ALPHA™ System and subsequent Cold Absorption System where the SO_3 is absorbed by counter-current contact with circulating 98.5% H_2SO_4 (identical to absorption systems used in DCDA plants). The gases leaving the Cold Absorption System returns to the SO_2 Generator via the SO_2 Recycle Blower.

A small portion of the recycle gas is sent to the Purge Gas Scrubber to control the inert gas concentration in the gas entering the CORE-S™ Reactor. This purge gas consists mainly of the inert gases contained in the oxygen feed.

Strong acid (98.5% H_2SO_4) is produced in the Cold Absorption System and is further cooled to less than 40°C before being sent to storage tanks.

CORE-SO2™ for Hydrometallurgical Facilities

CORE-SO2™ is ideally suited for hydrometallurgical facilities due to its following design features:

1) Ultra-low SO_2 and acid mist emissions, < 0.1 kg SO_2/t H_2SO_4 and <0.005 kg mist / t H_2SO_4 are easily achievable.

2) No CO_2 emissions – ever. Electric heaters are used to start up the acid plant. No waste streams, other than impurities in the sulphur, are produced.

3) Low capital cost, smaller equipment, modular construction, high quality due to shop fabrication instead of field fabrication.

4) Turndown to idle is possible without damaging the equipment. This is important during initial ramp-up after construction when the hydrometallurgical plant is not operating at full capacity. Generally, less acid storage capacity is required which also decreases capital cost.

5) Optimized power production and consumption from the superheated steam generated in the process.

6) High single train production capacity, up to 13,000 t/d, which means multiple trains are not required which decreases initial capital cost and ongoing sustaining capital costs.

7) Nitrogen and other gases, such as argon, can be generated as by-products from the oxygen plant and possibly sold, increasing value.

ENHANCED SUSTAINABILITY WITH CORE-SO2™

The ongoing mission to decrease CO_2 emissions applies to metal producing facilities. A proposed utility block flow diagram for a hydrometallurgical plant based on CORE-SO2™ with zero CO_2 emissions is shown in Figure 7. Electric package boilers are used to provide back-up steam and renewables (wind, solar, and/or hydroelectric) provide supplemental electricity generating capacity.

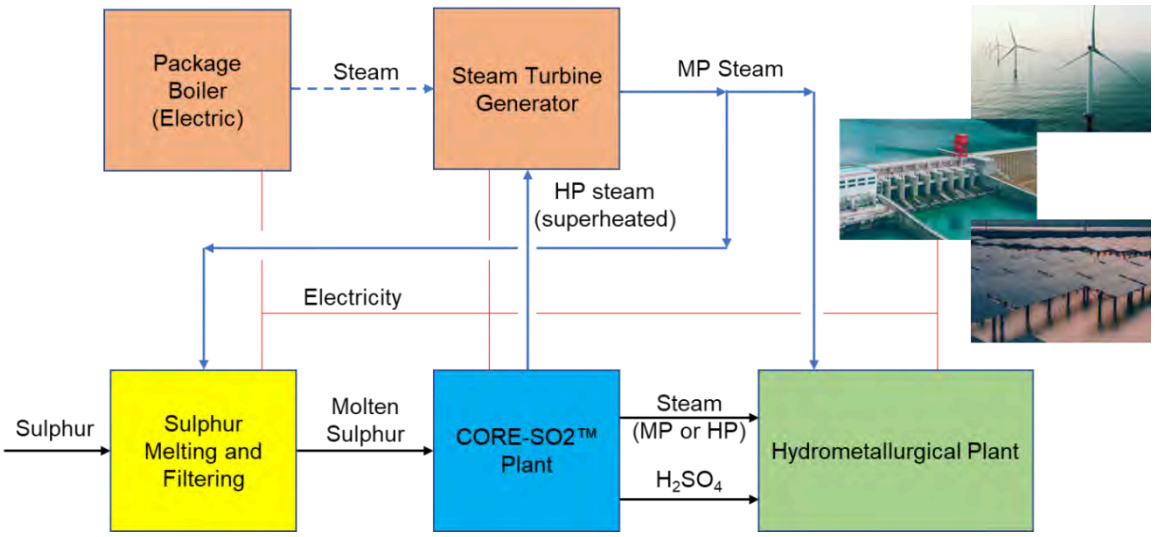

Figure 7. Zero CO_2 Emission Hydrometallurgical Facility

CONCLUSIONS

Sulphuric acid is used at hydrometallurgical facilities to leach valuable metals (Ni, Cu, Co, REE and others) from ores and concentrates. This acid is commonly produced on-site in conventional DCDA type acid plants. These plants recover energy to produce high pressure superheated steam that is used to generate electricity.

Careful consideration must be given in the design phase to the acid, steam and electricity balances that are required during normal operation. Start-up, transient and turndown operations must be clearly defined and the acid plant and its associated utility systems appropriately designed to cater for these conditions to ensure high efficiency, low-cost operations are maintained.

Hydrometallurgical production of the metals needed for the energy transition can be enhanced by selecting a CORE-SO2™ acid plant which emits no CO_2 and ultra-low quantities of SO_2 and acid

mist. Coupling CORE-SO2™ with renewable power results in the possibility of a metal production facility with zero CO_2 emissions.

REFERENCES

1. Environmental Protection Authority, Perth, Western Australia, Bulleting 1093, April 2003, Ravensthorpe Nickel Project, Change to Environmental Conditions, Table 1, 3.

2. Government of Western Australia, Department of Environment Regulation, Decision Document, Environmental Protection Act 1986, Part V, Murrin Murrin Operations Pty Ltd, License: L7276/1996/11, Amendment date: 4 June 2015, Category 52 – Power generation, 5.

3. Ramu Nickel Cobalt Project, Located in Madang Province – Papua New Guinea, NI 43-101 Technical Report, Report Prepared for Cobalt 27 Capital Corp, Behre Dolbear Australia Pty Limited, July 2019, 27.

4. NI 43-101 Technical Report, Ambatovy Nickel Project, Madagascar, CSA Global Report No. R501.2018, Effective Date: 30 June 2018, 134.

5. Kabbash, A., 2016. Tenke Fungurume looks to the future with second acid plant. Sulfuric Acid Today, Spring/Summer 2016, 2-5.

6. Freeport-McMoRan, 28 October 2011, Retrieved from https://energy-oil-gas.com /news/freeport-mcmoran/ on April 8, 2024.

7. Retrieved from https://noracid.cl/acido-sulfurico/ on June 10, 2024.

HPAL AUTOCLAVE PERFORMANCE: A COMPREHENSIVE DESIGN EXPLORATION

By

Niels Bussmann, Wolfgang Keller

EKATO Rühr- und Mischtechnik GmbH, Germany

Presenter and Corresponding Author

Wolfgang Keller
wolfgang.keller@ekato.com

ABSTRACT

The extraction of nickel from lateritic ore bodies in horizontal HPAL autoclaves has evolved into a well-established and standard process. While the geometric design of these autoclaves has remained unchanged since the second generation in the 1990s, their size has substantially increased, with volumes doubling. From a process point of view the crucial role of effective mixing in the multiple compartments of HPAL autoclaves persists.

This paper explores the intricate relationship between autoclave geometry and agitator design in standard setups, utilizing cold flow test results obtained from a 400-liter model autoclave. The findings highlight the continued importance of optimizing mixing processes within autoclaves and provide insights into potential vessel design variations to optimize both Capex and Opex costs.

Keywords: HPAL, autoclave, nickel, agitator design

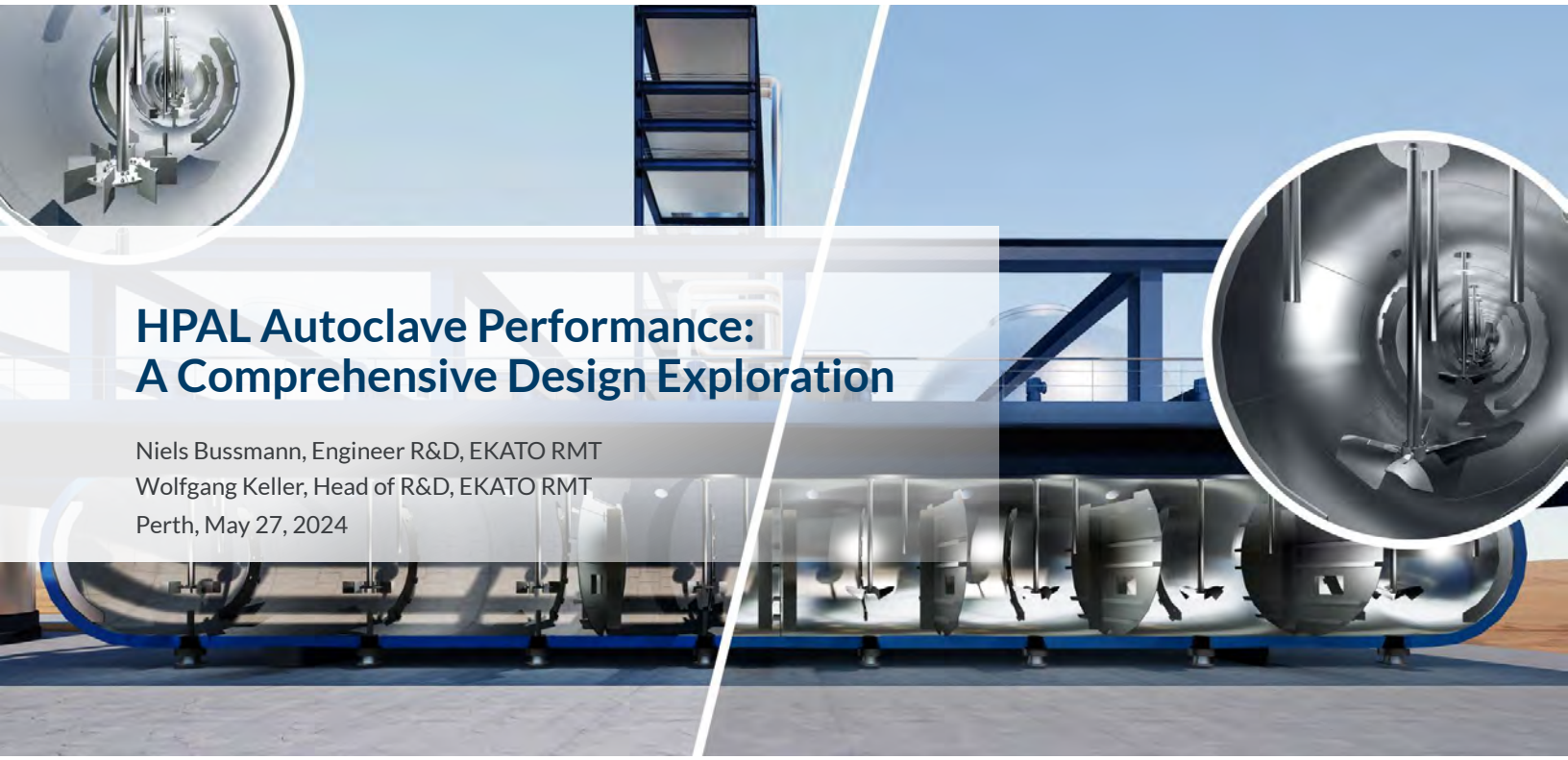

HPAL Autoclave Performance: A Comprehensive Design Exploration

Niels Bussmann, Engineer R&D, EKATO RMT
Wolfgang Keller, Head of R&D, EKATO RMT
Perth, May 27, 2024

HPAL Review / History

- EKATO supplies agitators for HPAL Autoclaves for more than 20 years
  - > 300 agitators installed
  - performed many optimizations related to the process performance
- Valuable feedback for many of the projects we were involved in (impellers, photos, onsite information and other data)
  - process results
  - power draw agitators
  - lifetime of the mechanical seal
  - lifetime of the impeller (abrasion)
  - HPAL geometric setups differ (baffles, compartment length, overflow weir geometry)
  - scale formation at impellers and other autoclave wetted surfaces
- Other activities
  - multiple CFD simulations

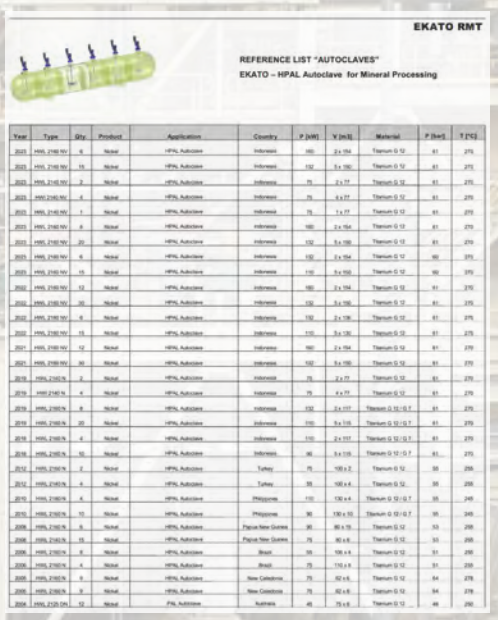
EKATO RMT

REFERENCE LIST "AUTOCLAVES"
EKATO – HPAL Autoclave for Mineral Processing

HPAL Review / History

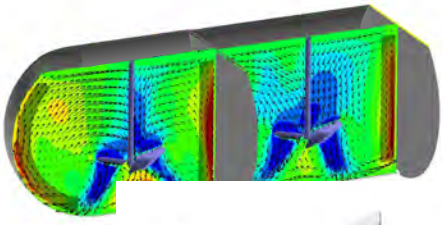



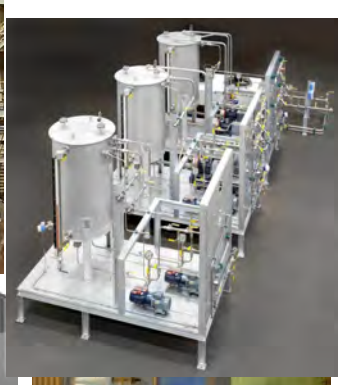
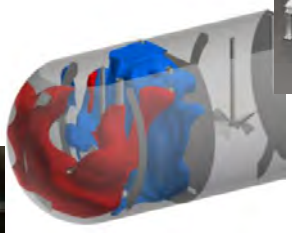
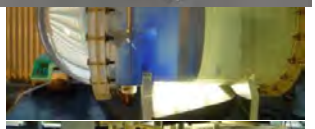


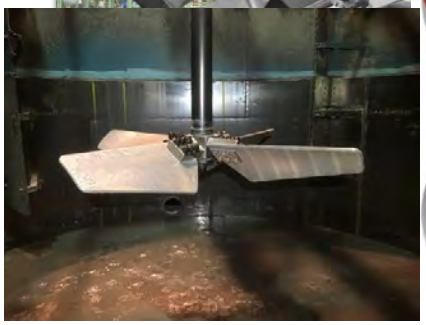
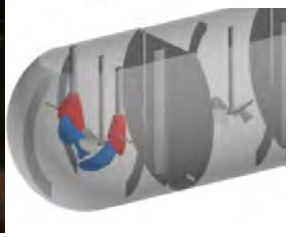


HPAL - Feedback







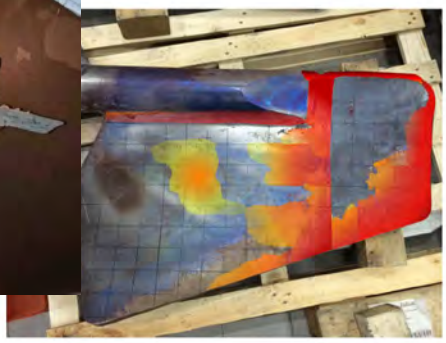


(Some) Challenges

- Scale formation
  - nickel and cobalt are the target metals, but other reactions dominate
  - iron and aluminum undergo leach-precipitation reactions
  - formation of e.g. Hematite and Alunite
  - majority forms in first compartments but in the entire autoclaves
  - regular cleaning required
  - not only process but mechanical impacts as well

- Remove / reduce number of inter-compartment walls and other internals
  - erosion near rat holes
  - reduced scale formation

Concept Study HPAL Setup / Exploration

- Impact of the geometric setup
  - number and location of baffles
  - number and location of overflow weirs / compartment walls
  - over- and underflow
- Goal: reduce the size of the wetted surface area in the autoclave
  - reduce scaling
  - reduce Capex
  - easier maintenance
- EKATO Technical Center in Germany
  - lab study 500 liter
  - basis for comparison: standard design
  - comparison of RTD measured
  - solids suspension / flow pattern
  - mechanical impact: power input, radial forces

Available Test Setups

Test possibilities at EKATO Technical Centre

~ 70 liters filling volume, 6 compartments

Scale-Up

~ 1 m³ filling volume, 2 compartments

Scale-Up

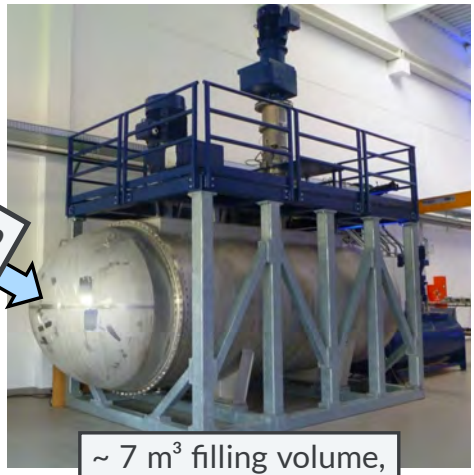

~ 7 m³ filling volume, 2 compartments

70 liter-scale for testing:
- blending times
- suspending behaviour
- residence time distribution
- feed point locations
- others

1 m³ and 7 m³-scale for testing:
- mechanical loads
- wear of e.g. impeller, baffles

Typical HPAL Autoclave – 'Standard'

ALTA 2024 28 27 - 31 May | Perth, Australia

Ore slurry Sulphuric acid Leached slurry

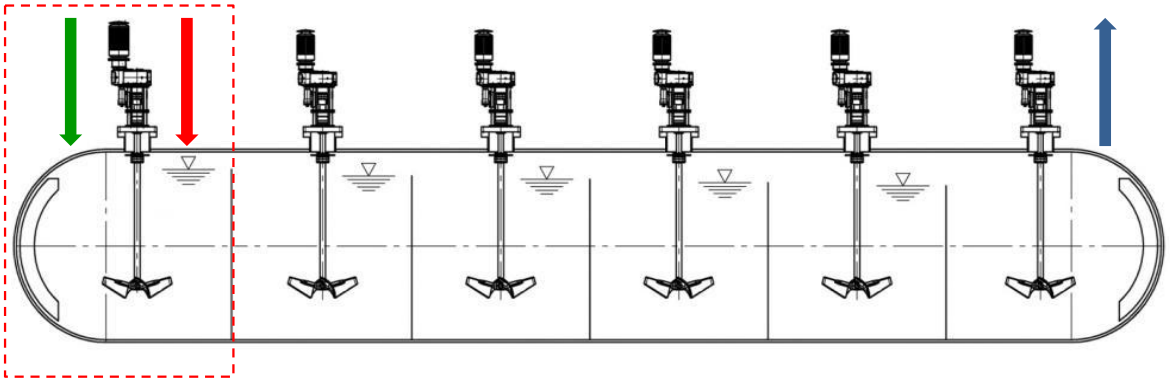

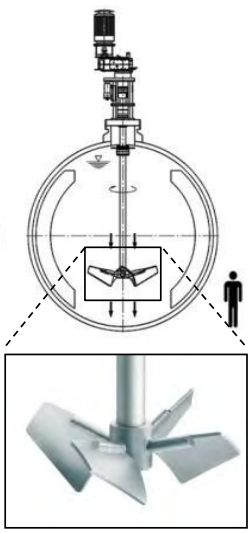

EKATO EPAL impeller

Main Mixing tasks are:
- no short – circuiting
- no acid hot spots (fast blending)
- homogeneous suspending

Test Setup

Our approach: 500 liters lab-trials – measurement of the residence time distribution

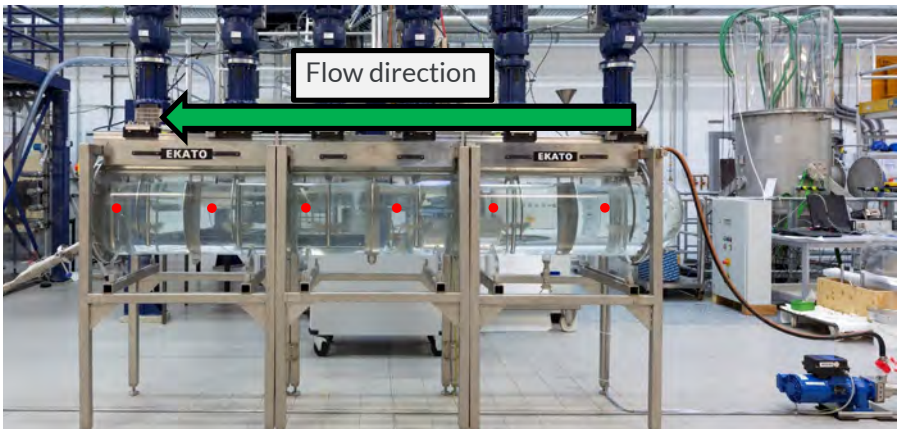

conductivity probes

Basis: Analysis of the typical design

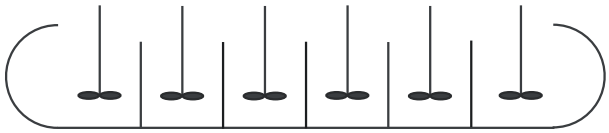

Step 1: Examination: what is the influence of each wall and baffle

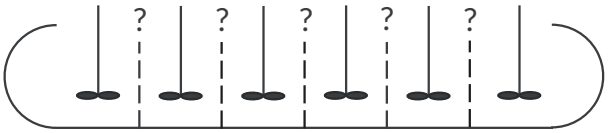

Residence Time Distribution

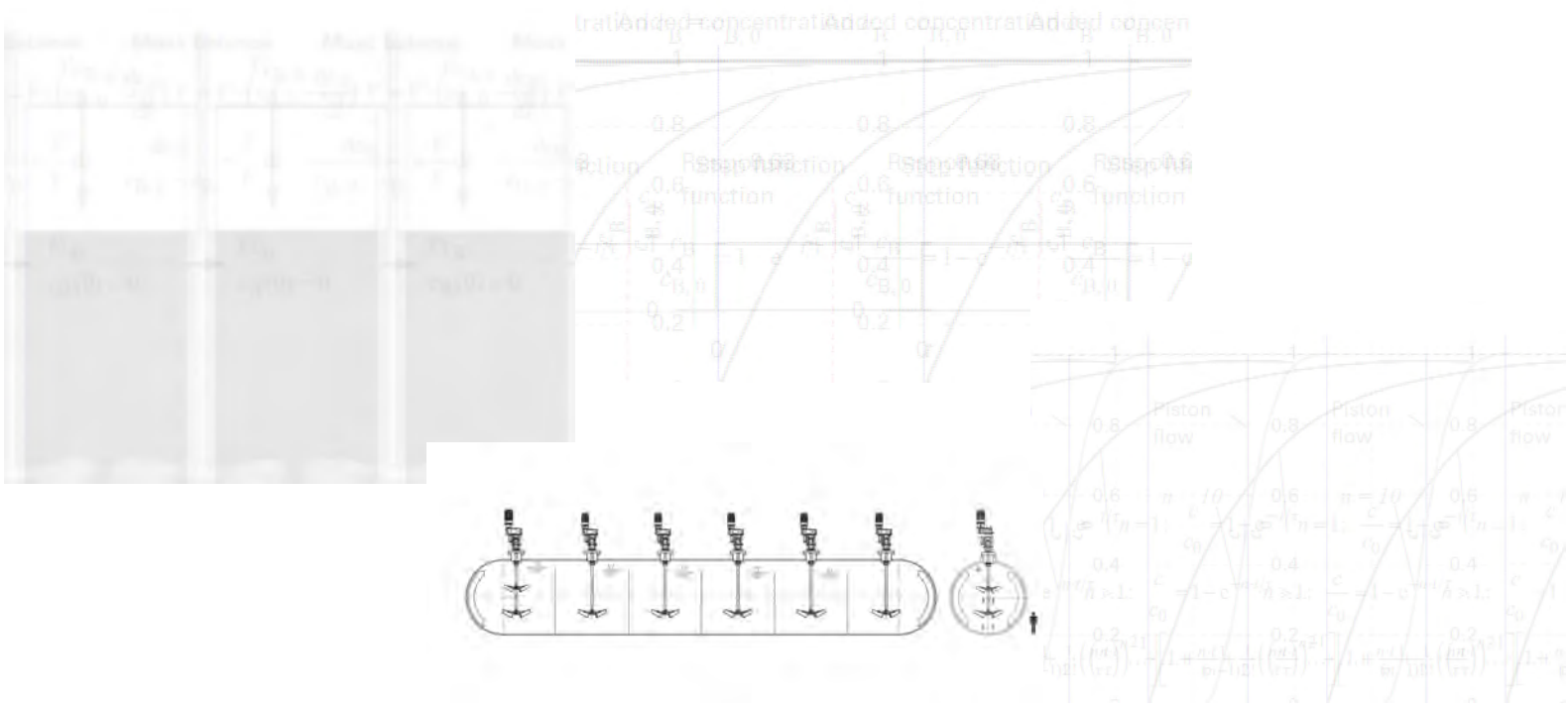

EKATO Concept Study

Our approach: 500 liters – lab-trials

Step 2: Comparison calc CSTR cascade & measured

- continuous addition of salt solution in compartment 1
- measurement of the conductivity in each compartment
- residence time 1 hour
- P/V or ratio blend time to residence time varied

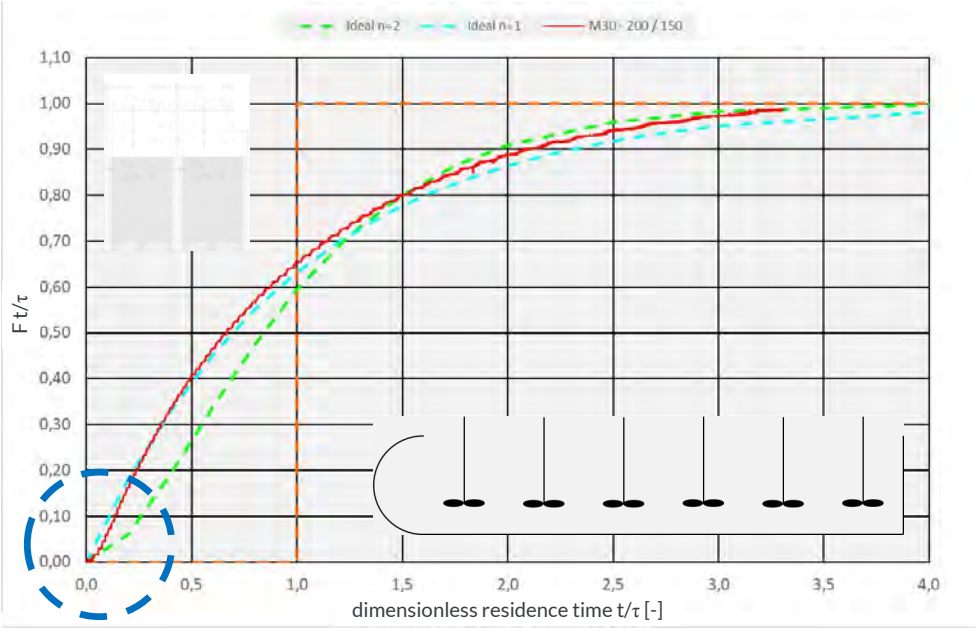

EKATO Concept Study

Our approach: 500 liters – lab-trials

Step 2: Comparison calc CSTR cascade & measured

- continuous addition of salt solution in compartment 1
- measurement of the conductivity in each compartment
- residence time 1 hour
- P/V or ratio blend time to residence time varied

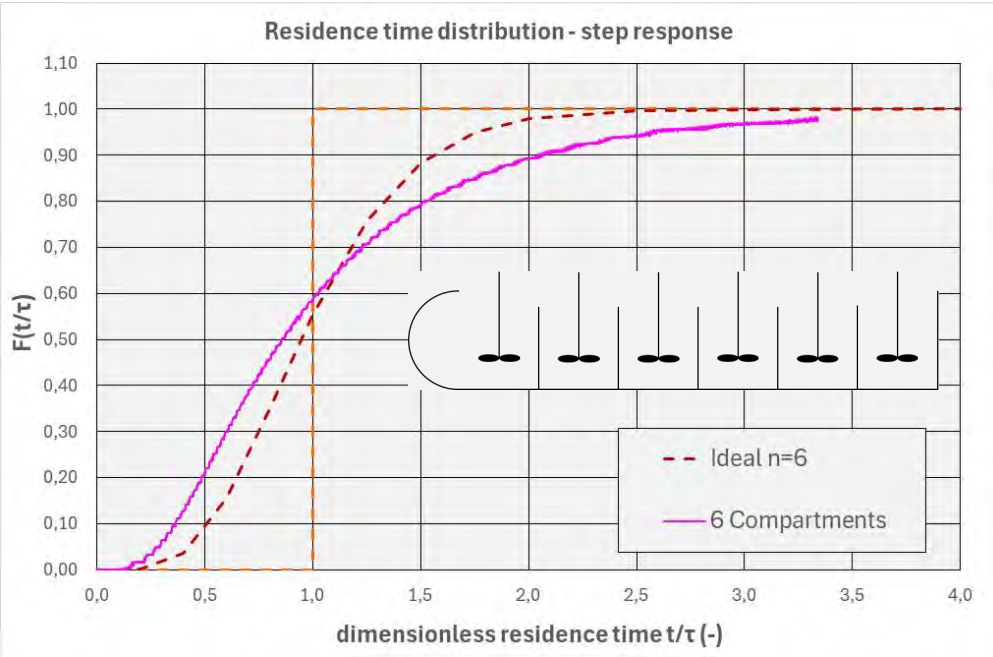

Residence Time Distribution – Impact of Shaft Speed

- increased shaft speed or power input results in short-circuiting
- scale-effect and probably less distinct in full scale

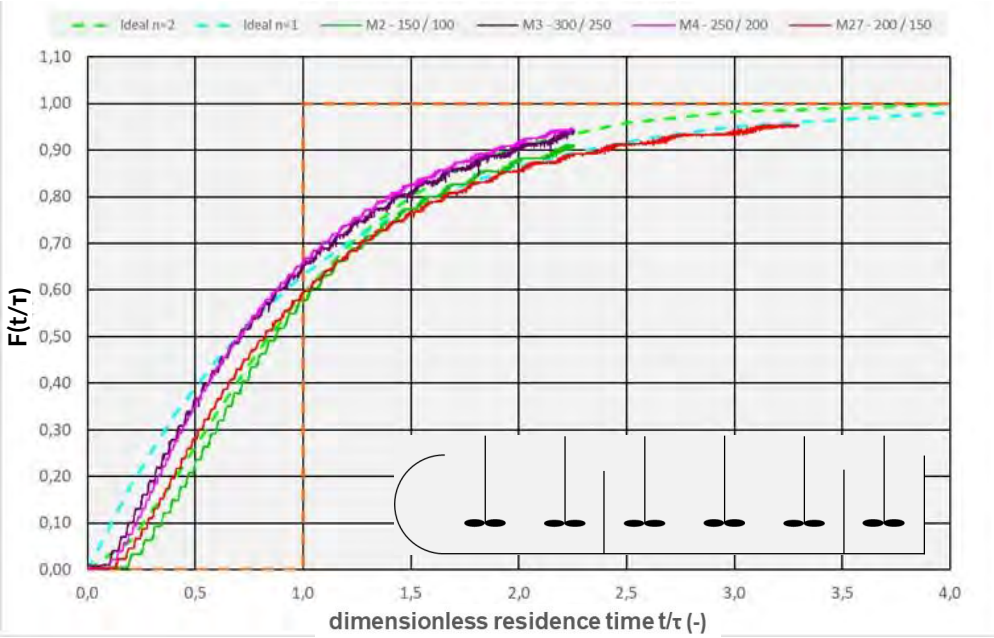

Residence Time Distributions

Over-flow concept

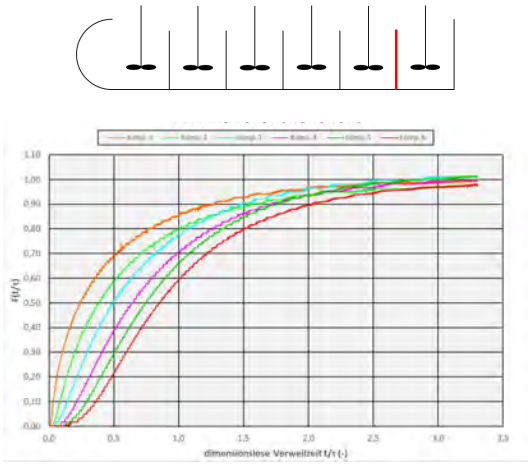

$t_{resp,C6}$=13.4 min

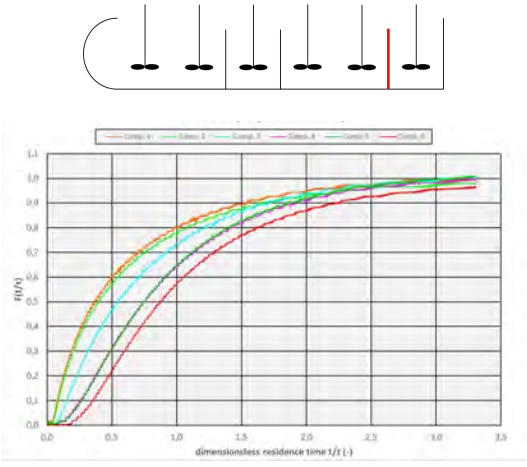

$t_{resp,C6}$=12.1 min

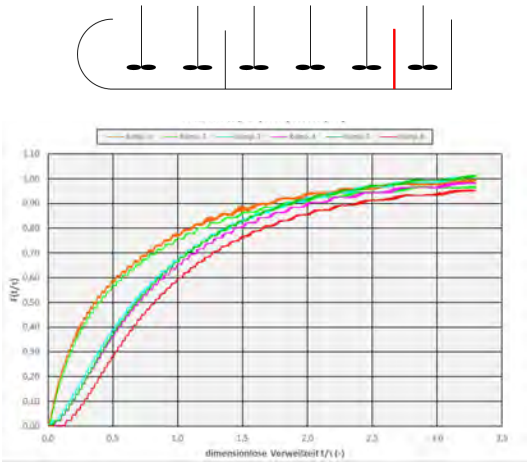

$t_{resp,C6}$=8.6 min

Residence Time Distributions

Response time in compartment 6 and residence time distribution

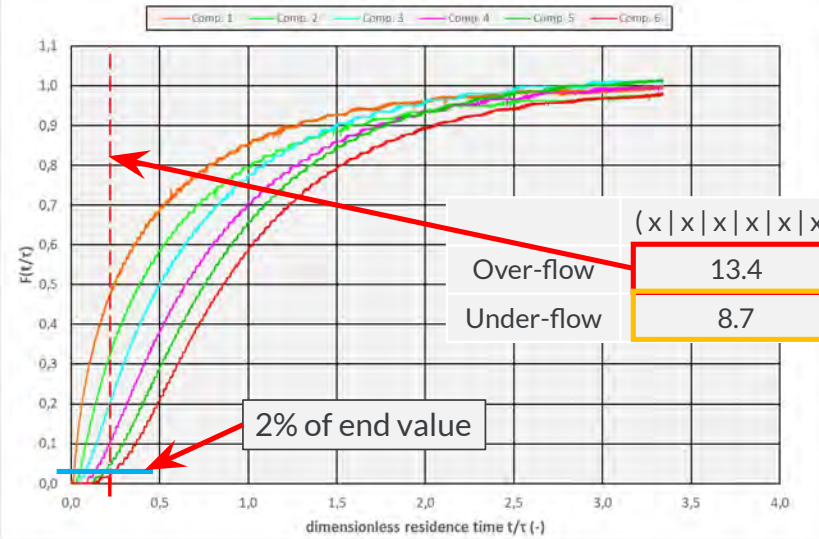

	(x|x|x|x|x|x)	(xx|x|xx|x)	(xx|xxx|x)	(xxxxxx)
Over-flow	13.4	12.1	8.6	3.4
Under-flow	8.7	7.3	6.0	

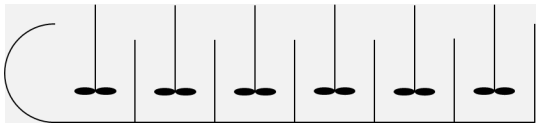

Residence Time Distributions

Under-flow concept

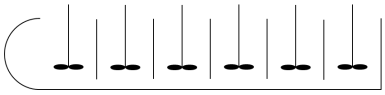

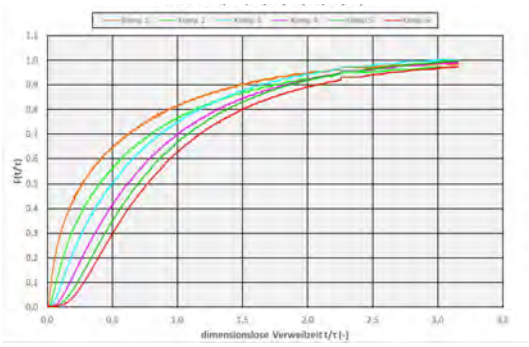

$t_{resp,C6}$=8.7min

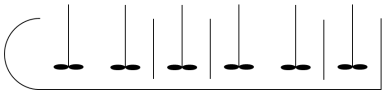

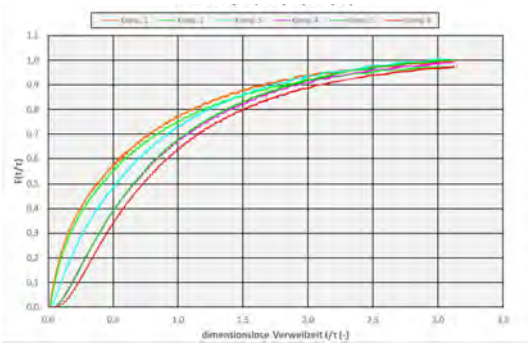

$t_{resp,C6}$=7.3min

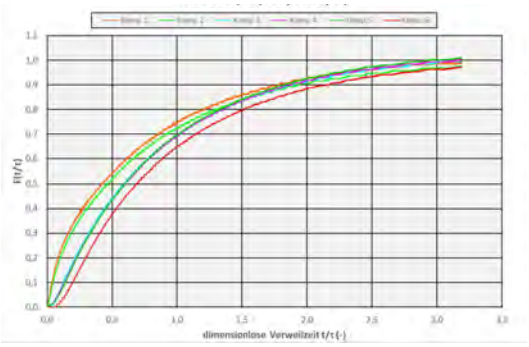

$t_{resp,C6}$=6.0min

Residence Time Distributions

Kick-Off question:

Can a difference in the residence time distribution between over-flow and under-flow be observed?

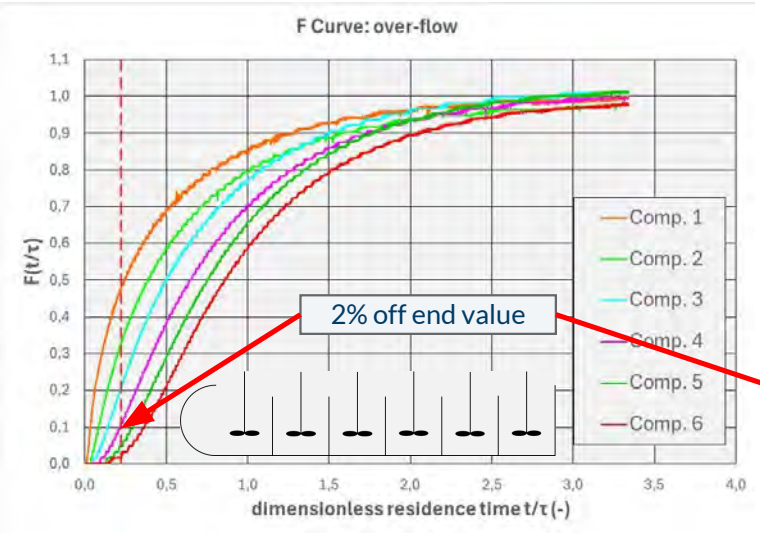

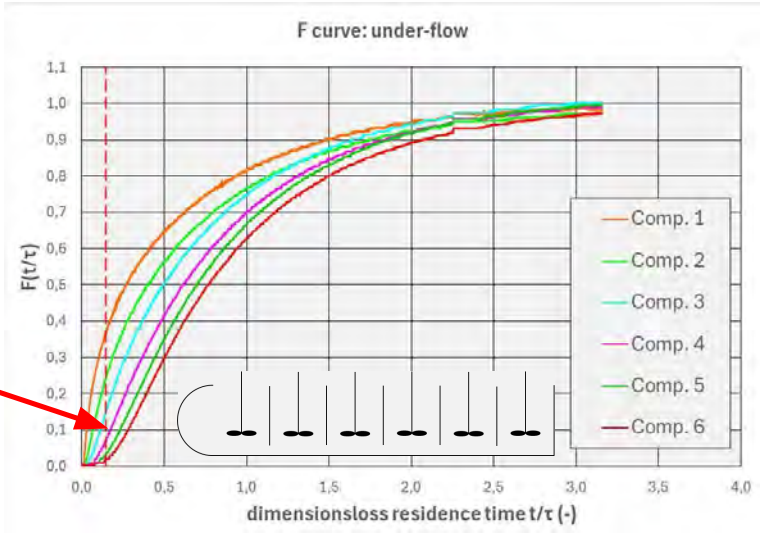

$t_{response,C6}$ = 13.4 min

$t_{response,C6}$ = 8.7 min

Residence Time Distributions Compartment 6

Results of the study

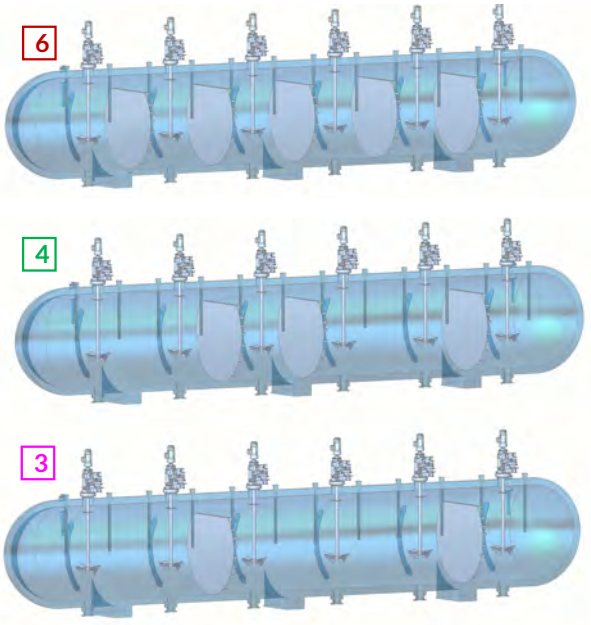

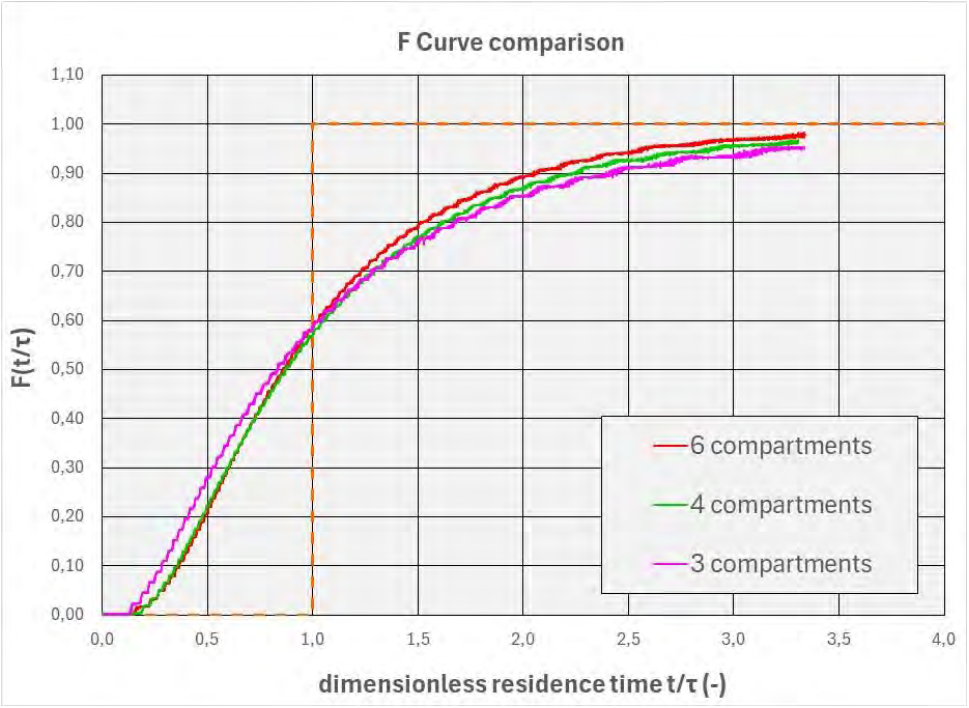

Residence Time Distributions Compartment 6

Results of the study

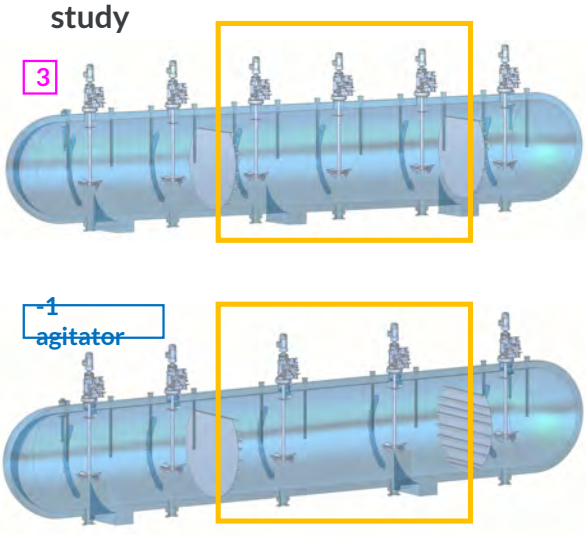

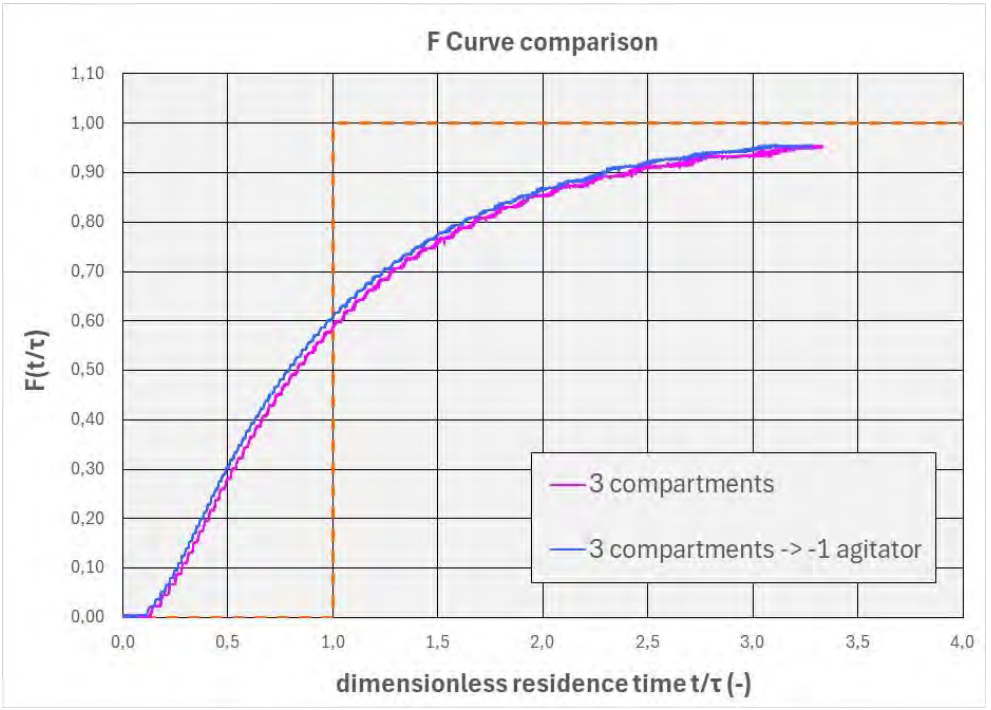

- Same distribution

EKATO Concept Study

Our approach: 500 liter – lab-trials

Step 3: Investigation of solids suspension, flow pattern and blending times

- measurement of blending time
- comparison of suspending behaviour

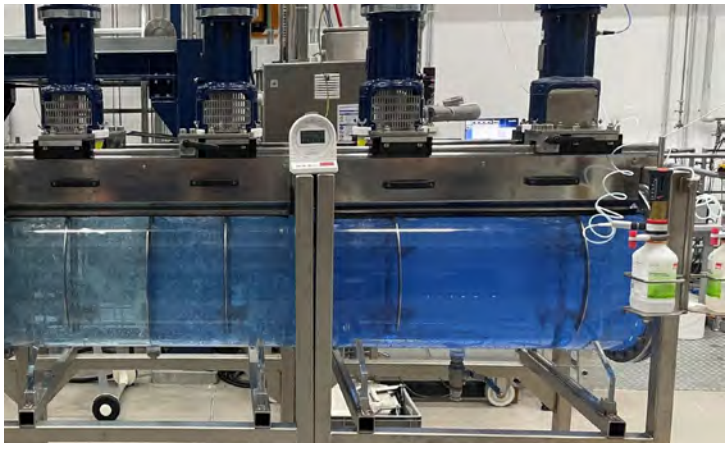

EKATO Concept study

Our approach: 500 liter – lab-trials

Step 4: Mechanical impact: power input, radial forces

- Do the two (or more) agitators in one compartment influence each other ?
  - **Yes, but not significantly !**

ADVANCED PROCESS SOLUTIONS

Summary and Conclusions

- Discussion
  - presentation for thought-provoking impulse / brainstorming
  - concept might be worthwhile for some users or new autoclaves to be built
  - comparisons as presented may allow to assess a possible impact on the leaching performance
  - test scale to full scale: results in test scale considered to be conservative since absolute length scale important
  - additional testing in our new 1 m diameter autoclave model with 3 compartments
  - transfer concept to POX and similar applications
  - CFD analysis after feedback
  - new impeller type under development (compartmentalization ?)
- Looking forward to your feedback / input

AUTOCLAVE OVERPRESSURE: THE HIDDEN VARIABLE

By

Rob Mock, Brant Mock

NOVA Hydromet Ltd., Canada

Presenter and Corresponding Author

Rob Mock
robm@novahydromet.ca

ABSTRACT

Autoclave systems have traditionally been plagued by multiple issues, some of which receive more attention than others. The authors' approach to pressure hydrometallurgy problem solving uses first principles to look beyond common practice to mathematics- and physics-based solutions which often run counter to engineering intuition. Perplexing but common autoclave system issues can include autoclave letdown throughput limitations, broken letdown valve trim, excessive letdown circuit erosion, improper sizing, reaction kinetics modelling miscalculations, and harmonic autoclave level control oscillations. These issues all have several things in common: they result in costly and often unnoticed losses; resolution to obvious issues usually happens very slowly; they are significantly interrelated, sometimes at more than one level; and the interrelated sciences are generally not well understood.

Overpressure in the autoclave and its discharge line is related to all these issues, as it affects the root causes of each. Several issues can be simultaneously addressed using the skilled application of multiple interdependent sets of first principle-based equations. A solid understanding of the related sciences and the added benefit of long industry experience help create solutions specific to each site. Autoclave overpressure provides the classic example of the absence of (or indifference to) complex but essential knowledge that leads to solutions and improvement. As a function of total autoclave pressure and discharge fluid temperature, overpressure can be understood as the partial pressure of non-condensable gasses in the autoclave vapour space. Despite its dominant and extensive effects, it is not directly measured and rarely indirectly derived. Without receiving much attention autoclave overpressure has effectively remained a hidden variable for decades.

Accordingly, overpressure fluctuates significantly in most autoclaves. That high variability is detrimental in multiple ways. Consequently, many autoclave sites incur millions of dollars in silent production losses each year. Throughput limitations of this type are often built into production baselines and are thus completely unknown to plant personnel. Strategies for better comprehending and managing autoclave overpressure leading to performance enhancement will also be presented, along with some descriptive mathematics essential to the relevant sciences.

Keywords:

Autoclave Overpressure, Autoclave Letdown, Throughput Limitation, Autoclave Control, Vapour Pressure

Autoclave Overpressure: The Hidden Variable

Rob Mock | robm@novahydromet.ca
Tatiana Tagieva | tatianat@novahydromet.ca

Overpressure Effects

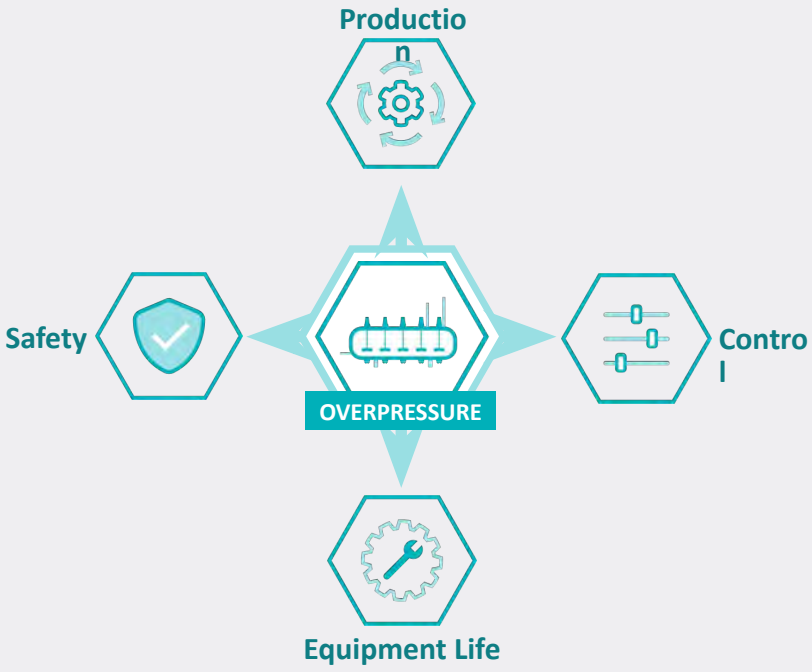

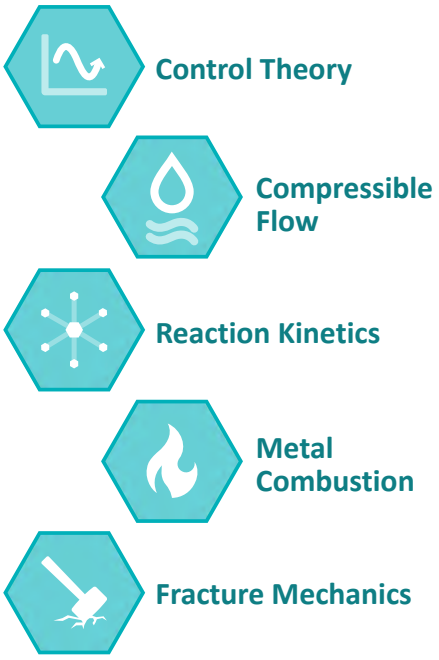

Autoclave Overpressure: The Hidden Variable

Overpressure = $P_{Autoclave}$ - P_{Vapour}

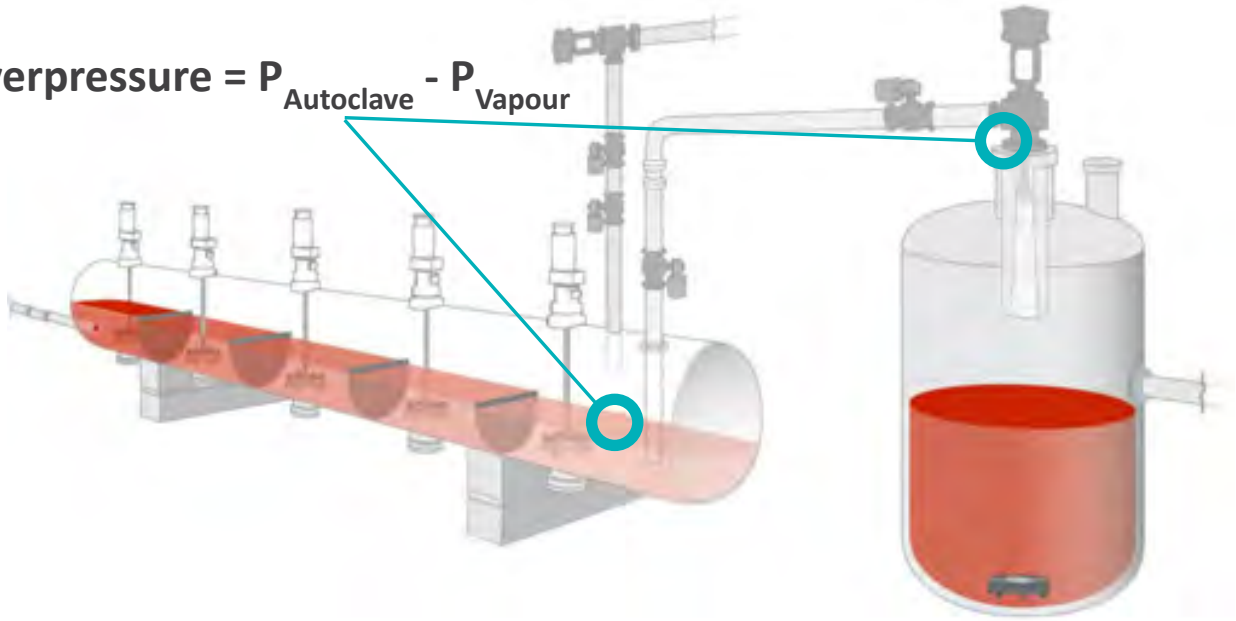

novahydromet.ca

What is Overpressure?

Partial Pressures

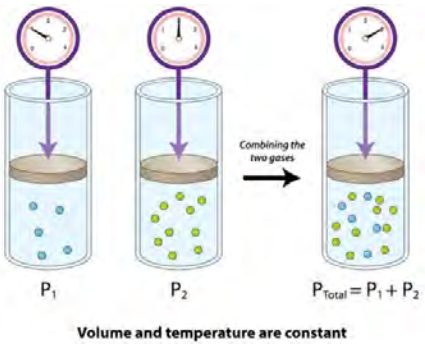

Steam Dome

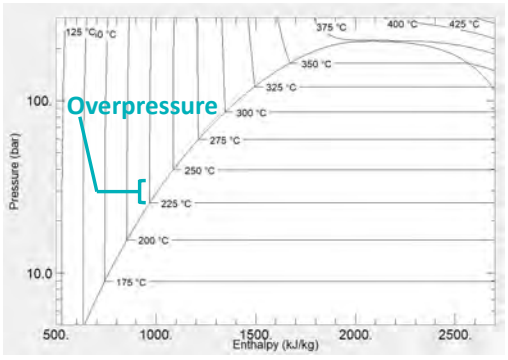

Simplifying Variables

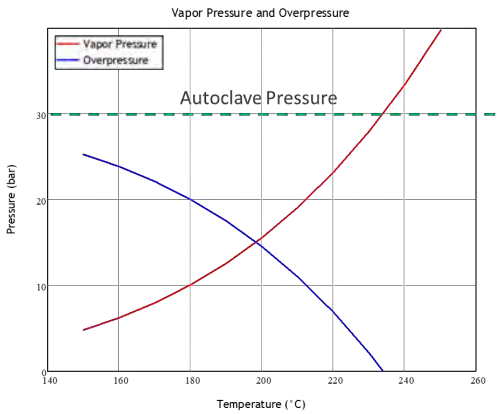

Overpressure: driving force for the flashing flow

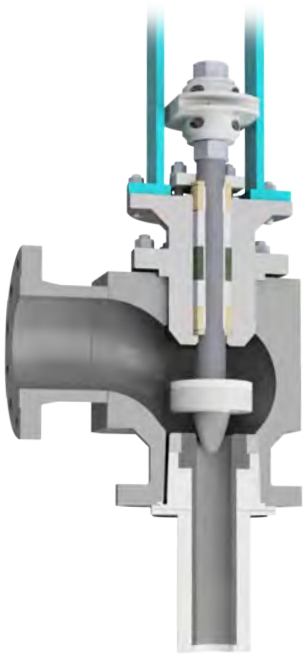

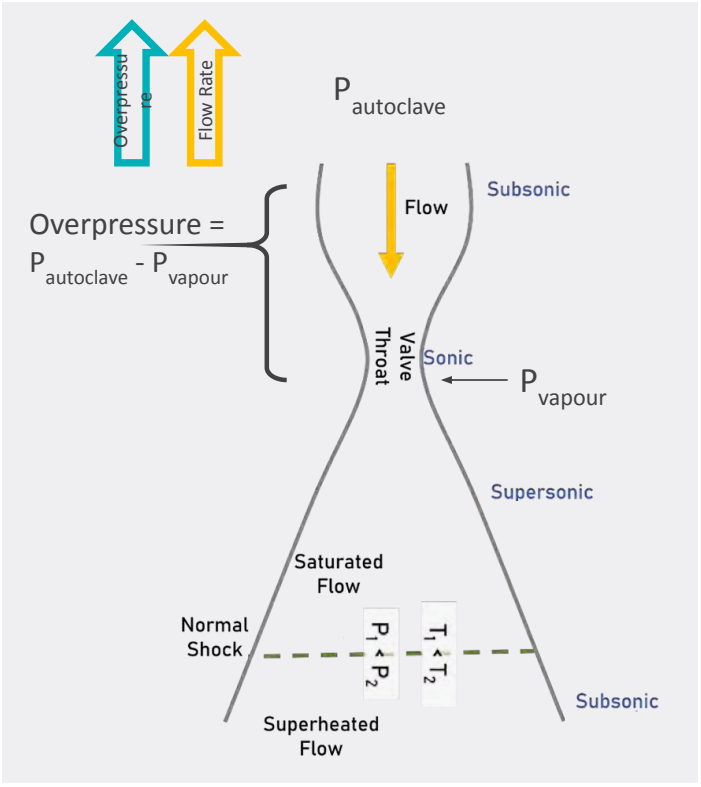

Multiphase Compressible Flow

Converging Diverging Nozzle

Gas Dynamics

Mass Flow is Sensitive to Overpressure

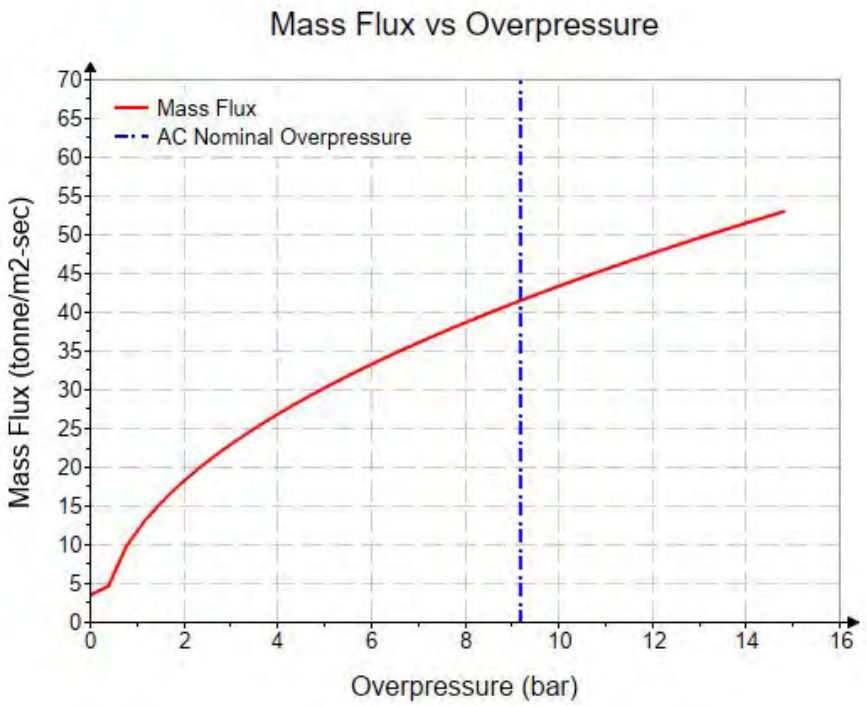

Statistical Representation of Overpressure

μ_P = 32 bar
σ_P = 0.30 bar

μ_{OP} = 8 bar
σ_{OP} = 1.7 bar

μ_T = 221 °C
σ_T = 3 °K

Trim Damage vs. Throughput Limitation

Accelerated Trim Damage

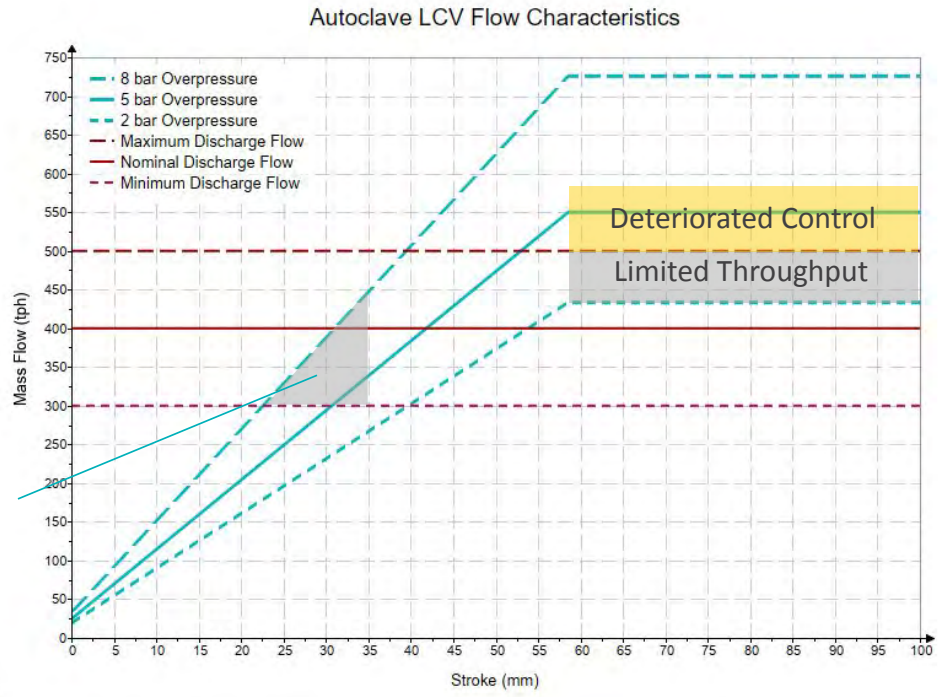

Obvious and Hidden Losses

Obvious
Trim Failure Losses

0.1-1% production loss + spare parts

Hidden
Throughput Limitation Losses

1-5% production loss

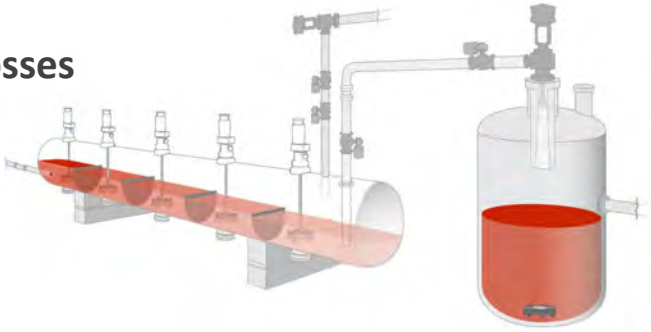

novahydromet.ca

Adding Crushing to Sieving

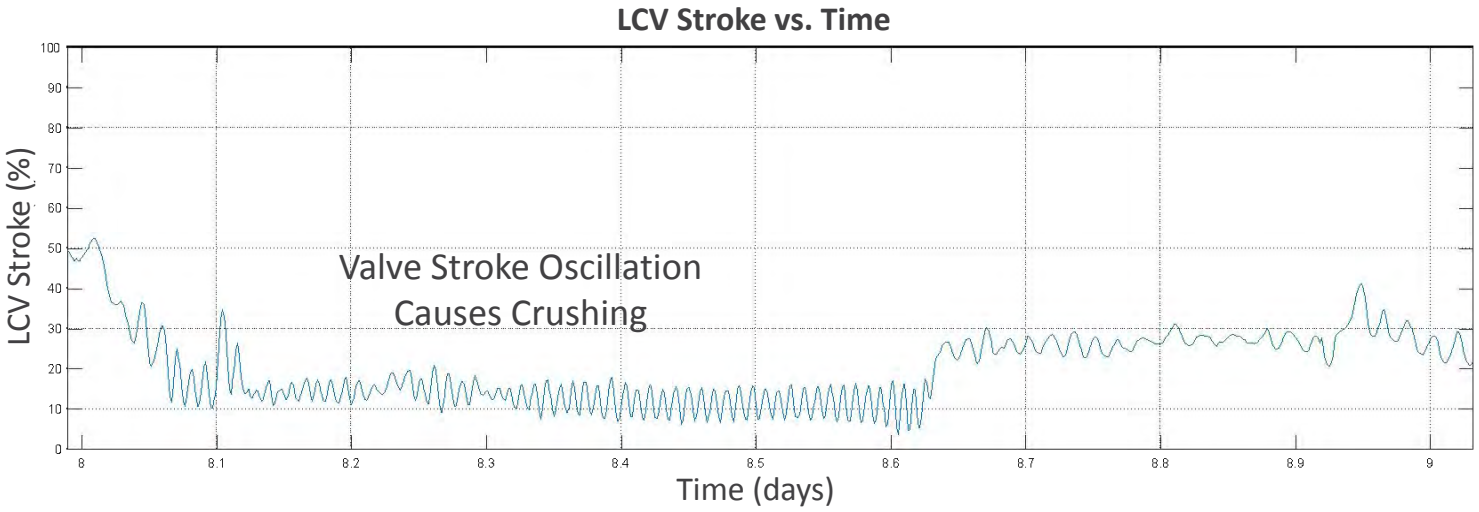

Data Science 1010 1010 Control Theory

Overpressure Affects Level Control

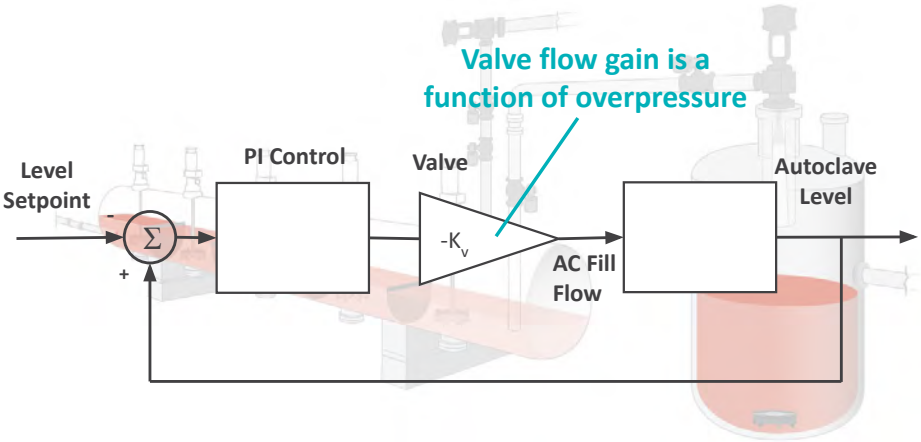

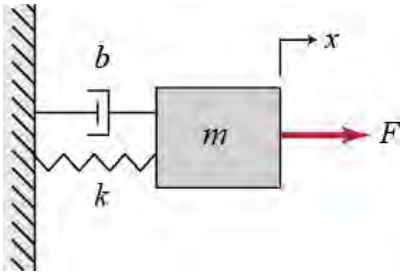

Underdamped

Damped

Overdamped

Micro Scale Overpressure

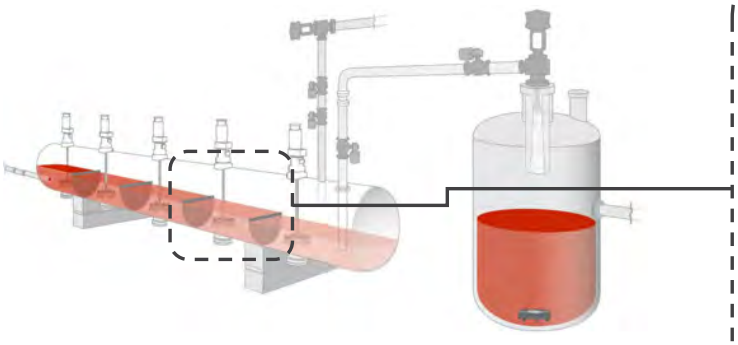

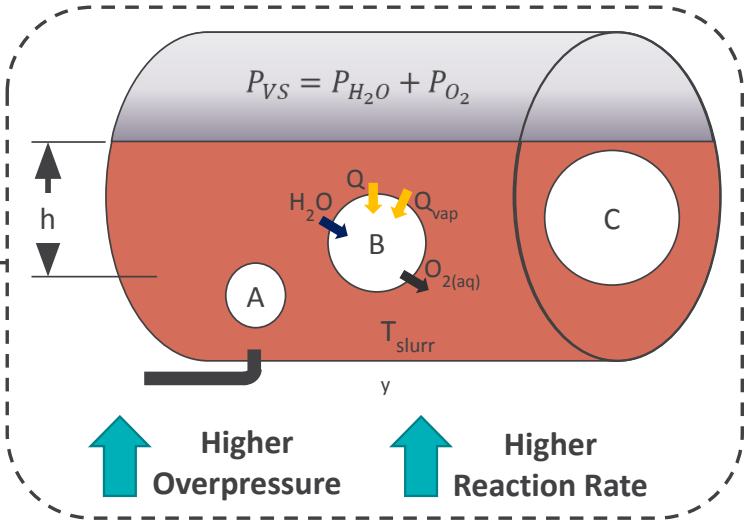

Partial Pressure

Diffusion Mass Flux

Solubility

Temp. Dependence

Gas Diffusion

Overpressure Control

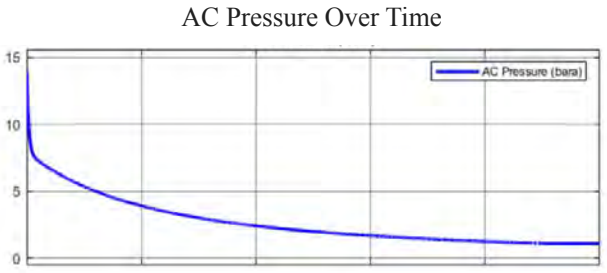

4.8 tph fixed gas flow

small margin

Autoclave Temperature Control

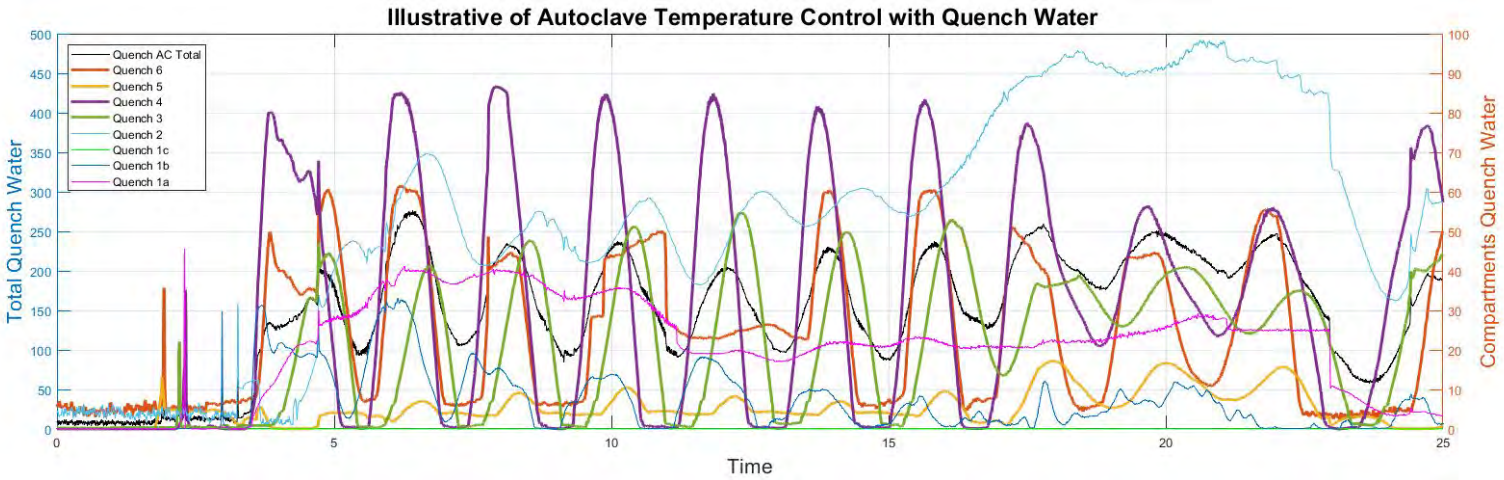

Temperature Control → Overpressure → Level Control

Overpressure Control Value Proposition

Low Capital Investment

Little or No Hardware Required

Optimize Your Process

Leverage Existing Data and Assets

High Return Potential

Increase Throughput

novahydromet.ca

LONG-TERM EXPERIENCES AND NEW DEVELOPMENTS IN AUTOCLAVE LININGS FOR HIGH-PRESSURE LEACHING AND PRESSURE OXIDATION PROCESSES

By

Dr. Daniel Kessler, Thomas Feldhaus, Stefan Henneking, Oliver Kams, Horst Feldheiser

DSB Saeurebau GmbH Koenigswinter, Germany

Presenter and Corresponding Author

Dr. Daniel Kessler
Daniel.Kessler@didiersb.de

ABSTRACT

Common processes to extract metals from refractory ores or laterite ores rely on high pressure applications in autoclaves, e.g. High Pressure Acid Leaching (HPAL) to extract nickel and cobalt or Pressure Oxidation (POX) in cases of copper, gold, zinc, etc.
In both processes ore is mined, crushed and a slurry is created by addition of water or acid. This slurry is treated at elevated temperature and pressure (e.g. T>200°C, P>30 bar) in an autoclave. To return the slurry to atmospheric conditions, an array of flash vessels is used.
Via decantation and selective precipitation the desired metal, metal oxide or metal salt can be accumulated and purified.
As each step requires a specific corrosion protection lining, different lining setups were used in autoclaves, flash vessels, etc.
Especially for high pressure applications in autoclaves and flash vessels combined linings of membranes, bricks and inserts of PTFE, titanium or Inconel are used.
Looking at various ore processing plants around the world, different kinds of membranes are combined with different types of brick linings aiming for a long-lasting and efficient corrosion protection.
Membranes protect the steel vessels against chemical attack. Widely used in pressure vessels are lead membranes, glass fiber reinforced coatings or rubber linings. Also explosion plated titanium or welded on Inconel is partially used.
The main task of the additional brick lining is to protect the membrane against abrasion or mechanical impact. Acid resistant ceramic bricks, carbon bricks, graphene bricks or different specialties are widely used. Depending on the local load (e.g. liquid phase, gas phase, transition zone) different types of mortars are used to install the brick lining.
During the presentation, we will look back on decades of experience with different lining combinations and show pros and cons in application, operation, maintenance, repair and relining

Keywords: HPAL, POX, Corrosion Protection, Combined Linings, Autoclave, Flash Vessel

INTRODUCTION

In the realm of metallurgy, the pursuit of efficient ore processing methodologies has been an enduring quest, driven by the imperative to extract valuable metals from increasingly complex ores. Among the arsenal of techniques, high-pressure acid leaching (HPAL) and pressure oxidation (POX) stand out as transformative methodologies, offering unparalleled opportunities to unlock the latent value of ores once deemed refractory.

HPAL involves subjecting ore slurries to elevated temperatures and pressures in the presence of sulfuric acid, facilitating the dissolution of valuable metals such as nickel, cobalt, and copper. Meanwhile, POX entails the oxidation of sulfide minerals under high temperature and pressure conditions, leading to the liberation of encapsulated metals and rendering them amenable to subsequent extraction.

Within this context, the autoclave emerges as the pivotal apparatus orchestrating the intricacies of HPAL and POX processes. An autoclave, essentially a robust pressure vessel, serves as the crucible wherein ore slurries undergo the rigors of elevated temperature and pressure conditions. Operating akin to a metallurgical alchemist's cauldron, the autoclave catalyzes the dissolution of minerals, liberating metals from their mineralogical confines and facilitating their downstream recovery.

Image 1: Inside View of a POX Autoclave during relining.

AUTOCLAVES

Autoclaves play a central role in both High-Pressure Acid Leaching (HPAL) and Pressure Oxidation (POX) processes, yet their operational characteristics and design nuances vary significantly between the two methodologies.

In HPAL processes, autoclaves are primarily tasked with facilitating the dissolution of valuable metals from ore concentrates through the application of elevated temperature and pressure conditions in the presence of sulfuric acid. These autoclaves are typically constructed from materials resistant to the corrosive nature of sulfuric acid, such as high-grade stainless steel or specialized alloys. The temperature and pressure regimes within HPAL autoclaves are tailored to promote the dissolution of specific metal sulfides, ensuring optimal

extraction efficiencies while mitigating undesirable side reactions. Additionally, HPAL autoclaves often incorporate agitators or stirrers to enhance mass transfer and promote uniform mixing of the ore slurry with the acid solution, thereby maximizing metal recovery rates.

In contrast, autoclaves utilized in POX processes are engineered to catalyze the oxidative dissolution of sulfide minerals present in refractory ores, liberating encapsulated metals for subsequent extraction. Unlike HPAL autoclaves, which rely on sulfuric acid as the leaching agent, POX autoclaves operate under oxygen-rich atmospheres at elevated temperatures and pressures, driving the oxidation of sulfide minerals to soluble metal species. Consequently, POX autoclaves are constructed with materials capable of withstanding oxidative environments and are often lined with refractory bricks or coatings to resist high temperatures and abrasive slurries. The design of POX autoclaves prioritizes efficient gas-liquid-solid contact to facilitate the oxidation reactions, typically incorporating spargers or gas injection systems to disperse oxygen throughout the ore slurry and promote reaction kinetics.

While both HPAL and POX autoclaves share the fundamental objective of enhancing metal recovery from refractory ores, their distinct operating principles necessitate tailored designs and operational parameters. By understanding the nuanced differences between autoclaves employed in HPAL and POX processes, metallurgical engineers can optimize process performance and maximize the extraction of valuable metals from challenging ore sources.

FLASH VESSELS

Flash vessels are integral components in the metallurgical processing of ores, particularly in autoclave applications such as High-Pressure Acid Leaching (HPAL) and Pressure Oxidation (POX). These vessels play a crucial role in separating the liquid and gas phases following the high-pressure treatment of ore slurries, thereby facilitating efficient metal recovery and process optimization.

In HPAL processes, flash vessels are strategically positioned downstream of the autoclave to exploit the sudden reduction in pressure that occurs when the slurry exits the autoclave. As the high-pressure slurry is depressurized upon entering the flash vessel, the sudden drop in pressure induces flash vaporization of volatile components, including water and sulfuric acid. This vaporization effectively separates the liquid and gas phases, allowing the acidic solution laden with dissolved metals to be collected for further processing. Meanwhile, the liberated gases, which may include steam and sulfur dioxide, are vented or recycled for subsequent use within the process, thereby minimizing energy consumption and environmental impact.

Similarly, in POX applications, flash vessels serve as critical components for phase separation and gas-liquid disengagement following the oxidative treatment of sulfide ores. As the ore slurry exits the high-pressure autoclave and enters the flash vessel, the abrupt reduction in pressure triggers the release of dissolved gases, primarily carbon dioxide and sulfur dioxide, generated during the oxidation of sulfide minerals. This gas liberation promotes the separation of the gas and liquid phases, allowing the oxidized slurry to be collected for downstream processing, while the off-gases are typically directed to gas treatment systems for purification or environmental control.

The utilization of flash vessels in autoclave applications offers several advantages for metallurgical processing. By effectively separating the liquid and gas phases, flash vessels enable the recovery of valuable metals from ore slurries with enhanced efficiency and selectivity. Moreover, the controlled release and management of gases within flash vessels contribute to process safety and environmental compliance, minimizing the risk of gas emissions and ensuring regulatory compliance.

Overall, flash vessels represent indispensable components in the arsenal of equipment employed in autoclave-based metallurgical processes, playing a pivotal role in optimizing metal recovery, enhancing process efficiency, and maintaining operational integrity.

GENERAL LINING SETUPS – COMBINED LININGS

The setup of corrosion protective linings in Pressure Oxidation (POX) autoclaves and flash vessels is meticulously engineered to withstand the harsh chemical environments encountered during the processing of refractory ores. This dual-layered approach, comprising a membrane for the protection of the steel substrate and a brick lining consisting of acid-proof ceramic bricks, ensures robust corrosion resistance and prolonged equipment lifespan.

1. Membrane Lining: The first line of defense against corrosion in POX autoclaves and flash vessels is the application of a membrane lining directly onto the steel substrate. This membrane serves as a barrier between the corrosive process fluids and the underlying steel, preventing direct contact and corrosion-induced degradation. Membrane linings are typically composed of synthetic polymers or elastomers that exhibit excellent chemical resistance to acidic solutions, high temperatures, and mechanical stresses. Common materials used for membrane linings include fluoropolymers like PTFE

(polytetrafluoroethylene) or PVDF (polyvinylidene fluoride), as well as elastomeric compounds such as EPDM (ethylene propylene diene monomer) or chlorobutyl rubber. These materials form a flexible and impermeable barrier that effectively shields the steel substrate from corrosive attack, extending the service life of the equipment.

2. Brick Lining: In addition to the membrane lining, POX autoclaves and flash vessels are equipped with a secondary layer of protection in the form of acid-proof ceramic brick linings. These brick linings are installed atop the membrane lining to provide additional mechanical strength, abrasion resistance, and thermal insulation. Acid-proof ceramic bricks are composed of dense and chemically inert materials, such as silica or silicon carbide, which exhibit exceptional resistance to acidic environments and high temperatures. The bricks are tightly fitted and bonded together using acid-resistant mortars, forming a continuous and durable protective layer. The brick lining acts as a sacrificial barrier, absorbing the brunt of the corrosive attack from the process fluids and shielding the underlying membrane lining and steel substrate from direct exposure. Additionally, the thermal insulation properties of the brick lining help to maintain uniform temperature distribution within the vessel, optimizing process performance and energy efficiency.

By combining a membrane lining for direct corrosion protection of the steel substrate with a brick lining of acid-proof ceramic bricks for mechanical strength and thermal insulation, POX autoclaves and flash vessels are equipped to withstand the rigors of high-pressure oxidative leaching processes. This multi-layered approach to corrosion protection ensures the integrity and longevity of the equipment, enabling efficient and reliable processing of refractory ores while minimizing downtime and maintenance costs.

Image 2: Rubber Membrane in an Autoclave.

Image 3: Beginning of brick lining on top of the membrane.

Image 4: Almost completed brick lining within an autoclave.

FINITE ELEMENT METHOD

The Finite Element Method (FEM) is a powerful numerical technique used to model and analyze complex engineering systems, including autoclaves used in metallurgical processes such as Pressure Oxidation (POX). FEM can be employed to predict and assess potential interferences between the internal brick lining and the steel vessel of these autoclaves, offering valuable insights into structural integrity, stress distribution, and potential failure modes.

Here's how the Finite Element Method can be utilized in this context:

1. **Geometry Modeling**: The first step involves creating a detailed geometric model of the autoclave, including its steel vessel, internal brick lining, and any other relevant components. This model accurately represents the dimensions, shapes, and material properties of each component, capturing the intricacies of the autoclave's internal structure.
2. **Mesh Generation**: The geometric model is then discretized into a finite number of smaller elements, or "mesh," using specialized software. The meshing process divides the autoclave geometry into finite elements, each of which is associated with specific material properties and geometric characteristics. The mesh density and element types are chosen to ensure accurate representation of the structural features and stress distribution within the autoclave.
3. **Material Properties**: Material properties, including mechanical properties such as elasticity, yield strength, and thermal expansion coefficients, are assigned to each element based on the properties of the steel vessel, brick lining, and any other components. These material properties are essential for accurately simulating the behavior of the autoclave under various loading conditions.
4. **Boundary Conditions**: Boundary conditions, such as applied loads, constraints, and thermal conditions, are defined to simulate the operating conditions experienced by the autoclave during POX processes. These boundary conditions mimic the effects of internal pressure, temperature gradients, and mechanical forces acting on the autoclave.
5. **Analysis**: The finite element model is subjected to numerical analysis, wherein the software solves a system of equations derived from the principles of solid mechanics, heat transfer, and fluid dynamics. This analysis predicts the distribution of stresses, strains, displacements, and temperature gradients within the autoclave, providing insights into potential areas of concern, such as regions of high stress or deformation.
6. **Interference Detection**: By analyzing the results of the finite element analysis, engineers can identify potential interferences or conflicts between the internal brick lining and the steel vessel. These interferences may manifest as excessive stresses, deformations, or contact pressures at the interface between the two components. Engineers can assess the severity of these interferences and explore mitigation strategies, such as adjusting the design parameters, optimizing material selection, or refining the manufacturing process.
7. **Validation and Optimization**: The finite element model can be validated against experimental data or benchmark simulations to ensure its accuracy and reliability. Additionally, the model can be used iteratively to explore design variations, optimize structural configurations, and enhance the performance and durability of the autoclave.

By leveraging the Finite Element Method, engineers can effectively predict and mitigate potential interferences between the internal brick lining and the steel vessel in POX autoclaves, ensuring their structural integrity, reliability, and safety throughout the demanding conditions of metallurgical processing.

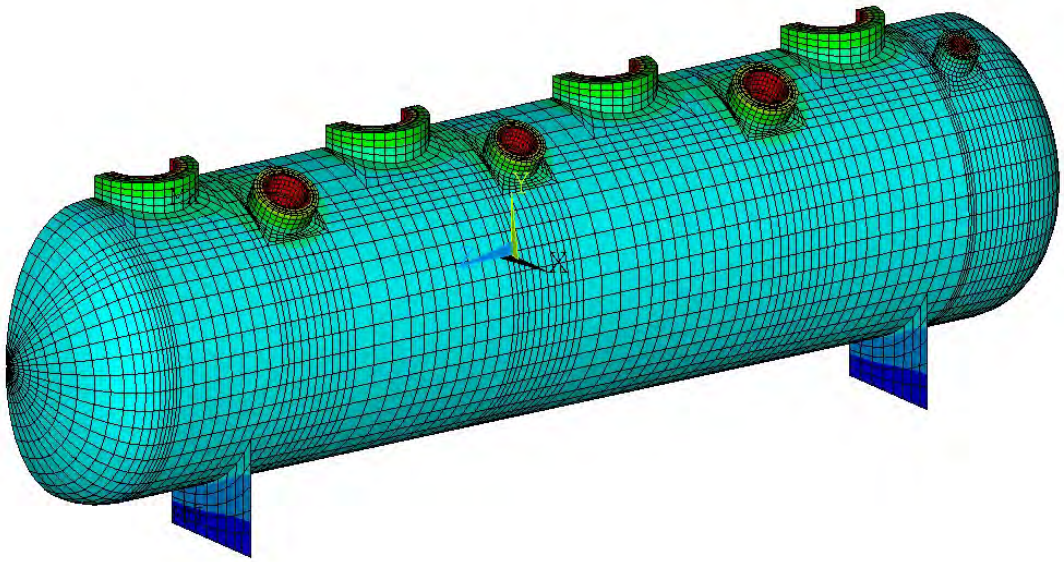

Image 5: FEA-model of an Autoclave: Expansion of brick lining inside an autoclave, Temperature distribution

MEMBRANES

Regarding the different parts of a Vessel lining the membrane is the most critical. It must provide an impervious seal to protect the steel against the corrosive, acidic media.
Membranes which are used for Autoclaves, Heater- and Flash Vessels are in general:

- Reinforced Plastic membranes (GRP)
- Elastomeric Rubber Linings
- Flexible thermoplastic sheet lining
- Plastic sheets made out PVDF, PTFE, and ECTFE
- Lead as sheet material or homogenous clad bonded
- Metal overlay welding like Inconel-cladding

INCONEL MEMBRANES / METAL OVERLAYS

Inconel, a family of nickel-chromium-based superalloys renowned for their exceptional corrosion resistance, mechanical strength, and high-temperature performance, finds widespread application as a membrane lining in autoclaves utilized in metallurgical processes such as Pressure Oxidation (POX). Here's how Inconel linings serve as robust barriers against corrosive environments within these autoclaves:

1. **Corrosion Resistance**: Inconel alloys, particularly grades such as Inconel 625 and Inconel 718, exhibit outstanding resistance to corrosion from a wide range of aggressive chemicals, including sulfuric acid, hydrochloric acid, and acidic solutions encountered in POX processes. The high nickel content in Inconel imparts excellent resistance to both oxidizing and reducing environments, making it an ideal choice for applications where corrosion is a primary concern.
2. **High-Temperature Performance**: POX autoclaves operate under elevated temperatures ranging from 150°C to 250°C or higher, depending on the specific process requirements. Inconel alloys maintain their mechanical strength and corrosion resistance at elevated temperatures, ensuring long-term integrity and reliability of the membrane lining even under harsh thermal conditions. This high-temperature stability allows Inconel linings to withstand the demanding thermal cycling and operating conditions experienced during POX processes without degradation or failure.
3. **Mechanical Strength**: Inconel alloys possess excellent mechanical properties, including high tensile strength, fatigue resistance, and toughness, which are essential for withstanding the mechanical stresses and pressures exerted on the membrane lining within the autoclave. The inherent strength of Inconel ensures structural integrity and dimensional stability of the lining, preventing deformation, buckling, or rupture under operating conditions.
4. **Compatibility with Process Fluids**: Inconel linings are compatible with a wide range of process fluids and chemicals commonly encountered in metallurgical processing, including acidic solutions, high-

pressure steam, and corrosive gases. The inert nature of Inconel minimizes the risk of contamination or chemical reactions with the process fluids, ensuring purity and integrity of the processed materials and final product.

5. **Fabrication and Installation**: Inconel membranes can be fabricated using various techniques, including welding, forming, and machining, to achieve precise dimensions and configurations tailored to the specific geometry of the autoclave. The membrane lining is securely installed onto the steel substrate using welding or mechanical fastening methods, creating a robust barrier against corrosive attack while maintaining tight seals and interfaces to prevent leakage.

Overall, the use of Inconel as a membrane lining in POX autoclaves provides a reliable and durable solution for protecting the steel substrate against corrosion and thermal degradation, thereby ensuring the long-term performance and integrity of the equipment in demanding metallurgical processing environments. However, material and installation price is very high. The main drawback is repairability or maintenance, which is usually not easy and needs to be designed carefully. Usually special welding equipment is needed which cannot be used in any point of an autoclave or which would require a rotation of the complete vessel.

LEAD MEMBRANES

The use of lead as a membrane lining in autoclaves, particularly in metallurgical processes like Pressure Oxidation (POX), serves as a specialized solution for corrosion protection in highly acidic and aggressive environments. Here's how lead membranes offer unique advantages and considerations:

1. **Corrosion Resistance**: Lead is renowned for its exceptional resistance to corrosion, particularly in acidic environments. In POX processes where sulfuric acid or other aggressive chemicals are present, lead provides a robust barrier against corrosion, preventing degradation of the steel substrate and ensuring long-term integrity of the autoclave.
2. **Chemical Inertness**: Lead is chemically inert and does not react with most acids or corrosive substances encountered in metallurgical processing. This inert nature ensures that the lead membrane remains stable and impervious to chemical attack, maintaining its protective properties over extended periods of operation.
3. **Malleability and Formability**: Lead possesses excellent malleability and formability, allowing it to conform closely to the contours of the autoclave's internal surfaces. This capability enables the fabrication of seamless lead membranes that provide complete coverage and protection, minimizing the risk of corrosion at joints or seams.
4. **Sealing and Insulation**: Lead membranes can be tightly sealed against the steel substrate, forming a continuous and impermeable barrier that prevents the ingress of corrosive fluids and gases. Additionally, lead exhibits moderate thermal insulation properties, helping to mitigate temperature differentials and maintain uniform conditions within the autoclave.
5. **Environmental Considerations**: While lead offers superior corrosion resistance, its use raises environmental and health considerations due to the potential for lead leaching or contamination. Special precautions must be taken during the fabrication, installation, and maintenance of lead membranes to prevent exposure to lead dust or fumes. Proper ventilation, personal protective equipment, and waste management practices are essential to ensure worker safety and environmental compliance.
6. **Durability and Maintenance**: Lead membranes require periodic inspection and maintenance to ensure their continued effectiveness in corrosion protection. Although lead is highly durable and resistant to degradation, factors such as mechanical damage, erosion, or exposure to extreme temperatures may compromise the integrity of the membrane over time. Regular inspections and repairs are necessary to address any signs of wear or damage and to prolong the service life of the lead lining.

In summary, the use of lead as a membrane lining in autoclaves offers unique advantages in terms of corrosion resistance, chemical inertness, and formability, making it well-suited for protecting steel substrates in aggressive metallurgical processing environments. However, careful consideration of environmental and health considerations is essential to ensure safe handling and operation of lead-lined autoclaves.

Compared to Inconel, lead shows a lower resistance at temperatures higher than 100°C. Homogeneous lead lining can only be installed in the 6 o’clock position (rotation of an autoclave may be needed during installation or repair). Lead panels (cladding on profiles) can be installed regardless of the orientation. But in this case the membrane is not completely attached to the substrate. Vacuum within this gap improves the lifetime.

GLASS FIBRE REINFORCED PLASTICS (LAMINATES BASED ON FURANIC RESINS)

Glass fiber-reinforced plastics (GRP), particularly those based on furanic resins, serve as versatile and durable membrane linings in autoclaves, offering a combination of corrosion resistance, mechanical strength, and thermal stability. Here's an overview of GRP membranes in autoclave applications, with a focus on furanic resin-based compositions:

1. **Composition and Structure**: GRP membranes are composed of a matrix resin reinforced with high-strength glass fibers. Furanic resins, derived from furfuryl alcohol, serve as the matrix material in these membranes. Furanic resins offer excellent chemical resistance, particularly to acidic and corrosive environments encountered in metallurgical processes. The glass fibers provide reinforcement, enhancing mechanical properties such as tensile strength, flexural strength, and impact resistance.
2. **Corrosion Resistance**: Furanic resin-based GRP membranes exhibit superior corrosion resistance, making them well-suited for protecting steel substrates against aggressive chemicals, including sulfuric acid, hydrochloric acid, and acidic solutions present in POX autoclaves. The chemically inert nature of furanic resins ensures long-term stability and integrity of the membrane lining, even in highly corrosive environments.
3. **Mechanical Strength and Durability**: GRP membranes offer high mechanical strength and durability, thanks to the reinforcement provided by glass fibers. This combination of materials results in membranes with excellent load-bearing capacity, dimensional stability, and resistance to deformation under mechanical stress. GRP membranes can withstand the rigors of autoclave operation, including high pressures, temperature fluctuations, and mechanical agitation, without compromising their structural integrity.
4. **Thermal Stability**: Furanic resin-based GRP membranes exhibit good thermal stability, allowing them to withstand the elevated temperatures encountered in autoclave processes. These membranes maintain their mechanical properties and dimensional stability over a wide range of operating temperatures, ensuring reliable performance under thermal cycling and transient heating conditions.
5. **Fabrication and Installation**: GRP membranes can be fabricated using various techniques, including hand lay-up, filament winding, or compression molding, to achieve precise dimensions and configurations tailored to the specific geometry of the autoclave. The membranes are securely bonded to the steel substrate using adhesives or mechanical fasteners, ensuring tight seals and interfaces to prevent leakage and corrosion ingress.
6. **Environmental Considerations**: Furanic resin-based GRP membranes offer environmental advantages compared to traditional materials such as lead or certain polymers. Furanic resins are derived from renewable biomass sources and can be formulated to minimize volatile organic compound (VOC) emissions during manufacturing. Additionally, GRP membranes do not pose the same health and safety risks associated with lead or certain plastics, making them a safer and more environmentally friendly option for autoclave linings.

In summary, glass fiber-reinforced plastics based on furanic resins offer a compelling combination of corrosion resistance, mechanical strength, thermal stability, and environmental sustainability, making them well-suited for membrane linings in autoclaves used in metallurgical processes like Pressure Oxidation. Their versatility and performance make them a preferred choice for protecting steel substrates and ensuring the long-term reliability and efficiency of autoclave operations. The unbeatable benefit of these organic membranes is of course their low price compared to metal membranes and their fast installation time.

PLASTIC SHEETING

Plastic sheets such as PVDF (Polyvinylidene fluoride), PTFE (Polytetrafluoroethylene), or ECTFE (Ethylene Chlorotrifluoroethylene) serve as effective membrane linings in autoclaves, offering a combination of chemical resistance, thermal stability, and non-stick properties. Here's how these materials are utilized as membranes in autoclave applications:

1. **PVDF (Polyvinylidene fluoride)**:
    - PVDF is a fluoropolymer known for its exceptional chemical resistance, mechanical strength, and thermal stability. These properties make it an excellent choice for membrane linings in autoclaves operating in corrosive environments.
    - PVDF membranes exhibit high resistance to a wide range of chemicals, including strong acids, bases, and organic solvents. This makes them suitable for protecting steel substrates against corrosion in processes involving acidic solutions, such as High-Pressure Acid Leaching (HPAL).

- PVDF membranes have good thermal stability, withstanding temperatures ranging from cryogenic to elevated levels without significant degradation. This allows them to maintain their mechanical properties and integrity under operating conditions encountered in autoclave processes.

2. **PTFE (Polytetrafluoroethylene)**:
   - PTFE, commonly known by the brand name Teflon, is a fluoropolymer renowned for its non-stick properties, chemical inertness, and high-temperature resistance. These characteristics make it an ideal choice for membrane linings in autoclaves.
   - PTFE membranes exhibit unparalleled non-stick properties, preventing the adherence of process fluids, solids, or contaminants to the membrane surface. This facilitates easy cleaning and maintenance of the autoclave, reducing downtime and improving operational efficiency.
   - PTFE membranes offer excellent chemical resistance to acids, bases, solvents, and other corrosive substances encountered in metallurgical processes. They provide reliable protection against corrosion, ensuring the longevity and integrity of the steel substrate in autoclaves.
3. **ECTFE (Ethylene Chlorotrifluoroethylene)**:
   - ECTFE is a fluoropolymer known for its combination of chemical resistance, mechanical strength, and thermal stability. It offers superior performance in aggressive chemical environments, making it suitable for membrane linings in autoclaves.
   - ECTFE membranes possess good mechanical properties, including high tensile strength, impact resistance, and dimensional stability. This ensures that the membrane maintains its integrity and functionality under mechanical stresses and pressures encountered during autoclave operation.

In summary, plastic sheets such as PVDF, PTFE, and ECTFE serve as versatile and reliable membrane linings in autoclaves, providing effective protection against corrosion, thermal degradation, and contamination. Their unique combination of properties makes them well-suited for a wide range of metallurgical processes, enhancing the durability, efficiency, and safety of autoclave operations. However, beside their brought chemical resistance, the diffusion resistance is comparably low (small molecules like water can diffuse easily through a PTFE membrane). Thus, usually a combination of an underlying coating or furanic GRP system together with a plastic sheet is used.

A “loose bond” connection (no complete bond between membrane and substrate) leads to mechanical stress within the sheets caused by the different thermal expansions. Especially at nozzles, penetrating the plastic sheet cylinder build up a potential stress point, leakages are the consequences.

FLEXIBLE VISCOELASTIC SHEET LINING

Flexible viscoelastic sheet linings, such as those made from carbon-based materials, offer unique advantages as membrane linings in autoclaves. Here's how these materials are utilized in such applications:

1. **Viscoelastic Properties**: Viscoelastic materials exhibit both viscous (flow) and elastic (recovery) behavior under stress, allowing them to deform and conform to irregular surfaces while maintaining their structural integrity. This property makes them ideal for lining autoclaves with complex geometries, as they can easily adapt to the contours of the interior surfaces without sacrificing durability or effectiveness.
2. **Chemical Resistance**: Flexible viscoelastic sheet linings are engineered to provide resistance to a wide range of chemicals, including acids, bases, solvents, and corrosive substances commonly encountered in metallurgical processes.
3. **Application**: Viscoelastic sheet linings can be applied by butting adjacent sheets together. Seams are fused together with joint stripes. The sheets are attached to the metal surface by an open flame
4. **Temperature Resistance**: Viscoelastic materials exhibit good temperature resistance, allowing them to withstand the moderate to high temperatures encountered in autoclave processes. Polyurea, for instance, can withstand temperatures ranging from sub-zero to over 100°C, making it suitable for a wide range of metallurgical applications, including both low-temperature leaching processes and high-temperature oxidation reactions.
5. **Balancing different thermal expansion factors**: Viscoelastic membranes are intended to act as an expansion joint between steel and brick and thus balancing the different thermal expansion (thermal expansion of steel usually two to three times higher than the expansion coefficient of the brick lining).

The viscoelasticity allowing the membrane to act as an expansion joint, creates also the main drawback of this kind of membrane when in operation over a longer time period. During operation of a POX autoclave or a flash vessel, the membrane is heated to an elevated temperature e.g. 80°C. This results in a tremendous softening

of the material allowing the membrane to flow. Thus an almost liquid membrane is set under pressure between an incompressible steel surface and a stiff brick lining. As long as this liquid material does not find an open gap to escape it can fulfill its purpose. But in case this “pressurized” liquid will find a crack or an open gap (e.g. at nozzles, flanges or manholes) it will be squeezed out. In this case the function as expansion joint can no longer be fulfilled and the bricklining shifts closer to the steel surface with all possible consequences for the lining integrity.

Image 6: Viscoelastic membrane at 80°C (original sheet size: 65 mm x 115 mm, thickness approx. 11 mm) Surface pressure (below a standard ceramic brick 24 x 11.5 x 6.5 cm) ≈ 0,052 bar ≈ 0,005 MPa
After 20 h, 2 days, and 8 days.

ELASTOMERIC RUBBER LINING

Rubber linings serve as effective and versatile membrane linings in autoclaves, offering excellent corrosion resistance, flexibility, and durability. Here's how rubber linings are utilized in autoclave applications:

1. **Chemical Resistance**: Rubber linings, particularly those made from synthetic elastomers such as neoprene, EPDM (Ethylene Propylene Diene Monomer), or natural rubber, provide exceptional resistance to a wide range of chemicals, including acids, bases, solvents, and corrosive substances commonly encountered in metallurgical processes. This chemical resistance makes rubber linings well-suited for protecting steel substrates against corrosion in autoclaves used for processes such as High-Pressure Acid Leaching (HPAL) or Pressure Oxidation (POX).
2. **Flexibility and Conformability**: Rubber linings are inherently flexible and elastomeric, allowing them to conform closely to the contours of autoclave interiors, including irregular surfaces, weld seams, and joints. This flexibility ensures complete coverage and protection of the steel substrate, minimizing the risk of corrosion or leakage at vulnerable points. Rubber linings can be customized to accommodate complex geometries, ensuring uniform protection throughout the autoclave.
3. **Temperature Resistance**: Rubber linings exhibit good temperature resistance, allowing them to withstand the moderate temperatures encountered in most autoclave processes. While certain rubber formulations may have temperature limitations, such as neoprene or EPDM, new developments with new cross-linking systems offer enhanced temperature resistance and can withstand higher operating temperatures (up to 150°C). This versatility allows rubber linings to be tailored to specific process requirements, ensuring compatibility with a wide range of metallurgical applications.
4. **Mechanical Properties**: Rubber linings offer excellent mechanical properties, including high tensile strength, elongation at break, and tear resistance, which are essential for withstanding mechanical stresses and pressures encountered during autoclave operation. These materials can absorb impact and vibration, reducing the risk of damage or delamination, and providing long-term durability and reliability.
5. **Ease of Maintenance**: Rubber linings require minimal maintenance and can be easily repaired or replaced as needed to address wear, damage, or degradation over time. Routine inspections and maintenance activities, such as cleaning, patching, or recoating, help to prolong the service life of the rubber lining and ensure continued protection of the steel substrate. Even other membranes (e.g. lead membranes) could be repaired by rubber.
6. **Balancing different thermal expansion factors**: Due to its elastomeric behavior, rubber linings act as expansion joint between steel and brick surface. As explained above, the expansion coefficient of steel is much higher than the coefficient of the brick lining (combination of acid resistance brick and stiff mortar). However, rubber is an elastomeric material and thus cannot flow. Due to the cross-linking,

the rubber matrix cannot move. In case of open cracks or gaps runner material cannot be squeezed out.

In summary, rubber linings offer a robust and cost-effective solution for corrosion protection in autoclaves, providing excellent chemical resistance, flexibility, temperature resistance, and mechanical properties. Their versatility, ease of application, and durability make them well-suited for a wide range of metallurgical processes, enhancing the longevity, efficiency, and safety of autoclave operations.

SUMMARY

Autoclaves and flash vessels are the key equipment in hydrometallurgical ore processing plants like High Pressure Acid Leaching (HPAL) or Pressure Oxidation (POX). In most vessels a combined lining is used to protect the steel surface against chemical and mechanical attack. This combined lining usually consist of a membrane to protect the steel against corrosion and a brick lining to protect the membrane against mechanical impact and temperature. The interference between steel, membrane and brick lining can be analysed and predicted using a Finite Element Method (FEM). The main target in lining setup is to provide an impervious seal to protect the steel against the acidic and oxidizing media. Different types of membranes are in use. Inconel, lead, GRP, plastic sheeting, viscoelastic sheeting or rubber linings are the most common alternatives. Depending on resistance, applicability, repairability, price and other factors, all types exhibit different pros and cons which should carefully investigated when planning a new plant or maintenance at existing linings.

REFERENCES

1. Shneerson Ya. M., Chugaev L. V., Pleshkov M. A. Pressure oxidation technology in gold industry. *Globus*. 2012. No. 1. pp. 54–55.
2. Fedorov V. K., Shneerson Ya. M., Afanasiev A. V., Klementiev M. V. et al. Short summary of first year of the Pokrovskiy pressure oxidation hub operation. *Tsvetnye Metally*. 2020. No. 3. pp. 43–47.
3. Zaytsev P. V., Chugaev L. V., Pleshkov M. A., Shneerson Ya. M. et al. Pressure oxidation of double refractory gold-bearing concentrates. *Proceedings of the 4th International Congress "Non-Ferrous Metals-2012"*. Krasnoyarsk, 2012. pp. 561–567.
4. Kaya S., Topkaya Y.A. High pressure acid leaching of a refractory lateritic nickel ore. *Minerals Engineerin*g, 2011, 24, 11 p. 1188-1197.
5. Gultom T., Sianipar A., High pressure acid leaching: a newly introduced technology in Indonesia, *IOP Conf.: Earth Environ. Sci.* 2020, 413, 012025.
6. Guo X., Shi W., Tian Q., Leaching behavior of metals from limonitic laterite ore by high pressure acid leaching, *Transactions of Nonfer. Metals Soc. China*, 2011, 21, 1, p. 191-195.
7. Whittington B.I., Muir D., Pressure Acid Leaching of Nickel Laterites: A Review, *Min. Proc. And Extractive Metallurgy Review*, 1999, p. 527-599.
8. Uhlendorff A., E-Auto-Batterien: Nickel aus Indonesien statt Russland*, ISE AG* April 2023
9. Rubisov D.H., Papangelakis V.G., Model-based analysis of pressure oxidation autoclave behavior during process upsets, *Hydrometallurgy*, 1995, 39, 1-3, p. 377-389.
10. Ucyldiz A., Girgin I.,High Pressure Sulphuric Acid Leaching of Laterite Nickel Ore, *Physicochem. Probl. Miner. Process*. 216, 53, 1, p.475-488.
11. Korkmaz K., Comparative Study of high temperature and atmospheric acid leaching for the extraction of Nickel and Cobalt from refractory nickel laterite ores, 2014, *Middle East Technical University*
12. Conway M.H., Gale D.C., Sulfur's Impact on the Size of Pressure Oxidation Autoclaves, 1990, *JOM*, p.19-22.
13. Ambrosia M.I., Fundamentals of Partial Pressure Oxidation of Gold Bearing Sulphide Minerals, University of Queensland, Australia, 2020.
14. Thomas K.G., Pearson M.S., Pressure Oxidation Overview, 2016, *Chapter 21 in Gold Ore Processing*, Adams M.D., Elsevier
15. Tian Q., Dong B., Gua X., Wang Q., Xu Z., Li D., Valuable metals substance flow analysis in high-pressure acid leaching process of laterites, *J.Cent.South Univ.* 2023, 30, p.1776-1786.

DETAPIPE™ - CHANGING REACTIVE METAL PIPE SYSTEMS FOR HPAL AND POX OPERATIONS

By

Edgar E. Vidal

NobelClad, U.S.A.

Presenter and Corresponding Author

Edgar E. Vidal
evidal@nobelclad.com

ABSTRACT

Availability and supply chain concerns around titanium are always in the minds of designers and end users of High-Pressure Acid Leaching (HPAL) and Pressure Oxidation (POX) circuits. Because of the extreme conditions of temperature, pressure, and acidity, titanium alloys are often selected for components of these circuits, such as the autoclave itself, valves, pipe straights and elbows. Because of the relatively thick walls needed for these pipes and elbows, the cost of these components can become an economic concern for the project. Additionally, handling, fixturing, and repairing a solid titanium pipe adds technical challenges, particularly in remote operations.

NobelClad has developed a proprietary cylindrical cladding process to produce a titanium, zirconium, or tantalum cladded surface inside carbon or stainless-steel pipes – called DetaPipe™. In combination with explosion-cladded flanges (DetaClad™), these pipe spools and elbows utilize significantly less amount of titanium alloys, where these alloys become just a corrosion barrier and not part of the pressure boundary. Because of the unique characteristics of the cladding process, many different titanium alloys can be used, including those that have increased corrosion, erosion, and ignition resistance, which tend to be significantly more expensive when compared to pure titanium. Examples of combinations produced, along with mechanical, thermal, and fatigue characterizations performed, are presented.

Keywords: Clad pipes, explosive cladding, titanium, zirconium, tantalum, HPAL, POX, nickel extraction, refractory gold, acid leaching, autoclaves

DETAPIPE™ - CHANGING REACTIVE METAL PIPE SYSTEMS FOR HPAL AND POX OPERATIONS

Edgar E. Vidal

evidal@nobelclad.com

NobelClad – VP of Marketing & Business Development

Colorado School of Mines – Affiliate Faculty in Extractive Metallurgy

Abstract

Availability and supply chain concerns around titanium are always in the minds of designers and end users of High-Pressure Acid Leaching (HPAL) and Pressure Oxidation (POX) circuits. Because of the extreme conditions of temperature, pressure and acidity, titanium alloys are often selected for components of these circuits such as the autoclave itself, valves, pipe straights and elbows. Because of the relatively thick walls needed for these pipes and elbows, the cost of these components can become an economic concern for the project. Additionally, handling, fixturing, repairing a solid titanium pipe adds technical challenges particularly in remote operations. NobelClad has developed a proprietary cylindrical cladding process to produce a titanium, zirconium or tantalum cladded surface on the inside of carbon or stainless-steel pipes – called DetaPipe™. In combination with explosion cladded flanges (DetaClad™), these pipe spools and elbows utilize significantly less amount of titanium alloys, where these alloys become just a corrosion barrier and not part of the pressure boundary. Because of the unique characteristics of the cladding process, many different titanium alloys can be used, including those that have increased corrosion, erosion and ignition resistance, which tend to be significantly more expensive when compared to pure titanium. Examples of combinations produced, along with mechanical, thermal and fatigue characterizations performed are presented.

- Keywords: Clad pipes, explosive cladding, titanium, zirconium, tantalum, HPAL, POX, nickel extraction, refractory gold, acid leaching, autoclaves

Present at ALTA2024

Dr. Edgar E. Vidal

Vice President of Marketing and Business Development
Affiliate Faculty of The Kroll Institute for Extractive Metallurgy – Colorado School of Mines

Specializes in developing technologies and business opportunities related to selection and development of materials and processes. Professor of Extractive Metallurgy

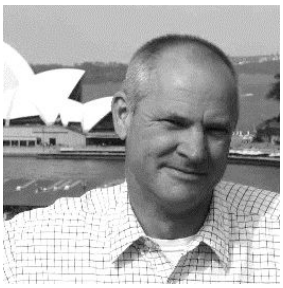

Alex Van Leeuwarden

Managing Director at International Engineering Solutions Pty Ltd
Agent for NobelClad – Australia

More than 40 years' experience in industry from an engineering and maintenance perspective for: mechanical equipment, thermal applications (pyrometallurgical), corrosion resistant applications (hydrometallurgical), abrasion resistant applications, for existing operations or on newly constructed plants.

NobelClad is Global

- 200 employees
- 13 languages

Pennsylvania, United States

Rhineland-Palatinate, Germany

Use of Titanium Piping and Components

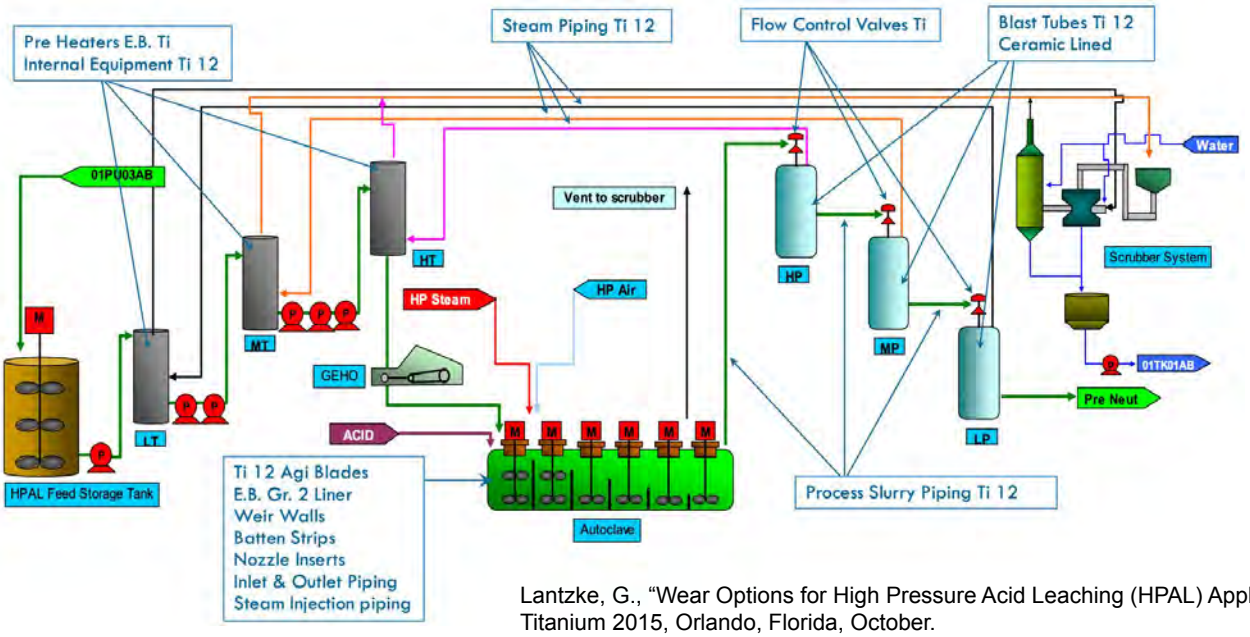

Lantzke, G., "Wear Options for High Pressure Acid Leaching (HPAL) Applications," Titanium 2015, Orlando, Florida, October.

Use of Titanium Piping

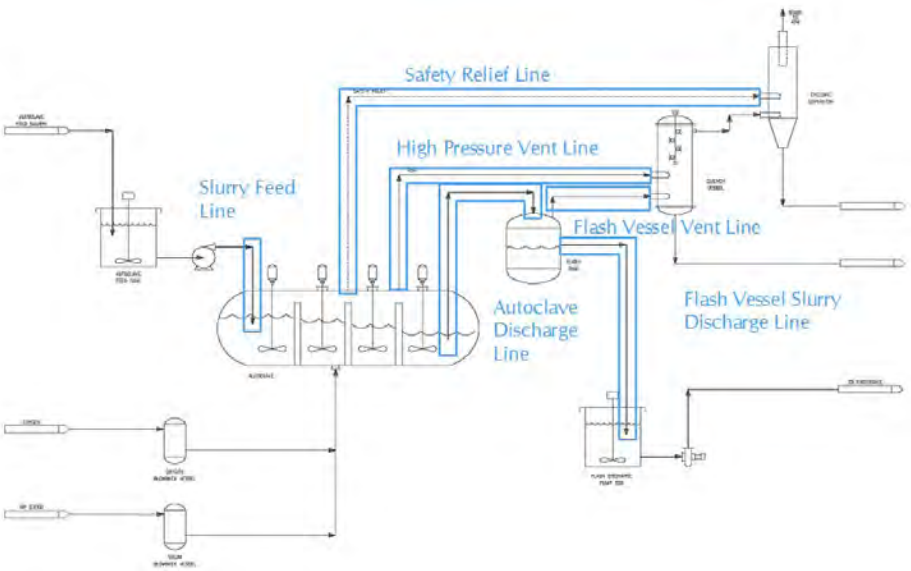

Mercer, L.N., Clappison, J., "Design and Fabrication of Titanium Piping for Pressure Hydrometallurgy Service," Titanium 2010, Orlando, Florida, October.

- Pressure Class 300#
  - Slurry feed lines
  - High pressure vent line
  - Autoclave discharge line
  - Safety relief line
- Pressure Class 150#
  - Flash vessel vent and slurry discharge lines
  - Slurry sampling lines
- Suitable for HPAL and POX

Pressure and Temperature Ratings for Titanium Grades 2, 2H and 12

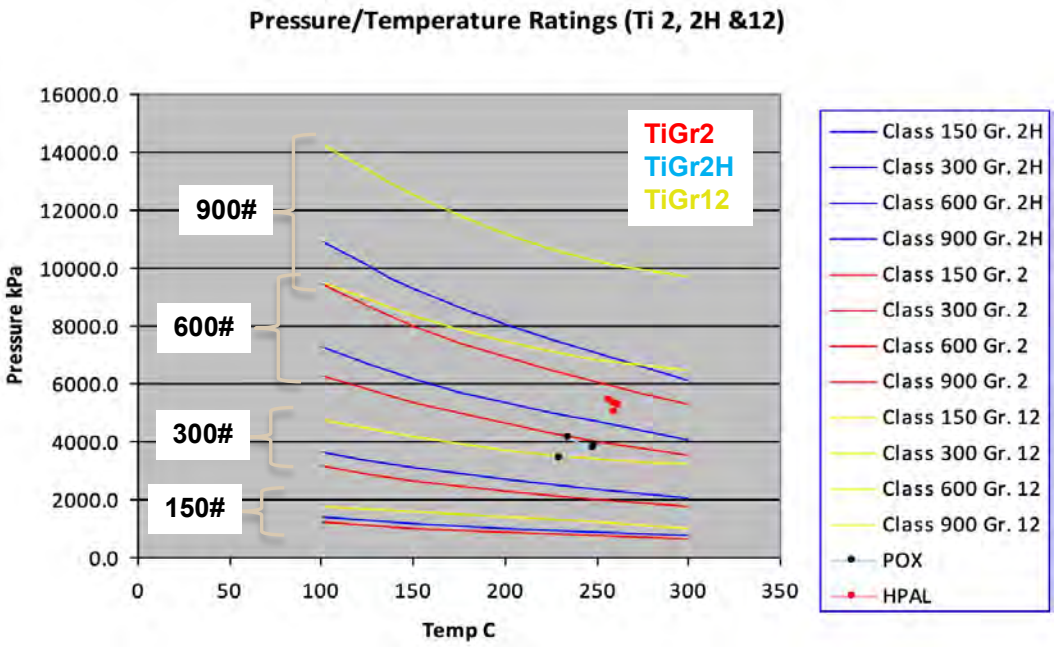

- Based on ASME B16.5 Appendix A equations
- Pressure/Temperature conditions of HPAL/POX are shown (red and black dots)
- Three case studies based on using:
  - TiGr2: #600, #900
  - TiGr12 #300, #600
  - Selection is to comply with ASME B16.34 for valves

Mercer, L.N., Clappison, J., "Design and Fabrication of Titanium Piping for Pressure Hydrometallurgy Service," Titanium 2010, Orlando, Florida, October.

Limitations of Working with Solid Titanium Pipes

Table 2 – Case Study Design Conditions

	Case Study 1 POX		Case Study 2 POX		Case Study 3 HPAL	
Material	Ti Grade 2H	Ti Grade 12	Ti Grade 2H	Ti Grade 12	Ti Grade 2H	Ti Grade 12
Flange Rating	600#	300#	600#	600#	900#	600#
Corrosion Allowance mm (inch)	3 (0.1)		3 (0.1)		3 (0.1)	
Design Temperature °C (°F)	230 (446)		249 (480)		260 (500)	
Design Pressure kPa(g) (psig)	3392 (491)		3875 (562)		5000 (725)	

Table 4A – Maximum Wall Thickness for Welded 3D Bends

Max Thickness for 3D bend – Welded Pipe		
Pipe Diameter mm (inch)	Ti Grade 2/2H	Ti Grade 12
50 (2)	sch 80	sch 40
100 (4) -300 (12)	sch 120	sch 80

Table 4B – Maximum Wall Thickness for Seamless 3D Bends

Max Thickness for 3D bend - Seamless Pipe		
Pipe Diameter mm (inch)	Ti Grade 2/2H	Ti Grade 12
50 (2) -300 (12)	sch 160	sch 160

- The valve ratings override the design criteria for the pipe flanges
- Ti stubs with ASTM A150 carbon steel lap joint flanges are utilized to reduce cost
  - However, the pressure/temperature rating of titanium still rules since it is lower than carbon steel
- The actual titanium wall thickness is not based on the flanges, but the actual pressure/temperature of the process
- Ti pipe thickness is limited by its fabricability into 3D bends

Mercer, L.N., Clappison, J., "Design and Fabrication of Titanium Piping for Pressure Hydrometallurgy Service," Titanium 2010, Orlando, Florida, October.

There is a solution: DetaPipe™ Titanium or Zirconium or Tantalum

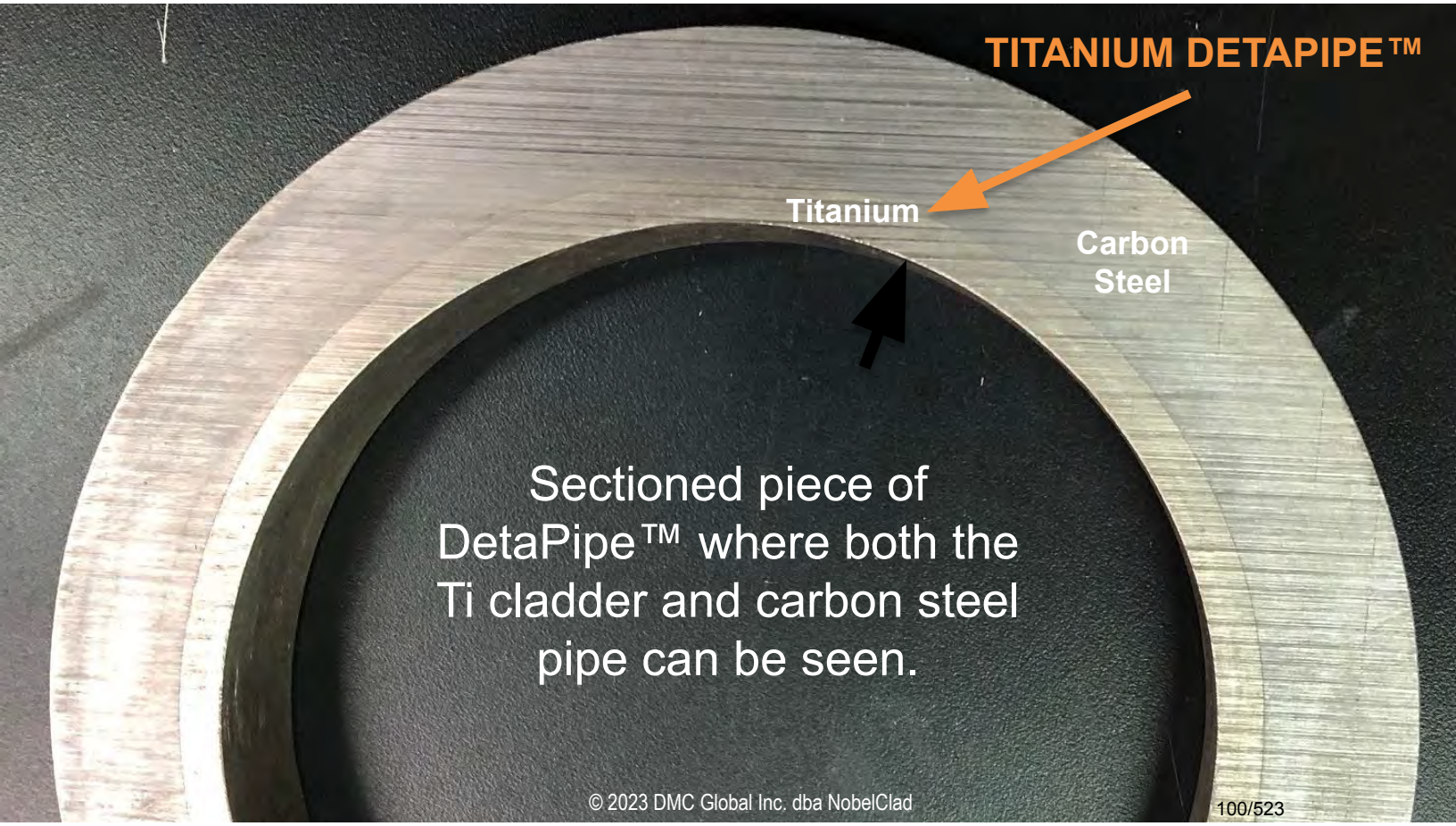

Sectioned piece of DetaPipe™ where both the Ti cladder and carbon steel pipe can be seen.

What is Being overcome with DetaPipe™

- Rather than a pipe completely made of titanium, we only use the minimum corrosion allowance thickness of titanium since it is a cladder (e.g. 3-mm)
- The pipe thickness is still designed for the the pressure/temperature of the process, but now, there is no issue with the pressure/temperature rating of titanium being lower than carbon steel
- The maximum thickness of walls for making a 3D bend is not an issue anymore since the pipe it self is carbon steel
- ASME B16.5 and B31.3 still apply, but much easier to implement since it is carbon steel.
- External pipe maintenance and fixturing is simple using carbon steel compared to titanium
- DetaPipe™ can be made using indifferently with seam-welded or seamless titanium

NobelClad has performed extensive thermomechanical Tests to ensure the reliability of the product

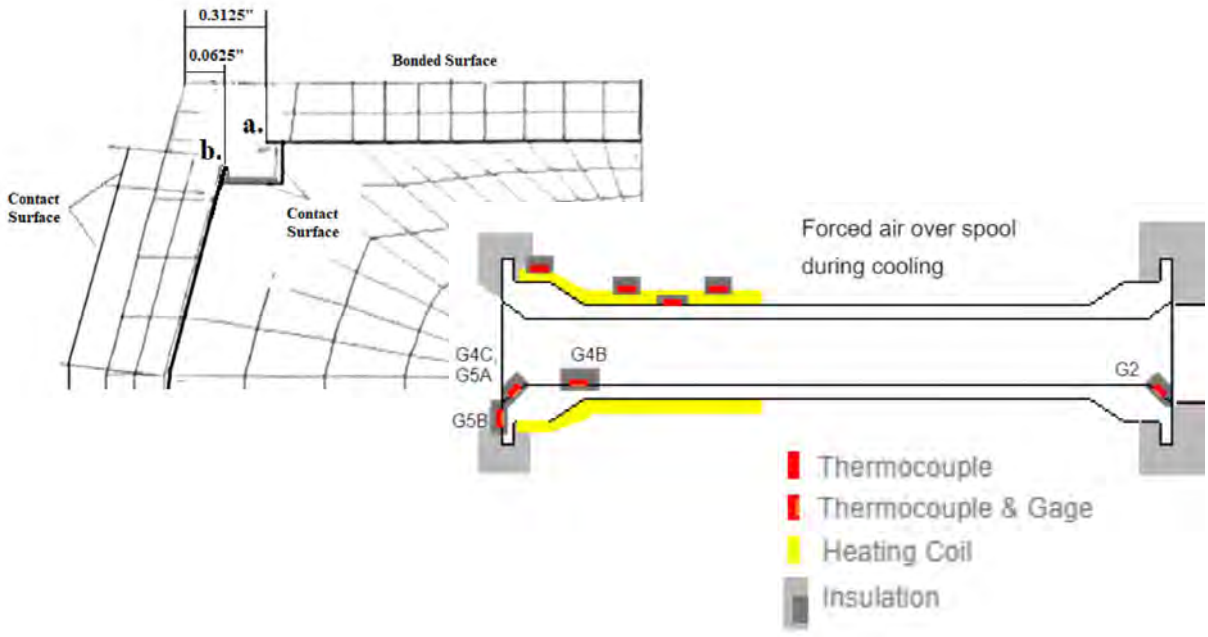

Markl / Hinnant Load Frame for Bending Fatigue Tests

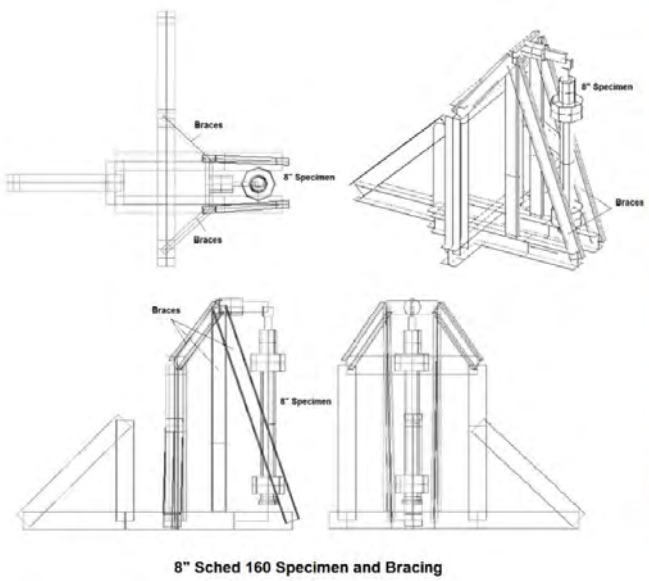

8" Sched 160 Specimen and Bracing

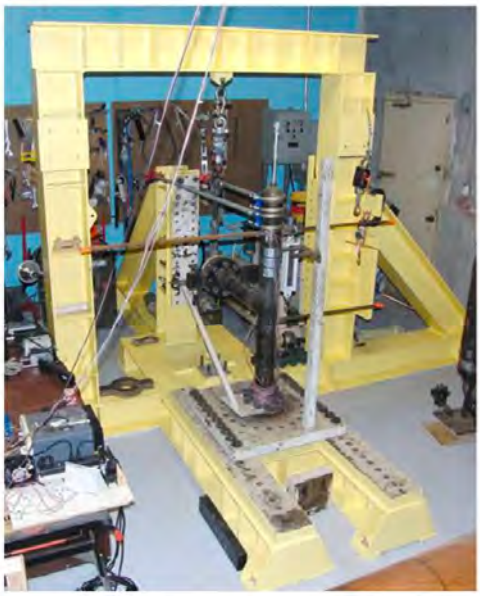

Phased Array UT Analysis of the Flange Weld – 8” 1500# Pipe

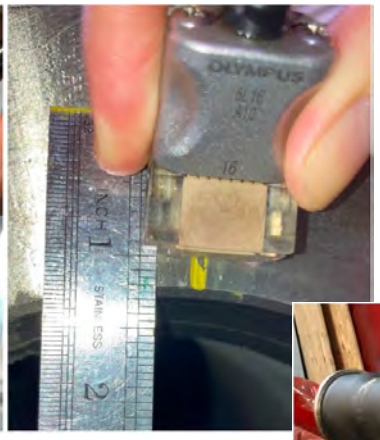

DetaPipe Under Thermal Cycling to 200C and 250 bar – Checked Every ~100 cycles

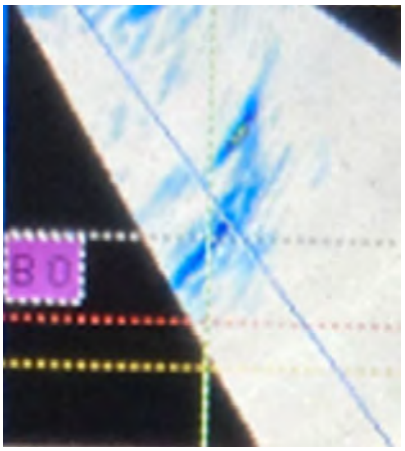

Reference flaw location at 0° and 0 cycles

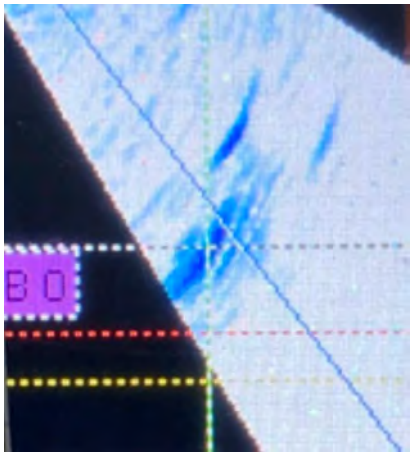

Reference flaw location at 0° and 183 cycles

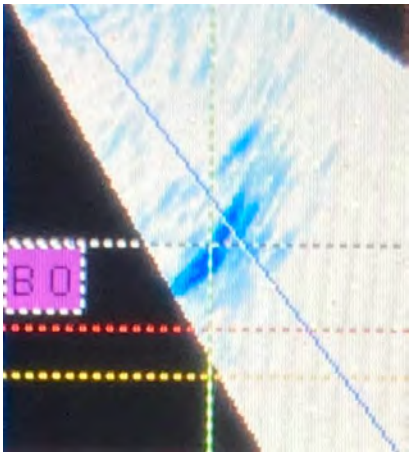

Reference flaw location at 0° and 1602 cycles

DetaPipe™ Pipe Spool Evaluation

- FEA & Cycle Fatigue Failure Analysis
  - Thermal cycling > 200°C and > 250 Bar
  - 1600+ cycles no cracks
- Exceeds performance of B31.3 for solid titanium
- Can it withstand thermal and pressure cycling?
  - 1600+ cycles
- PT of ID & Surface of Flange face welds
- Thermal cycling at pressure, temperature and bending moment

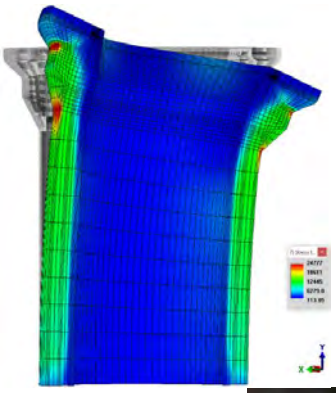

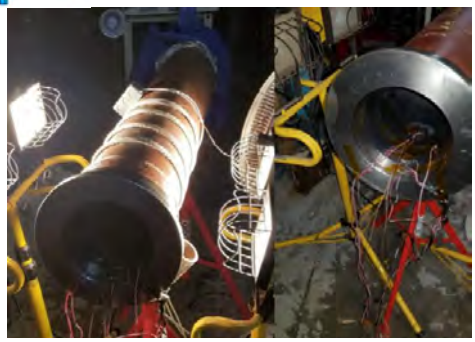

DetaPipe™ Elbow – R&D product advancement

1st trial elbow assembly 1.5D radius

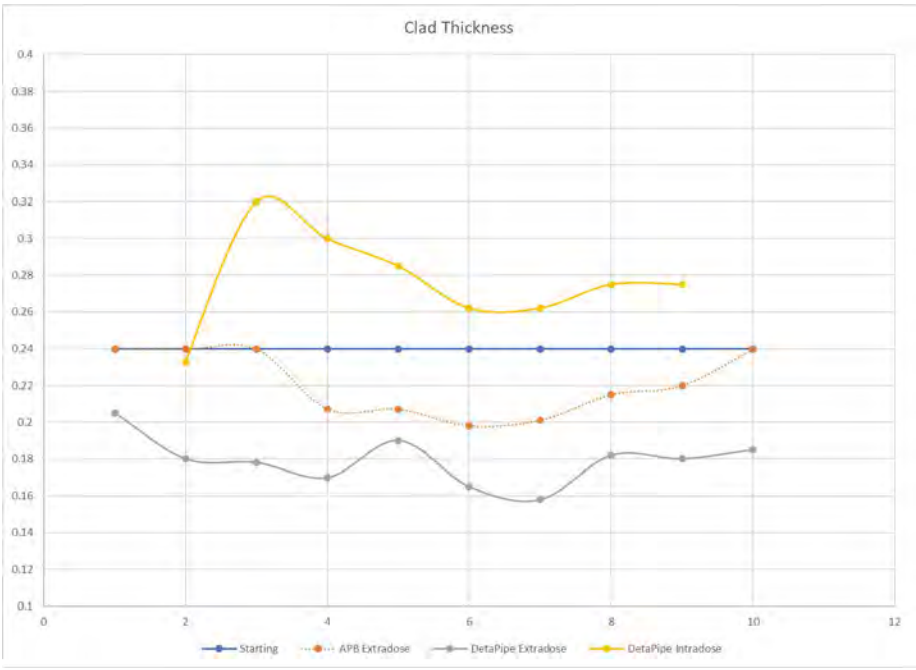

DetaPipe™ Elbow – R&D product advancement

2nd trial elbow

- 16” NPS, Sch 40 LR Elbow
- 14” NPS Ti-Gr.2, Sch 40 LR Elbow with Ti-Gr.2 pipe

Example of 10D DetaPipe™ elbow pipe spool with Grayloc® hubs

DetaPipe™ Tee development

DetaPipe™ Product Testing

- Liquid penetrant testing (PT) of welds
- Hydrostatic test
- Dimensional inspection
- Radiographic inspection (RT)
- Certification package includes:
  - Raw material certifications, PT, RT and partial data (where applicable) of the pressure welds and hydro test of the spool prior to cladding
- DetaPipe™ is made to NobelClad's DETA-221 internal specification for cladding

NobelClad Brings Value Added to your Solution

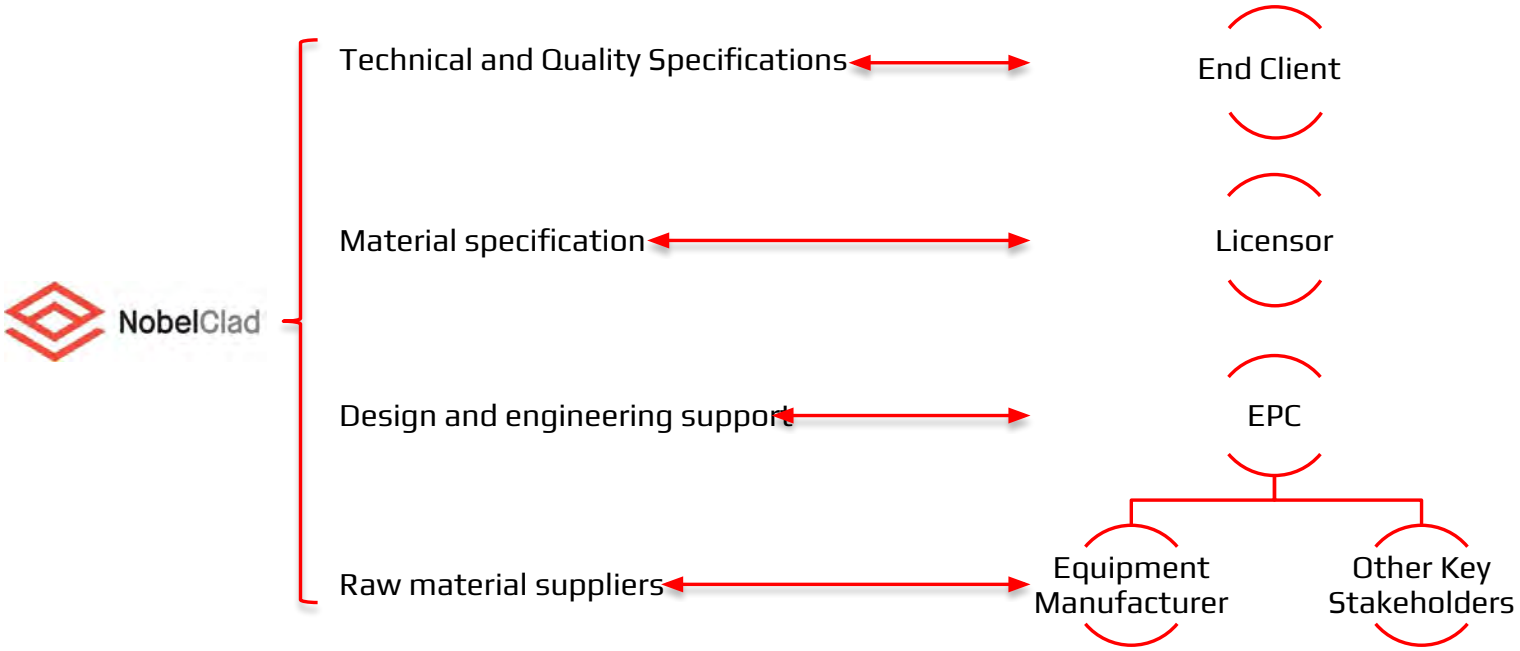

IMPLEMENTATION OF SELECTIVE OXIDATION AT LIHIR GOLD OPERATIONS PAPUA NEW GUINEA

Presenting Author

Johm O'Callaghan
Consultant

stardustantares@gmail.com

ABSTRACT

On 10 December 2014 Lihir Gold Operations changed from full oxidation of gold containing auriferous sulfides to selective oxidation.

Most of the gold at Lihir is contained in high-arsenic pyrite or arsenian pyrite and this pyrite is the target for preferential or selective oxidation. The installed and fixed cryogenic oxygen supply capacity is used to oxidise arsenian pyrite in preference to low-grade "barren" pyrite thereby maximising gold production.

This paper briefly describes the history of the Lihir process plant and the implementation of the selective oxidation process using the new operating strategy.

Specific lime, cyanide, and other reagent usage in the downstream Carbon-in-Leach gold recovery circuit has remained largely unchanged.

Other deposits of similar mineralogy may benefit from a selective oxidation approach.

Keywords: *arsenian pyrite oxidation*

INTRODUCTION

The Lihir Gold operation is located on the eastern side of Niolam Island in the New Ireland Province of Papua New Guinea (PNG), within the collapsed caldera of an ancient volcano. As Niolam Island is the principal island of the Lihir Group, it is generally referred to as Lihir Island see Figure *1* below. An aerial view of Lihir in Figure *2* shows the treatment plant in the foreground with the open-cut mine in the background.

Gold was discovered in 1982 and was followed by a major exploration program between Kennecott and Niugni Mining Limited. The first drilling occurred in 1983. Over 340 holes and 83,000m of drilling and associated metallurgical test work supported the final bankable Feasibility Study which was completed in 1992. Gold recovery using whole ore pressure oxidation was the selected treatment process. Construction of the mine, process plant and all related infrastructure commenced in 1995 and the plant was commissioned in May 1997.

In 1988, the RTZ Corporation (now Rio Tinto) acquired Kennecott from BP Minerals America, thereby taking over as the Lihir Joint Venture partner with Niugini Mining Limited. Lihir Gold Limited (LGL) was incorporated in Papua New Guinea in June 1995.

Newcrest Mining Limited (Newcrest) purchased Lihir Gold Limited following the merger of Newcrest

and LGL in August 2010 and subsequently completed a major plant upgrade (Million Ounce Plant Upgrade – MOPU Project) that was already underway at the time. Additional crushing, grinding, pressure oxidation and carbon in leach (CIL) capacity as well as new support infrastructure was part of the upgrade. On 6 November 2023 Newmont Corporation completed the acquisition of Newcrest.

Considerable reserves remain at Lihir, and long mine life is expected.

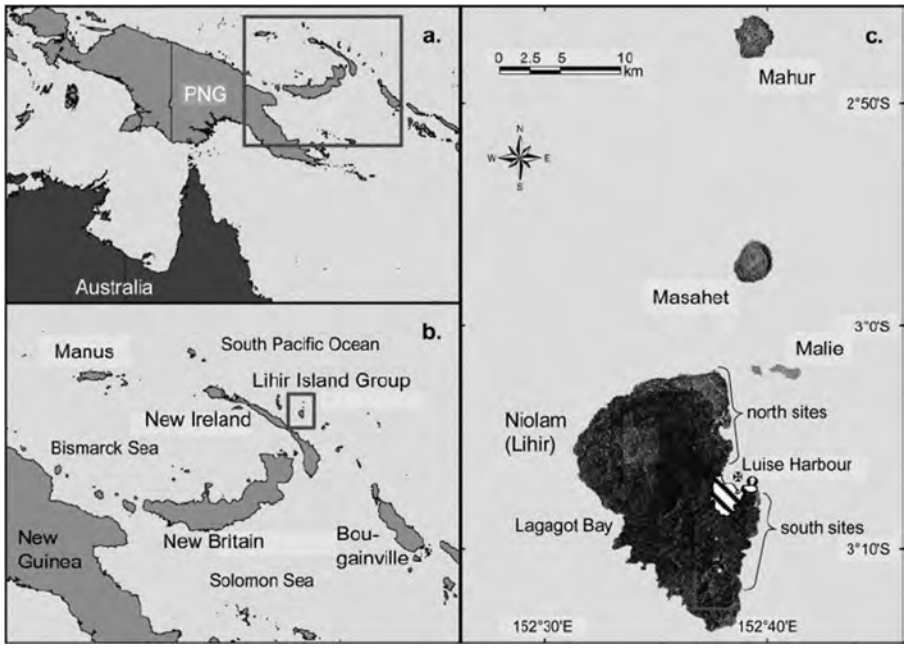

Figure 1 - Location of Lihir Island


Figure 2 - Aerial View of the Lihir Gold Mine

Sherritt Research Centre conducted the original Lihir pressure oxidation test work as a pre-treatment process ahead of gold recovery via cyanidation. There are several references documenting the process development for Lihir (Ketcham et al, Collins et al and Ketcham and O'Reilly). A key feature of the original process design was high sulfur oxidation for ores containing high gold and sulfur grades. The strategy for the original owners and then LGL for the MOPU project was to target the high gold and high sulfur "boiling zone" areas of the orebody. Initially a

declining cut-off grade strategy was adopted which led to stockpiling of medium to low grade ores containing low Au:S ratio ores (mainly Argillics). Gardner et al describes the different ore types and domains at Lihir. (Note Au:S ratio = gold g/t and sulfur %w/w and all references to sulfur therein refers to sulfide sulfur).

Soon after purchase and faced with low gold prices, Newcrest took the value-based choice to adopt a lower gold grade processing feed cut-over strategy. Large scale stockpiling of medium grade ores was discontinued, and treatment of previously stockpiled "medium grade" ores commenced. The large Kapit Flat stockpile generated by the previous owners would be treated rather than relocated off the final major pit of the orebody - Kapit. In addition, future ROM grade ores from Kapit would be treated rather than stockpiled.

The new mining strategy required treatment of lower Au:S ratio and lower sulfur (sS) grade ores to maximise gold production.

On 10 December 2014 Lihir Gold Operations changed the plant operating strategy from "full oxidation" of gold containing auriferous sulfides to selective oxidation. As most of the gold at Lihir is contained in arsenian pyrite this is the target for *preferential* or selective oxidation. This allows increased throughput of lower Au:S ratio ores as only part of the sulfur needed to be oxidised. The installed and fixed cryogenic oxygen supply capacity is used to always oxidise arsenian pyrite in preference to low-grade "blocky" pyrite thereby maximising gold production.

THE LIHIR PROCESS

At a pre-treatment process technology level, the Lihir process has not fundamentally changed over time. Pressure oxidation of gold containing auriferous pyrite remains the pre-treatment process prior to final gold recovery by Carbon-In-Leach (CIL).

The original overall block flowsheet for the Lihir process is shown in Figure *3* below (re-drawn from Collins et al). Chloride washing of autoclave feed slurry was practiced.

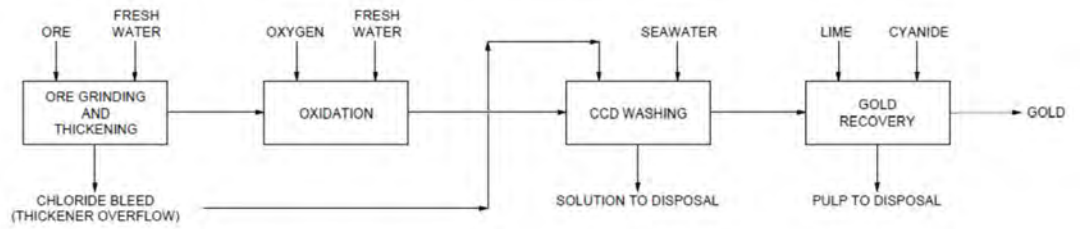

Figure 3 – Original Overall Lihir Flowsheet (Collins et al)

To accommodate declining sulfur grades over time, equipment additions, modifications, and enhancements were made. The decline in sulfur and gold grades over time (especially in the first 10 years of operation) is shown in the attached graphs (Figure 4 and Figure 5)

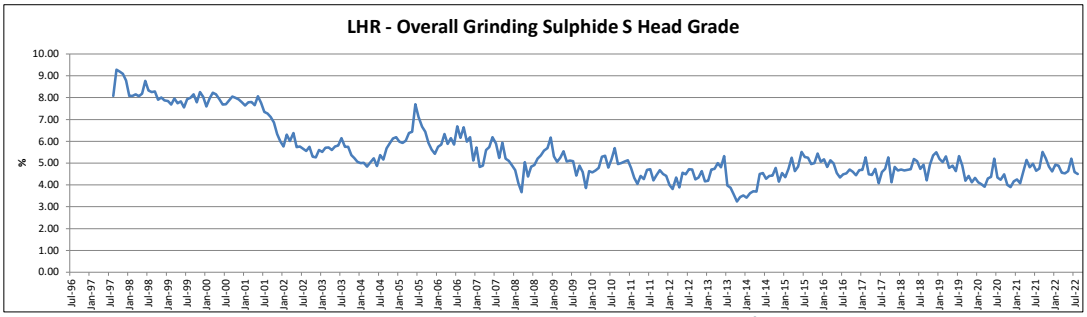

Figure 4 - Lihir Mill Feed Sulfide Sulfur, %S

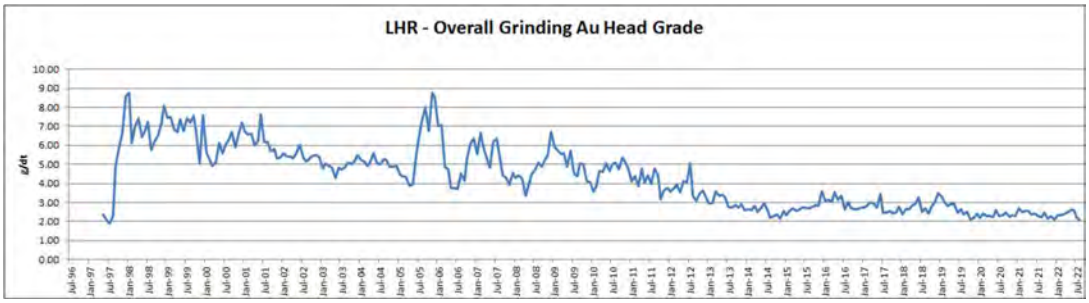

Figure 5 – Lihir Mill Feed Gold, g/t

With treatment of all ore types including those with lower grades of gold and sulfur the Au:S ratio has reduced to around 0.5 which is close to the Mineral Resource average for Lihir. Initially the Au:S ratio was higher at 0.8 to 1 (or higher) in line with the original declining cut-off grade strategy of targeting high gold and sulfur ores. This trend of Au:S ratio in mill feed is shown below in Figure 6.

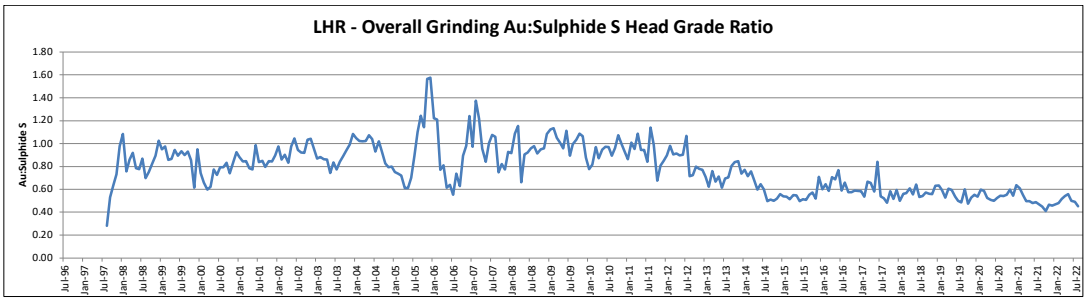

Figure 6 - Lihir Mill Feed Au (g/t):S (%)

Prior to 2015 with a fixed amount of oxygen available and in “full” oxidation mode then preference was given to high Au:S ratio ores, demanding proportionally higher mining rates to supply these ores.

Hence it was clear that “full oxidation” of low Au:S ratio ores (especially treatment of lower grade stockpiled ores) required a different approach as gold production would clearly be reduced with a fixed oxygen plant capacity.

After extensive mineralogy and gold deportment investigations (Gardner et al) it was verified that gold deports preferentially to micro-crystalline arsenian pyrite. Importantly this high-gold fraction is very reactive and oxidises rapidly in the autoclaves. The high-gold microcrystalline pyrite fraction occurs in all ore types at Lihir in varying amounts hence all ore types display some response to

selective oxidation. Note that the low-grade “blocky” pyrite always oxidises to some extent however due to the slow kinetics it is preferentially present in autoclave discharge.

In early August 2014 a selective oxidation plant trial was completed which showed preferential oxidation of gold containing pyrite with high gold CIL recoveries after only ~ 70% oxidation. On 10 December 2014 the plant operating strategy was changed from ‘full” oxidation to selective oxidation. The gold within microcrystalline pyrite became the primary target for selective oxidation. The installed and fixed cryogenic oxygen supply capacity is now used to always oxidise arsenian pyrite in preference to low-grade “barren” pyrite thereby maximising gold production.

A minimum sulfide oxidation of 50% was set initially however some ores require higher oxidation and some less. In typical day-to-day operation the % oxidation varies as throughput and/or feed sulfur grade varies. This is discussed more later.

Brief History of the Lihir Flowsheet

The flowsheet as installed in 1997 is shown below in Figure 7 . The main features were: -

Single stage crusher with a single SAB milling circuit
Fresh water ex Londolovit River
Three autoclaves with single stage flash and seawater flash steam quench
CCD wash for acid and soluble sulphates removal
1 x NCA (CIL) for final gold recovery
Whole ore feed only; no flotation and no pre-heating

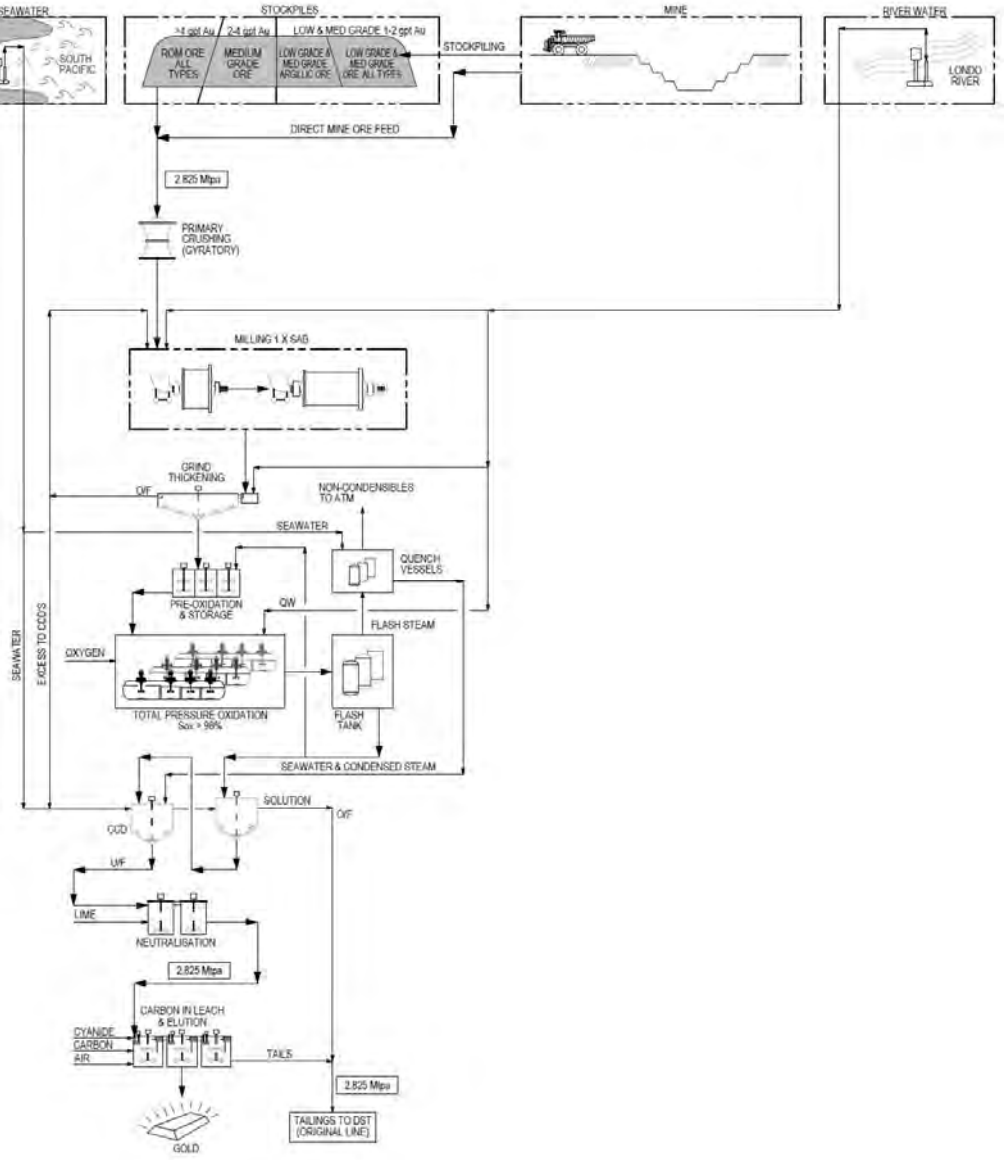

Figure 7 - Lihir Original Flowsheet circa 1997

In circa 2003, three direct contact heat exchangers and a pebble crushing circuit were installed. This allowed increased throughput with declining sulfur grades while ensuring the autoclaves were not restricted by autoclave temperature (McDonald).

After extensive piloting a flotation circuit was added in addition to a second grinding circuit in circa 2006 (the original flotation pilot plant has only recently been demolished). A dedicated concentrate thickener was also installed. The flotation plant was used on an as needs basis.

In 2010-2011 a major plant upgrade commenced associated with the addition of Kapit Ore Reserves. Known as the Million Ounce Plant Upgrade (MOPU) project the key equipment installed included:-

- Two jaw crushers and one additional grinding circuit SABC (HGO2)
- Two additional pre-oxidation tanks
- One additional autoclave roughly twice the size of the original three (AC4).
- Two additional flash/quench circuits for AC4
- Installation of a common Oxidised Slurry Tank system for all autoclave discharges
- Additional CIL capacity – NCA2
- New tailings disposal line
- Additional oxygen plant
- Other infrastructure

The design of the new MOPU autoclave is well described in Hewitt et al. Figure 8 shows flotation added to the overall block flowsheet.

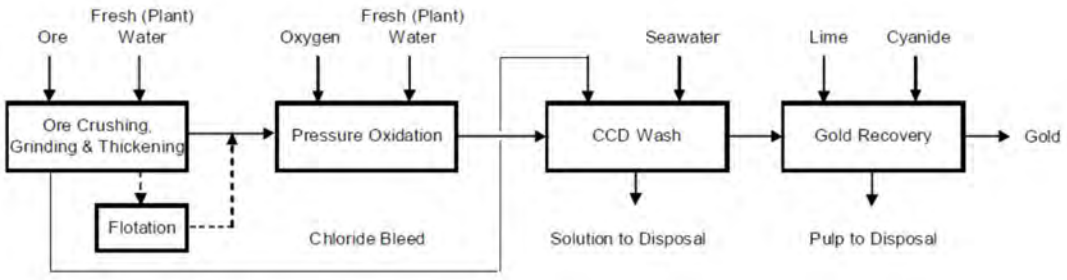

Figure 8 - Lihir Flowsheet with Flotation (after Hewitt et al)

The flowsheet with the MOPU equipment added is shown below in Figure 9

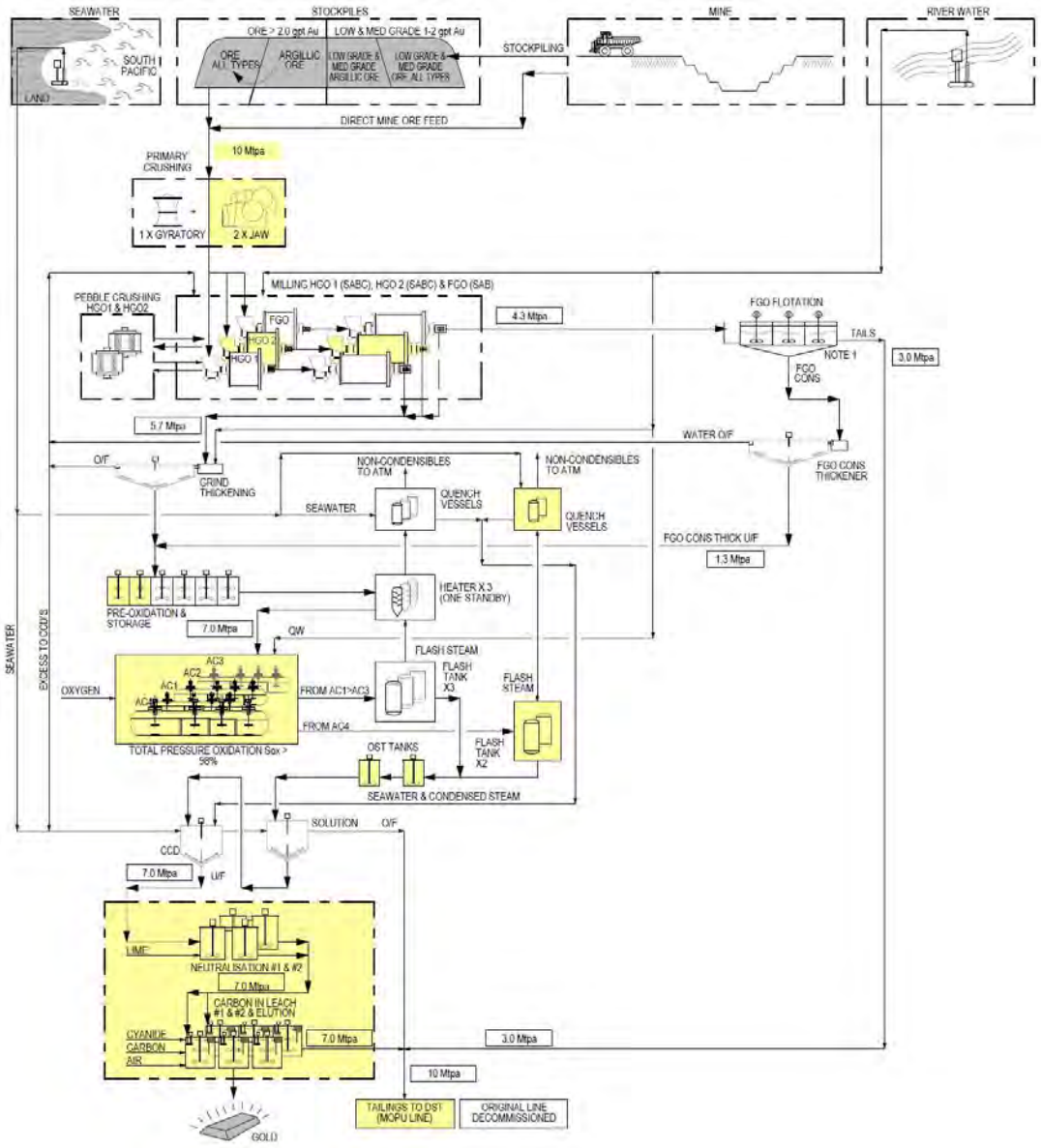

Figure 9 - Lihir Flowsheet post MOPU Upgrade

As the MOPU expansion project was nearing completion Lihir was acquired by Newcrest. To accommodate the new mining strategy requiring treatment of lower sulfur ores Newcrest installed a second and larger flotation circuit, considering recent processing lessons from its Cadia Mine.

From 1997 until the end of 2014 the pressure oxidation process was operated in nominally “full oxidation” mode.

With the change to selective oxidation of lower sulfur ores (and reduced Au:S ratio ores) on 10 December 2014 increased mill throughput was possible thereby maximising gold production.

As there was some latent grinding capacity available at the time this allowed an immediate increase in throughput. Excess mill capacity (above autoclave capacity) is sent to flotation which is now essentially a mass rejection process. Flotation became an integral part of the Lihir process rather than being used ad-hoc to upgrade low sulfur ores.

Sulfur oxidation is allowed to vary between 50 and 100% (subject to additional controls described further below) and hence autoclave sulfur throughput has increased substantially. While a slight reduction in CIL recovery has occurred, this is vastly offset by increased throughput.

Some limited recovery of gold from flotation tailings does occur. When floating partially oxidised stockpiled ores fine oxidised solids are recovered from flotation tailings using cyclones and the fines are sent to the CIL circuits directly. If fine sulfides are to be recovered these can be sent directly to the autoclave for oxidation.

The process plant flowsheet as it stands today is shown below in Figure 10.

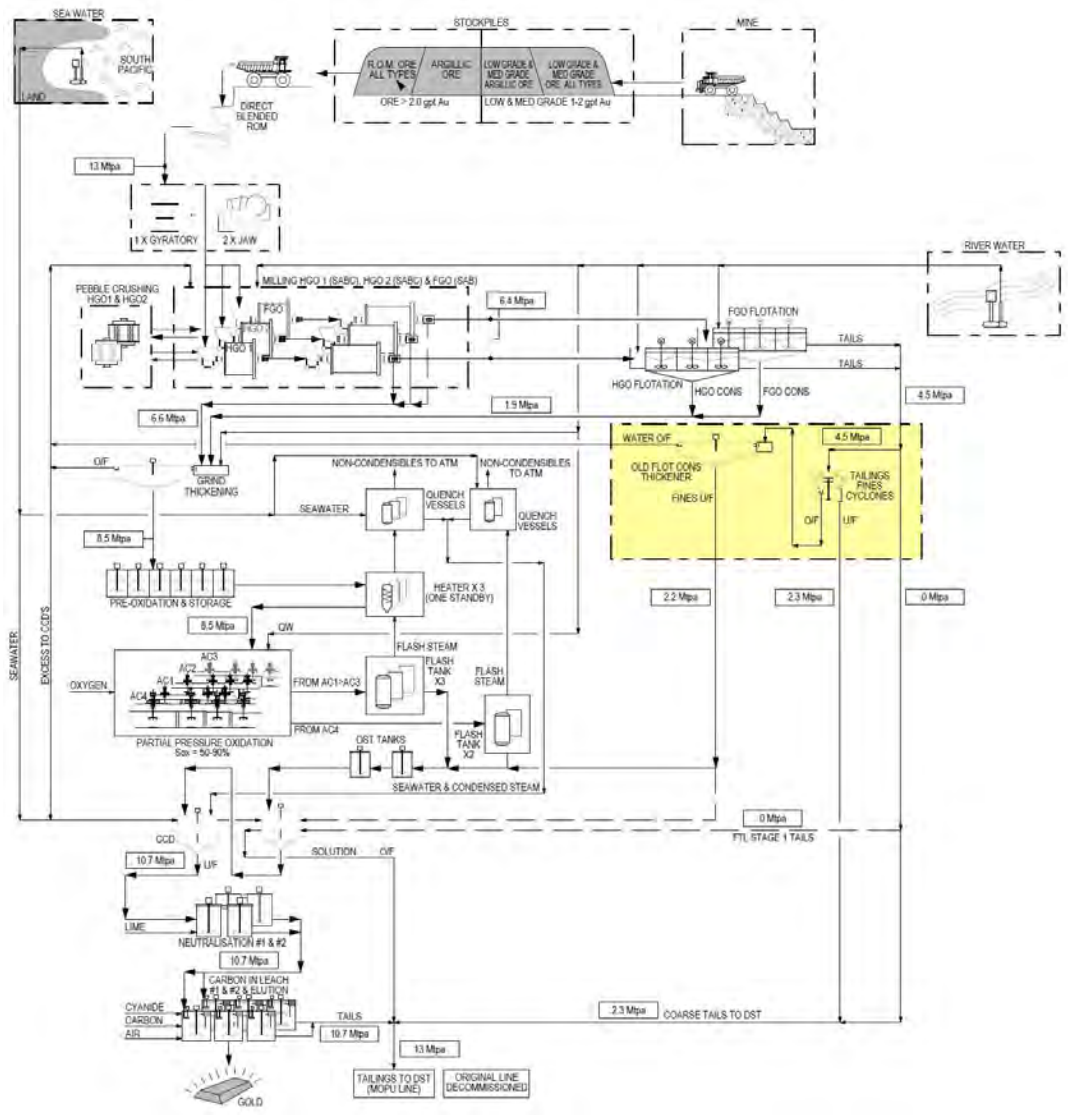

Figure 10 - Lihir Flowsheet Current

Selective Oxidation at Lihir

On 10 December 2014 at roughly 3 pm in the afternoon the plant operation changed from nominally "full" oxidation to selective oxidation. Latent milling capacity was immediately used and over the next several years mill throughputs were progressively de-bottlenecked, and the milling circuits modernised.

Originally the descriptor "partial oxidation" was used for the new process and while technically correct – part of the sulfide sulfur is being oxidised - the term selective oxidation is more accurate since the plant is operated to ensure that liberated high-gold microcrystalline pyrite is oxidised preferentially to low-gold (blocky pyrite). Gardner et al describes the different pyrite species and some examples of the typical gold content of each of the pyrite types is shown in Figure 11 below.

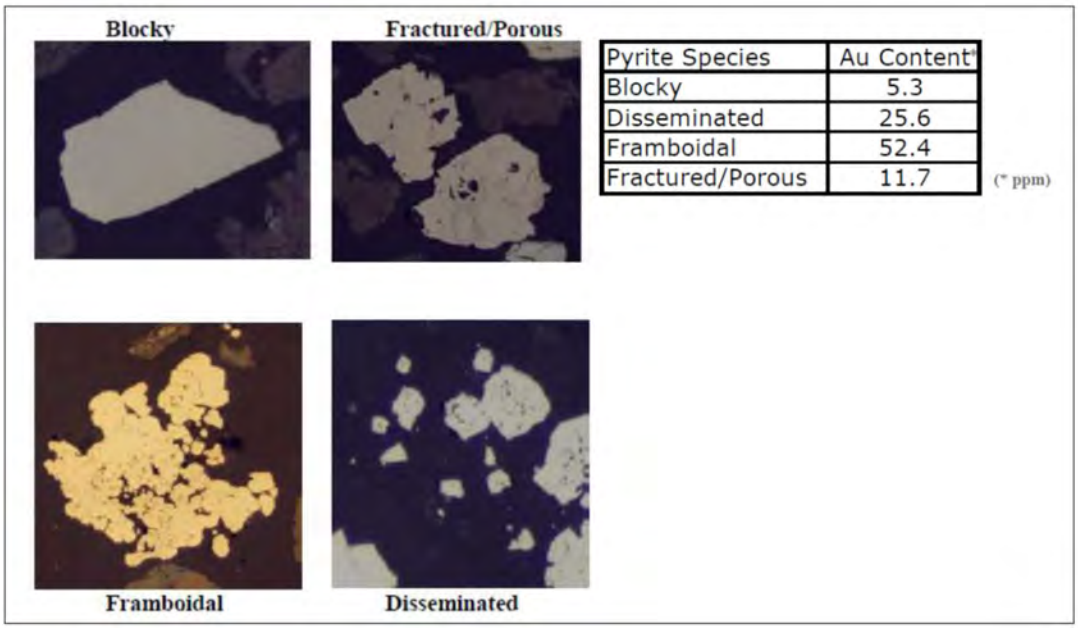

Pyrite Species	Au Content*
Blocky	5.3
Disseminated	25.6
Framboidal	52.4
Fractured/Porous	11.7

(* ppm)

Figure 11 - Pyrite Speciation at Lihir (after Gardner et al)

The proportion of blocky and reactive pyrite varies throughout the orebody and operation down to 40 and even 30% oxidation is possible without significant gold loss. However, for future higher Au:S ratio ores it is likely that increased oxidation will be required. This is subject to on-going testing and analysis.

The optimum operating point for Lihir is to keep increasing sulfur throughput to the autoclaves such that all the available oxygen is used to oxidise the reactive microcrystalline arsenian pyrite only. At this point Lihir would be producing at the maximum gold production rate possible. However, for several practical reasons, operation occurs at just above the minimum ORP (oxidation reduction potential) or oxidation level. Of course, some blocky pyrite is always oxidised but at a much slower rate. Essentially inherent differences in pyrite oxidation kinetics are being exploited at Lihir.

Controlling the process plant to maximise gold production using selective oxidation is referred to as the Lihir Operating Strategy (LOS) and is described below.

Lihir Operating Strategy (LOS)

The operating strategy at Lihir using selective oxidation is very different to the original design of "full oxidation" of high gold grade ores (and high Au:S ores). With a fixed oxygen supply capacity (currently 140 tph) the objective is to operate the autoclave facility such that all high gold arsenian pyrite is oxidised preferentially while minimising oxidation of blocky pyrite. This is achieved by maintaining high autoclave sulfur throughputs until either of the following conditions is met.

- Minimum total sulfur oxidised is 50% (can be lowered with Plant Manager approval)

  OR

- Minimum autoclave discharge slurry solution potential is 360 mV (ref Ag-AgCl, saturated)

Together these limits are described as the Lihir Chemistry Limit (LCL) and the objective is to always operate at the LCL.

Shown below in Figure 12 and Figure 13 are some typical daily trends for ORP and % oxidation. In this instance operation was close to the LCL. Compliance with the LOS is monitored continuously, and the process controlled to ensure gold production rate is always maximised.

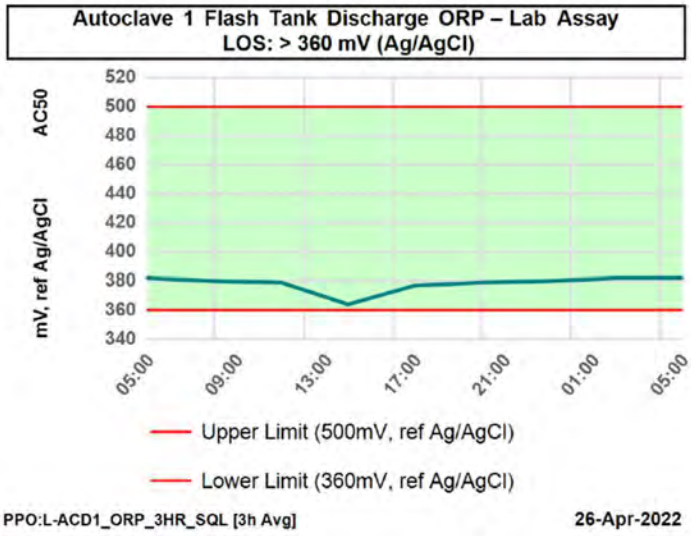

Figure 12 - Example ORP Trend - Autoclave 1

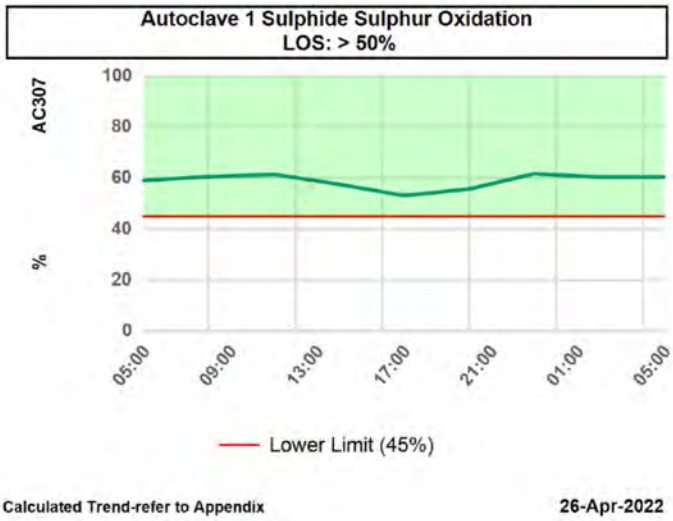

Figure 13 - Example Oxidation Trend - Autoclave 1

Other key aspects of the LOS are: -

Some ore blending should be practiced (not currently implemented)
Mill throughput is always maximised (with excess capacity sent to flotation)

- All available oxygen is used.
- Autoclave mass throughput is maximised (to maximise overall recovery by minimising the fraction of ore sent to flotation)
- Minimum and maximum autoclave feed sulfur grades are 5 and 12% (% w/w)
- The mill grind size maximum is P80 of 210 µm (see discussion later)
- Maximum oxygen utilisation is always targeted.

In theory autoclave mass throughput could continue to be increased while operating in selective oxidation mode. However, other constraints need to be satisfied including (but not limited to) autoclave feed pump capacity and final downstream carbon-in-leach (CIL) gold recovery circuit capacity. The most fundamental limit is that the autoclave energy balance must be satisfied, and the autoclave needs to be kept at the required operating temperature. For autoclave feed slurry densities typically encountered at Lihir roughly 4 to 4.5% sulfide sulfur must be oxidised to achieve this. Mass throughput is controlled to achieve minimum “front-end” temperatures. The LOS nominates a minimum of 5% sulfur grade in autoclave feed.

With the flotation circuits, milling of lower sulfur grade ores is possible and excess milling capacity over autoclave capacity is sent to flotation. High throughputs through the flotation circuits are possible and, often “full flotation” is achieved with only concentrate sent to the autoclaves. Gangue is rejected, and sulfur (and gold) grades are increased. However, on average the autoclaves receive a mixture of whole ore and flotation concentrate.

Importantly the split of milled ore to flotation is controlled by the level in the buffer storage (pre-oxidation) tanks between the grinding and autoclave areas. As level increases in the pre-oxidation tanks more ore is sent to flotation and more concentrate is treated in the autoclaves. When level drops, less ore is directed to flotation and effectively more “whole ore” is treated in the autoclaves.

The overall flowsheet showing LOS operation is shown in Figure 14 below.

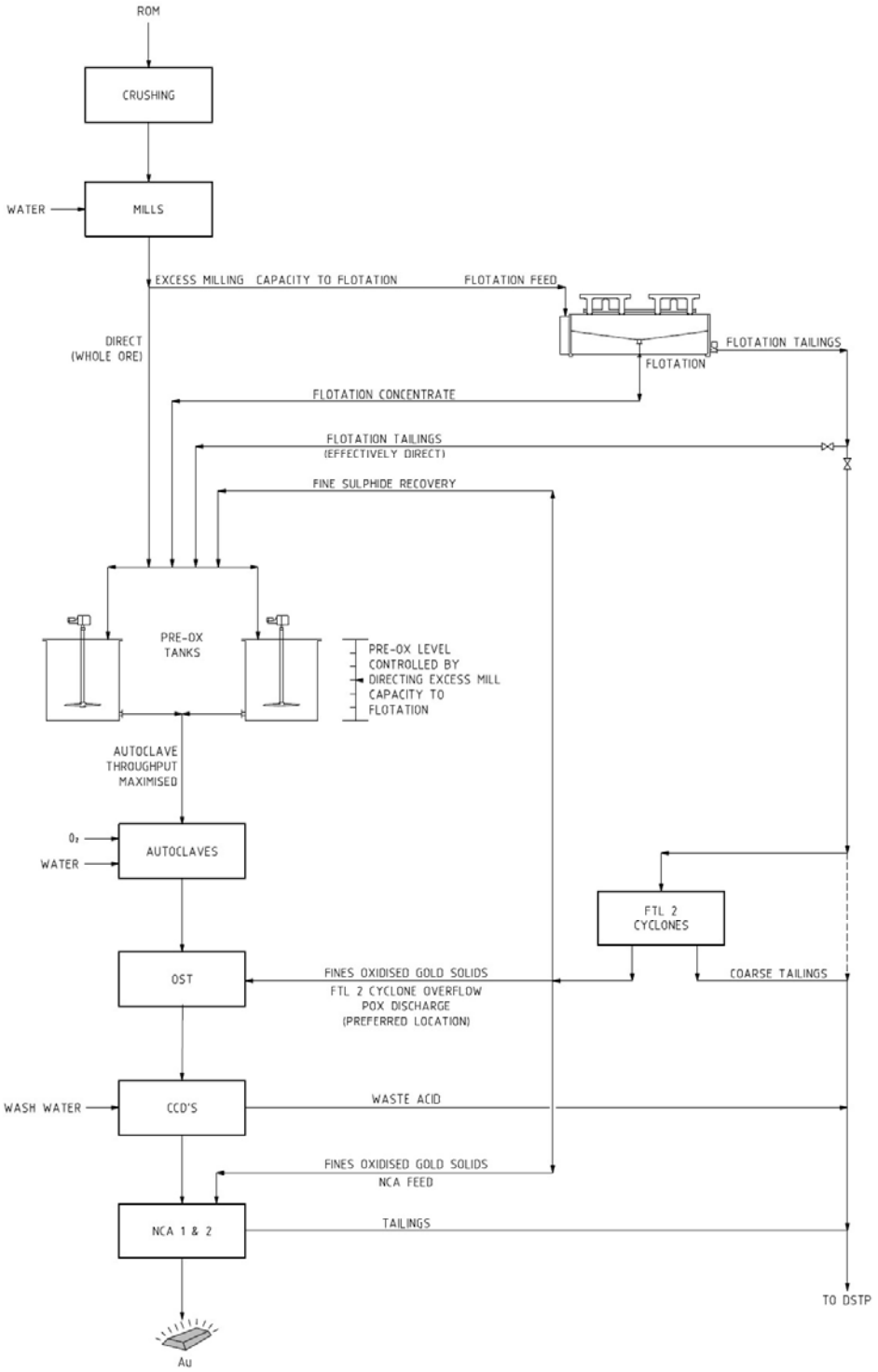

Figure 14 - Lihir Flowsheet showing LOS Operation

The four POX autoclaves at Lihir are horizontal pressure vessels with individually agitated compartments each with oxygen injection (the last compartment oxygen is now isolated). Cold water addition is used to control temperatures in individual compartments if and as needed. Cold feed slurry is introduced at the feed end of the autoclave ("front end") and slurry cascades over compartment walls until exiting under pressure from the last compartment. Feed slurry can be partially heated (to a maximum of 95 ^{o}C), however due to the nature of the reactor configuration there is almost always a gradient in the temperature profile and the front-end compartments are typically operated approximately 5^{o}C lower than the target autoclave temperature (of 210 ^{o}C).

The LOS is an example of a self-correcting process. If "front-end" temperatures drop, then throughput is reduced. At a fixed mill throughput more ore is sent to flotation and the mix of whole ore and flotation concentrate changes and autoclave feed sulfur increases. "Front-end" temperatures increase as additional reactive microcrystalline pyrite is oxidised in the first few compartments with a higher oxygen utilisation (there is also a higher total concentration of sulfur as well). Oxygen utilisation is a strong function of feed sulfur grade at Lihir.

In theory, higher autoclave throughput is possible if operation closer to true autothermal operation could be achieved. Over the last eight years internal autoclave modifications like compartment wall removal and feed splitting between the first and third agitators have been made allowing higher mass throughputs at lower % sulfur oxidised and lower autoclave feed sulfur grade.

Lihir Operating Performance – Before and After Introduction of Selective Oxidation

In the following figures, Lihir performance before and after the change to selective oxidation is shown and described.

Grinding and Flotation

Total mill throughput rate (tonnes/operating hour) is shown in Figure 15. The increase with the second and third mill installation in 2006-07 and 2012 is clearly seen. From early 2015 to 2020 progressive mill de-bottlenecking work was completed. Higher throughput rates of lower Au:S ores and lower % sulfur ores can now be treated by selective oxidation with excess mill capacity over autoclave capacity directed to flotation (see Figure 14).

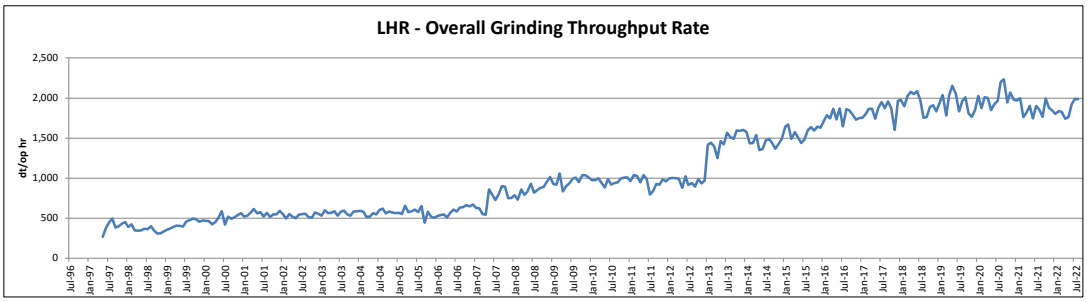

Figure 15 - Lihir Total Mill Throughput t/op.h

As installed mill power has not increased the average grind size has subsequently increased see Figure 16 below. The increase in average grind size has been partially offset by softer stockpile ores (Argillics mainly) being treated. The LOS allows grind size to vary up to a maximum of P80 of 210 µm beyond which mainly hydraulic issues with coarse particles start to occur in several parts of the plant. There is no grind size target at Lihir except to grind as fine as possible with the installed power. While some reduction in flotation and POX/CIL recovery occurs with coarser grinds the increased throughput and gold production vastly outweighs the incremental loss. Contributing to the relatively minor gold loss with grind size is likely preferential grinding of softer

microcrystalline pyrites, although this requires further study. Note that some grind size information is missing in the trend below.

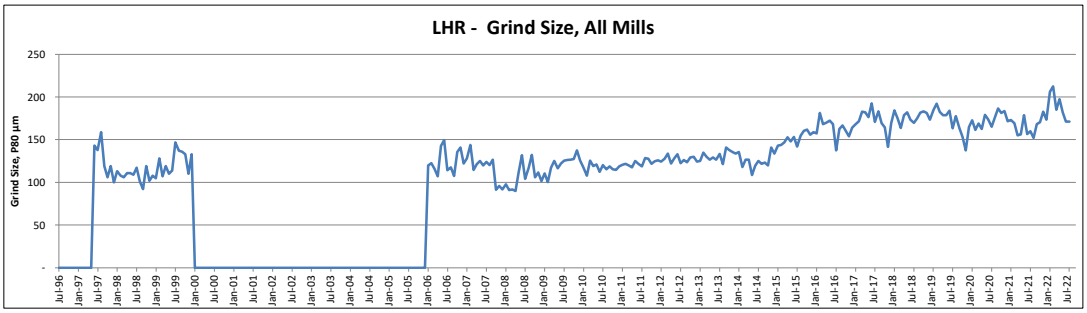

Figure 16 - Lihir Milling Circuit Grind Size, micron

Gold recovery in flotation is shown below in Figure 17 (note that recovery of sulfur is typically 2-5% higher). Flotation recovery is impacted by a combination of poor floating ores, oxidised stockpiled ores, high viscosities due to a high proportion of fines (mainly Argillics) and presence of smectites and a coarser grind. However, even with reduced recovery increased overall mill throughput using flotation for mass rejection leads to additional gold production at a lower unit cost ($US/oz). Note: there was no flotation at Lihir prior to approximately January 2007.

Work continues with optimisation of the flotation circuits at Lihir to minimise gold loss.

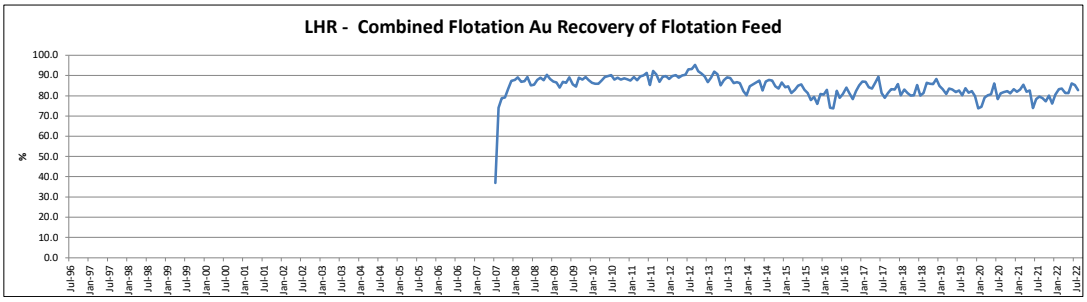

Figure 17 - Lihir Flotation Circuit Recovery

Pressure Oxidation (POX)

The autoclave feed sulfur mass flow in dry tonnes sulfur/month is shown below in Figure 18. The increase in sulfur mass throughput from 2015 is clear. From 2019 there was increased treatment of difficult stockpile ores with lower sulfur grades. Throughput through mills and autoclaves was impacted by smectite clays and excessive fines from Kapit Flat stockpile (mainly Argillic) ores. High and variable viscosity impacted milling rates and oxygen utilisation within the autoclaves.

However, as the operation moves into fresh ore from the third major orebody at Lihir (the Kapit orebody) then autoclave feed sulfur throughput (and hence gold production) is expected to increase.

Treatment of the residual Kapit Flat stockpile overlying the Kapit pit, is now essentially complete. While Argillic ores from the top of the Kapit orebody are to be treated, it is expected that fresh ore viscosity impacts will be lower in the near term.

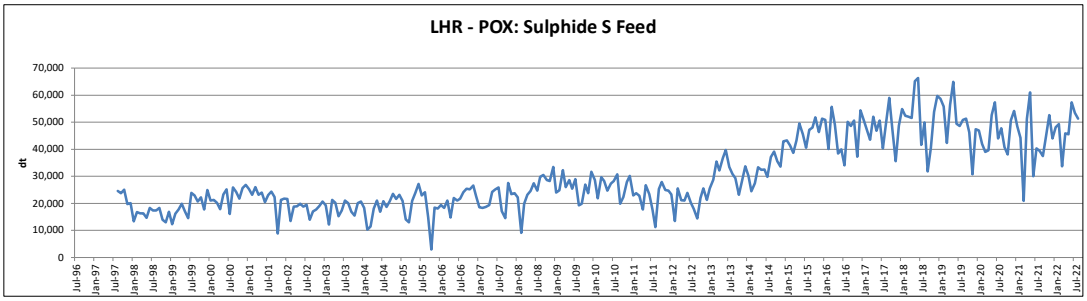

Figure 18 - Autoclave Feed Sulfide Sulfur Throughput

Autoclave availability Figure 19 also impacted sulfur mass throughput with erratic performance particularly evident during 2019-2021 (planned shutdowns are included in this trend).

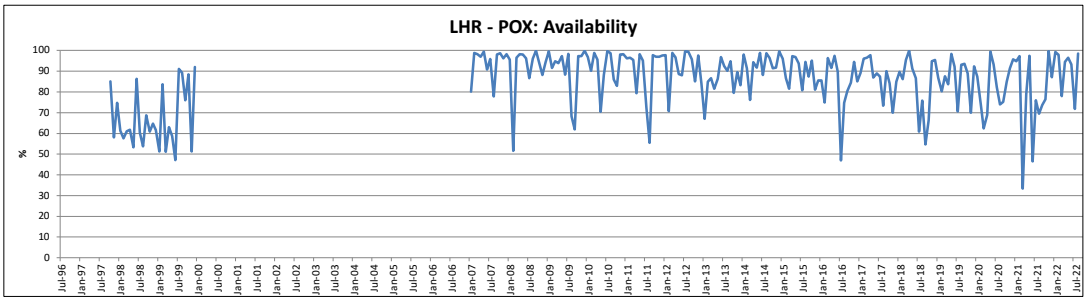

Figure 19 - Lihir POX Availability

Autoclave feed gold grade (g/dt) and sulfur grade (%) is shown below in Figure 20 and Figure 21.

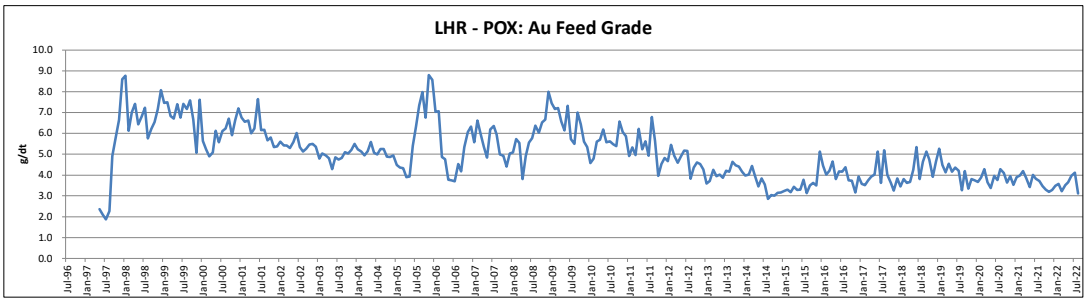

Figure 20 - Lihir Autoclave Feed Gold Grade, g/t

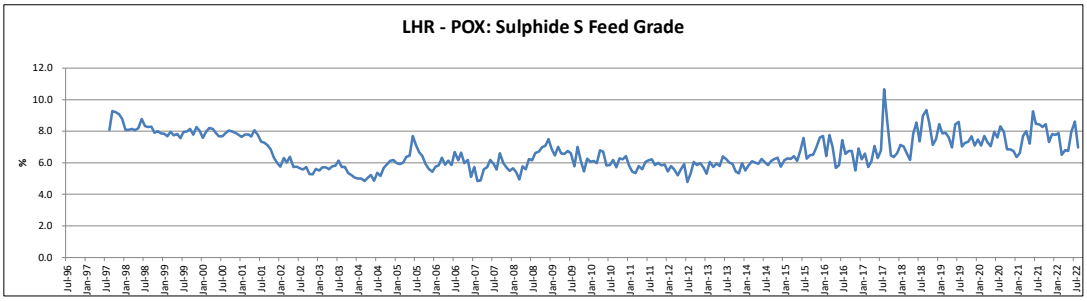

Figure 21 - Lihir Autoclave Feed Sulfide Sulfur Grade, %

The Au:S ratio in autoclave feed is shown below in Figure 22. Generally reflecting the mill feed Au:S ratios.

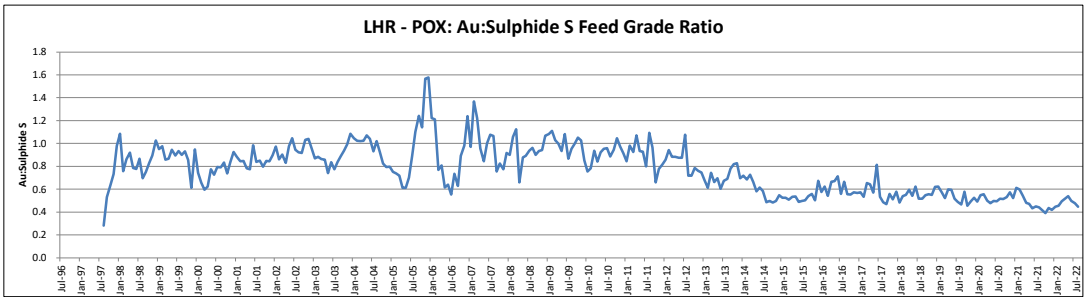

Figure 22 - Lihir Autoclave Feed Au:sS Ratio

POX sulfur oxidation is shown below in Figure 23. Interestingly and importantly some "partial oxidation" was practiced as early as 2006. Operators at the time empirically noticed that oxidation could be relaxed by increasing the amount of sulfur treated without a significant reduction in CIL gold recovery. During this period of operation, the autoclave discharge % sulfide sulfur (sS) was targeted at a maximum allowable value of around 1.0 - 1.3%. With the current LOS this is allowed to be much higher– see Figure 24.

The reduction in % oxidation from around Aug-Sept 2014 was due to selective oxidation plant trials and testing. Then finally on 10 December 2014 the operation formally switched to selective oxidation.

There is no oxidation target at Lihir, and oxidation extent is allowed to vary. The oxidation at any point in time is an outcome of the mine sulfur grade and the availability (and throughput) of mills, autoclaves, and oxygen plants. For a fixed mill throughput and mine sulfur grade with an autoclave off-line then the total amount of oxygen that can be added in the POX circuit is lower and hence the % oxidation can be lower. Conversely, for a fixed autoclave throughput and oxygen capacity and fixed mine sulfur grade then if a mill is offline the autoclaves can operate at a higher % oxidation.

While oxidation and autoclave feed sulfur grade can vary over the short term (often just a few hours) the oxygen flow to the autoclaves is fixed and the roughly same mass of sulfur is being burnt. Autoclave temperatures remain relatively steady. Depending on mine feed and plant equipment availability then oxidation may typically vary from 50% to 80%.

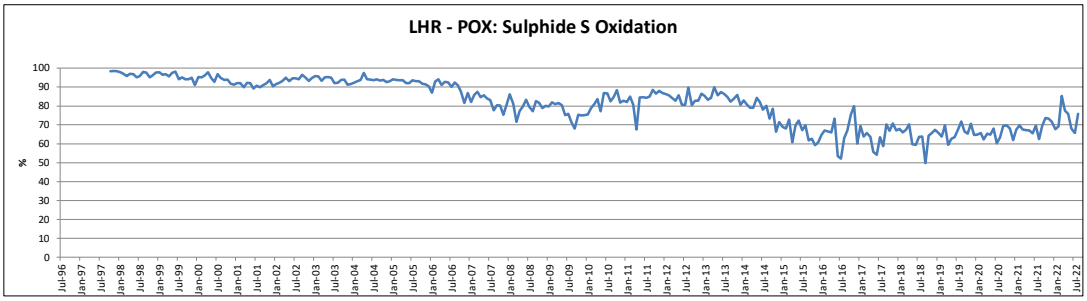

Figure 23 - Lihir Autoclave Sulfide Sulfur Oxidation

The impact of the LOS is more clearly seen in Figure 24 below where % sulfur in autoclave discharge slurry is shown. A value of 2.5-3% sulfur in autoclave discharge is now typical. While there is increased gold in autoclave discharge the autoclave feed sulfur and gold sulfur grades must increase since a minimum of 4 - 4.5% sulfur must be oxidised to maintain reaction temperature.

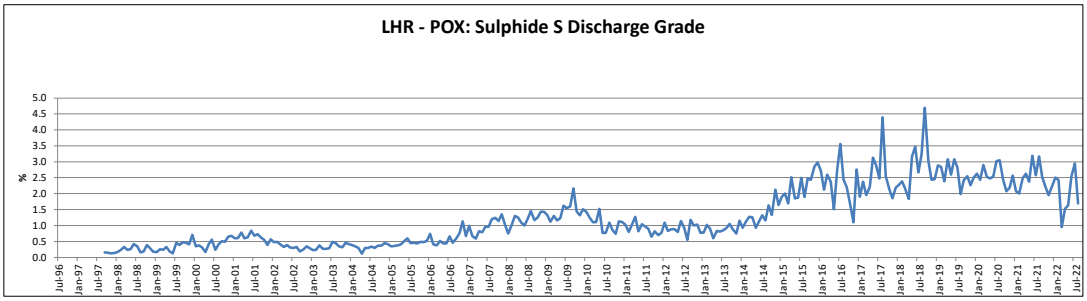

Figure 24 - Autoclave Discharge Solids, % Sulfide Sulfur

The autoclave oxygen:sulfur ratio is shown in Figure 25. The stoichiometric ratio for the oxidation of pyrite is 1.87 t oxygen/t sulfur. As clearly seen, operation well below this value (down to 1.2) has occurred since the introduction of selective oxidation as only part of the total sulfur is being oxidised. Note: some operational data is missing.

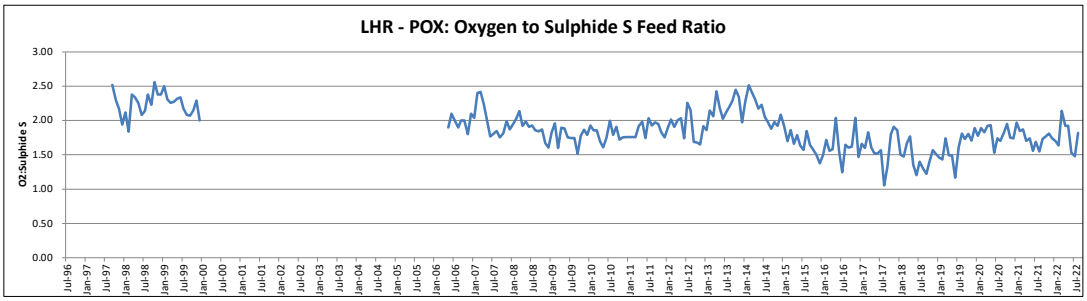

Figure 25 - Autoclave Oxygen : Sulfide Sulfur Ratio

Gold Recovery

Many controls are in place to ensure that all the high gold arsenian pyrite is burnt. One Key Performance Indicator (KPI) that is monitored daily is the gold in CIL solids to CIL feed % sulfur ratio. See Figure 26. Typically, this value is 0.10 - 0.2. Values >> 0.25 may indicate issues within the cyanide leach process itself or the presence of significant non-sulfide gangue containing gold like silicates or carbonates.

Note: NCA refers to Neutralisation, Cyanidation and Absorption. NCA uses CIL technology. A significant amount of neutralisation of autoclave discharge solids is required at Lihir.

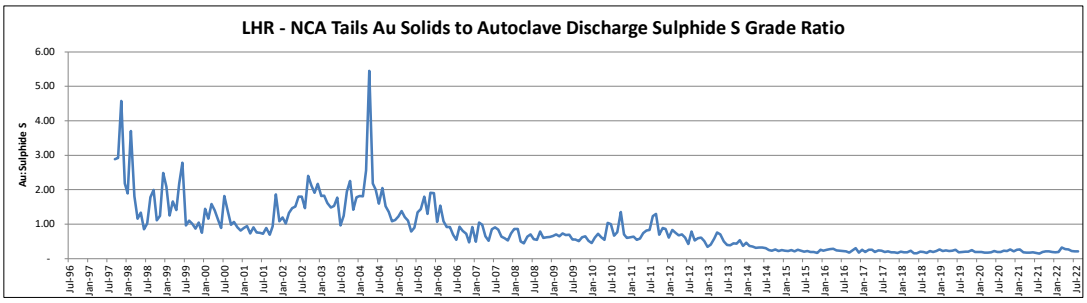

Figure 26 - Lihir NCA (CIL) Au:S Ratio

Interestingly neither CIL terminal gold grade nor overall extraction have changed significantly since 2015 despite reduced oxidation in the autoclaves. See Figure 27 and Figure 28 below.

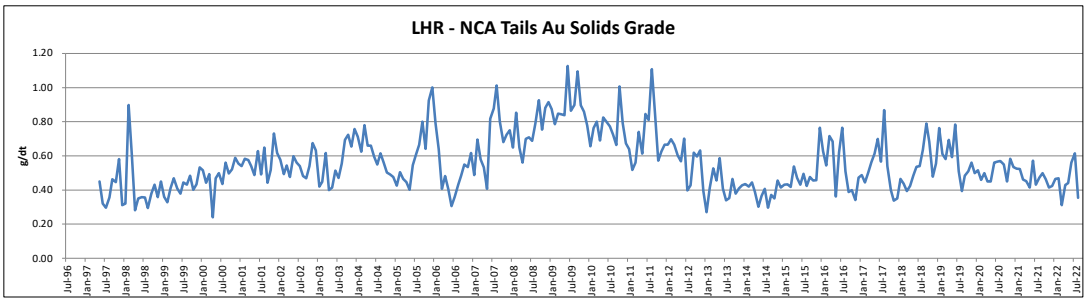

Figure 27 - NCA (CIL) Tails Gold Grade, g/t

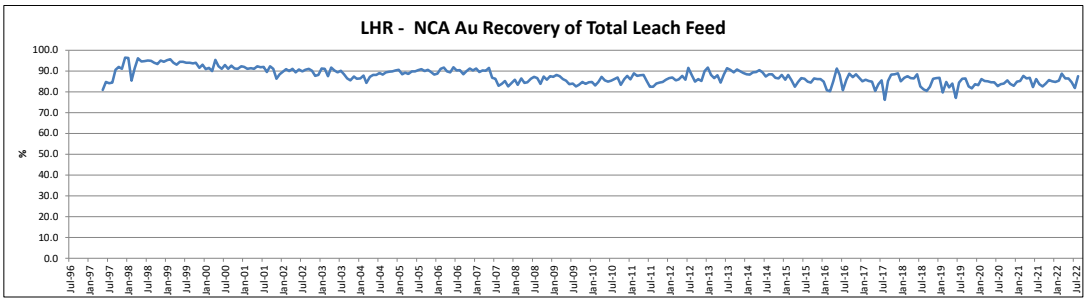

Figure 28 - Lihir NCA (CIL) Gold Recovery, %

A plot of gold extraction from solids vs oxidation is shown below in Figure 29 for the years 2015, 2016 and 2017. Hence this represents a wide range of ore types and variable mixtures of flotation concentrate and whole ore. For ore treated since 10 December the gold extraction vs oxidation is a reasonably flat line. Most oxidation since December 2014 has been in the region of 60 to 75%.

One reason for this is that the % oxidation has not dropped significantly despite much higher autoclave sulfur feed rates. This is due to the increase in autoclave oxygen utilisation as feed sulfur grade increases. More of the added oxygen is used for oxidation rather than being vented. An added benefit of the LOS.

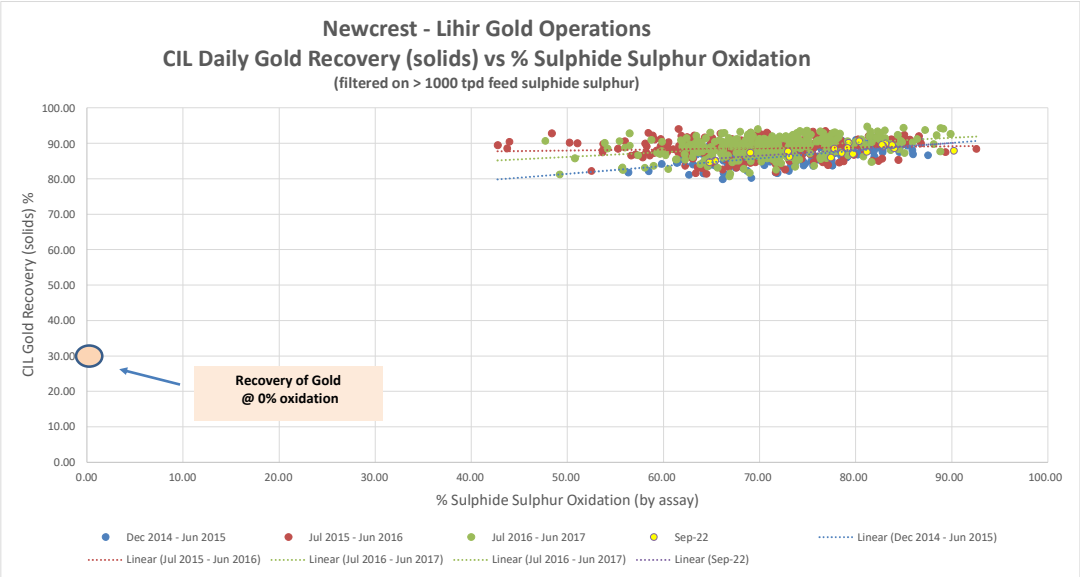

Figure 29 - CIL Gold Extraction (solids) vs Sulfide Sulfur Oxidation

Cyanide, Lime, and Activated Carbon Usage

Cyanide usage in terms of kg (NaCN)/d tonne of CIL feed as shown in Figure 30 has increased since 2017. In 2019-2021 a higher proportion of stockpile ore leading to viscous autoclave discharge necessitated increased dilution of CIL feed slurries and increased cyanide usage. Some increase in cyanide addition is also occasionally required when treating higher autoclave feed sulfur ores due to increased copper concentrations in solids. Copper as chalcopyrite is concentrated in flotation and some additional cyanide usage on CIL feed is expected. Residual sulfur from autoclave discharge may also partially consume cyanide and dissolved oxygen and to compensate the CIL circuits at have been converted to using oxygen rather than air. Work continues optimising cyanide and oxygen addition.

Note: some reagent data is missing in the following trends.

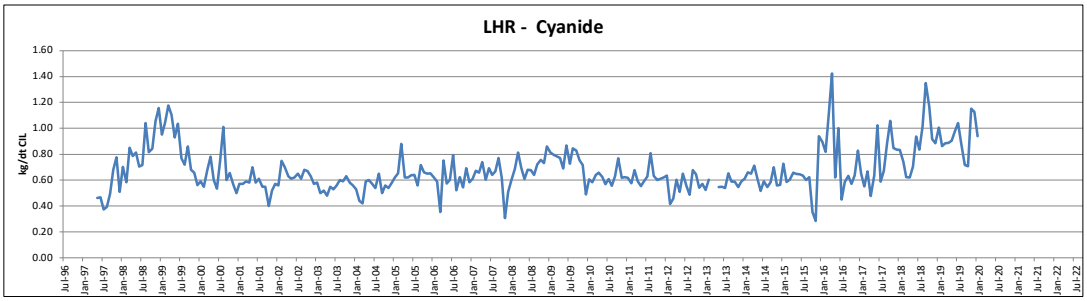

Figure 30 - Lihir Cyanide (NaCN) Usage, kg/t CIL Feed

Interestingly in terms of kg NaCN/dry tonne of mill throughput then usage is ~ 0.6 kg/t – in-line with the original design is shown below in Figure 31

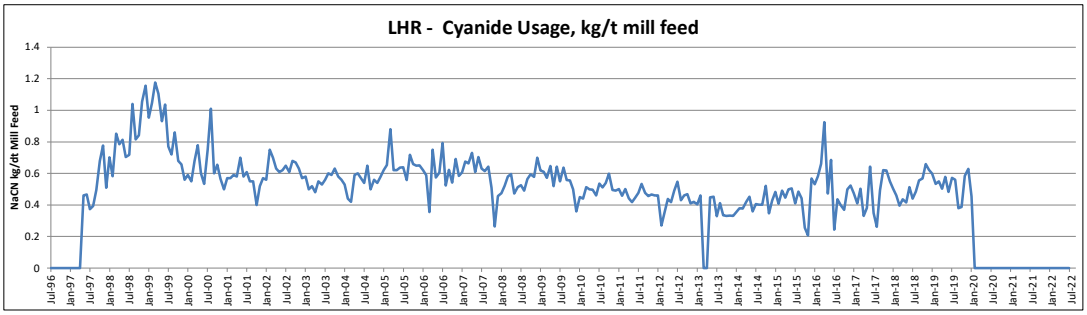

Figure 31 - Lihir Cyanide Usage (NaCN), kg/dt Mill Feed

Lime usage has been relatively steady (although considerable variation is often seen month to month). Consistent with cyanide, dilution (with seawater) in the CIL circuit since 2019 has led to slightly increased lime usage in terms of usage per to CIL feed, Figure 32.

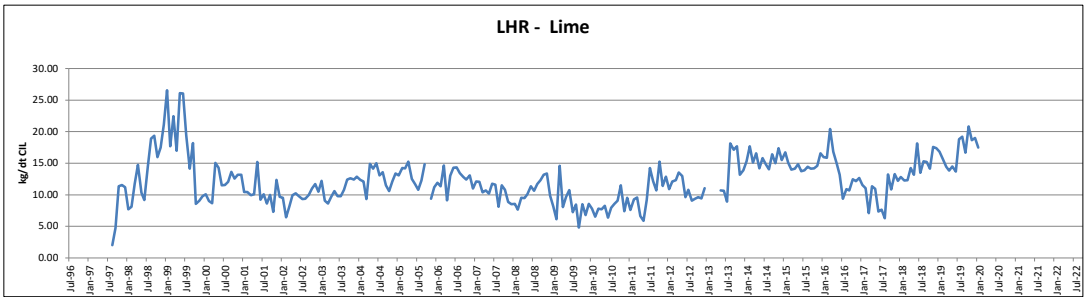

Figure 32 - Lihir Lime Usage, kg/dt CIL Feed

Again, expressed in terms of lime usage per dry tonne of mill feed, lime usage has not changed significantly during the period of selective oxidation at Lihir. See Figure 33.

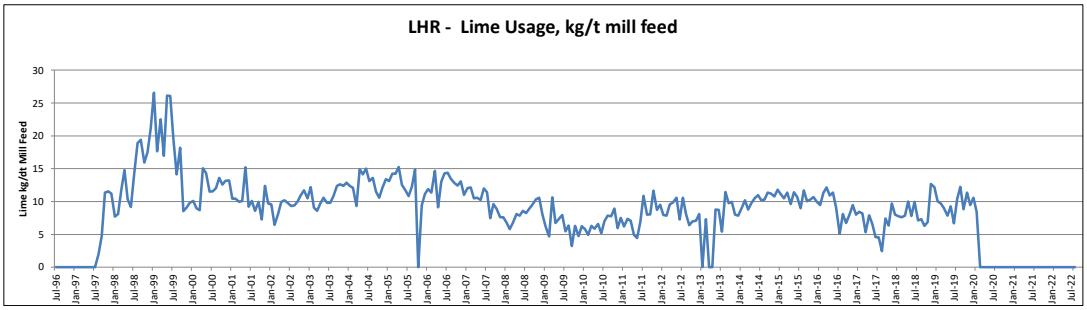

Figure 33 - Lihir Lime Usage, kg/dt Mill Feed

Activated carbon usage has increased in the last few years during treatment of the Kapit Flat stockpile. Work continues to optimise and reduce carbon usage.

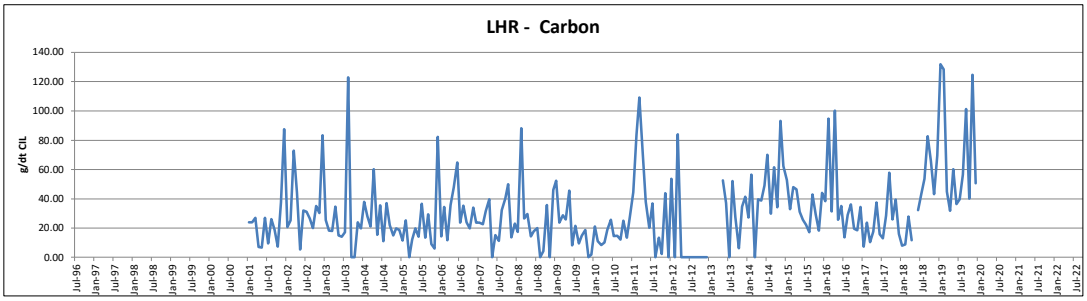

Figure 34 - Lihir Activated Carbon Usage, g/dt CIL Feed

POTENTIAL APPLICATION TO OTHER REFRACTORY GOLD SULFIDE DEPOSITS

Selective oxidation may be applicable to other similar deposits. "Partial Oxidation" test work should always be completed to understand the relationship between recovery and oxidation for every refractory gold pyrite/arsenian pyrite/arsenopyrite deposit. High oxidation with commensurate high recovery is not necessarily the economic optimum for ores with a "flat" gold extraction vs oxidation profile as seen in Figure 29.

For example, the Lone Tree deposit in Nevada is another example of a POX project that utilised partial oxidation. Gold was deported into a fine-grained pyrite containing most of the gold and a coarse pyrite containing little gold. "Gold was concentrated in numerous fine-grained (< 10 µm) aggregates of porous pyrite, marcasite and arsenous pyrite mineralization. Coarse pyrite and arsenopyrite contained a very small portion of the total gold" (Simmons, p74). The papers of Cole, Janhunen and Lenz and G.L. Simmons give further description of the Lone Tree project.

The Lihir Operating Strategy and the use of selective oxidation has been patented (see references below).

CONCLUSIONS

Selective oxidation at Lihir exploiting favourable pyrite-gold mineralisation has been successfully implemented at Lihir. Increased gold production has been achieved since December 2014.

As the major costs at Lihir are essentially fixed then the unit cost of production has been reduced.

Notably specific cyanide and lime consumption in the gold recovery circuit has not materially changed with the introduction of selective oxidation.

ACKNOWLEDGEMENTS

The assistance of the following individuals is acknowledged. Mr Ian Clatworthy for updating Life of Mine data and graphs and Ms Tamala Anam for provision of Lihir Metallurgical Accounting information.

REFERENCES

V.J., Ketcham et al (1993). The Lihir Gold Project; Process Plant Design. *Minerals Engineering*. Vol 6, Nos 8-10, pp 1037-1065

M.J., Collins et al (1993). The Lihir Gold Project; Pressure Oxidation Process Development. *International Symposium on Hydrometallurgy, Salt Lake City, USA* Chapter 38, pp 611-628

V.J., Ketcham and J.F O'Reilly (1994). Pressure oxidation circuit design for the Lihir Project, Papua New Guinea. *AusIMM Proceedings of the PNG Geology, Exploration and Mining Conference 1994, Lae. Rogerson, R. (Ed), pp 219-229*

K Gardner, D Seaman, and J O'Callaghan (2017), Ore Deposit Knowledge – The Value of Continuous Improvement, *Proceedings of COM 17 | The Conference of Metallurgists hosting World Gold and Nickel Cobalt*

J.A. Cole, W.J. Janhunen and J.C. Lenz (1995), Santa Fe Pacific Gold's First Pressure Oxidation Circuit; Year One at Lone Tree. *Presented at the SME Annual Meeting, Denver, Colorado - March 6-9, 1995*

G.L. Simmons, Development of low-temperature pressure oxidation at Lone Tree. *Minerals and Metallurgical Processing, May 1994.*

McDonald, A, Lihir Gold Five Years On – Maximising Throughput and Capital Utilisation. *Eighth Mill Operators' Conference, Townsville, Queensland, 21-28 July 2003, pp 115-120*

Patent: WO 2020/160611 A1*, Processing Ores Containing Precious Metals, Priority Date: 5/2/2019*

Patent: WO 2021/003521 A1*, Processing Gold Containing Ores, Priority Date: 5/7/2019*

PROPOSED BACTERIAL HEAP LEACHING OF ORE SORTER PRODUCTS AT ANAX METALS' INNOVATIVE WHIM CREEK PROJECT

By

Tony Parry, [2]Geoff Laing, [3] Wendy Beets,

Nexus Bonum, Australia
[2]Anax Metals Ltd, Australia
[3]Anax Metals Ltd, Australia

Presenter and Corresponding Author

Tony Parry
tony.parry@nexusbonum.com

ABSTRACT

Anax Metals Limited ("Anax") is planning to re-commence mining and processing operations at the historic Whim Creek mining centre located 120 km southwest of Port Hedland, with a vision to developing a strategic polymetallic ore processing hub in the Pilbara.

The Whim Creek Project is a joint venture between Anax (80%) and Develop Global Limited (20%). Oxide ore was mined from Whim Creek and Mons Cupri volcanic-hosted massive sulphide (VMS) deposits by Straits Resources Limited (now Aeris Resources Ltd) in the mid-2000's and processed through a heap leach and SX/EW plant to produce around 15,000 tpa of copper cathode. Much of the heap leach infrastructure remains.

Anax acquired its interest in the Project in late 2020. In April 2023 a Definitive Feasibility Study ("DFS") to produce 10,000 to 12,000t of copper equivalent metal per year from sulphide ore was completed. The Whim Creek DFS flowsheet to treat copper-zinc-lead sulphide ores with significant precious metals credits is innovative, incorporating two stages of sensor-based ore sorting prior to further metallurgical processing. The first stage primary ore sorters will upgrade the ROM ore into higher grade pre-concentrates which will then be processed in a new purpose built copper-zinc-lead concentrator to produce saleable sulphide concentrates.

The rejects from the Primary ore sorters will be further treated in a secondary ore sorting circuit to produce a 'middlings' pre-concentrate and barren rejects that potentially can be used as commercial aggregates. It is intended to treat the middlings pre-concentrates in the existing heap leach circuit (after refurbishment) to produce copper metal (from SX-EW) and a separate zinc sulphate by-product stream. The Whim Creek copper mineralisation is primarily chalcopyrite and therefore Anax believes that the proposed heap leach operation will need to incorporate bacterial leaching in order to achieve satisfactory copper recoveries.

This paper describes the proposed innovative pre-concentration circuit, the bacterial heap leach test work undertaken by Anax using ore sorter middlings pre-concentrates generated in ore sorting test work, as well as discussing the refurbishment requirements and circuit modifications likely to be required for a re-start of the existing heap leach and SX-EW infrastructure.

The bacterial leaching test work was conducted using native bacterial cultures extracted from remnant fluids in the Whim Creek pits. Column leaching test work has produced excellent results, as announced by Anax in June 2023[1]. The tests confirmed that bacterial column leaching test work delivered 79-80% copper extraction and over 90.

zinc extraction from the ore sorter middlings. Bioleaching test work is ongoing with larger column tests underway and optimisation of conditions to further improve both copper and zinc extraction. Meanwhile, Anax has progressed studies into the refurbishment of the heap leach and SX-EW infrastructure, the key elements of which are also described in this paper.

Keywords: Whim Creek, bacterial heap leach, bioleaching, chalcopyrite ore.

[1] "Bioleaching Success to Boost Whim Creek Metal Production", Anax Metals Ltd, ASX release, 18 June 2023

PROPOSED BACTERIAL HEAP LEACHING OF ORE SORTER PRODUCTS AT ANAX METALS INNOVATIVE WHIM CREEK PROJECT

[1]Tony Parry , [2]Geoff Laing

[1] Nexus Bonum, Australia
[2]Anax Metals Ltd, Australia

PRESENTATION BY ANAX AND NEXUS

- INTRODUCTION – ANAX METALS AND NEXUS BONUM
- ANAX METALS' WHIM CREEK PROJECT
- BIO LEACHING RESULTS – LAB TEST WORK
- DEVELOP GLOBAL JV – EMERGING PROCESSING HUB OPPORTUNITY
- CHALCOPYRITE LEACHING – CHALLENGES AND OPPORTUNITIES
- CONCLUSIONS

WHO WE ARE

ANAX METALS:

- **Aquired 80% interest in the Whim Creek Project**, from Develop Global Limited (ASX:DVP) in 2020.
- Strategy to **fast-track the re-start of copper and base metal production** at the site, utilising **smart technology** to realise processing efficiencies and reduce capex.
- **Completed a DFS,** secured final regulatory approvals to commence mining operations.
- **Implementing Pilbara Consolidation Strategy:** development of a processing hub at Whim Creek capable of treating more than 20ktpa copper (eq) from our own deposits and other regional assets.

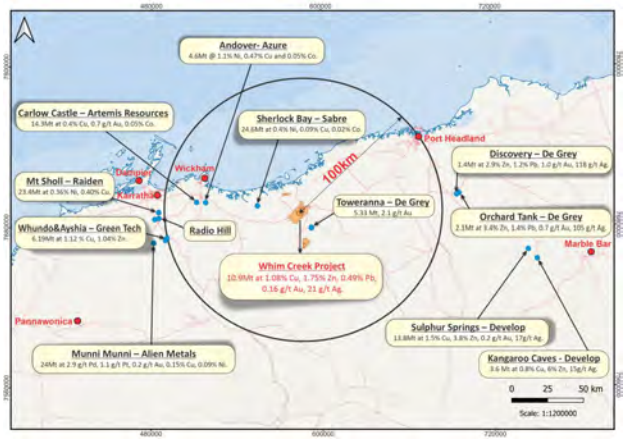

NEXUS BONUM:

- Established in 2014, as a specialist consultancy **focused on ore sorting and associated pre-concentration technologies.**
- Combined **metallurgical and engineering expertise**.
- Design and manage comprehensive **test work** programs, technical and economic evaluations, **Scoping Studies, PFS** and **Definitive Feasibility Studies.**

WHIM CREEK HISTORY

- Copper mining commenced in the late 1800's with DSO ore shipped from the port at Balla Balla
- Processing facilities followed in the early 1900's
- Straits Resources Oxide Heap Leach Operations between 2004 and 2009
- Blackrock/Venturex turned the upper lift over in 2018/19
- Anax acquired Whim Creek June 2020 – focus on existing infrastructure and establishing primary mineralisation resources

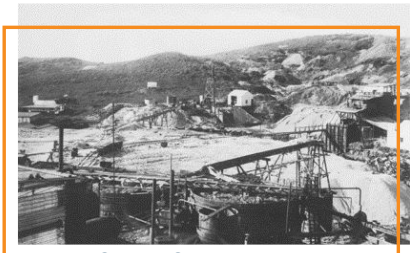

Whim Creek Copper Mine 1900

Whim Creek Copper Mine 2024

PRIMARY MINERALISATION IDENTIFIED BY ANAX (DFS Published Resources):

COPPER	000 Tonnes	Cu %	Zn %	Pb %	Ag ppm	Au ppm	ZINC	000 Tonnes	Cu %	Zn %	Pb %	Ag ppm	Au ppm
Measured	990	1.62	1.42	0.61	38	0.28	Measured	70	0.16	4.56	1.79	53	0.23
Indicated	6,390	1.22	0.71	0.17	13	0.14	Indicated	1,230	0.40	7.55	2.20	58	0.27
Inferred	1,820	0.86	0.32	0.07	5	0.04	Inferred	430	0.34	5.07	1.75	27	0.10
TOTAL Copper Resources	**9,200**	**1.19**	**0.71**	**0.20**	**14**	**0.13**	**TOTAL Zinc Resources**	**1,750**	**0.37**	**6.75**	**2.05**	**50**	**0.22**

FLY-THROUGH

THE ANAX FLOWSHEET – USING TECHNOLOGY TO TRANSITION TO SULPHIDE ORE TREATMENT

Two Parallel Process Streams – Concentrator and Heap Leach

- Whim Creek - **fully permitted site**
- **Low Capex development** option by <u>using concentrator and heap</u>
- **Ore Sorters and Jigs are 'gatekeepers'** to determine concentrator/heap feed split

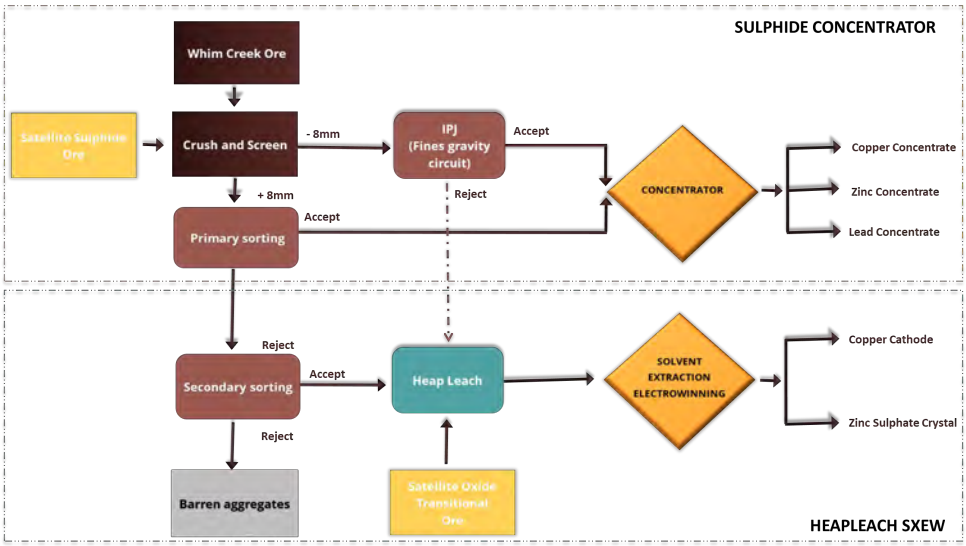

WHIM CREEK – A PROCESSING HUB WITH SORTING, CONCENTRATOR AND HEAP LEACH FACILITIES [1]

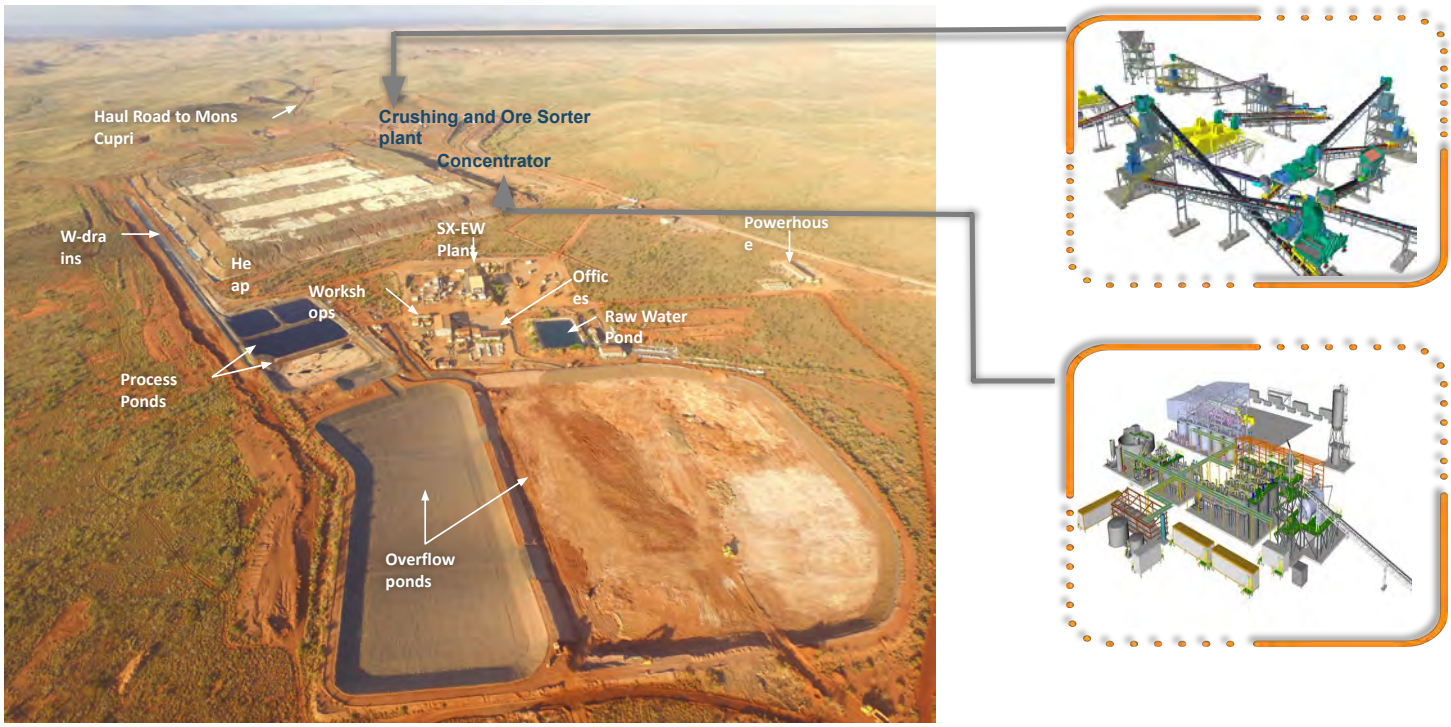

1. ASX announcement 11 September 2023 - Bioleaching Scoping Study

THE ANAX FLOWSHEET – USING TECHNOLOGY TO DELIVER A ROBUST PROJECT

High Grade Ore Feed – Massive/semi massive sulphides

- **Higher Grade Feeds** – Most feed goes to milling/flotation

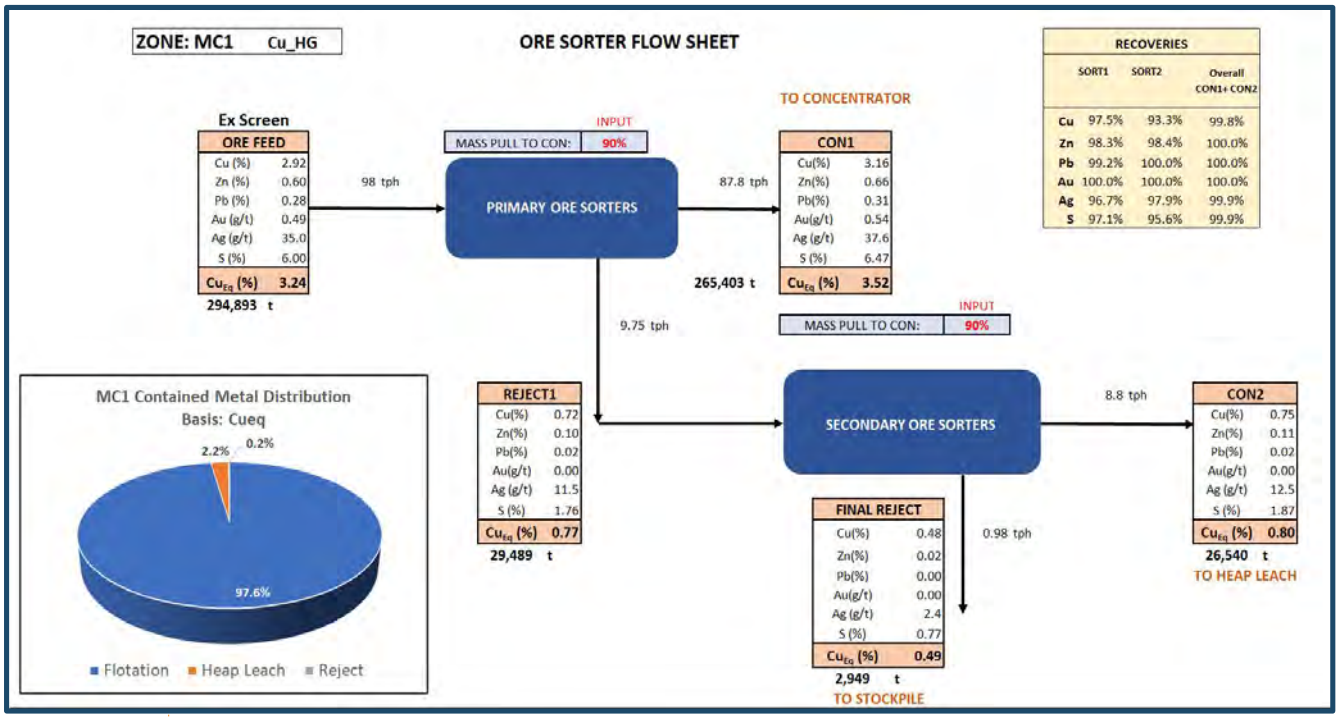

THE ANAX FLOWSHEET – USING TECHNOLOGY TO DELIVER A ROBUST PROJECT

Low Grade Copper Ore Feed – Stringer Zones

- **Lower Grade Feeds** – Increase focus on secondary sorter and heap leach

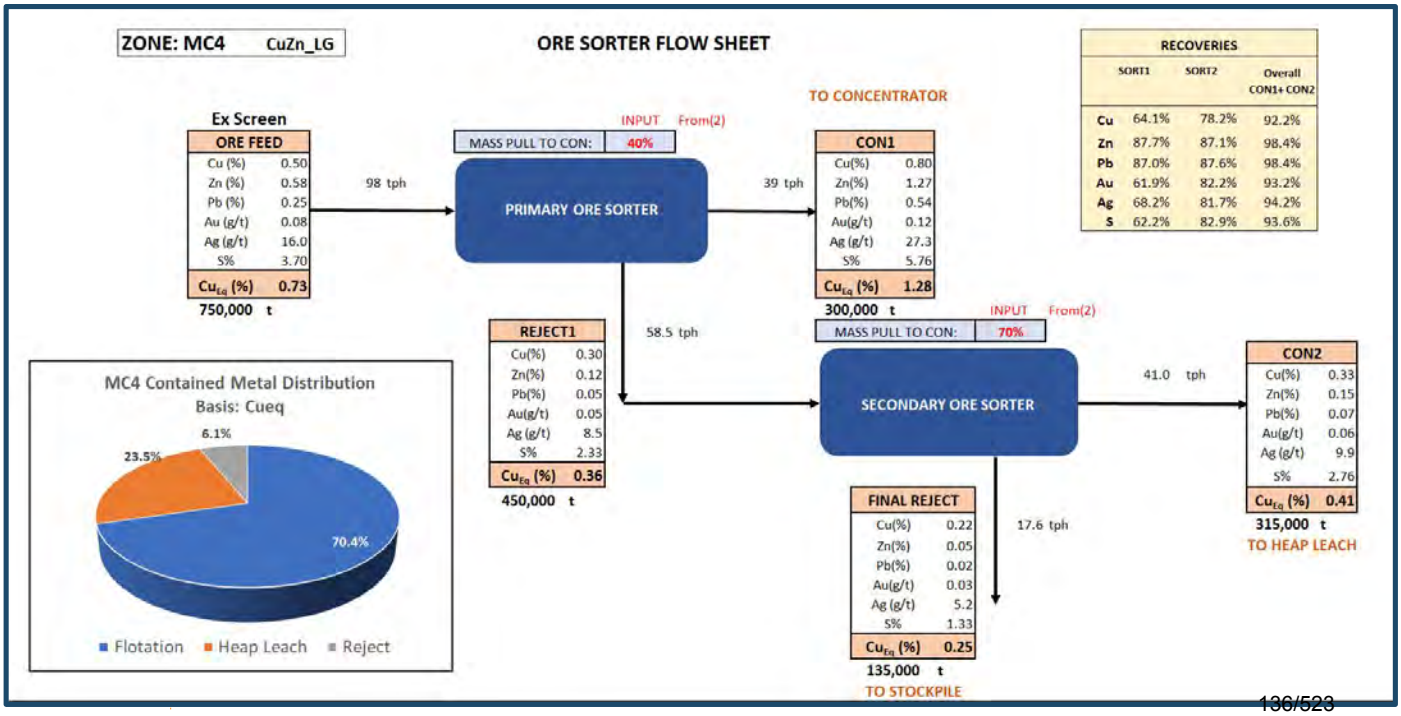

WHIM CREEK HEAP LEACH TEST WORK

ANAX ORE PRE-CONCENTRATION AND FLOTATION TEST WORK

Extensive test work program completed

- ✔ Domain-specific ore sorting bulk tests.
  - Whim Creek Ore Bodies: Massive sulphide and stringer zones
  - Satellite Ore Bodies: Salt Creek, Evelyn
- ✔ Fines (<8mm) gravity upgrade (Gekko jig).

Flotation test work on bulk ore sorter pre-concentrates

- ✔ Domain-specific flotation strategies developed.

Heap Leach Test Work on ore sorter 'middlings'

ANAX BIOLEACHING TEST WORK

Staged test work program has progressed to 1.0m columns

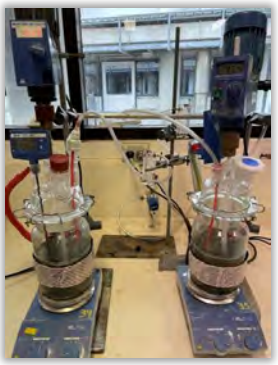

Early 2021: Bioleach amenability tests – BioHeap cultures

2021/2022: Bioleach amenability tests followed by small column (0.5m) leach tests – BV cultures

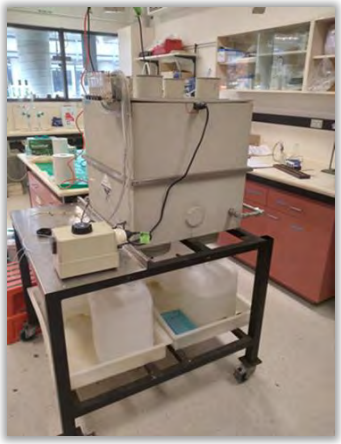

2023-present: Small column tests (0.5m) progressed to larger column (1.0m) tests – CSIRO and Whim Creek cultures tested

BUREAU VERITAS SMALL COLUMNS (0.5M) BIO LEACH TESTS

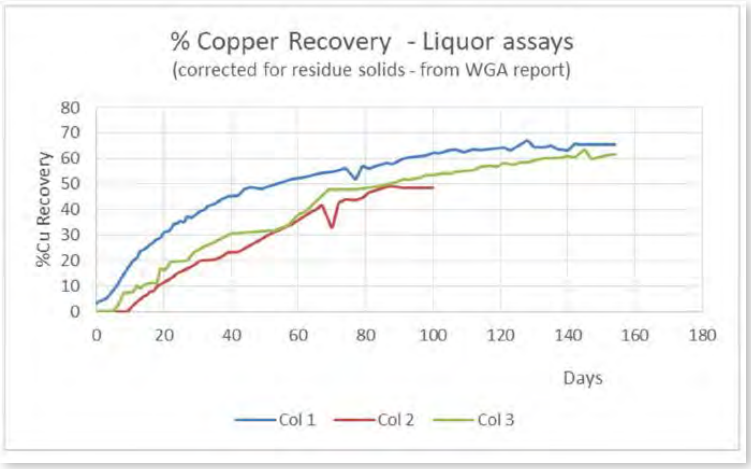

BV Cultures : ~60-70% Cu Recovery and ~80% Zinc Recovery

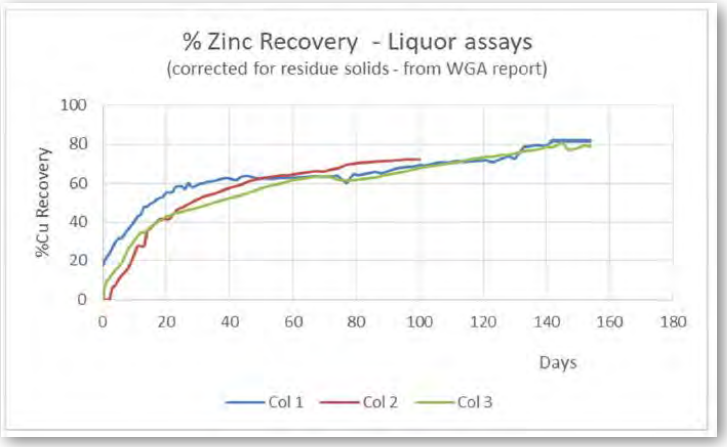

- Temp 50C
- Head 0.92% Cu and 0.15% Zn
- Agglomeration
- P_{100} 3.35mm
- pH 1.8 - 2.0
- Control of Fe levels and ORP

CSIRO SMALL COLUMN (0.5M) BIO LEACH TESTS

Promising Results using Ore Sorter Middlings Products

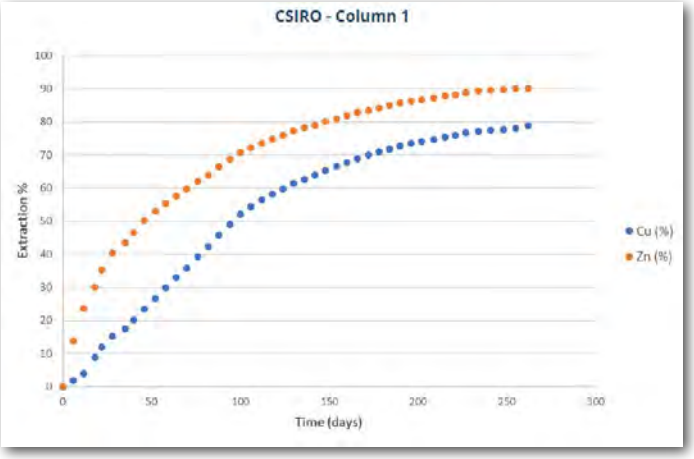

CSIRO and Anax Whim Creek Cultures :
~80% Cu Recovery and ~90% Zinc Recovery

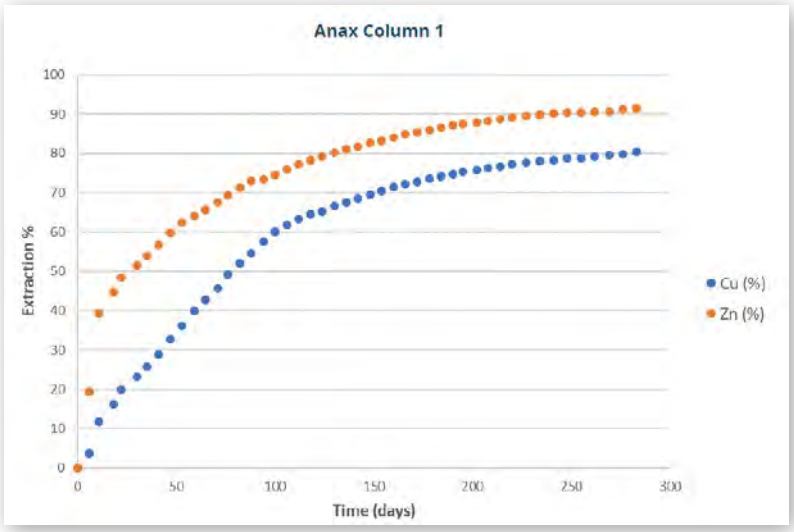

- Temp 45 – 60C
- Head 0.94% Cu and 0.21% Zn
- Agglomeration
- P_{100} 3.35mm
- pH 1.8 - 2.0
- Control of Fe levels and ORP

CSIRO LARGE COLUMN TESTS

- Tests on-going
- ~10kg per column
- Assessing feed size (3.35mm, 6.4mm)
- Agglomeration/no agglomeration
- Assess higher bed temp (60C) to enhance kinetics

FURTHER INNOVATIVE WHIM CREEK BIO LEACH INITIATIVES – focus on acid consumption

ACID CONSUMPTION

HEAP DESIGN

Ore sorting to remove acid consuming gangue → Sulphur doping of ore → Supplemental acid and heat from tank leaching elemental sulphur, IPJ fines and pyrite concentrates → Heap configuration to maximize leaching

ANAX HEAP LEACH SCOPING STUDY (Sept 2023)

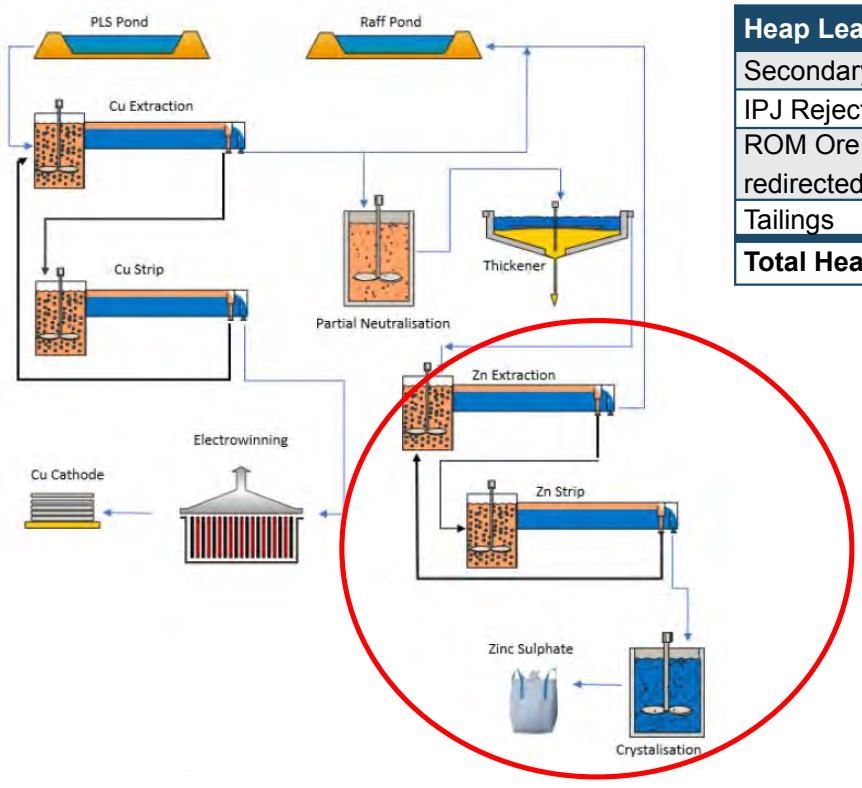

Heap Leach Feed Type	Kt
Secondary Sort Rejects	788
IPJ Rejects	300
ROM Ore (transitional ore + new sulphide ore + redirected ore)	751
Tailings	354
Total Heap Leach Feed	**2,193**

ANAX DFS FINANCIALS

Includes Heap Leach Scoping Study

Metric	Concentrator (DFS)	Heap Leach Contribution**	Combined Project [2]
Pre-Production Capex	$ 71M	($10 M)	$ 71 M
Operating Costs (mining, processing, freight and admin)	$ 628 M	$ 46 M	$ 674 M
Operational Cashflow	$ 451 M	$ 85 M	$ 536 M
Free Cashflow (before financing and tax)	**$ 340 M**	**$ 71 M**	**$ 411 M**
IRR	54.3%	n/a	55.3%
Payback	20 months	n/a	23 months
NPV (7%)	$ 224 M	n/a	$ 270 M

**Reported on a 100% Project Basis. Anax has an 80% interest in the project and will contribute 80% of costs and receive 80% of financial outcomes.*
***Heap Leach Capex to be committed in Y2 of operations and paid from operating cashflow*

HEAP LEACH PROCESSING HUB – EMERGING OPPORTUNITIES

WHIM CREEK HEAP LEACH TO BECOME PROCESSING HUB?

- Develop Global and ANX confirms Scoping Study
- Oxide/Transitional Ores from Develop Global's Sulphur Springs project may be treated on the Whim Creek heap
- Anax and Greentech confirm Base Metal Alliance collaboration
- Oxide/Transitional Ores from Greentech's Whundo project may be treated on the Whim Creek heap
- Hub Concept – Processing option from a number of stranded deposits in the Pilbara

CHALCOPYRITE LEACHING – CHALLENGES AND OPPORTUNITIES

Seen as potentially important to provide additional copper to meet demand

MiningNews.net

25 March 2024

MINERS

Spare SX-EW capacity could be utilised on primary copper ore, says Goldman Sachs

'Big copper' doing a lot of testwork on new technologies able to use existing infrastructure

"We believe new leach technologies may be able to economically compete with proposed new concentrators such as those at Escondida and Bagdad."

Rio Tinto, which has a 30% stake in Escondida, could also add to the output from primary ore by utilising its Nuton bio-heap leaching technology.

MAJORS FOCUSSING ON DEVELOPING VIABLE PRIMARY COPPER ORE HEAP LEACH

Passivation is the big challenge with chalcopyrite leaching

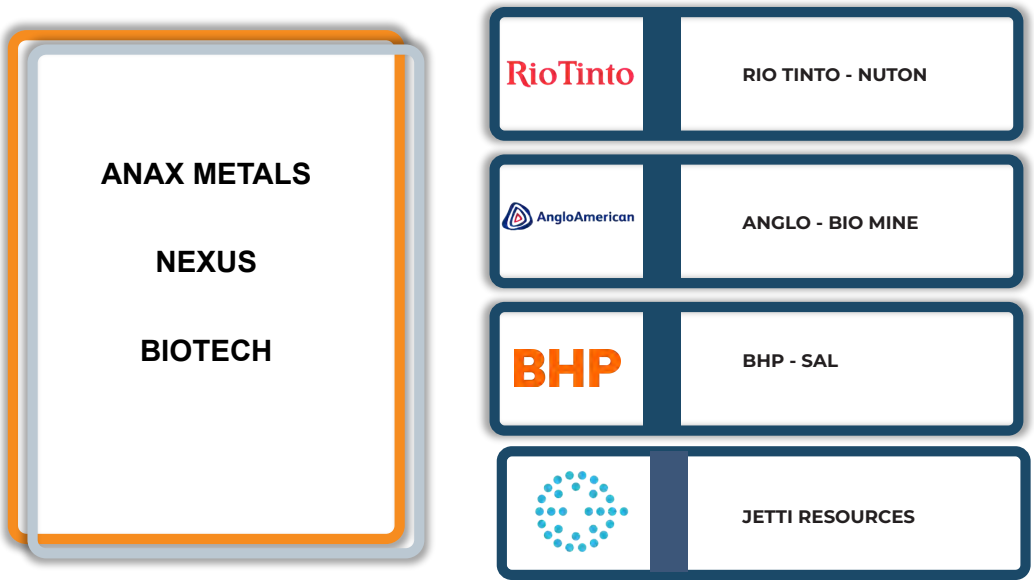

WRAP UP

- BIO LEACHING OF PRIMARY COPPER ORES RECEIVING STRONG GLOBAL FOCUS TO 'CRACK THE NUT'
- BIO LEACH USING EXISTING HEAP LEACH INFRASTRUCTURE TO PLAY A KEY ROLE ANAX METALS' WHIM CREEK PROJECT
- INNOVATIVE FLOWSHEET WITH 'GATEKEEPER' PRE-CONCENTRATION TECHNOLOGY OPTIMISES THE FEED SPLIT TO CONCENTRATOR AND BIO HEAP
- PRIMARY ORE BIO LEACHING RESULTS SHOWING PROMISING RESULTS
- WHIM CREEK HEAP LEACH FACILITY SPARE CAPACITY WILL BE KEY TO DRIVING PILBARA HUB PROCESSING CONCEPT
- DEVELOP GLOBAL JV – EMERGING HUB OPPORTUNITY

SOLUTION RATE TECHNIQUES FOR COLUMN COPPER ORE LEACHING TESTING

By

Fernando Zeballos, Julio Ayquipa,

Compañía de Minas Buenaventura S.A.A., Peru

Presenter and Corresponding Author

Fernando Zeballos
fernando.zeballos@buenaventura.pe

ABSTRACT

To run a laboratory column leaching testwork of a copper ore, the most recommendable method would be to use columns with similar or equal height of operating or designed heap lift. The main reason why it is always not possible is because full height columns demand more ore and during the project study stages it could be a restriction because the representative samples come from drill cores mainly, which are used to other project purposes also.

In the other hand, the most common solution rate used for columns leaching testing, independently of a column height, is a single rate equal to solution rate considered for industrial heap operation. When applied a full and unique solution rate for all columns size without considering the mass of ore loaded in each column, then final kinetic results will be different, hence, will be needed to use equivalence factors to standardize and analyse the testwork results, and finally use the data for heap design.

With the necessity to start a variability column leaching testwork using samples by mine bench height to support the FS of Trapiche project, in Buenaventura was run a laboratory test with three different column heights (1 m, 3 m and 6 m), using the same composite crushed and agglomerated copper ore and the same leaching conditions, but equivalent irrigation solution rates. Solution rates were based on full scale eight meters lift height (around 5 L/m^2-h) and reduced proportionally in function of ore mass loaded to each column. Ore weight is proportional to each column height. All leaching columns test has the same diameter (six inches) and were operated at 25 °C.

Considering a leaching cycle of 184 days, it was obtained an average copper extraction of 72% and similar kinetic curves for all three leaching columns. This indicate that the application of reduced *Irrigation Rate* or equivalent solution rate technique could be applied to short leaching columns and the copper extraction behaviour will be the same as if full-size columns had been used. This technique is being applied to the Trapiche project variability metallurgical leaching campaign (105 columns) with one meter columns height, so it is aligned with the little availability of core drilling samples. Variability metallurgical testwork results will be used to develop the copper extraction and acid consumption geometallurgical project models.

Keywords: column leaching, solution rate, leaching kinetics, copper leaching

INTRODUCTION

The Trapiche project is located in the Apurimac region, Peru. It is a mainly secondary copper ore hydrometallurgical project which currently is in a Feasibility Study phase. In the last years it was performed several metallurgical column leaching tests in a laboratory located in Lima city (around 300 masl), but to has a better approach to environment *in situ* conditions (4,650 masl) it was constructed a metallurgical laboratory on site, where were developed the last column leaching tests and it is performing the metallurgical variability tests campaign to support the Feasibility Study. All tests were carried out using sample composites, but for the variability metallurgical testwork it is using individual samples corresponding to a height bench that come from half diamond drill cores.

Copper extraction, acid consumption and leaching cycle are very key parameters in a copper hydrometallurgical project due to impact that have in CAPEX (initial pad), OPEX (acid consumption) and revenue (recovery), so to generate this data from representative samples from drill hole cores that allows populating the block model and finally to obtain a reasonable geometallurgical model is necessary to try a laboratory procedure that proves to be robust, reproducible and easy to scale-up to different columns or industrial lift heap. As it is known, the amount of sample from diamond drill cores is not abundant enough to carry out tests with large and/or full-size columns, the exception could be to run some column tests to study hydrodynamic of solution percolation, pH ore temperature profiles, and geotechnical parameters where composite samples can be used.

Before initiate the metallurgical variability campaign and in parallel to the parameters optimization testwork it was performed three tests using different column heights to know the copper extraction kinetics during all leaching cycle using solution rates adjusted regarding each column heigh and based on a design industrial lift of 8 m and *Irrigation Rate* of 5.0 L/h-m^2. The ore used in this test was a single composite formed with sections from drill cores of Trapiche project and performed on site project metallurgical laboratory.

Testwork conditions and results are described hereinafter in this paper. It is important to highlight that copper extraction curves were very similar for each column independent of column height (1m, 3m and 6m). It was not shown the same behaviour in the case of gangue acid consumption and related parameters, it could be due to the air injection flow, which was supplied as an unique value for each column despite of its heigh.

MATERIAL AND LABORATORY TESTS PROCEDURE

Materials Used for the Tests

Column leaching tests were performed in the facility constructed on site to carry out the project variability metallurgical testwork campaign to support the Trapiche Feasibility project stage. These tests are part of metallurgical leaching parameters optimization program developed previously to initiate the metallurgical variability test program.

These tests were performed using a general composite sample of Mixed ore as was classified in the project due to medium content of copper soluble in acid and sodium cyanide based on sequential copper chemical assay.

Composite sample chemical assay of total copper and sequential copper (also known as diagnostic leaching) are presented in Table 1 to follow:

Table 1. Copper Ore Chemical Assay

Copper assay	CuT	CuS	CuCN	CuR
Content, %	0.483	0.224	0.174	0.085

The sequential copper assay reports the copper soluble in a solution of sulphuric acid (CuS), copper soluble in a solution of sodium cyanide (CuCN) and the non-soluble copper in these solutions is considered as residual copper (CuR). The total copper content in the sample (CuT) is assayed separately.

Sequential copper assay could be reported in percentage also, as it is shown in Table 2 where is included the Leachability Index (LI) which is intended as the theoretical copper leachable (copper oxides and secondary copper sulphides) by a conventional leaching operation.

Table 2. Copper Diagnostic Leaching and the Leachability Index

Parameter	LI	CuS	CuCN	CuR
Content, %	82.4	46.4	36.0	17.6

In the other hand, as a reference the complete chemical assay of composite head sample by Atomic Absorption (AA) and Inductively Coupled Plasma (ICP) is shown in Table 3.

Table 3. Composite Sample Chemical Assay

Element	Unit	Value
AA Assay		
Cu	%	0.483
Fe	%	3.244
ICP Assay		
Al	%	5.88
Ca	%	0.34
K	+%	3.78
Mg	%	0.38
Mn	%	0.02
Na	%	0.90
S	%	2.35
Ti	%	0.03
Zn	%	0.02
Ag	ppm	3.15
As	ppm	379
Ba	ppm	757
Be	ppm	1
Bi	ppm	<5
Cd	ppm	<2
Co	ppm	22
Ni	ppm	34
P	ppm	109.5
Sb	ppm	9
Sc	ppm	6
Sn	ppm	5
Sr	ppm	169
V	ppm	95
W	ppm	<1
Y	ppm	8
Zr	ppm	4

The composite was prepared using different samples collected from half diamond drilling cores and crushed to reach a P_{80} of ½ inch as can be seen in the particle size distribution (PSD) shown in Figure 1(a). In figure 1(b) is shown the distribution of sequential copper assay, total iron assay and retained ore weight by mesh also.

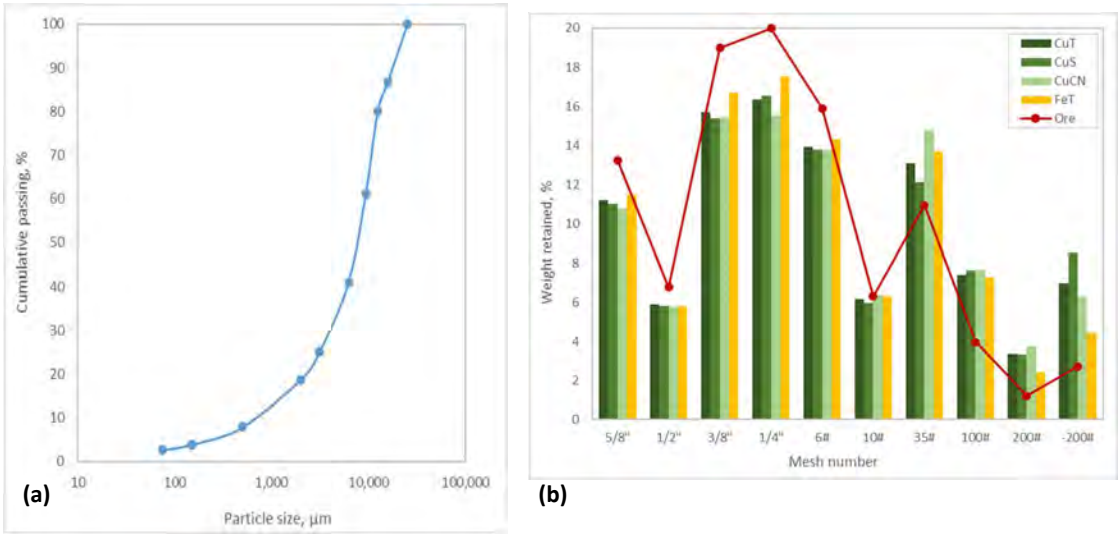

Figure 1. PSD, Copper, and Iron Distribution by Mesh Size of Sample Used in Tests

Columns used for this test has three heights: 6 m, 3 m and 1m. These PVC columns has a diameter of 6 inches, and it were isolated using fiberglass and a heat tracing system to maintain the temperature columns at 25 °C. Figure 2(a) shows the metallurgical laboratory facility on site and current columns distribution in Figure 2(b).

Figure 2. Metallurgical Laboratory at Site and Test Columns Distribution

Laboratory Procedure

The composite for these tests was divided in three samples to treat separately each sample and load each one in different heigh columns. Characteristics of the tests are described in Table 4.

Table 4. Characteristics of Each Column Test

Characteristic	Units	Column – 6 m	Column – 3 m	Column – 1 m
Ore dry weight	kg	150.1	77.2	26.2
Ore moisture	%	0.62	0.62	0.62
Agglomerate moisture	%	5.8	6.0	6.2
Curing time	days	3	3	3
Leaching cycle	days	184	184	184
Acid for curing	kg/t	5.3	5.3	5.3
Irrigation rate	L/h-m^2	3.8	1.9	0.6
Solution/ore rate (at 184 days)	m^3/t	2.0	1.9	1.9

As can be seem in Table 4, the key parameter for this test is the *Solution/Ore Rate*. It should be the same for each column independent of column heigh, hence the variable *Irrigation Rate* should be adjusted for each column regarding to its heigh or better, the ore weigh loaded into it.

Reference for variable solution *Irrigation Rate* by each column height in this case is the project heap heigh lift of 8 meters and its *Irrigation Rate* of 5.0 L/h-m^2.

Ore preparation before load the columns, curing process and operation of each column are described to follow:

- **Agglomeration**: it was used an intermediate leaching solution (ILS) with next characteristics: Cu = 1.898 g/kg, free acid = 1.67 g/kg, total iron = 21.26 g/kg, Fe^{3+} = 10.76 g/kg and added sulphuric acid 5 kg/t reaching an ore final moisture around 6% (See Table 4).
- **Curing:** time curing for these columns was 3 days at ambient temperature.
- **Leaching period**: in this project and due to project area restrictions, the leaching period should be around 184 days.
- **Leaching solution**: it was used a raffinate solution which free acid was suitably adjusted. Characteristics of leaching solution are as follow: Cu = 0.25 g/kg, free acid = 20 g/L, total iron = 21.26 g/kg and a ratio Fe^{3+}/Fe^{2+} = 1.02.
- **Temperature**: columns temperature operation is 25 °C, maintained constant by means of an insulation cover and heat tracing.
- **Controls and chemical Assay**: every day of leaching cycle up to day 56 it was collected a sample per day to perform a chemical assay of copper, total iron, ferrous iron and additionally do measurement of pH, Eh and free acid. After day 56, samples for chemical assay were collected every five days up to day 184.

Irrigation regime was constant and continuous for each column from day 4 to day 184. Additionally, it was maintained in similar way a countercurrent air flow of 0.6 m^3/h-m^2.

TESTS RESULTS

To follow are presented the results obtained in these tests for the 184 days leaching period. This information is about copper extraction results, acid consumption, pH and REDOX potential among other parameters.

Copper Leaching

Once started the irrigation operation in each leaching column and after the tree curing days, solution took around other three days to start dripping into the container that collects the pregnant leaching solution (PLS) under the column. A sample was collected every day from this container to perform a chemical assay and solution control up to day 56, onwards and up to day 184, samples were collected every five days.

Copper extraction measured from first day that columns dripped PLS and during all leaching cycle are represented in curves shown in Figure 3 below.

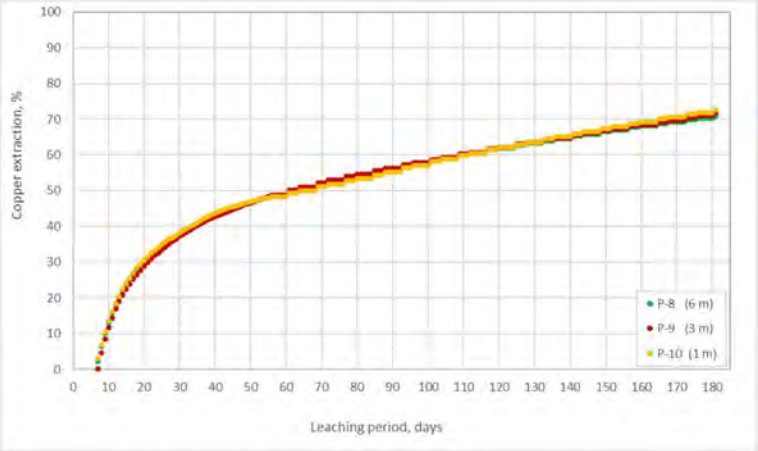

Figure 3. Copper extraction During the Leaching Cycle for Each Column

As can be seen in Figure 3, the copper extraction behaviour in each column is similar along the leaching cycle. Final copper extraction for each column has close values with a slightly greater extraction in the smaller columns, maintaining an inversely proportional relationship between copper extraction and heigh column: column 6m: 70.3%, column 3m: 71.0% and column 1m: 71.8%.

Acid Consumption

Regarding to the gangue acid consumption (GAC), initially the consumed acid was very similar in each column test, but around the day 56 after starting the test, the GAC began a different behaviour suggesting acid generation in the 1 m column as can be appreciated in Figure 4. As per the data obtained and shown in Figure 4 it is possible to note that the gangue acid consumption has a directly proportional relationship with column height (Figure 4a) once most of copper oxides were leached, it can be inferred observing the column tests kinetics in Figure 3 compared with the copper acid soluble (CuS) of sequential copper assay.

It should pay attention over the acid consumption, there is a different behaviour in function of column height. In this case, using an ore with secondary copper minerals as chalcocite and covellite and other sulphides as pyrite in addition to the copper oxides which the copper leaching is strictly based in a chemical reactions mechanism, it seems that when copper oxides are spent, start an sulphides oxidation mechanism that generate acid in the system and it appear as less acid consumption value along the leaching cycle (Figure 4a) or reducing the GAC regarding to copper extracted rate as is shown in Figure 4b.

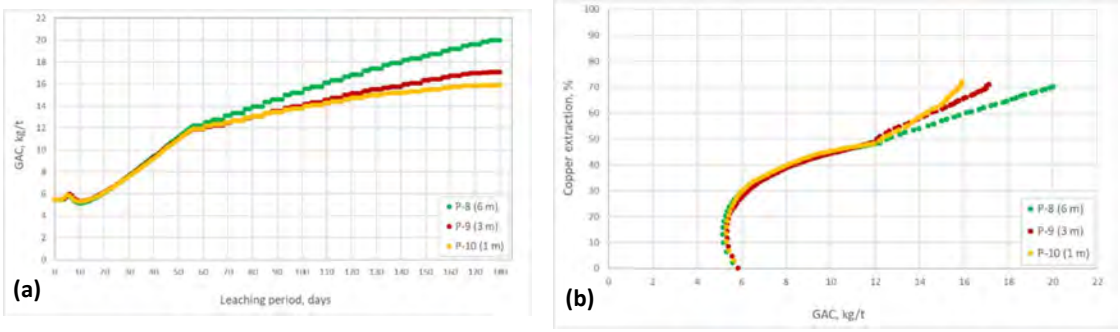

Figure 4. Ganga Acid Consumption by Each Column Test

Other Leaching Parameters

Main parameters that directly affect the copper leaching are the extraction kinetics and gangue acid consumption, but it depends on other parameters that are key to support good results and aid the understanding of kinetics and GAC behaviour. One of these parameters is the *Total Iron* (FeT) dissolved in the PLS (Figure 5a) and related to this and the quality of the bacterial activity is the ferric ion content in the PLS or even better the ferric ion to ferrous ion ratio (Figure 5b).

The *Total Iron* dissolved in PLS has an inversely proportional relationship with column heigh (Figure 5a). Despite the difference in *Total Iron* in the solution, the Fe^{3+}/Fe^{2+} ratio is very similar along the time in all three columns (Figure 5b).

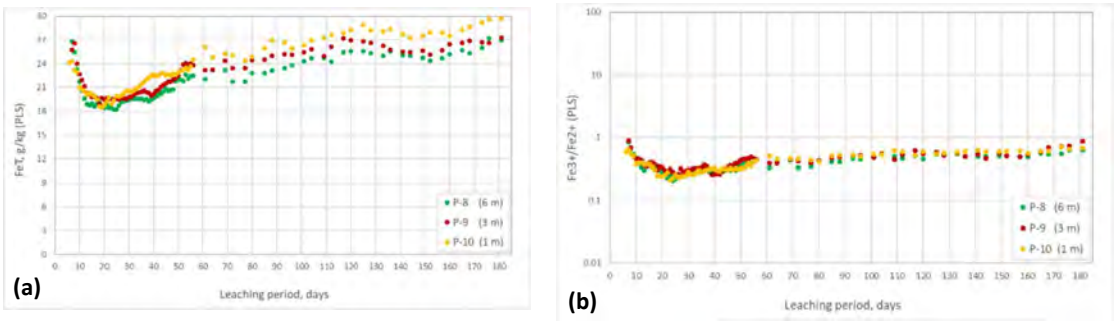

Figure 5. Total Iron and Ferric-Ferrous Ratio in PLS

The tendency is that as the columns are smaller, the acid consumption is less and therefore the free acid in the solution is higher as is shown in Figure 6a. Due to the Fe^{3+}/Fe^{2+} ratio is similar for each column independent of its height, the electrochemical potential or oxidation-reduction potential (ORP) is similar also for all columns as can be seen in Figure 6b. ORP values reported are regarding the Ag/AgCl electrode.

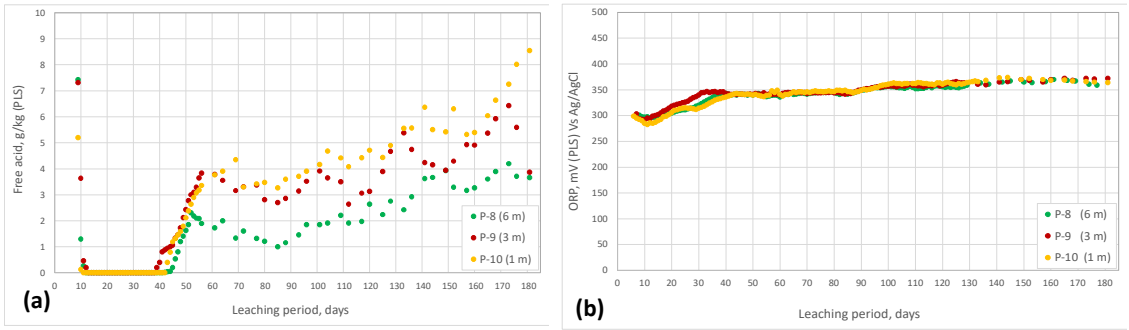

Figure 6. Free Acid and Electrochemical Potential in PLS

DISCUSSION

Copper extraction by acid leaching using different height columns and applying an adjusted solution rate in accordance with the column height (columns ranging from 1 m to 6 m) or even better regarding to the ore weight loaded in each column shown similar leaching curves or in other words, the copper extraction kinetics is equivalent in each case. It is highly recommendable in this type of tests is to use the ore weight instead the column height to reach more accuracy in results.

Despite that leaching curves are very similar for each column height, copper extraction at 184 days of irrigation is slightly different as can be seen in Table 5. It could be attributed to small deviations in operation, experimental error and the supplied air rate which was the same flow for all columns and perhaps should be treated in the same way of leaching solution rates. The main operating leaching parameters are reported in Table 5 or illustrated in Figure 7.

Although the copper extraction can be considered with similar results with a little difference in final copper extraction values (range of 1.8% among columns), the gangue acid consumption (GAC) has different behaviour mainly after leaching the copper soluble in acid (CuS) of sequential copper assay, it could be due to the different level of pyrite oxidation as consequence of air flow which is the same in all columns and consequently the lowest columns, so it would be receiving a higher rate of air per weight of ore. It is consistent with less acid consumption in shorter columns as well as the higher *Total Iron* concentration and *Free Acid* in the PLS. In the case of the Fe^{3+}/Fe^{2+} ratio and ORP, these variables are strongly related and despite of little variations in final values at 184 days, these curves along all leaching cycle has a similar behaviour.

Table 5. Test Results at 184 Days for Each Column

Column height	Cu recovery %	GAC kg/t	FeT g/kg	Free acid g/kg	Fe^{3+}/Fe^{2+}	ORP mV
6 m	71.2	20.4	26.5	4.3	0.6	364
3 m	72.3	17.5	26.9	4.7	0.9	374
1 m	73.0	15.9	28.6	7.0	0.6	368

It is important to note that although these tests were conducted under a bioleaching process, *Total Iron* in solution was high and there is an apparently important bacterial activity evidenced by the lower acid consumption in shorter column, the Fe^{3+}/Fe^{2+} ratio was under 1.0 in all columns. For variability test campaign it was reached a highly oxidative process with Fe^{3+}/Fe^{2+} ratio major than 1.0 and ORP higher than 450 mV (Ag/AgCl), so it is defined by the Nernst equation which can be used to determine one of the two values.

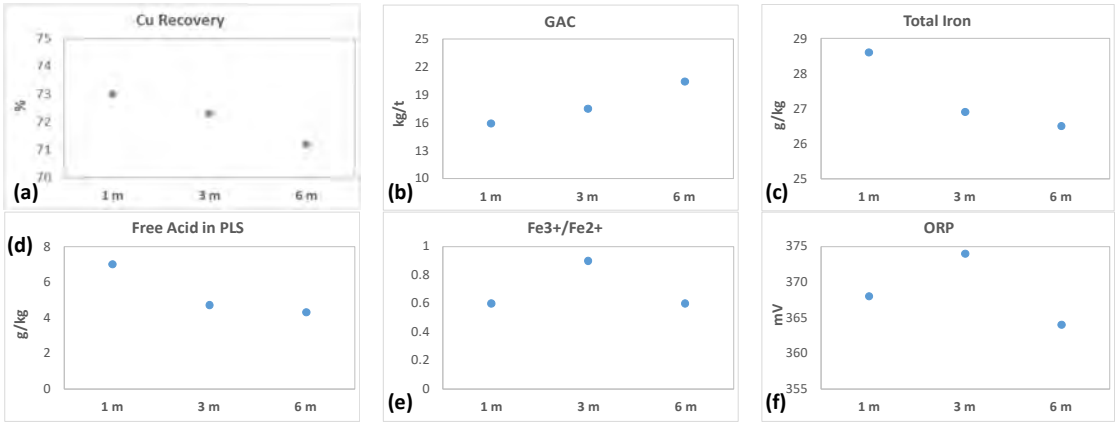

Figure 7. Graphic Representation of Test Results at 184 Days for Each Columns

CONCLUSIONS

- The findings in this study demonstrate that it is possible to obtain a similar copper leaching kinetics in short columns regarding to full-size column leaching that represent the heap lift (v. gr. 6 m). The key parameter to reach it is the implementation of the variable irrigation solution rate in function of column heigh or even better to ore weight loaded to the column. The *Solution/Ore* rate (m^3/t) is proposed as a main parameter to manage any test with different column sizes and to be used as scale-up factor to the industrial leaching. This is aligned with what was proposed by E. Rood (2000) and H. Lizama, et al. (2004).

- The copper extraction results obtained in this test can support the metallurgical variability program due that it is possible to use smaller sample weight for a column leaching test without any important bias in recovery or the necessity to a complex model for the copper recovery scale-up. It is well known that representative samples available from drill cores to perform a column leaching metallurgical campaign are not abundant in any project.

- Acid consumption presented a different behaviour of copper extraction, with an apparently acid generation mainly in shorter columns, it is possibly due to pyrite oxidation by Fe^{3+} ion and bacterial activity. Higher *Free Acid* concentration in PLS and lower GAC is aligned with higher *Total Iron* in the PLS and higher air to ore rate also.

- Together with variability metallurgical program should be carried out another test similar to this but paying special attention, furthermore of kinetics and variable *Irrigation Rate*, to which are the causes of variable acid consumption and related parameters as *Total Iron* in the solution and the oxygen dissolved which is related to the air injection flow rate.

ACKNOWLEDGMENTS

The authors would like to thank the staff and management of the Proyecto Trapiche and the VP of Projects Management and Innovation of BVN for their support and provision of data to prepare this paper. The views of the authors do not necessarily present those of the Company.

REFERENCES

1. Edwin A. Rood. Solution Application Techniques for Column testing, Randol Copper Hydromet Roundtable 2000. Randol International, Golden, pp. 49–52, 2000.

2. H.M. Lizama, J.R. Harlamovs, D.J. McKay, Z. Dai. Heap Leaching Kinetics are Proportional to the Irrigation Rate Divided by Heap Height. Minerals Engineering, 2004.

3. S.W. Robertson and P.J. Van Staden. The Progression of Metallurgical Testwork During Heap Leach Design. Hydrometallurgy Conference 2009, The Southern African Institute of Mining and Metallurgy, 2009.

4. J. Marsden, L. Todd and R. Moritz. Effect of Lift Height, Overall Heap Height, and Climate on Heap Leaching Efficiency. SME Annual Meeting Denver, Colorado - March 6-9, 1995.

5. Vaikuntam Iyer Lakshmanan, Raja Roy and V. Ramachandran Editors. Innovative Process Development in Metallurgical Industry - Concept to Commission, 2016.

MODELING COPPER LEACHING IN HEAP SYSTEMS CONSIDERING COMPETING REACTION MECHANISMS AND COUPLED DISSOLUTION WITH REPRECIPITATION (CDR) PROCESSES

By

Eric O. Ansah, Jay R. Black and Ralf R. Haese

School of Geography, Earth and Atmospheric Sciences, The University of Melbourne, Australia

Presenter and Corresponding Author

Eric O. Ansah
eaowusu@student.unimelb.edu.au

ABSTRACT

Chalcopyrite, an abundant source of copper, is noted to undergo slow dissolution under ambient conditions due to the formation of secondary minerals at the chalcopyrite surface also referred to as surface passivation. Although the passivation mechanism has been extensively studied, present models do not adequately account for it. Hence, passivation limiting copper recovery from chalcopyrite was explored and demonstrated by implementing a surface passivate model (SPM) in this reaction pathway modelling (RPM) study. In addition, the role of different gangue minerals and different chalcopyrite dissolution mechanisms were assessed, and the state of saturation was determined for various minerals to constrain limiting conditions for copper recovery. RPM with different rate laws describing proton-promoted, ferric-iron promoted, and combined ferric-iron-proton promoted chalcopyrite dissolution in the presence of gangue minerals in chloride system were used.

The reaction mechanism that facilitated the fastest dissolving of chalcopyrite and the largest mobilisation of copper was that induced by ferric iron. Nonetheless, the production of iron-hydroxy sulphates (like jarosite), iron oxide (hematite), and various gangue minerals inhibited the mobilisation of copper, underscoring the significance of precisely depicting primary and secondary reactions, their co-location, and their reaction behaviour.

The SPM was able to simulate jarosite surface covering of the chalcopyrite surface, reducing the reactive surface area and hindering chalcopyrite dissolving in the process. On the other hand, because covellite was consistently undersaturated in trial models, the SPM was unable to simulate the incongruent dissolution of chalcopyrite, resulting in a copper sulphide layer deficient in iron.

Additionally, the dissolution of chalcopyrite may be positively impacted by the presence of gangue minerals like hematite and gypsum, but negatively impacted by the presence of silicates like feldspar and muscovite.The results of this investigation are significant because they offer fresh perspectives on the simultaneous processes governing copper recovery in heaps and the most effective modelling techniques for these reactions..

Keywords: Chalcopyrite dissolution, reaction path model, competing reaction rates, copper recovery, jarosite, heap leaching, surface-passivate model.

MODELING COPPER LEACHING IN HEAP SYSTEMS CONSIDERING COMPETING REACTION MECHANISMS AND COUPLED DISSOLUTION WITH REPRECIPITATION (CDR) PROCESSES

By: Eric O. Ansah

eaowusu@student.unimelb.edu.au

Apoorv Jyoti, Jay R. Black, Ralf R. Haese

University of Melbourne

Funding: George Lansell and Melbourne Research Scholarships
Appreciation: TrACEES and MCFP platform
(Graham, Ling, Raveen, Anders, Hoa, etc.)

Motivation

Energy Transition

How to produce more copper, whilst preserving water, to meet growing energy demands?

Source: iStock (2022)

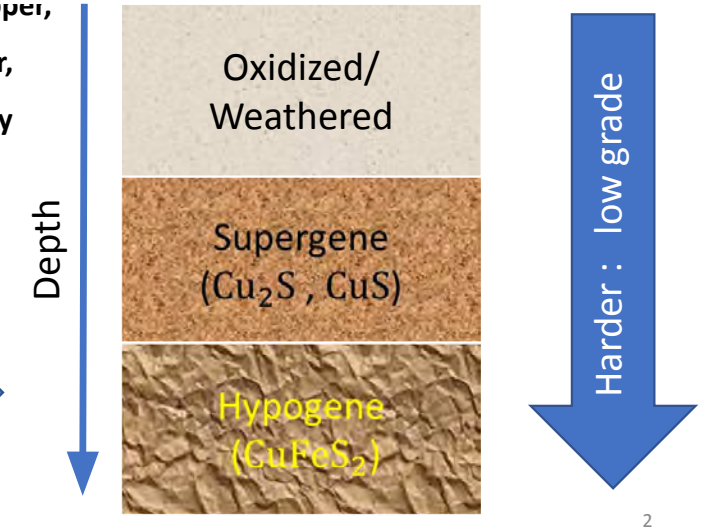

Heap leaching and its low recovery challenge

Source: Jex Technologies

unreacted

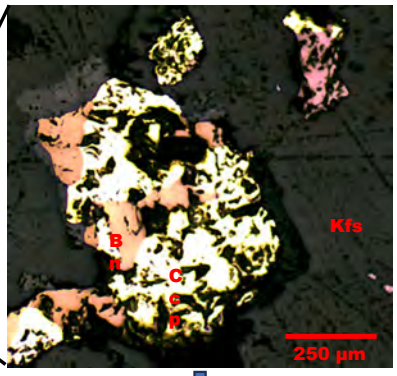

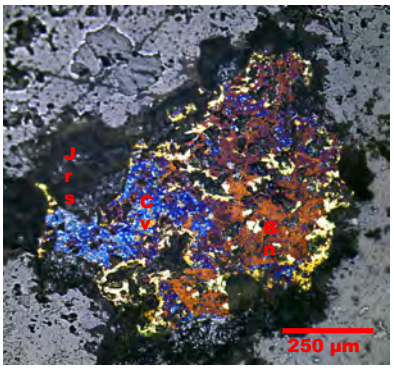

reacted

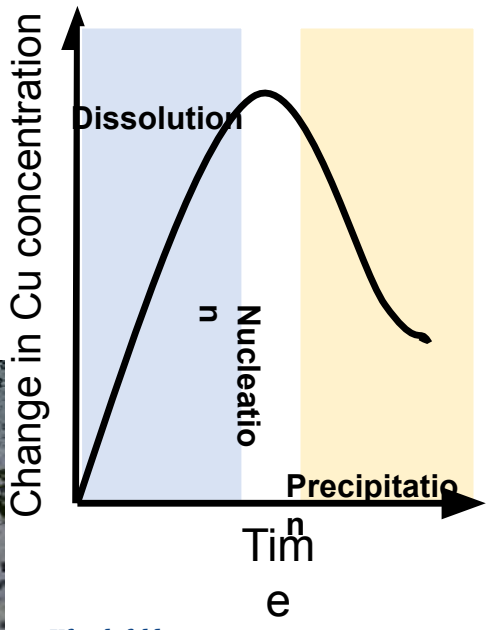

Kfs – k-feldspar
Ccp – chalcopyrite
Bn – bornite
Cv – covellite
Jrs - jarosite

Coupled dissolution with reprecipitation (CDR)

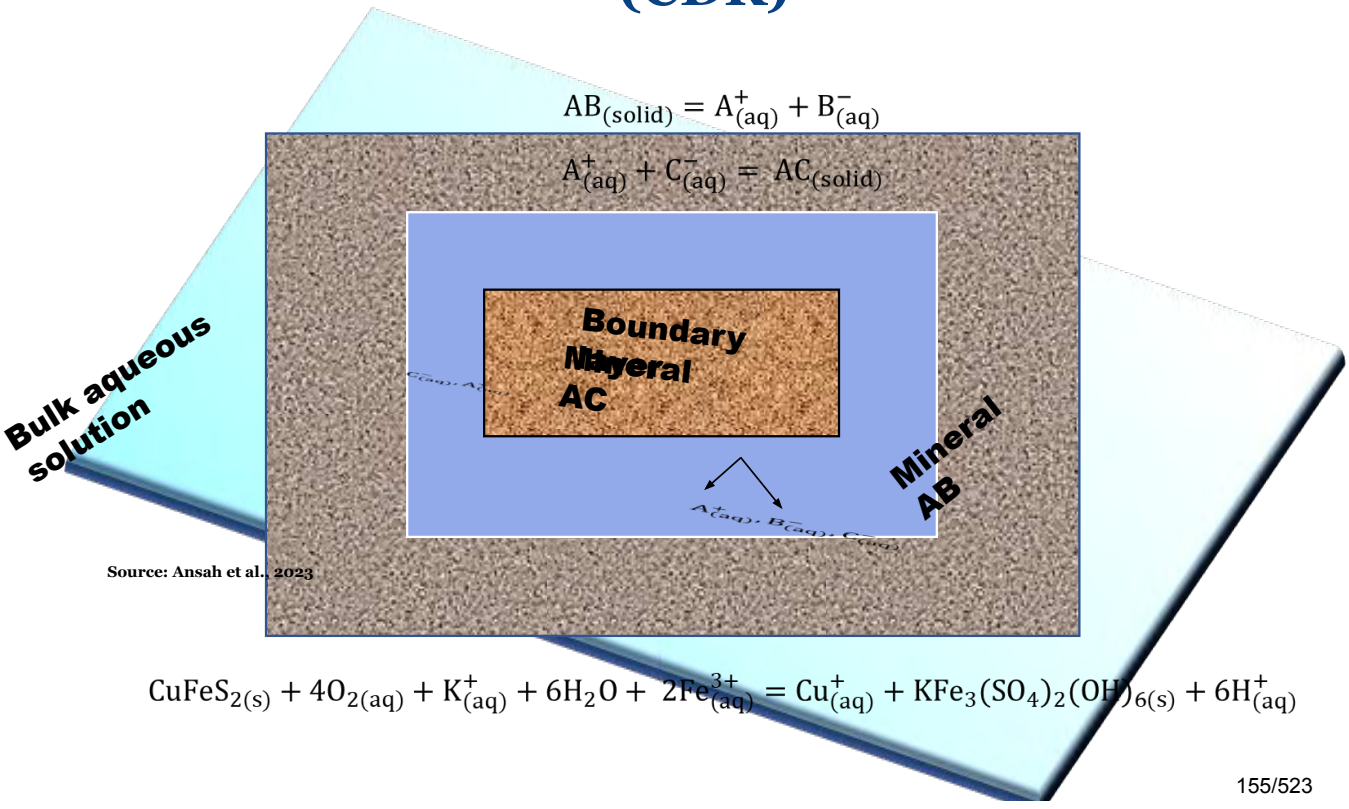

Source: Ansah et al., 2023

$$CuFeS_{2(s)} + 4O_{2(aq)} + K^+_{(aq)} + 6H_2O + 2Fe^{3+}_{(aq)} = Cu^+_{(aq)} + KFe_3(SO_4)_2(OH)_{6(s)} + 6H^+_{(aq)}$$

Passivation mechanism(s)

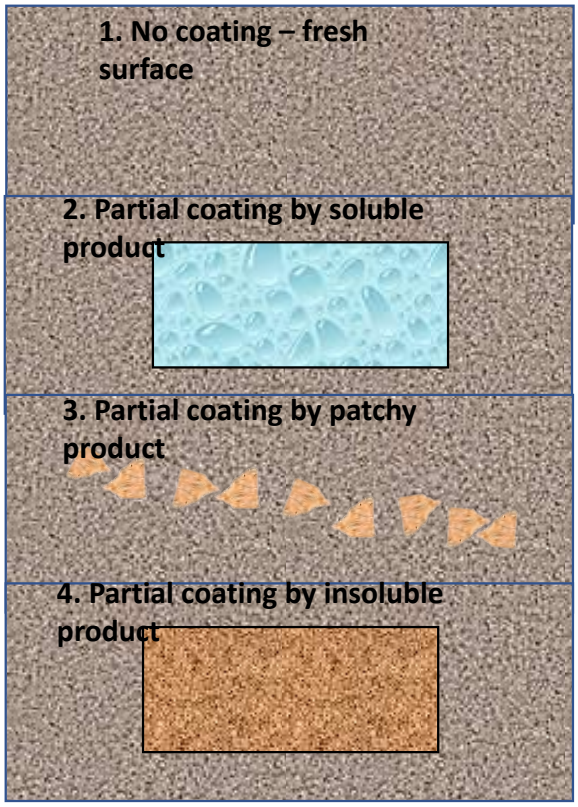

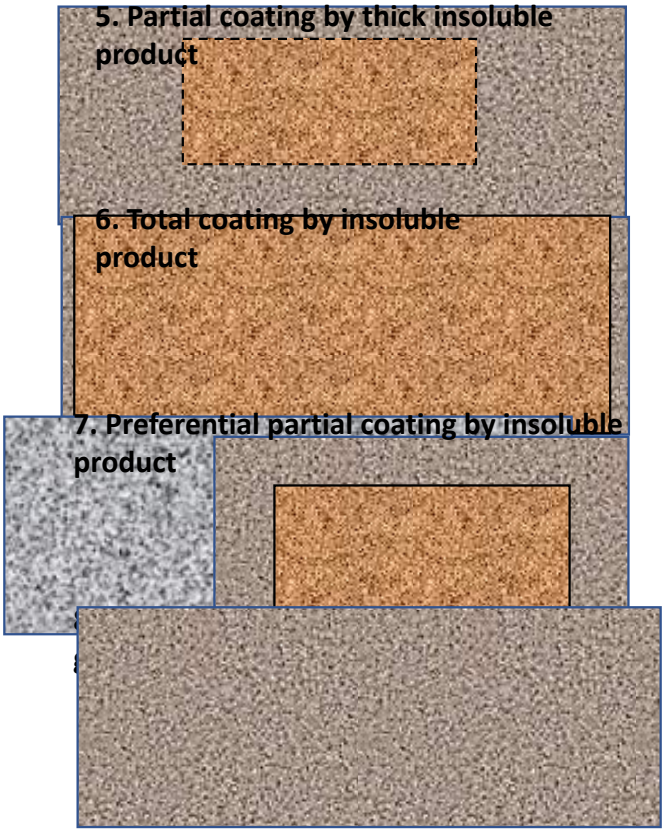

Source: Ansah et al., 2023

Heap leaching and its low recovery challenge

Source: Jex Technologies

unreacted

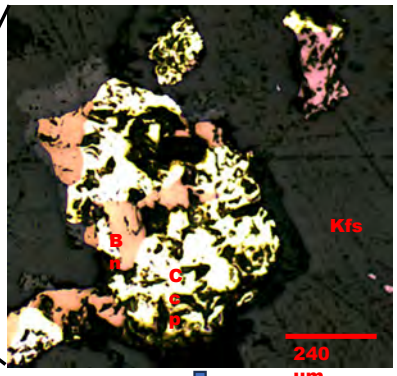

reacted

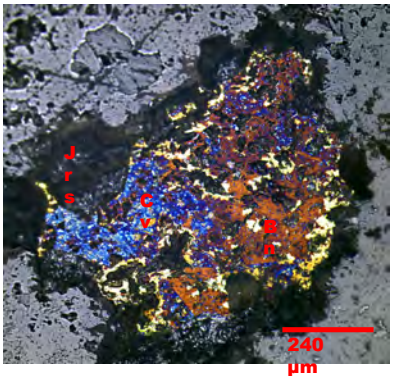

1. Mineral surface area controls CDR
2. Growth of a secondary mineral influences the reactive surface of the primary mineral

Kfs – k-feldspar
Ccp – chalcopyrite
Bn – bornite
Cv – covellite
Jrs - jarosite

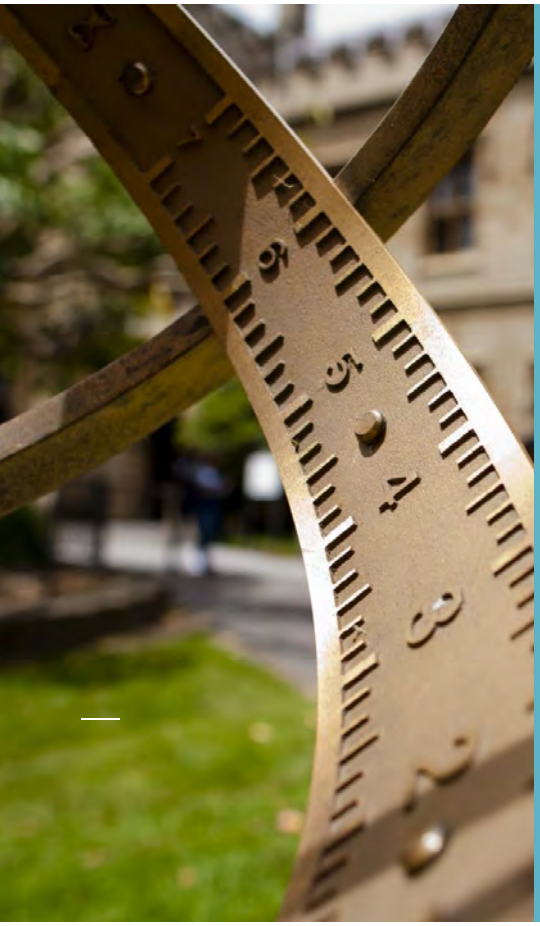

3. How to model?

Introducing a surface-passivate model to handle surface area variation

Objectives

1. How to best model various chalcopyrite reaction mechanisms and rate laws?

2. What effect do distinct types of gangue minerals (e.g., silicates, oxides, sulphates, etc.) have on Cu liberation from chalcopyrite?

3. What is the influence of precipitate (such as jarosite and gypsum) formation on
   - ✔ Surface area
   - ✔ Element (copper) mobilization?

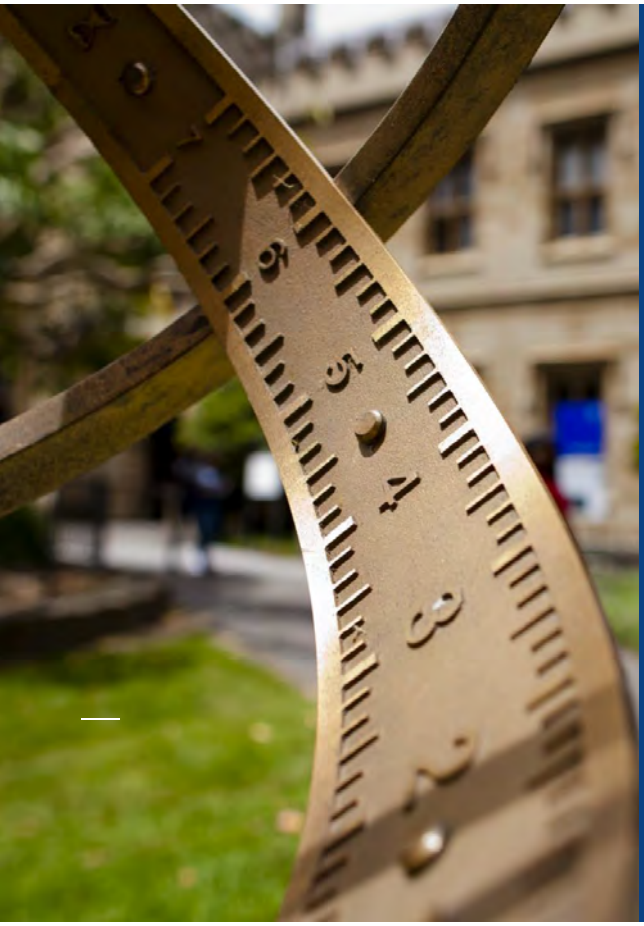

Materials & Methods

Model conditions

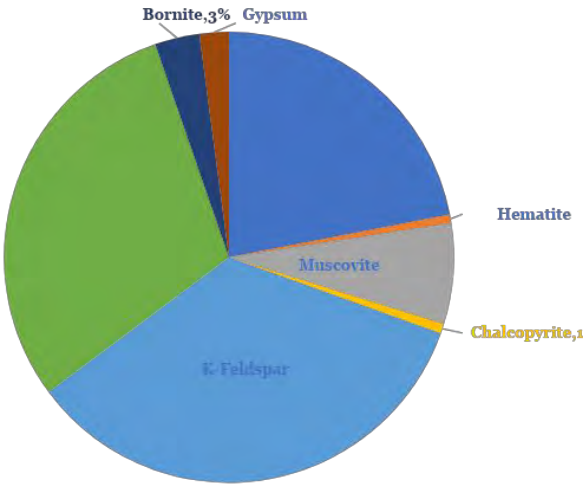

1. The initial fluid for proton-promoted simulations was 0.0316 M HCl with no Fe^{3+}.
2. 0.1 M $FeCl_3$ solution was used in the ferric-iron promoted and combined ferric-iron-proton promoted cases.
3. The model is simulated at Eh of 650 mV SHE and pH 1.5 under ambient conditions.
4. The solution master species and solution species of Al, Ca, Cu, Cl, Fe, H, K, Mg, Na, O, S, and Si from the llnl.dat were used.
5. The models were run to simulate 1 to 5000 days of reaction.
6. The equilibrium rate constants for the aqueous species and mineral phases were taken from the Lawrence Livermore National Laboratory (LLNL) thermodynamic database (llnl.dat) with a few supplementary phases added (e.g., anhydrite, bornite and muscovite) from the wateq4f.dat database of PHREEQC

Redox constraints

$$Fe^{3+}_{(aq)} + e^- = Fe^{2+}_{(aq)}$$

$$O_{2(aq)} + 4H^+_{(aq)} + 4e^- = 2H_2O$$

$$Cu^{2+}_{(aq)} + e^- = Cu^+_{(aq)}$$

$$SO^{-2}_{4(aq)} + 9H^+_{(aq)} + 8e^- = HS^-_{(aq)} + 4H_2O$$

Large kinetic rate constant (1E10) was assumed for the redox reactions, thereby behaving as equilibrium reactio

Case 1 – comparison of different rates and reactions of chalcopyrite dissolution

a

Proton-promoted (non-oxidative) dissolution of chalcopyrite (Lazaro and Nicol, 2003):

$$CuFeS_{2(s)} + 2H^+_{(aq)} = Cu^{2+}_{(aq)} + Fe^{2+}_{(aq)} + 2HS^-_{(aq)}$$

The rate law for proton-promoted chalcopyrite dissolution (Kimball et al., 2010):

$$r = 10^{-1.52} e^{-28200/RT} [H^+]^{1.68}$$

b

Ferric-iron promoted (oxidative) dissolution of chalcopyrite (Lu et al., 2000):

$$CuFeS_{2(s)} + 4Fe^{3+}_{(aq)} = Cu^{2+}_{(aq)} + 5Fe^{2+}_{(aq)} + 2S^0_{(s)}$$

The rate law for ferric-iron promoted chalcopyrite dissolution (Rimstidt et al., 1994):

$$r = -1.78 \times 10^{-7} [Fe^{3+}]^{0.43}$$

c

Combined ferric-iron-proton promoted dissolution of chalcopyrite (Kimball et al., 2010):

$$CuFeS_{2(s)} + 16Fe^{3+}_{(aq)} + 8H_2O_{(aq)} = Cu^{2+}_{(aq)} + 17Fe^{2+}_{(aq)} + 16H^+_{(aq)} + 2SO^{-2}_{4(aq)}$$

The rate law for combined feric-iron-proton promoted chalcopyrite dissolution (Kimball et al., (2010):

$$r = 10^{1.88} e^{-\frac{48100}{RT}} [H^+]^{0.8} [Fe^{3+}]^{0.52}$$

Case 2 - Influence of gangue minerals on combined ferric-proton chalcopyrite dissolution

Quartz: $SiO_{2(s)} + 2H_2O_{(aq)} = H_4SiO_{4(ss)}$

k-Feldspar: $KAlSi_3O_{8(s)} + 4H^+_{(aq)} = Al^{3+}_{(aq)} + K^+_{(aq)} + 2H_2O + 3SiO_{2(ss)}$

Anhydrite: $CaSO_{4(s)} = Ca^+_{(aq)} + SO^{2-}_{4(aq)}$

Albite: $NaAlSi_3O_{8(s)} + 8H_2O = Na^+_{(aq)} + Al(OH)^-_{4(aq)} + 3H_4SiO_{4(aq)}$

Muscovite: $KMg_3AlSi_3O_{10}(OH)_{2(s)} + 10H^+_{(aq)} = K^+_{(aq)} + 3Mg^{2+}_{(aq)} + Al^{3+}_{(aq)} + 3H_4SiO_{4(aq)}$

Hematite: $Fe_2O_{3(s)} + 6H^+_{(aq)} = 2Fe^{3+}_{(aq)} + 3H_2O$

The rate expression for k-feldspar, albite, muscovite, hematite, gypsum/anhydrite in pure H_2O (neutral pH), acid (promoted by H^+) and base (promoted by OH^-) (Palandri and Kharaka, 2004 and references therein).

$$r = k^{298.15K}_{\text{acid}} e^{\frac{-E_{\text{acid}}}{R}\left(\frac{1}{T}-\frac{1}{298.15K}\right)} a^{n_1}_{H^+}(1-\Omega^{p_1})^{q_1} + k^{298.15K}_{\text{neutral}} e^{\frac{-E_{\text{acid}}}{R}\left(\frac{1}{T}-\frac{1}{298.15K}\right)} a^{n_2}_{H^+}(1-\Omega^{p_2})^{q_2} + k^{298.15K}_{\text{base}} e^{\frac{-E_{\text{acid}}}{R}\left(\frac{1}{T}-\frac{1}{298.15K}\right)} a^{n_3}_{H^+}(1-\Omega^{p_3})^{q_3}$$

Case 3 - Influence of passivate (jarosite and gypsum) on combined ferric-proton chalcopyrite dissolution taking account into gangue minerals

The precipitation of secondary minerals requires

1. aqueous speciation
2. the calculation of the state of mineral saturation for each computational iteration
3. the implementation of either thermodynamic or kinetic control of the precipitation process

Jarosite: $2SO_{4(aq)} + K^+_{(aq)} + 6H_2O + 3Fe^{3+}_{(aq)} = KFe_3(SO_4)_2(OH)_{6(s)} + 6H^+_{(aq)}$

Gypsum: $Ca^+_{(aq)} + SO^{2-}_{4(aq)} + 2H_2O_{(aq)} = CaSO_4.2H_2O_{(s)}$

The reaction rate expression for jarosite (Elwood Madden et al., 2012):

$$r = 10^{-6.487}[H^+]^{0.899} + 10^{-10.964}[OH^-]^{0.392}$$

Limitations of the Model

1. Focussed only on the kinetic rate-dependent process of chalcopyrite dissolution in stagnant or very slow-moving liquid coupling dissolution of gangue minerals and precipitation of secondary phases.

2. Heap hydrodynamics was not considered despite having the potential to affect this rate-dependent process.

3. For the sake of simplicity, a microbe-free model of a solely chemical heap system under ambient conditions was used.

4. An open system that was equilibrated with oxygen, where the oxygen was modelled to be constant during the simulation period.

5. Surface tension and gravity were not considered

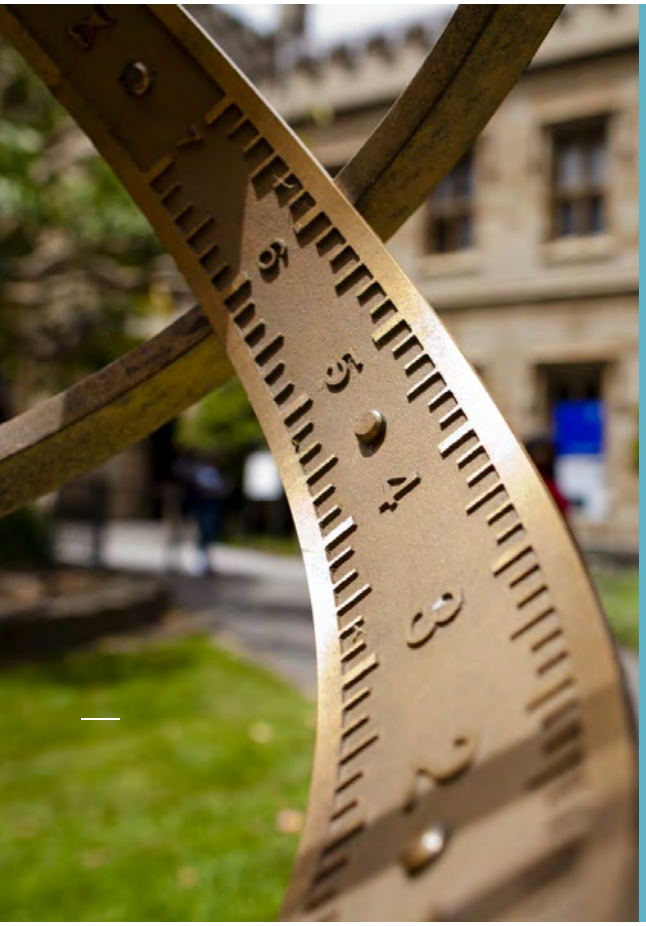

Results & Discussion

Case 1 – comparison of different rates and reactions of chalcopyrite dissolution

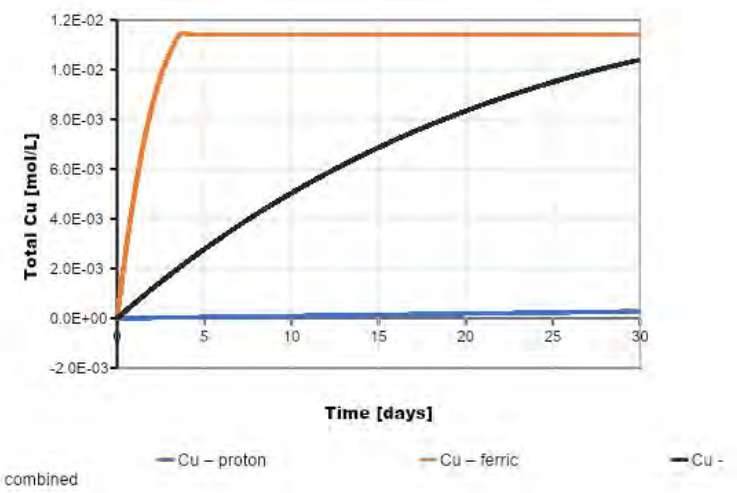

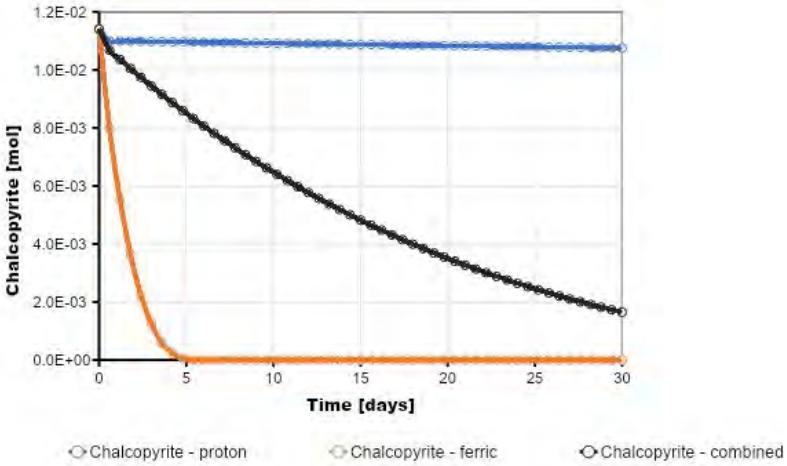

Ferric- promoted > Combined ferric-proton > Proton-promoted

Case 1 – comparison of different rates and reactions of chalcopyrite dissolution

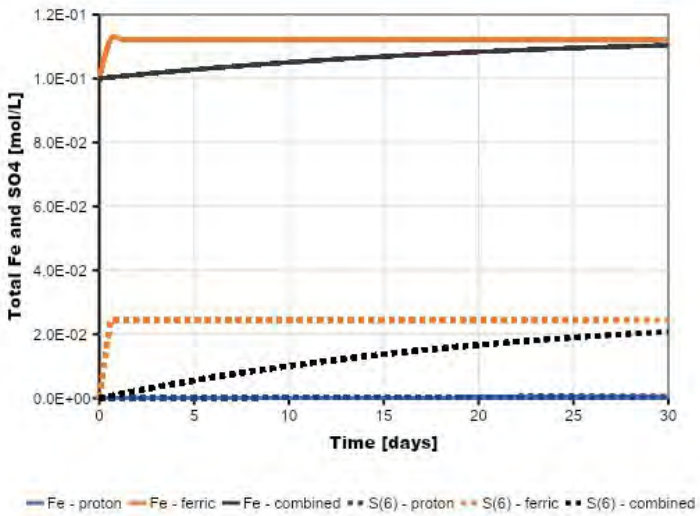

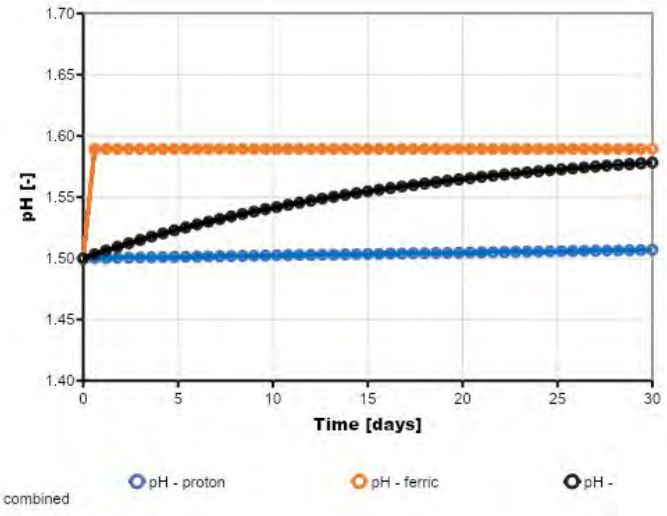

- Fe consumption/release controls chalcopyrite dissolution

- Sulphate release controls pH but H2S appears not to influence pH

Case 2 - Influence of gangue minerals on combined ferric-proton chalcopyrite dissolution

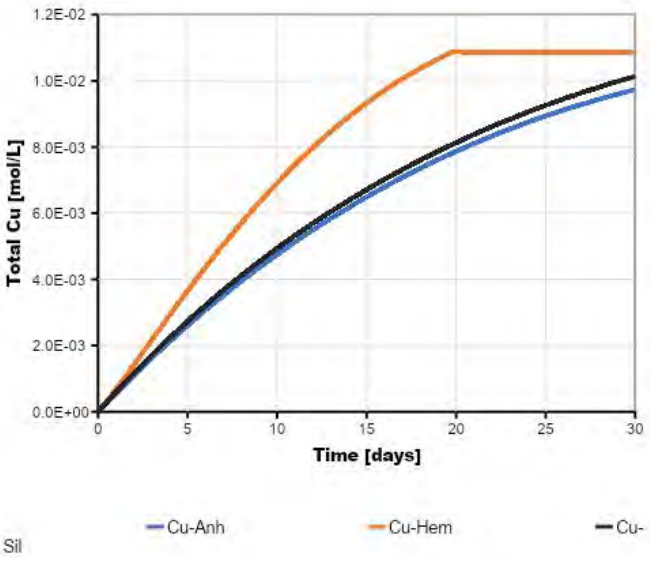

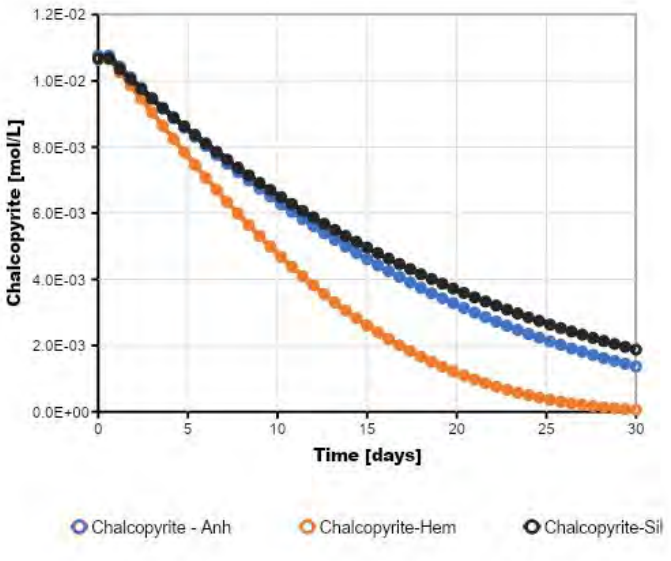

Hematite (Hem) > Silicate (Sil) > Anhydrite (Anh)

Hematite (Hem) > Anhydrite (Anh) > Silicate (Sil)

Case 2 - Influence of gangue minerals on combined ferric-proton chalcopyrite dissolution

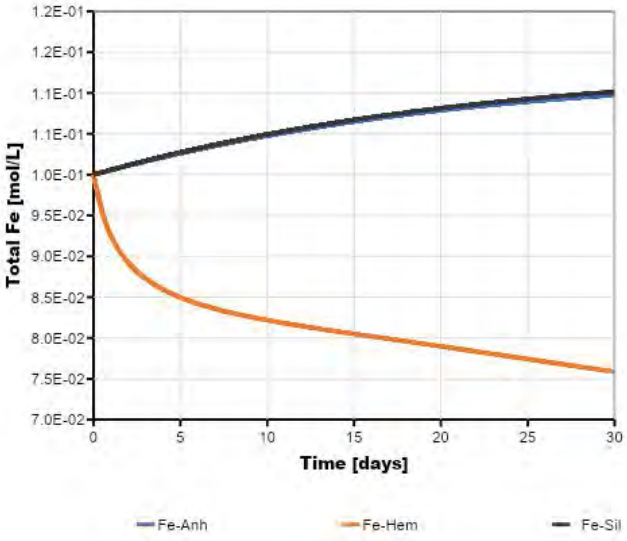

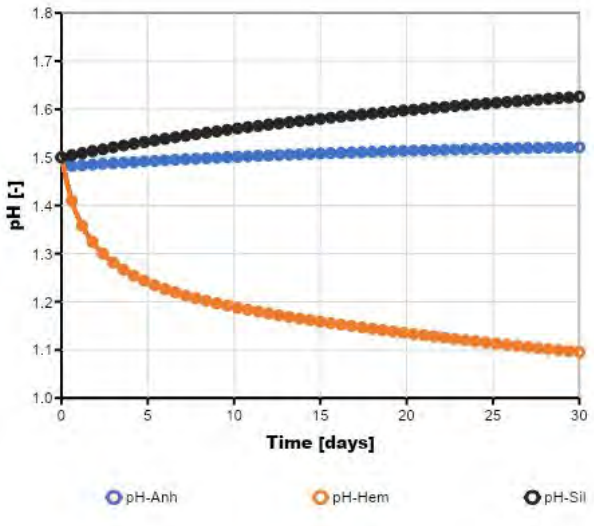

- Hematite dissolution releases Fe and hematite reprecipitation leads to pH decline

- Sulphate release increases pH. Possible occlusion of Cu by anhydrite

- Silicate dissolution consume protons

History Matching of Experimental Data (Role of surface area)

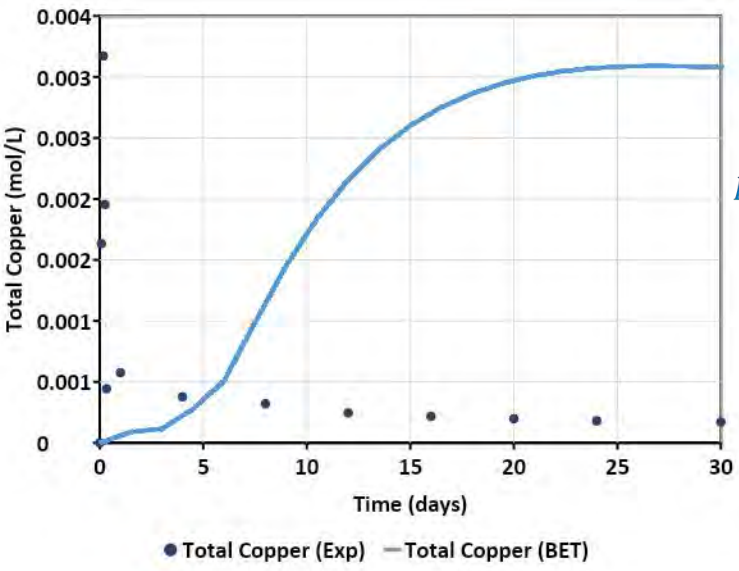

BET = EXTERNAL + INTERNAL SURFACE AREA

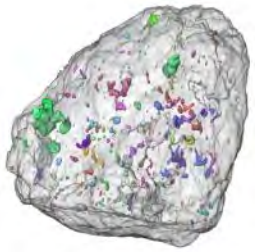

Coloured is copper mineral and grey is siliclastic gangue.

$$Rate, R_{(CP-D)t} = (r * A_{CP-D})$$

$$A_{CP-D} = S_{A_i}.M_{wi}.n_i$$

Where, $A_{CP-D}[\frac{m^2}{g}]$ is the reactive grain surface area of a specific mineral, $S_{A_i} = S_{A\_BET}\ [\frac{m^2}{g}]$ is the overall BET specific surface area that was experimentally determined, r is the dissolution rate constant , n_i is the mole fraction of a specific mineral individual mineral phase in the total rock ore, $M_{wi}\ [\frac{mol}{g}]$ is the molecular weight of a specific mineral

Ansah et al 2022

History Matching of Experimental Data

$$Rate, R_{(CP-D)t} = (r * A_{CP-D})$$

$$A_{CP-D} = S_{A_i}.M_{wi}.n_i.f$$

Where, $A_{CP-D}[\frac{m^2}{g}]$ is the reactive grain surface area of a specific mineral, $S_{A_i} = S_{A\_BET}\ [\frac{m^2}{g}]$ is the overall BET specific surface area that was experimentally determined, r is the dissolution rate constant, n_i is the mole fraction of a specific mineral individual mineral phase in the total rock ore, $M_{wi}\ [\frac{mol}{g}]$ is the molecular weight of a specific mineral and f [−] is the surface reactivity factor

Ansah et al 2022

Case 3 - Modelling the growth of a secondary mineral related to the reactive surface of the primary mineral

$$Rate, R_{(CP-D)t} = (r * A_{CP-D})$$

$$A_{CP-D(t)} = A_{CP(0)} * [n_d - K_p(n_p)^{\rho}]$$

$$A_{CP-D(t)} \geq 0$$

The overall precipitation rate coupled to the chalcopyrite dissolution rate

1. Surface-passivate modelling (SPM + TST)

$$A_{CP-D(t)} = A_{CP(0)} * (n_d)^{\rho}$$

The overall precipitation rate not coupled to the chalcopyrite dissolution rate

2. No surface-passivate modelling (TST)

Here, $A_{CP(0)}$ [m^2/mol] is the original chalcopyrite mineral specific surface, n_p [mol] is the amount of precipitated mineral, ρ [-] is a sphericity factor (assumed to be 0.67 for uniformly dissolving spheres, n_d [mol] is the amount of dissolving mineral remaining, and K_p [-] is a proportionality factor modifying the amount of precipitate in contact with dissolving mineral

SPM – surface passivate model; TST – transition state theory

Case 3 - Modelling the growth of a secondary mineral related to the reactive surface of the primary mineral

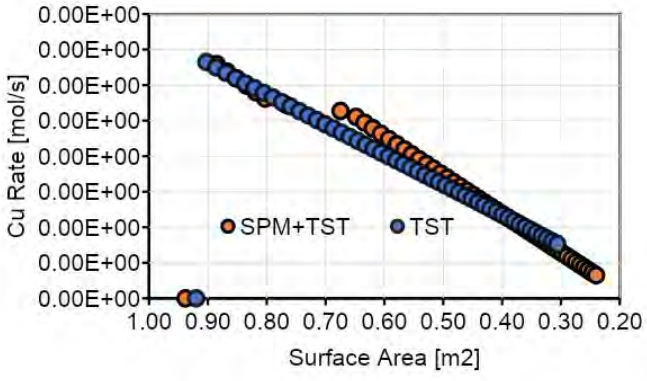

1. With SPM, there is a further decline in the Cu release rate as the surface area of the chalcopyrite is further reduced by the precipitated jarosite.

2. Considering SPM, there is less copper release than a model where this was not accounted for.

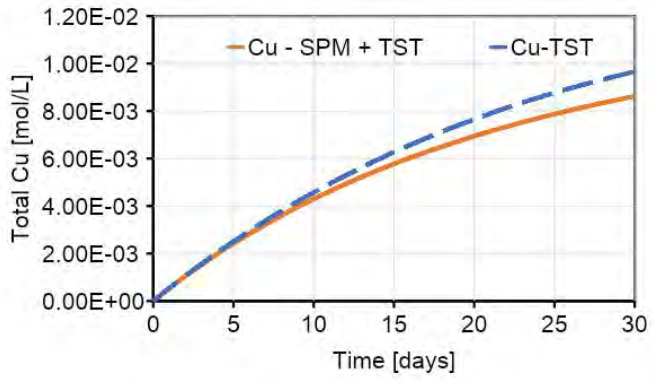

SPM – surface passivate model; TST – transition state theory (Ansah et al., 2023,…Minerals Engineering)

Case 3 - Influence of passivate (jarosite and gypsum) on combined ferric-proton chalcopyrite dissolution taking account into gangue minerals

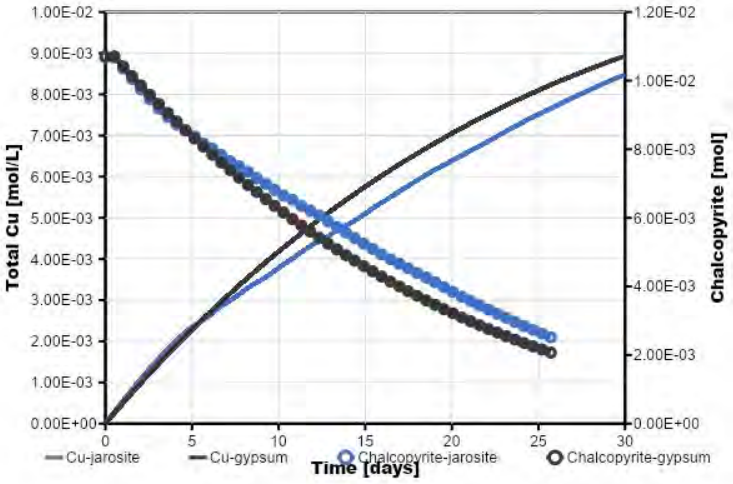

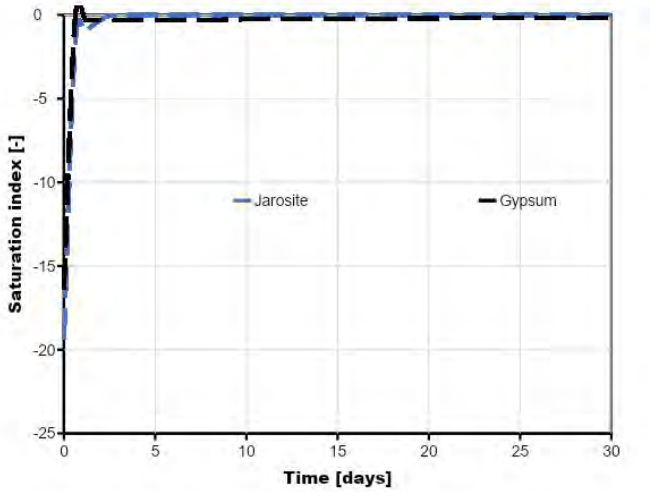

Gypsum > Jarosite

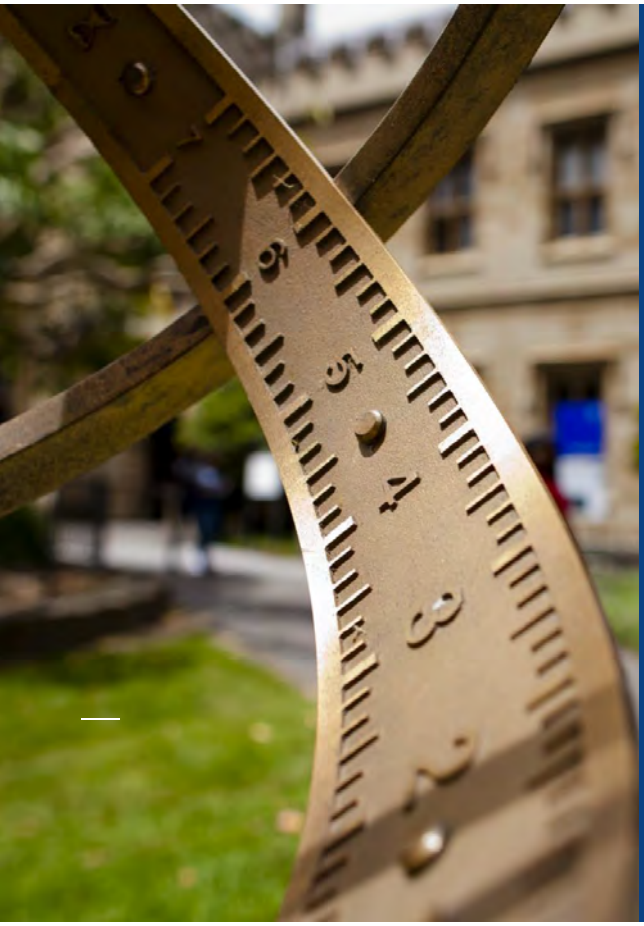

Limitation of the model: incongruent dissolution

Incongruent dissolution of chalcopyrite in acid-only

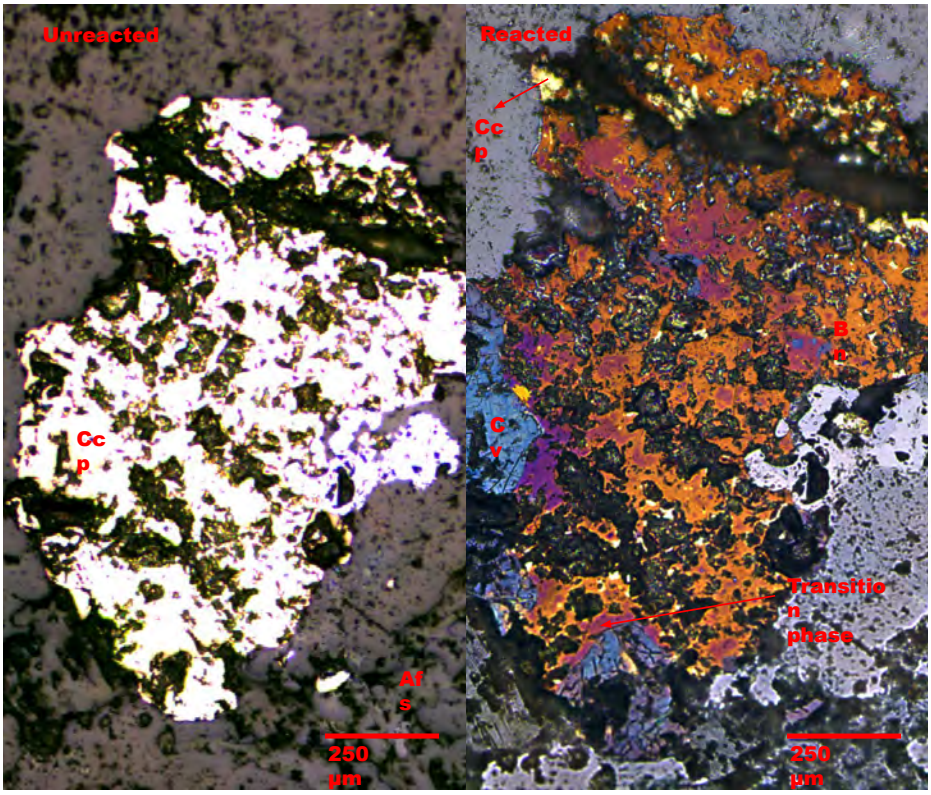

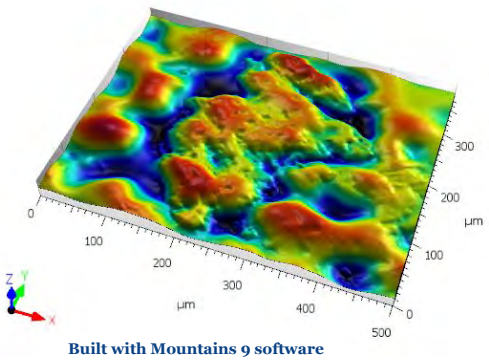

Precipitatio
n

Dissolutio
n

Afs – Alkaline feldspar (KAlSi3O8)
Ccp – chalcopyrite (CuFeS2)
Bn – bornite (Cu5FeS4)
Cv –covellite (CuS)

Leaching in acid-only

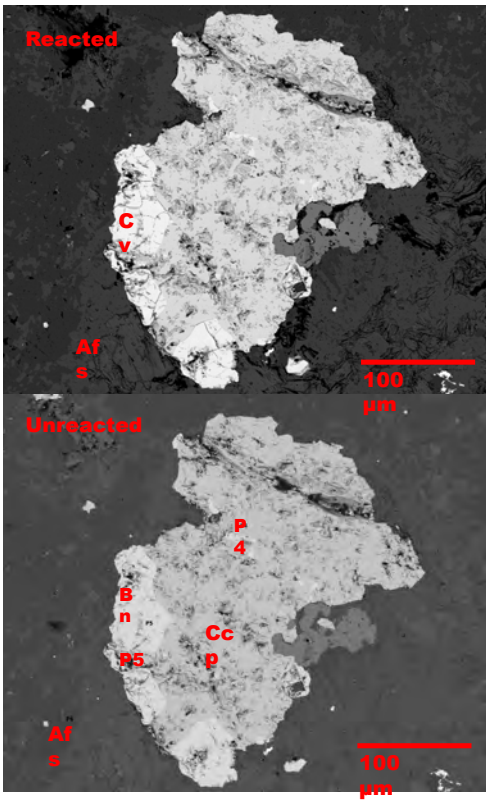

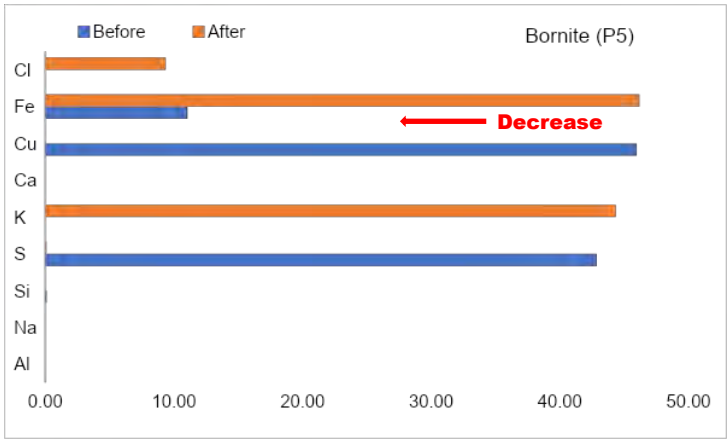

Negligible change

Afs – Alkaline feldspar (KAlSi3O8)
Ccp – chalcopyrite (CuFeS2)
Bn – bornite (Cu5FeS4)
Cv –covellite (CuS)

How to model Incongruent dissolution of chalcopyrite ???

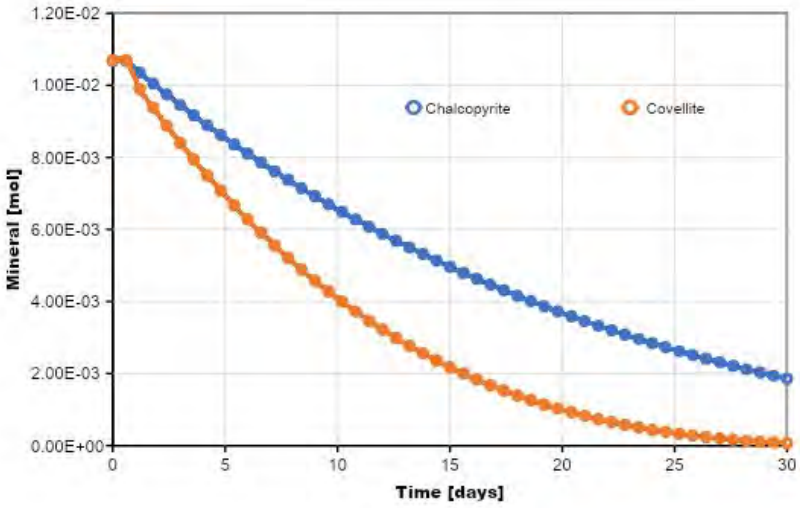

- Why does covellite precipitate, if it is highly undersaturated (~ -110) throughout the simulation?

- Why is the copper flux from chalcopyrite dissolution the highest when covellite (CuS) passivates the surface?

- Shouldn't we expect copper mobilised by chalcopyrite dissolution to precipitate as covellite and thereby reducing the dissolved copper concentration?

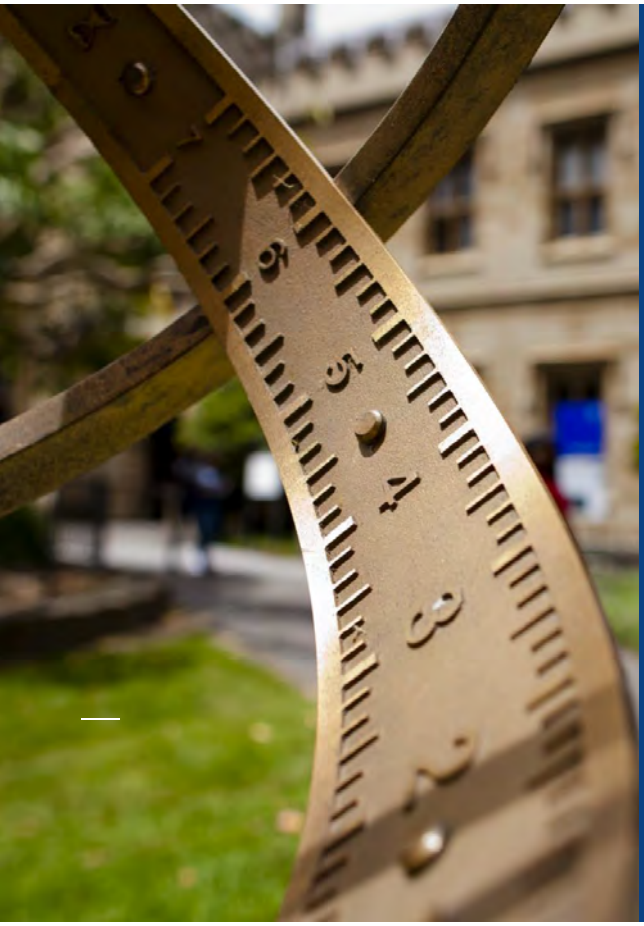

2. Limitation of the model: role of thickness and porosity of passivate layer

Passivation mechanism(s)

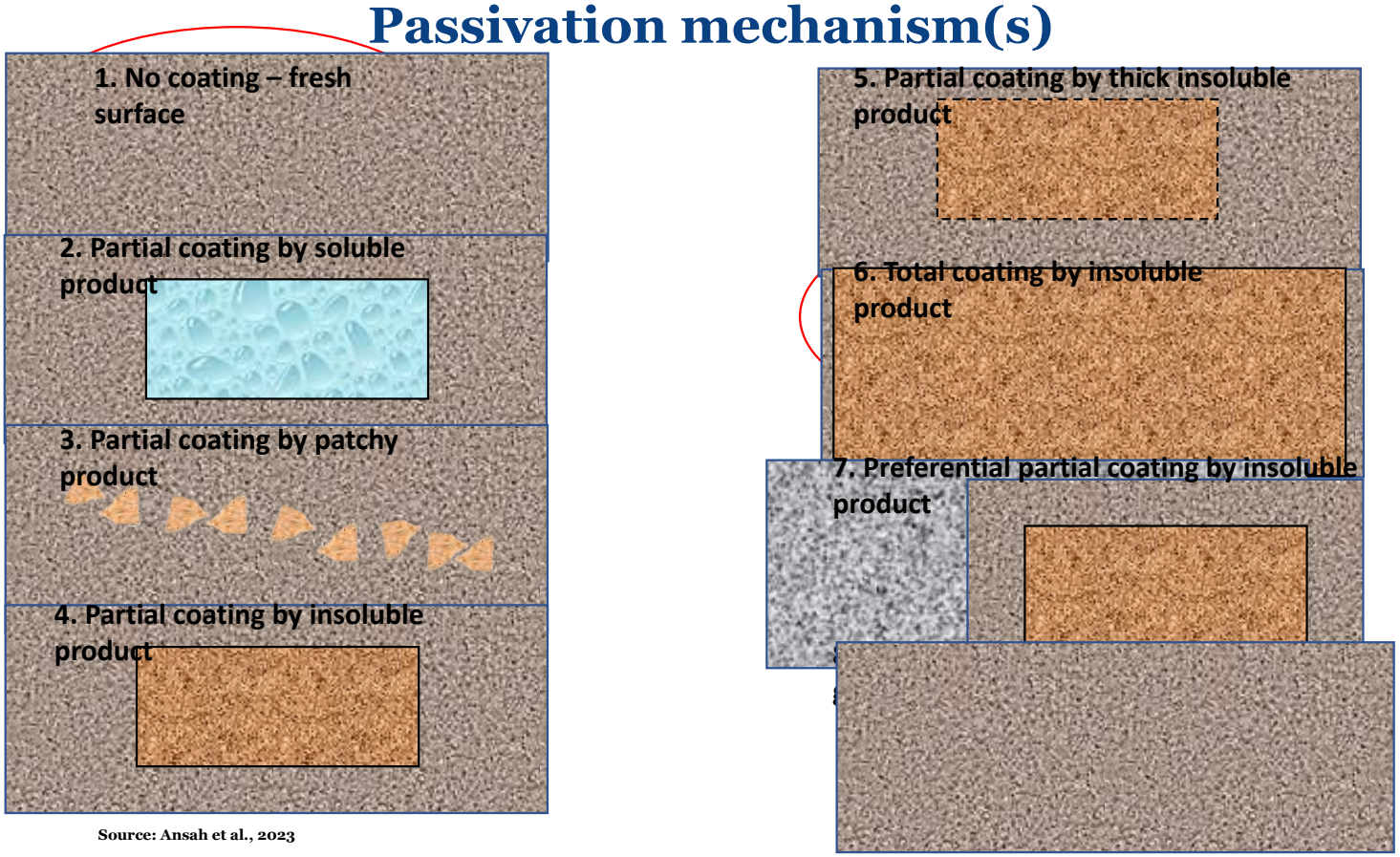

Source: Ansah et al., 2023

How to tackle passivation, where to look?

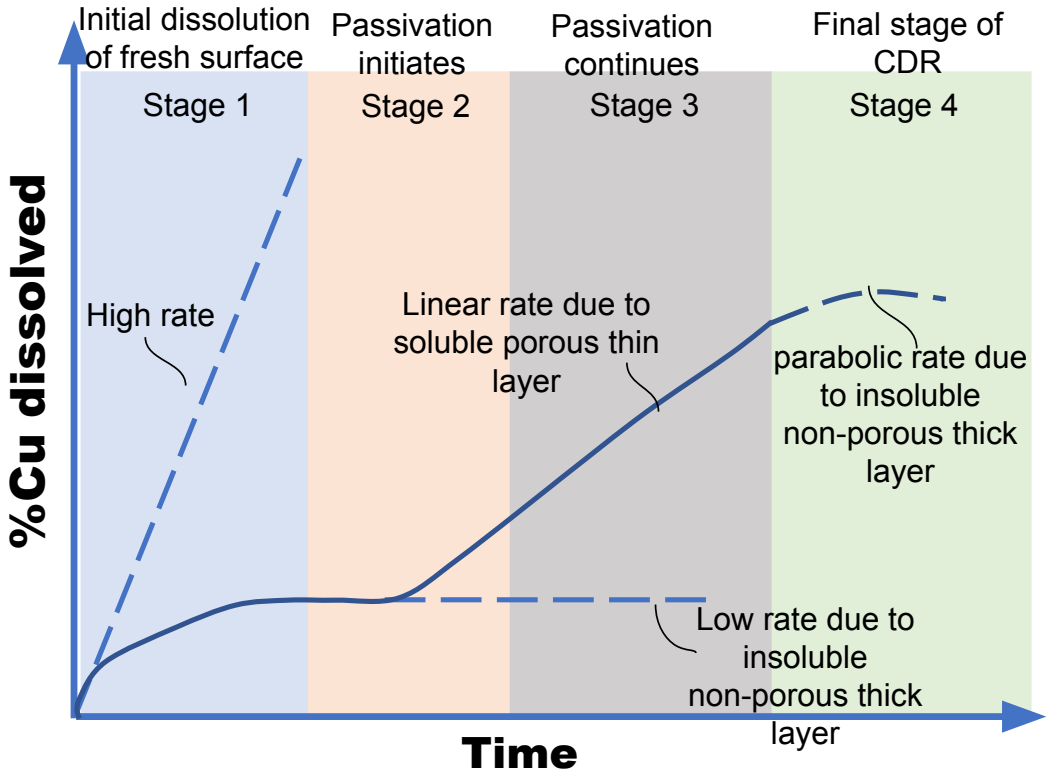

Edited after Klauber, 2008 and references therein

So, what...,?

1. Accurate representation of different rate laws and reaction mechanisms is important during modelling of chalcopyrite and gangues in heap leaching.

2. The mineral surface area is critical for modelling and understanding chalcopyrite leaching.

3. Need to consider the role of secondary minerals on the original surface area of a chalcopyrite during heap leach modelling.

4. Incongruent dissolution of chalcopyrite leading to residual Cu-S rich phase (e.g., covellite) remains a mystery to model.

5. Future models should consider porosity and thickness of passivate on chalcopyrite dissolution.

Ralf and all group members of Peter Cook CCS Center

TrACEES, MCPF, and SGEAS of Unimelb

THANK YOU (MEDAASE!)

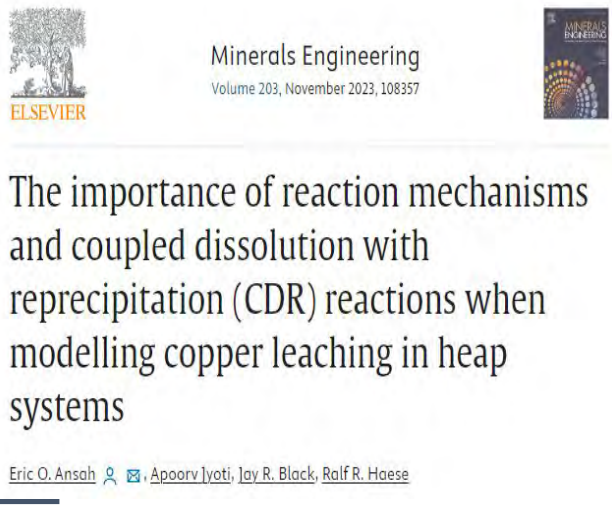

INTEGRATION OF HYDROMETALLURGY PROCESS AND MINERAL CARBONATION TECHNOLOGY

By

Yasunori Nozoe, [2]Sho Fujimoto, [2]Toru Matsuzawa

JGC Corporation, Japan
[2]JGC Japan Corporation, Japan

Presenter and Corresponding Author

Yasunori Nozoe
nozoe.yasunori@jgc.com

ABSTRACT

The metal smelting and refining field is facing a dilemma to satisfy the social demand to reduce carbon dioxide (CO_2) emissions while maintaining supply chains by fulfilling the increasing demand for metal resources, such as for batteries and magnetics, as high-grade mineral resources continue to become depleted. Regardless of the market requirements, the need to respond to such social demands cannot be ignored.
Carbon dioxide capture, usage and storage (CCUS) is one of the measures to reduce CO_2 emissions, and JGC has been developing its own technology by focusing on a CCUS using mineral carbonation (CO_2 mineralization).
CO_2 mineralization is a technology that reacts with and solidifies CO_2 by forming chemical compounds with calcium and magnesium (Ca and Mg) sources such as basic rocks. As to the methodology of the reaction, a high-pressure method is commonly known, but JGC has been focusing instead on a method at atmospheric pressure.
In the beginning, a CO_2 mineralization method using activated serpentine had been studied, however, a simplified economic study showed a negative result in terms of profitability due to its limited income based on carbon credits and magnesium carbonate sales revenue alone.
Conversely, in the field of nickel hydrometallurgy, acid leaching processes, such as high-pressure acid leach (HPAL), are attracting attention in recent years because the process produces nickel sulphate and mixed hydroxide precipitate (MHP) as the precursor materials of lithium-ion batteries (LiB) from nickel laterite ores. However, high-Mg ores have no affinity to the acid leaching process, as its Mg consumes the acid reagent and lowers the feasibility, therefore, high-Mg ores have not been actively processed but probably stockpiled at mine sites. JGC has developed a method to integrate the acid leaching process and CO_2 mineralization, which converts high-Mg ore into a nickel resource and reduces CO_2 emissions at the same time.
This paper introduces the abovementioned JGC's methodology and results of laboratory tests using actual nickel laterite ore samples and describes the improvement in a simplified economic study.

Keywords: carbon dioxide mineralization, sequestration, mineral carbonation, acid leach, nickel laterite ore

INTRODUCTION

CO_2 mineralization technology is a technology that fixes CO_2 as carbonate by reacting with calcium and magnesium, and sources of calcium and magnesium can be obtained from waste concrete, steel slag, coal ash, seawater, etc. While the most promising source is said to be basic rocks such as serpentine and olivine.
Conventionally, a method of activating serpentine by calcining, capturing CO_2 through sequestration, and crystallizing for storage had been proposed [(1)].

Serpentine dehydration:
$Mg_3Si_2O_5(OH)_4$ (s) . $(MgO)_3(SiO_2)_2$ (s) + $2H_2O$ (v)

Carbon dioxide gas dissolution:
CO_2 (g) + OH^- (aq) □ HCO_3^- (aq)

Magnesium dissolution:
$(MgO)_3(SiO_2)_2$ (s) + $6H^+$ (aq) □ 3 Mg^{2+} (aq) + $2SiO_2$ (s) + $3H_2O$ (l)

Crystallization:
$5Mg^{2+}$ (aq) + $4HCO_3^-$ (aq) +$6OH^-$ (aq) □ $Mg_4(CO_3)_4$ $(Mg(OH)_2)$ $4H_2O$ (s)

JGC investigated CO_2 mineralization by applying waste concrete, seawater, and basic rocks (serpentine and olivine) as sources of the calcium and magnesium and dissolving the calcium and magnesium from these sources by varying the reacting conditions from pressurized to atmospheric and from high temperature to ambient and established a method to sequestrate CO_2. Particularly, a method to mineralize CO_2 by dissolving Mg in basic rocks at atmospheric and ambient condition was established. Although the amount of magnesium extracted is small due to the lower partial pressure of CO_2 compared to the high-pressure method, it can be positioned as a method that is easy to conduct because the equipment cost is lower, and operation and maintenance are easier than high-pressure/high-temperature methods. Moreover, an improvement of magnesium dissolution was achieved by grinding the magnesium source in the reactor system continuously to renew the residual surface and to reveal the activated part of the magnesium source. The laboratory test result showed the improvement in the amount of magnesium dissolved, that is, the concentration of magnesium in the liquid, by approximately six times.

Figure 1: Improvement of Mg dissolution by grinding in the reactor system

Based on the laboratory test results using serpentine, the amounts of CO_2 mineralized and emitted were estimated. In this estimation, CO_2 emission was derived from energy consumption by assuming Natural Gas (NG) fuels and NG power generation. As shown in Figure 2 it was confirmed that the amount of CO_2 fixed for storage is expected to exceed the amount of CO_2 emission.

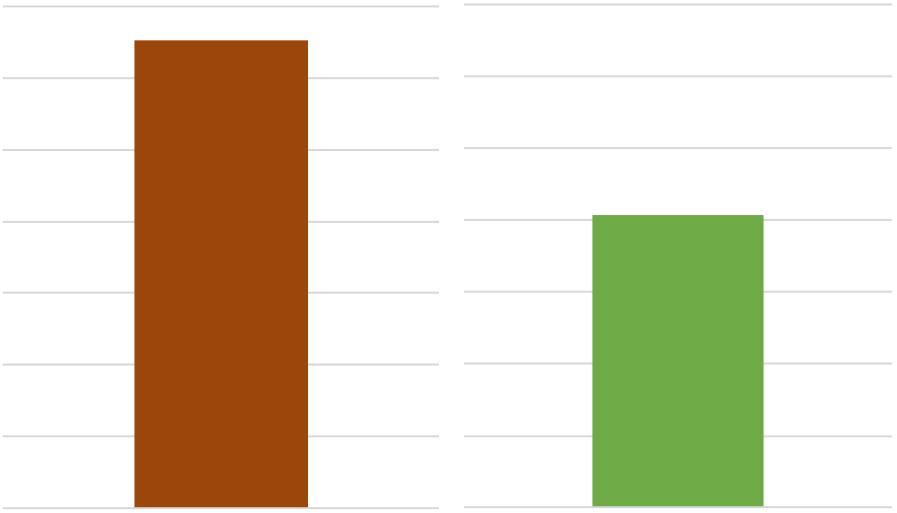

Figure 2: Balance of CO_2 fixation and emission based on lab tests using serpentine

Further to the above, the income from carbon credits was calculated from the net CO_2 fixation amount (CO_2 fixation amount - CO_2 emissions) and the unit price of carbon credits (assumed to be 150 USD/ton-CO_2) and compared with the operating costs calculated from the consumptions of heat and electrical power in the process. The unit prices of the heat and electrical power were assumed to be 3 USD/GJ and 0.1 USD/kWh, respectively. As shown in Figure 3, it was found that CO_2 mineralization using serpentine would not be feasible in terms of profitability.

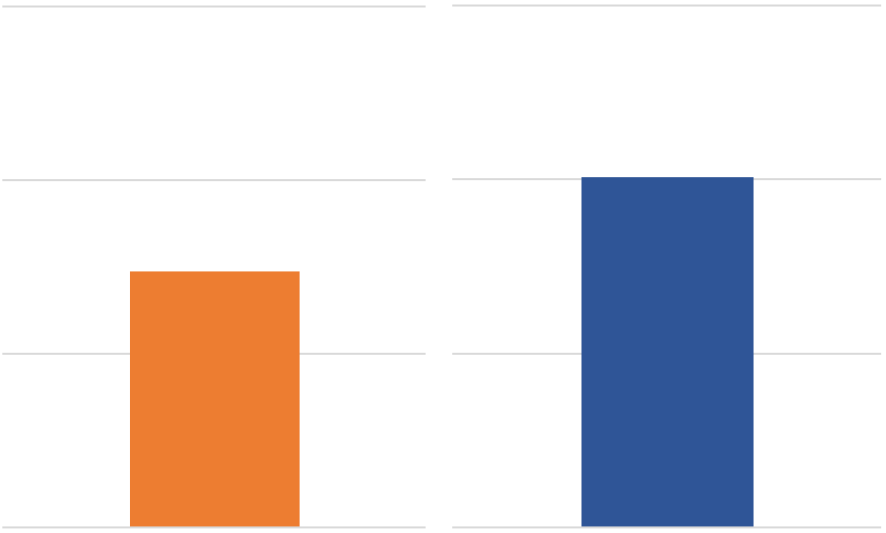

Figure 3: Income from carbon credit vs expenses for energies consumed in the process

JGC's idea to improve the economic feasibility of CO_2 mineralization is to integrate CO_2 mineralization technology with metallurgical processes. In addition to the fundamental benefits of not only reducing CO_2 emitted from the metallurgical processes, but also revenue from metal products and cost savings by sharing common facilities such as infrastructures and utilities, there are additional opportunities to convert low grade difficult-to-processing ores that are untapped and stockpiled at mine sites to processable ores, especially when looking at nickel acid leaching as a hydrometallurgical process. This is to say, in the acid leaching process, high-Mg ores are left untouched because the magnesium in the ore consumes the leaching agent

sulfuric acid, whereas carbonation processing removes the magnesium from the ore and as a result expands the amount of nickel resources that can be processed in an economically feasible way.
A schematic block flow diagram of the integration process is shown in Figure 4.

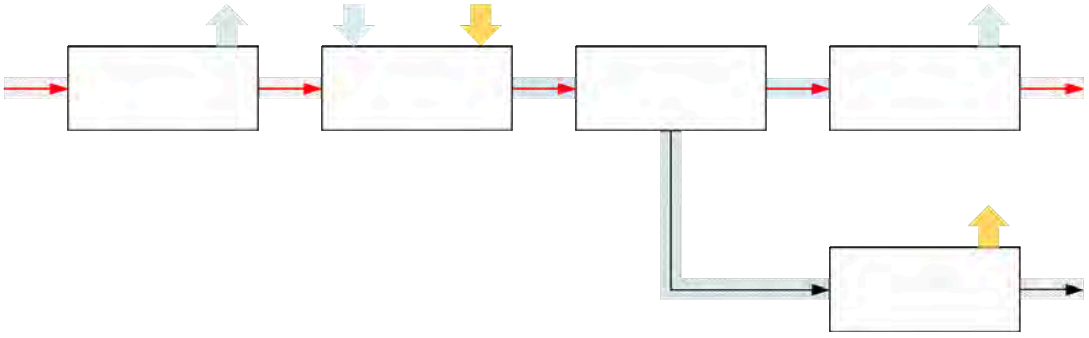

Figure 4: Integration of CO_2 mineralization and Ni acid leaching processes

Figure 5 shows a profile of a typical laterite deposit. Normally, an acid leaching process treats laterite mainly existing in the surface layer, and the nickel grade is at most about 1 wt%, but profitability is ensured because there is less magnesium, which consumes the leaching agent sulfuric acid. High-Mg ores have generally been processed using a pyrometallurgy/smelting method, which consumes a lot of energy, but the high nickel grade makes it profitable.

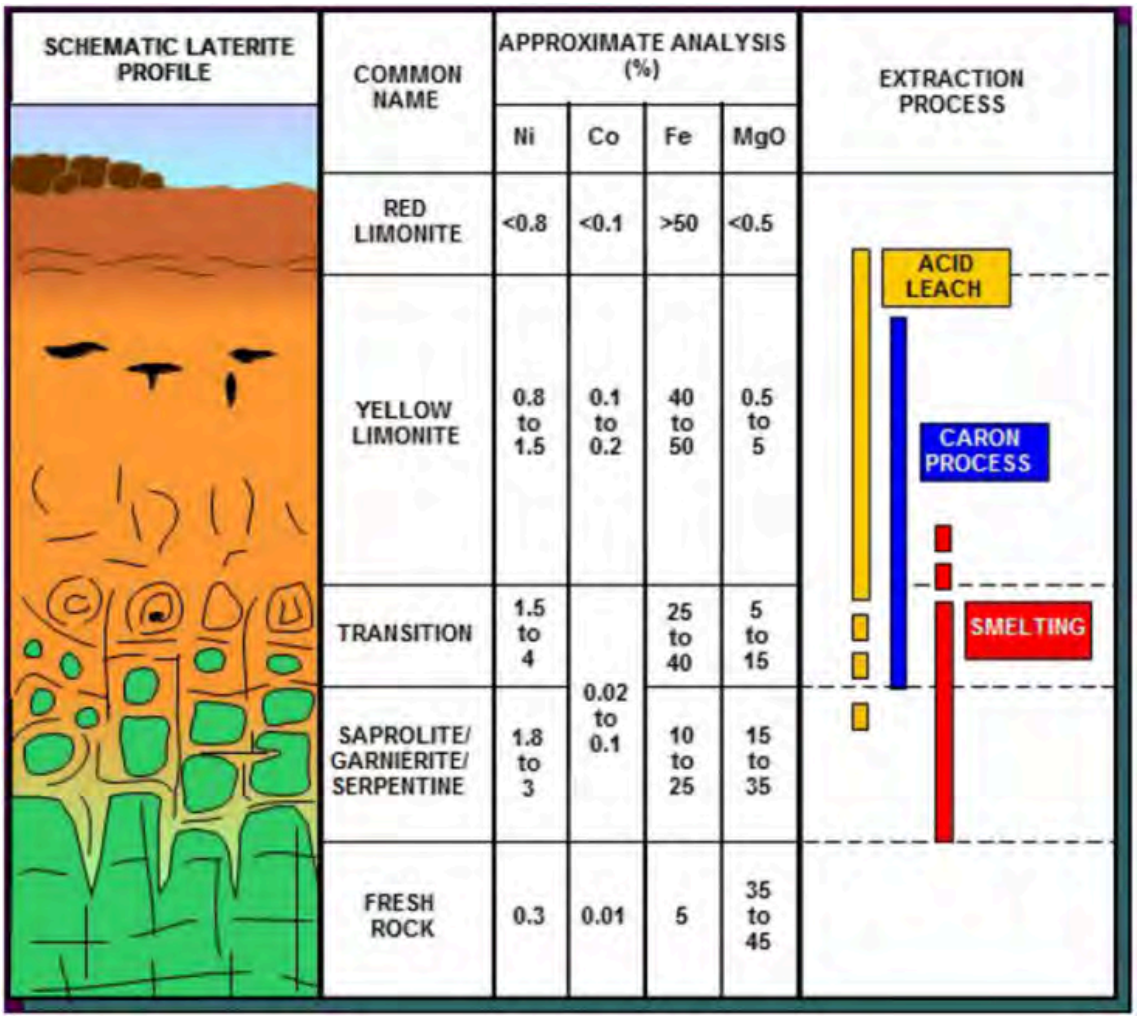

Figure 5: Schematic Laterite Profile (Elias 2002)

Assuming that a laterite ore with a nickel content of 1 wt% and a magnesium content of 20 wt% is used as a feedstock for an acid leaching process (HPAL, etc.), the cost impact of reducing magnesium in the ore and reducing CO_2 through CO_2 mineralization was estimated.
The magnesium in the ore consumes sulfuric acid in the leaching reactor, and at the downstream neutralization process with limestone it generates another CO_2.

$$MgO\ (s) + H_2SO_4\ (aq) \rightarrow MgSO_4\ (aq) + H_2O$$
$$MgSO_4\ (aq) + CaCO_3\ (s) \rightarrow MgO\ (s) + CaSO_4\ (s) + CO_2\ (g)$$

The amount of CO_2 generated when ore containing 20 wt% of magnesium is processed in an acid leaching plant was estimated, and the carbon credit for reducing magnesium in the ore through CO_2 mineralization treatment was calculated based on the amount of magnesium in the residue after mineralization. In addition, the amount of sulfuric acid consumed by the acid leaching plant from magnesium remaining in the residue without being extracted during the CO_2 mineralization process was estimated and compared it in a graph along with carbon credits.
In this study, the carbon credit was assumed to be 150 US$/t-$CO_2$ and the sulfuric acid cost was 150 US$/t-Acid (see the estimation conditions in Table 1 below).

Table 1: Assumptions for economical study

Mg content in the ore	20 wt%
Free acid at the outlet of acid leaching	50 g/L
Carbon credit	150 US$/t-$CO_2$
Sulfuric acid cost	150 US$/t-Acid

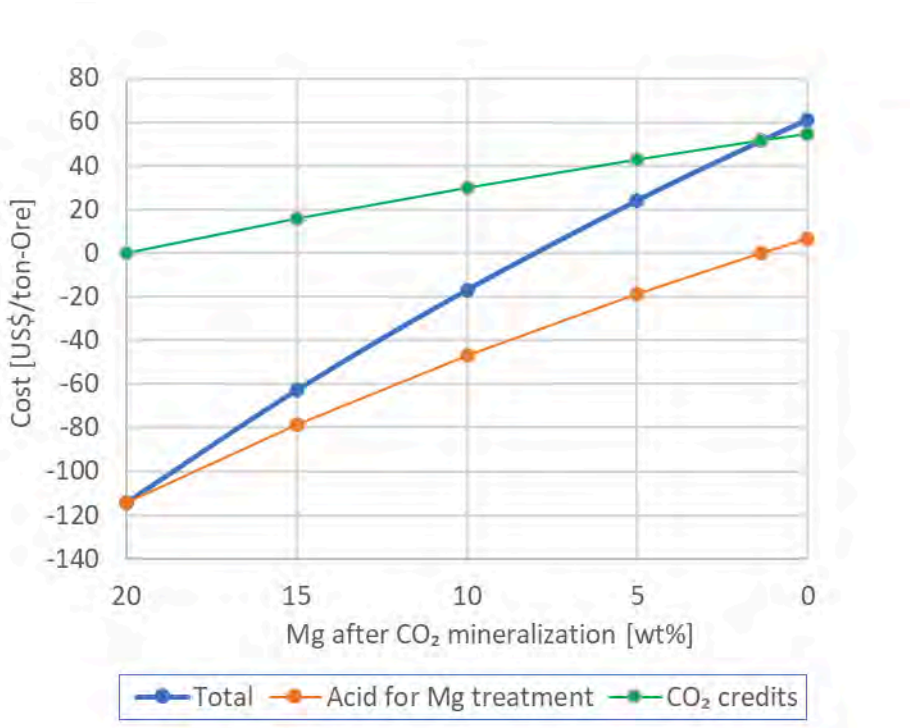

Figure 6: Economical study for carbon credit and acid consumption by magnesium

When ore feedstock containing 20 wt% of magnesium is processed as is in the acid leaching plant without mineralization, the sulfuric acid consumed by the magnesium in the ore is approximately equivalent to 115 US$/ton-Ore. Reducing magnesium in the ore through CO_2 mineralization reduces sulfuric acid consumption in the acid leaching plant and increases carbon credits simultaneously. Reducing the residual magnesium in the ore after CO_2 mineralization to 8 wt% offsets the cost of sulfuric acid consumed by residual magnesium and the carbon credits. If the residual magnesium in the ore after CO_2 mineralization treatment is further reduced, the economic efficiency of CO_2 mineralization becomes superior.

EXPERIMENTAL APPARATUS / TEST CONDITIONS

High-Mg nickel laterite ores were collected from various areas and subjected to laboratory tests.
In this laboratory test, calcined ore, water, and alumina balls were placed in a separable flask with a capacity of 2000 ml, and CO_2 was supplied while stirring with an agitator to dissolve magnesium. A photo of the equipment used in the laboratory test and a photo of the ore sample used in the test are shown in Figure 7, and the composition of the ore is shown in Table 2.

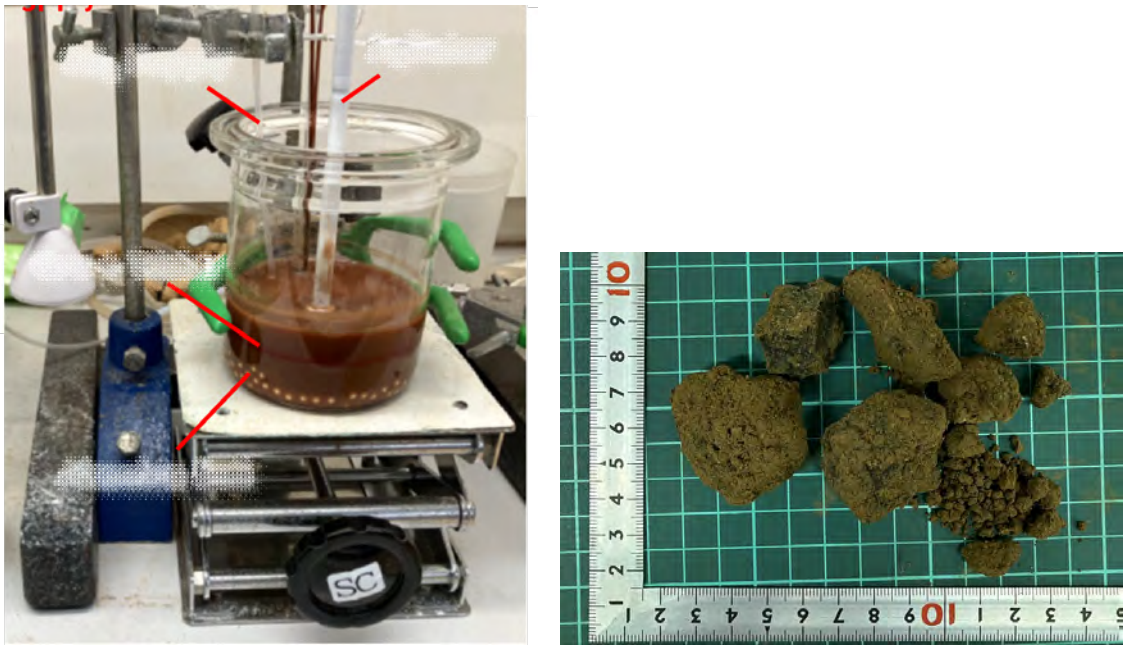

Figure 7: Experimental apparatus (left) and ore sample (right)

Table 2: Composition of ore sample

Composition	[wt%]
Ni	0.90
Fe	6.82
Co	0.02
Mg	22.4
Si	19.7
C	1.66
S	0.01
Al	0.08
Ca	0.01

The test procedure is summarized in below Table 3.

Table 3: Test Procedure

Comminution	The ore sample was crushed to obtain particles under 150 μm.
Calcination	Calcine the ore at 500 – 700° C for 30 minutes using muffle furnace.
Magnesium dissolution	Calcined ore, water, and alumina balls were put in the flask, and CO_2 gas was supplied while stirring with the agitator to dissolve magnesium.
Crystallization	After magnesium dissolvement, residues were removed from Mg dissolved solution. Then crystallize magnesium carbonate by air bleeding to the solution.

In the magnesium dissolving process, JGC's unique method (patent pending) to grind the ores in the reactor system was simulated by stirring the ore slurry together with alumina balls, that is, allowing the reaction to

occur while renewing the residual surface and exposing the activated part of the calcined ore through abrasion.
In the past laboratory test result using serpentine showed the improvement in the amount of magnesium dissolved, that is, the concentration of magnesium in the liquid, by approximately six times. (See Figure 1)

TEST RESULTS

Calcination

The image of weight loss observed in the results of TG (Thermogravimetry) for laterite ore is shown in Figure 8. Similar to serpentine, a significant weight loss was observed above 500° C, which is considered to be due to the removal of crystal water in the ore. Based on the TG results, the calcining temperature was set at 500-700° C.

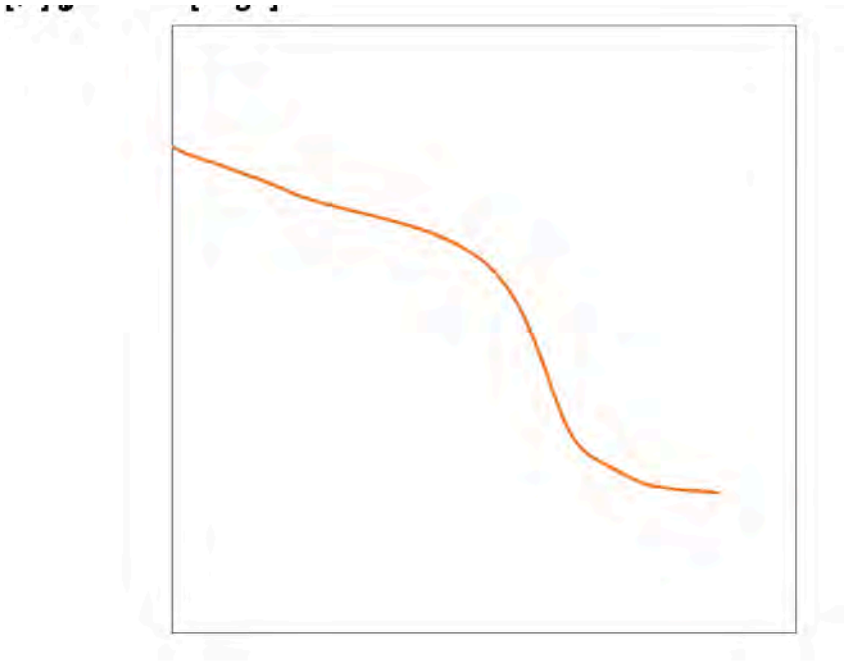

Figure 8: TG trend in ore sample calcination

Magnesium dissolution

One of the results of changes in magnesium concentration in the liquid during the magnesium dissolution tests is shown in Figure 9. Although the final magnesium concentration differed depending on the test conditions, there was a tendency for the magnesium concentration to reach a plateau in about 2 hours under most conditions. Furthermore, it has been confirmed that nickel loss from the ore into the magnesium carbonate solution was negligible.

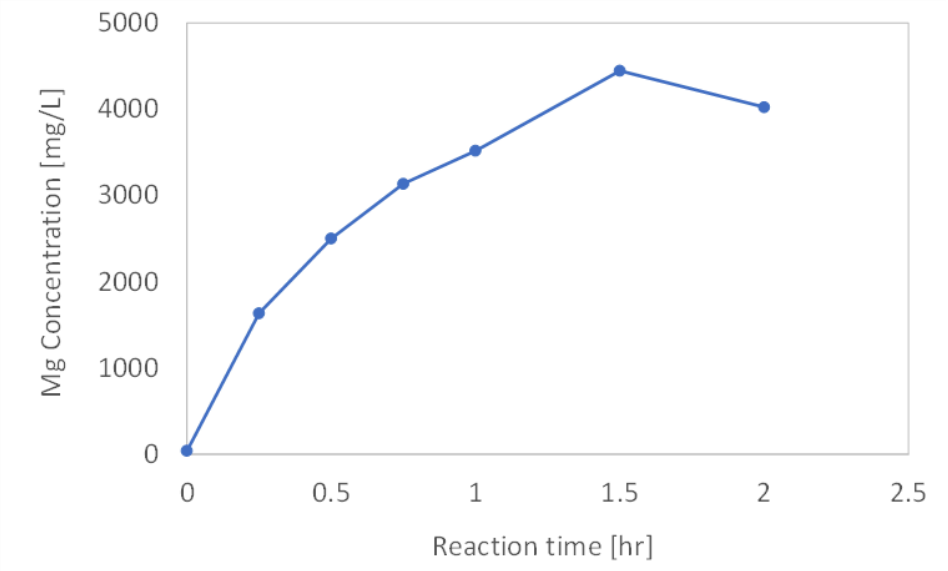

Figure 9: Magnesium concentration in the dissolution test

Crystallization

A photograph and SEM (Scanning Electron Microscope) image of magnesium carbonate obtained from the crystallization test are shown in Figure 10. White crystals with a needle-like structure were obtained.

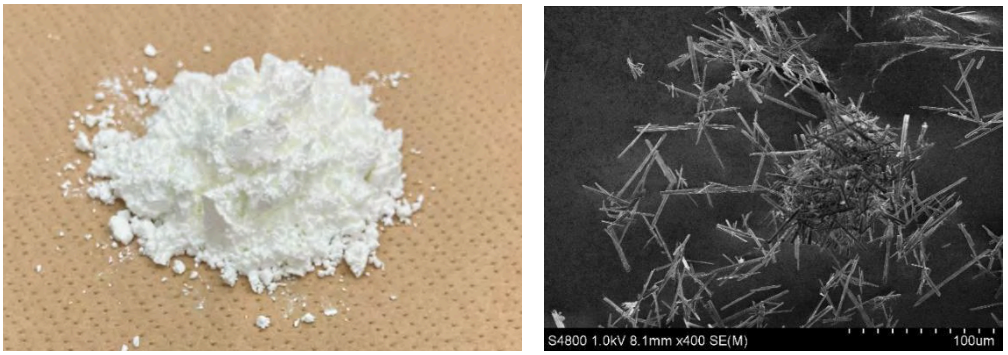

Figure 10: Photo (left) and SEM image (right) of magnesium carbonate obtained from crystallization

The results of XRD analysis for the obtained crystallized carbonate are shown in Figure 11. The XRD results showed that there were no sharp peaks, and it was difficult to identify the crystallized substances by XRD. Nesquehonite ($MgCO_3 \cdot 3H_2O$), Hydromagnesite ($Mg_5(CO_3)_4(OH)_2 \cdot 4H_2O$) and Dypingite ($Mg_5(CO_3)_4(OH)_2 \cdot 5H_2O$) are known as Mg-$CO_2$-$H_2O$ type magnesium carbonate[(2)]. It has also been reported that amorphous magnesium carbonate is produced as a precursor of magnesium carbonate hydrate[(2)].
To identify the crystallized material, TG analysis of the crystallized material was performed, and the results are shown in Figure 12. Since it matches well with the TG trend of the reagent Hydromagnesite, the crystallized product is considered to be Hydromagnesite.

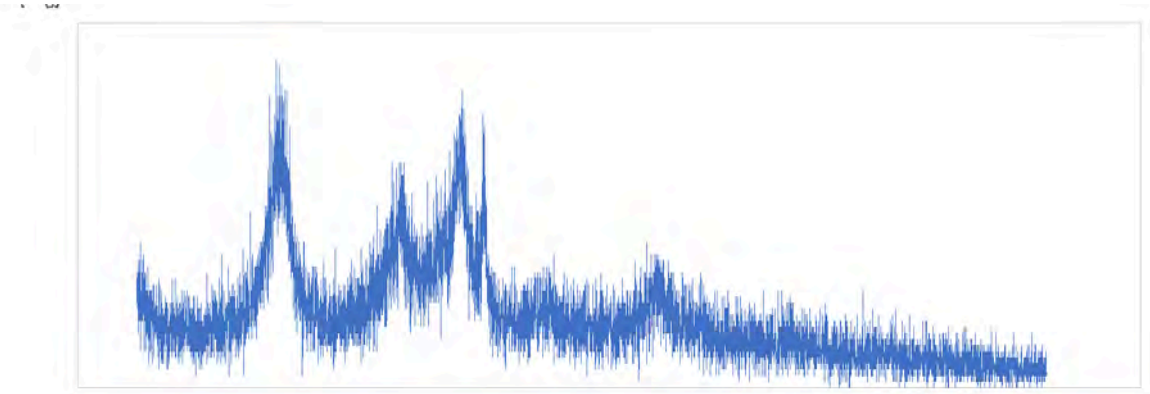

Figure 11: XRD analysis of crystallized material

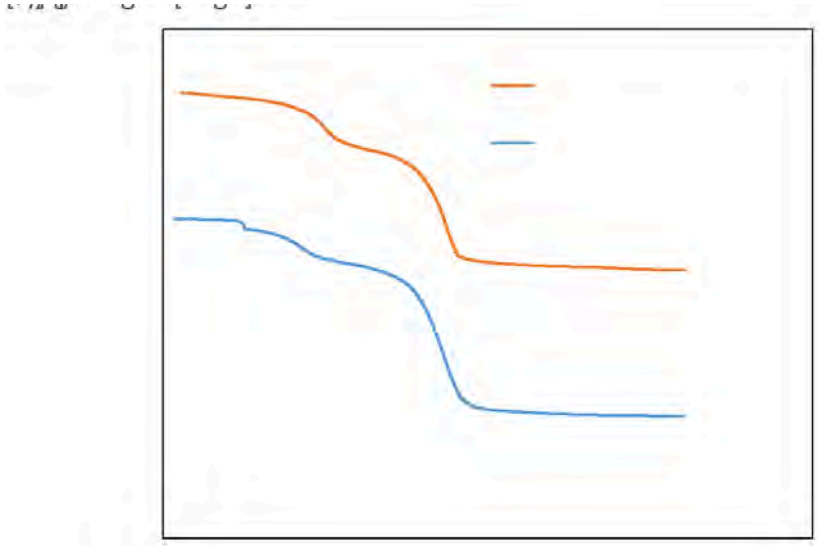

Figure 12: TG analysis of crystallized material

Transition of ores/residues structures through calcination to magnesium dissolution

Figure 13 shows SEM images of the ore samples, calcined ores and residues after magnesium dissolution for the past serpentine test and laterite ore test. Corresponding specific surface areas are shown in Table 4, where measurement of the surface areas SA are shown in the left column and calculations based on the equation (1) – a calculation of the surface areas Sω based on the particle size distributions by assuming all the particles being spherical bodies - are shown in the right column.

$$S_\omega = \frac{\sum n_i d_i^3}{\sum n_i d_i^2} \quad (1)$$

ni : number of particles sized *di*

ρ : density

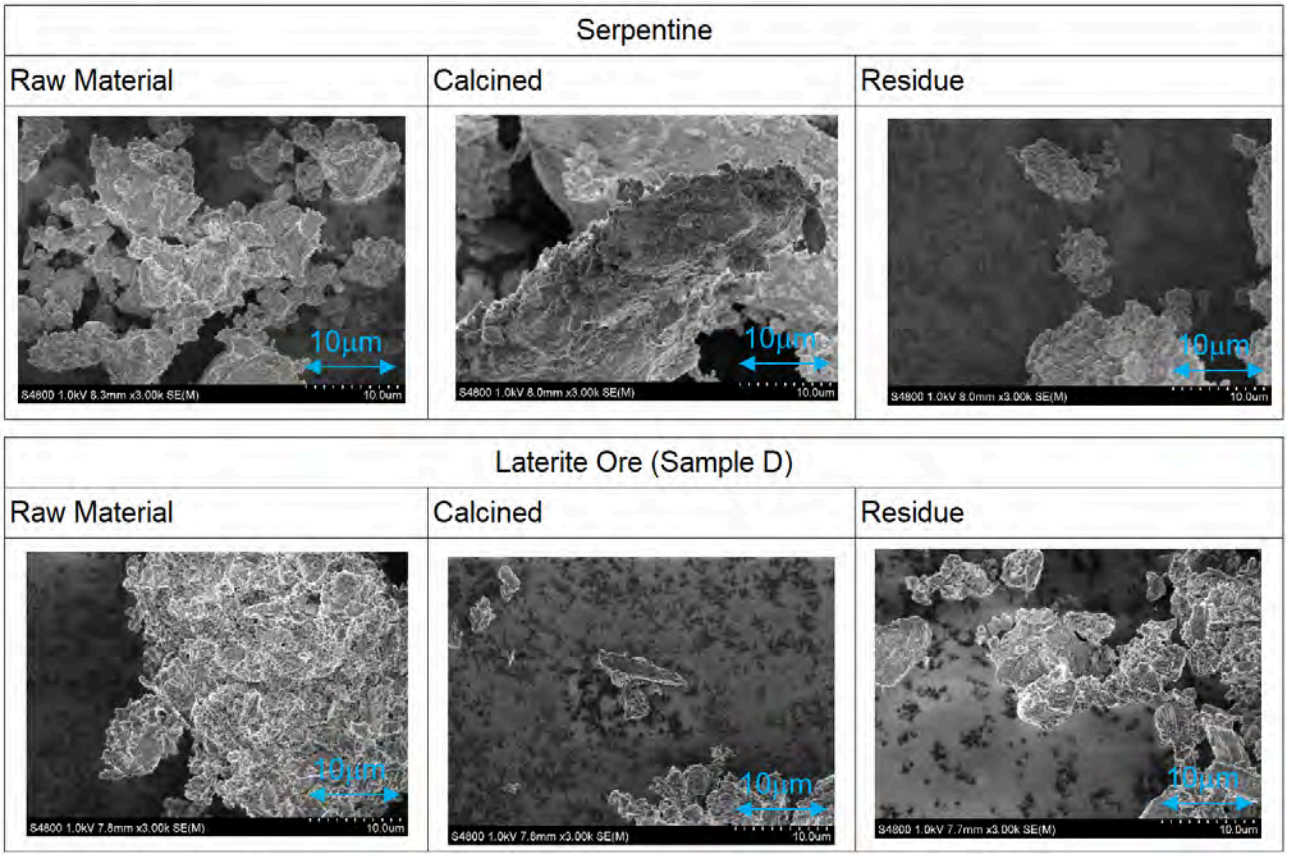

Figure 13: SEM Images of ore samples, calcined ores and residues

Table 4: Surface Areas of ore samples, calcined ores and residues

	Measured Surface Area: SA(m^2/g)		Calculated Surface Area: S_ω(m^2/g)	
	Serpentine	Laterite Ore	Serpentine	Laterite Ore
Raw Ore	17	127	1.58	0.03
Calcined	34	110	1.44	0.31
Residue	81	234	0.97	1.27

From the SEM images and specific surface areas, it was found that the surfaces of all these solid contents were porous, and the surface areas increased due to the process through calcination and magnesium dissolution reaction. It can be assumed that through calcining and Mg dissolution process, the surface of the ores would become porous as hydroxides and magnesium compounds being removed from the structures.

The SA and Sω of the serpentine represent such a phenomenon (SA increased by five times while Sω maintained and even reduced a bit).

When comparing the serpentine and the laterite ore, it is presumed that the laterite ore (raw ore, calcined and residues) were more porous, but increase in SA through the process was relatively low while Sω increased considerably. This is to say, laterite ore may remain with a potential to increase in porousness, i.e., to increase activated parts.

ECONOMIC STUDY

Study conditions/assumptions

Based on the laboratory test results of CO_2 mineralization using nickel laterite ore with a magnesium content of 22 wt% and assumptions derived from the laboratory test results, the amount of CO_2 fixed in the mineralization process and the power and heat consumptions to operate the facility were estimated. The energy and heat consumptions were converted into CO_2 emissions using the specific CO_2 emissions

intensity for LNG fuels and LNG power generations. Table 5 below summarizes the estimation conditions for the study.

Table 5: Conditions/assumptions for economical study

Mg content in the ore	22 wt%
Moisture content in the ore	20 wt%
Rate of mineralized CO_2	83 %
Mg utilization (dissolution) rate	41 %
CO_2 emissions intensity	
Electrical power	0.4 kg-CO_2/kWh (NG power)
Heat	50 kg-CO_2/GJ (NG fuel)

Study result

Comparing the amount of CO_2 fixed in the mineralization process and the equivalent amount of CO_2 emissions required to operate the mineralization facility shown in Figure 14 below, the amount of CO_2 fixed well exceeds the amount of CO_2 emissions.
Most of CO_2 emissions come from energy sources such as calcining heat (including free water drying) and crystallization energy, and it is possible that a large part of them can be reduced by using green electricity and green fuel.

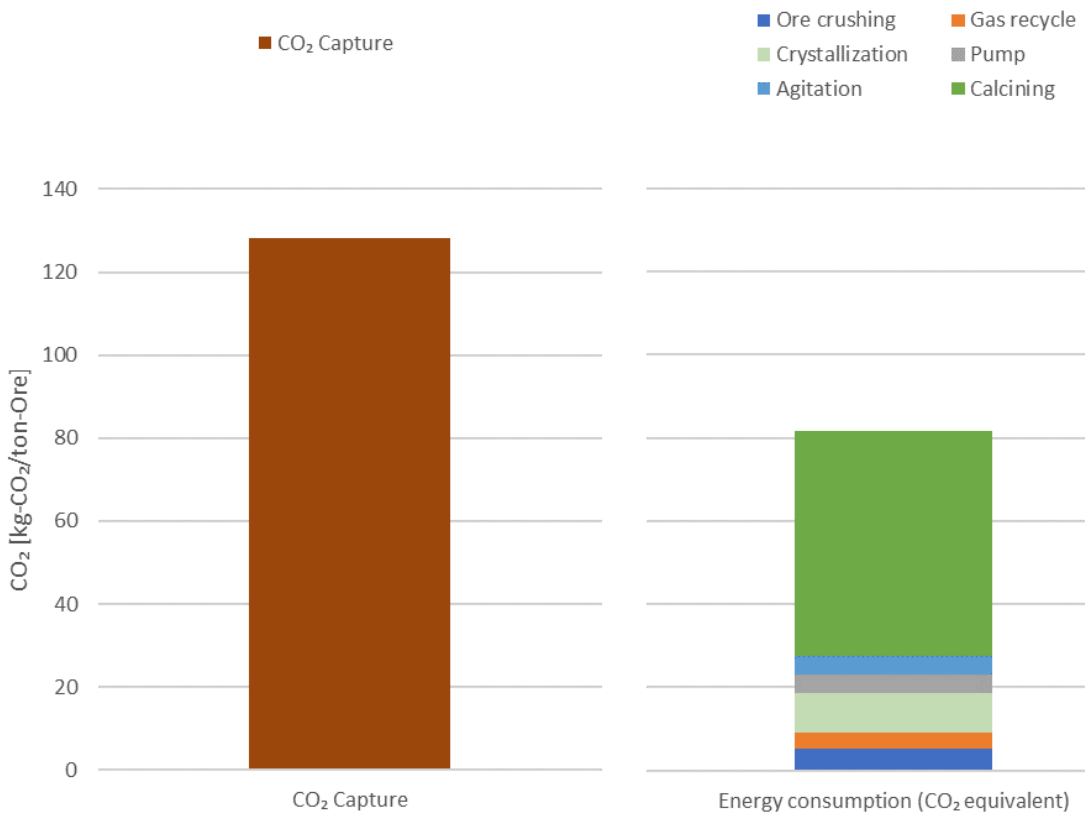

Figure 14: Comparison of CO_2 fixed vs emitted as energies consumed in the mineralization process

The test results using the actual laterite ores showed above explains that the utilization (dissolution) rate of magnesium in the mineralization process is not high, and the magnesium remaining in the residue consumes sulfuric acid in the acid leaching process and generates CO_2 in the neutralization process. This has not resulted in a significant reduction in CO_2 emissions.
If high-Mg ores can be converted to ores processable in the acid leaching method, it is expected that the range of ore resources will expand and production of nickel and cobalt will increase, and the profitability of CO_2 mineralization will be improved.
Furthermore, by optimizing the magnesium concentration in the feedstock of nickel acid leaching process and the operating conditions of the mineralization process in accordance with the properties of the nickel

laterite ores, e.g., magnesium contents, it is expected to improve the magnesium dissolution rate and reduce the energy consumption.

DISCUSSION

According to the test results and economic study results, although the effect of removing magnesium from the high-Mg ore was observed similarly with serpentine, the current level of magnesium utilization (dissolution) is only about 40%, whereas the magnesium remaining in the residue will consume the leaching agent in the acid leaching process and generate another CO_2 emission in the neutralization process at the downstream.
Therefore, it is necessary to reduce the magnesium in the residue before feeding to acid leaching process as much as possible. As a guideline, when CO_2 mineralization is applied to 20 wt%-Mg ore, if the magnesium remaining in the residue could be reduced to about 8 wt%, that is, the amount of magnesium dissolved can be increased to about 60%, the integration process of CO_2 mineralization and acid leaching technology reduces overall CO_2 emission.
Figure 15 shows a simple calculation of the overall CO_2 emissions when blending the residue from CO_2 mineralization of 20 wt%-Mg ore with Mg-free nickel laterite ore. As discussed above, the magnesium utilization (dissolution) rate directly dominates the effectiveness of CO_2 emission or reduction, and the effectiveness in whichever emission or reduction is eased off by ore blending with CO_2 mineralization residue.

It is also necessary to consider reducing the energy required for mineralization, including the calcination process, and supplying the energies from sources other than fossil fuels.

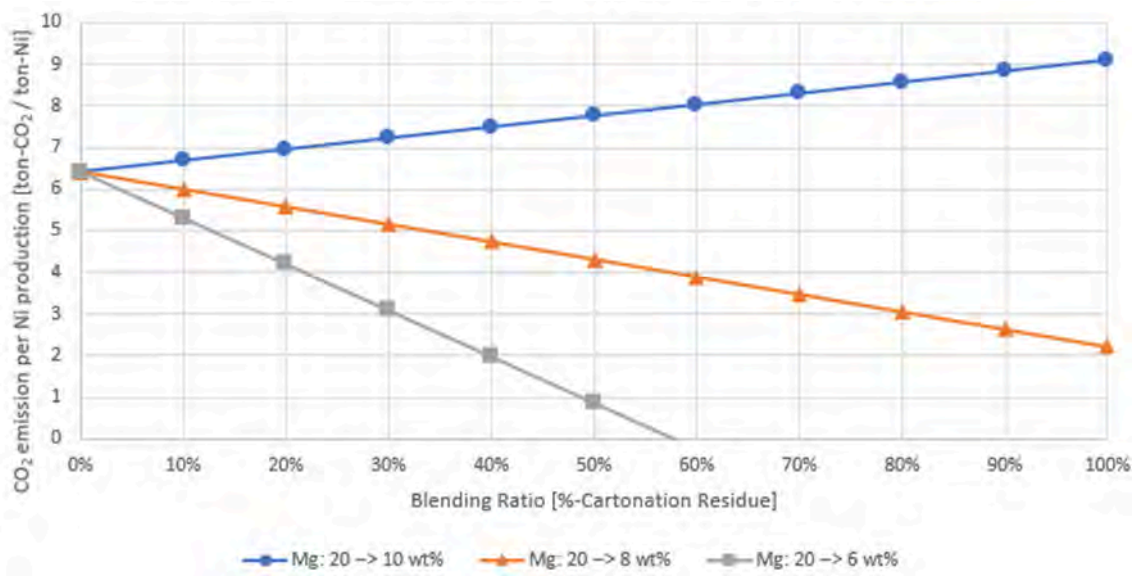

Figure 15: Effect of Mg reduction from high-Mg ores in CO_2 mineralization process

Ideas to improve magnesium dissolution

Ore particle size

It would be possible that the reactivity can be improved by pulverizing the high-Mg ore more finely and exposing the surfaces to be activated. However, it is necessary to keep it within a range that does not affect sedimentation.

Activation of magnesium in ore

It would be possible to improve the ore activation by extending the calcining time or by applying internal heating method by using microwaves or the like to ensure even calcining and to prevent inactivated portions from remaining.
Since it has been reported possible to modify serpentine into highly active olivine [(3)(4)], the application of microwave calcining technology seems promising.

Adjustment of dissolution temperature

Figure 16 shows Magnesite Saturation Indexes [(5)] a measure of degree of supersaturation, defined as the base 10 logarithm of the ion activity product divided by the solubility product constant. Although the solubility of carbon dioxide becomes lower at higher temperatures, the solubility of Mg-CO_2-H_2O type magnesium

carbonate increases even at higher temperatures, and there would be a sweet spot to optimize the magnesium dissolution by adjusting the dissolving temperature.

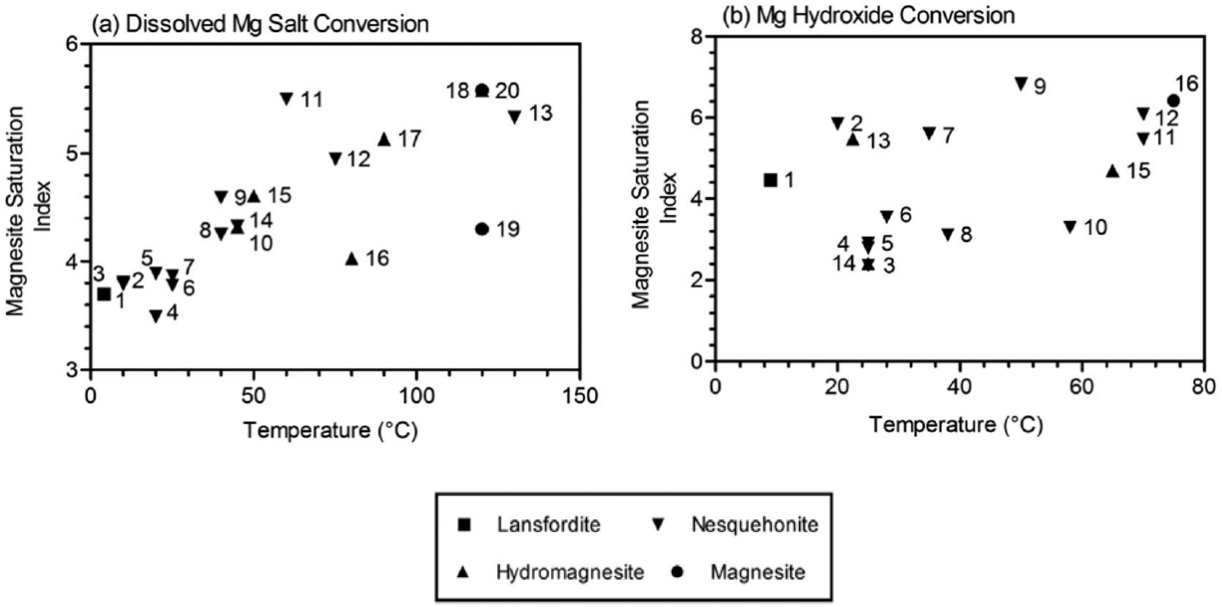

Figure 16: Summary of literature data versus simulated magnesite saturation indexes [5]

Ideas to improve energy consumption

Alternative energies

Although LNG is assumed as the power and heat sources in the study, it is possible to reduce CO2 emissions by applying green fuels (hydrogen, ammonia fuel), and green electricity. The microwave mentioned above is also an alternative method that uses electricity, so it is expected that both problems can be solved at the same time.

CONCLUSION

A reaction similar to the CO_2 mineralization reaction observed in serpentine was confirmed in lab tests using nickel laterite ores by JGC's method at atmospheric pressure.

It was suggested that the integration of CO_2 mineralization and nickel acid leaching process could satisfy both the reduction of CO_2 emissions and profitability.

Future challenges include optimizing the amount (concentration) of magnesium dissolution by adjusting conditions and methodologies in comminution and calcining process.

ACKNOWLEDGEMENTS

The authors would like to thank the staff and management of Sumitomo Metal Mining Co., Ltd for supplying nickel laterite ore samples from various areas.

REFERENCES

1. Ilies Tebbiche, Louis-César Pasquier, Guy Mercier, Jean-Francois Blais, Sandra Kentish. 2021. Mineral carbonation with thermally activated serpentine; the implication of serpentine preheating temperature and heat integration. Chemical Engineering Research and Design,172, 159–174.

2. Genichiro Yamamoto, 2022. Structure of amorphous magnesium carbonate and Crystallization process of magnesium carbonate hydrate mineral

3. Erin R. Bobicki, Qingxia Liu, Zhenghe Xu, 2014. Microwave heating of ultramafic nickel ores and mineralogical effects

4. J. Forster, R. Elliott, D. Boucher, E. R. Bobicki, 2021. High-temperature microwave properties and phase transitions of ultramafic nickel ores

5. Edward J. Swanson, Kyle J. Fricker, Michael Sun, Ah-Hyung Alissa Park, 2014. Directed precipitation of hydrated and anhydrous magnesium carbonates for carbon storage

BREAKING FREE OF THE NEW MINE DEVELOPMENT CATCH-22

By

Matt Schneider, Alistair Barron, Grant Wellwood,

Idoba, Australia

Presenter and Corresponding Author

Matt Schneider
Mathew.Schneider@idoba.com

ABSTRACT

Developing a new mine is one of the toughest endeavours out there, yet our renewable future requires a lot of minerals, from new mines sympathetic to the sustainability cause (low-impact, efficient, safe). Overlay the industry's historically low success rate and the rising cost of capital, and you have an extremely challenging environment for developing new mines. Consequently, many projects get stuck in the "Study Phase Catch-22" (can't advance beyond scoping phase without investment, can't get investment without advancing beyond scoping phase). Decisions informed by directed experience and system's thinking is one of the keys to breaking out of this cycle, however for many proponents this is their first mine development project therefore creating another catch-22.

To formulate an assistance tool, we started by imagining being able to see the components of a proposed value chain laid out visually to show the key linkages, and then being able to flex elements of the system as a function of time to immediately see the financial and process implications of doing so. Inspired by AusIMM's Technical Economic Analysis (TEA) guidelines, we then built a bespoke dynamic driver model (DDM) based tool to support decision makers.

Hosted on the Akumen platform, the DDM approach to TEA elevates the process from the flaky and opaque world of spreadsheets, offering transparency, rigour as well as the power of artificial intelligence (AI). This tool not only facilitates the evaluation of alternate processing futures, it also enables the go-forward option to be shared with potential investors interactively so they can undertake genuine due diligence. Moreover, having assisted projects break out their scoping study catch-22, the DDM remains a project team asset that can grow with the project, informing and supporting decisions as it passes through the rest of study phase and then on into production.

To illustrate these points, this paper focusses on a common scoping stage decision around the inclusion of ore sorting, which is frequently hailed as a game-changer especially for struggling projects. By working through this decision, the paper both validates the importance of TEA, as flagged by the AusIMM's, and demonstrates the benefits of realising it in the form of a DDM.

Keywords: Study phase, Techno Economic Analysis, TEA, Dynamic Driver Model, DDM, Akumen, Ore Sorting

Breaking Free of the New Mine Development Catch-22

Charting a Path Forward

Matthew Schneider

idoba

The challenge of developing new mines

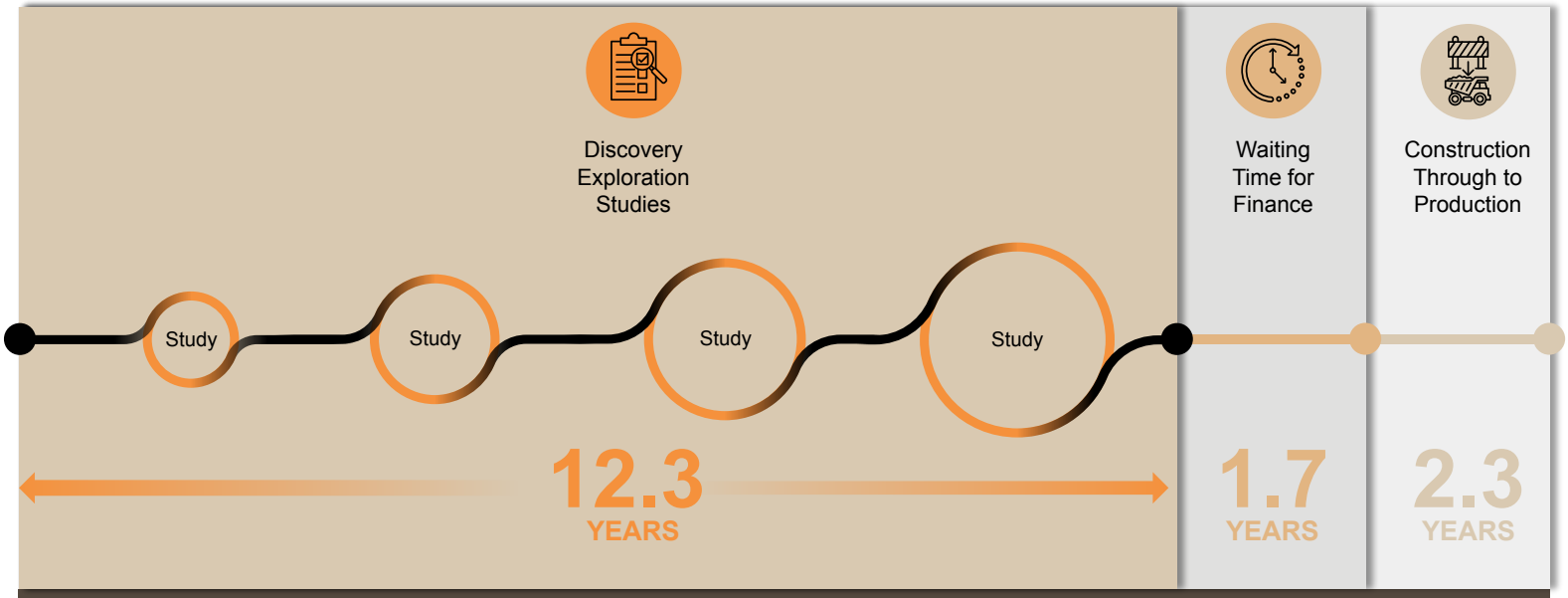

New mines are crucial for a sustainable future but face challenges to develop efficiently and safely. Modern mines take >16 years from Discovery to Production, often delayed by the “Study Phase Catch-22”.

Long development timelines and specific mineral feasibility durations

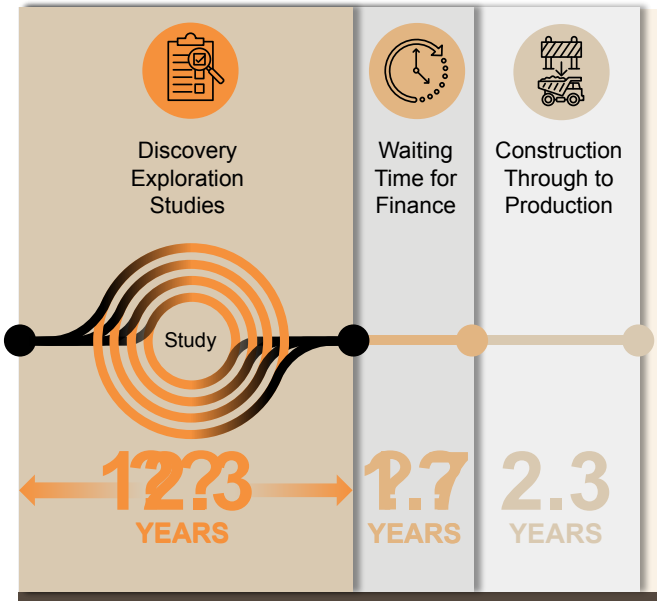

Gold, Lithium, Zinc and Nickel all have substantial feasibility times due to longer exploration and permitting.

On average, **Copper mines** have one of the longest exploration and discovery time frames, **roughly around 12.9 years**

What if we could streamline the discovery process and run multiple study scenarios simultaneously to optimise yield and operational efficiency?

Optimising mineral processing with Akumen

- **Two-step process**: High-level mass balance model and techno-economic model for financial metrics.
- **Dynamic driver modelling**: Tailored for each operation using standard components and process inputs.
- **Goals**: Maximise copper recovery and gangue rejection, using partition coefficients and bond work index.

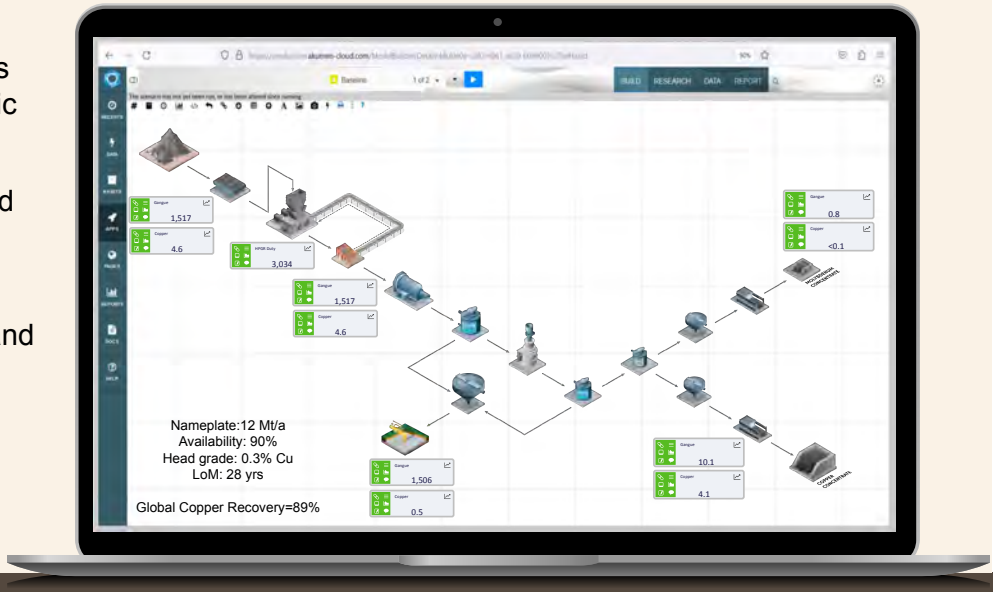

Analysis: Run “what if” scenarios with Akumen to explore trade-offs.

Scenario 1 | NO Ore Sorter (Units=dmt/h)

- Here we see a **Level 1 DDM** mass balance for the base case, **NO sorter**.

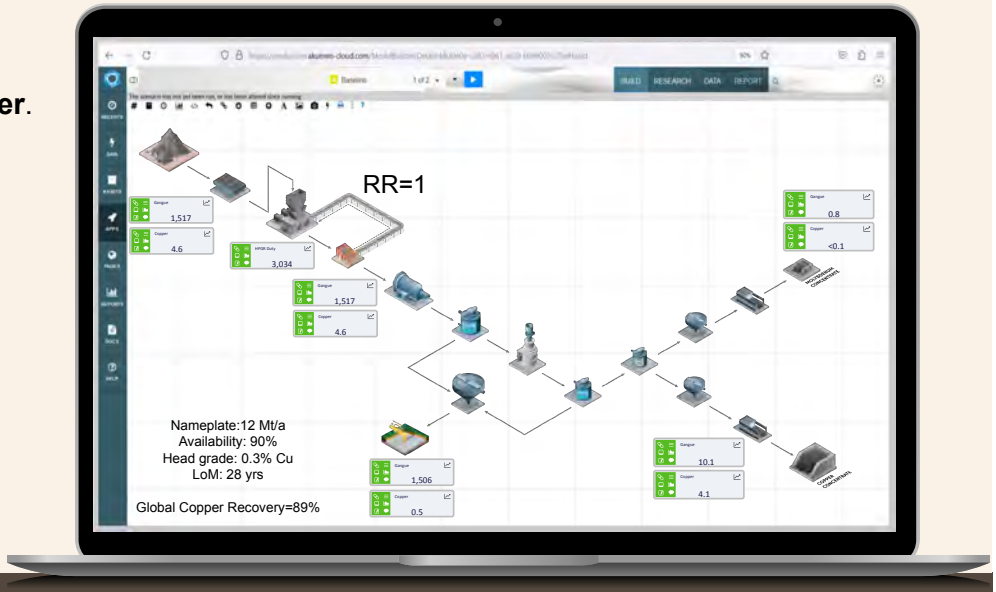

The recycle ratio around the HPGR is around **1** and the global recovery is **89%**

Scenario 2 | WITH Ore Sorter (Units=dmt/h)

- In this **With Sorter** case we see coarse gangue being rejected from the ore sorter with some loss of copper.
- However, the size of the HPGR recirculating load is reduced by 80% which means the HPGR can be smaller.

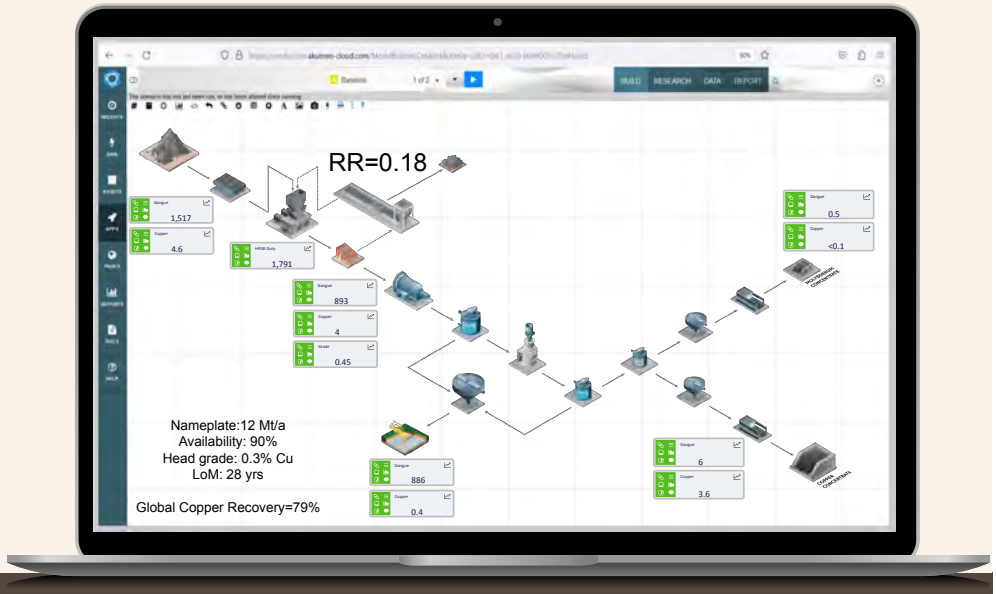

Analysis: Run “what if” scenarios with Akumen to explore trade-offs.

The techno-economic analysis Ore Sorter trade-off

- While these Level 1 models are not the final solutions in themselves, they are tools that can help guide the way through the early stages of study (scoping) ahead of the expensive detailed study and make **better decisions early in the study process**.

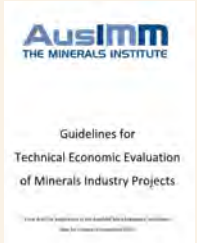

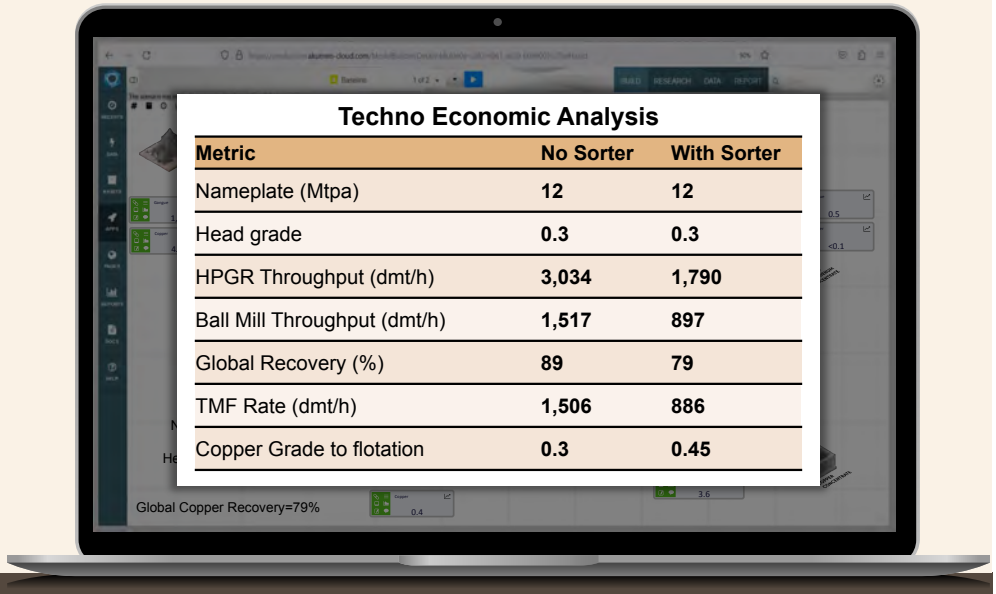

Lowering the capital ask like in this example can help break out of the **‘Study Phase Catch 22’**

The techno-economic analysis, Financial transparency

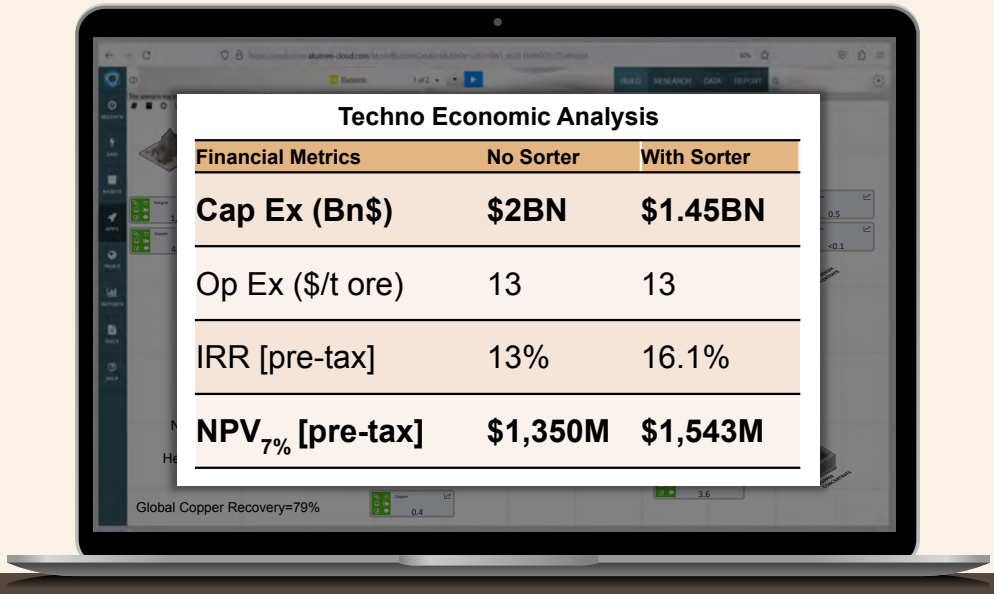

Lowering the capital ask like in this example can help break out of the **'Study Phase Catch 22'**

Final thoughts

- Modern mines take >16 years from Discovery to Production, often delayed by "Study Phase Catch-22"
- These new mines are crucial for a sustainable future, but face challenges to develop efficiently and safely
- By running "what if" scenarios:
  - better techno-economic trade-off decisions can be made earlier
  - decision makers and stakeholders are more engaged, leading to novel ways to **break out of the 'Study Phase Catch 22'**
  - leverage digital technologies to help solve the critical minerals shortage

idoba

idoba is reshaping mining with cutting-edge software products, our DiiMOS™ platform and expert consulting. We help our clients intelligently navigate complex challenges, from boosting productivity to meeting ESG goals.

Mathew Schneider Matt.Schneider@idoba.com

Dr. Grant Wellwood Grant.Wellwood@idoba.com

TECHNO ECONOMIC EVALUATION OF THE ATLAS MATERIALS PROCESS

By

Mike Dry

Arithmetek, Canada

Presenter and Corresponding Author

Mike Dry
mike.dry@arithmetek.com

ABSTRACT

This paper presents the results of a study comparing the techno-economics of producing nickel-cobalt hydroxide from saprolite for a new process being developed by Atlas Materials, against atmospheric tank leaching with sulphuric acid.

The new route entails leaching saprolite with hydrochloric acid, precipitation of iron and aluminium hydroxides, precipitating the nickel and cobalt as a mixed hydroxide product, oxidation and precipitation of manganese, precipitation of magnesium and calcium as hydroxides and passing the remaining sodium chloride through a chlor-alkali section to regenerate hydrochloric acid and sodium hydroxide for recycle to the upstream parts of the process.

Process modelling was used to generate detailed mass-energy balances for each route, then the balances were used to calculate preliminary estimates of the capital and operating costs associated with the processing routes examined. These numbers were used to examine the techno-economics of the two routes.

Keywords: Saprolite, novel technology, economics

INTRODUCTION

The drive to net-zero carbon requires a major shift away from the burning of fossil fuels. Achieving that requires a major shift in the power generation and transportation industries, particularly the development of storage batteries if the use of intermittent sources of renewable energy is to become viable. That represents a massive increase in demand for the metals needed for these storage batteries.

Nickel is one of these critical metals. Historically, much of the global supply of nickel and cobalt came from sulphide ores, but as these reserves become depleted the processing of laterite ores is becoming increasingly important. The pressure leaching of limonite at Moa Bay began in the late 1950s, and the pyrometallurgical processing of saprolite to ferronickel is well established. A third major source of nickel and cobalt (and manganese), sea nodules, may well become important, but has not yet gained a place in the pantheon of resources being exploited (and its advent might, for various non-technical reasons, not be imminent).

In this context, a previous study[1] examined the techno-economic merits of selected established and proposed circuits for the processing laterite ores, limonite, saprolite, and mixtures thereof. For each case a process model (numerically rigorous mass-energy balance, based on publicly available information, was built and the output was used to calculate estimates of the capital and operating costs. The broad approach and the conclusions reached have been described previously[1,2]. Recently, Atlas Materials published information on a novel low-carbon approach to the processing of saprolite[3]. This present study now extends the previous one, adding this new option to those already examined.

SAPROLITE

The saprolite composition assumed previously was used in this extension of the study for consistency in evaluating the various alternatives. Table 1 lists its elemental analysis and Table 2 the suite of minerals used to represent it. It should be noted, however, that Atlas Materials specify a value of 1.8% Ni for a saprolite originating from New Caledonia[3]. The purpose of this exercise is to evaluate the Atlas materials process on the same basis as the processes previously examined, not to validate or otherwise any specific application of either technology.

Table 1 – Saprolite analysis, mass %.

Ni	1.60
Co	0.02
Al_2O_3	0.86
Cr_2O_3	0.67
Fe_2O_3	11.99
CaO	0.15
MgO	27.33
MnO	0.18
Na_2O	0.05
K_2O	0.03
SiO_2	40.0

Table 2 – Saprolite mineralogy, mass %

Ni_2SiO_4	2.9
CoO	0.03
$Al_2O_3 \bullet H_2O$	1.0
$FeCr_2O_4$	1.0
$Fe(OH)_3$	15.6
$Ca_3Si_2O_7 \bullet 3H_2O$	0.3
$Mg_3Si_2O_5(OH)_4$	41.1
$Mg_4Si_6O_{15}(OH)_2 \bullet 6H_2O$	37.7
$MnSiO_3$	0.33
Na_2SiO_3	0.10
K_2SiO_3	0.05

ATMOSPHERIC TANK LEACH

The atmospheric tank leach (ATL) circuit was part of the previous exercise; its description is repeated here for convenience and clarity. Figure 1 illustrates the process model used to represent this circuit. The incoming saprolite is mixed with recycled water and leached in agitated tanks with sulphuric acid from the sulphur-burning acid plant. The leach is heated by addition of steam from the acid plant. The leached slurry is first contacted with recycled base metal hydroxide precipitate from downstream to re-dissolve co-precipitated nickel and cobalt and to partially consume the free acid left after the leach. The partly neutralised slurry is neutralised further with limestone to precipitate the bulk of the iron and aluminium while co-precipitating essentially no nickel or cobalt. The resulting iron-aluminium slurry is thickened and washed with recycled process water in a counter-current decantation train, and the washed residue leaves the circuit. The supernatant is neutralised further with more limestone, to precipitate essentially all the remaining iron and aluminium. Some nickel and cobalt are co-precipitated in this step, and the underflow from the subsequent thickening step is recycled. The remaining solution is dosed with magnesium oxide to precipitate the bulk of the nickel and cobalt as hydroxides. The hydroxide slurry is thickened, the underflow is filtered, and the filter cake is washed with fresh water. The washed filter cake leaves the circuit as the mixed hydroxide product commonly called MHP. The supernatant and filtrate are combined limed, precipitating the remaining nickel and cobalt as hydroxides, along with gypsum. The precipitate is thickened and recycled. The remaining solution is limed again to precipitate the magnesium and manganese into a hydroxide-gypsum residue that leaves the circuit after thickening. The supernatant from the final thickening step is recycled as process water.

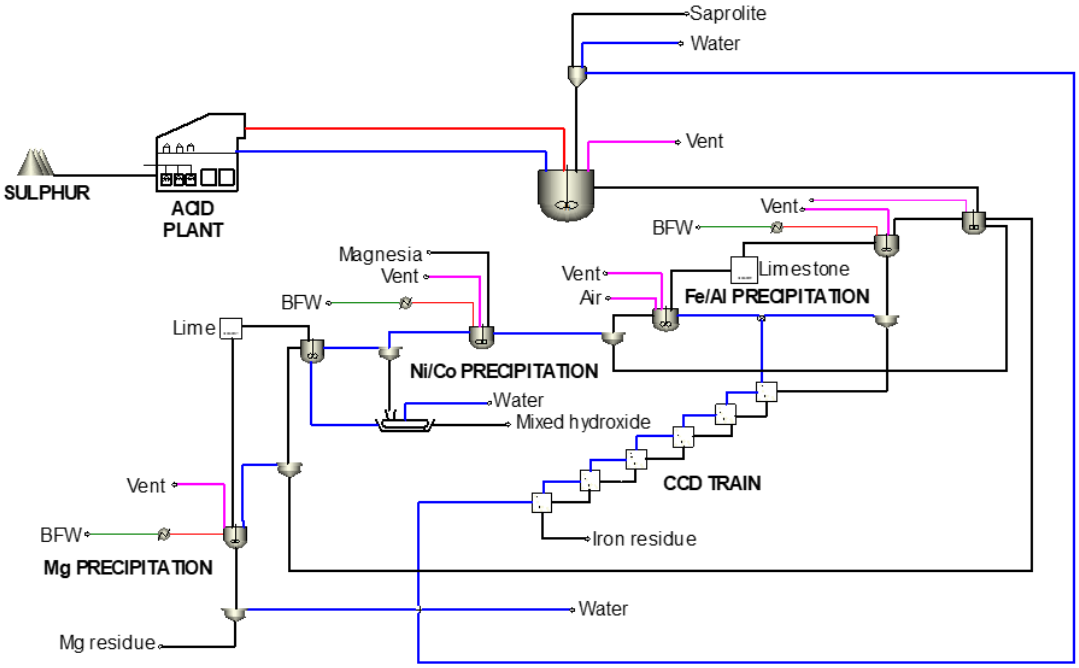

Figure 1 – ATL circuit.

ATLAS MATERIALS CIRCUIT

The Atlas materials circuit has been described elsewhere[3]. Figure 2 illustrates the process model built to represent this circuit. Incoming saprolite is mixed with recycled solution and the slurry is leached with recycled and make-up hydrochloric acid. The extents of dissolution for nickel, iron and magnesium were taken from published information[3]. The extent of dissolution of cobalt was assumed to be the same as that of nickel, and the extent of dissolution of aluminium was assumed to be the same as that of iron. The leached slurry is thickened and filtered. The filter cake is washed with water and removed as a silicate residue to be sold as an ingredient for cement making. The resulting solution is neutralised with recycled sodium hydroxide in two counter-current stages, precipitating the trivalent cations (Fe, Al, Cr) as hydroxides. The precipitate is filtered out, washed with water and discarded. The remaining solution is neutralised further with more recycled sodium hydroxide, precipitating the nickel and cobalt as a mixed hydroxide precipitate (MHP) that is recovered by thickening and filtration, the filter cake being washed with water and exiting as the desired product. The remaining solution is oxidised with sodium hypochlorite, precipitating the manganese as manganese dioxide that is recovered by thickening, filtration and washing with water. The washed manganese dioxide leaves the circuit. The residual solution is almost pure sodium/potassium chloride. Remaining traces of divalent cations (Ca and Mg) are removed using ion exchange, the resin being stripped with acid and the spent eluant discarded as an effluent. The purified solution is partly concentrated by evaporation to manage the overall water balance of the circuit. The energy balance over the evaporation section is closed using steam from the chlor-alkali section and by mechanically re-compressing and recycling some of the steam driven off in the evaporation

step. The remaining solution is then passed through a conventional chlor-alkali electrolysis process to regenerate hydrochloric acid and sodium hydroxide for recycle.

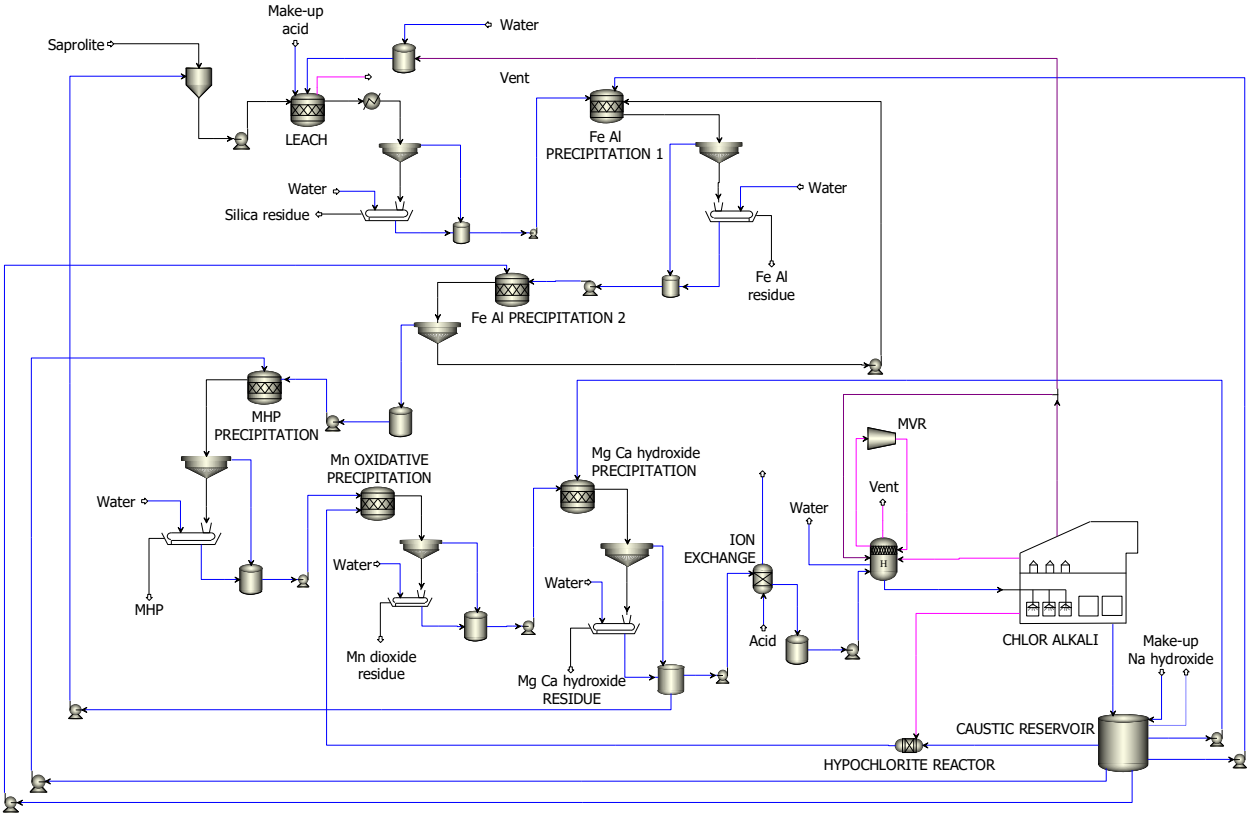

Figure 3 illustrates the part of the process model representing the chlor-alkali circuit. The black dashed lines represent energy flows. In the chlor-alkali section, the incoming pure NaCl brine is electrolysed in chlor-alkali electrolysis cells, generating sodium hydroxide in the exit solution and evolving chlorine and hydrogen at the anodes and cathodes, respectively. The current efficiency for chlorine production was assumed to be 97 percent, the balance due to the evolution of oxygen at the anodes.

Figure 2 – Atlas Materials circuit.

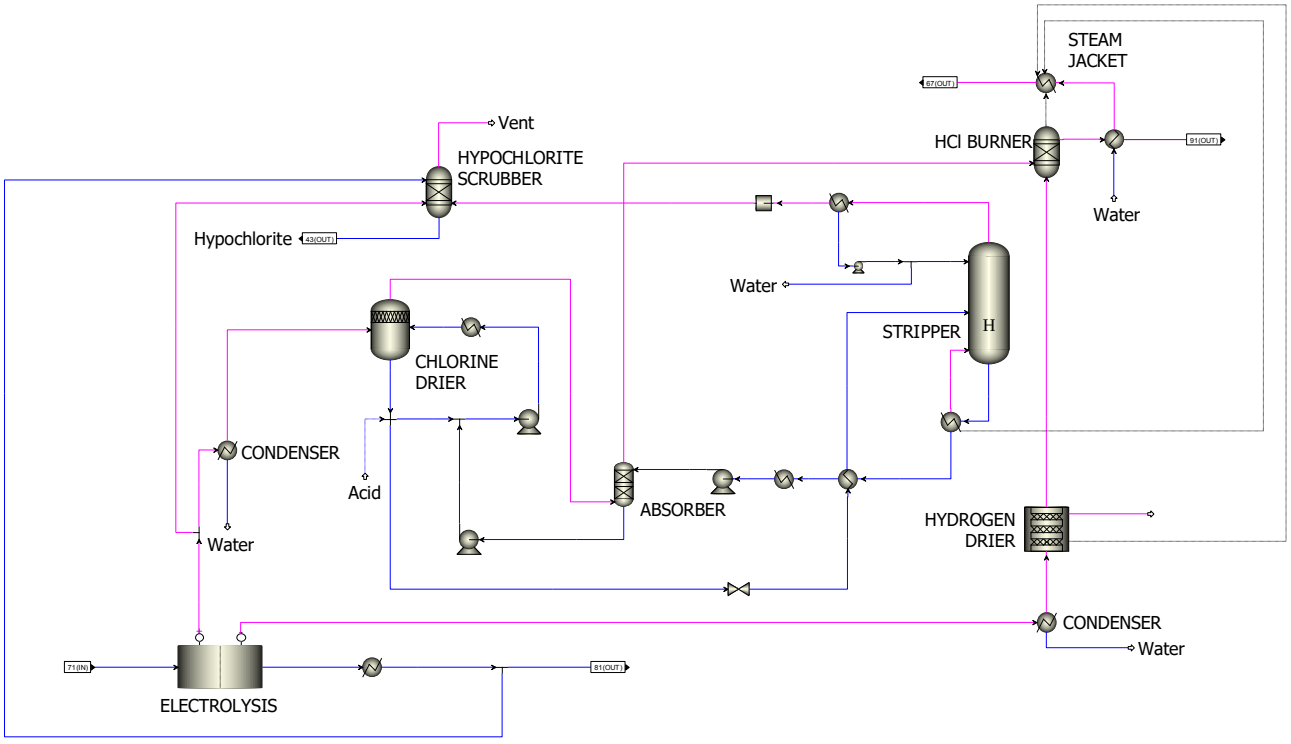

Figure 3 - Chlor-alkali circuit.

Some of the chlorine from the anodes, plus the residual chlorine in the vent gas from the striper in the chlorine drying loop, is reacted with sodium hydroxide in part of the solution ex the chlor-alkali cells, making the sodium

hypochlorite needed to oxidise manganese to manganese dioxide. The rest of the chlorine is dried by contact with circulating sulphuric acid, removing about 99 percent of the water. The temperature is controlled in this loop by cooling the recirculating acid with cooling water. The partially dried chlorine is contacted with concentrated sulphuric acid in an absorber column, removing essentially all the remaining water. The concentrated sulphuric acid is regenerated in a stripping column and recycled. Energy to the reboiler of the stripping column comes from steam generated from the exothermic reaction between the dried hydrogen and chlorine in the HCl burner. The hydrogen from the cathodes is dried by adsorption into silica gel, with the energy for regenerating the silica gel also coming from the steam generated in the HCl burner.

The dried chorine and hydrogen are reacted to hydrochloric acid in the HCl burner. The heat of reaction is captured as steam that is used in the two drying steps in the chlor-alkali section and in the evaporation stage upstream of the chlor-alkali section.

CAPITAL AND OPERATING COSTS

The main reason for selecting atmospheric tank leaching with sulphuric acid as the comparative baseline for this study is that both the ATL and Atlas Materials processes use acid leaching at ambient pressure and progressive neutralisation to purify the solution ex leaching and to recover the base metals as MHP. A secondary reason is that, in the previous study[1], the economics of the ATL process came out very close to those of the RKEF process, a pyrometallurgical option that is also used to process saprolite.

Table 3 and Table 4 list the costs of the various reagents and utilities consumed by the two circuits, the various unit costs and the calculated variable operating costs. For the ATL circuit the variable costs are dominated by the costs of elemental sulphur and waste disposal. For the Atlas Materials circuit, the dominant variable cost is for the electricity used in the chlor-alkali electrolysis.

The capital cost previously estimated for the ATL process (in 2015) was escalated to 2023 using the Chemical Engineering Process Cost Index (CEPCI) values for 2015 (556.8) and 2023 (790.8), bringing the cost for the installed process equipment up from $397 million to $564 million. The capital costs calculated for the Atlas Materials circuit are listed in Table 5. The methodology for estimating the capital cost has been detailed elsewhere[2]. The capital costs for the mine and other non-process infrastructure were estimated using a correlation based on other laterite projects[1]. These costs were assumed to be the same for both processes.

Table 3 – Reagent & utility costs, ATL.

Item	Amount	Unit cost	Opex/t
Sulphur per tonne dry feed	240 kg	$130/t	$31
Magnesia, as 100% MgO	9 kg	$300/t	$3
Limestone,as $CaCO_3$	21.0 kg	$500/t	$11
Electricity per tonne dry tonne feed	33 kWh	$0.05/kWh	$2
Fresh water per tonne dry feed	2435 kg	$1/t	$2
Waste disposal, per tonne dry feed	2126 kg	$15/t	$32
Reagent & utility cost, per dry tonne feed			$80
Annual reagent & utility cost, $ million (27 kt/y Ni)			$144

Table 4 – Reagent & utility costs, Atlas Materials.

Item	Amount	Unit cost	Opex/t
Make-up acid per tonne dry feed (36% HCl)	102 kg	$130/t	$12
Make-up caustic per tonne dry feed (100% NaOH)	3 kg	$300/t	$1
Acid to IX per tonne dry feed (10% HCl)	0.2 kg	$500/t	$0.1
Electricity per tonne dry tonne feed	2265 kWh	$0.05/kWh	$114
Fresh water per tonne dry feed	481 kg	$1/t	$0.5
Cooling water make-up, per tonne dry feed	1 kg	$1/t	$0.001
Waste disposal, per tonne dry feed	946 kg	$15/t	$14
Reagent & utility cost, per dry tonne feed			$142
Annual reagent & utility cost, $ million (28 kt/y Ni)			$253

Table 5 – Capital cost estimate, $ million, Atlas Materials.

Process equipment not including the chlor-alkali plant	824
Chlor-alkali capex ($600 per annual tonne chlorine)[4,5]	818
Mine & infrastructure	594
Combined capital cost	2236

METAL PRICES

Revenue, of course, depends on the selling prices of the various products. This is not information that is freely published for nickel and cobalt in intermediates such as MHP, and establishing reliable numbers for the selling prices the products is not a trivial exercise. One reference[6] claims that the nickel in MHP fetches 70-80 percent of the LME price of nickel, whilst another[7] puts the discount from LME nickel at 5-10 percent. Information for cobalt is scarcer than for nickel. One reference[8] puts the selling price of cobalt in MHP at 55-63% of the metal price. The same reference gives the "payable indicator" for nickel in mixed hydroxide as 70-76%. It might be that the whole market for nickel and cobalt in intermediate products is in flux[9]. For want of anything better, the economic calculations presented below are based on 80 percent of the prices of metallic nickel and cobalt.

Because ventures processing ores and minerals are planned for decades of operation, using short-term projections of metal prices is not the best way to evaluate overall economics[10]. Figure 4 shows just over a century of price data for nickel and cobalt, inflation-indexed to 2022 currency. The dashed lines are the long-term average, plus or minus one standard deviation. (The vertical solid lines show when the US dollar was decoupled from gold.) From this history, the long-term average prices for nickel and cobalt are US$9.05/lb and US$32.75lb, respectively, or $19 910 per tonne for nickel and $72 050 per tonne for cobalt. These numbers were assumed for this study.

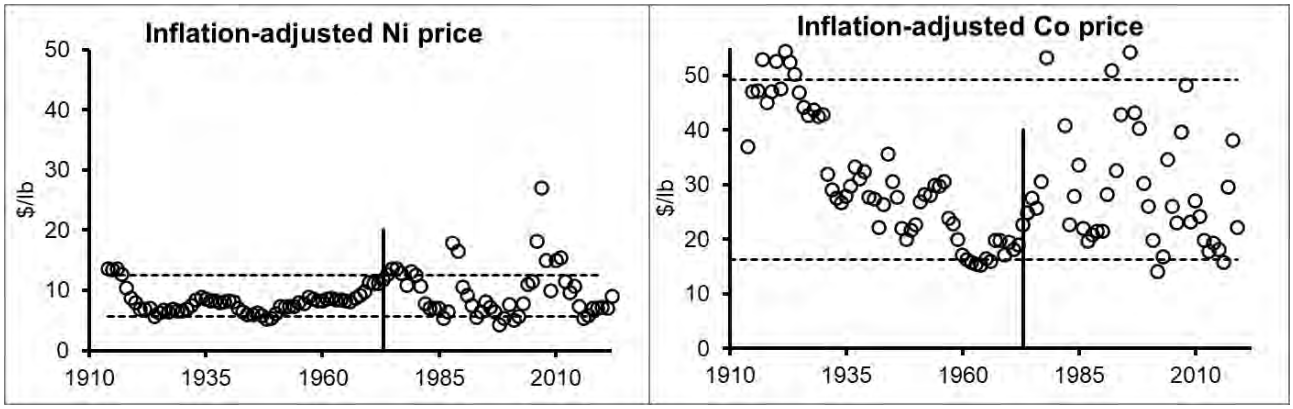

Figure 4 – Nickel and cobalt price data.

Figure 5 shows a century of long-term price data[11] from Metal Bulletin, adjusted to 2015 currency. From this history, the long-term average for nickel is $14 044/tonne, or $6.39/lb, not overly different from the data in Figure 4, if the 2015 value is converted to 2022 values ($16 073/t).

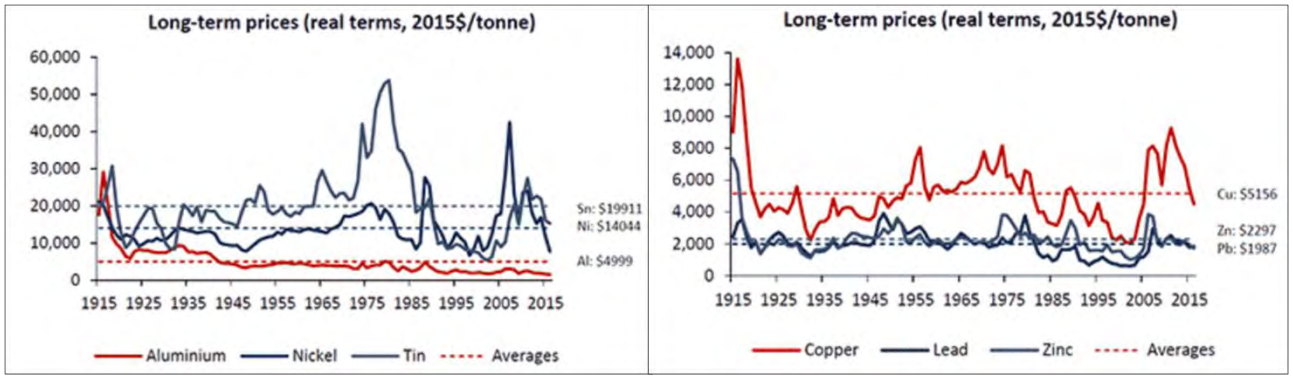

Figure 5 – Historical price data (source: Metals Bulletin)

RESULTS

Assuming the same mine and other infrastructure for both circuits, a two-year construction period and that in both cases commissioning will be progressive (25% of design in the first year of operation, 50% in the second year, 75% in the third year and 100% thereafter) leads to the cash flow calculations shown in Table 6 and Table 7. Figure 6 shows the same results graphically.

Table 6 – Cash flows, $ million, ATL.

Year	1	2	3	4	5	6	7	8	9	10	11	12	13	14	15	16	17	18	19	20	21	22
Capex	579	579																				
Fixed costs			4	4	4	4	4	4	4	4	4	4	4	4	4	4	4	4	4	4	4	4
Variable costs			36	72	108	108	108	108	108	108	108	108	108	108	108	108	108	108	108	108	108	108
Revenue			114	227	341	455	455	455	455	455	455	455	455	455	455	455	455	455	455	455	455	455
Margin	-579	-579	73	151	229	343	343	343	343	343	343	343	343	343	343	343	343	343	343	343	343	343
Tax, 30%	0	0	0	0	0	0	0	97	103	103	103	103	103	103	103	103	103	103	103	103	103	103
Profit	-579	-579	73	151	229	343	343	245	240	240	240	240	240	240	240	240	240	240	240	240	240	240
IRR					-28%	-10%	0%	4%	7%	9%	11%	12%	13%	14%	15%	15%	16%	16%	16%	16%	17%	17%

Table 7 – Cash flows, $ million, Atlas Materials

Year	1	2	3	4	5	6	7	8	9	10	11	12	13	14	15	16	17	18	19	20	21	22
Capex	1118	1118																				
Fixed costs																						
Variable costs			64	127	191	254	254	254	254	254	254	254	254	254	254	254	254	254	254	254	254	254
Revenue			129	259	388	518	518	518	518	518	518	518	518	518	518	518	518	518	518	518	518	518
Margin	-1118	-1118	66	132	198	264	264	264	264	264	264	264	264	264	264	264	264	264	264	264	264	264
Tax, 30%	0	0	0	0	0	0	0	0	0	0	0	2	79	79	79	79	79	79	79	79	79	79
Profit	-1118	-1118	66	132	198	264	264	264	264	264	264	262	185	185	185	185	185	185	185	185	185	185
IRR					-45%	-29%	-19%	-13%	-8%	-5%	-2%	0%	1%	2%	3%	4%	4%	5%	5%	6%	6%	6%

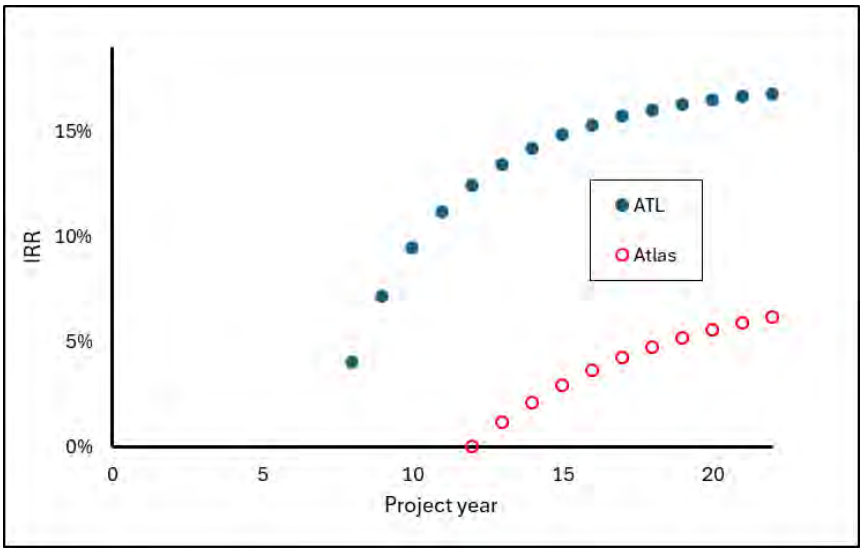

Figure 6 – Internal rate of return versus project year.

These calculations indicate the Atlas Materials Process to be significantly weaker, economically, than the ATL process. To reach the same IRR as the ATL process, the capital cost of the Atlas Materials process, excluding the number for infrastructure and non-process capital, which is the same for both processes, would need to be 20 percent of the number calculated. The capital cost calculations for the process equipment used the same methodology for both processes; that large an error in the relative capital cost numbers is extremely unlikely. For the Atlas materials process, the capital cost of the chlor-alkali plant was not calculated in the same way as the rest of the process equipment because the requisite equipment for electrolysis is not in the costing databases, therefore the estimate of $600 per annual tonne of Cl_2 produced is based on information from the literature[4,5]. However, even reducing that from $600 per annual tonne to zero increases the 20-year IRR for the Atlas Materials process from 6% to 11%, compared to 17% for the ATL process.

This analysis is based on economics as generally assumed at present. Before summarily dismissing the Atlas Materials process, it might be prudent to examine it against the ATL process using potential future economic assumptions. A partial list of such future assumptions could be:

- The cost of CO_2 emissions could go much higher than it is at present.
- The price of renewable electricity could change if/when new generation technology emerges.
- When the burning of fossil fuels stops, the availability and price of sulphur will change dramatically.

If the cost of CO_2 emissions becomes high enough, there would be a corresponding benefit to capturing and sequestering atmospheric CO_2. The calcium/magnesium hydroxide residues from both the Atlas Materials and the ATL processes could conceivably be used for CO_2 sequestration because both calcium and magnesium hydroxide, when exposed to the atmosphere, combine slowly with atmospheric carbon dioxide, making stable carbonates. The process models for the two circuits predict the numbers shown in Table 8 for the incremental gains for capturing and holding CO_2. The ATL total is negative because CO_2 is emitted from the limestone added in the first neutralisation stage and the lime and magnesia used are made by calcining limestone and magnesite, emitting one mole of CO_2 per mole of CaO or MgO, not counting the emissions from the fuel burned to supply the energy needed. Adding these numbers to the economics gives the results shown in Figure 7. While it does improve the Atlas Materials case appreciably, a carbon price of $150 per tonne of CO_2 is not enough to overcome the other differences.

Table 8 - CO_2 capture potentials.

CO_2 capture, per dry tonne feed ($150/t CO_2)		
Ca,Mg hydroxide (Atlas)	253 kg	$38/t feed
Ca, Mg hydroxide (ATL)	297 kg	
CO_2 ex lime (ATL)	-299 kg	
CO_2 ex MgO (ATL)	-10 kg	
CO_2 ex neutralisation (ATL)	-30 kg	
Total for ATL	-42 kg	-$6/t feed

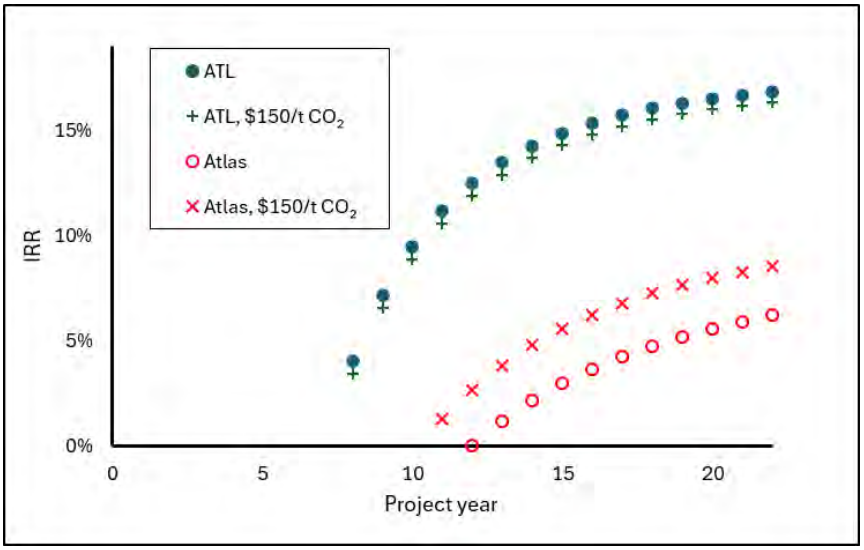

Figure 7 – Effect of carbon pricing.

That raises an interesting question: all else being equal, what carbon price would make the economics of the Atlas Materials process competitive with those of the ATL process? This was examined by simple trial and error, changing the carbon price. At a carbon price of $630/t CO_2 the IRR curves for the Atlas Materials and the ATL processes become almost the same, as shown in Figure 8. Whether or not the carbon price will go to that level is outside the scope of this study.

The dominant operating cost of the Atlas Process being for electricity, a drop in that cost would impact the Atlas Process. Figure 9 shows how a major drop in the cost of electricity would affect the economics of the Atlas Materials process. Whether or not such those lower prices for electricity will ever occur is a subject outside the scope of this paper.

A possibly more plausible scenario would be that the sulphur price rises. Figure 10 shows recent data for the production and consumption of sulphur[12,13]. By far the most sulphur comes from the oil and gas industry, and over half of the total production goes into the manufacture of fertilisers. When the production of oil and gas is terminated or drastically reduced by the global drive to zero carbon, the global supply of sulphur will be severely disrupted, which will affect its price. Were the price of sulphur to double, the impact on the Atlas Materials circuit would be nil because that process does not use sulphur. The effect on the ATL process would, of course, not be zero.

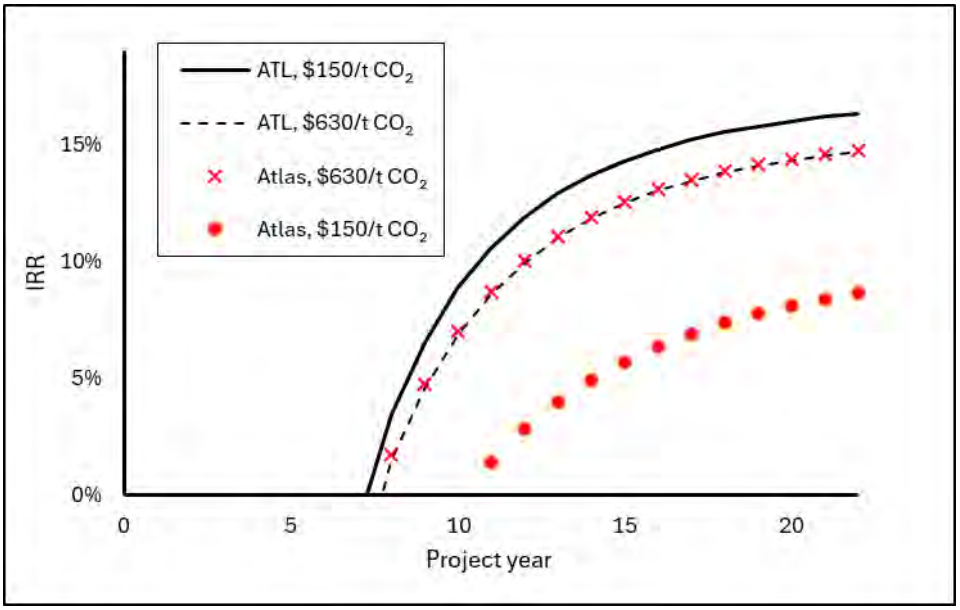

Figure 8 – Economics at $640/t CO_2.

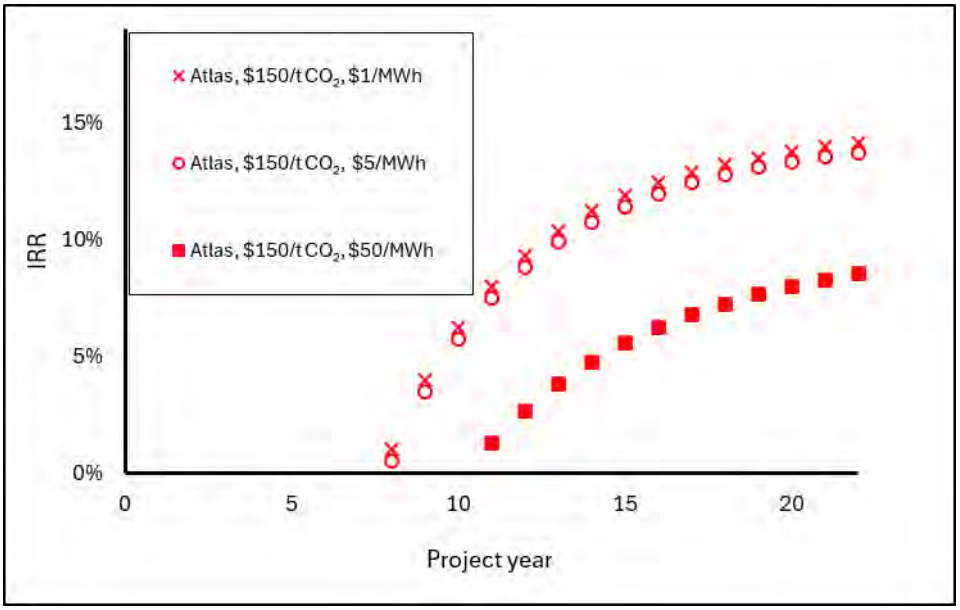

Figure 9 – Effect of electricity price.

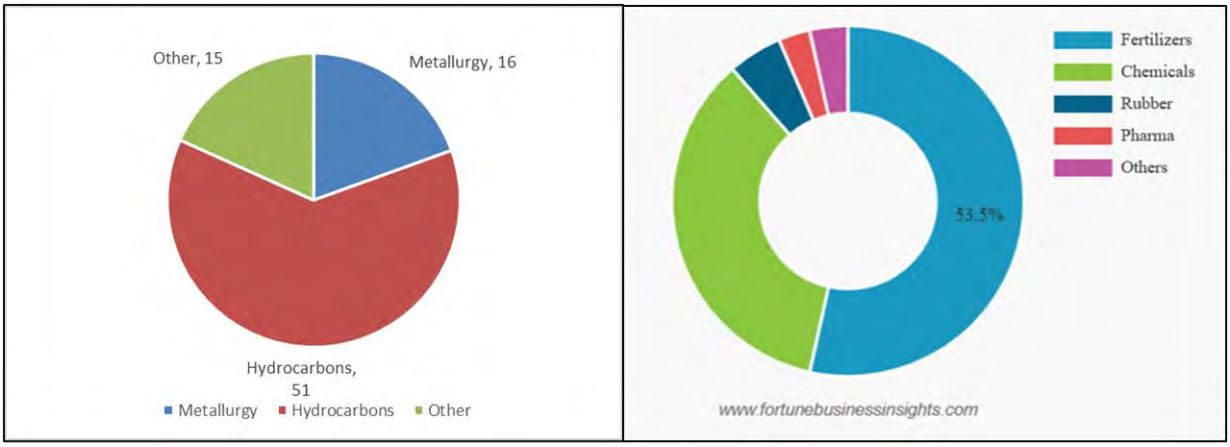

Figure 10 – Sulphur production and consumption.

Figure 11 shows slightly over a century of sulphur price data, adjusted to 2022 currency. Over the past century, the sulphur price has stayed mostly in the channel defined by the long-term average plus or minus one standard deviation, i.e. between $121 and $350 per tonne. The assumption of $130 per tonne used in the baseline of this study may well be too optimistic, the long-term average being $235 per tonne.

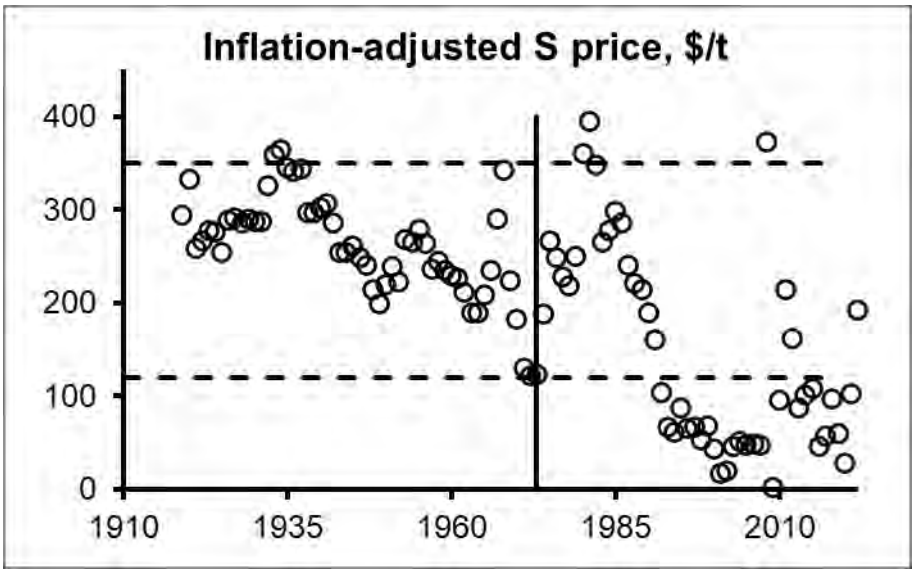

Figure 11 – Sulphur price history, 2022 currency.

Figure 12 shows the impact of higher sulphur and lower electricity prices on the economics of the ATL and Atlas Materials processes. Doubling the sulphur price from $130 to $260 per tonne would affect the economics of the ATL process appreciably but pulling its IRR down to that of the Atlas materials process at an electricity price of $50/MWh would need a sulphur price of about $600 per tonne. Given that the oil and gas tap may well be closed off at some stage, it might be prudent to not discount this as a future possibility. Against that, however, would be the impact of such a rise in the price of sulphur on the global fertilizer industry, and hence on the agricultural industry. Other sources of sulphur would probably become viable, for example its recovery from disseminated sulphide ores[14] or perhaps pyrite roasting with the production of sulphuric acid[15]. Other chloride- and nitrate-bases processes[1] may also be implemented, merely to avoid requiring sulphur for processing laterites. Evaluating the probability of such a drastic shift in the price of sulphur is an exercise well beyond the scope of this paper.

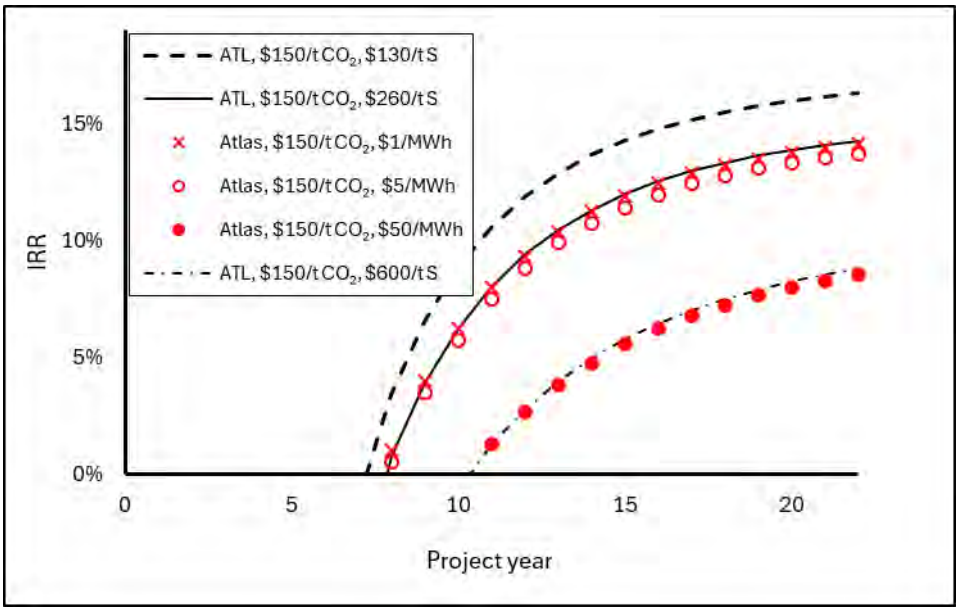

Figure 12 – Summary of the techno-economics.

CONCLUSION

This study adds a new process to those previously examined for treating saprolite. Under the assumptions of today, namely a sulphur price of $130/tonne, a carbon price of $150 per tonne of CO_2 and an electricity price of $50/MWh, the economics of the Atlas Materials process are distinctly inferior to those of the atmospheric tank leaching process and by extension from the previous study[1], also to those of heap leaching, the RKEF route and two other proposed routes, Neomet and DNi (now Altilium).

For the economics of the Atlas Materials process to match the economics of the other processes, taking the ATL process as the proxy for the others, some combination of the following would be needed:

- The carbon price rising to about $650 per tonne of CO_2.
- The sulphur price rising to about $600 per tonne.
- The price of electricity dropping to 10% or less of the $50/MWh assumed as the baseline in this study, plus the sulphur price doubling to $260 per tonne.

ACKNOWLEDGEMENT

Bryn Harris of NMR360 reviewed this paper and made several most helpful suggestions. His input is gratefully acknowledged.

REFERENCES

1. Dry, M. Technical & Cost Comparison of Laterite Treatment Processes Part 3. Alta NCC, Perth, Australia, May 2015.
2. Dry, M. Early Evaluation of metal Extraction Projects. Alta NCC Conference, May 2013.
3. Ley, J. and Dreisinger, D. Low Carbon Nickel and Cobalt production from Nickel Saprolite Ores using the Atlas Materials Process. Alta NCC, May 2023, Perth, Australia.
4. Chlor-Alkali Process Economics - Thunder Said Energy (accessed 2024-05-14).
5. Estimated Capital Costs of Hydrogen, Chlor-Alkali, and CO 2 Electrolyzers | Download Scientific Diagram (researchgate.net) (accessed 2024-05-14)
6. Yang, Y., Perry, C. MHP emerges as preferred route to sulfate for international nickel market. Fastmarkets, August 9, 2022. https://www.fastmarkets.com/insights/mhp-emerges-as-preferred-route-to-sulfate-for-international-nickel-market/ (accessed 2024-03-04)
7. Milewski, A. Mixed hydroxide precipitate — the new class one nickel. Mining.com, October 3, 2021. Mixed hydroxide precipitate — the new class one nickel - MINING.COM (accessed 2024-03-04).
8. Yang, J. Cobalt metal sustains price rally; longer-term oversupply challenges loom. Fastmarkets, March 22, 2023. https://www.fastmarkets.com/insights/cobalt-metal-sustains-price-rally/ (accessed 2024-03-04)
9. Metals, 28 June 2022. Nickel sulfate vs metal: Is the market shifting towards new pricing mechanisms? https://www.spglobal.com/commodityinsights/en/market-insights/blogs/metals/062822-china-nickel-sulfate-lme-pricing-mechanisms (accessed 2024-03-05).
10. Dry, M. Laterite and the commodity price cycle. Alta NCC, Perth, Australia, May 2018.
11. Fastmarkets MB Research. Commodity prices: a 100-year history. Fastmarkets MB Research (metalbulletinresearch.com) (accessed 2024-03-05-05)
12. USGS 2021 Annual Tables.
13. https://www.fortunebusinessinsights.com/sulfur-market-102143 (accessed 2023-04-07)
14. Dry, M. Potential of Pyrrhotite in Addressing Sustainability: Replacing Oil Industry Sulphur and Carbon. Alta NCC Conference, Perth, Australia, May 2023.
15. Runkel, M., Sturm. P. Pyrite roasting, an alternative to sulphur burning. SAIMM Journal, Volume 109, August 2009. https://www.saimm.co.za/Journal/v109n08p491.pdf (accessed 2024-05-12).
16.

INNOVATIVE TECHNOLOGIES FOR THE EXTRACTION OF NICKEL, COBALT AND MANGANESE FROM LATERITE CRUSTS

By

Maxim Seredkin, [2]Semyon Zakharyan

ERM, Sustainable Mining Services, Australia
[2]Kazakhmys Smelting LLC, Kazakhstan

Presenter and Corresponding Author

Maxim Seredkin
maxim.seredkin@erm.com

ABSTRACT

ERM Sustainability Mining Services team (formerly CSA Global) has worked on innovative technologies for extracting nickel, cobalt and manganese from laterite mineralisation since 2018. This work commenced on Kazakh Ni-Co-cobalt laterite deposits with Ni grades from 0.3–1.3% (average 0.7% Ni) and cobalt grades around 300–500 ppm. In these deposits, Ni-Co mineralisation is comprised mostly of high-magnesium silicates, commonly nontronite, with minor amounts of Ni-Co in limonite.

Modern processing of Ni-Co ores generally involves either pyrometallurgical or hydrometallurgical methods. Hydrometallurgical methods, including AAL, HPAL and heap leaching, are the most common. However, these conventional approaches have not been economic for the Ni-Co laterite deposits in the Urals and Kazakhstan due to the prevalence of Ni-silicate mineralisation and overall low grades.

The successful development of *in situ* recovery technology for extracting copper and gold from regolith/weathering crusts was identified as a potential opportunity to extract Ni-Co from the Ni-Co enriched regolith in the Urals and Kazakhstan. Initial laboratory and pilot investigations – using sulfuric acid as the lixiviant – were completed on the Tochilnogorskoe, Kungurskoye and Rogozhinskoe deposits in the Urals. However, it was quickly recognised that sulfurous acid is a superior lixiviant for Ni-Co laterite deposits. This approach was successfully demonstrated in pilot tests on the Ekibastuz-Shiderty deposit in 2017.

CSA Global prepared the first formal Scoping Study on the use of ISR at Ekibastuz-Shiderty using the Clean TeQ process to treat Ni-Co pregnant solutions using a combination of IX, SX and neutralisation of pregnant solutions.

Subsequently, Kaznickel completed extensive ISR tests, over the course of 2021-2022, at the Gornostay Project using sulfuric acid as the lixiviant. This extended pilot test work resolved numerous issues in operating the test polygon and achieved a stable leaching regime. Kazniclel also developed an improved IX technology for processing pregnant solutions.

At the same time, the research by the authors identified potential improvements for the extraction of Ni-Co from Severgino Ni-Co laterite deposit, TPK, Kazakhstan, followed by:

- Selective sorption of Ni from low-grade Ni-Co laterite leach solutions, followed by removal of iron from the resin using soft acid solutions, and desorption of Ni by 7-10% ammonium hydroxide, producing an eluate of Ni ammine complexes such as $Ni(NH_3)_4(OH)_2$, $Ni(NH_3)_6(OH)_2$ etc. These complexes are easily dissociated to produce $Ni(OH)_2$, with ammonia recycled to the IX process.
- Improved heap leaching outcomes using enhanced agglomeration approaches that are more manageable than ISR. Poor permeability is the main issue with the heap leaching of clay-rich materials typical of regolith deposits. A polymeric additive that is stable with aggressive acid leaching was identified for improved agglomeration and permeability. The dynamics of heap leaching using this approach are much better than those of ISR.

Processing using sulfurous acid was found to be favourable for the leaching of manganese from weathering crusts by both ISR and heap leaching. Mn grades in pregnant solutions were 50–60 g/L. MnO_2 was produced directly from these solutions by electrowinning. However, Mn oxide mineralisation is often associated with elevated calcium, leading to gypsum permeability blockages (colmatation). In these cases, hydrochloric acid is better lixiviant than sulfurous acid, with Mn precipitated as the hydroxide. Recovery of the HCl by sulfuric acid improves the economics of this approach.

Keywords: in situ recovery, heap leaching, nickel, cobalt, manganese, technology, laterite, deposits

Innovative Technologies for the Extraction of Ni, Co & Mn From Laterite Crusts

PRESENTED BY:

DR. MAXIM SEREDKIN
TECHNICAL DIRECTOR – ISR LEAD
ALTA 2024: 28/05/2024

Sustainability is our business

Agenda

1. Why innovative technologies in the Ural-Kazakhstan province
2. Past pyrometallurgical operations
3. Overview of Ni-Co extraction technologies
4. Heap Leaching & In-Situ Recovery
5. Development the innovative technologies
6. Improvements of the innovative technologies
7. Applicability of new technologies for other regions

Why innovative technologies in the Ural-Kazakhstan province

- Innovative technologies were developed in the Ural – Kazakhstan Ni-Co laterite province due to two factors:
- In the past deposits in this province were subject to pyrometallurgical operations which are now uneconomic.
- The Ural-Kazakhstan province hosts Mesozoic Ni-Co mainly nontronite deposits with low average grade 0.3–1.3% Ni, 300–500 ppm Co.

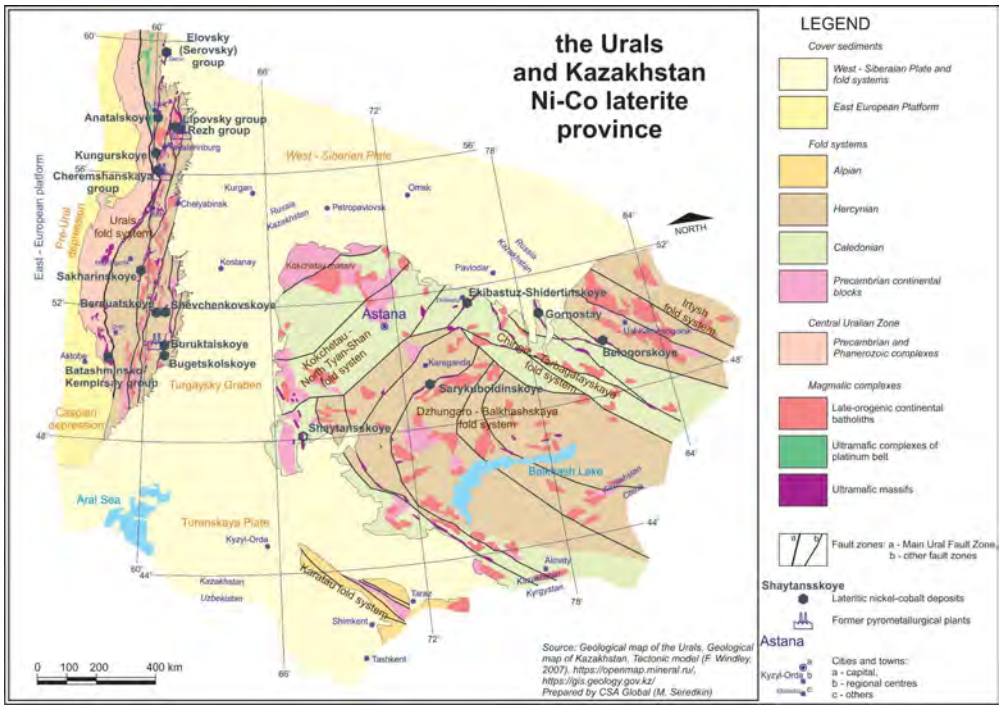

Mineralisation in the Ural-Kazakhstan Ni-Co laterite province

Cover / Overburden sediments (1) and Redeposited weathering crust (2)

Limonite mineralisation

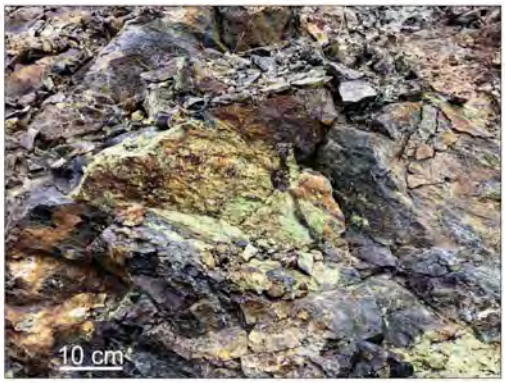

Relict of nontronite in limonite zone

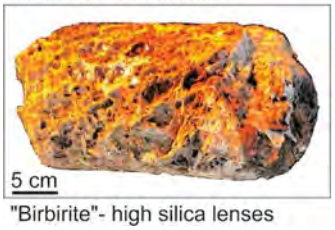

"Birbirite"- high silica lenses

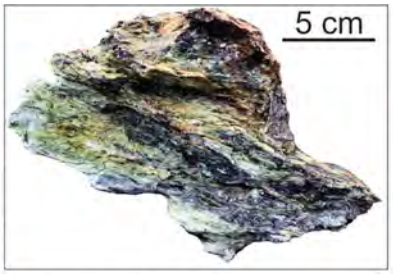

Nontronite with lens of manganese mineralisation

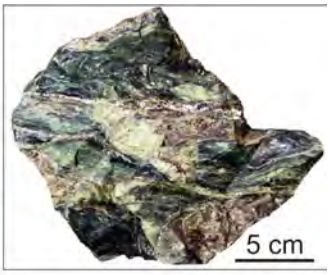

Nontronite with silicification

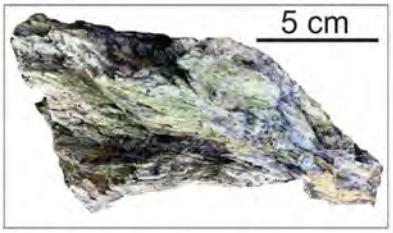

Silicified nontronite (green opal)

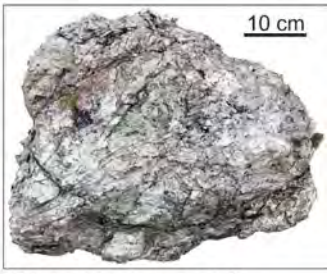

Nontronitised serpentinite

Location of the Ural-Kazakhstan Ni-Co laterite province

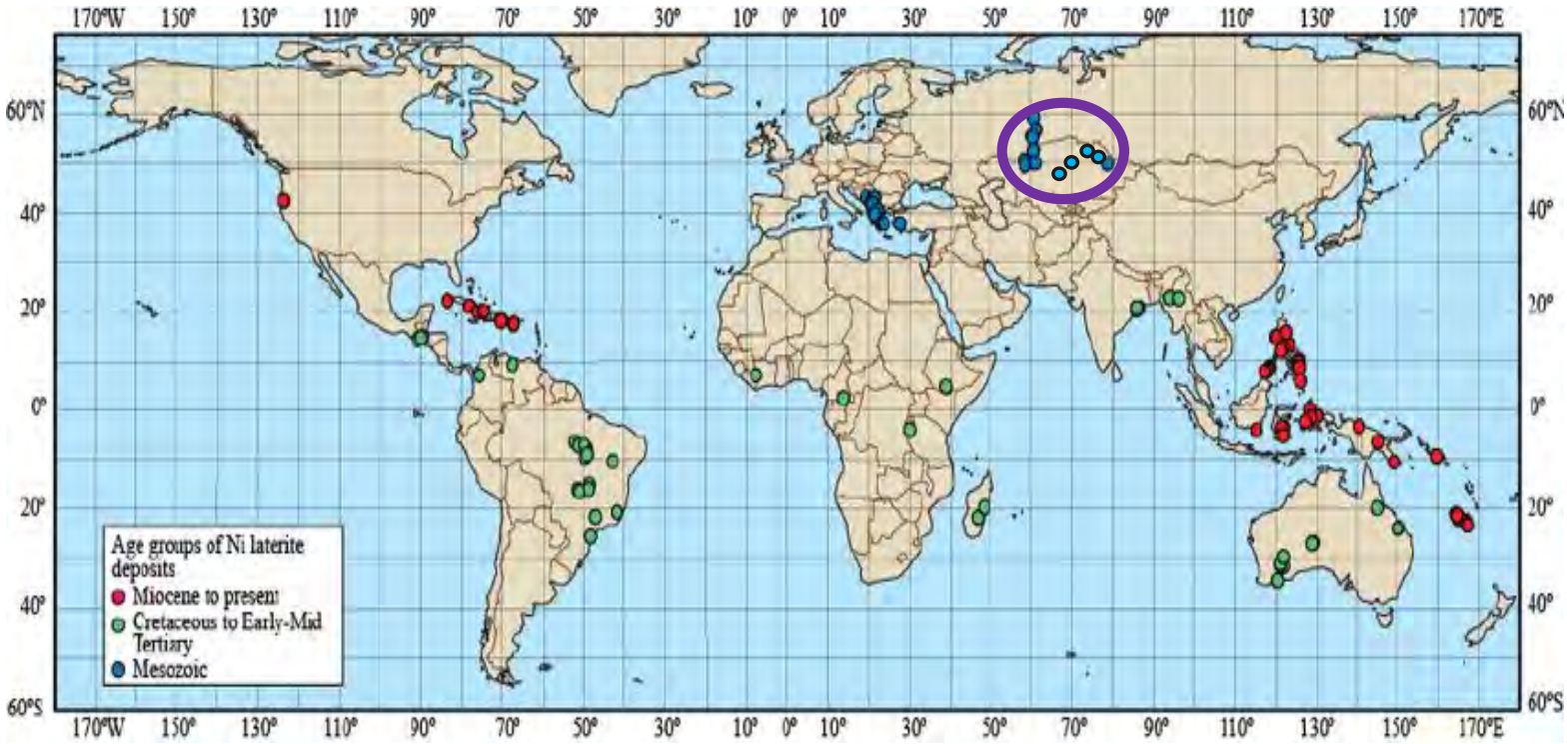

Past pyrometallurgical operations

	2002	2003	2004	2005	2006	2007	2008	2009	2010	2011	2012	2013	2014	2015	2016	2017	2018	2019	2020	2021	2022	2023	2024
New technologies	Initial development														Application in test regime								
	YouzhUralNickel Operation Plant														YouzhUralNickel Idle Plant								
	UfaleyNickel Operation Plant															UfaleyNickel Idle Plant				UfaleyNickel Demolished Plant			
	RezhNickel Operation Plant															RezhNickel Idle Plant							

Energy intensive technologies with high emissions

Class of the process		Type of the process	Products
	Pyrometallurgy	Smelting of Saprolite ore	Ferronickel production
	Pyrometallurgy	Smelting of Limonite ore	Nickel pig iron
	Combination of Pyrometallurgy and Hydrometallurgy	Caron process for Limonite ore: Reduction at high temperature Ammonium leaching, SX processing of pregnant solutions	SX with following precipitation Ni and Co products

Conventional CAPEX and OPEX intensive technologies

Class of the process		Type of the process	Products
	Hydrometallurgy - HPAL	For low-magnesium ore Processing of pregnant solutions by sulfidisation and SX	Ni and Co products (MHP, sulphates etc)
	Hydrometallurgy - HPAL	For low-magnesium ore Processing of pregnant solutions by IX and SX – CleanTeQ process	Ni, Co, Sc products (MHP, sulphates etc)
	Hydrometallurgy – AL (tank leaching)	Leaching by Sulphuric acid Limonite and saprolite ore	Ni and Co products (MHP, sulphates etc)
	Hydrometallurgy – AL (tank leaching)	Leaching by Hydrochloric acid Saprolite ore	Ni and Co products (MHP, sulphates etc)

Innovative technologies

Class of the process	Type of the process	Products
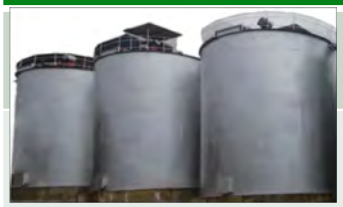 Hydrometallurgy – AL (tank leaching)	Leaching by Sulphurous acid Co-Mn limonite ore	Co and Mn products (MHP, sulphates etc)
Hydrometallurgy – AL (tank leaching)	Leaching by Nitric acid (DNi process) Limonite and saprolite ore	Ni, Co, Sc, Mg products (hydroxides / oxides)
 Hydrometallurgy – Heap leaching	Leaching by Sulphuric acid Limonite and saprolite ore	Ni and Co products (MHP, sulphates etc)
Hydrometallurgy – Heap leaching	Leaching by Sulphurous acid Limonite and saprolite ore	Ni and Co products (MHP, sulphates etc)
 Hydrometallurgy – In-Situ Recovery	Leaching by Sulphuric acid Limonite and saprolite ore	Ni and Co products (MHP, sulphates etc)
Hydrometallurgy – In-Situ Recovery	Leaching by Sulphurous acid Limonite and saprolite ore	Ni and Co products (MHP, sulphates etc)

Heap leaching for Nickel-Cobalt

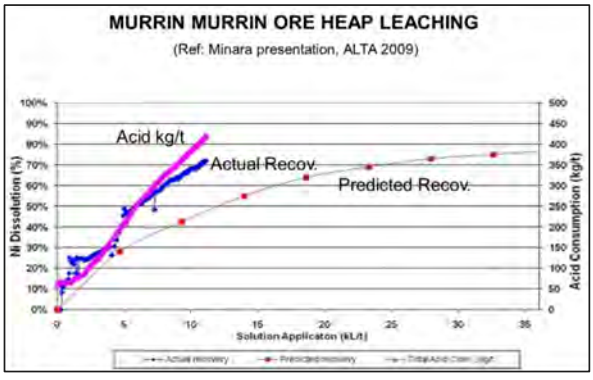

ALTA, 2009

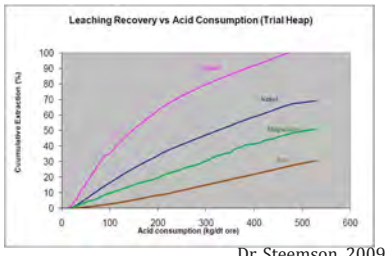

Dr. Steemson, 2009

In 2016-2017, Brazilian Nickel successfully demonstrated large-scale heap leaching, purification and recovery of Ni and Co from Piaui ore.

The company started commercial operation in 2022, expecting full-scale operation could produce an average of 25,000 tpa of Ni and 900 tpa of Co

In-Situ Recovery for Nickel-Cobalt

- In situ recovery (ISR) is one of the most effective methods to address mining costs.
- The key feature of ISR is transferring a significant proportion of the hydrometallurgical processing of mineralised bodies to the subsurface, to directly obtain solutions of metals.

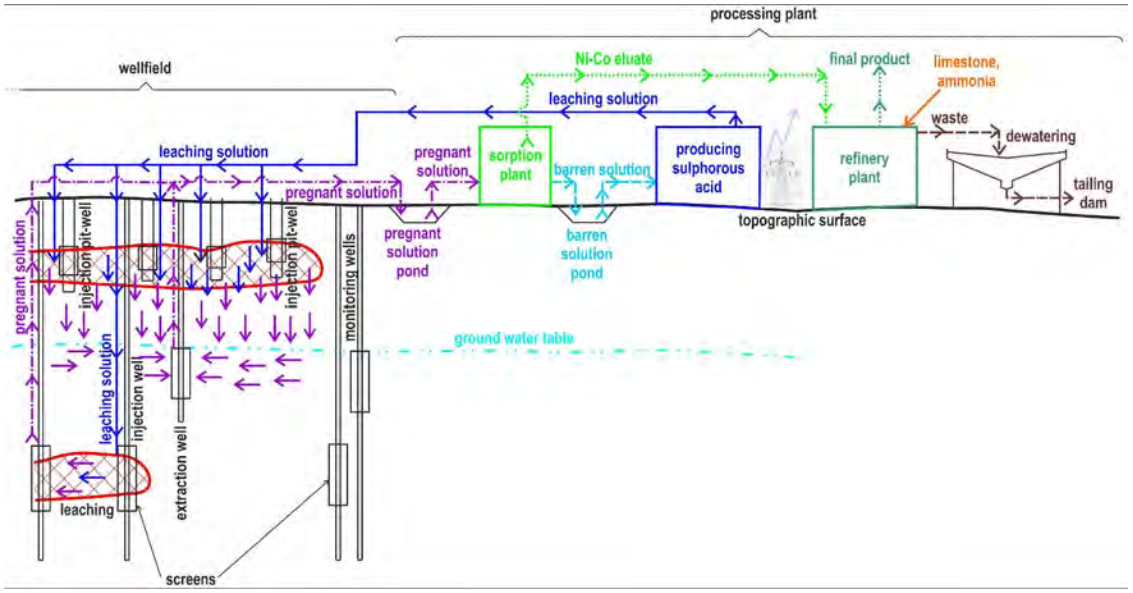

In the Urals-Kazakhstan Province ISR was considered the most effective innovative method for Ni-Co extraction

History of Nickel-Cobalt ISR development

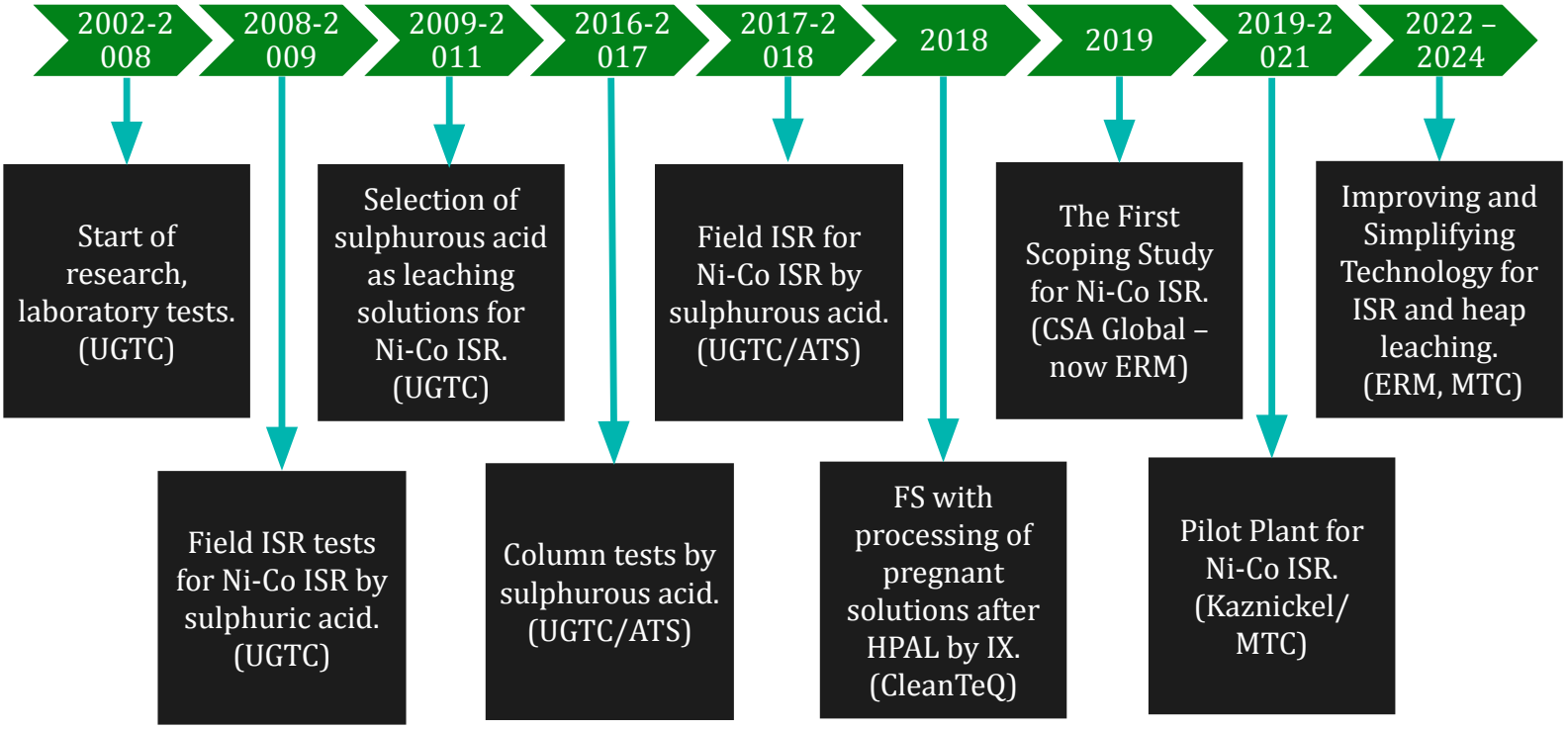

History of Nickel-Cobalt ISR development

- ISR was tested widely in the Ural-Kazakhstan Ni-Co laterite province
- ISR by Sulphuric acid was tested in the initial period on the Urals Ni-Co deposits
- ISR by Sulfurous acid was tested and is currently developing on the Kazakhstan Ni-Co deposits

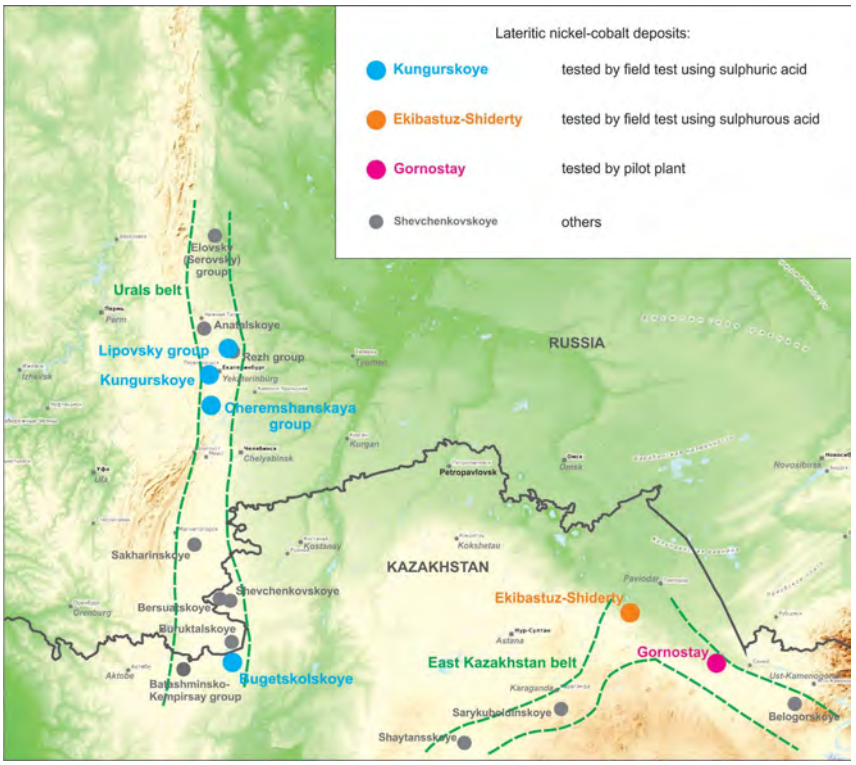

Initial period of R&D of Ni-Co ISR technology

The most complete field test was performed on the Rogozhnsky deposit (South Ural) (personal communications).

- Period: 2008-2009
- Tonnage: 410 t @ 0.61%Ni @ 2.5 t Ni
- Duration: 8 months
- Leaching Solution (Lixiviant): Sulphuric Acid
- Nickel recovery 8% (1% in month)
- Nickel grade in pregnant solutions up to 750 mg/L (average in the best month 500 mg/L)
- Acid consumption – 20 t (~50 kg/t or ~400 kg/t for target nickel recovery 65%
- L/S: 2.1 m^3/t or ~17 m^3/t for target nickel recovery 65%.

Investigation of leaching using sulphurous acid

- Successful investigations of sulphurous acid as a lixiviant for leaching Ni-Co laterite mineralisation – limonite and silicate
- Column tests for investigations of leaching dynamics, components recovery and acid consumption

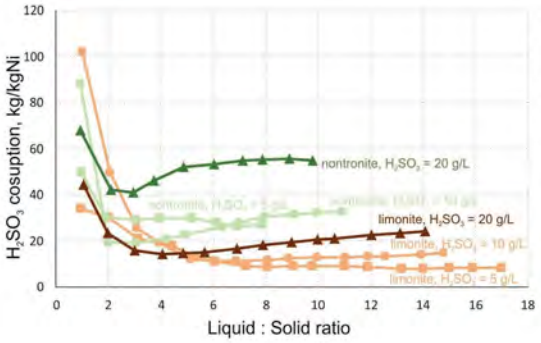

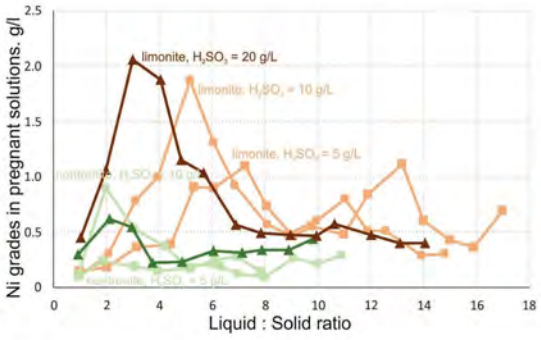

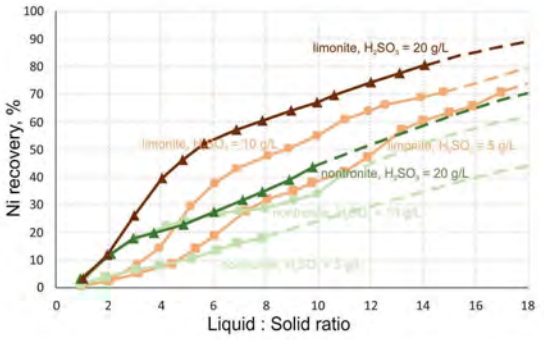

Field test at the Ekibastuz-Shiderty deposit in 2017-2018

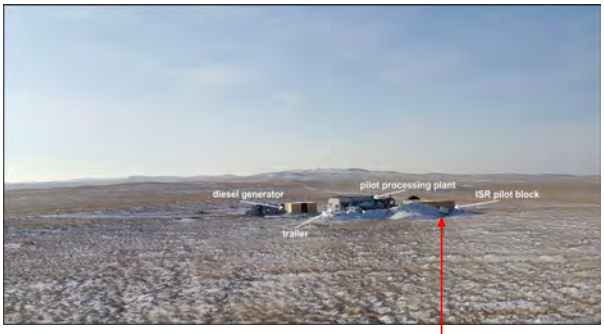

Test results demonstrate a principal opportunity to produce a final product of nickel and cobalt cathode from pregnant solutions after ISR by IX processing and, following neutralisation, SX and electrowinning processes

Nickel cathode

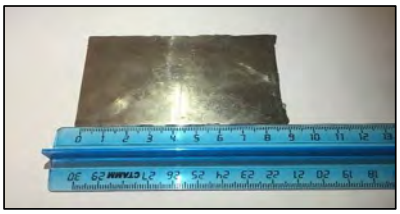

Cobalt cathode

The first Scoping Study for Ni-Co ISR Hydrogeology

The average measured permeability by classical hydrogeological tests is:

- 0.1-0.3m/day

And in fractured zones up to 5m/day

However, permeability after acidification is probably higher and average pumping rate is 1.6 m^3/hour

Groundwater table is located in fractured serpentinites usually

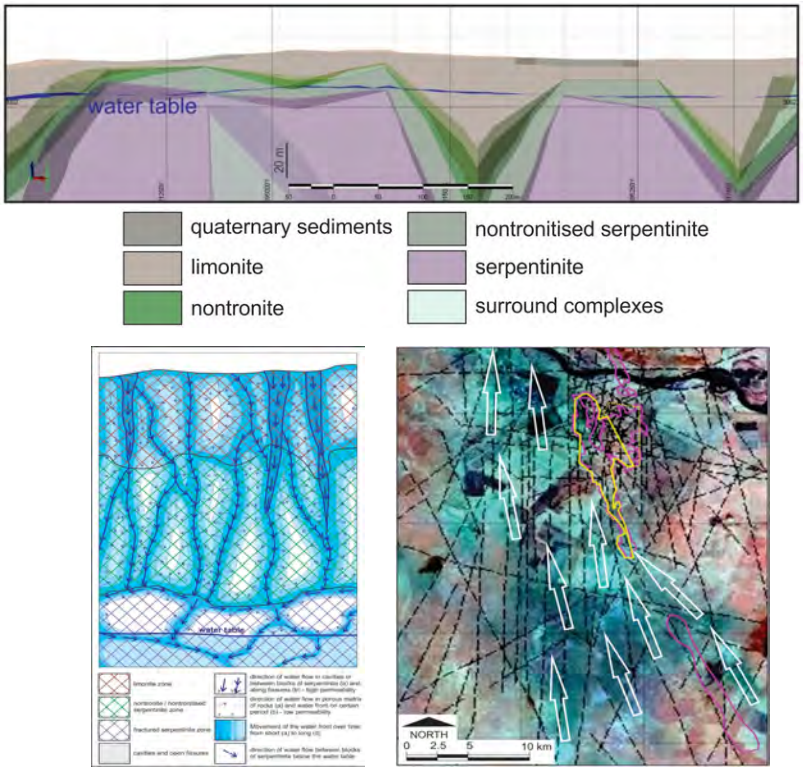

The first Scoping Study for Ni-Co ISR Mining Scheme

- Operational cells above the water table (infiltration ISR) emulate heap leaching with vertical movements of leaching solutions and collection of pregnant solutions at the water table.
- Operation cells below the water table (filtration ISR) are classical style of ISR, with sub-horizontal movement of pregnant solutions.

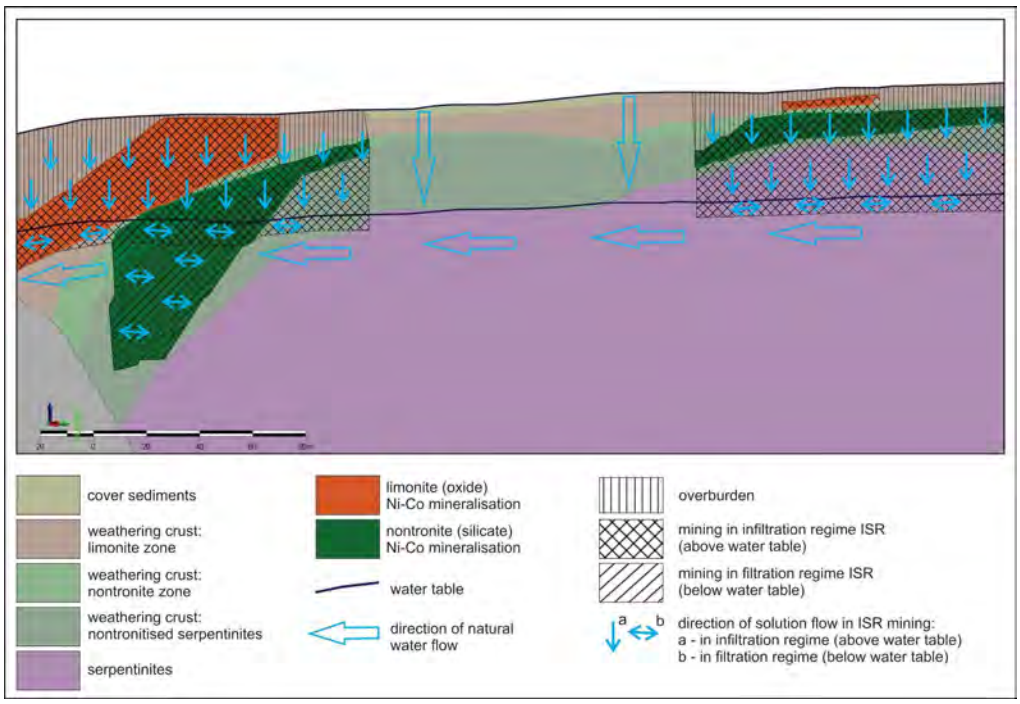

The first Scoping Study for Ni-Co ISR Lixiviant

Sulphurous acid preparation is part of the Sulfuric acid plant and may be implemented on site easily for preparation lixiviant from lump sulphur

A sulphurous acid plant was designed for the Mt Thirsty cobalt project in Western Australia

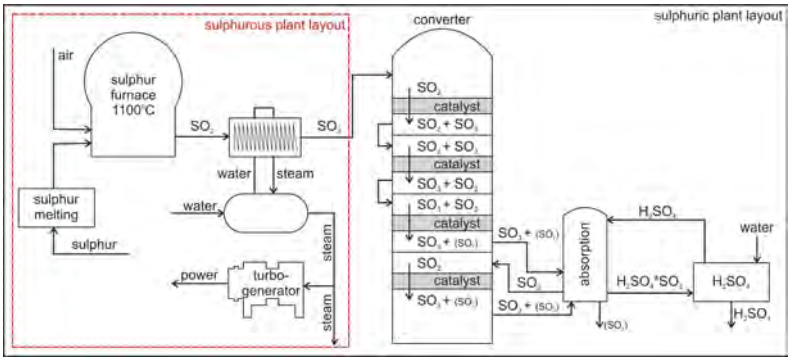

The first Scoping Study for Ni-Co ISR Processing of solutions

- ERM Sustainable Mining Services (formerly CSA Global) prepared the first Scoping Study for Ni-Co ISR based on UGTC tests, the CleanTeQ flowsheet.
- Processing of pregnant solutions by Ion Exchange (sorption to resin) and following processing of eluate – neutralisation, solvent extraction and crystallisation of the final product.
- Power and steam will be produced in a Sulphurous acid plant, and the project will have **<u>almost zero carbon dioxide emissions</u>** due to the generation of steam and electrical power.

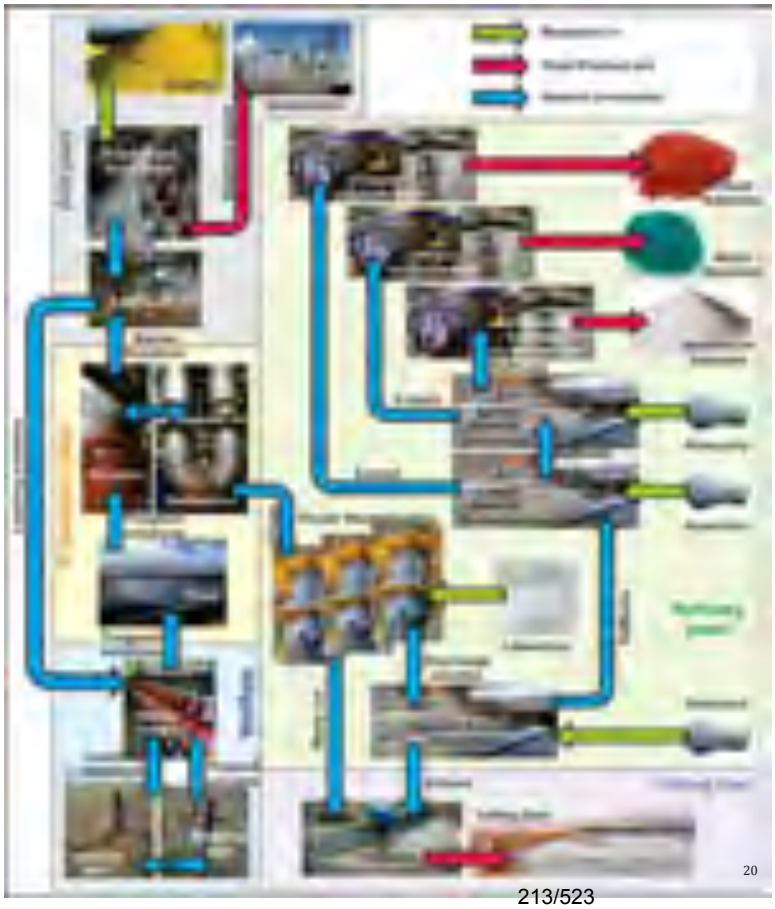

The first Scoping Study for Ni-Co ISR
Final products

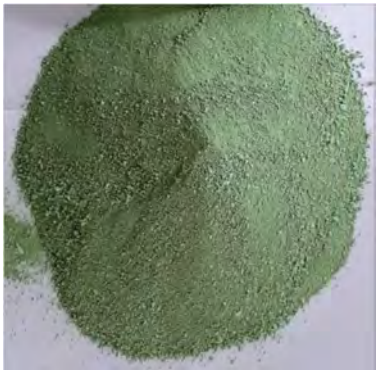

Option 1 – production Mixed Hydroxide Precipitate (MHP)

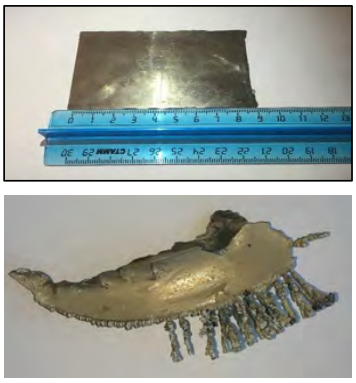

Option 2 – production Cathode Ni and Co

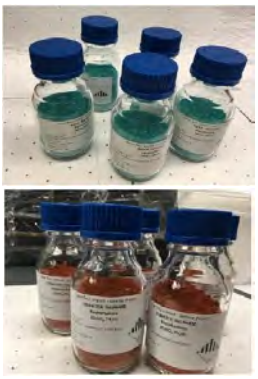

Option 3 – production sulphate of Ni and Co

Pilot operation of the Gornostay deposit

Kaznickel team constructed a Pilot Block and Plant at the Gornostay project in 2018:

- Wellfield
- Acidification block
- IX block
- Neutralisation
- Precipitation MHP

Pilot operation of the Gornostay deposit

- Kaznickel uses mixed sulphurous and sulphuric acid for nickel leaching.
- The average pumping rate of pumping wells is 1.6 m^3/hour.
- Kaznickel has achieved the stable work of ISR operation block
- Nickel grade in pregnant solutions reached up to 350 mg/L, with an average of 150-200 mg/L, comparable to estimated parameters in the Scoping Study.

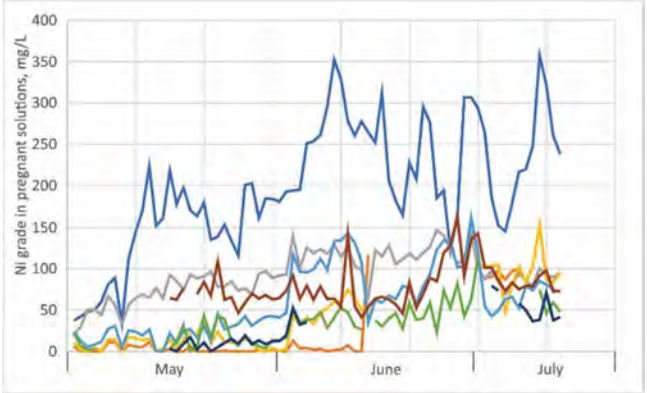

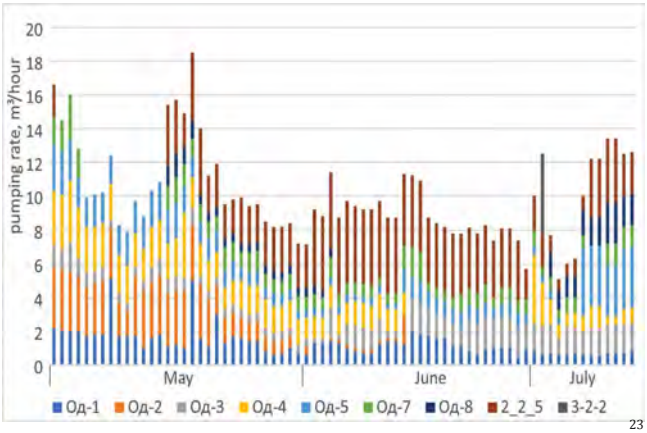

Manganese leaching by Sulphurous acid

- Manganese mineralisation with a low average MnO grade (17%) was tested for leaching by sulphurous acid
- Manganese recovery by sulphurous acid reaches >90% whereas by sulfuric acid is less than 20%
- The best results were for SO_2 gas as lixiviant with Mn grade in pregnant solutions up to 40 g/L
- Manganese was extracted from pregnant solutions in MnO_2 form by electrowinning

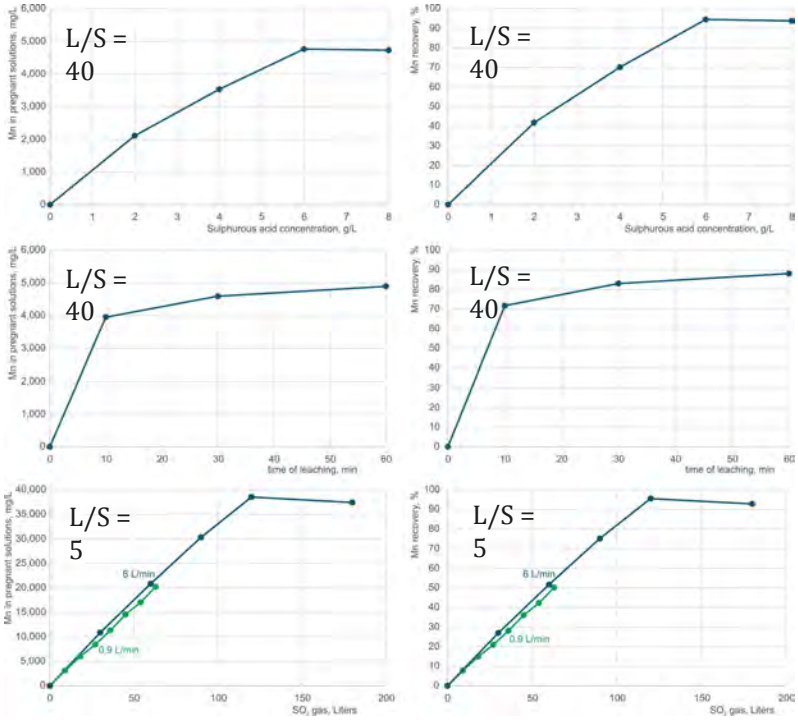

Challenges of developed technologies

- Very low permeability of material with high clay content in heap leaching

- ISR above water is poorly managed and sweep factor can be very high up to 50% as demonstrated the San-Manuel copper project

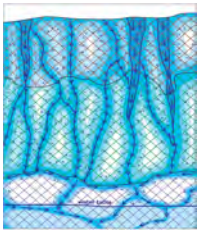

- Very complicated the CleanTeQ flowsheet is for poor pregnant solutions, may require two stages of sorption for production eluate with an acceptable grade of nickel

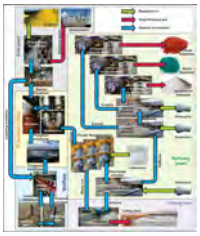

Tests for the potential improvements

Initial agglomerates

Column leaching

Agglomerates after leaching

- Polymeric agglomerate was found to be stable in acid heap leaching

Tests for the potential improvements

- Selective sorption of Ni on Lewatit TP-220 resin, followed by removal of iron from the resin using 'soft' acid solutions
- Desorption of Ni by 7-10% ammonium hydroxide, producing an eluate of Ni ammine complexes such as $Ni(NH_3)_4(OH)_2$, $Ni(NH_3)_6(OH)_2$ etc.
- Ammine complexes are easily dissociated to produce $Ni(OH)_2$, with ammonia recycled to the IX process

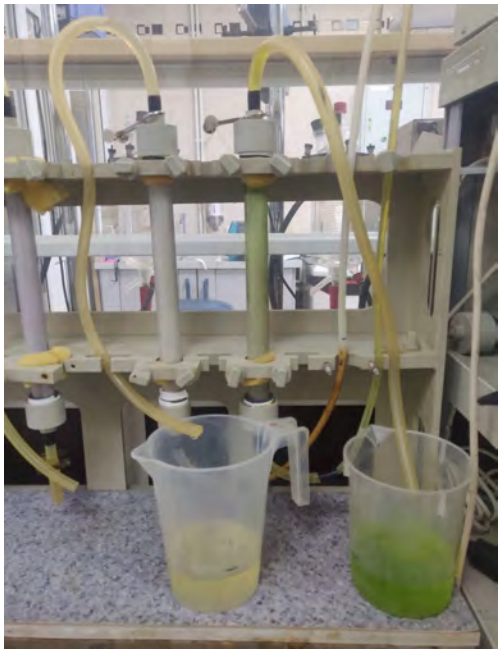

Distribution of technologies to other regions

- Ni-Co laterite deposits in the Urals-Kazakhstan province are poor and geology complicated, and technologies are still developing to be economic
- However, all found solutions are applicable to Ni-Co laterite deposits in other regions with classical zonation and higher Ni-Co grades

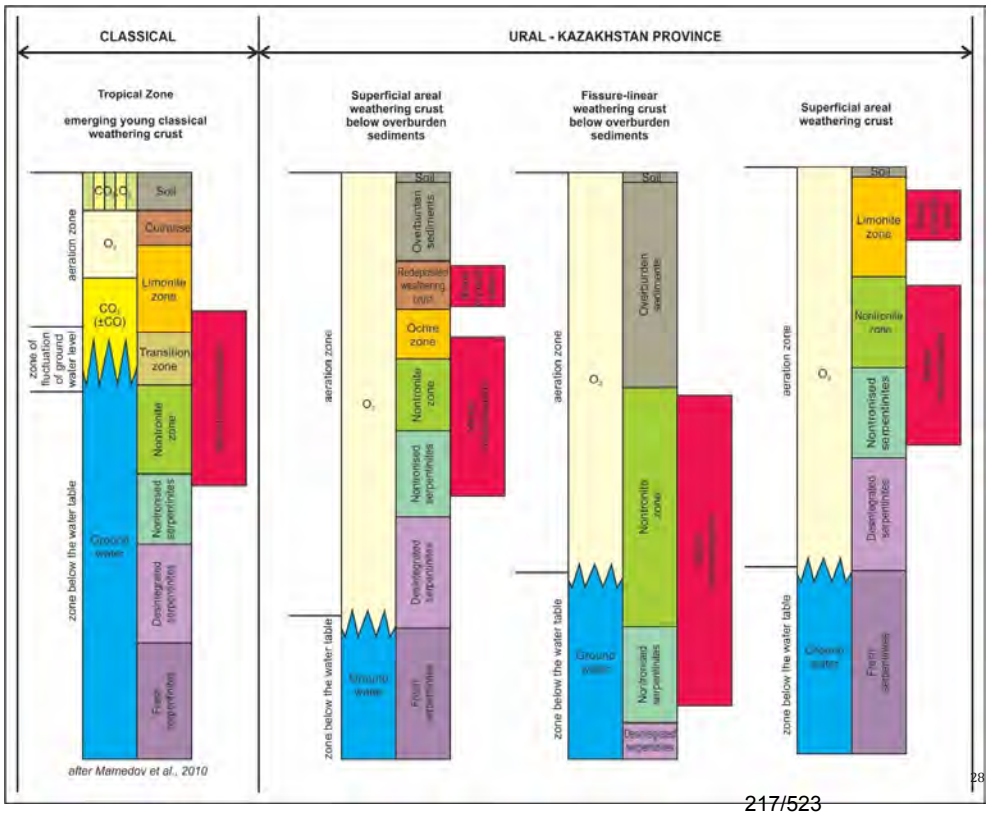

Application of this approach to other regions

- Mineralisation above the water table can be extracted by heap leaching and below the water table by ISR
- Sulphurous acid is recommended as the preferred lixiviant

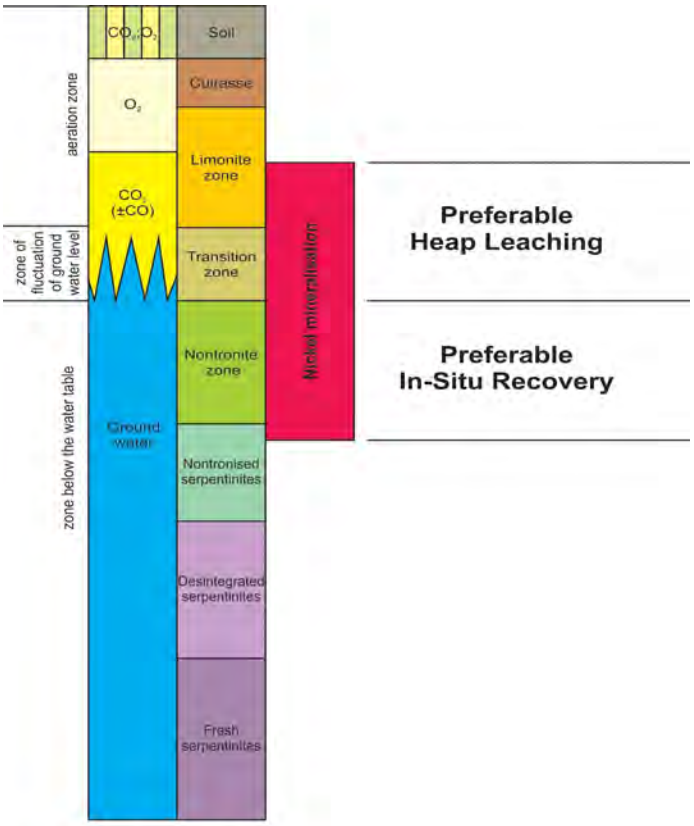

Based on materials from: Mamedov et al., 2010

EVALUATION OF CARBONATE AND PHOSPHATE BASED BIOCEMENT FOR IN-SITU BARRIER OPERATIONS

By

Pelin Polat, [2]Carlos Rodriguez Navarro, Abhijit Mukherjee, Navdeep K Dhami

School of Civil and Mechanical Engineering, Curtin University, Perth, Australia
[2]Department of Mineralogy and Petrology, Uni of Granada, Spain

Presenters and Corresponding Authors

Pelin Polat
pelin.polat@postgrad.curtin.edu.au
Navdeep K Dhami
navdeep.dhami@curtin.edu.au

ABSTRACT

In-situ recovery (ISR) refers to the hydrometallurgical method for extracting metals through specifically designed chemical interactions. ISR is being employed widely in mining for recovering an increasingly diverse range of metals including uranium, copper, nickel and gold. One of the foremost challenges in the ISR operation is to protect the surrounding geoenvironment and groundwater from the harsh lixiviants used in the process. Therefore it is critical to establish an environmentally conscious strategy to build barriers around.

This research aims to explore the potential of biogenically created carbonate (as limestone, magnesium carbonate) and phosphate (as hydroxyapatite, struvite) based barriers in various ISR-related environments. Created by natural biogeochemical activities of microbes in geological formations (microbialites, beach rocks), biocement has emerged as a potential biogeotechnical solution for a variety of engineering applications due to its significant advantages of low carbon footprint, low viscosity and recyclability. While majority of the research has focused on microbially induced calcium carbonate-based cement which faces challenges at low pH conditions, not much has been explored in developing low pH tolerant phosphate based biocement.

In this study, a range of microbial metabolic pathways, role of extra polymeric substances, substrates and their impact on formation of struvite and apaptite biocements has been demonstrated. The impact of biogenic phosphate and carbonate cements on acid and alkaline lixiviant tolerance has also been analysed. Overall, the outcome of this research has significantly improved our understanding of microbially induced biomineralisation process and widened the scope of biocement barriers as containment in ISR-related environments.

Keywords: In-Situ recovery, Biocement, Microbial carbonate, Microbial phosphate, lixiviant

Evaluation of Phosphate and Carbonate Based Biominerals For In-situ recovery (ISR) operations

Presenter: Pelin Polat
PhD student
School of Civil and Mechanical Engineering
Curtin University
WA, Australia

Content

- Introduction to ISR
- Barriers and containments in practice
- Biocementation
- Our research
- Outcomes

Background

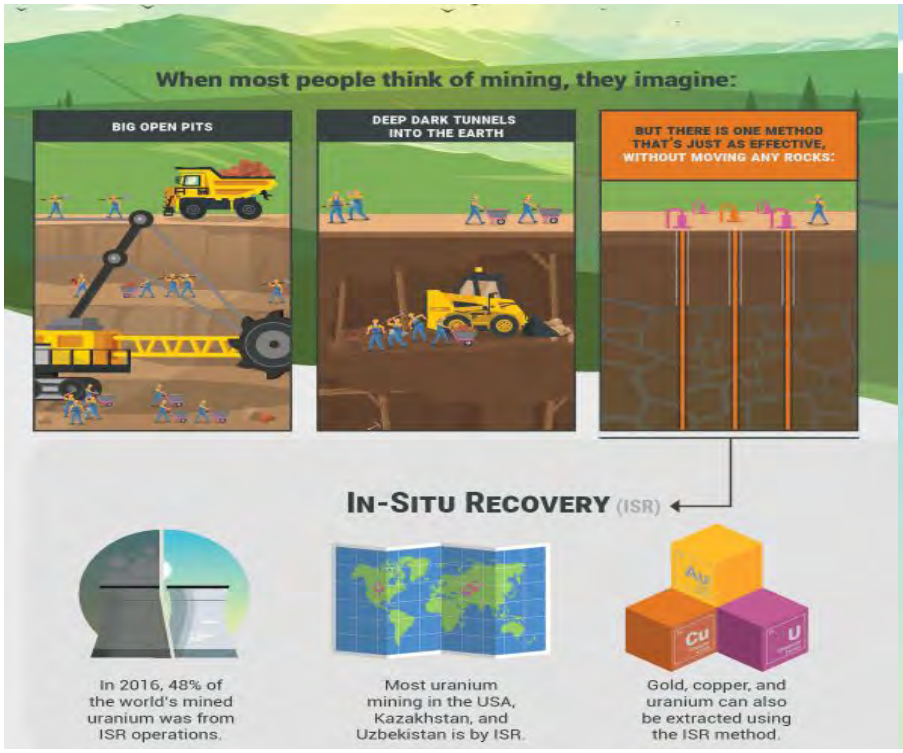

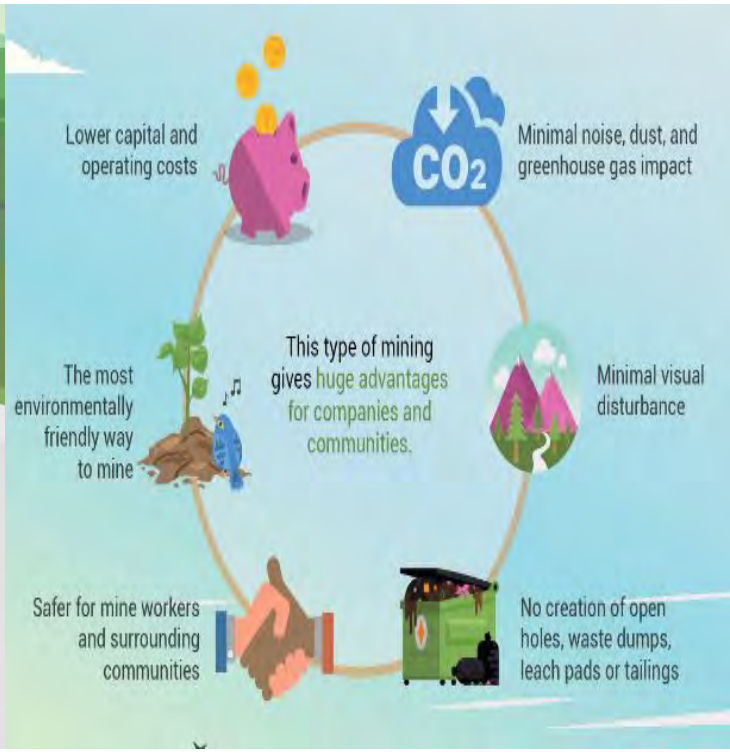

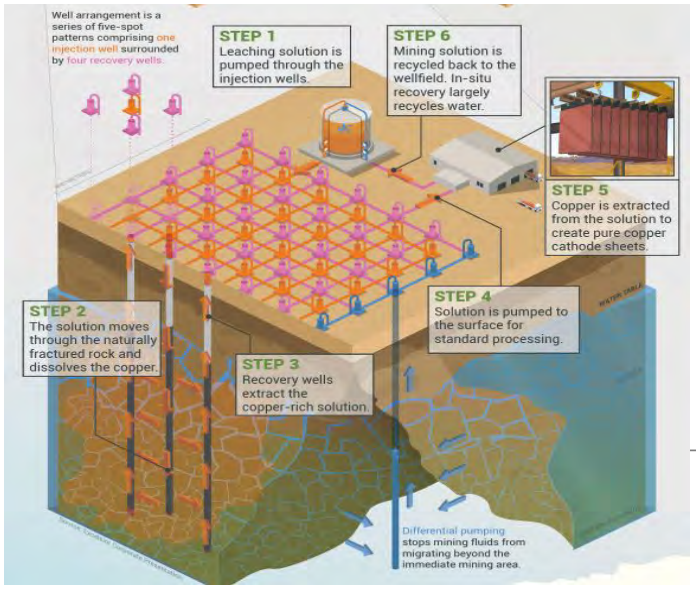

Commonly used lixiviants in ISR operations

Lixiviant	Co-reagents	Conditions	Dissolved metal species
Glycine	NaOH, oxygen	High pH	Au, Cu, Co, Fe, Si, Al, Ni, Zn, Ca,
Sulfuric Acid		Low pH	Cu, Ni, Sc, Re, REES, Y, Se, Mo, V, U
Ammonium sulfate	Ammonia, oxygen	High pH	Cu
Water		Brine	K, Na, Li

Challenges of ISR

- **Containment of leaching agents**
- Monitoring and managing subsurface fluid flow
- Ensuring minimal disturbance to surrounding ecosystems
- Addressing potential groundwater contamination concerns

Different types of barriers and containments in practice

The Problems With Current Barrier And Containment In Practice

- **Inefficacy**
- **Viscosity**
- **Environmental toxicity**
- **Cost**

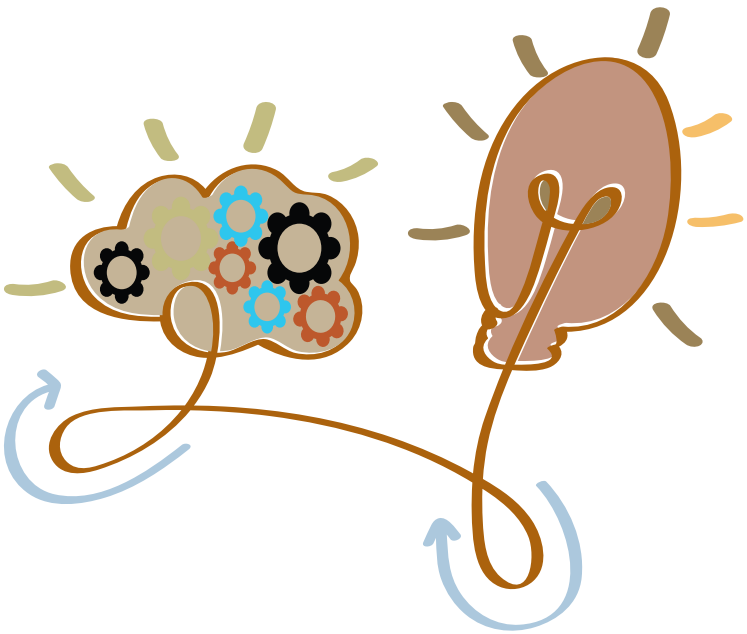

Get inspiration from…. Nature

Microbially induced mineral precipitation (biocementation)

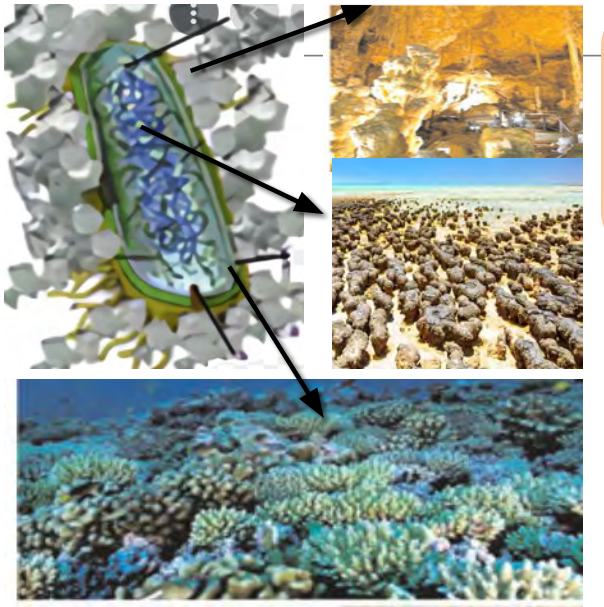

Natural process by which microbes form inorganic minerals and polymers as part of their basic metabolic activities

Recorded in a range of geological structures varying from travertines, corals, stromatolites to beach rocks in terrestrial and marine environments

Wide range of minerals can precipitate

- Carbonates
- Phosphates
- Sulphides
- Oxides
- Silicates

Bio-mineralization of calcium carbonates in natural structures (A) Corals (B) Stromatolites (C) Limestone cave www.sciencedaily.com

(Murugan, et al. 2021; Dhami, et al., 2013)

Bacterial metabolic routes in MIMP

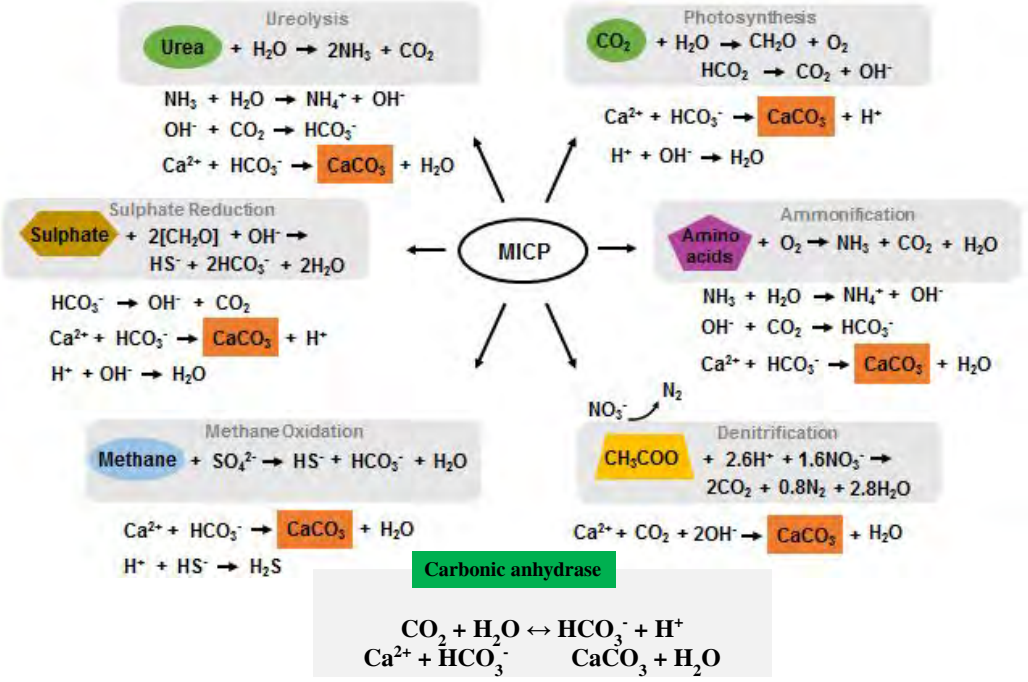

Benefits of MIMP

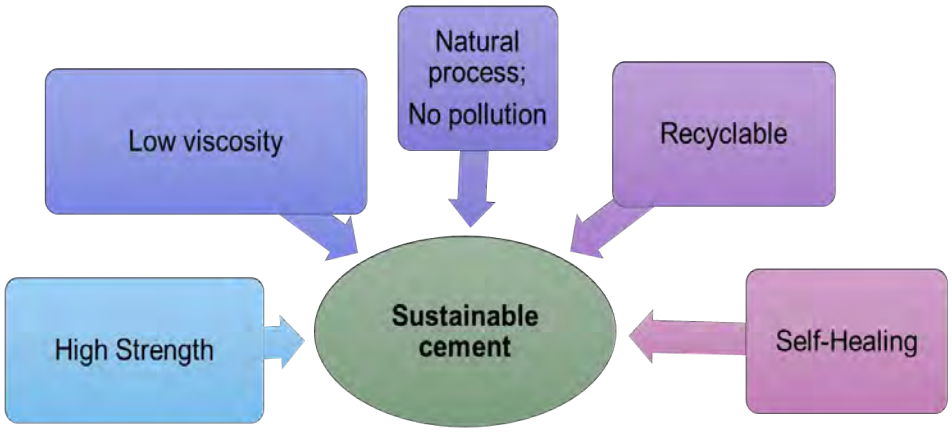

Microbially induced calcium carbonate precipitation (MICP)

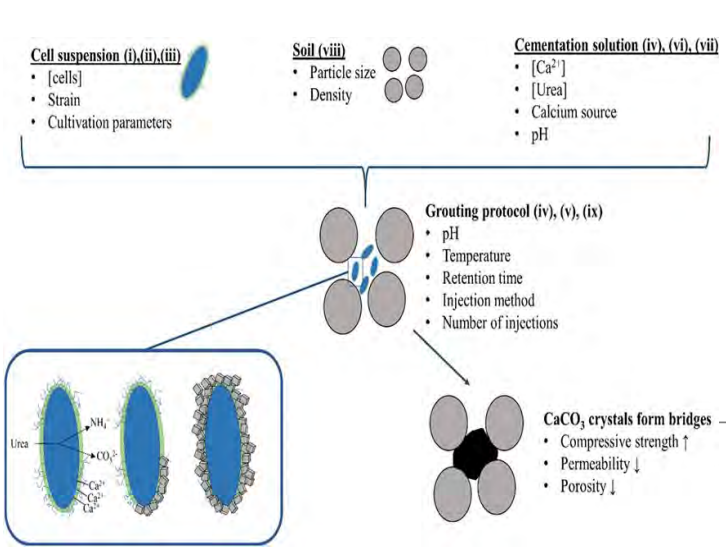


REVIEW PAPER

Erosion mitigation with biocementation: a review on applications, challenges, & future perspectives

Anant Aishwarya Dubey · Navdeep Kaur Dhami · K. Ravi · Abhijit Mukherjee

RESEARCH PAPER

Biopolymer-biocement composite treatment for stabilisation of soil against both current and wave erosion

Anant Aishwarya Dubey · Jack Hooper-Lewis · K. Ravi · Navdeep Kaur Dhami · Abhijit Mukherjee

WM&R

Effective method for upcycling construction and demolition waste into concrete: A life cycle approach

Abhijit Mistri, Venkata Ravi Sankar Cheela, Brajesh Kumar Dubey, Navdeep Dhami, Sriman Kumar Bhattacharyya, Abhijit Mukherjee and Sudhirkumar V Barai

Limitations of MICP

- Extreme conditions such as lower pH conditions
- By-products and Uncontrolled Growth
- Obtaining Uniform Treatment
- Economic

(Phillips et al., 2013, Farah et al., 2016, Zhu and Maria 2016 Hart et al.,2012)

Microbially induced phosphate precipitation

- Wide range of phosphate compounds can precipitate
- Tricalcium phosphate
- Struvite
- Apatite
- Baricite
- Vivianite
- Variscite

BACTERIAL ENZYMES
Acid phosphatases enzymes
Such as *Bacillus sp. and Pseudomonas sp.*

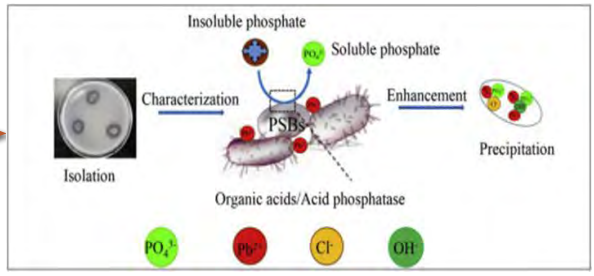

Advantages of bio-phosphates as grout material

- Nontoxic
- Better performance and stability under low pH conditions
- Can be extracted from natural sources as fertilizers and bones of livestock

(Qian C, 2018)

Hydroxyapatite (HAP) $Ca_5(PO_4)_3(OH)$

$$10\ Ca(OH)_2 + 6\ H_3PO_4 \rightarrow Ca_{10}(PO_4)_6(OH)_2 + 18\ H_2O$$

- Thermodynamically stable in its crystalline state
- Similar composition to bone mineral
- Biological sources or wastes such as mammalian bone, marine or aquatic sources, shell sources, and plants and algae and also from mineral sources
- Can be synthesised chemically or microbiologically

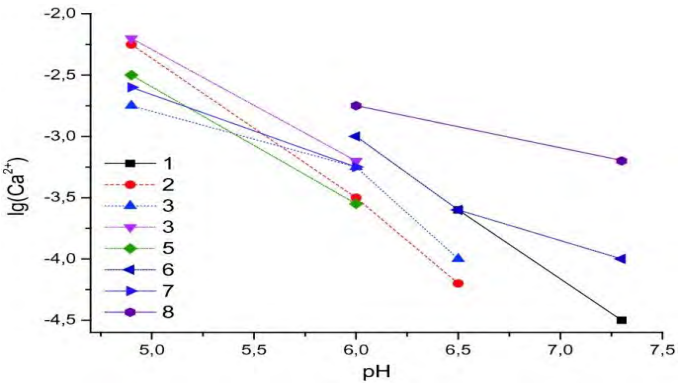

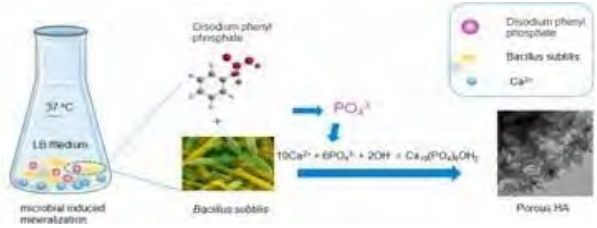

Experimental data on hydroxyapatite solubility in aqueous solutions at different pH from literature sources: (1) Rootare et al. (1962), (2) Wier et al. (1971), (3) Avnimele et al. (1973), (4) Chuong (1973), (5) McDowell et al. (1977), (6) Bell et al. (1978), (7) Verbeeck et al. (1980), (8) Mahapatra et al. (1982)

Methodology

Sporosarcina pasteurii ATCC 11891

Gram positive
Ureolytic bacterial culture
Has the ability to precipitate calcite
(Dhami et al., 2012)

Bacillus subtilis ATCC 6051

Gram-positive
Biofilm producing
Ureolytic bacterial culture
capable of producing nano-hydroxyapatite

(Yu et al., 2021).

ATCC13525

Gram – negative
Strong biofilm producing
Capable of producing nano-hydroxyapatite
(Turner et al., 2017)

Bacteria + Cementation Fluid

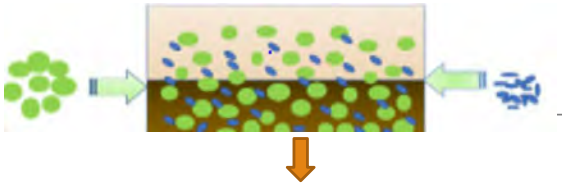

Growth condition optimization
Enzyme activity measurements

Crystal precipitation

Crystal analyses
Scanning Electron Microscopy
X- ray Diffraction
Nanomechanical characterisation
Acid Solubility Test

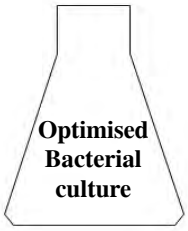

+

Mine tailings

- Mineral Characteristic
- Hydraulic characterisation
- Service life assessment

Results

. Growth curve for 3 different cultures

.

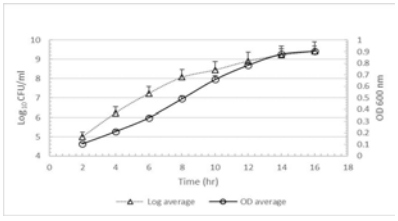

S. pasterurii

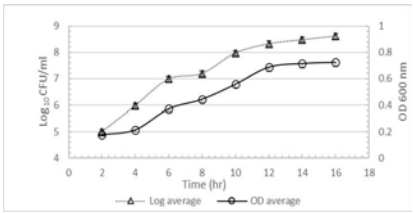

B. subtilis

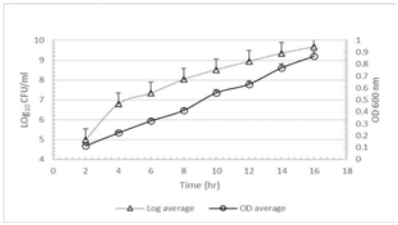

P. fluorescence

- optical density (OD 600 nm) and the corresponding bacteria concentration (CFU ml) are plotted vs. time. Data of concentration curves are reported until the stationary phase

. Urease and Alkaline Phosphatase Enzyme Activities

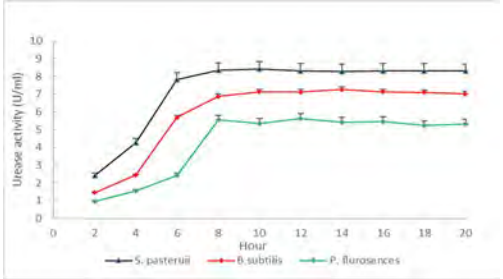

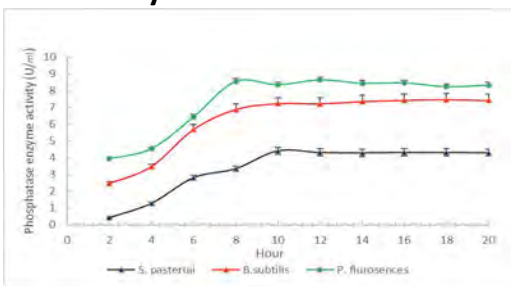

. Concentration of soluble calcium ions, phosphate and pH over the time

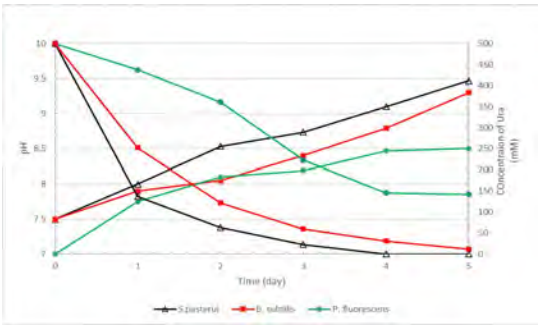

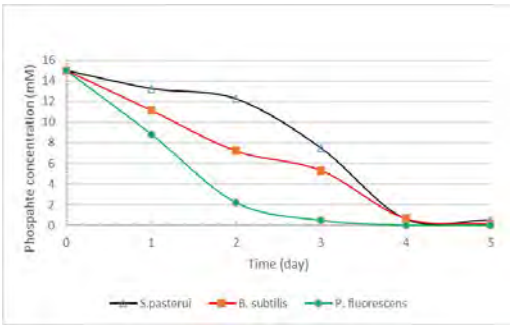

- Dry weight of insoluble precipitate

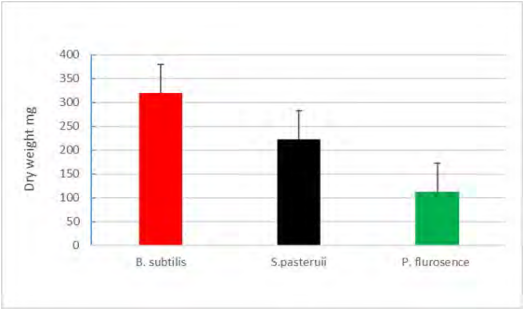

- Precipitation by *S. pasteurii*

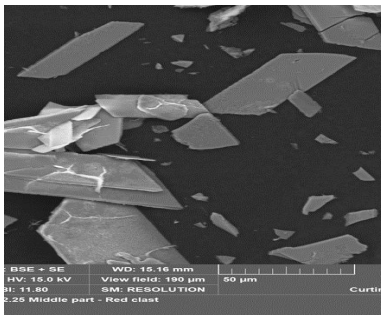

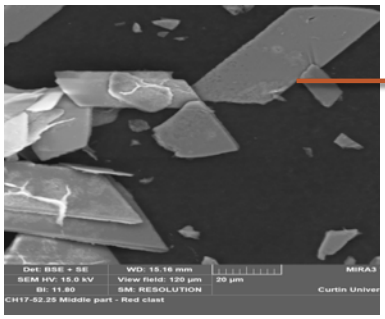

- XRD results

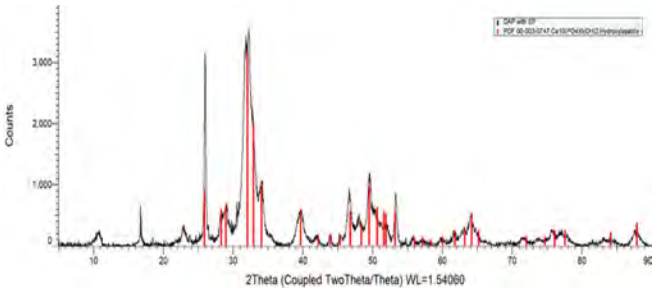

- Precipitation by *B. subtilis* Hydroxyapatite

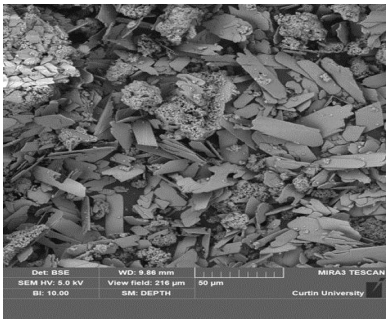

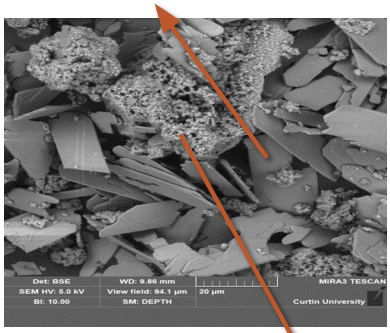

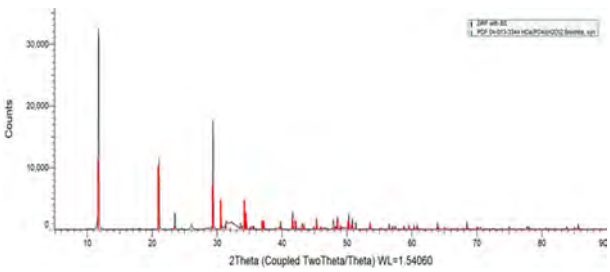

Brushite

Precipitation by *P. flurosence*

XRD results

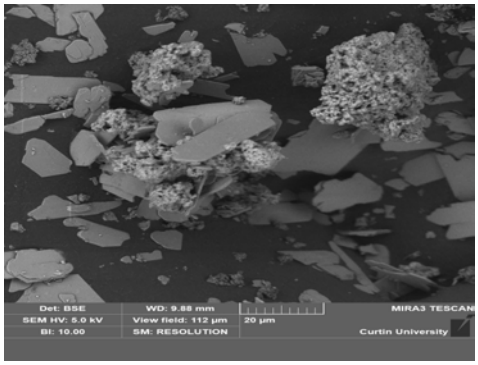

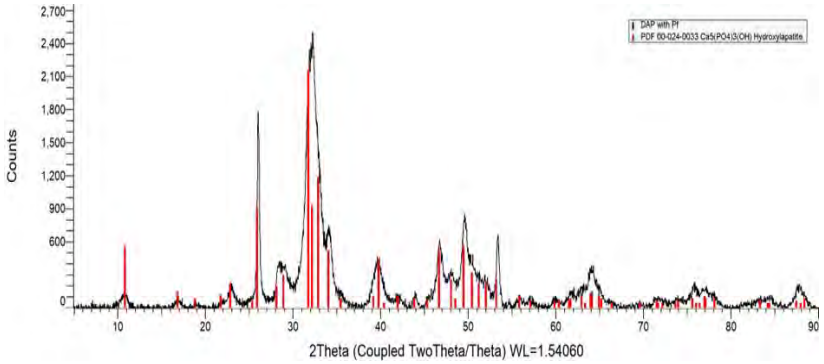

Raman Analysis For HAP Precipitation

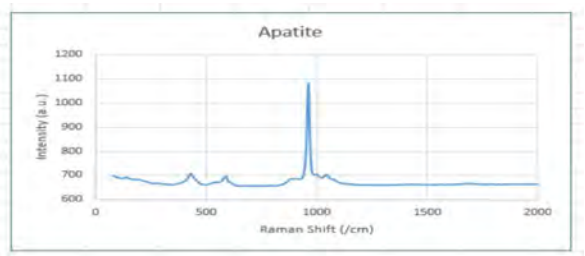

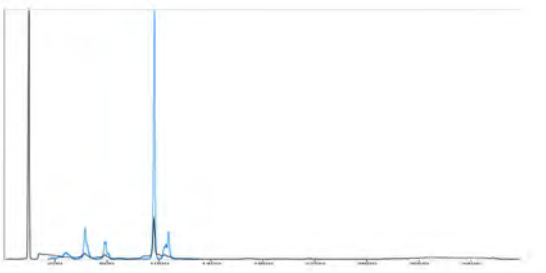

Nanoindentation Results For HAP

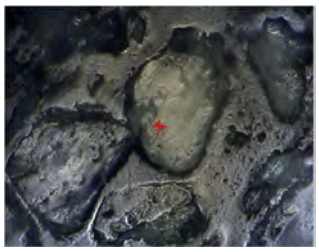

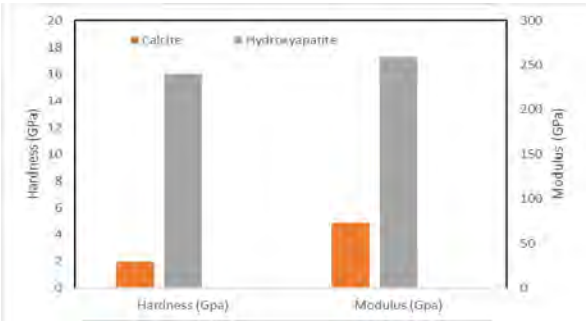

- **Abiogenic precipitation**

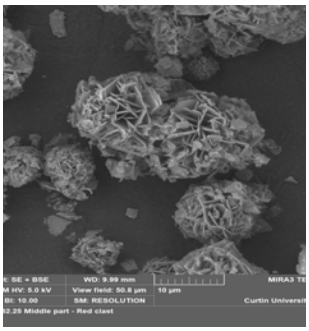

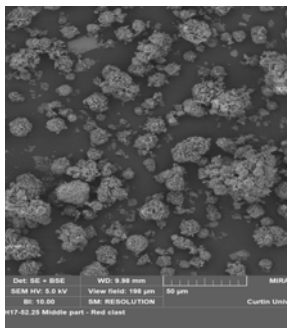

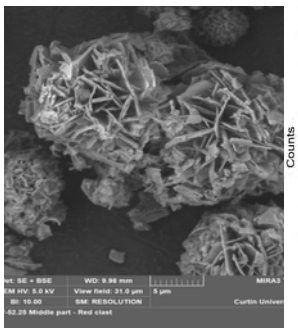

- XRD results

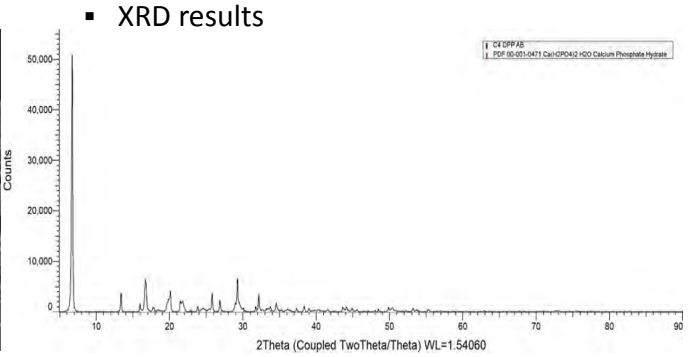

- Raman result

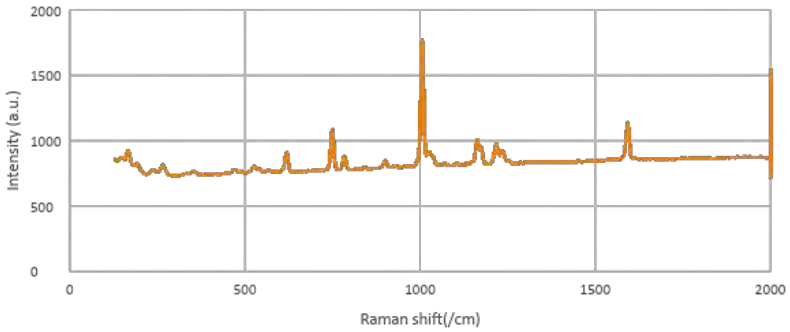

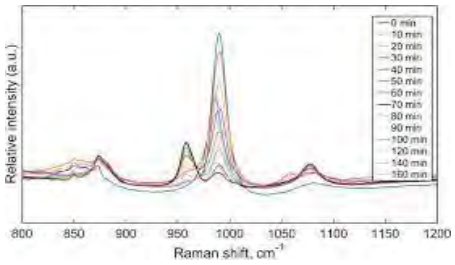

Hang, B. 2018

. The impact of biofilm production on mineral precipitation

B.subtilis **vs** ***S.pasteurii***

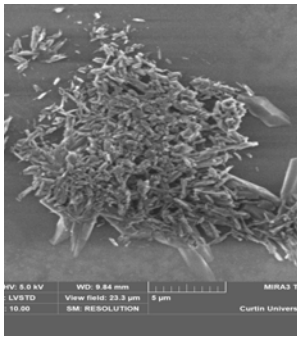

6hr after treatment

12hr after treatment

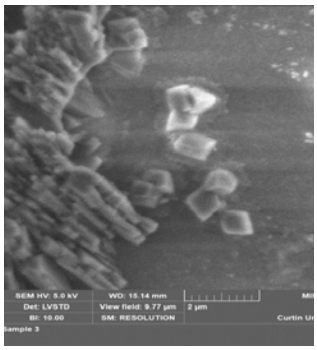

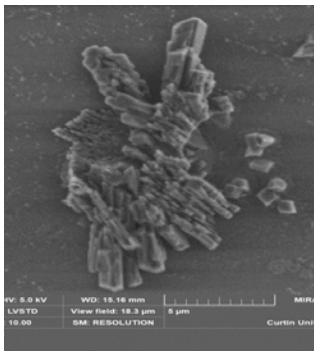

6hr after treatment

12hr after treatment

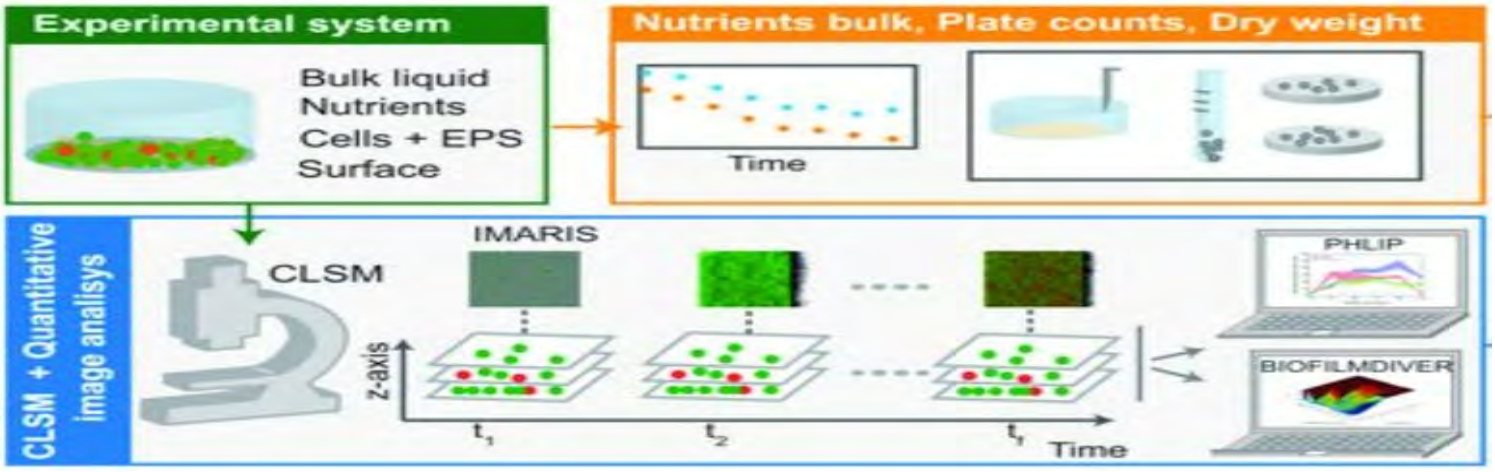

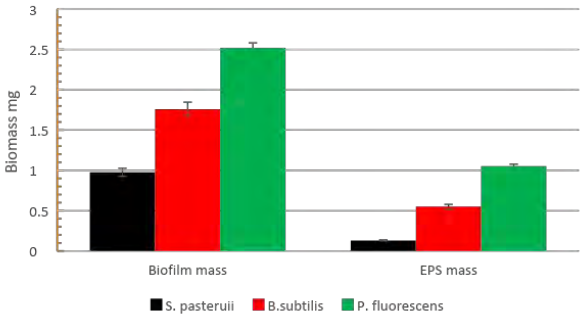

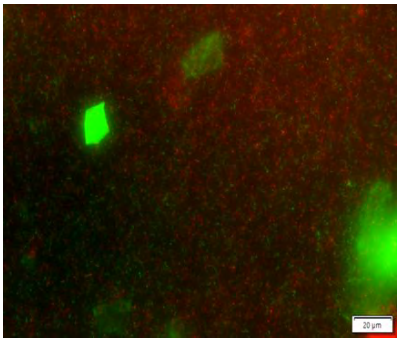

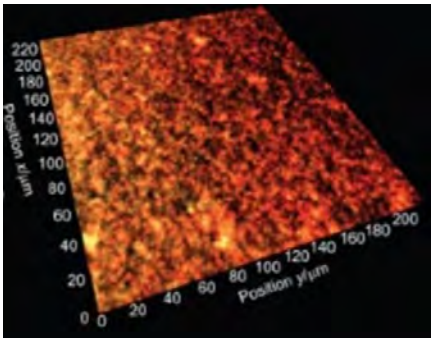

. Acid solubility of Biogenic Hydroxyapatite/ Calcite

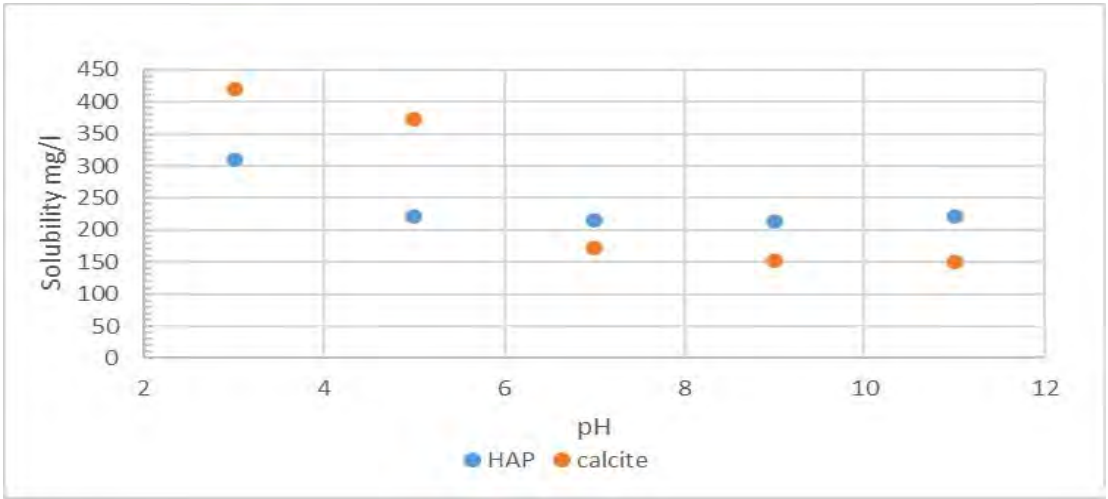

Ongoing Experiments

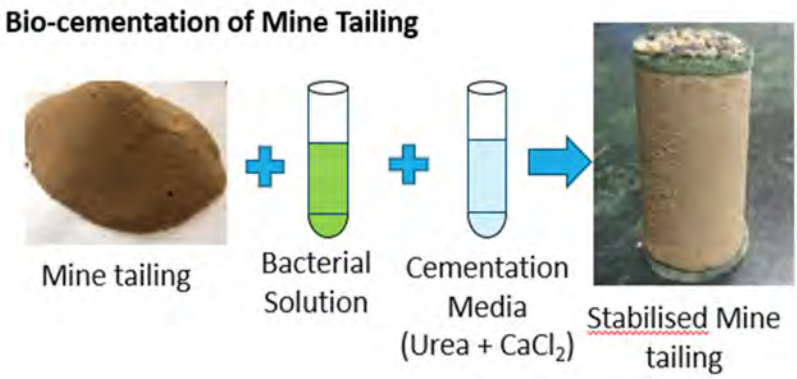

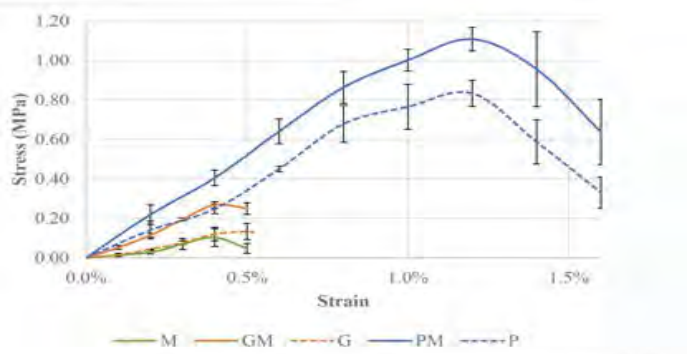

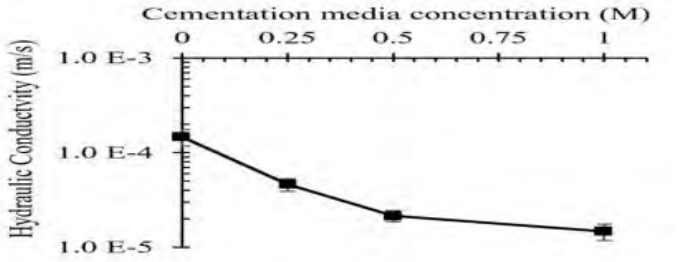

Findings

- Successful production of phosphate biocement as hydroxyapatite achieved
- Bacterial culture plays a crucial role in determining the morphological-mineralogical-nanomechanical properties of precipitated hydroxyapatite
- Biofilm and extrapolymeric substance producing cultures can create uniformity in HAP crystal orientation and pattern
- Biogenic hydroxyapatite demonstrates higher stability in pH environments (>5)
- Co-precipitation of carbonate and phosphate biocement offers promising solution for sustainable barriers
- Further studies to be conducted to investigate the efficacy of biocement barriers under simulated subsurface conditions over longer durations

Acknowledgments

References

Gat D, Ronen Z, Tsesarsky M. Soil Bacteria Population Dynamics Following Stimulation for Ureolytic Microbial-Induced CaCO3 Precipitation. Environmental Science & Technology. 2016;50(2):616-624. doi:10.1021/acs.est.5b04033

Whiffin VS, van Paassen LA, Harkes MP. Microbial Carbonate Precipitation as a Soil Improvement Technique. Geomicrobiology Journal. 2007;24(5):417-423. doi:10.1080/01490450701436505

1Dejong JT, Mortensen BM, Martinez BC, Nelson DC. Bio-mediated soil improvement. Ecological Engineering. 2010;36(2):197-210. doi:10.1016/j.ecoleng.2008.12.029

14. Hammes F, Verstraete* W. Key roles of pH and calcium metabolism in microbial carbonate precipitation. Reviews in Environmental Science and Biotechnology. 2002;1(1):3-7. doi:10.1023/A:1015135629155

Yu X, Jiang J. Mineralization and cementing properties of bio-carbonate cement, bio-phosphate cement, and bio-carbonate/phosphate cement: a review. Environmental Science and Pollution Research. 2018;25(22):21483-21497. doi:10.1007/s11356-018-2143-7

Qian C, Yu X, Wang X. Potential uses and cementing mechanism of bio-carbonate cement and bio-phosphate cement. 2018;8(9):095224. doi:10.1063/1.5040730

Maxwell RF, Krista G, David F, Melanie JF. Physiological and genetic characterization of calcium phosphate precipitation by Pseudomonas species. Scientific Reports. 2018;8(1):1-14. doi:10.1038/s41598-018-28525-4

Sassoni E, Naidu S, Scherer GW. The use of hydroxyapatite as a new inorganic consolidant for damaged carbonate stones. Journal of Cultural Heritage. 2011;12(4):346-355. doi:10.1016/j.culher.2011.02.005

Naidu S, Blair J, Scherer GW. Acid-Resistant Coatings on Marble. American Ceramic Society. Journal of the American Ceramic Society. 2016;99(10):3421-3428. doi:10.1111/jace.14355

.Sassoni E. Hydroxyapatite and Other Calcium Phosphates for the Conservation of Cultural Heritage: A Review. Materials (Basel, Switzerland). 2018;11(4) doi:10.3390/ma11040557

Cardew PT, Davey RJ. The Kinetics of Solvent-Mediated Phase Transformations. Proceedings of the Royal Society of London. Series A, Mathematical and Physical Sciences (1934-1990). 1985;398(1815):415-428. doi:10.1098/rspa.1985.0043

Putnis A, Putnis CV. The mechanism of reequilibration of solids in the presence of a fluid phase. Journal of Solid State Chemistry. 2007;180(5):1783-1786. doi:10.1016/j.jssc.2007.03.023

Wang L, Ruiz-Agudo E, Putnis C, Menneken M, Putnis A. Kinetics of calcium phosphate nucleation and growth on calcite: Implications for predicting the fate of dissolved phosphate species in alkaline soils. 2012

Pedrosa ET, Putnis CV, Putnis A. The pseudomorphic replacement of marble by apatite: The role of fluid composition. Chemical Geology. 2016;425(C):1-11. doi:10.1016/j.chemgeo.2016.01.022

Turner RJ, Renshaw JC, Hamilton A. Biogenic Hydroxyapatite: A New Material for the Preservation and Restoration of the Built Environment. ACS Appl Mater Interfaces. 2017 Sep 20;9(37):31401-31410.

doi: 10.1021/acsami.7b07927. Epub 2017 Sep 5. PMID: 28737897.

Hart, Peter & Colson, Gary & Burris, Jeffery. (2012). Application of Carbon Dioxide to reduce water side lime scale in heat exchanges. J. of Science and Technology for Forest Products and Processes. 1. 67-70.

CLAYS CONTAINED IN MINERAL ORES AND THEIR EFFECTS ON SOLID-LIQUID SEPARATION PROCESSES

By

Francesco Kaswalder, [2]Andrea Grosso, [3] Andrew Hawkey,

Diemme Filtration Srl, Italy
[2]Diemme Filtration Srl, Italy
[3]Diemme Filtration Srl, Australia

Presenter and Corresponding Author

Andrew Hawkey
andrew.hawkey@diemmefiltration.com

ABSTRACT

Dry stacking of filtered tailings usually requires a low cake residual moisture to meet the specifications from geotechnical engineers. The growing demand for minerals has resulted in lower and more complex grades of ores being mined and processed. Many such ores contain varying amounts of clays. The filtration process can be hindered by the presence of clays and it's important to understand the filtration characteristics of these ores at a very early stage in the flowsheet design.

Other solid-liquid separation process can be affected by the presence of clays, including thickening. Thickening, even in the beneficiation stage, can be severely compromised, leading to lower process efficiencies downstream (e.g. leaching). Poor thickening performance caused by non-ideal mineralogy (particularly clay content) can force the process designer to consider filtration as a more appropriate solid-liquid separation option (in some cases, even replacing counter-current decanting thickeners).

Some clays affect solid-liquid separation processes more than others. A comprehensive characterization of the ore that includes detection and identification of clay types is important. Standard physical-chemical characterization of mineral slurries includes tests for density, solid concentration and solid (and liquid) specific gravity. More thorough characterization can include tests for yield stress, particle size distribution and morphology, as well as element analysis and mineral phase detection. Some of these tests require sophisticated instruments and highly-experienced technicians.

Phyllosilicates (clays) are one of the most common components of mineral ores and tailings, together with quartz, feldspar and other aluminosilicates. Their content is not necessarily predominant but their presence, even in small concentrations, can influence slurry behavior and filter cake permeability and moisture content. A comprehensive study of clay detection and quantification, including correlation with dewatering properties was recently carried out by Diemme Filtration's R&D laboratory. Some of the results and conclusions of that study are presented here. The paper also uses real project examples to illustrate how the presence of clays in mineral ores can change the flow sheet design and influence the sizing of filtration equipment.

Keywords: solid-liquid separation; thickening; filtration; dry stacking, mine tailings, filter presses, clays; beneficiation; leaching

INTRODUCTION

Dry stack tailings (DST) management offers a more sustainable and safe solution in many situations than conventional slurry storage (by 'dry', we actually mean filtered cake which contains moisture but within a certain limit). Mining sites where dry stacking is used are increasing and many projects with very high throughput needs are currently under operation or development. The attention of the mining sector towards the sustainability of the process, combining minimisation of risk of failures, environmental footprint and maximum water recovery is pushing the development of this strategy and related technologies. To achieve the best practice level, the creation of partnerships between mine owners, engineering companies and equipment manufacturers has been essential.

One critical aspect of filtered tailings storage is related to the economical assessment of the overall process. This topic is much debated in the mining industry, mainly because of the high complexity of the variables involved and the related uncertainly. Cost of tailings dams are often underestimated and the benefits of DST at the time of site closure are not taken into proper consideration. The acceptance of the DST process as a viable option is largely dependent on a simpler (and short-sighted) cost evaluation, placing all emphasis on the CAPEX and OPEX of the particular design.

Currently, for DST, the use of a filter press for tailings dewatering is the most popular technology, combining substantial flexibility in regard to the variation of slurry characteristics with very high throughput capability and final cake moisture achievable. The high level of customization offered by this technology to match the slurry characteristics and final cake moisture target is a distinct advantage. However, to avoid excess capital costs, care must be taken to ensure that thorough testing is done so that the optimum plate pack configuration is selected, rather than a more expensive configuration (possibly leading to a larger filter sizing) that may be uneconomic.

The set-up of a filter press process involves many different variables, such as:

- Plate type: recessed (i.e. fixed volume) or membrane (i.e. variable volume, allowing cake consolidation by pressure squeezing), chamber thickness
- Feeding (and, in some cases, squeezing) pressure
- Application of compressed air blowing to achieve cake desaturation, and optimization of air consumption
- Filter cloth selection

Any one of these items can have a strong impact on both OPEX and CAPEX of the equipment. Use of membrane plates instead of fixed-volume ones, for example, presents a significant higher cost but can be necessary in order reach the required cake moisture. The use of compressed air blowing is often necessary to prevent liquefaction and to reach a specified cake moisture level, but the compressor and its energy demand can increase the costs capital and operating costs significantly.

In figure 1, below, a graph showing the typical moisture range achievable with different filter configurations on copper tailings (the same application as the case study discussed later in the paper) is reported. It clearly shows the importance of the target definition for a proper process configuration.

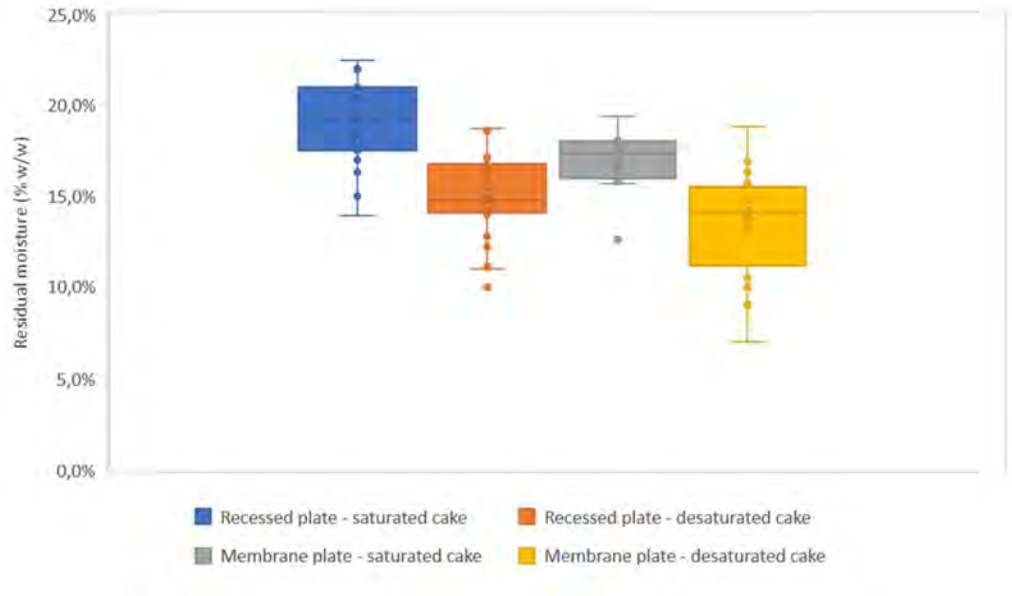

Figure 1: cake moisture vs dewatering process for different copper tailings

The material physical-chemical characteristics have a strong impact on the performance achievable, both in terms of throughput (by affecting the filtration time), and cake moisture. Each parameter has its own contribution, and this makes a full understanding of the system challenging. The particle size distribution plays an important role, considering that the building of the cake determines many process outcomes such as filtration time, cake permeability for cake blowing (desaturation), and the final moisture content of the cake. Figure 2, below, shows clearly that that generally, materials with a coarser particle size distribution form drier filter cakes (but its very important to know what the P10 of the distribution is to be able to predict cake permeability with confidence).

Another important feature that can affect the filtration performance is the mineralogy. This determines the particle shape and the way they pack to form a cake. This is particularly important for the fine fraction (below 4 microns), because of the presence of phyllosilicates. These are characterized by a plate-like structure and can contribute to a very high specific cake resistance, causing long filtration times and higher residual moistures. The worst case occurs when swelling clays (i.e. smectites) are present. Their impact is substantial from the geotechnical behaviour to the filterability of the material, leading to stricter moisture targets and lower dewatering efficiencies. Figure 3, below, shows an example from a case study comparing two different copper tailings coming from the same mine but taken from two different parts of the ore body. Both contain a significant amount of clay but sample A presents no smectite phases. However, sample B has a smectite content of around 2% w/w. The impact on proctor compaction and filtration time (considering two different chamber thicknesses) are evident.

With the rising global demand for minerals and the reduction of average mineral grade, mining and minerals processing industries are encountering progressively many more complexities. For these reasons, as in the case of copper production reported in the following figure, the demand for copper has continued to rise over the decades as new technologies evolve thereby impacting ore production. The result of this confluence is an increasing amount of tailings generated that must be managed by stressing existing structures.

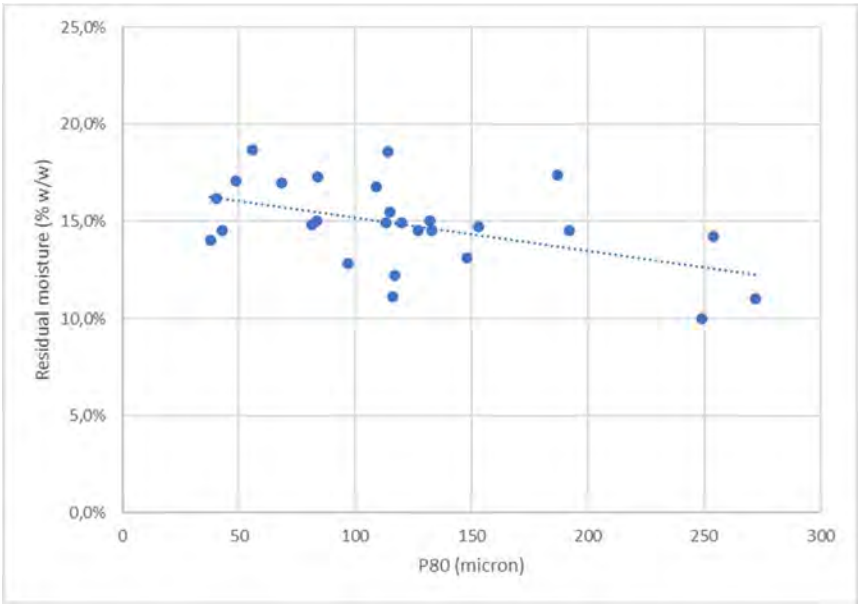

Figure 2: cake moisture vs P80 for different copper tailings

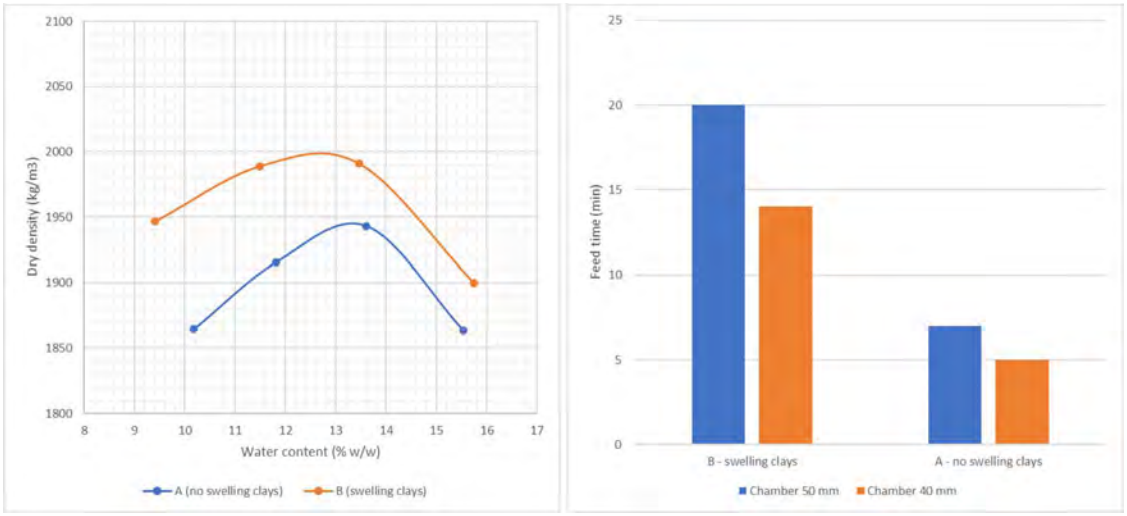

Figure 3: proctor curves and filtration times of two copper tailings with different swelling clays content

In the following section, a case study is presented, describing the strategy behind the design and sizing of the dewatering equipment and how all these aspects are involved.

CASE STUDY AND METHODOLOGY

The case study presented here is related to the design and installation of the first Diemme GHT.5000.F Domino in the SPCC Toquepala copper mine in Peru. This filter press is the biggest currently available, capable of reaching a filtration area of up to 25 m^2 and a total volume of up to 600 liters per single chamber, with a plate size of 5000 x 5000 mm. This filter has been especially developed for high capacity tailings dewatering plants, typically higher than 35,000 tonnes per day of dry solids.

The unit is part of a demonstration plant built to evaluate the use of stacking filtered tails in place of the current thickened-surry tailings dam. The demonstration plant capacity is nominally 8,000 tonnes per day (although higher throughputs have been achieved) and the required cake moisture, based on geotechnical studies and dry stack design needs, is below 15% w/w. The next step will be a full-scale plant with an overall capacity of 80,000 tonnes per day.

The filter sizing was based on the findings of detailed bench-scale filtration tests, carried out in a laboratory. A summary of the main findings and the sizing, commissioning and start-up of the industrial filter will be presented in the next session.

RESULTS AND DISCUSSION

The main results of the tailings characterisation are reported in table 1, below.

Table 1: Tailings characteristics

Slurry data	Particle size distribution	Elemental analysis	Phase analysis
Density = 1.54 Kg/l	P10 = 2.65 µm	SiO2 = 42.8%	Quartz = 41.8% w/w
Solid content = 56.0% w/w	P50 = 22.0 µm	Al2O3 = 14.0% w/w	Chalcopyrite = 1.02% w/w
	P80 = 153 µm	Fe2O3 = 4.6% w/w	Muscovite = 55.2% w/w
		SO3 = 4.03% w/w	Clinochlore = 1.9% w/w
		K2O = 3.74% w/w	
		Others <3% w/w	

The characterization data are useful to guide the initial configuration of the test filter. The tailings sample shows an average-to-coarse particle size distribution, with presence of fine sand and silty-clayey fractions. The amount of phyllosilicates is relatively high but there's no evidence of the presence of swelling clays, therefore the slurry is expected to show fast filterability and the cake will most likely be permeable allowing desaturation (with compressed air) but also well consolidated. Taking all this into account, the first stage of testing was focused on the plate/chamber configuration.

The following different configurations were tested:

- Recessed chamber filtration with different feed pressures
- Membrane chamber filtration with final squeezing with different pressures
- Addition of cake blowing in both recessed and membrane options

To simulate the filtration process, a bench pilot filter has been used. This equipment was designed by Diemme Filtration to produce results that can be scaled to any possible industrial filter setup, no matter how large. The bench filter, shown in figure 4, below, consists of one single filtration chamber with a filtration area of 0.0077 m^2 connected to the feed tanks. Figure 5, below, reports the results of the first test campaign.

Figure 4: Diemme filtration bench rig

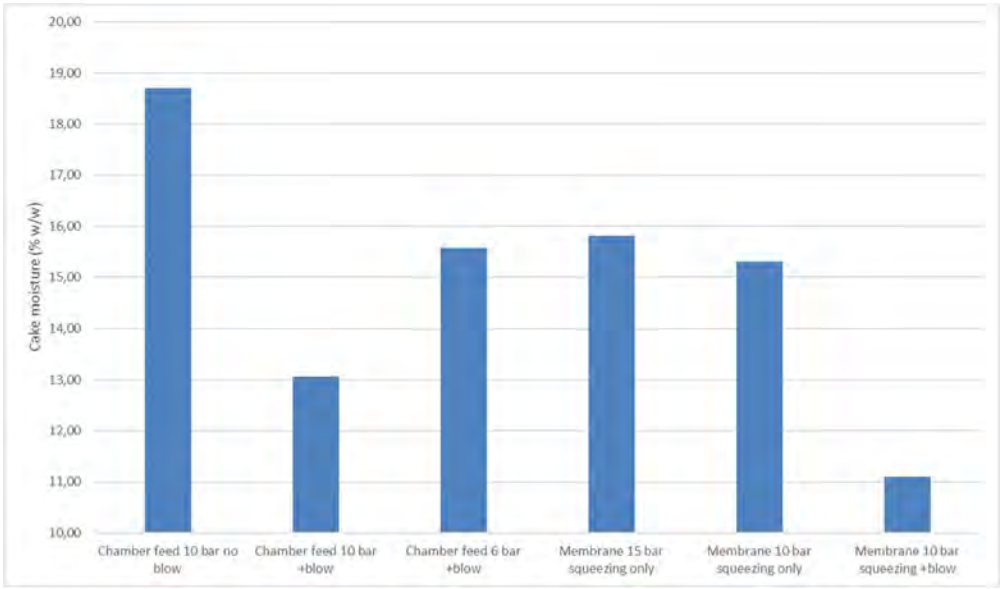

Figure 5: preliminary test campaign results

The best results were obtained using cake blowing, both in the recessed and membrane configuration. Considering that the fixed volume chamber option is significantly cheaper than the membrane (variable-volume chamber) one, and that it reaches the desired moisture, it can be considered as the best one in terms of cost effectiveness. The second stage of the of testing focused on optimizing the blowing phase with a recessed configuration, considering the blowing time and air consumption as variables (see Figure 6, below). The selected chamber thickness was 50 mm to maximize the filter throughput; thinner chambers were not required in this case as there was good cake permeability.

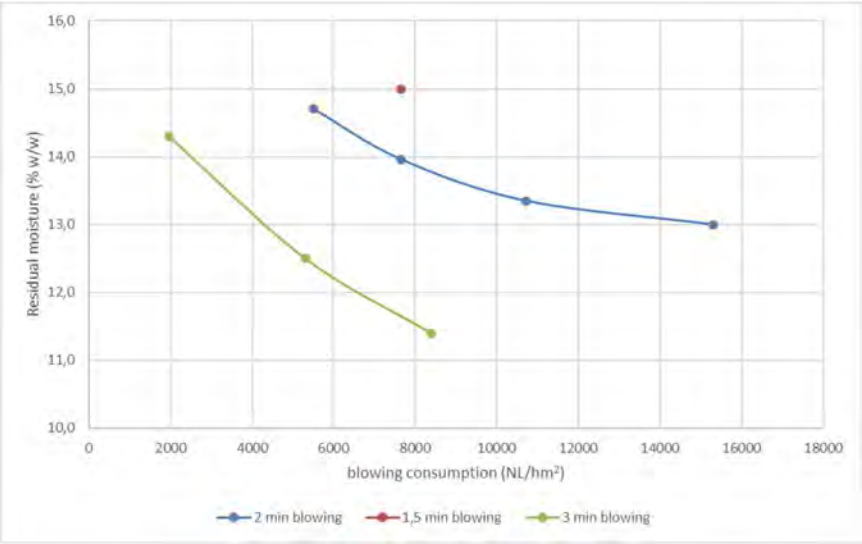

Figure 6: optimization of blowing phase in recessed configuration

Based on these results a blowing time of two minutes has been considered. The final sizing is based on the cycle time reported in table 2.

Table 2: cycle time

Cycle phase	Time (min)
Filter filling	2.0
Cake compacting	3.5
Cake blowing	2.0
Non-process time	8.0

The sizing resulted in one GHT.5000.F Domino equipped with 141 plates, with a total filtration area of 2850 m^2 and a total chamber volume of 71 m^3. It is designed to reach 8000 tonnes per day of solid throughput. The installation of the filter at site was successfully completed in less than three months. After this, the commissioning and ramp-up phases lasted for other three months each. Pictures of the Domino filter press and the overall demonstration plant (where it is possible to see the dry stacking) are reported in Figures 7 and 8.

Figure 7: GHT.5000.F Domino operating at Toquepala mine

Figure 8: Demonstration plant

An important feature of the filter press is the implementation of the AIDA system, the software developed by Diemme Filtration for remote process monitoring, support, and maintenance by means of data collection and, most importantly, data analysis. The AIDA system has been a vital tool in assisting the fine process tuning and filter optimization. The first results are very promising, Figures 9 and 10 report the data taken from AIDA showing how the filter is matching the required performances both in terms of hourly productivity and cake dryness.

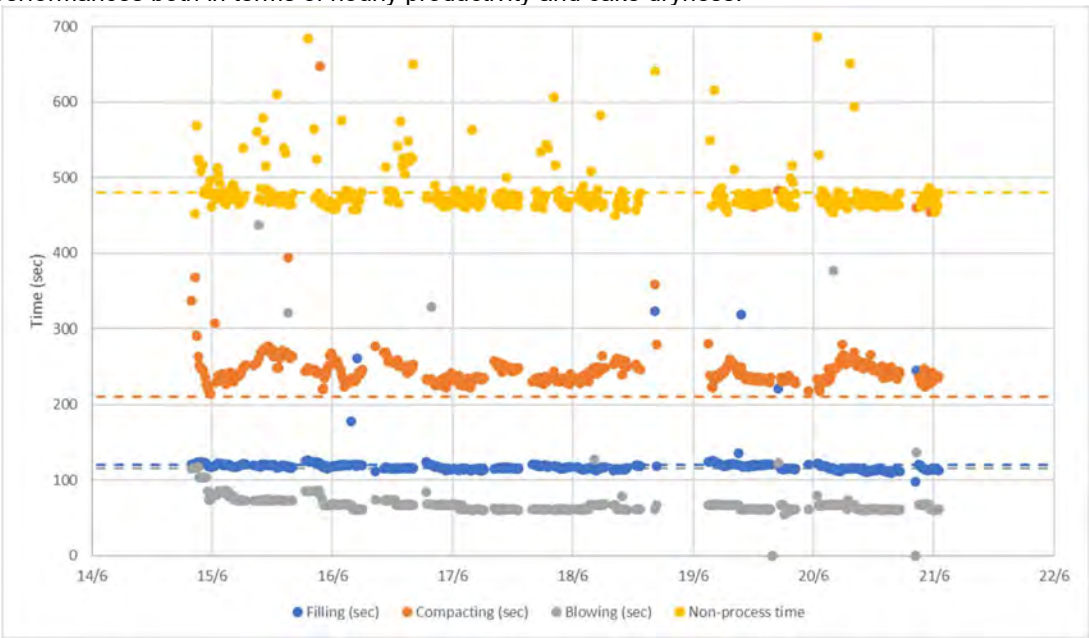

Figure 9: cycle time (different phases). Points are data coming from AIDA, dotted line are related to the sizing parameters

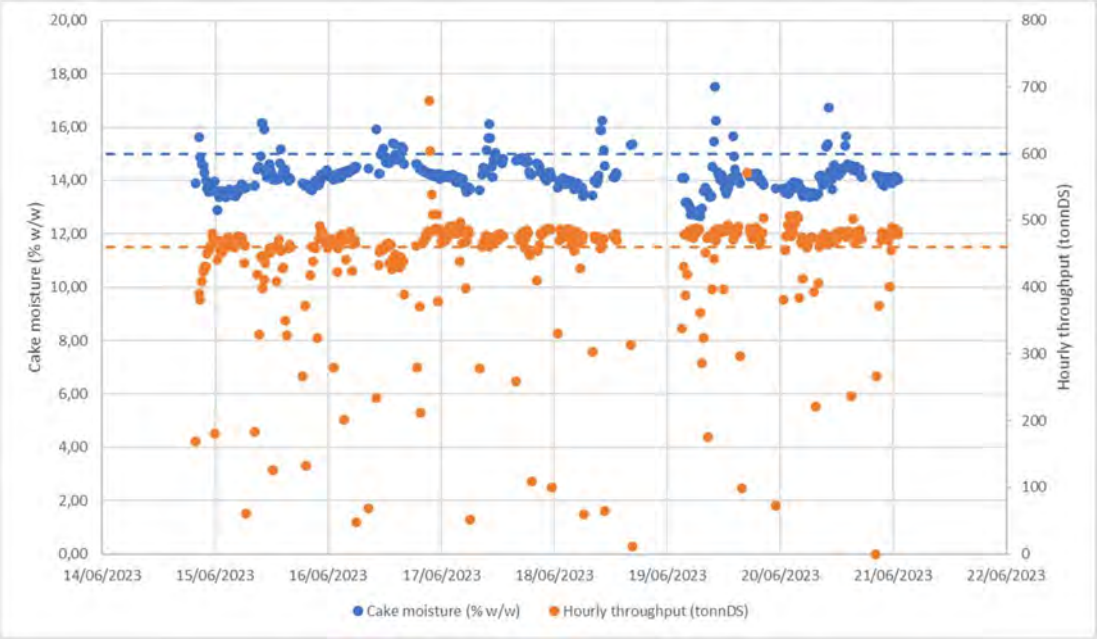

Figure 10: hourly throughput and cake moisture. Points are data coming from AIDA, dotted line are related to the sizing parameters

In figure 10, a trend of the total throughput obtained during the first week of continuous operation is reported. By means of a constant monitoring of the process parameters the cycle time and the overall availability of the filter have been optimized showing an increasing trend of the total productivity that is currently close to 10,000 tonnes per day. This optimization stage is focusing mainly on the cycle phases (particularly the blowing time) and the filter availability.

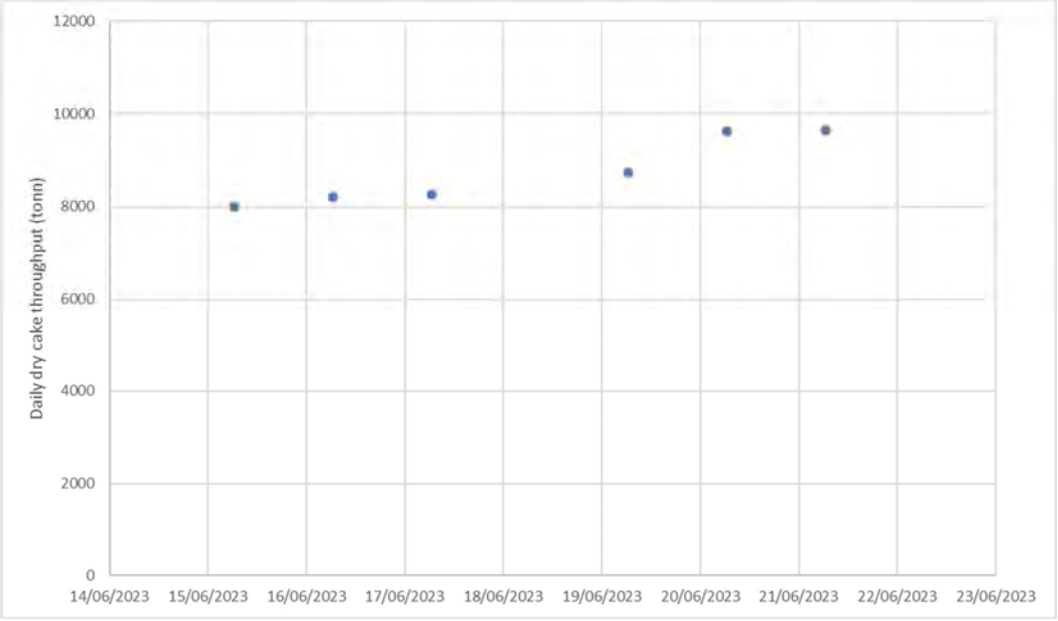

Figure 11: daily throughput

CONCLUSION

The perspectives of applying dry stack disposal for big sized projects (with throughputs overcoming 100000 tonnes per day) are increasingly promising. The related costs of this technology are still an important cause of debate; the development of the new dewatering equipment with increased capacity and optimized CAPEX and OPEX related, together with a thorough study of the process and the material characteristics carried out case by case are of upmost importance during the economical

assessment of the projects.

The installation of the first GHT.5000.F Domino filter press, here presented, leads in this direction. The successfully operation of the demo plant will be an important step to demonstrate the environmental and economical sustainability of the dry stacking applied to large mining plants. The first results and feedback coming from the plant are very positive. The findings coming from the material characterization and process study and the use of real time data monitoring have proven to be vital in the optimization process.

BIBLIOGRAPHY

Cooke, R., T.L.G. Gerritsen, Y. Mladinic, I. Oyarzun, T. Tran. 2023. The tailings management partnership agreement, a unique industry collaboration to achieve safer tailings facilities. In: G.W. Wilson, N.A. Beier, D.C. Sego, A.B. Fourie and D. Reid (editors), *Paste 2023. Proceedings of 25th International Conference on Paste, Thickened and Filtered Tailings*. Banff, Alberta (CA). ISBN 978-1-55195-493-6

Grosso, A., F. Kaswalder and A. Hawkey, 2021. Clay-bearing mine tailings analysis and implications in large filter press design. In: A.B. Fourie and D. Reid (editors), *Paste 2021. Proceedings of 24th International Conference on Paste, Thickened and Filtered Tailings*. Perth (AU). ISBN 978-0-6450938-0-3

Julien, M., 2023. The evolution of practice in the field of mine waste and water management in the last 10 years with supporting examples. In: G.W. Wilson, N.A. Beier, D.C. Sego, A.B. Fourie and D. Reid (editors), *Paste 2023. Proceedings of 25th International Conference on Paste, Thickened and Filtered Tailings*. Banff, Alberta (CA). ISBN 978-1-55195-493-6

Kaswalder, F., D. Collini, N. Masciocchi, A. Guagliardi, 2014. X-rays techniques: a new version for the field of wastewater filtration. *Filtration + Separation* nov-dec 2014 36-39

Kaswalder, F., D. Collini, A. Grosso and N. Finocchiaro, 2018. Filter press dewatering process: analysis of the physical-chemical features affecting the cake build-up. In: *Proceedings of Filtech 2018*. Cologne (DE)

Stickland, A., 2023. Mineral tailings filtration: lessons learnt from wastewater sludge filtration. In: *Proceedings of Filtech 2023*. Cologne (DE). ISBN 976-3-941655-21-8

Whittering, R., M. Pyle and G. Lane. 2019. Filtered dry stack tailings: the "state of play" for high capacity tailings filter plants. In: *Proceedings of Filtech 2019*. Cologne (DE).

MICROWAVE PROCESSING OF ORES – COMMERCIAL REALISATION OF A STEP CHANGE FOR THE MINERALS INDUSTRY

By

Sam Kingman, [1]Andrew Batchelor, [2]Richard Bearman, [3]Herman Purutyan, [3]David Craig

Faculty of Engineering, University of Nottingham, UK
[2]Bear Rock Solutions, Australia
[3]Jenike & Johanson, USA

Presenter and Corresponding Author

David Craig
dacraig@jenike.com

ABSTRACT

As ore bodies age and grades decline, increasingly higher embodied energy input is required for comminution to maintain production, which increases costs and the carbon footprint of these operations. A step-change in energy reduction is required to meet the future demand of these processes. Microwave technology has long been suggested as a route to significant energy reduction and enhanced recovery in mineral processing. Until recently, however, the work was at an academic level with little or no vision for deployment in the mining industry.

We present for the first time a defined pathway to commercial application of microwave technology for the mining industry. This builds on our previous work which has successfully demonstrated this technology at over 150 t/hr. We consider the integration of microwave engineering with bulk solids handling at scale and also present details of a route to commercial delivery. We will focus our paper upon the value proposition that this technology can deliver. In particular, we consider the impact of induced fractures on conventional grinding/flotation circuits, on the performance of leach systems and on new flowsheets with the potential to deliver a paradigm shift in carbon emissions from mineral processing circuits.

Keywords: comminution, microwaves, carbon footprint

MICROWAVE PROCESSING OF ORES – COMMERCIAL REALISATION OF A STEP CHANGE FOR THE MINERALS INDUSTRY

Sam Kingman[1], Andrew Batchelor[1], Richard Bearman[2], Herman Purutyan[3], David Craig[3]
[1] Faculty of Engineering, University of Nottingham, UK
[2] Bear Rock Solutions, Perth, Australia
[3] Jenike & Johanson, Tyngsboro, MA, USA
Presenter: David Craig dacraig@jenike.com

Presentation overview

- Why is innovation needed?
- Existing comminution technology
- Basic principle of microwave comminution technology
- Development history
- Where are we now?
- Value proposition
- What are the potential benefits?

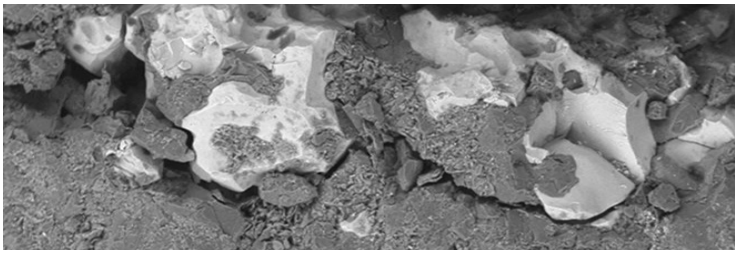

Mining industry drivers

Why is comminution innovation needed?

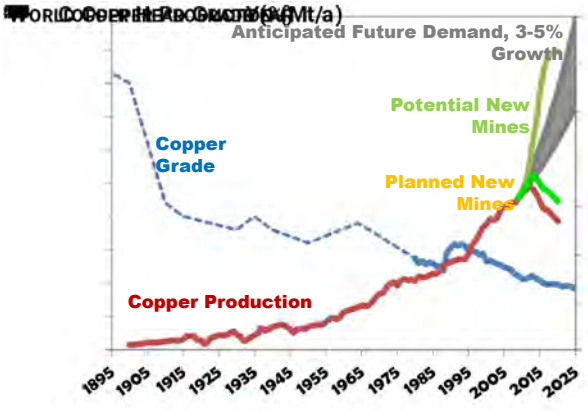

Higher Embodied Energy

- Decreasing Copper Grade
- Decreasing Grain & Grind Size
- Increasing Ore Hardness

Limited Mining Activity

- Growing Demand & Production
- Rising Costs (Utilites, Remote Locations)
- Falling Deposit Discovery

Typical Mine Site Energy Consumption

Energy reduction benefits

Increase Competitiveness

Fight Climate Change (i.e., decarbonization)

Mining industry drivers

Why is comminution innovation needed?

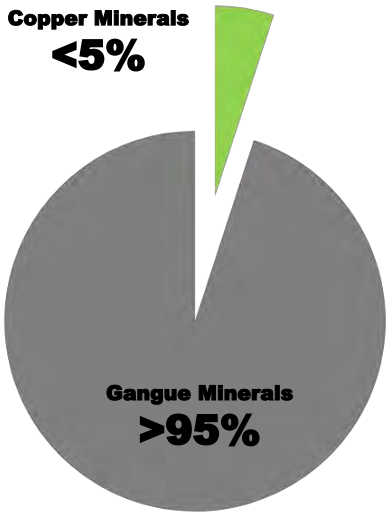

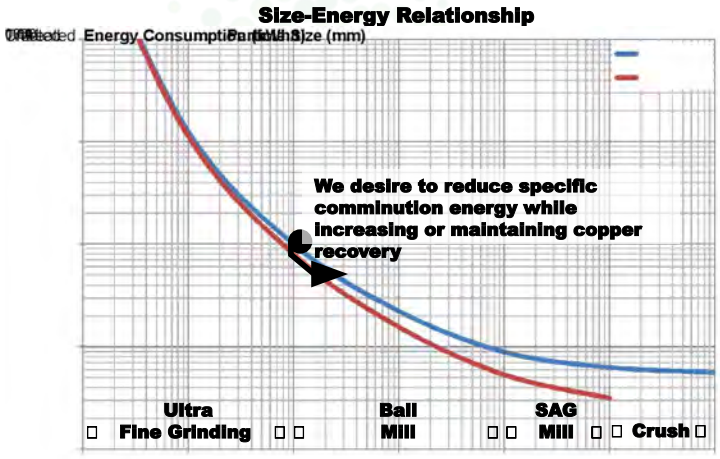

Existing comminution solutions

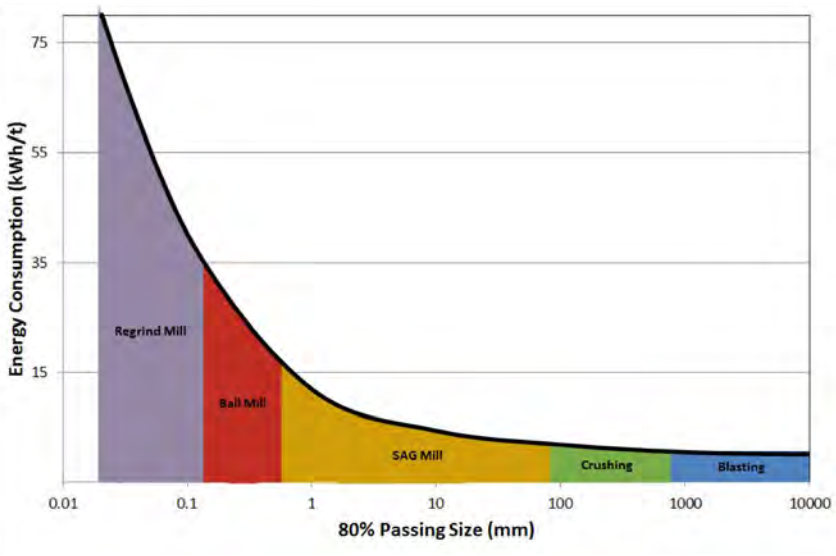

SAG mill

Ball mill

HPGR
(per FLS)

Microwave technology poised to complement existing solutions

Microwave technology – what is it?

- Rocks contain mixtures of minerals with varying abilities to heat due to microwave application
- SHOT applies high-intensity electrical microwave energy to cause differential heating and generate thermal stresses primarily at the mineral-grain interface
- Overall effect controlled by mineralogy and texture

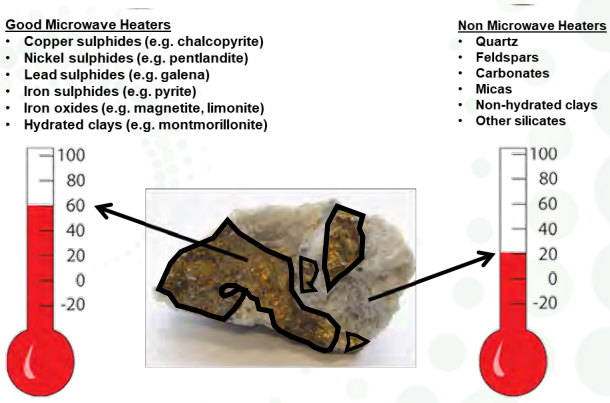

Energy usage:
0.3 to 3 kWh/t (typically <1 kWh/t)
i.e., << HPGR, Ball, SAG

Microwave technology – what is it?

- Benefits:
  - Competency reduction: Micro-fractures at the mineral-grain boundaries
  - Enhanced recovery: Preferential grain boundary cracking frees the valuable mineral at larger grain size

Micro-Fracture
(energy reduction, liberation)

Macro-Fracture
(leaching pathways)

Microwave technology – history

- Developed by University of Nottingham
  - 20+ years of experience and have demonstrated world-class capability in the application of microwaves in mineral processing
- Lead developer
  - Professor Sam Kingman is a Pro-Vice- Chancellor and was Director of the National Centre for Industrial Microwave Processing (NCIMP). Published over 175 refereed journal papers and he is an inventor on over 150 patents within 29 patent families in the field of industrial microwave processing
  - Worked with a wide variety of mining companies during the early development phase of microwave processing
- Team and Facilities
  - World-first design for industrial system, using power intensifying methods
  - Test facilities and research teams in-place

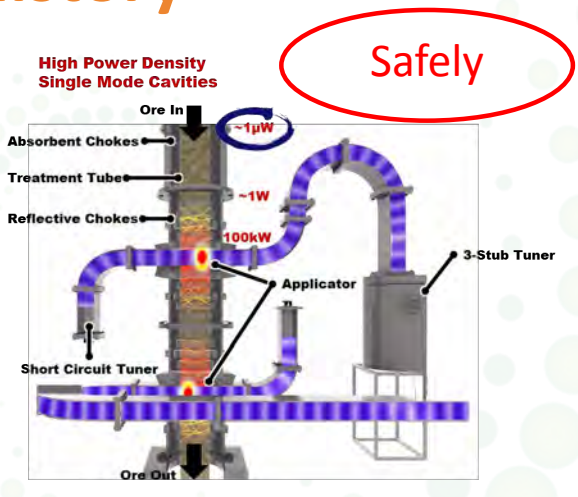

Integrated Materials Handling & Electromagnetic Design

Continuous Treatments

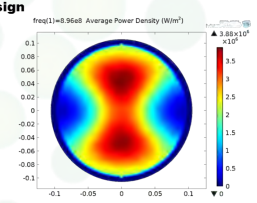

We are we?

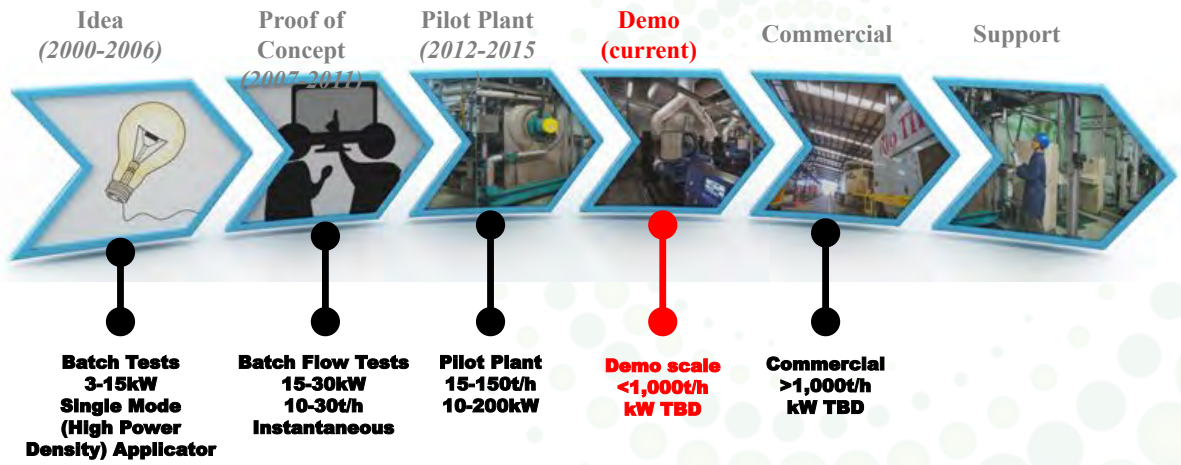

Microwave technology – pilot plant

- Designed, built and proven circa. 2012 to 2015
- 2 x 100 kW (896 MHz) microwave generators (AT01)
- 15 to 150 t/hr
- Up to 4 tonnes per batch run

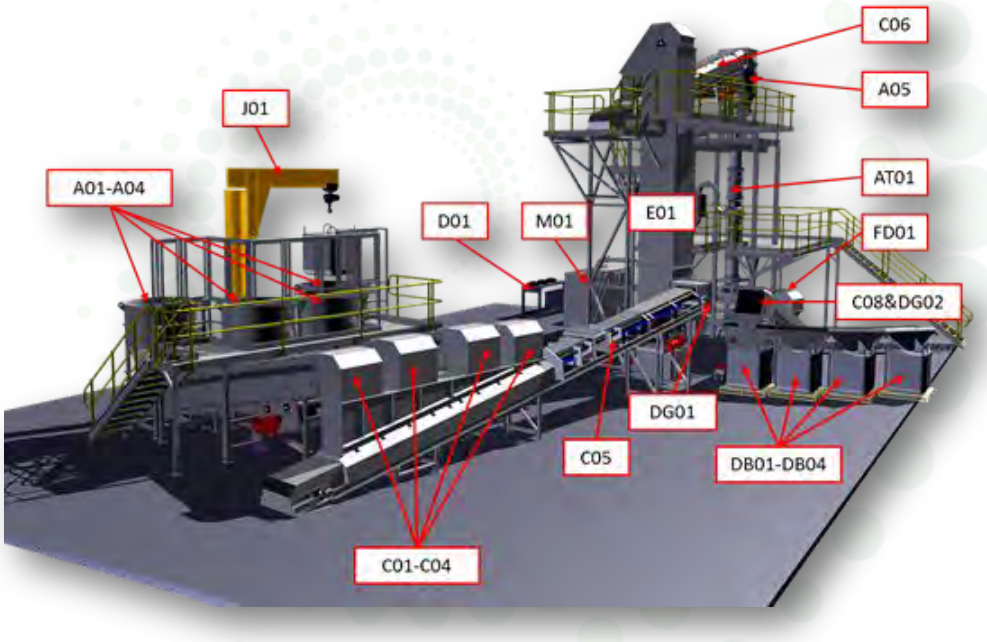

SHOT microwave system

Demo scale

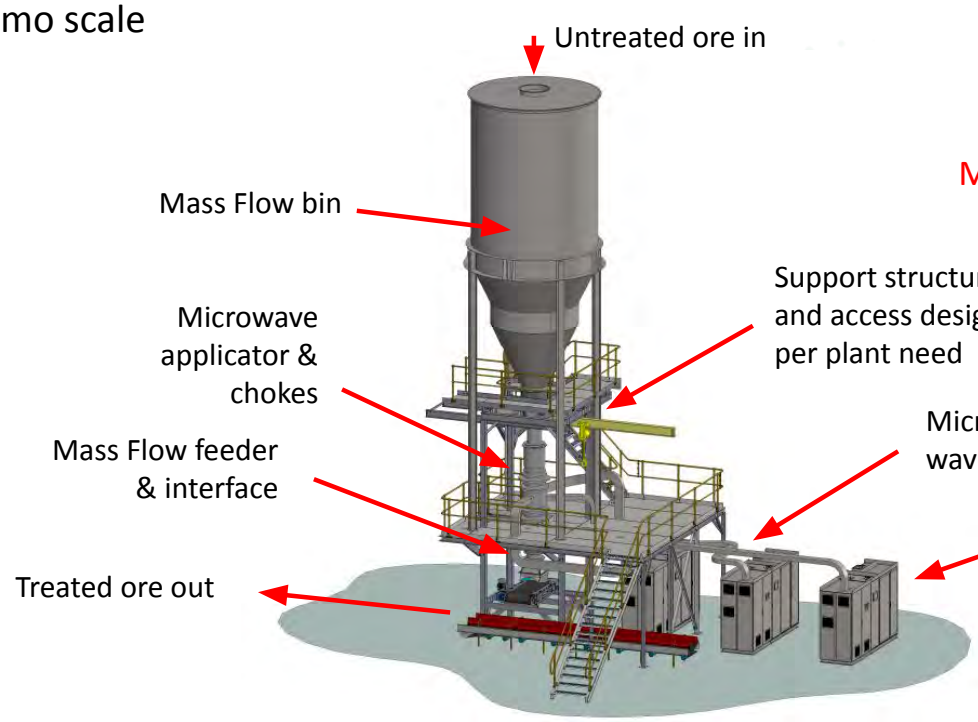

300 to 800 t/hr
PSD < 80 mm
0.3 to 3 kWh/t
Multiple 100 kW generators

"Patent protected"

SHOT microwave system

Demo scale

- Customizable
  - Designed for each particular application & ore
  - Positioning within plant can be fine-tuned for optimal energy reduction
- Comprised of:
  - Mass flow storage bin, microwave applicator & chokes, mass flow feeder, and microwave generator(s) and waveguides
- System design important

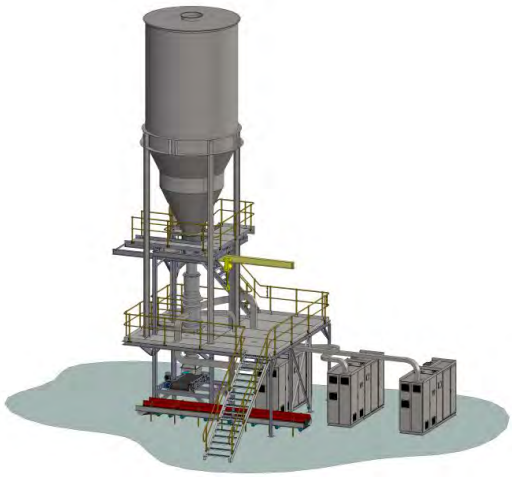

SHOT solution partners

Jenike & Johanson are materials handling specialists and the engineering and equipment supply vendor for the SHOT system

The University of Nottingham are microwave process design experts and assess ore amenability to the SHOT system

Bear Rock Solutions are an experienced mineral processing consultancy providing client interaction, process modelling and value proposition definition services

Fight Climate Change

Increase Competitiveness

Transform the Mining Cycle

SHOT microwave system “kit”

- Solution: Microwave system equipment “kit”
- Underlying design process:
  - Evaluate ore for success using microwave technology
  - Ore tests
    - Microwave properties (e.g., dielectric properties and heating potential) – for design of generator, waveguides, applicator & chokes
    - Flowability properties – for design of materials handling equipment
  - Conceptual design
  - Detailed design
  - Equipment fabrication & supply

Importance of bulk solids handling

- Small footprint
- Suitable materials of construction
  - Electrical properties, mechanical properties, wear
- Low complexity
- Control of ore residence time
  - Unimpeded and stable solids flow
- Control of ore presentation to microwaves
  - Voidage, segregation, blockage, loads

Flow path diameter

Microwave & bulk solids technology

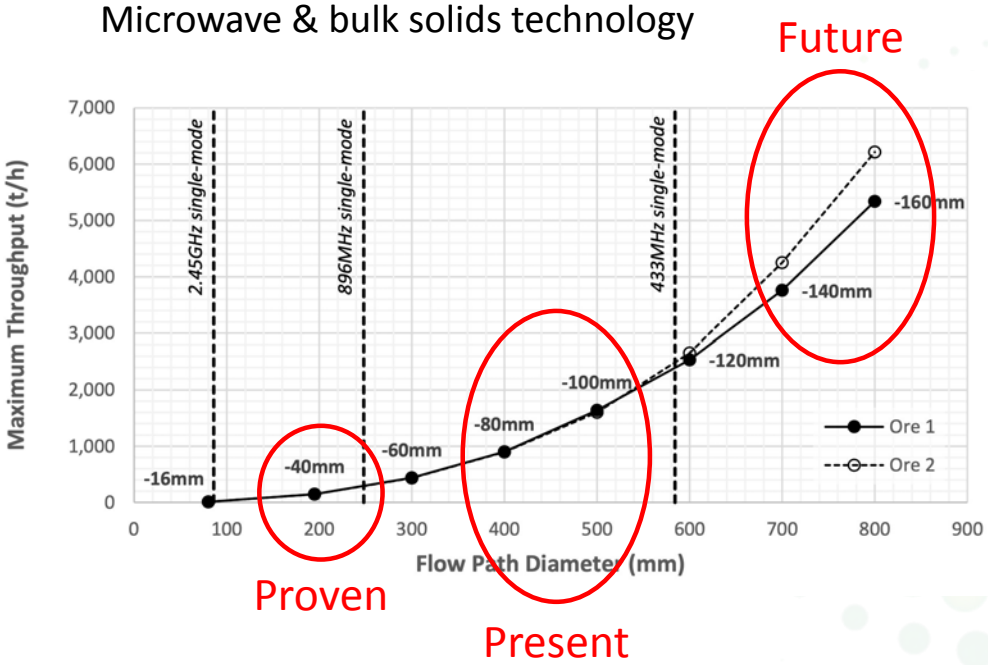

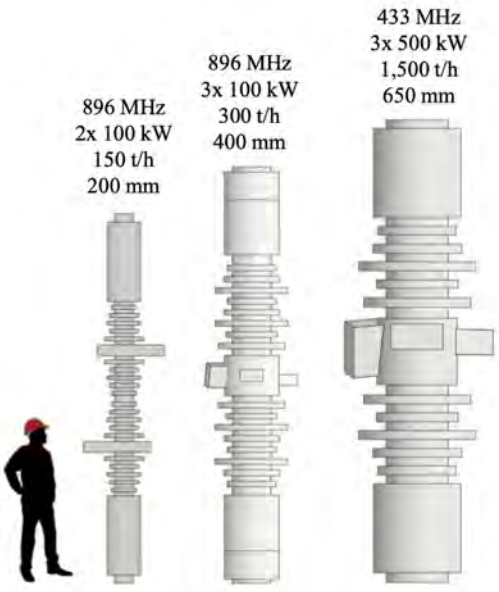

Value propositions

- Reduced ore competency
  - Reduced comminution energy requirement
- Enhanced liberation
  - Increased mineral recovery
  - Achieve mineral recovery at a coarser size
  - Aid preferential liberation
- Increased throughput
- Assist pre-concentration
- Increased heap leaching pathways
- Reduced water consumption
- Reduced grinding media consumption
- Reduced equipment wear

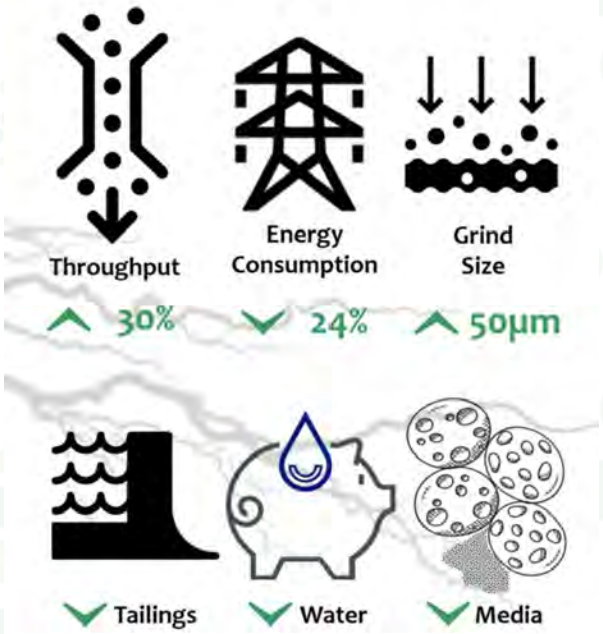

Example results

Flow sheet simulations

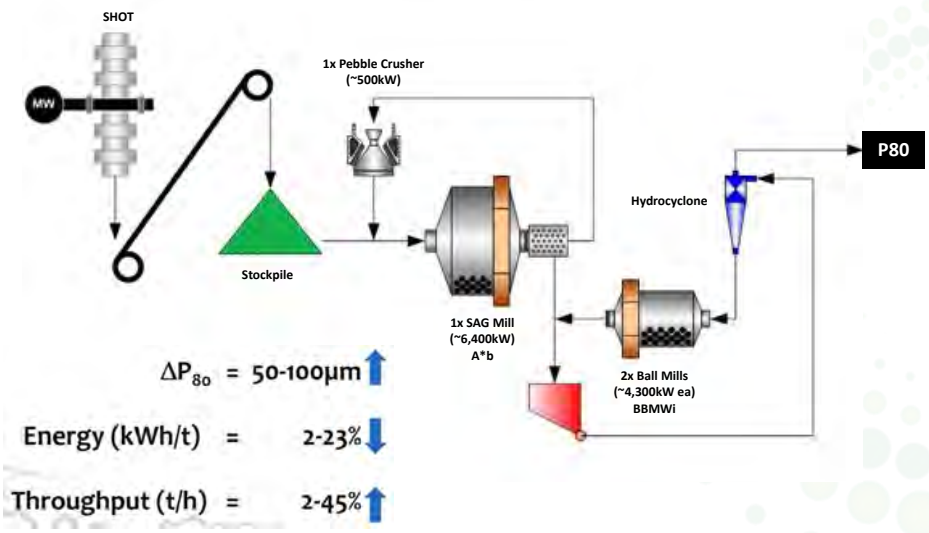

Ore 2	Untreated	Treated	Treated
A*b	39.3	44.8	44.8
BBMWi (kWh/t)	13.69	12.69	12.69
Product Size P80 (µm)	190	190	290
Total Power (kW)	15,081	14,988	14,638
Throughput (t/h)	1,500	1,590	1,756
	-	+6.0%	+17.1%
Specific Energy (kWh/t)	10.5	9.4	8.3
	-	-10.5%	-20.9%

Ore 3	Untreated	Treated	Treated
A*b	44.9	48.1	48.1
BBMWi (kWh/t)	9.27	9.19	9.19
Product Size P80 (µm)	190	190	290
Total Power (kW)	15,907	15,904	15,717
Throughput (t/h)	1,670	1,700	1,970
	-	+1.8%	+18.0%
Specific Energy (kWh/t)	9.5	9.4	8.0
	-	-1.8%	-16.2%

Liberation and recovery improvement

Example for porphyry copper ores after microwave treatment

- Increased liberation at same grind size
  - ΔLiberation ~5 to 10%
- Equivalent liberation at a coarser grind size
  - ΔP_{80} ~50 to 100 µm

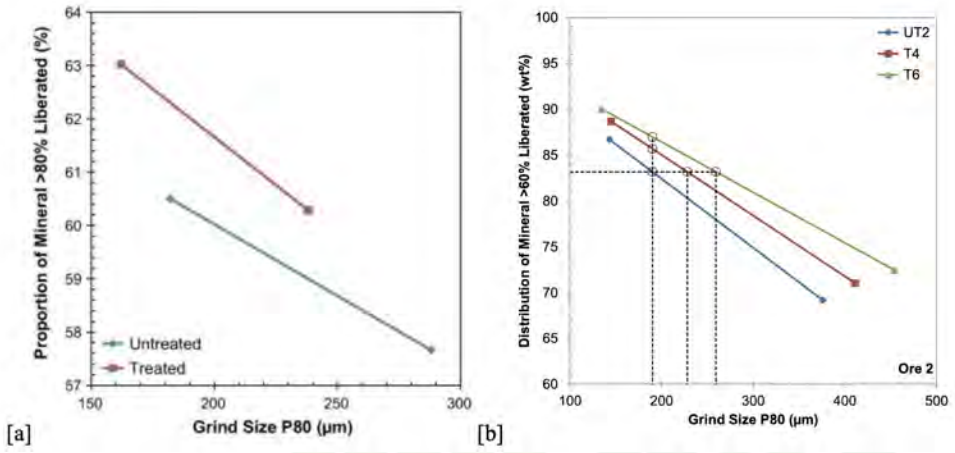

Heap leaching

The best way to save energy is to not grind the rock to begin with!

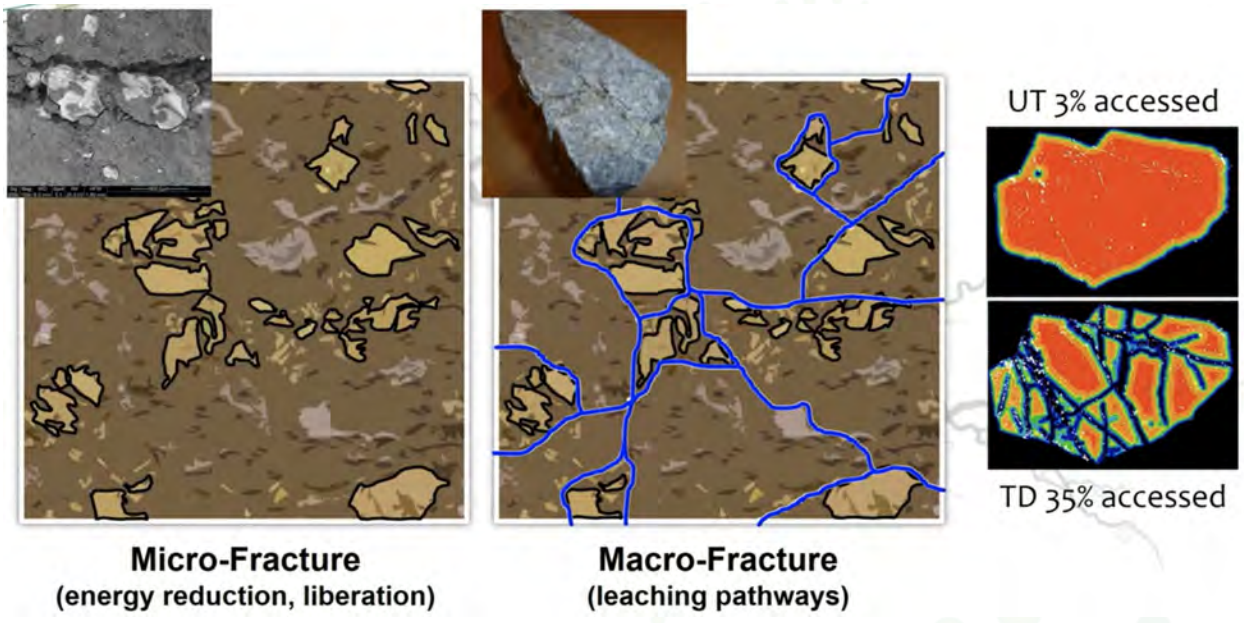

Improvement in leaching

Gold leaching at fine grind sizes

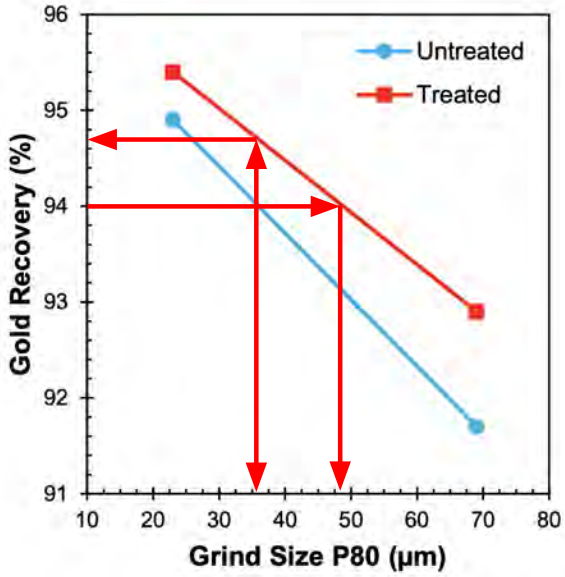

Conclusions

- Microwave electrical comminution solution is proven both theoretically and at 150 tph pilot lab scale
- Presently available for industrial systems at ~300 to 800 t/hr at ~<1 kWh/t using 100 kW microwave generators
- Major benefit:
  - Fracture along mineral grain boundary seen to be critical leap forward in comminution technology
- Complements existing comminution solutions
  - Combined solution results in overall energy reduction, which ultimately results in positive environmental impact including decarbonization

Conclusions (cont.)

- Benefits can include:
  - Up to 70 μm increase in grind size for equivalent liberation
  - Up to 30 μm increase in grind size for equivalent recovery
  - Up to 1% increase in recovery at existing plant grind sizes
  - Up to 10% increase in plant throughput or reduction in specific comminution energy at existing plant grind sizes
  - Up to 30% increase in throughput or 20% reduction in specific comminution energy at coarser grind size for equivalent liberation

- *Ultimately needs to be engineered to particular site and material*

EXTENDING AUTOCLAVE SERVICE LIFE BEYOND THE THIRD DECADE

By

Evelyn Ng

Callidus Group, Australia

Presenter

Evelyn Ng
evelyn.ng@callidusgroup.com.au

ABSTRACT

Autoclaves are critical fixed assets integral to the high-pressure acid leaching (HPAL) process. Traditionally, these vessels are engineered with a thirty-year operational lifespan, aligning with the projected lifespan of mining operations. Throughout this designated lifespan, regular maintenance efforts are directed toward repairing corrosion and erosion damage within the autoclave lining. However, a critical knowledge gap exists regarding the viability of extending the autoclave's service life beyond its designed duration.

Despite the initial design parameters, instances arise where the operational lifespan of an autoclave needs to be prolonged, particularly when the mine's lifespan is extended. Comprising formed carbon steel and explosion-bonded titanium, the autoclave's structure blends mechanical strength with cost-effectiveness. The titanium-clad lining is a vital protective layer, shielding the vessel's interior against high-temperature acidic slurry's corrosive and erosion effects.

Given the considerable size of autoclaves, their construction entails multiple plates of carbon steel and explosion-bonded titanium, meticulously shaped to form the vessel's cylindrical body with hemi-heads at each end. The interior is rendered seamless by strategically welding titanium batten strips, ensuring a tight seal containing the pressurized acidic slurry.

Routine maintenance shutdowns are inevitable to address issues such as leakage, corrosion, and erosion within the autoclave lining. Repair procedures involving the removal and replacement of batten strips and subsequent welding pose concerns regarding the impact of the titanium cladding's material properties. Notably, the potential formation of intermetallic compounds and consequent cracking in the autoclave wall lining remains a looming threat.

This presentation aims to unveil findings regarding the critical threshold of titanium cladding thickness that must not be compromised to mitigate the risk of intermetallic formation and subsequent structural integrity issues. By offering essential insights into long-term maintenance strategies for autoclaves, this research bridges the knowledge gap essential for ensuring the sustained efficiency and safety of HPAL processes.

Keywords: High-Pressure Acid Leach, HPAL, severe service, autoclave, explosion bonded, clad titanium, cladding, carbon steel, sulphuric acid, equipment, corrosion, erosion, performance, high temperature, weld repair, properties, performance, batten strips, cracks, failure, NDT, non-destructive testing, hardness, x-ray fluorescence, intermetallic, microscopy, energy dispersive spectroscopy, SEM, EDS.

Beyond limits: Titanium nitride's game-changing role in hydrometallurgical production

Evelyn Ng
Callidus Group, Australia

Titanium use in HPAL is extensive

Titanium is the material of choice in HPAL for its corrosion resistance and strength-to-weight ratio.

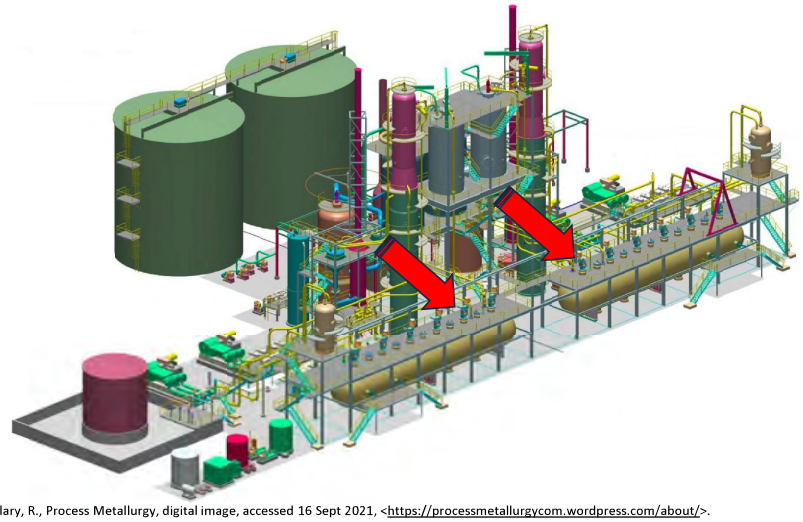

Clary, R., Process Metallurgy, digital image, accessed 16 Sept 2021, <https://processmetallurgycom.wordpress.com/about/>.

Equipment that is predominantly fabricated from Ti or Ti alloy:

- Pre-heater vessels
- Pre-heater towers
- Autoclave lining
- Discharge valves
- Let down valves
- Feed valves
- Vent valves
- All piping

HPAL discharge ball valves are critical equipment

The discharge valves are subject to the most severe conditions.

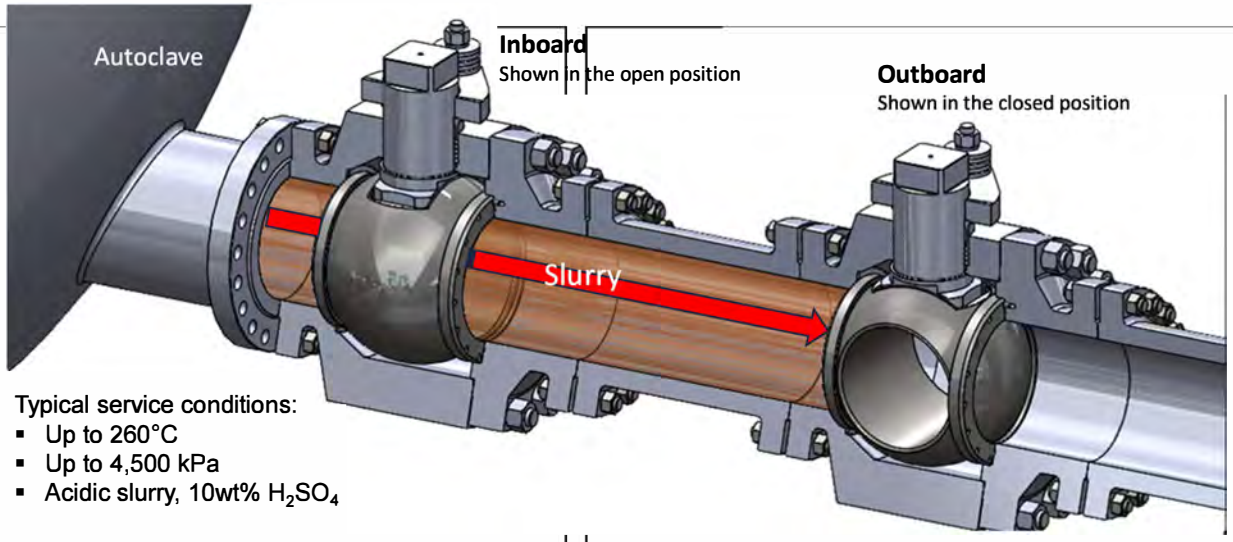

Typical service conditions:

- Up to 260°C
- Up to 4,500 kPa
- Acidic slurry, 10wt% H_2SO_4

Ceramic coatings are applied on the valve trim

The typical failure mechanism is coating delamination, with a 6- to 12-month lifespan.

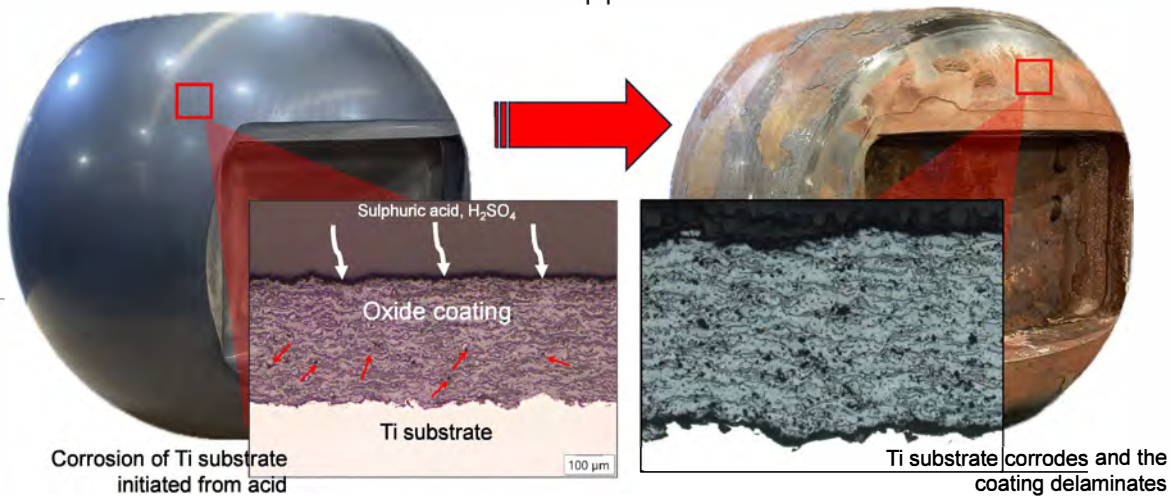

Innovation in surface modification at Callidus

Patented FM-1500™ applied on discharge titanium valve trim

FM-1500™ designed for severe service trim

FM-1500™ installed as a retrofit or repair to a client's OEM valve.

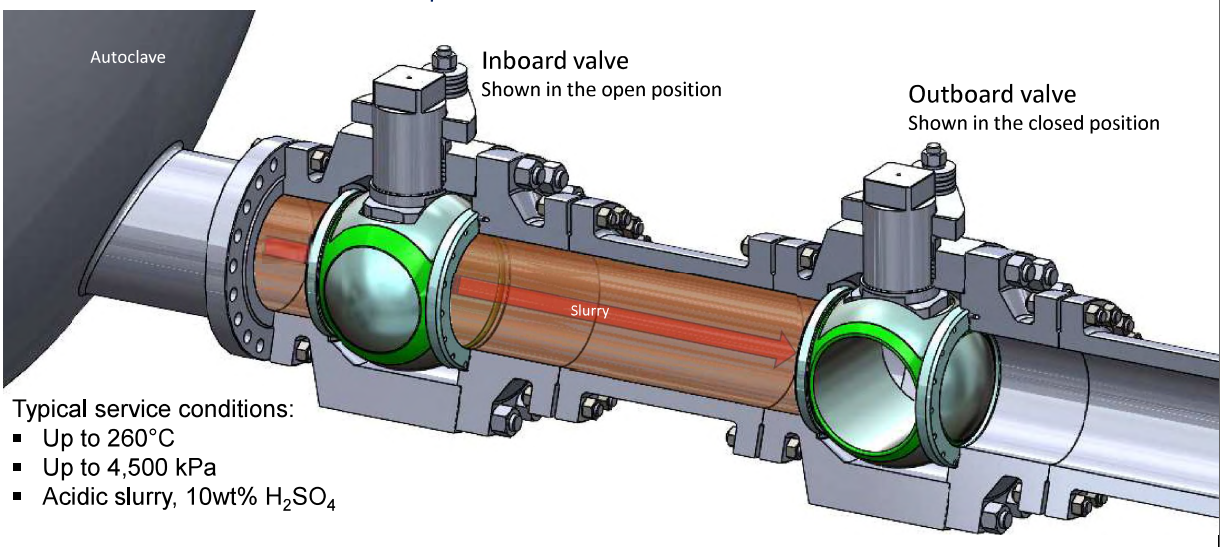

Typical service conditions:

- Up to 260°C
- Up to 4,500 kPa
- Acidic slurry, 10wt% H_2SO_4

A closer look at FM-1500™

Innovating with Titanium Nitride. Patented material and design.

Experimenting with Titanium Nitride (TiN)

Evolution of innovation at Callidus

Titanium nitride (TiN) surface modification

Turning an unfortunate event into something purposeful.

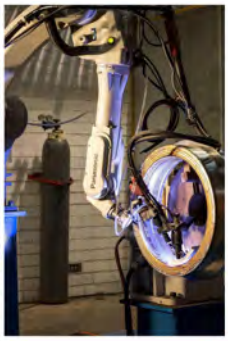

Ti weld quality, optimal vs inferior → Purposefully hardening the surface → Use of robotic welding for consistent quality

Callidus' suite of titanium surface modifications

Over a decade committed to innovating surfaces for erosion- and corrosion-resistance.

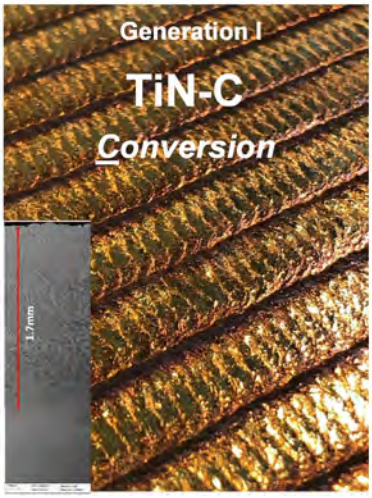

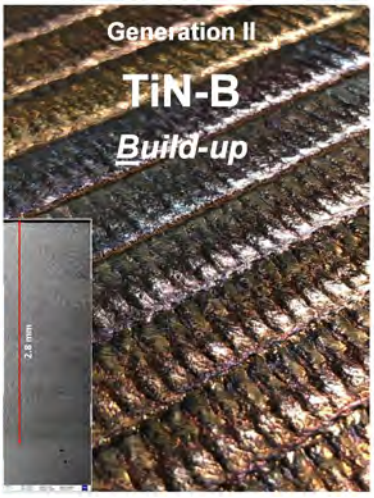

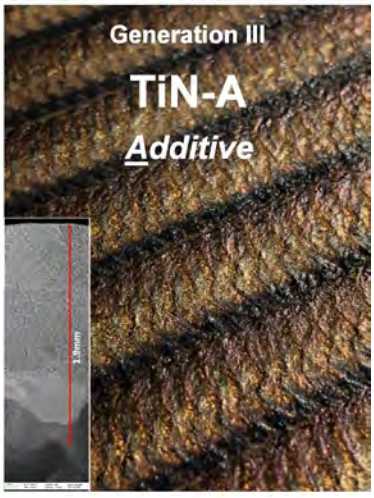

TiN-C material properties

Painful to manufacture as valve trim but still highly applicable.

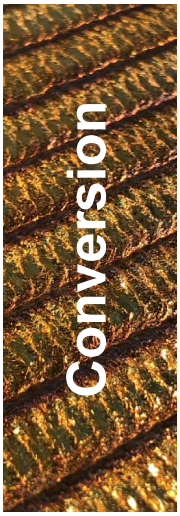

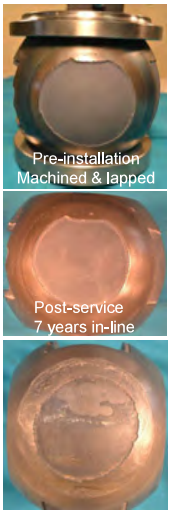

Penetrant testing

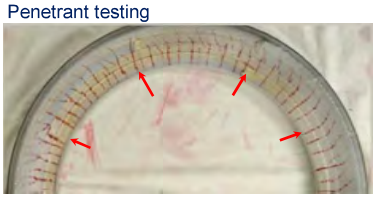

Hardness profile

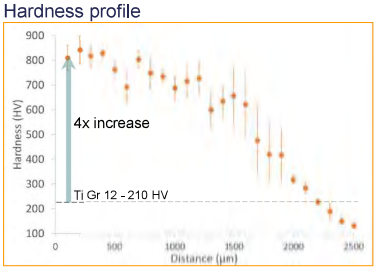

Wear (G65) & high stress abrasion (B611)

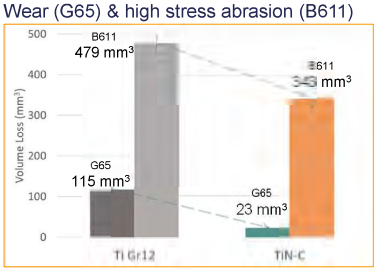

Corrosion rate

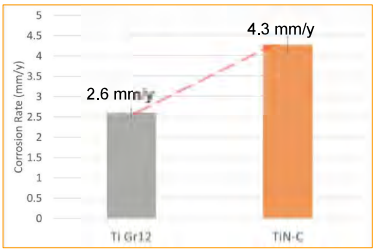

Step change using TiN-C for erosion resistance

Significantly increasing the service life of mining components.

Without TiN-C

With TiN-C surface modification

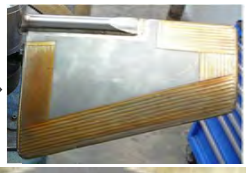

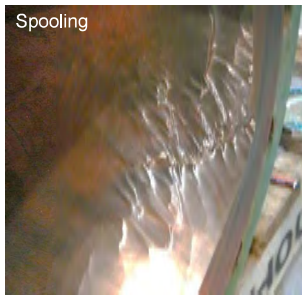

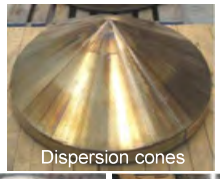

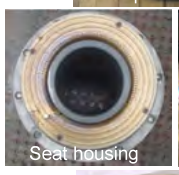

TiN-B material properties

A novel solution to a recurring failure.

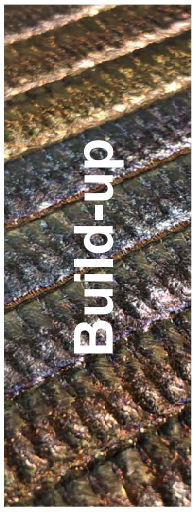

Hardness profile

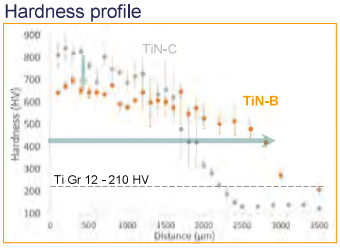

Wear (G65) & Abrasion (B611)

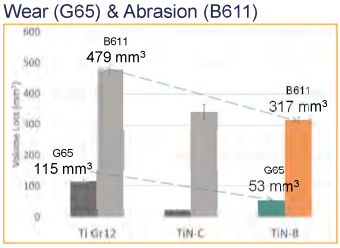

Corrosion rate

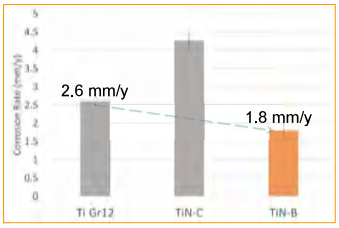

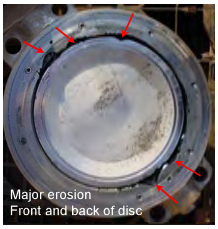

As-received butterfly valve, 4 months in-line

TiN-B on sealing areas

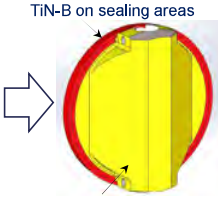

Refurbished disc front & back, 2.5 years in-line

TiN-A on trim is FM-1500™

Designed for discharge valve location. Erosion- and corrosion-resistant.

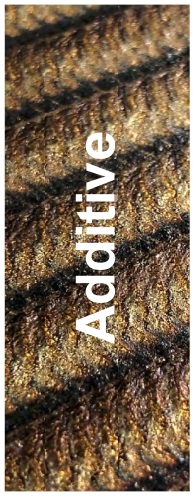

TiN-A material properties

Surpassing previous generations on all counts concerning valve trim.

Hardness profile

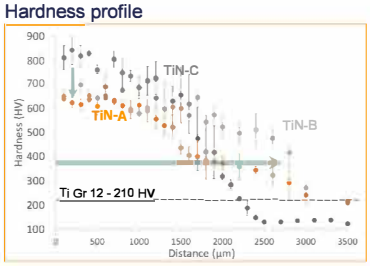

Wear (G65) & Abrasion (B611)

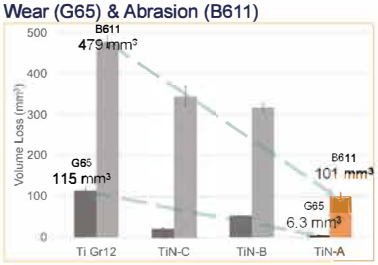

Corrosion rate

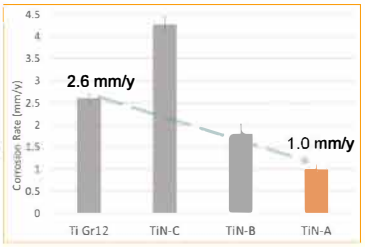

Pin-on-disc

Simulation of loading applied on mated surfaces in-service

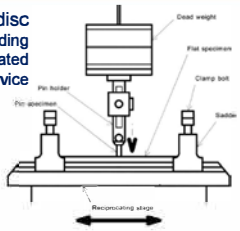

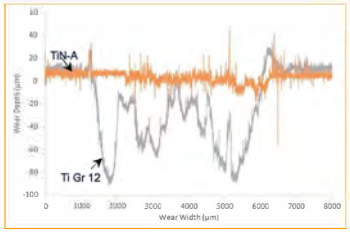

Penetrant testing

Case study

FM-1500™ trial results

Who wins for best performance?

FM-1500™ is a game-changer for the discharge valve location.

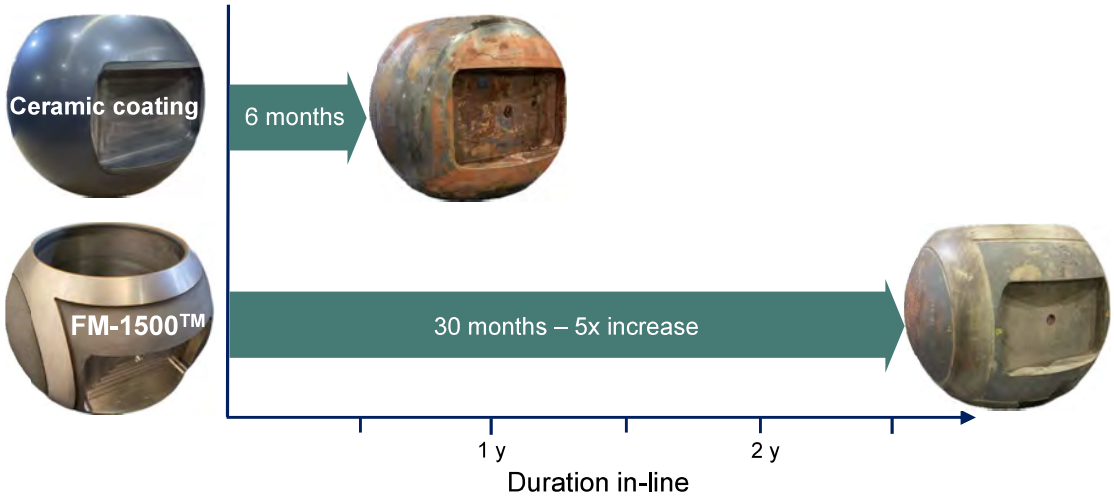

FM-1500™ inspection after 30 months in service

Bands show superficial surface marks and light scoring. No delamination or galling.

How was the valve operated during the trial?

A case study exemplifying severest of severe service.

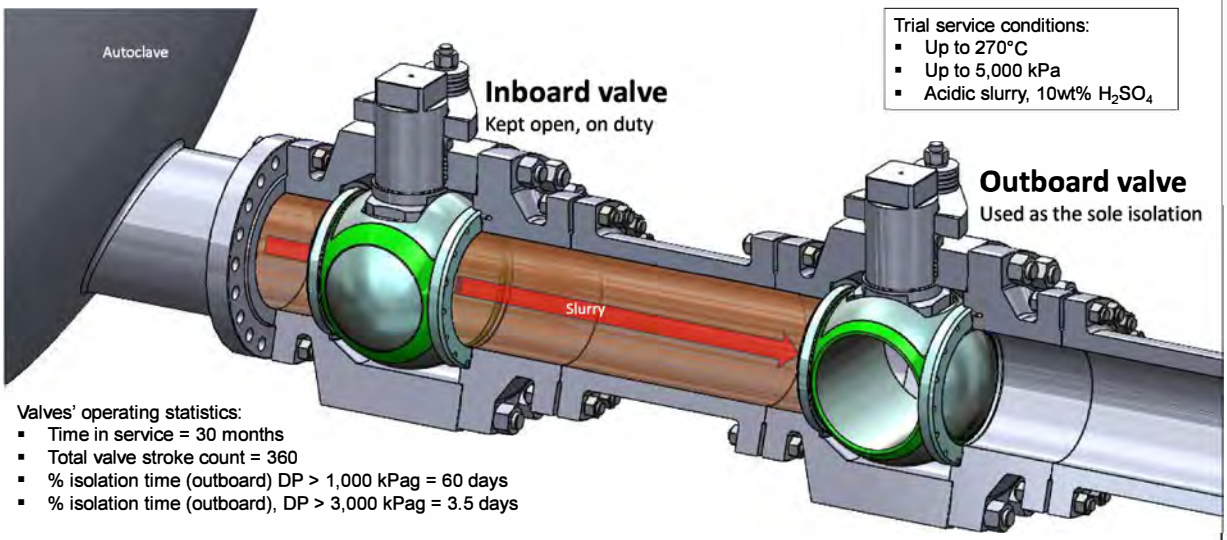

Trial service conditions:
- Up to 270°C
- Up to 5,000 kPa
- Acidic slurry, 10wt% H_2SO_4

Valves' operating statistics:
- Time in service = 30 months
- Total valve stroke count = 360
- % isolation time (outboard) DP > 1,000 kPag = 60 days
- % isolation time (outboard), DP > 3,000 kPag = 3.5 days

Closing takeaways

- Evolution of TiN surface modifications developed and applied to solve clients' equipment issues. Demonstrative of Callidus' ongoing investment into R&D.
- FM-1500™ for severe service ball valve trim designed for erosion and corrosion resistance.
- Callidus supports the end user to achieve optimum performance through technical, operational, and engineering support to key OEMs to assist with product improvements and development.

MORE OUT OF TAILINGS:
METAL AND ACID PRODUCTION, CIRCULARITY AND ENERGY TRANSITION

By

Dr. Jörg Hammerschmidt, Maciej Wrobel,Dr. Sepehr Mozaffari, [2]Marcus Runkel, [3]Darryl Harris

Metso, Germany
[2]Metso, USA
[3]Metso, Australia

Presenter and Corresponding Author

Darryl Harris
darryl.harris@metso.com

ABSTRACT

The need to “extract more from less’ is not a byword that sits well in the mining industry. Head grade degradation, basically processing ever more ore to produce ever less final product with an inevitable increase in waste, is a fact for many operations.

The need for more circular solutions required for the emerging energy transition (i.e. the demand for ever more non-ferrous and critical minerals) requires us to rethink what we can do differently. The processing of tailings from the copper ore processing offers significant potential to recover valuable elements like copper, cobalt, and nickel as well as to produce sulphuric acid for different applications in the fertilizer and metallurgical industry. Perhaps the time is right for a well proven industrial process to be part of the push towards a true circular economy?

We intend to present our views on the renaissance of a technology value chain – the roaster-gas cleaning acid plant - widely used in the past and its applicability to the current scenarios. This process chain is capable of utilising virgin pyrite ores as well as pyrite tailings, with a view to maximum extraction of valuable ferrous, non-ferrous and critical minerals, reducing acid mine drainage, production of clean energy as well as providing a ‘regionalised’ sulphuric acid supply. When these commodity flows are considered in total as revenue streams, return on investment is, in many cases positive – substantiating the claim that one can obtain ‘more out of ore’.

Keywords: fluid bed technology, roasting, tailings, pyrite, metal recovery, sustainable, circular solution, acid production, battery metals, valuable metals; CFB, fertilizer

****

INTRODUCTION

Australia holds some of the world’s largest recoverable resources of critical minerals like cobalt, lithium, manganese, rare earth elements, tungsten, and vanadium. The country’s commitment to becoming a renewable energy superpower aligns with the growing demand for these minerals. The Australian Government’s measures in the 2023–24 Budget highlight its commitment to a net-zero economy, leveraging its mineral resources(1). Additionally, in December 2023, they revised the Critical Minerals List and introduced a new Strategic Materials List. These actions recognize the importance of specific materials in the global shift toward net-zero emissions and broader strategic applications(2).

The existence of diverse pyrite and sulphide deposits in Australia offers ample opportunities for mining companies to explore, invest, and contribute to sustainable resource utilization. For instance, one example to highlight the importance of managing pyrite-rich materials in Australia is overcoming pyrite challenges in Queensland’s Ore Reserves and Mine Tailings. Rresearchers are collaborating with several companies to extract copper from resources considered too difficult to process due to high pyrite levels. Using innovative processing solutions are essential to meet metal demand to achieve the target, which is to recover more base metals from pyrite and reduce losses to tailings(3). Additionally, for mining operations, recovering fresh, reusable water from tailings is highly valuable.

This significance is particularly pronounced in Australia, where conditions of aridity, high evaporation, and poor-quality groundwater are common[4].

The critical minerals industry in Australia is intrinsically linked to the issue of tailings. As the extraction and processing of these minerals often result in the production of large volumes of tailings, the management of these by-products is a significant concern. Tailings contain residual minerals that were not initially targeted for extraction but may now be valuable in the context of decarbonisation and the transition to renewable energy. For instance, cobalt, a critical mineral for battery technology, can often be found in the tailings of copper mines. Therefore, the challenge for Australia's critical minerals industry is not just about increasing production to meet global demand, but also about innovating and improving the efficiency of mineral extraction processes to reduce tailings and potentially recover valuable minerals from them. This approach aligns with the broader goals of sustainable mining and circular economy, turning a waste product into a resource, and contributing to the decarbonisation efforts. In 2022, Australia witnessed limited growth in its mining operations, contributing only 3% to global growth. Despite maintaining its status as a significant producer, it was overtaken by Indonesia as the second-largest producer of cobalt and nickel. Also, it is estimated that Australia has the potential to double its share of mined supply growth from 2022-30, potentially reaching up to 6%[5].

TAILINGS IN MINING AND METALS INDUSTRY

Pyrite is a common mineral in many types of metal ore deposits, and it is often found in association with other minerals that contain gold, copper, cobalt, and zinc amongst others. Pyrite-containing tailings are commonly produced in mining operations that extract these types of minerals. The amount of pyrite present in the tailings can vary depending on the specific deposit and the extraction process used. Sulphur content in pyrite tailings concentrate is typically anywhere between 30-50 wt%. In the past, sulphuric acid used to be produced from Pyrite concentrate as the main source of sulphur. Today Pyrite is a by-product of the mining industry that often ends up in tailings. Beside the requirements for circular economy, there are industry wide discussions, if future sulphur demand will be challenged by energy transition and de-carbonization. The usage of Pyrite could also address this topic at least locally, where elemental sulphur from oil and gas industry is imported.

It is estimated that there are thousands of pyrite tailings dams around the world. A 2017 report by the International Council on Mining and Metals (ICMM) estimated that the mining industry produced between 10 and 20 billion tonnes of tailings annually. Most of the pyrite tailings originates from copper mining and mainly consists of sulphur, Iron, SiO_2, Al_2O_3, CaO as well as valuable non-ferrous metals[6].

Globally, there are 580 operations exploiting copper, with 190 cases from where resources and reserves are reported. Copper production in Australia for 2023 was over 1 million tons per year (tpy) with about half of it being exploited by the 5 biggest mines Olympic Dam, Cadia Mine, Mount Isa Mine, Ernest Henry Mine and Prominent Hill Mine (Figure 1)[7]. With approximately 197 tons of tailings generated for every 1 ton of copper produced, this makes about 200 million tpy of tailings alone for Australia. The sulphuric acid amount produced out of these tailings would amount to roughly 15 million tpy as compared to world production in 2021 of 260 million tons.

Figure 1: Australian Critical Minerals at Operating Mines and Major Deposits[2]

As global ore grades further deplete over time, the volume of tailings per ton of metal is continuously increasing. The mine operator has the challenge of treating an increased volume of mineral to maintain same metal production rate, this increases tailings waste and the associated operational costs. Mining operations inevitably generate waste and tailings, but there are strategies to ensure their sustainable management. Although mining waste is an established part of the industry, the methods of handling it can be modified[6]. According to Australia's Department of Climate Change, Energy, the Environment and Water's 'National Waste Report 2022', the mining sector produced substantial waste in 2020–21, totalling 620 million tons (Mt), a notable increase from 502 Mt in 2018–19. Approximately 96% of this mining waste was stored in tailings dams, which serve as storage place for mining by-products following ore extraction.

Figure 2 below presents the estimated mining waste by commodity indicating that the most wastes are produced from gold ores, followed by iron ore and copper ore mining[8].

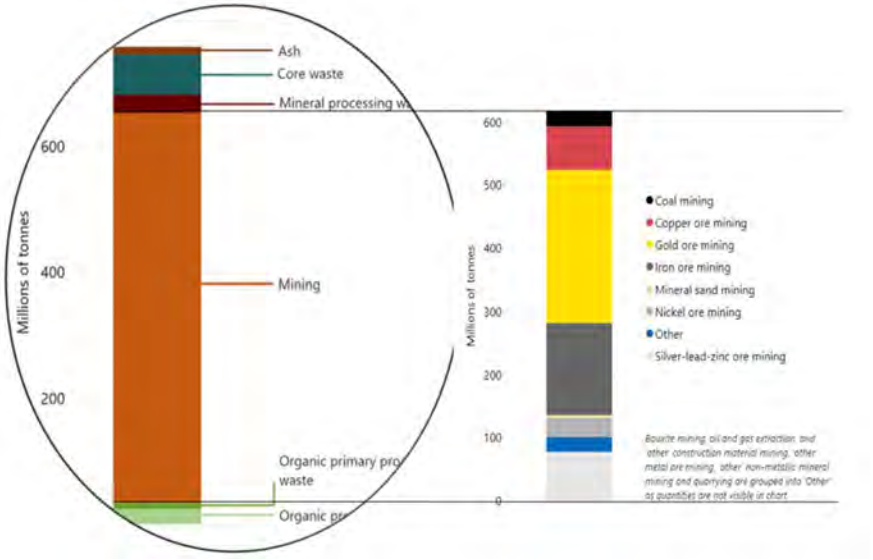

Figure 2: Estimated Mining Waste by Commodity in Australia, 2020–21 (Redrawn; Derived from[8])

It is important to note that processing of pyrite and tailings is indeed crucial for several reasons: pyrite-rich tailings can lead to acid mine drainage (AMD) when exposed to air and water. This acidic runoff can harm ecosystems, contaminate water sources, and affect aquatic life. Therefore, proper processing helps prevent AMD by neutralizing or encapsulating pyrite, minimizing its environmental impact. In addition, tailings often contain valuable minerals that were not efficiently extracted during primary processing. So, by reprocessing tailings, Australia can recover additional metals such as copper, cobalt, gold, or zinc, contributing to resource sustainability. Furthermore, unprocessed tailings pose safety risks, especially if they are unstable or prone to collapse. Therefore, proper processing ensures tailings are stable, reducing the risk of dam failures or environmental disasters[9]. Also, under the legal and regulatory compliance for tailings management, Australian mining regulations require responsible management of tailings. Therefore, processing tailings aligns with legal obligations and demonstrates commitment to environmental stewardship. In summary, the processing of pyrite and tailings is essential for environmental protection, resource utilization, safety, and compliance with industry standards of the country and understanding their effects is critical for responsible resource management[10]. At some locations, mining companies are legislated by the government to take care of the existing dumps before receiving new permits. At the same time, as attention to environmental, social, and governance (ESG) increases, mining companies are more aware of environmental issues and the related increasing costs. In conclusion, proper management of tailings is crucial for ensuring the safe and sustainable production of minerals and metals. A large amount of these tailings contains ferrous material in the form of pyrite as the main component. By upgrading the concentrate to a calcine or further processing it for metals recovery, Co, Cu, Ni, Zn, Ag, and Au can be recovered. In addition, sulphide-bearing tailings can be considered as relevant feedstock for acid production and potential Fe rich calcine from the hydrometallurgical retreatment can potentially be evaluated for further value recovery.

Australia's approach to managing tailings balances resource recovery with ecological sustainability. To cope with the future challenge of circular economy, technology requires adaptation. The amount of Pyrite to be processed requires a significant increase of the throughput of existing plant units to reduce capital intensity. We, at Metso, are working to increase the capacity of individual roasters using our unique knowledge of this technology. Recycling mine tailings can help reduce the volume of tailings for disposal, mitigate water contamination, and generate new revenue streams such as valuable metals extraction, sulphuric acid production, and energy generation. Dependent on the composition of the pyrite, the local acid market, and the volume of tailings to be processed, several different processing scenarios can be offered by Metso.

Today metallurgical processing plants are focusing on all valuable metal recoveries from the pyrite concentrate. The roasting process can be seen as a pretreatment process before processing the calcine in a downstream hydrometallurgical process for the recovery of the valuable metal. However, important revenue streams, such as sulphuric acid, steam and in some cases iron oxide may well add further revenue upsides to the project.

Figure 3 shows all relevant material streams for a conceptual evaluation.

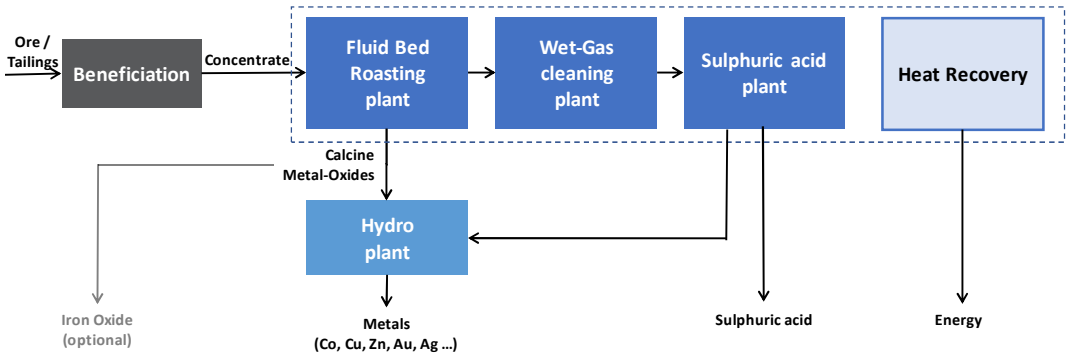

Figure 3: Metals Value Chain of Pyro / Hydro Metallurgy

CONCEPTS OF PYRITE ROASTING

Whilst the fundamentals of the roasting process have not changed significantly, each plant has its specifics and optimum key plant configuration. Over the last sixty years, Metso (including former Outotec and Lurgi companies) has built more than 470 fluid bed applications. Approximately two thirds of these references are based on the bubbling fluid bed technology (BFB) and the rest employ circulating fluid bed technology (CFB). In the following sections, three roasting plants related to pyrite are briefly described.

In the past the capacity of a pyrite roasting plant has been typically based on the sulphur content of the feed pyrite and market requirement and few plants reached beyond 1,000 t/d for one fluid bed roaster. In general, the bubbling fluid bed technology has been applied for more than 165 pyrite roasters.

Figure 4 shows the latest reference of Metso installed roaster at Mazidağı/Turkey which has a total capacity of 2 x 750 t/d pyrite based on the BFB technology.

Figure 4: Pyrite Roasting Plant at Mazidağı/Turkey[11]

The process chain starts with the roaster, followed by a boiler system. The off-gas with some dust entrainment is further cleaned in the cyclone system and finally in the hot-electrostatic precipitator (H-ESP). Hot solid product (calcine) is discharged from the plant from the roaster down to the H-ESP and cooled down further. After the hot gas cleaning, the off-gas enters the wet gas cleaning section, which traditionally includes the quench tower (Otovent), gas cooling tower, wet-ESP, and any impurity removal steps. Finally, the purified SO_2 gas enters the sulphuric acid plant for conversion to sulphuric acid.

Figure 5: Gold Roasting Plant at NGM, Nevada/USA[12] (left) and Resolute Mininig - Gold Roaster at Syama / Mali (right)

The NGM Carlin gold roaster (
Figure 5, left) was designed in the 1990s for a throughput of 2 x 3,900 t/d and operates today around 30% higher than initially designed, which is a credit to the operation/maintenance philosophy locally employed. The fluidizing air is recycled from the H-ESP off gas back to the roaster and enriched with preheated oxygen before it enters the CFB[13].

A third example is the roasting plant at Syama in Mali (
Figure 5, right) and this operation consists of a single roasting train and is designed to operate a maximum capacity of 590 t/d with a sulphide-sulphur equivalent of minimum 31.1 %[14].

The application of the CFB technology allows for both gold roasters mentioned above to produce a significantly more homogeneous temperature distribution in the roaster, enhancing production efficiency in the downstream leaching process. The key advantage of the CFB over the BFB technology is to obtain higher throughput in a single fluid bed reactor. For the Mazidağı plant, two roasters are installed in parallel (total 1,500 t/d). If higher capacity is required at a specific location (e.g., above 2,000 t/d), circulating fluid bed technology could be applied to handle all the material in a single unit.

The two pyrite projects at Mali and Cengiz are at the lower end of current sulphuric acid production capacity globally but form the basis for any future plants in this capacity range. The sulphuric acid industry however is defined by sulphur burning and metallurgical off gases with much higher capacity than currently exist for a roasting plant configuration.

The circulating fluid bed technology for high throughput is more defined by whole ore roasting, such as the NGM gold roaster, alumina calcination or the Enefit oil shale combustion. All these applications from Metso are already operating with much higher solid throughput rates. Metso is now combining all this experience from different projects in the sulphuric acid and fluid bed industry, as well the experience from metallurgical acid plant projects to meet the demands of the market for higher throughput pyrite plants. The next logical step from this trend in pyrite roasting is therefore to build pyrite roasting plant with higher acid production and higher solids throughput utilizing CFB technology. Metso is minimizing the technical risk of development by applying a proven technology for the renaissance of roasting for the treatment of pyrite tailings. This step is now in focus and already applied in ongoing development and engineering projects. This future step is demonstrated in Figure 6 as a future reference base with capacities of approx. 1,500 – 3,000 t/d of concentrate and acid production of 2,000 – 3,500 t/d.

The operation area and size and number of roasters of the future references are defined by the amount of concentrate as well as by the sulphur content and with this, the formation of energy in the roaster. Typical sulphur content in the pyrite concentrate is in the range of 30 – 50%. Therefore, beside the capacity, the sulphur content and acid production are also shown in Figure 6. A lower sulphur content allows a higher solids throughput in the plant. The figure shows an orientation for the possible capacity increase marked as future reference base. The feed capacity for a pyrite tailings roaster can reach ca. 3,000 t/d with a 30 % sulphur content, however the capacity will be lower if the sulphur content is higher. A fine example to illustrate this trend is Metso's gold roaster reference at NGM in Nevada which treats whole ore with only ~3 % sulphur. With this low energy content, one roaster unit can operate with throughputs up to ~ 5 000 t/d. This gold roaster is a unique solution as the intention there is only gold recovery, however it clearly shows that the handling and treatment of such a huge volume of material in one fluid bed roaster based on CFB-technology is possible (see also Figure 6). The large throughput roasters follow the development under the Circoroast® approach, which combines increased heat recovery with traditional roasting technology.

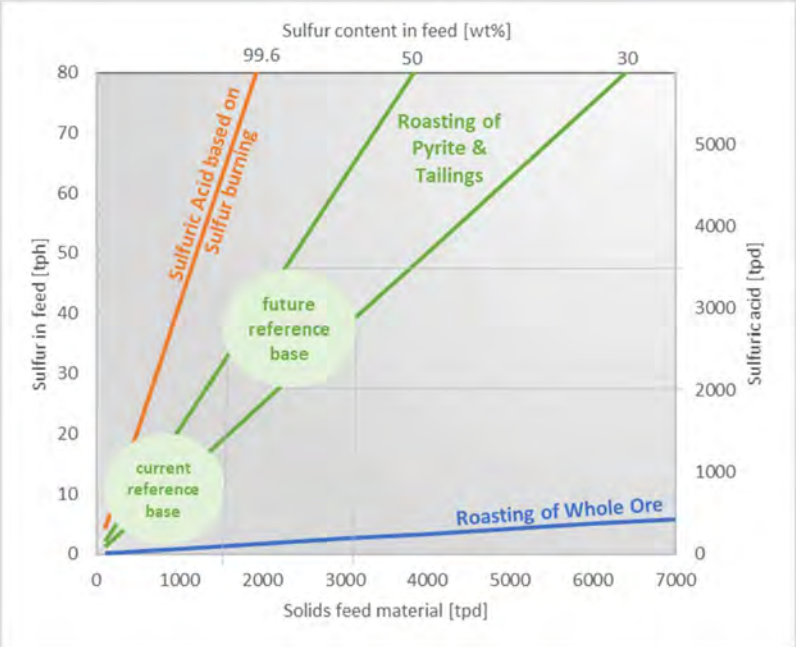

Figure 6: Roasting & Sulphuric Acid plant Capacity Trends

Metal Recovery

The composition of the pyrite concentrate varies depending on the ore body. Table 1 shows a typical composition of pyrite concentrates that has been analyzed in recent projects or are already treated today in existing operations.

For economical evaluation of a concentrate, all valuable metals must be considered. Combined with the local market situation for sulphuric acid and power generation a project can become economical. The basis for all evaluations is the described fluid bed roasters above. The economics of the metal recovery section depends on the metal content and the market value of the metals. Today due to the above-described trend to electromobility and energy transmission the most important factor is the cobalt content. With a value of 26,000 Euro/t, it is far above all other metals in the concentrate. However also copper and zinc can bring additional revenues to the project.

The composition of pyrite concentrate typically encompasses a range of elements, each playing a distinct role in its overall properties and applications. As shown in Table 1, sulphur (S) and iron (Fe) stand as primary constituents, forming the backbone of pyrite's chemical structure. Beyond these foundational elements, pyrite concentrate often contains trace amounts of other metals, which can be categorized into different groups based on their significance and utility. Firstly, critical elements such as zinc (Zn), copper (Cu), and cobalt (Co) are commonly present, each contributing to various industrial processes and applications. These elements are integral in sectors like electronics, renewable energy, and infrastructure development, highlighting their importance in modern technologies. Additionally, silver (Ag) and gold (Au) are often found within pyrite concentrate, representing valuable precious metals that hold significant economic and industrial significance.

In the context of upgrading pyrite concentrate for downstream processing while simultaneously recovering energy and producing sulphuric acid, the elemental composition assumes paramount importance. The S- content within the concentrate is of particular significance, as it serves as the primary source for sulphuric acid production. Pyrite's high sulphur content makes it an ideal feedstock for sulphuric acid manufacturing, a process vital in various industrial sectors including fertilizer production, chemical synthesis, and metal extraction. Additionally, the Fe content in the concentrate holds potential for energy recovery through processes such as pyrometallurgical smelting or hydrometallurgical leaching. By harnessing the exothermic reactions associated with these processes, valuable energy can be generated, contributing to the overall sustainability and efficiency of downstream operations. Moreover, the presence of base metals such as Zn, Cu, and Co further enhances the economic viability of the upgrading process. These metals can be selectively extracted and purified through hydrometallurgical techniques, yielding additional revenue streams while

facilitating the production of high-purity products for various industrial applications. Furthermore, the recovery of precious metals like Ag and Au presents opportunities for further value addition, as these metals command high market prices and are in demand across diverse sectors. Therefore, by strategically leveraging the elemental composition of pyrite concentrate, it becomes possible to optimize downstream processing while concurrently recovering energy and producing sulphuric acid, thereby maximizing resource utilization and minimizing environmental impact.

Table 1: Typical Pyrite Compositions

Element		Pyrite/Tailings	Calcine
		content (wt%)	
Sulphur	S	48 - 52	1 - 3.0
Iron	Fe	40 - 45	60 - 65
Base Metals	Zn	0.1 - 0.5	0.2 - 0.8
	Cu	0.5 - 0.9	0.8 - 1.4
Critical Elements	Co	0.7 - 1.3	1 - 1.7
	Ag	> 10 g/t	
	Au	> 1 g/t	

Based on the latest reference plant with a concentrate feed rate to the roaster of 500,000 tpy a calcine amount of around 375,000 tpy is produced. In addition to the solids feed and production rates, sulphuric acid of around 750.000 tpy is produced as well as and energy of 140 GW in one year.

Pyrite concentrates with high metal content tend to be more economically valuable due to their potential applications in metal production and energy. In addition, having a high sulphur and iron content in the concentrate would make the metallurgical process very attractive with acid and energy as the by-products.

When the gold content is high in pyrite concentrates, however, in modern practice, such pyrite is often bypassed for further treatment in the hydrometallurgical process. Despite this, the presence of low non-ferrous metals can be viewed as an advantage because it enables the production of a calcine with high iron content and low sulphur content. This strategic utilization aligns with efficiency and resource optimization. In ferrous industry, the presence of non-ferrous metal in the calcine is a common challenge so where the non-ferrous metal content is low, it can be added into the feed stream in the steel production process. In addition, the other main concern would be the calcine sulphur content. However, the content can be reduced during the roasting process, resulting in calcine suitable for steel industry, acid, and energy.

For the pyrites with high base metal content, test work must be carried out and the target of these tests is always to increase the recovery of valuable metals, such as cobalt, copper, zinc, silver, gold, etc. whilst keeping the iron portion in solid form. Only with a low Fe-content in leaching-solution, then it is possible to avoid producing high amounts of waste and selling the final residues to the ferrous industry. The results of the recovery rates can vary from one pyrite concentrate to another and the complete process chain, roasting as well as leaching, must be tested. In the Mazıdağı plant a pressure autoclave leaching has been implemented[15], since it was confirmed by testwork that better results in recovery of the metals as well as for the consumables acid, steam, and solubility of iron were achievable[16].

In another internal project, we also analyzed pyrite and made atmospheric leaching tests. Table 2 shows the recovery development in relation to the roasting temperature, leaching temperature and acidity. The recovery in these test campaigns has been on the lower side. Based on a roasting and leaching test series the process condition with the overall best performance has been conducted. While a conventional roasting process at (or above) 850 °C followed by atmospheric leaching results in lowest recovery rates, the combination of correct process conditions can result in excellent overall plant efficiencies. Starting out at low roasting temperatures (less than 700 °C) and atmospheric leaching, the metals recovery rate is still below its potential. Looking at table below, the extraction rate of metals is at about 60-70%. Increasing the roasting temperature and acid concentration further results in improved recovery rates in some cases, however high amount of unwanted iron is leached as well (Test 3) at certain process condition under atmospheric leaching.

Table 2: Metals Recovery Rates Based on Roasting and Leaching Conditions

Test	Roasting	Leaching		Extraction Rates			
No.	Temp.	Temp.	Acid	Co	Cu	Zn	Fe
	°C	°C	g/l	%	%	%	%
1							
2							
3							
4							
range	*640-850*	*20-220*	*35-100*	*24-95*	*33-95*	*19-97*	*0.1-11*

In Test 4, we observe a remarkable metal recovery rate, exceeding 95%, while minimal iron leaching occurs. The process involves a roasting of the feed material at a temperature of 820 °C, followed by a high-pressure and high-temperature autoclave leaching to achieve the optimal metal recovery while minimizing acid usage. The overall best plant performance can be reached at optimized roasting temperature and optimized autoclave leaching. The high recovery rates of around 85 to 98% found in laboratory conditions match typically what can be achieved in the industry, although industrial applications tend to operate at the higher end of this spectrum. With respect to a gold roasting plant, the operating temperature window is normally lower, however when operated in combination with autoclave leaching the extraction is optimized. There are several advantages for this change in roasting process conditions for the metal recoveries, which are related to better heat recovery, lower effluents, and higher acid production in the roaster. All these factors are important for an attractive and feasible process.

Sulphuric Acid Production

Apart from metal recovery, the demand for the sulphuric acid will further increase in the decades to come. As the availability of elemental sulphur from the oil and gas industry reduces, new sources must be found or re-developed. In the past, pyrite was already one of the main sources for sulphuric acid production and it can certainly fill some of the expected gap in demand. The surge in low-carbon technologies, including batteries, lightweight vehicle motors, and solar panels, will intensify mineral mining. Ores that are rich in cobalt and nickel will play a crucial role. By 2050, cobalt demand could soar by 460%, nickel by 99%, and neodymium by 37%. Remarkably, all these metals rely on substantial sulphuric acid extraction. Simultaneously, global population growth and dietary shifts will boost sulphuric acid demand. The phosphate fertilizer industry, a major consumer, will drive this increase. Therefore, balancing supply and demand become pivotal for sustainable resource management[17].

In the context of Australia, the potential sulphuric acid shortage highlighted in the study could have significant implications for various industries in the country. Australia heavily relies on sulphuric acid in vital sectors such as mining, agriculture, and manufacturing. A shortage of sulphuric acid could disrupt mining operations, leading to economic consequences due to reduced production of key commodities like copper and gold. It would also impact agriculture, hindering crop yields and fertilizer production, affecting both domestic food security and export potential. Additionally, such a shortage would impede the manufacturing of industrial chemicals and green technology products, hampering Australia's transition to a low-carbon economy. Moreover, environmentally damaging sulphur mining practices could worsen, leading to habitat destruction and pollution, further harming Australia's environment. Thus, ensuring a stable sulphuric acid supply is essential for Australia's economic resilience and environmental sustainability.

According to a recent study on the global demand for sulphuric acid and its potential crisis in the future showed that over 246 million tonnes of sulphuric acid are used worldwide annually. However, as the green economy grows and agriculture intensifies, demand could surge to over 400 million tonnes by 2040 (
Figure 7). Currently, more than 80% of global sulphur supply comes from fossil fuel desulphurization to reduce sulphur dioxide emissions. Yet, decarbonization efforts will reduce fossil fuel production, potentially causing a shortfall of 100 to 320 million tonnes of sulphuric acid by 2040. Addressing this challenge is crucial to avoid environmentally damaging mining[17].

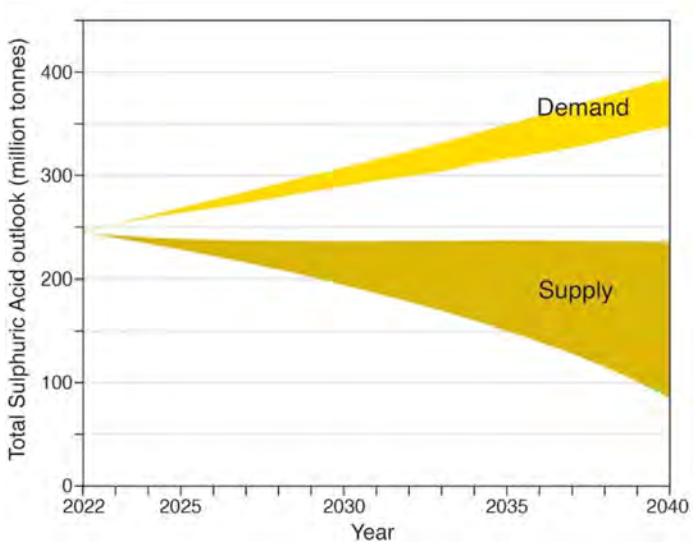

Figure 7: Estimated Future Supply and Demand of Sulphuric Acid[18]

ECONOMIC EVALUATION OF PYRITE ROASTING

On the earnings side it is particularly important to use a realistic local market value for the acid. Many projects are failing by using wrong or very conservative figures for the local acid price. The biggest revenue at the Mazidağı project in Turkey emanated from the cobalt and acid recovery. In 2018 the metals import has been reported at $270 million a year[19]. The acid in this project is used at site in the fertilizer plant. With an annual production of 750,000 t of fertilizer, the production meets the entire fertilizer requirements of the region[20].

As a reference study case we assumed a pyrite roaster plant based on CFB technology a capacity of 2,000 t/d pyrite plant with the metal composition of Cu 0.5%, Co 0.5%, Zn 0.2%, Ag 5 g/t, Au 1 g/t, the earnings are shown in Table 3. For a hypothetical operating cost on essential plant units (including leaching) the ROI is about 150 MEuro per year. Of course, this number is dependent on initial capex cost and market unit rates as shown in table below.

Table 3: Project Example of Earnings Based on Revenue Streams

item	amount		price		total/year	
Co	3162	t	26000	Euro/t	82.2	Mio€
Sulphuric Acid	999600	t	60	Euro/t	60.0	Mio€
Au	632.4	kg	54000	Euro/kg	34.1	Mio€
Cu	3162	t	7600	Euro/t	24.0	Mio€
Power	184960	MWh	40	Euro/MWh	7.4	Mio€
Zn	1264.8	t	2800	Euro/t	3.5	Mio€
Ag	3162	kg	670	Euro/kg	2.1	Mio€
CO_2	to be evaluated by location					
Tailings	future regulations may apply					
Groundwater	future regulations may apply					
Total Earnings					**213.4**	**Mio€**

SUMMARY

Australia, with its vast geological reserves and expertise in mineral extraction, stands at the forefront of a global transition. The Critical Minerals Strategy 2023–2030 is a visionary roadmap unveiled by the Australian government to explore how this strategy aligns with our collective goal of a sustainable

future. By extracting these vital minerals, Metso paves the way toward a cleaner future. Such dedication aligns with net-zero goals, tackles mine waste issues, and fulfills the worldwide need for environmentally responsible metal extraction.

In conclusion, the application of the high-capacity roasting process applying CFB technology can contribute to a planet positive development. While the transmission to electromobility and renewable energy is accelerating, the request for valuable metals as cobalt is increasing. Besides sulphuric acid and CO_2-free energy production, this allows for studying the economics of recovery for cobalt, copper, zinc, gold, and silver from pyrite feed sources. This is then dependent on the compositions of the feed material, as previously discussed in the article.

REFERENCES

1. Australian Government - Department of Industry, Science and Resources, “Critical Minerals Strategy 2023-2030,” 2023.
2. Australian Trade and Investment Commission (Austrade), “Australian Critical Minerals Prospectus,” 2024.
3. The University of Queensland, “Overcoming pyrite challenges in Queensland’s ore reserves and mine tailings,” The University of Queensland, [Online]. Available: https://smi.uq.edu.au/overcoming-pyrite-challenges-queensland%E2%80%99s-ore-reserves-and-mine-tailings. [Accessed March 2024].
4. Commonwealth Scientific and Industrial Research Organisation (CSIRO) , “Resourceful, Issue 26: Sustainable resources,” 2022. [Online]. Available: https://www.csiro.au/en/work-with-us/industries/mining-resources/Resourceful-magazine/Issue-26/Tailings. [Accessed March 2024].
5. Cobalt Institute, “Cobalt Market Report 2022” 2023.
6. M. Runkel, J. Hammerschmidt, M. Wrobel and J. Calvo, “Finding New Life for Tailings: Sustainable Technology for Co, Cu, Ni, and Zn Production,” in *Proceedings of the 62nd Conference of Metallurgists, COM 2023*, Toronto, Canada, 2023.
7. mine.nridigital.com, “Wrapped: Australia’s six biggest copper mines in 2023,” [Online]. Available:https://mine.nridigital.com/mine_australia_jan24/copper-biggest-mines-australia. [Accessed March 2024].
8. The Department of Climate Change, Energy, the Environment , “National Waste Report 2022,” 2023.
9. D. P. Mohapatra and D. M. Kirpalani, “Process effluents and mine tailings: sources, effects and management and role of nanotechnology.,” *Nanotechnology for Environmental Engineering,* vol. 2, no. 1, 2017.
10. Australian Government Department of Industry, Science and Resources, “Tailings Management - Leading Practice Sustainable Development Program for the Mining Industry,” 2016.
11. Database, Metso Q-bank (company data bank).
12. “Google Maps,” Gold Roasting Plant at NGM, Nevada/USA, [Online]. Available: https://goo.gl/maps/8cMBckESE9xHYAAP7, 02/2023. [Accessed February 2024].
13. J. Hammerschmidt, J. Güntner, B. Kerstiens and A. Charitos, “Roasting of gold ore in the circulating, fluidized-bed technology,” in *Gold Ore Processing (2nd Edition) by Adams, Mike D. - Chapter 24*, Elsevier, 2016, pp. 393 - 409.
14. A. Charitos, C. Mattich, J. Hammerschmidt, J. Wilson, T. Kerr and D. Landwehr, “Capacity and product quality optimization of the Syama roaster,” in *7th World Gold Conference, Conference of Metallurgists (COM 2017)*, Vancouver, Canada, 2017.
15. Metso, “Calcine pressure leaching – Eti Bakir case study,” Metso, [Online]. Available: https://www.mogroup.com/insights/blog/mining-and-metals/calcine-pressure-leaching-eti-bakir-case-study/. [Accessed 3 2024].
16. K. Haavanlammi, H. Laitala and M. Canbazoglu, “Pressure Leaching of Copper-Cobalt-Zinc Containing Calcine with the Outotec Pressure Oxidation Process,” in *Proceedings of the 58th Annual Conference of Metallurgists*, 2019.
17. M. Maslin, L. Van Heerde and S. Day, “Sulfur: A potential resource crisis that could stifle green technology and threaten food security as the world decarbonises.,” *The Geographical Journal,* vol. 188, pp. 498-505, 2022.

18. “Sulfuric acid: the next resource crisis that could stifle green tech and threaten food security,” 2022. [Online]. Available: https://theconversation.com/sulfuric-acid-the-next-resource-crisis-that-could-stifle-green-tech-and-threaten-food-security-186765. [Accessed March 2024].
19. H. Guldag, “Cengiz starts cobalt production in Mazidagi,” 2018. [Online]. Available: https://www.pressreader.com/turkey/TR-Monitor/20181029/281629601264587. [Accessed February 2024].
20. “Mazidagi Phospate Plant,” Cengiz Holding, [Online]. Available:https://etibakir.com.tr/plants/mazidagi-phospate-plant/?lang=en. [Accessed February 2024].

DILUENT SELECTION AND ITS IMPACT ON PERFORMANCE

By

Jia Tian Lee

ExxonMobil Chemical Asia Pacific, Singapore

Presenter and Corresponding Author

Jia Tian Lee, Singapore
jiatian.lee@exxonmobil.com

ABSTRACT

The diluent is an important component in the solvent extraction process. While its main role is to solubilize and carry the extractant, the composition and physical properties of a diluent can have a significant impact on the overall performance of the system. The choice of diluent can potentially optimize the solvent extraction process by improving extraction efficiency, phase disengagement, crud formation and diluent losses. In selecting a diluent, trade-offs that exist between the diluent properties should be considered to come to an optimum solution.

In addition, diluents constitute a large proportion of the mining chemicals used in a solvent extraction plant and hence its impact on the safety, health, and environmental aspects of plant operations cannot be understated. Over the years, diluent requirements have changed together with the continuous evolution of safety and environmental standards in the mining industry. The right diluent will enable a safe working environment without compromising on technical performance.

ExxonMobil's Escaid™ fluids have developed over the years to meet the evolving needs of the mining industry. They have been used globally in the extraction of copper, nickel, cobalt, uranium and other valuable metals. The Escaid fluids portfolio feature product grades with a range of volatilities and chemical types to support mining operations. The presentation will compare several diluents to provide insights on how the composition and properties of the diluent influence the solvent extraction process. The safety, health and environmental characteristics of the diluents will also be examined to show how the choice of diluents can help enhance industrial hygiene, improve personnel safety and potentially reduce environmental impacts.

Keywords: Solvent extraction, diluent, workers' exposure, safety, environment

ALTA 2024

Diluent Selection and Its Impact on Performance

Lee Jia Tian
Customer Application Development Technical Professional
ExxonMobil Chemical Asia Pacific
✉ **jiatian.lee@exxonmobil.com**

ExxonMobil

Industry Challenges and Potential Solutions

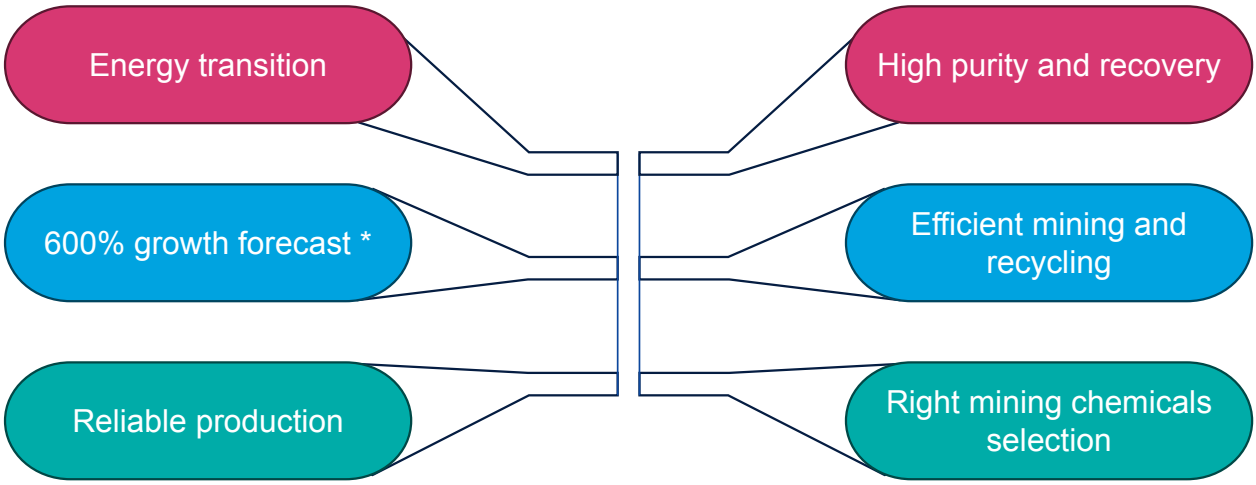

*By 2040, compared to 2020
Source: IEA (Link: https://www.iea.org/reports/the-role-of-critical-minerals-in-clean-energy-transitions/executive-summary)

Technology Reconnect

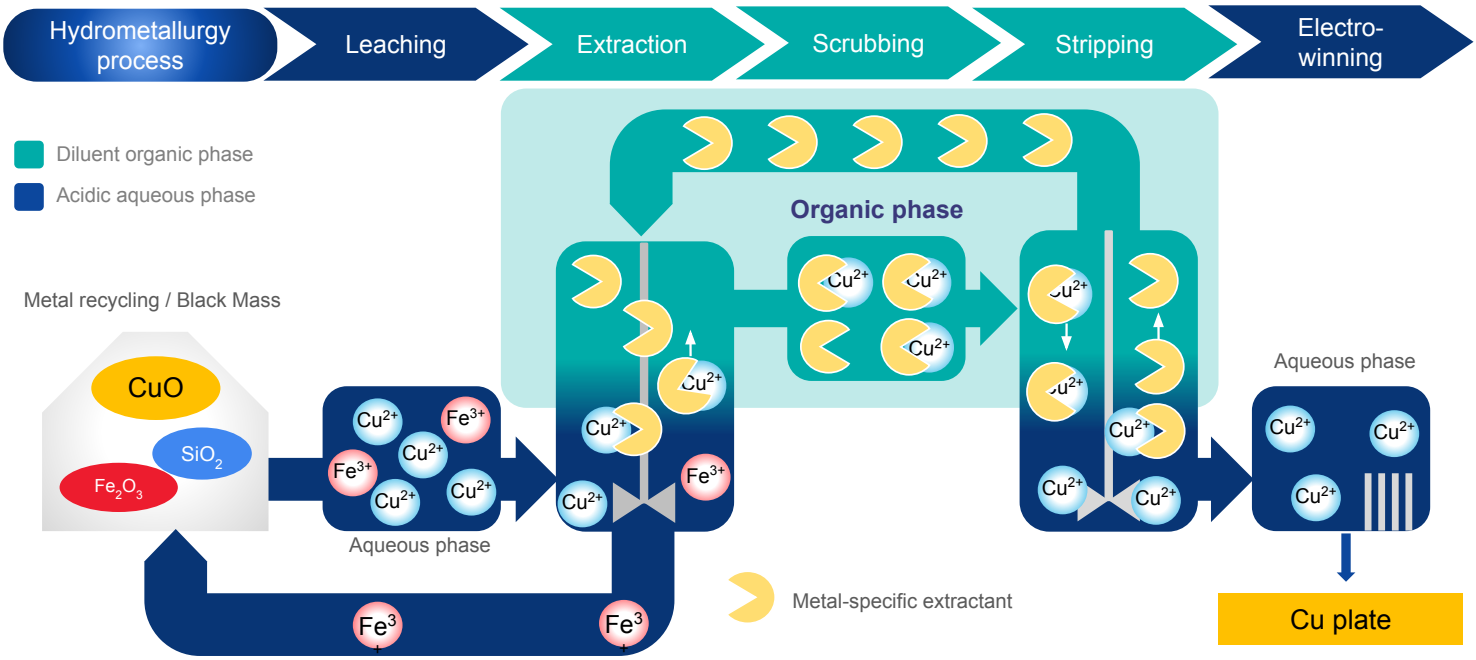

Diluent Selection Considerations

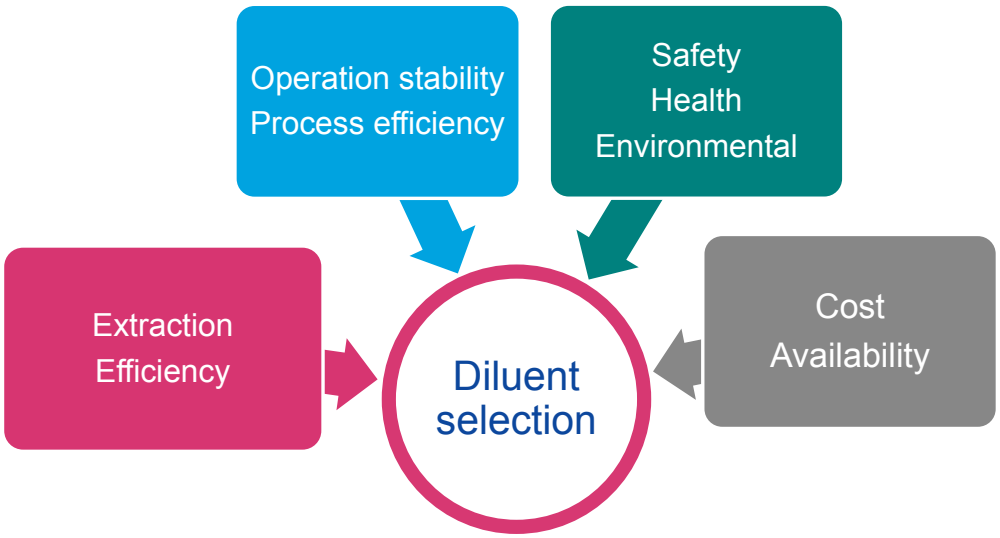

Diluent selection comprises of balancing the effects to reach an optimum compromise.

Extraction Efficiency

Efficiency

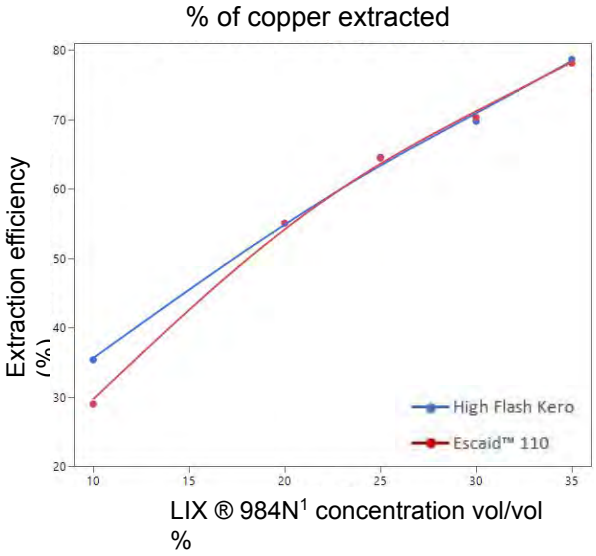

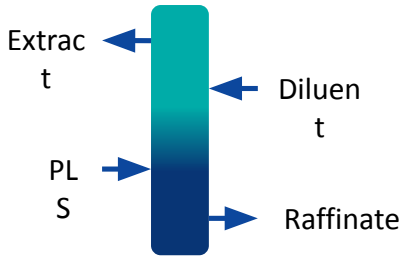

Lab scale extraction performed with copper nitrate solution. pH compensated with sulfuric acid.
Pregnant leach solution (PLS) :
[Cu] 15.2 g/l – pH: 2.11

Equivalent extraction efficiency on 1 stage for aromatized & dearomatized diluent

[1]LIX™ is a brand of an extractant produced by BASF

Data generated by or on behalf of ExxonMobil.

Diluent Losses

Cost

Process

- Escaid™ 110 fluid shows **lower entrainment losses** and **lower crud formation** vs. high flash kerosene

Lower diluent / extractant consumption
Potential for lower operating cost

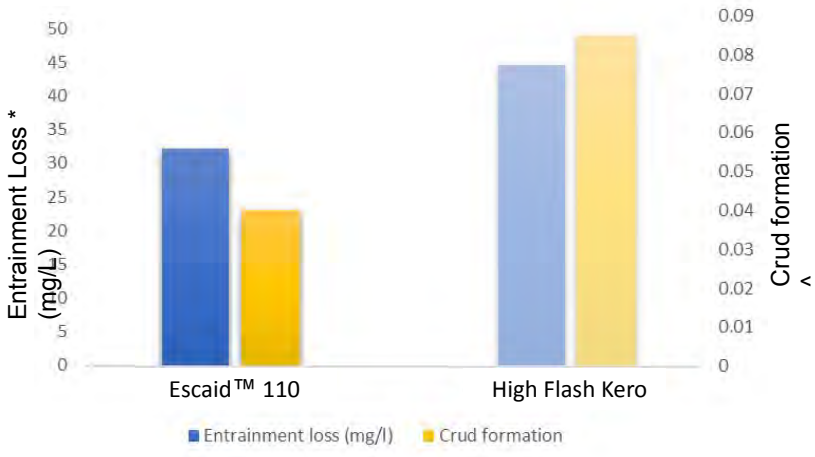

* Entrainment loss refers to trace organic fluid (15% LIX 984 N PLS 5 with pH=1.83) in aqueous phase measured via molecular absorption spectrophotometry following contact with the organic phase (O/A=1) and subsequent extraction with cyclohexane

^ Crud formation refers to ratio of total volume sludge / total volume organic

Lower diluent losses when comparing Escaid™ 110 fluid against high flash kerosene

Data generated by or on behalf of ExxonMobil.

Potential for lower health and environment risk

SHE

Property	Escaid™ 110 fluid (typical)	High flash kerosene (typical)
Aromatics (wt%) [UV/GC]	0.001	23
GHS hazard categories (environment)	-	Aquatic Chronic 3
Aquatic toxicity - Rainbow Trout	LL_0 > 1000 mg/l	LL_{50} = 41.4 mg/l

Source: Data from tests performed by or on behalf of ExxonMobil. All data are typicals. Typical values may vary over time

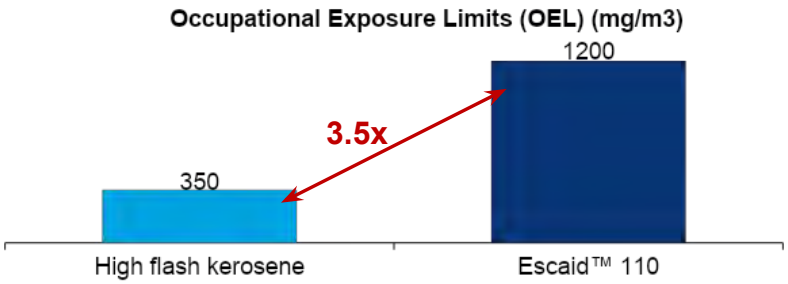

Potential benefits:

Not classified for environment (GHS)

- No aquatic toxicity classification
- Readily biodegradable (OECD 301F)

Lower risk of workers' overexposure

- Escaid™ 110 fluid has a higher OEL compared to high flash kerosene
- Lower health hazard (inhalation)
- Greater margin for safe use

Regional presence, global reach

Availability

Harmonized and globally available products enable rapid scale up and consistency of quality across regions.

Battery Recycling Opportunity

2 Million

Ton by 2030*

Global Annual Li-ion Batteries Available for Recycling

+90 %

Recovery

+95 %

Purity

Enabled by Hydrometallurgy and Solvent Extraction^ (SX)

*Source: BNEF- Lithium-Ion Battery Recycling.
^Source: Chagnesa A, Pospiech B, A brief review on hydrometallurgical technologies for recycling spent lithium-ion batteries. Journal of Chemical Technology and Biotechnology. 88: 1191-1199 (2013)

Flowsheet Example

Leaching with Sulfuric Acid → Extraction of Impurities (Mn, Mg…) with DEPHA → Extraction of Cobalt with Cyanex™ 272 → Extraction of Nickel with EM's Neodecanoic Acid → Extraction of Lithium with Cyanex 936 P

Escaid™ 110 fluids can be a suitable diluent for all solvent extraction steps.

Escaid™ fluids

A product range to match various process requirements while delivering advantages over traditional kerosene alternatives.

Key properties Methods	Escaid™ 110 fluid	Escaid™ 115 S fluid	Escaid™ 120 fluid
Distillation range (°C) ASTM D86	207-240	222-241	235-265
Aromatics content (%wt) UV Test Method	<0.01	<0.05	<0.1
Viscosity at 25°C (cSt) ASTM D445	2.09	2.41	3.16
Flash point (°C) ASTM D93	82	93	103
Density at 15°C (kg/dm^3) ISO 12185	0.795	0.796	0.822
Occupational exposure limit (mg/m^3) ExxonMobil data	1200	1200	1200

Source: Data from tests performed by or on behalf of ExxonMobil. All data are typical. Typical values may vary over time.

Escaid™ fluids in summary

Escaid™ fluids are **high performance extraction diluents** that can provide value in solvent extraction (SX) and also battery recycling:

The wide portfolio of ExxonMobil solvents can support innovation and process development in the field of solvent extraction.

Escaid™ fluids are globally available to ensure worldwide support.

Interested in learning more?

Access the deck via the QR code

Lee Jia Tian
Customer Application Development
Technical Professional

Phone: +65 8798 8298

Email: jiatian.lee@exxonmobil.com

Follow us

@XOM_chemical
linkedin.com/showcase/exxonmobil-chemical
@ExxonMobil
@ExxonMobil
instagram.com/ExxonMobil

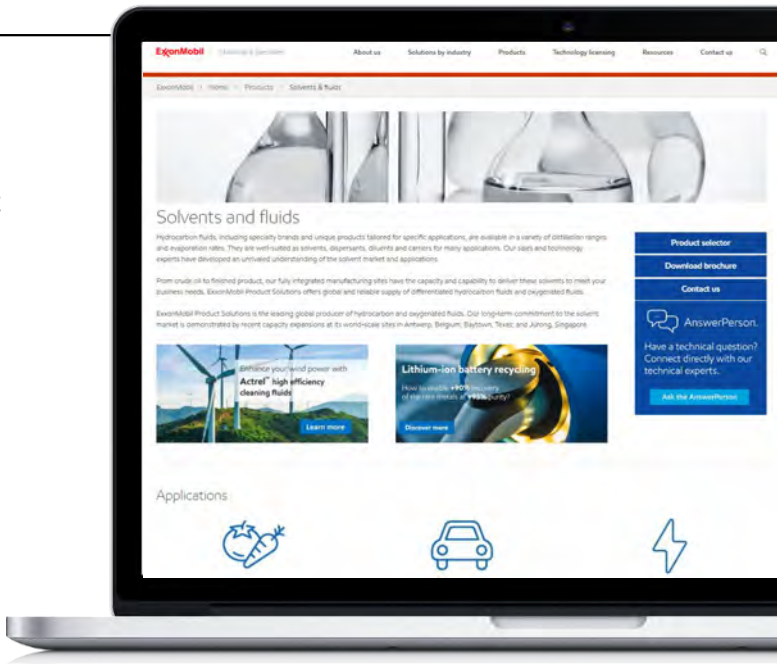

www.exxonmobilchemical.com

ExxonMobil

Diluent Losses

Cost | Process

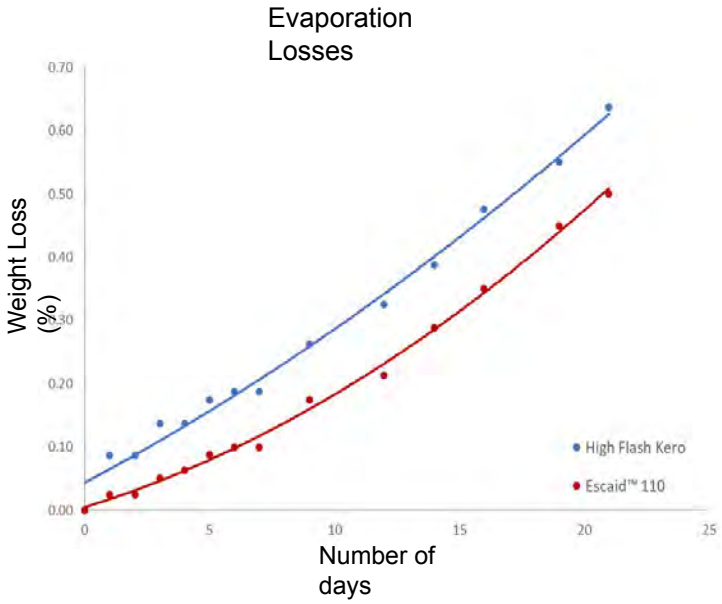

- Escaid™ 110 shows **lower weight loss from evaporation** vs. high flash kerosene
- Lower volatility reduces frequency of diluent top-ups and diluent's property variations over time

Potential for lower operating cost and improved process stability

Lower diluent losses when comparing Escaid™ 110 against high flash kerosene

Data generated by or on behalf of ExxonMobil.

Diluent selection considerations

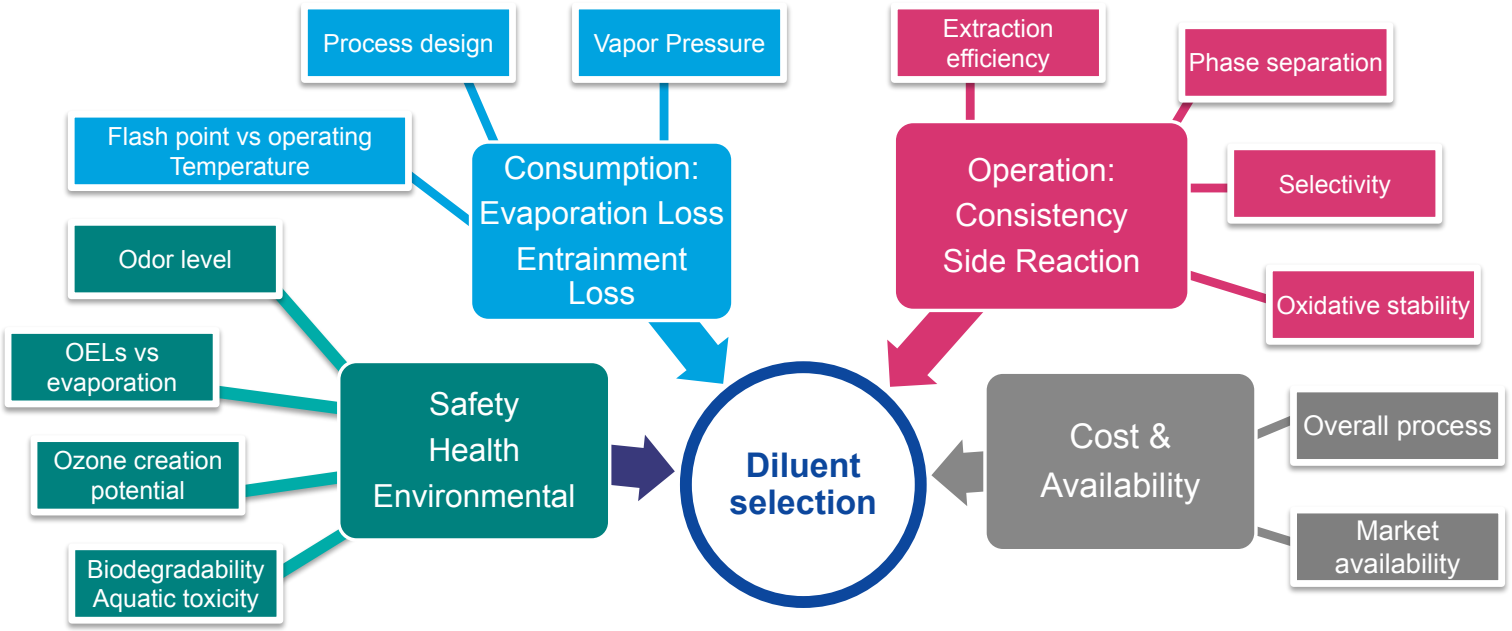

Diluent selection is based on defined requirements

BENEFITS OF GTL G80 MINING DILUENT IN COPPER SX FOR LOW- AND HIGH- GRADE COPPER ORE

By

Miguel Rivera Torrente, [2]Clio Deferm, [2]Peter Tom Jones, [2]Koen Binnemans, [3]Peter Haig

Shell Global Solutions International, The Netherlands
[2]SOLVOMET-KU Leuven, Belgium
[3]Peter Hague, Consultant, Australia

Presenter and Corresponding Author

Miguel Rivera Torrente
m.riveratorrente@shell.com

ABSTRACT

Shell GTL G80 is a synthetic, aliphatic mining diluent supplied by Shell into copper solvent extraction (CuSX) operations which represents the 4th generation of SX Diluents. G80 is produced from natural gas via the gas-to-liquids (GTL) process, resulting in a mixture of hydrocarbon distillate different from common market diluents.

In this work, we present the benefits of using G80 as the organic phase with various extractants of the LIX® and ACORGA® brands. Among others, good phase disengagement, copper loading and extraction/stripping kinetics were observed in laboratory tests carried out under common operating SX conditions. This was associated to the hydrocarbon composition of GTL G80, which consists almost exclusively of linear and lightly (methyl, ethyl) branched iso-paraffins, as opposed to other diluents which may contain naphthenes and aromatics.

Furthermore, the effects of high extractant concentration, commonly used for the recovery in Sub-Saharan oxidic deposits, were also studied. Specifically, we evaluated the impact of ~30%v/v concentration of various oximes in viscosity at different temperatures. Despite the low aromatic content of GTL G80 (< 300 ppm), the range of viscosities determined by standard methods was acceptable for most SX operations. In addition, different lab tests showed that the evaporation rate was lower than common aromatic and dearomatized diluents, likely resulting in less top-up necessary. These different parameters were benchmarked against an aromatic (20%) diluent, as well as aliphatic diluents produced from mineral oil.

Keywords: 4th Generation SX diluent, Copper, Synthetic Aliphatic, Iso-paraffins, Low Aromatic, Low Evaporation

Benefits of GTL G80 Mining Diluent in Copper SX for Low- and High-Grade Copper Ore

Miguel Rivera Torrente[1], Xiahoua Li[2], Clio Deferm[2], Peter Tom Jones[2], Koen Binnemans[2], Peter Haig[3]

1. Shell Global Solutions International B.V. – Amsterdam, The Netherlands, m.riveratorrente@shell.com
2. SOLVOMET R&I Centre, KU Leuven – Leuven, Belgium
3. SX Consultant – Brisbane, Australia

Definitions & cautionary note

Cautionary Note

The companies in which Shell plc directly and indirectly owns investments are separate legal entities. In this presentation "Shell", "Shell Group" and "Group" are sometimes used for convenience where references are made to Shell plc and its subsidiaries in general. Likewise, the words "we", "us" and "our" are also used to refer to Shell plc and its subsidiaries in general or to those who work for them. These terms are also used where no useful purpose is served by identifying the particular entity or entities. ''Subsidiaries'', "Shell subsidiaries" and "Shell companies" as used in this presentation refer to entities over which Shell plc either directly or indirectly has control. The term "joint venture", "joint operations", "joint arrangements", and "associates" may also be used to refer to a commercial arrangement in which Shell has a direct or indirect ownership interest with one or more parties. The term "Shell interest" is used for convenience to indicate the direct and/or indirect ownership interest held by Shell in an entity or unincorporated joint arrangement, after exclusion of all third-party interest.

Forward-Looking Statements

This presentation contains forward-looking statements (within the meaning of the U.S. Private Securities Litigation Reform Act of 1995) concerning the financial condition, results of operations and businesses of Shell. All statements other than statements of historical fact are, or may be deemed to be, forward-looking statements. Forward-looking statements are statements of future expectations that are based on management's current expectations and assumptions and involve known and unknown risks and uncertainties that could cause actual results, performance or events to differ materially from those expressed or implied in these statements. Forward-looking statements include, among other things, statements concerning the potential exposure of Shell to market risks and statements expressing management's expectations, beliefs, estimates, forecasts, projections and assumptions. These forward-looking statements are identified by their use of terms and phrases such as "aim"; "ambition"; "anticipate"; ''believe''; "commit"; "commitment"; ''could''; ''estimate''; ''expect''; "goals"; ''intend''; ''may''; "milestones"; ''objectives''; ''outlook''; "plan"; ''probably''; "project"; ''risks''; "schedule"; ''seek''; ''should''; "target"; ''will''; "would" and similar terms and phrases. There are a number of factors that could affect the future operations of Shell and could cause those results to differ materially from those expressed in the forward-looking statements included in this presentation, including (without limitation): (a) price fluctuations in crude oil and natural gas; (b) changes in demand for Shell's products; (c) currency fluctuations; (d) drilling and production results; (e) reserves estimates; (f) loss of market share and industry competition; (g) environmental and physical risks; (h) risks associated with the identification of suitable potential acquisition properties and targets, and successful negotiation and completion of such transactions; (i) the risk of doing business in developing countries and countries subject to international sanctions; (j) legislative, judicial, fiscal and regulatory developments including regulatory measures addressing climate change; (k) economic and financial market conditions in various countries and regions; (l) political risks, including the risks of expropriation and renegotiation of the terms of contracts with governmental entities, delays or advancements in the approval of projects and delays in the reimbursement for shared costs; (m) risks associated with the impact of pandemics, such as the COVID-19 (coronavirus) outbreak, regional conflicts, such as the Russia-Ukraine war, and a significant cybersecurity breach; and (n) changes in trading conditions. No assurance is provided that future dividend payments will match or exceed previous dividend payments. All forward-looking statements contained in this presentation are expressly qualified in their entirety by the cautionary statements contained or referred to in this section. Readers should not place undue reliance on forward-looking statements. Additional risk factors that may affect future results are contained in Shell plc's Form 20-F for the year ended December 31, 2023 (available at www.shell.com/investors/news-and-filings/sec-filings.html and www.sec.gov). These risk factors also expressly qualify all forward-looking statements contained in this presentation and should be considered by the reader. Each forward-looking statement speaks only as of the date of this presentation, **28th May 2024**. Neither Shell plc nor any of its subsidiaries undertake any obligation to publicly update or revise any forward-looking statement as a result of new information, future events or other information. In light of these risks, results could differ materially from those stated, implied or inferred from the forward-looking statements contained in this presentation.

Shell's Net Carbon Intensity

Also, in this presentation we may refer to Shell's "Net Carbon Intensity" (NCI), which includes Shell's carbon emissions from the production of our energy products, our suppliers' carbon emissions in supplying energy for that production and our customers' carbon emissions associated with their use of the energy products we sell. Shell's NCI also includes the emissions associated with the production and use of energy products produced by others which Shell purchases for resale. Shell only controls its own emissions. The use of the terms Shell's "Net Carbon Intensity" or NCI are for convenience only and not intended to suggest these emissions are those of Shell plc or its subsidiaries.

Shell's net-zero emissions target

Shell's operating plan, outlook and budgets are forecasted for a ten-year period and are updated every year. They reflect the current economic environment and what we can reasonably expect to see over the next ten years. Accordingly, they reflect our Scope 1, Scope 2 and NCI targets over the next ten years. However, Shell's operating plans cannot reflect our 2050 net-zero emissions target, as this target is currently outside our planning period. In the future, as society moves towards net-zero emissions, we expect Shell's operating plans to reflect this movement. However, if society is not net zero in 2050, as of today, there would be significant risk that Shell may not meet this target.

Forward-Looking non-GAAP measures

This presentation may contain certain forward-looking non-GAAP measures such as **[cash capital expenditure]** and **[divestments]**. We are unable to provide a reconciliation of these forward-looking non-GAAP measures to the most comparable GAAP financial measures because certain information needed to reconcile those non-GAAP measures to the most comparable GAAP financial measures is dependent on future events some of which are outside the control of Shell, such as oil and gas prices, interest rates and exchange rates. Moreover, estimating such GAAP measures with the required precision necessary to provide a meaningful reconciliation is extremely difficult and could not be accomplished without unreasonable effort. Non-GAAP measures in respect of future periods which cannot be reconciled to the most comparable GAAP financial measure are calculated in a manner which is consistent with the accounting policies applied in Shell plc's consolidated financial statements.

The contents of websites referred to in this presentation do not form part of this presentation.

We may have used certain terms, such as resources, in this presentation that the United States Securities and Exchange Commission (SEC) strictly prohibits us from including in our filings with the SEC. Investors are urged to consider closely the disclosure in our Form 20-F, File No 1-32575, available on the SEC website www.sec.gov.

GTL Manufacturing

Best affordable synthetic available

The GTL process converts natural gas into oil products

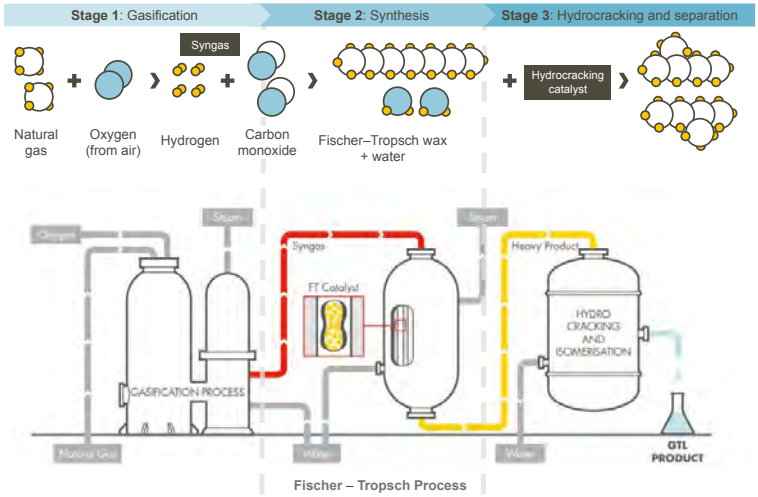

Unlike crude-oil derived products, GTL is synthetic, offering

- enhanced quality, consistency and stability
- increased control over the synthesising process – enabling, for example, more precise best ratios to be determined for desired applications
- **higher product purity**, resulting in lower emissions and better performance

Crude oil derived solvents

Normal-paraffins | **Iso-paraffins** | **Cyclo-paraffins** (naphthenes) | **Aromatics**

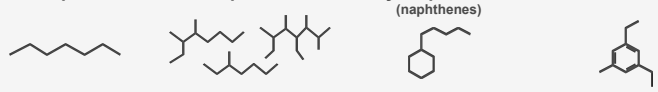

Synthetic iso-paraffins

Shell GTL solvents

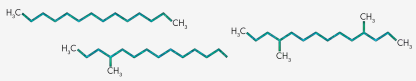

BI = Low

BI = Branching index (# branches / # all C atoms)

Conventional iso-paraffins
(Alkylates – Shellsol T / ShellSol TD)

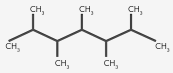

BI = High

1–2% cyclo-paraffins

Why use Shell GTL?

Large product portfolio and reliable global supply chain

- Meeting your requirements through constant innovation and a wide range of performance fluids
- Over 3500 GTL patents

Property	G70	G80	G85	G100
Density, kg/m^3	777	767	778	786
Distillation: Initial point, °C	177	200	198	237
Distillation: Dry point, °C	345	260	343	343
Flash point, °C	68	84	86	104
Aniline point, °C	95	87	95	98
Viscosity at 40°C , cSt	2.6	1.8	2.9	3.5
Aromatics, %	**0.02**	**0.03**	**0.02**	**0.02**

Global network of regional hubs for GTL solvents and fluids

Large distributor network with **strong** supply chain experience to get the product to your where and when you need it

Instant support through a strong customer service coverage globally

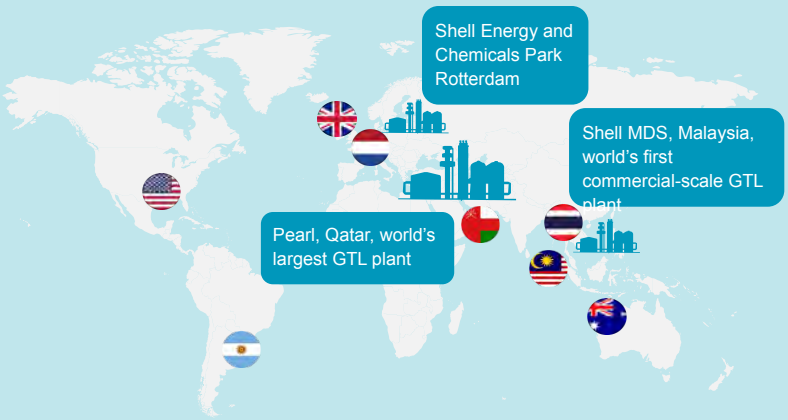

Shell GTL Solvents and Fluids in metal extraction

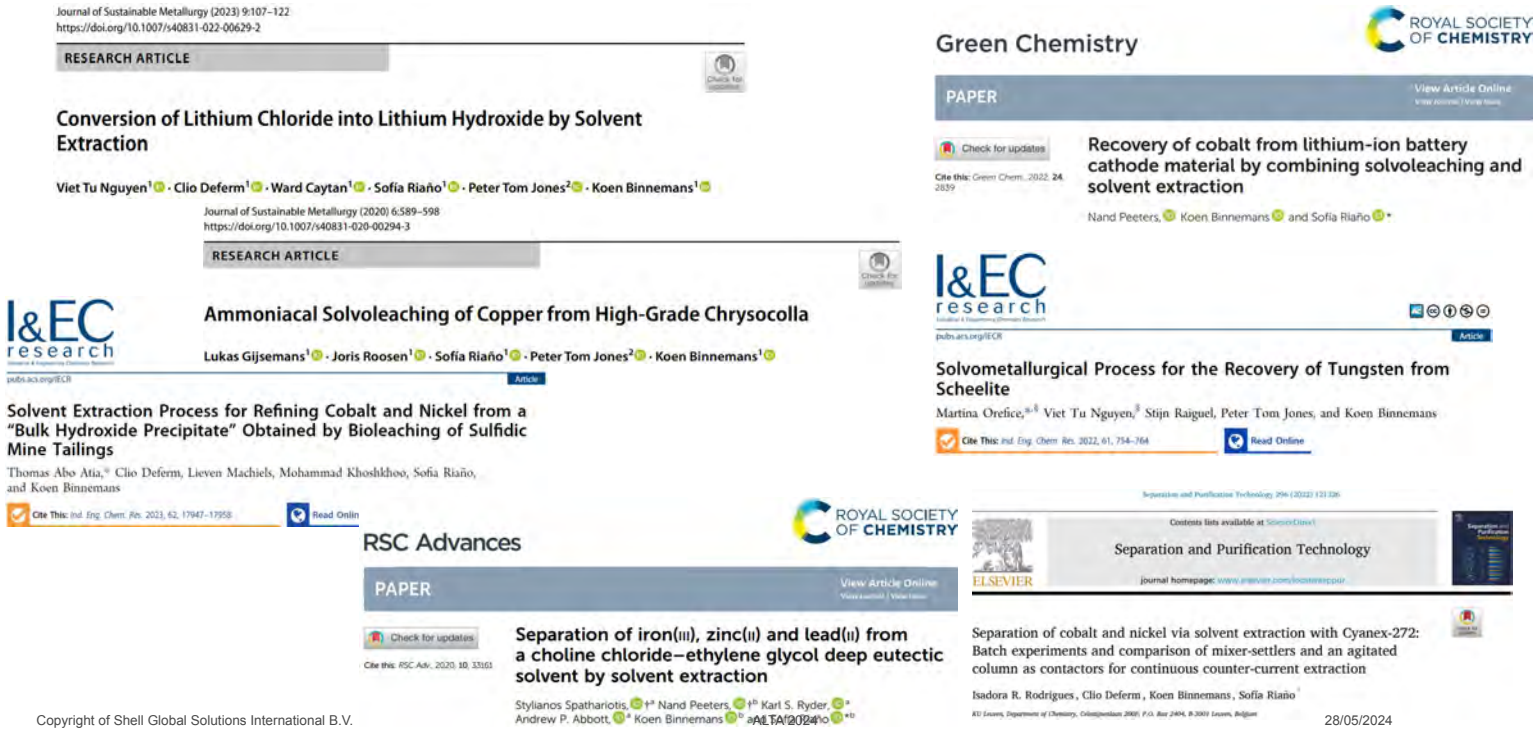

Shell GTL G80 vs competing diluents

Property	Method	Shell GTL Fluid G80	21% Aromatic Diluent	0% Aromatic Diluent
Initial Boiling Point, °C	ASTM D86	205	195	192
Final Boiling Point, °C	ASTM D86	265	245	250
Aromatics, %wt	GC	<0.04	19	0.8
Cycloparaffins, %wt	GC	<1	24	46
Flash point, °C	ASTM D93	84	75	74
Viscosity at 25°C, mm^2/s	ASTM D445	2.4	1.9	2.4
Color, Saybolt	ASTM D156	+30	+30	+30
Density at 15 °C, kg/l	ASTM D4052	0.767	0.811	0.808
Sulphur, ppm	ASTM 5453	<1	<5	<1
Vapour pressure at 20 °C, kPa	Calculated	0.01	0.013	0.016

Shell GTL G80 vs competing diluents

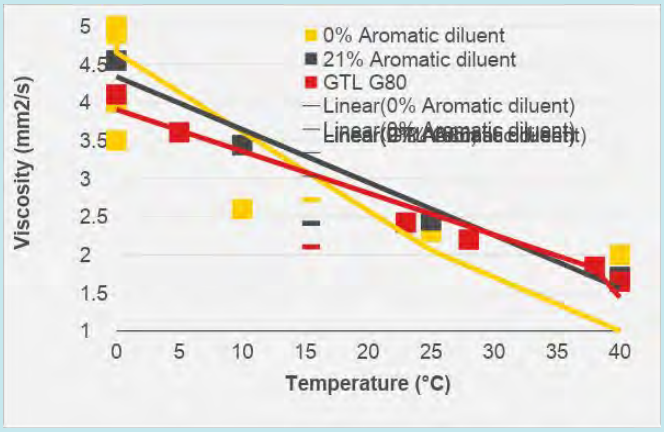

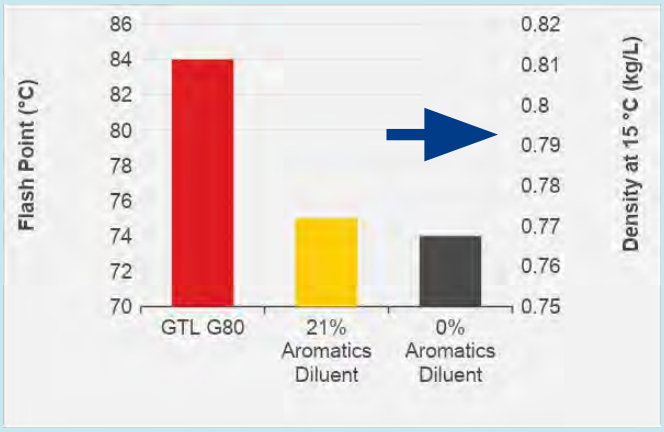

- **Viscosity below 4.0 mm²/s in the 0 to 40 °C range**
- **Combined with flash point above 83 °C and lower density**

Density and/or specific gravity measured following the ASTM D4052 method.
Viscosity measured according to the ASTM D445 method.
Flash point determined by the ASTM D93 method.

Accelerating solvent extraction with Shell GTL G80

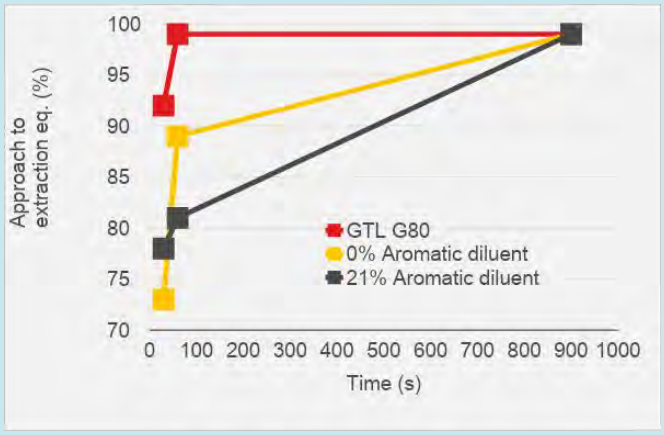

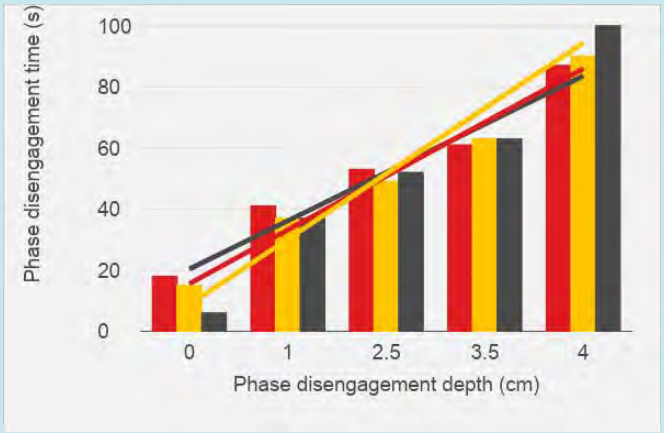

- Up to **20% faster extraction** kinetics**

Extraction tests of synthetic pregnant leach solution (PLS) with:
6.0 g/L Cu and 3.0 g/L Fe, pH = 2.0 (H_2SO_4).
10%vol of LIX® 984N[1] extractant,
O/A = 1, T = 25 °C

[1]LIX® is a brand of an extractant produced by BASF. [2]ACORGA® is a brand of an extractant produced by Syensqo.
Measured by or on behalf of Shell Global Solutions International B. V.
**Depending on extractant, ore and operational parameters.

Accelerating solvent extraction with Shell GTL G80

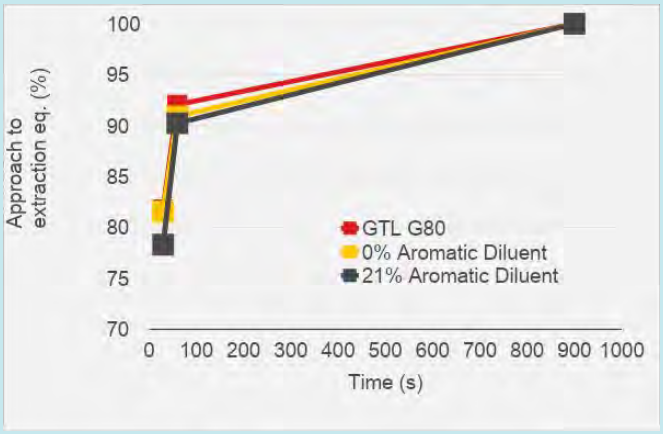

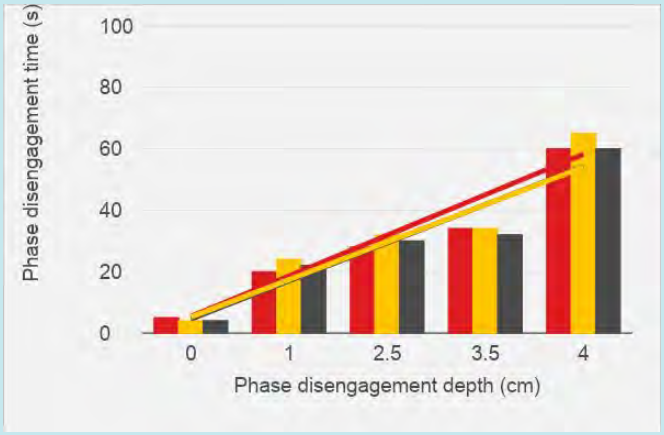

- **Faster stripping** kinetics**
- **Low phase disengagement time**

Extraction tests of synthetic pregnant leach solution (PLS) with:
6.0 g/L Cu and 3.0 g/L Fe, pH = 2.0 (H_2SO_4).
10%vol of ACORGA® M5640[2] extractant,
O/A = 1, T = 25 °C

[1]LIX® is a brand of an extractant produced by BASF. [2]ACORGA® is a brand of an extractant produced by Syensqo.
Measured by or on behalf of Shell Global Solutions International B. V.
**Depending on extractant, ore and operational parameters.

Accelerating solvent extraction with Shell GTL G80

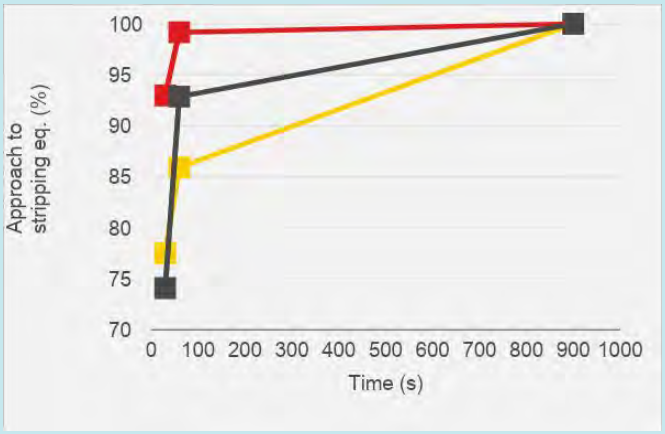

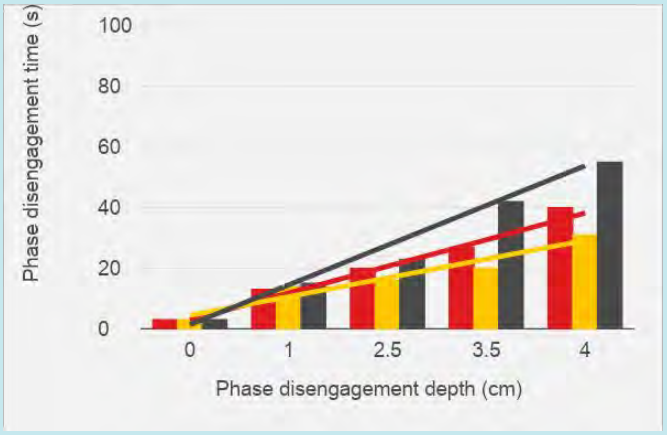

- **Faster stripping** kinetics**
- **Low phase disengagement time**

Stripping tests with simulated spent electrolyte and 10%vol LIX® 984N[1] :
35.0 g/L Cu and 160.0 g/L (H_2SO_4).
O/A = 1, T = 25 °C

[1]LIX® is a brand of an extractant produced by BASF. [2]ACORGA® is a brand of an extractant produced by Syensqo.
Measured by or on behalf of Shell Global Solutions International B. V.
**Depending on extractant, ore and operational parameters.

Accelerating solvent extraction with Shell GTL G80

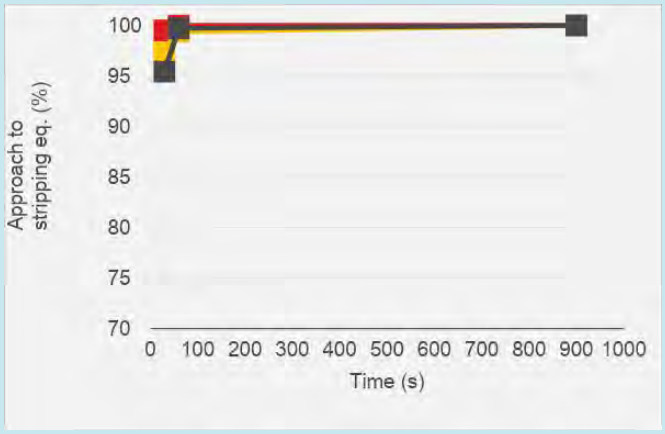

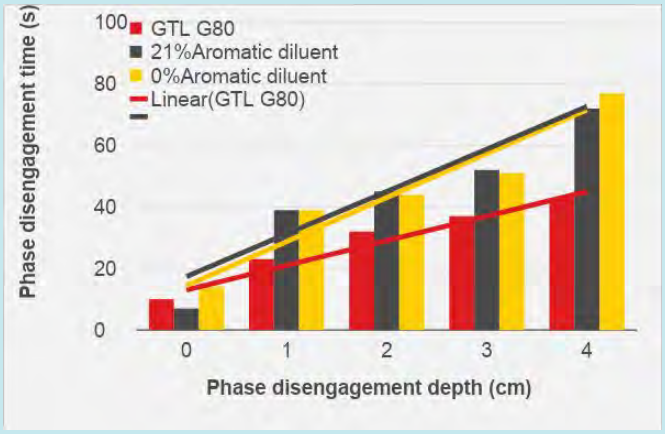

- **Faster stripping** kinetics**
- **Low phase disengagement time**

Stripping tests with simulated spent electrolyte and 10%vol ACORGA® M5640[2] :
30.0 g/L Cu and 150.0 g/L (H_2SO_4).
O/A = 1, T = 25 °C

[1]LIX® is a brand of an extractant produced by BASF. [2]ACORGA® is a brand of an extractant produced by Syensqo.
Measured by or on behalf of Shell Global Solutions International B. V.
**Depending on extractant, ore and operational parameters.

Extraction efficiency

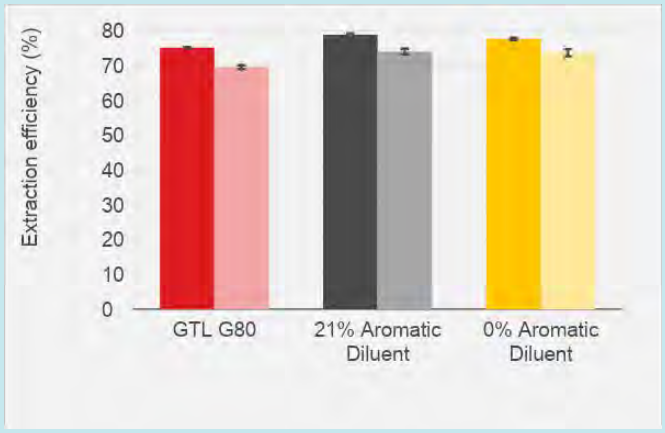

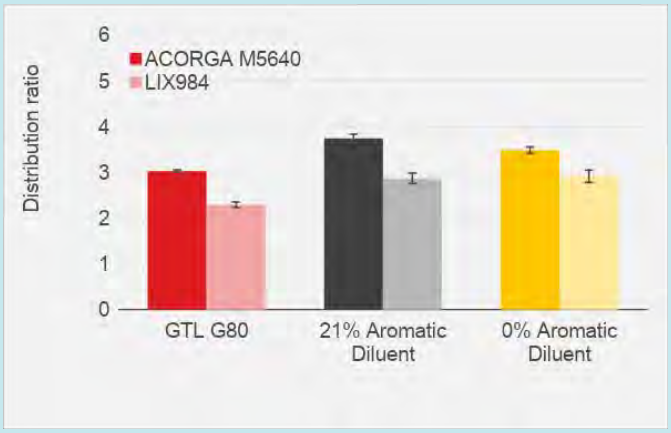

Extraction of synthetic pregnant leach solution (PLS) with:
6.0 g/L Cu and 3.0 g/L Fe, pH = 2.0 (H_2SO_4).
10%vol of leading oxime type extractant,
O/A = 1, T = 25 °C

$$\text{Ext eff}(\%) = \frac{Cu_{org}(900s)}{Cu_{org}(900s) + Cu_{aq}(900s)} \qquad D = \frac{Cu_{org}(900s)}{Cu_{aq}(900s)}$$

[1]LIX® is a brand of an extractant produced by BASF. [2]ACORGA® is a brand of an extractant produced by Syensqo.
Measured by or on behalf of Shell Global Solutions International B. V.
**Depending on extractant, ore and operational parameters.

Performance with both low- and high-grade ores

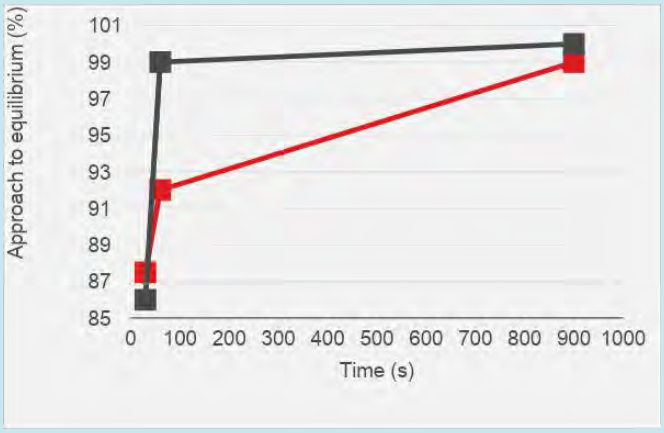

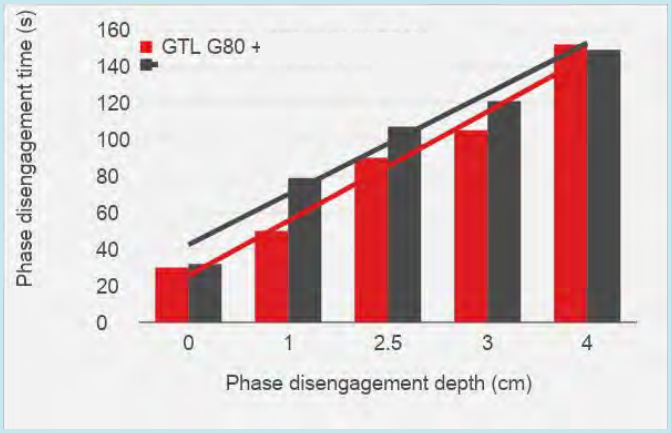

- **Low phase disengagement proven across SX reagents and Cu concentrations in PLS**

Stripping tests with simulated spent electrolyte and 35%vol LIX® 984N[1] :
35.0 g/L Cu and 160.0 g/L (H_2SO_4).
O/A = 1, T = 25 °C

[1]LIX® is a brand of an extractant produced by BASF. [2]ACORGA® is a brand of an extractant produced by Syensqo.
Measured by or on behalf of Shell Global Solutions International B. V.
**Depending on extractant, ore and operational parameters.

Performance with both low- and high-grade ores

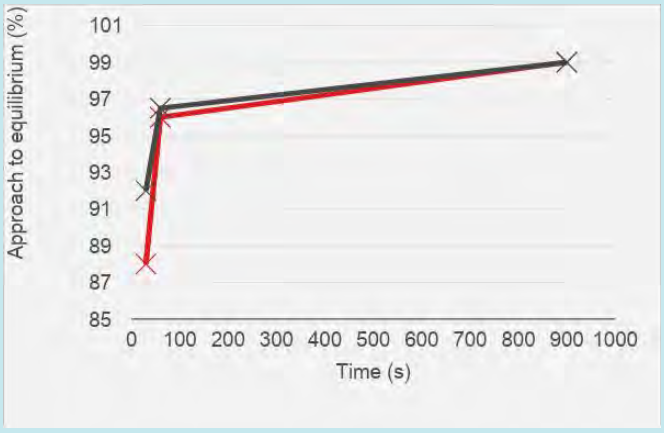

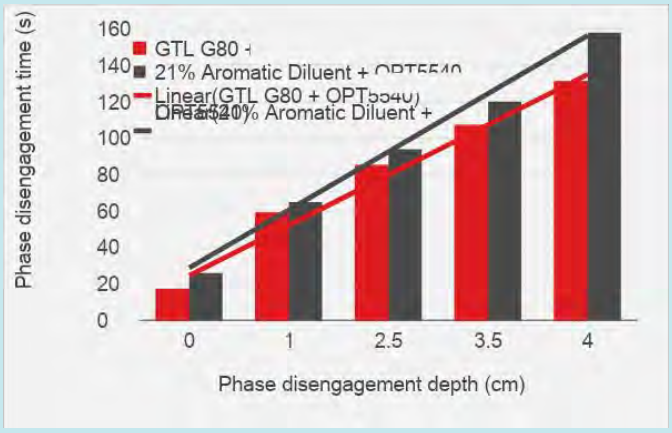

- **Low phase disengagement proven across SX reagents and Cu concentrations in PLS**

Stripping tests with simulated spent electrolyte and 35%vol ACORGA® OPT5540[2] :
30.0 g/L Cu and 150.0 g/L (H_2SO_4).
O/A = 1, T = 25 °C

[1]LIX® is a brand of an extractant produced by BASF. [2]ACORGA® is a brand of an extractant produced by Syensqo.
Measured by or on behalf of Shell Global Solutions International B. V.
**Depending on extractant, ore and operational parameters.

Copyright of Shell Global Solutions International B.V.
ALTA 2024
28/05/2024

Copper uptake after multiple contacts

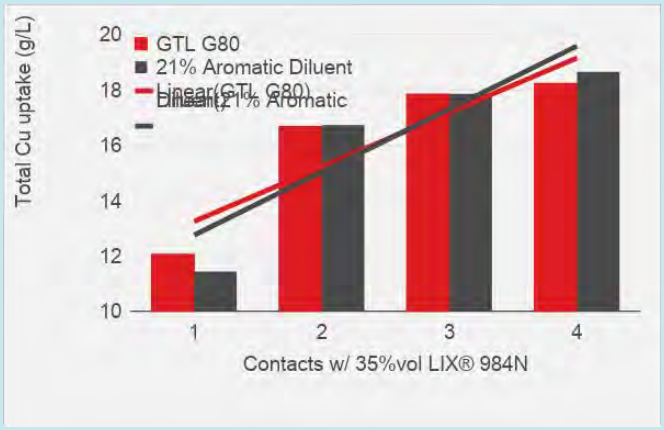

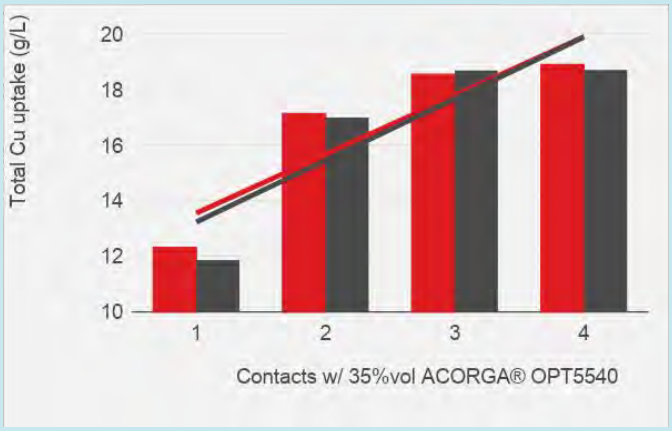

[A]Copper uptake of the organic phase measured after 900 seconds per contact by ICP-OES.
[B]Extraction tests of synthetic pregnant leach solution (PLS) with:
18.0 g/L Cu and 2.0 g/L Fe, pH = 2.0 (H_2SO_4).
35%vol of leading oxime extractant,
O/A = 1, T = 25 °C

[1]LIX® is a brand of an extractant produced by BASF. [2]ACORGA® is a brand of an extractant produced by Syensqo.
Measured by or on behalf of Shell Global Solutions International B. V.
**Depending on extractant, ore and operational parameters.

Diluent Losses in SX operations

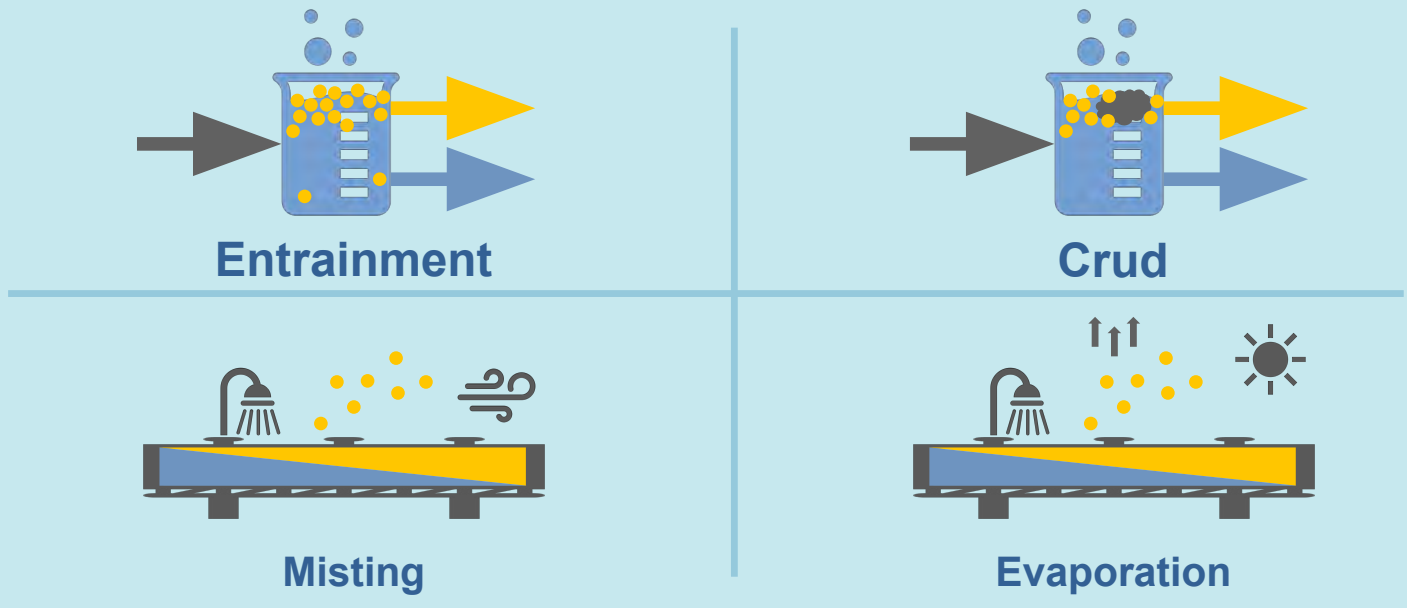

Performance with both low- and high-grade ores

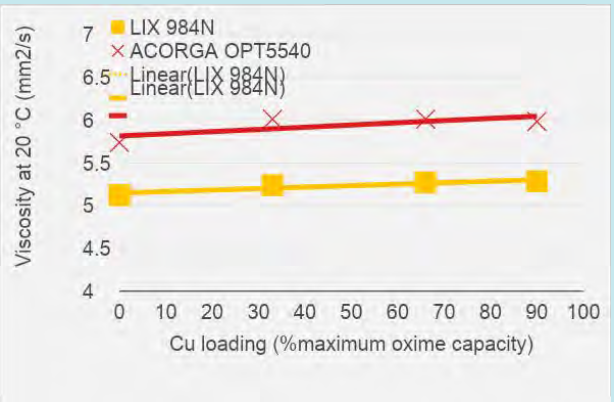

Viscosity performance at 35%vol extractant concentrations

Both at low- and high-grade copper loadings

[1]LIX® is a brand of an extractant produced by BASF. [2]ACORGA® is a brand of an extractant produced by Syensqo. Measured by or on behalf of Shell Global Solutions International B. V.
Viscosity determined as described in the ASTM D445 method at 20 °C with Ubbelohde viscometers.
Accelerated evaporation tests conducted in rotatory evaporator with reduced pressure under identical conditions.

Improved safety and reduced evaporation

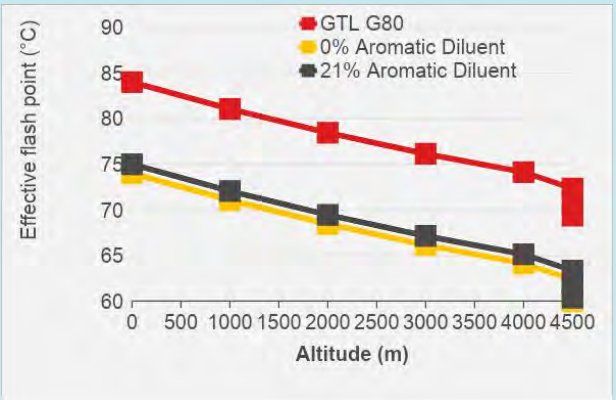

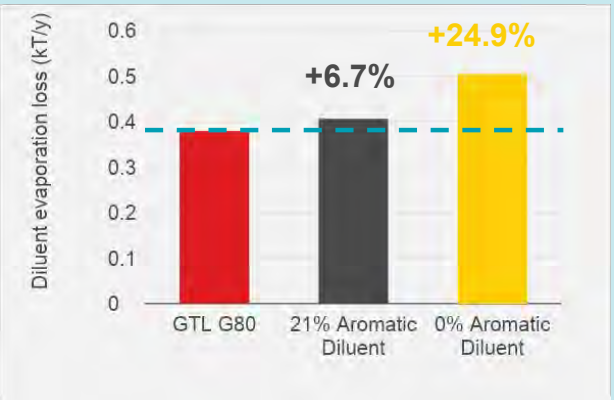

Better worker safety thanks to reduced risk of autoignition

Reduced evaporation leads to cost savings in diluent and extractant

Flash point determined according to ASTM D93. Model conditions of a selected location in the DRC (21 °C, 10 km/h wind, 25x25 m^2 mixer-settlers)
Flash point calculated as per: Yang et al. "Investigation on the dependence of flash point of diesel on the reduced pressure at high altitudes", *Fuel, (2016) 181, 836–842*
Evaporation as per: Mackay, D., Matsugu, R. S., "Evaporation rates of liquid hydrocarbon spills on land and water", *Canad. J. Chem. Eng. (1973), 51, 4, 434-439*

Excellent biodegradability

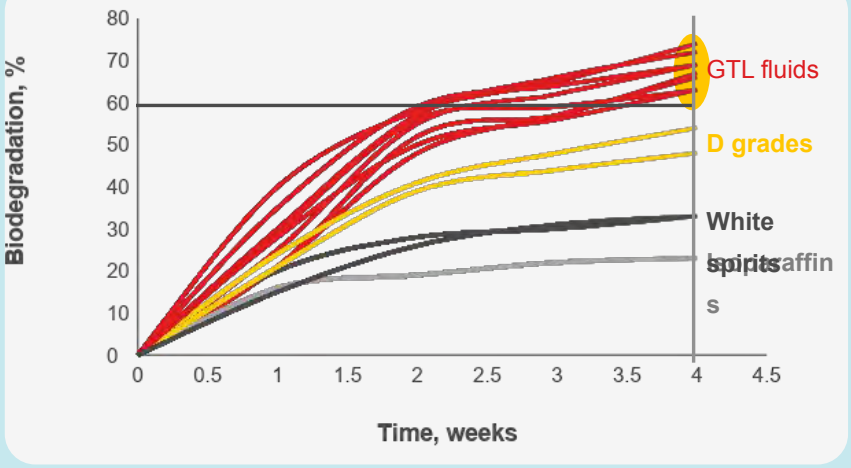

Reference: Christopher Hughes, Graham Whale (Shell), Chris Mead (Harlan Laboratories Ltd, Shardlow, UK), "Investigation into the biodegradability of hydrocarbons"

All Shell GTL Performance Fluids are "Readily biodegradable" according to OECD 301F (>60% biodegradation after 28 days) and have very low eco-toxicities.

Low toxicity and environmental impact

Property	Method	Shell GTL Fluid G80	21% Aromatic Diluent	0% Aromatic Diluent
GHS Labeling	(EC) No 1272/2008			
Toxicity to Aquatic Life		Non-toxic	Category 2, Toxic to aquatic life with long lasting effects	Non-toxic
Biodegradability	OECD 301F (in 28 days)	Readily biodegradable (>60%)	Biodegradable (<60%)	Readily biodegradable (>60%)
Components		C9-C16, n-alkanes, isoalkanes, < 2% aromatics	C12-C14, n-alkanes, isoalkanes, cyclics, aromatics (2-25%)	C12-C14, n-alkanes, isoalkanes, < 2% aromatics

Why use Shell GTL as a mining diluent?

Diluents play a critical role in the extraction of **copper, nickel, cobalt, zinc** and other metals

Environmental benefits

- Better anaerobic **biodegradability: >60%** degradation after 28 days*
- **Low aromatics** and polyaromatic hydrocarbons (PAH)
- **Non-ecotoxic** and non-phytotoxic
- High purity → **ensured quality** and stability

Health and safety benefits

- **Better worker safety**
- Low O_3 potential
- **Low misting** for less inhalation
- **Extremely low odour** and toxicity
- Non-skin sensitising and non-eye irritant

Technical benefits

- Carbon profile leads **to an optimal evaporation** profile with **low viscosity**
- Low density → **fast phase disengagement**
- Proven **Cu-Fe selectivity** and excellent stripping performance
- **High stability against oxidation** compared to aromatic diluents

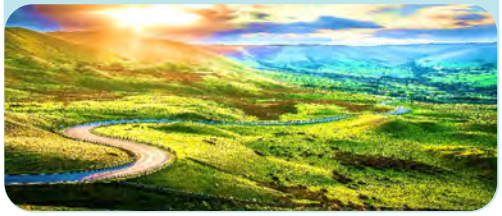

**According to OECD 301F tests*

Shell GTL G80 helping customers succeed

- Over 20,000 tons of product sold of G80 mining diluent in South Africa and the Copperbelt
- Trials planned in Arizona at one of the largest mining groups in the Americas
- Trials planned with the biggest players in Chile and Peru

Shell GTL G80 Diluent

- **Performance**
- **Supply**
- **Customer services**
- **Health and safety**
- **Environment**
- **Cost**

For more information, please contact your local Shell representative or technical support team at www.shell.com

INVESTIGATING THE IMPACT OF HIGH TEMPERATURE AGITATION LEACHING IN THE RATE OF OXIME DEGRADATION

By

Coralys Torres López, Andrew Nisbett, [2]Yi, Zhou

BASF Corporation, United States of America
[2]BASF Canada Inc, Canada

Presenter and Corresponding Author

Andrew Nisbett
andy.nisbett@basf.com

ABSTRACT

Agitation tank leaching is a widely used method in the African Copper Belt to facilitate the rapid dissolution of copper from mid to high grade copper ores. As ore grade has begun to decline and the relative abundance of secondary sulfide mineralization is increasing, plants have implemented or are considering treating calcined ore from a roaster to increase or supplement copper production. This process would cause an increase in the temperature of the pregnant leach solution (PLS) produced. The extraction step occurs in relatively mild acid conditions of 1-10g/L sulfuric acid, which is significantly lower than the 150-200g/L sulfuric acid level that copper solvent extraction (SX) reagents are contacted with in the stripping stage of most processes. However, the higher temperature range of 40-60°C is thought to be linked to an observable increase in the acid-catalyzed hydrolysis rate of the oxime reagents commonly used to selectively extract the copper from the PLS after agitation leaching.

This study shows the results of an experiment conducted to investigate the rate of hydrolysis observed from sustained contact with the PLS produced from these leaching conditions and temperatures. The results will be contrasted for the most common types of extractants currently used in the market and discuss the potential implications of those results.

Keywords: hydrolysis, agitation leaching, degradation

INTRODUCTION

African operations, particularly those in the African Copper Belt, are known for high ore grades and because of this the leaching of these ore bodies is typically done in agitation tanks.[1] Due to the mild temperatures and exothermic acidic leaching conditions, agitation tank leaching systems usually operate with temperatures between 35°C to 45°C, in which almost all the copper is leached in a matter of hours. Ultimately, resulting in a higher-temperature pregnant leach solution (PLS) going into the solvent extraction (SX) operation. Although the effect of higher temperatures in the SX circuit have positive effects on kinetics and copper transfer, the effect on diluent evaporation and degradation of the extractant are quite noticeable and negative. High temperatures lead to a faster loss by degradation of the extractant and as consequence the buildup of degradation products that negatively affect the physical operation of a plant by increasing entrainments.

As ore bodies around the world transition from easily leachable minerals to more refractory minerals, the processing route is likely to become more aggressive. Several operations in the Copperbelt are considering incorporating roasting or pressure leaching of sulfides into the overall flowsheet. The net effect of this will be an increase in the temperature of the PLS going to SX. Outside of the Copperbelt, several leaching technologies for primary sulfides are being proposed for heap and dump leach operations that will incorporate novel bacteria operating at higher temperatures[1]. Again, this will likely result in significantly higher PLS temperatures which will have to be accommodated in the SX plant.

In an SX operation, stripping stages typically have a much higher acid concentration and are run at higher temperatures than the extract stages. As expected, degradation of the oxime is higher in the strip stages than in extract. Questions have been posed by operators and technology developers as to how high a temperature can be tolerated in an SX plant with the commercially available extractants. Previous studies have investigated the effect of high temperature under stripping conditions and in this paper the effect of a higher temperature PLS was studied. Also, since there would be a need for extractants that can be more resistant to these aggressive conditions, BASF has developed a novel copper extractant that has greater stability at higher temperatures in addition to other beneficial properties like greater Cu/Fe selectivity and being nitration resistant.[2,3,4.] The degradation of this novel extractant and its blends with conventional oximes was also examined in this study.

OXIME DEGRADATION

Acid-catalyzed hydrolysis is usually the most common type of oxime degradation in SX plants. This degradation is favored because of the high concentration of acid in the circuit where the oximes are hydrolyzed to their respective aldehyde or ketone. The accumulation of these degradation products increases the viscosity of the organic phase, which in turns causes operational turmoil in terms of slower disengagement times and higher entertainment, ultimately increasing reagent consumption for the SX operation. The main factors that affect the rate of hydrolysis are impurities, polarity of the organic, amount of oxime on the interface, acid concentration and temperature.[2] The mechanism of the hydrolysis of oximes is illustrated in Figure 1.

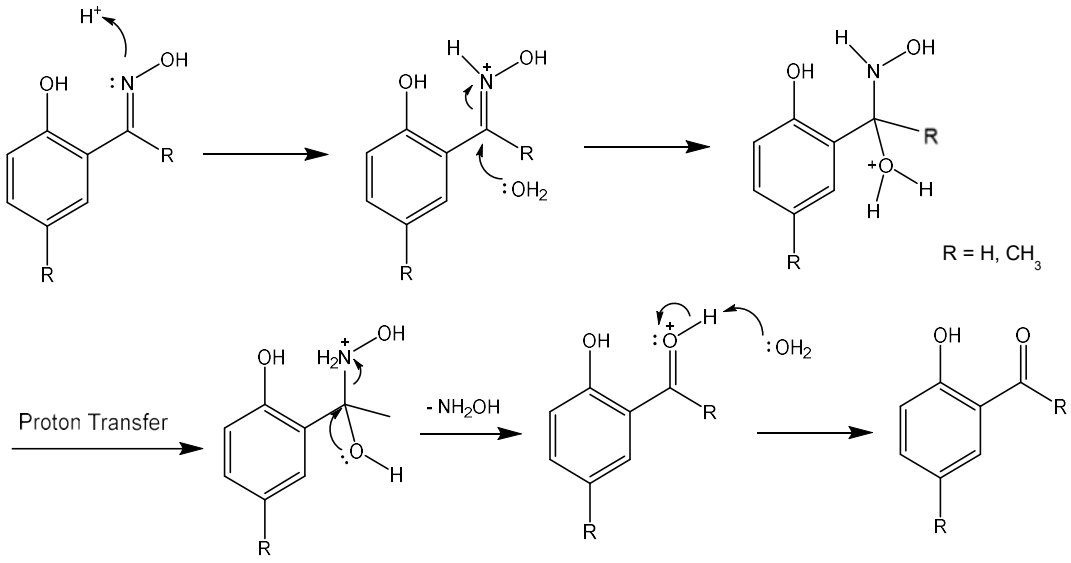

Figure 1. Acid-Catalyzed Hydrolysis of Oximes.

EXPERIMENTAL

Preparation of Aqueous Solution

A synthetic PLS containing 5g/L Cu^{2+}, 8g/L Fe^{3+}, 2g/L Fe^{2+}, and 5g/L H_2SO_4 was prepared by dissolving the required amounts of $CuSO_4 \cdot 5\ H_2O$, $Fe_2(SO_4)_3$, $FeSO_4$, and 97-98% H_2SO_4 in deionized water. The aqueous solution was prepared from reagent grade chemicals.

Preparation of Organic Solutions

Organic solutions targeting a max load of 8.4g/L Cu of LIX 860N-I, LIX 84-I, LIX 984N, LIX 10HS, LIX 2620HS, and LIX 0820HS, and a TXIB-modified aldoxime (found to be contaminated with a small amount of ketoxime) were prepared in SX-12. LIX 10HS is BASF's new-generation solvent extraction reagent, while the other two LIX HS reagents are blends of LIX 10HS and conventional oximes. These solutions were equilibrated with a standard strip solution containing 35g/L Cu^{2+} and 160g/L H_2SO_4. Then filtered through Whatman 1PS filter paper.

Procedure and Equipment

Degradation testing was performed by continuously stirring the organic extractant with the synthetic PLS. The test vessels used were three-necked 1L jacketed round bottom flasks, each connected in series to a recirculating water bath with a constant target temperature. An overhead mixer was connected via an airtight stopper to the flask and the stirring speed was maintained at 500 ± 25 RPM. Samples of the emulsion were taken so as to keep the aqueous to organic ratio constant at a 1:1 O/A. The organic and aqueous phases were separated and the organic fraction was max loaded with a standard extraction aqueous phase containing 6g/L Cu, 3g/L Fe and a pH of 2. The organic was also stripped with a 250g/L sulfuric acid solution. The max loaded sample was analyzed for Cu by Atomic Absorption Spectroscopy (AAS) and the stripped sample was analyzed for degradation and for oxime ratio by High Performance Liquid Chromatography (HPLC). Figure 2 shows the degradation testing setup.

Figure 2. Degradation Testing Setup.

TEST RESULTS

Degradation Tests

Degradation of oximes via acid-catalyzed hydrolysis is constantly happening within an operation. The concentration of the degraded oximes typically increases if the degradation rate is faster than the loss of organic via entrainment or removal. In this testing, organic was never removed other than the sample taken to quantify degradation. Therefore, buildup of the degraded products took place inside the test vessel. As plant processes are more dynamic and complex, the degradation rate seen in this study cannot be associated to a specific operation. Nonetheless, these laboratory simulations compared the relative rates of degradation between the different formulations tested and it can be reasoned that the relative trends could be seen in a plant.

Figure 3 shows the degree of hydrolysis of the reagents tested when contacted with the synthetic PLS at 50°C for 221 days. The most prone to degradation was the TXIB-modified aldoxime, followed by pure aldoxime, then blends containing aldoxime, then ketoxime and finally LIX 10HS. As expected, the aldoxime had a higher degradation rate than ketoxime. This is expected as the steric hindrance between the two functional groups is higher in the ketoxime because of the methyl group, making the ketoxime more resistant to the nucleophilic attack of water that leads to its degradation[2,6]. Blends that also contained a higher percent of aldoxime seemed to have a higher degradation rate than pure ketoxime and pure LIX 10HS. As the amount of aldoxime in the blend decreased, the more resistance the blend was to hydrolysis. Likewise, substituting a higher percent of the conventional oximes with LIX 10HS formulated blends that were more resistant to degradation, and with pure LIX 10HS being the most hydrolytically stable out of all the reagents tested.

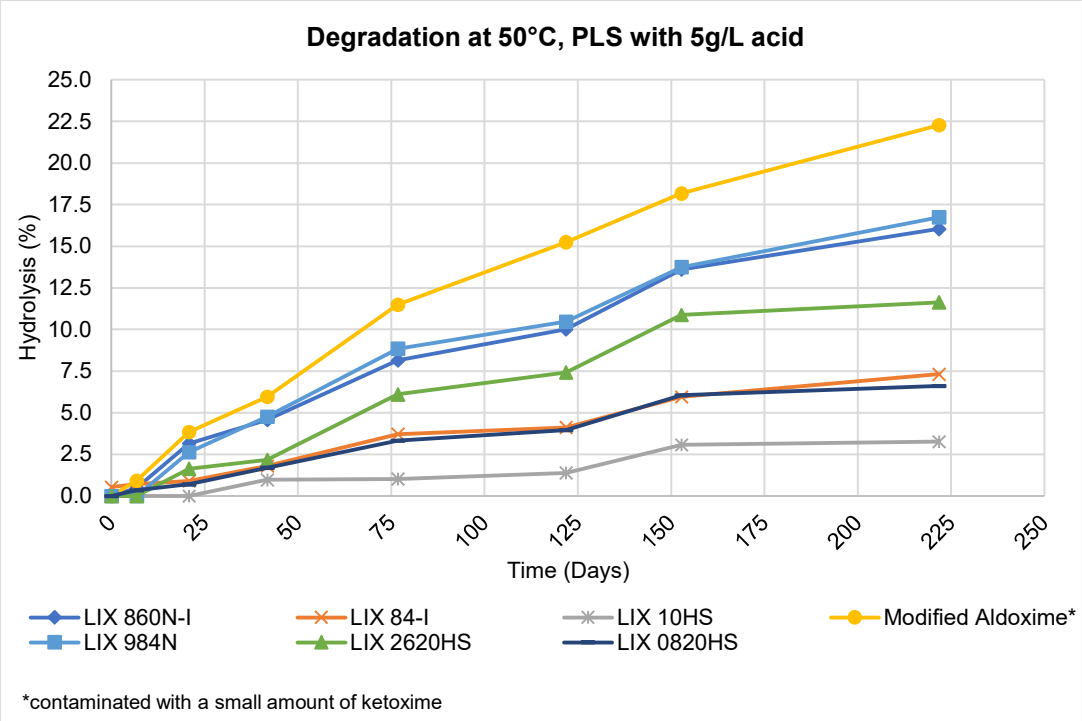

Figure 3. Hydrolysis Percent of Reagents Tested at 50°C.

The copper max load of the organic solutions correlates with the degradation data and can be used as another means to track degradation. The strength of the copper extractant decreases when the oxime functionality degrades as degradation products do not load copper. Hence, there is less oxime to extract copper from the PLS and a decrease in max load would be expected as shown in Figure 4. The max load trend shows an inverse relationship with the degradation data in the graph above.

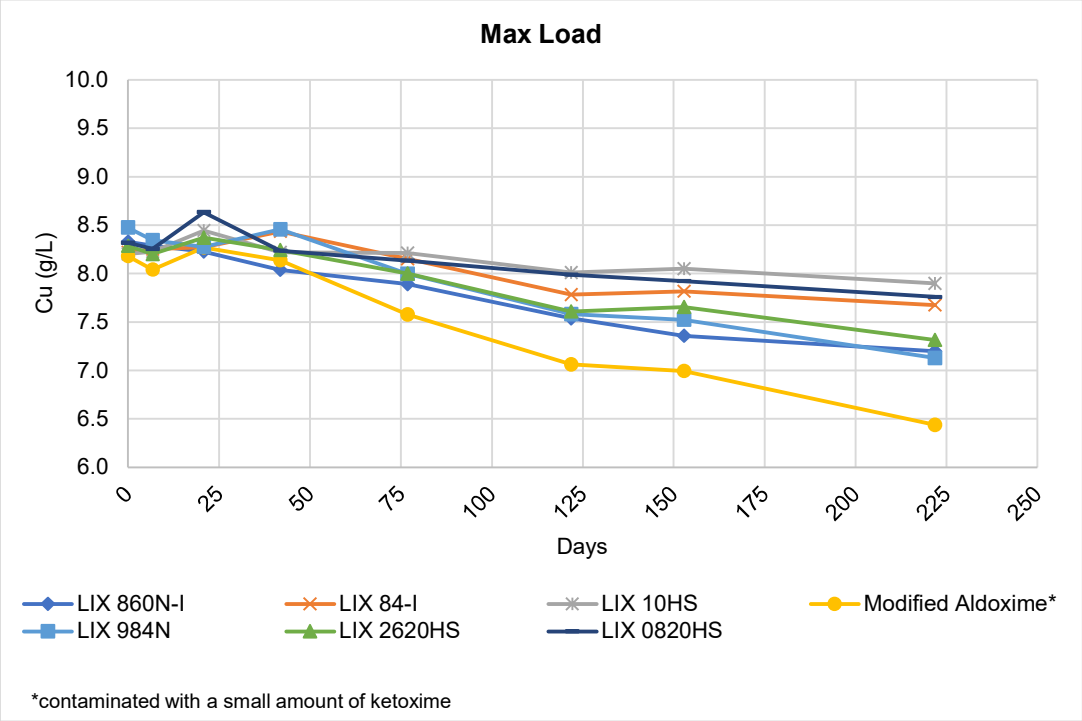

Figure 4. Max Load of reagents tested.

Degradation testing was also performed at an even higher temperature of 60°C. As already discussed, increasing the temperature accelerates the degradation of oximes. Therefore, in this study the effect of a 10°C increase in temperature was tested. These tests are still running at the time of paper submission, but preliminary data shows the same trend of degradation with the TXIB-modified aldoxime degrading the fastest, followed by pure aldoxime, then blends containing aldoxime, then ketoxime and finally LIX 10HS.

Figure 5 shows the degree of hydrolysis of the reagents tested when contacted with the synthetic PLS at 60°C for 57 days. By just increasing 10°C, the rate of acceleration is roughly twice as fast for the oximes tested. For example, at 60°C the degree of hydrolysis for the modified aldoxime at 57 days was calculated at 16%, while at 50°C temperatures at 57 days was calculated at ~8%. This shows that if an operation increases the temperature even by 10°C, a drastic negative effect on the health of the organic will most likely occur. All the negative effects of entrainment and evaporation, as well as the increase in reagent consumption would occur now at a more rapid pace.

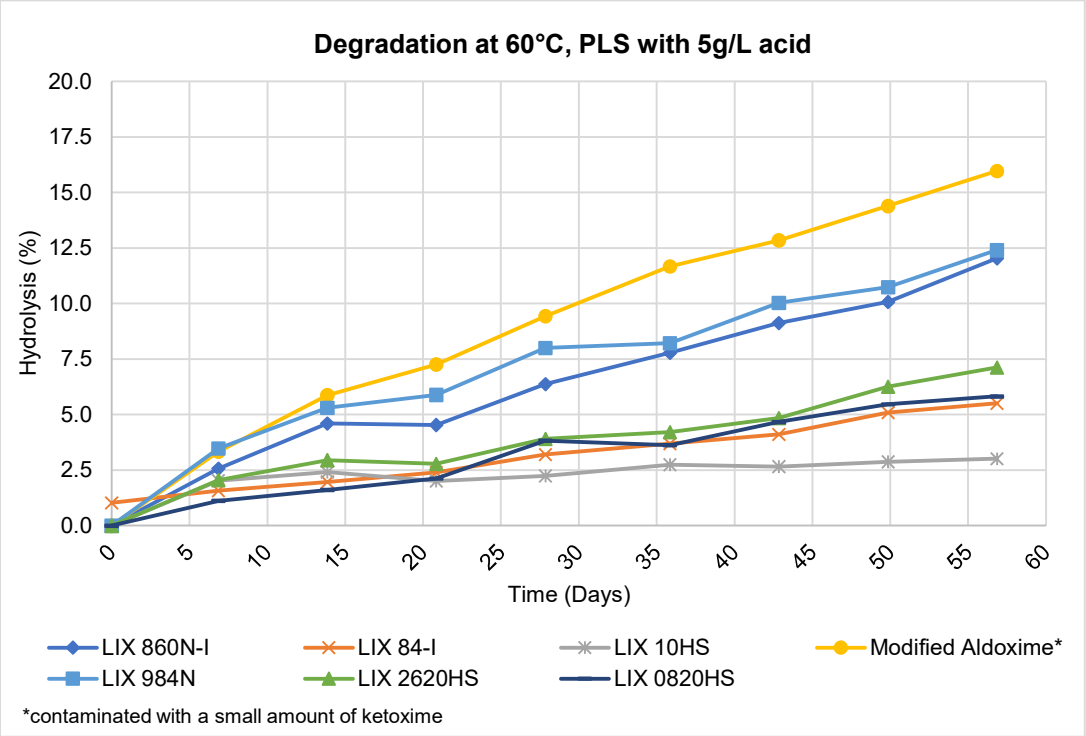

Figure 5. Hydrolysis Percent of Reagents Tested at 60°C.

Previous accelerated degradation testing has been done using a synthetic stripping stage electrolyte with a 180g/L acid concentration at 45°C.[2] It is known that degradation of oximes occurs faster in the stripping stages compared to extract stages due to the harsher conditions in stripping. Figure 6 illustrates the rate of hydrolysis for the modified aldoxime, pure conventional oximes and BASF high temperature extractants. As seen, the trend is similar to the ones found in the experiment for this paper, with the aldoximes degrading the fastest, followed by ketoxime and lastly the novel BASF high temperature reagents for solvent extraction.

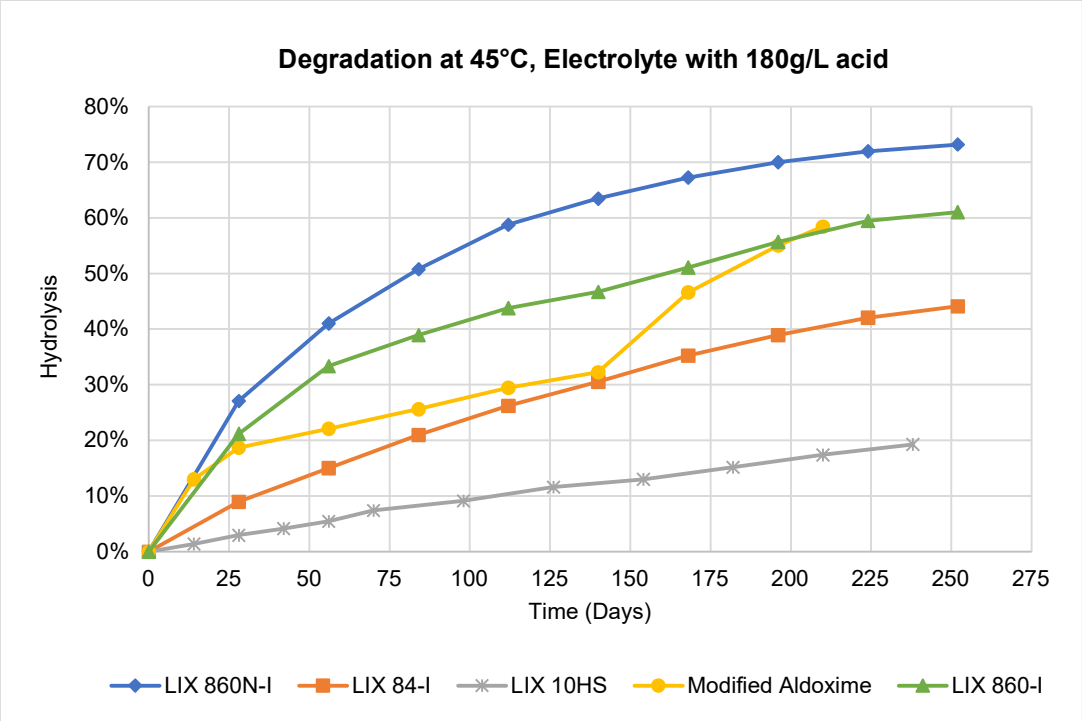

Figure 6. Degradation of different extractants at 45°C when contacted with a 180g/L H_2SO_4 synthetic electrolyte.[1]

CONCLUSIONS

Degradation by acid-catalyzed hydrolysis is inherent to a copper solvent extraction operation and the degree as to which it is controlled can have negative effects on the plant. As the industry considers more aggressive leaching and processing techniques that will result in higher temperatures in both extract and strip, the impact of accelerated degradation needs to also be considered. This is difficult to quantify in a static laboratory setting since an operating SX plant is a dynamic process and an equilibrium is always reached between the rate of degradation, the concentration of degraded products in the organic phase and organic make-up/losses. However, the test work results have shown that at 50°C degradation rates are high and are amplified significantly further with a 10°C increase to 60°C. BASF's novel extraction reagent LIX 10HS (and blends) have proven to provide higher resistance to degradation, even at higher temperatures, than the conventional ketoxime and aldoxime reagents.

Although not part of this study, the effect of higher temperature on the diluent component of the organic phase would also have to be considered and investigated.

ACKNOWLEDGMENTS

The authors would like to thank many of the colleagues in the BASF Tucson laboratory for their contributions in this project of collecting and analyzing samples, helping in the project setup and with intellectual support.

REFERENCES

1. Tinkler, O.S and Sole, K.C, 2023. Copper Solvent Extraction on the African Copperbelt : From historic origins to world-leading status. Journal of the Southern African Institute of Mining and Metallurgy, Volume 123, no 7, 349-356.

2. Bender, J. Emmerich, N. Nisbett, A., 2013. Development of a new generation of copper solvent extraction reagents. Proceedings Copper 2013.

3. Taute, J.J, Bwando, P., Chisakuta, G., Mitshabu, G., Nisbett, A., 2015. Copper Solvent Extraction: Status, Operating Practices and Challenges in the African Copper Belt. Copper Cobalt Africa, 8th Southern African Base Metals Conference, 281-290.

4. Bender, J., Yanez, H., Copp, R., McDonald, T., 2018. New generation of highly selective and degradation resistant reagents for copper solvent extraction. Hydroprocess 2018 10th International Seminar on Process Hydrometallurgy.

5. Taute, J.J., Archer, S.J. 2018. Techno-Economic Evaluation of ABSF's New High-Temperature Solvent-Extraction Reagent. Copper Cobalt Africa, 8th Southern African Base Metals Conference, 291-302.

6. Hurtado-Guzmán, C., Menacho, J. M. 2003. Oxime degradation chemistry in solvent extraction plants. Copper 2003-Cobre2003, Volume VI Hydrometallurgy of Copper (Book 2), 719-734.

MASS TRANSFER INTENSIFICATION IMPLEMENTING THE USE OF STATIC MIXERS IN Co/Ni SOLVENT EXTRACTION

Johan W. Bezuidenhout, [2]Burgert B. Hattingh and [2]Derik J. van der Westhuizen

School of Chemical and Mineral Engineering, North-West University, South Africa
[2]Chemical Resource Beneficiation, North-West University, South Africa

Presenter and Corresponding Author

Derik J. van der Westhuizen
derik.vanderwesthuizen@nwu.ac.za

ABSTRACT

Residence time plays a crucial role in any solvent extraction process. The mass transfer rate is significantly increased by reducing the oil droplet size of an oil-in-water dispersion. Therefore, residence time reduction through increased mass transfer rates is vital for optimising these processes. Recently, there has been a renewed interest in using static mixers to reduce the droplet size of these dispersions. Several studies have documented the efficacy of static mixers in reducing droplet size in these dispersions. However, characteristic equations of these static mixers have yet to be sufficiently developed. These equations describe the inherent efficiency of different static mixers in various separation systems.

This study seeks to develop characteristic equations for different static mixer configurations in a Co/Ni separation system. The parameters incorporated in these equations include the Sauter mean diameter of the oil droplets (d_{32}), the diameter of the pipe (D), the Weber number (We), Reynold's number (Re), and the number of static mixer elements used in the system (ne). The study considers the development of correlations with pre-determined fitting parameters (α,β,γ,δ) descriptive of each unique static mixer design. The characteristic equations take the following form:

$$\frac{d_{32}}{D} = \alpha We^{\beta} Re^{\gamma} ne^{\delta}$$

This study provides an approach to developing these characteristic equations using droplet size reduction in a Co/Ni solvent extraction system. The droplet size reduction was determined using existing settling velocity correlations. These characteristic equations were developed in various flow regimes for small-scale and large-scale applications. After creating these equations, a computational fluid dynamics (CFD) model was constructed in Star-CCM+ to verify the validity of these equations under different conditions.

The research conducted provides empirical confirmation that static mixers are not only able to decrease residence time in solvent extraction processes but also that static mixers exhibit different behaviour in different systems. The research results represent a further step towards optimising solvent extraction processes using static mixers.

Keywords: Solvent extraction, Static mixers, CFD, Co/Ni separation, Residence time

Mass Transfer Intensification Implementing the Use of Static Mixers in Co/Ni Solvent Extraction

Derik J. van der Westhuizen
derik.vanderwesthuizen@nwu.ac.za

[1]Johan W. Bezuidenhout, [1]Reynhard van der Berg [1]Burgert B. Hattingh, [2]Derik J. van der Westhuizen

[1]School of Chemical and Mineral Engineering, North-West University, South Africa
[2]RFA: Chemical Resource Beneficiation, Hydrometallurgy group, North-West University, South Africa

Introduction

South African mineral deposits

- RSA have the **world's 5th-largest mining sector** (gross domestic product value)
- **Mining companies** are key players in the **global** industry.
- SA holds the world's largest reported reserves of **Au** (30%), **PGMs** (88%), **Cr** (72%) and **Mn** (80%), and th 2nd-largest reserves of **Zr, V** and **Ti.**

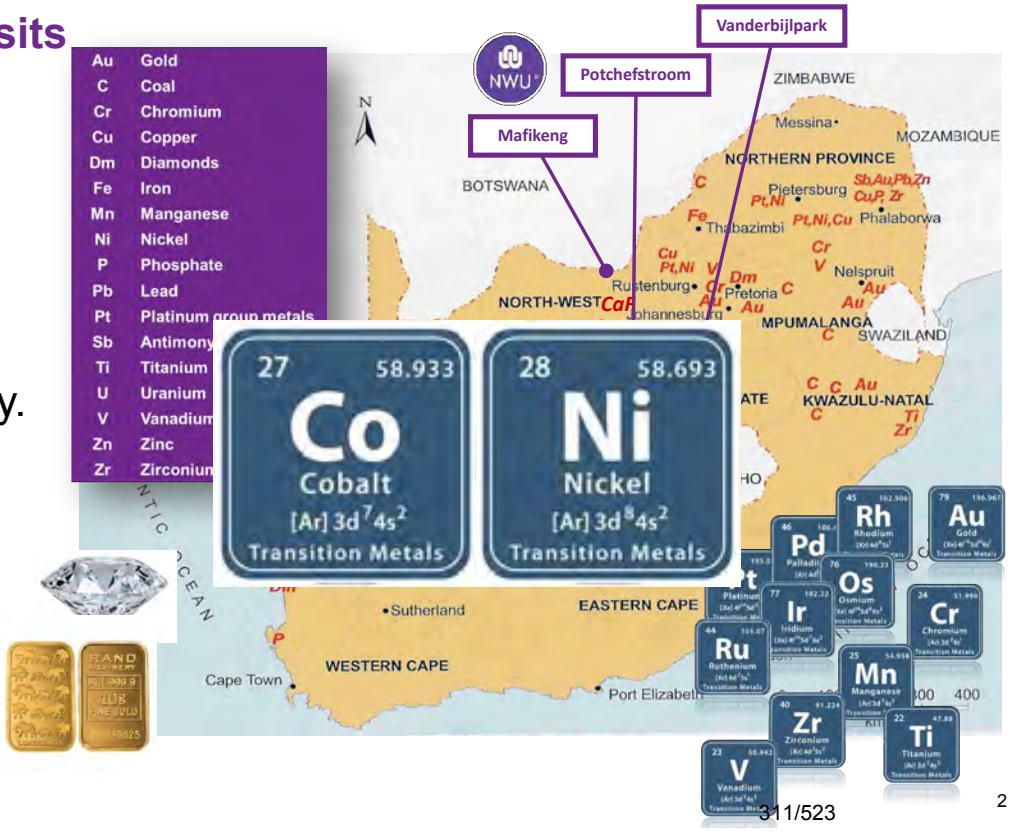

Pocket Guide to South Africa 2022/23: Mineral Resources

Introduction

South African mineral deposits

Country	Number of wins (years)
South Africa	**4** (1995, 2007, 2019, 2023)
New Zealand	3 (1987, 2011, 2015)
Australia	2 (1991, 1999)
England	1 (2003)

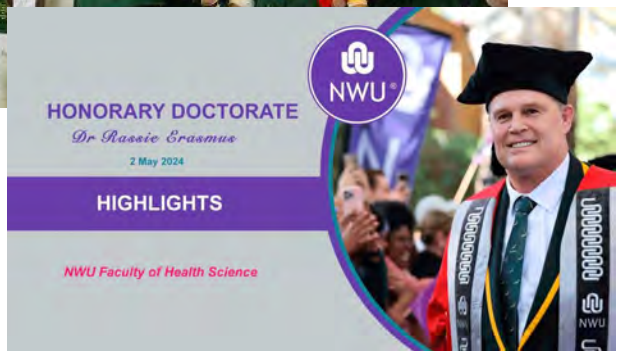

https://www.rugbyworldcup.com/

Introduction

Critical Minerals: Co/Ni

- Global Co/Ni demand is increasing
- Driven by:
  - stainless steel
  - electric vehicle
  - **energy storage solutions**

https://ardearesources.com.au/critical-minerals

Introduction

Co/Ni separation: SX

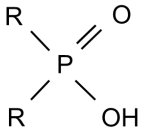

CYANEX® 272
(dialkyl phosphinic acid)

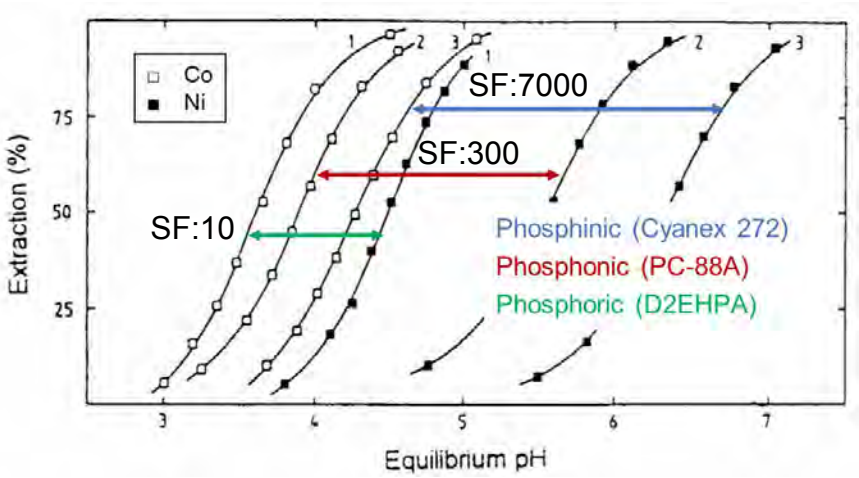

Cyanex 272:

- more stable to oxidative degradation by Co(III)
- more selective for Co over Ca
- minimises crud formation

Gordosky, HydroMet Short Course, 2011

Introduction

SX contactors: Mixer-settlers

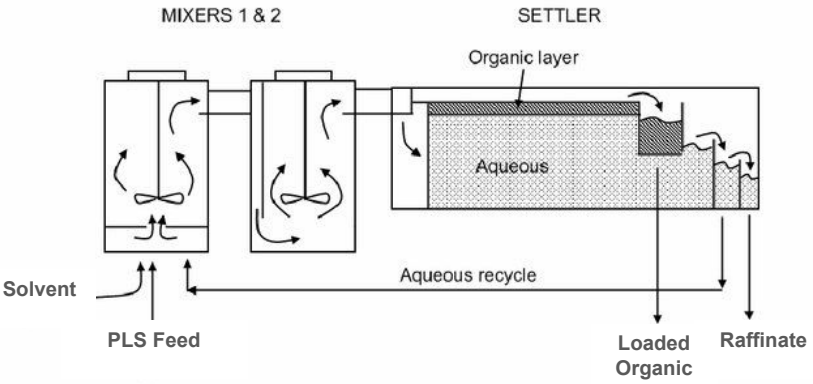

https://www.metso.com/portfolio/vsf-x-solvent-extraction-plant/

Introduction

SX contactors: Mixer-settlers

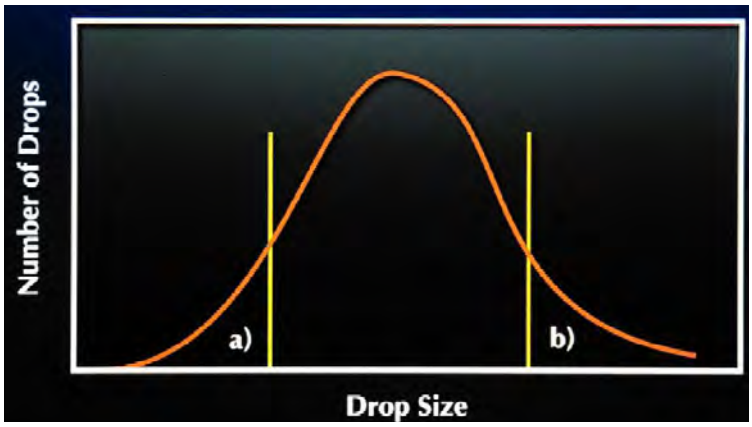

a) Drops too small: tend to entrain

b) Drops too large – slow transfer kinetics

Rule-of-thumb: 100-150 µm

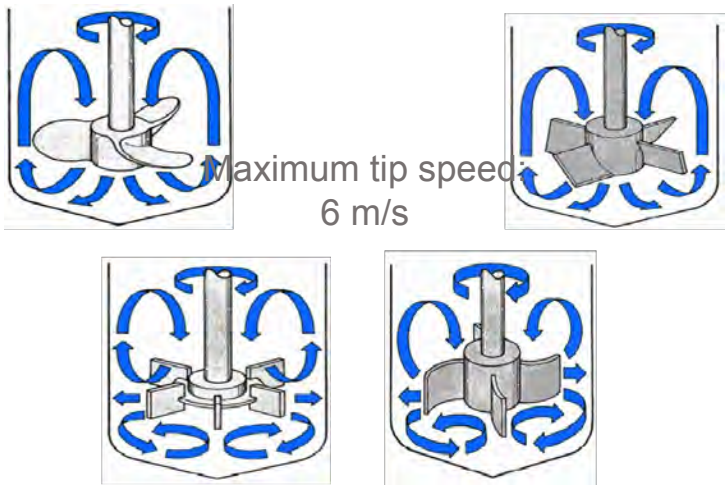

Courtesy of Johann Brits

Introduction

SX contactors: Mixer-settlers

Foaming

Cole, P.M., Hydrometallurgy, SX, TWP Projects Short Course, Wits Enterprise, 2011

Introduction

SX contactors: Mixer-settlers

Crudding



https://www.metso.com/portfolio/vsf-x-solvent-extraction-plant/

Introduction

SX contactors: Mixer-settlers



Organic Recovery Systems (Coalescers)


Courtesy of Peter Cole

Introduction

SX contactors: Pertraction (PX)

The "microfiltration" membrane:

- Does not filter
- Bubble point larger than 100 kPa
- Low diffusion resistance: thin (30 mm) and porous (40-50%)
- Compatible with solvent and feed: PP-HF & PE-potting

The contactor module:

- High area: 40-400 m^2
- Hydraulic diameter: 0.3-1 mm
- Low pressure drop: < 10 kPa/m @ V_{sup} = 2 cm/s
- Low cost: ± 50 USD/m^2

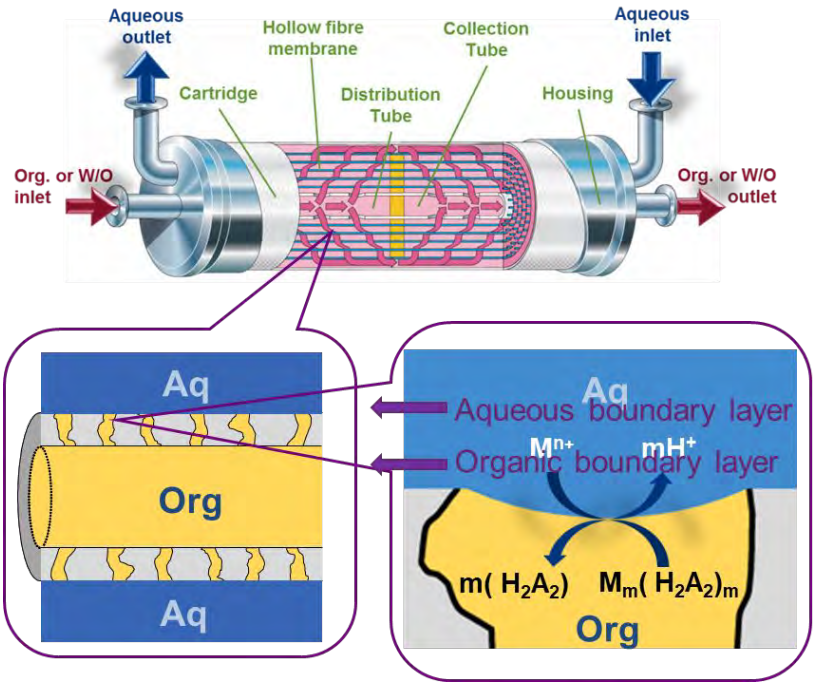

van der Westhuizen, D.J., et al., NWU, PCTWO2012/168915A

Introduction

SX contactors: Pertraction (PX)

Advantages

- High, well defined mass transfer area
- No flooding/crud: process control
- Less rotating equipment: maintenance
- Less solvent holdup & closed operation: safety
- Smaller footprint: CAPEX

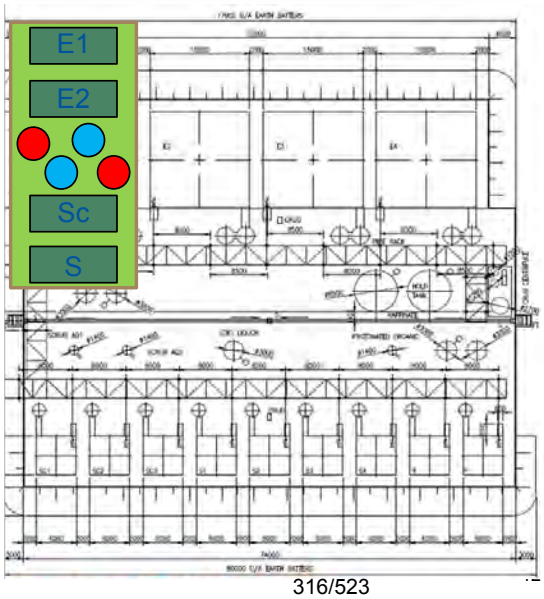

Challenges

- Membrane replacement cost
- No proven technology
- **Extra mass-transfer resistance**

van der Westhuizen, D.J., et al., NWU, PCTWO2012/168915A

Scope of study

SX contactors: Hybrid Pertraction (HPX)

"Rapid mixing and phase separation"

Hollow fibre membrane contactors

- Feed/Solvent Dispersion is fed into HFM
- Solvent droplets coalesce on fibre inner wall
- Solvent selectively permeates over membrane to module shell-side
- Aqueous Feed retained on lumen-side

van der Westhuizen, D.J., et al., NWU, Co/Ni-HPX Technical Report, 2023

Introduction

SX contactors: Hybrid Pertraction (HPX)

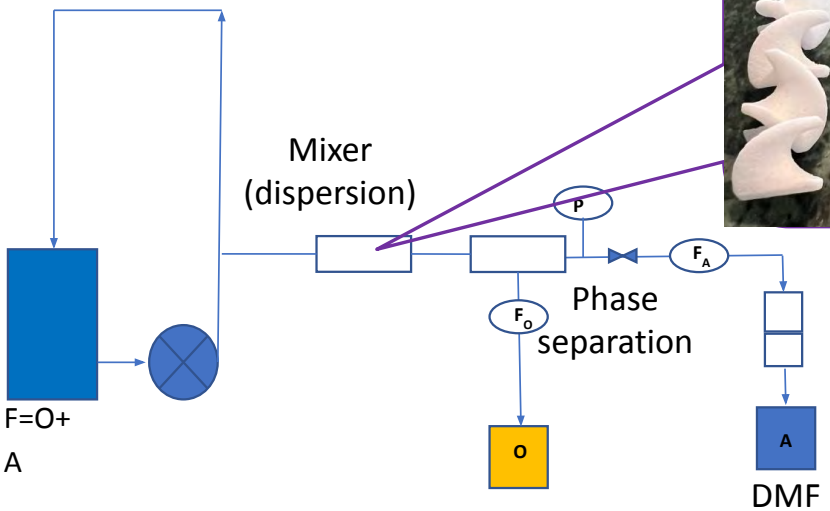

To maintain a transient flow regime:

- Kenics
- Sulzer SMX

van der Westhuizen, D.J., et al., NWU, Co/Ni-HPX Technical Report, 2023

Aim & Objectives

The aim of this study is to assess the suitability of static mixers to enhance the mass-transfer rate by reducing the Sauter mean diameter of the dispersion for a Co/Ni solvent extraction system.

- **Objectives:**
  - Prediction of the diffusion coefficients for a Co/Ni system
  - Comparison of the residence time and the Sauter mean diameter
  - Static mixer model determination and validation in a non-reactive system
  - Evaluation of the static mixer model in a reactive Co/Ni system
  - Assessment of phase separation in a hollow-fibre membrane

Methodology

Mixing optimisation

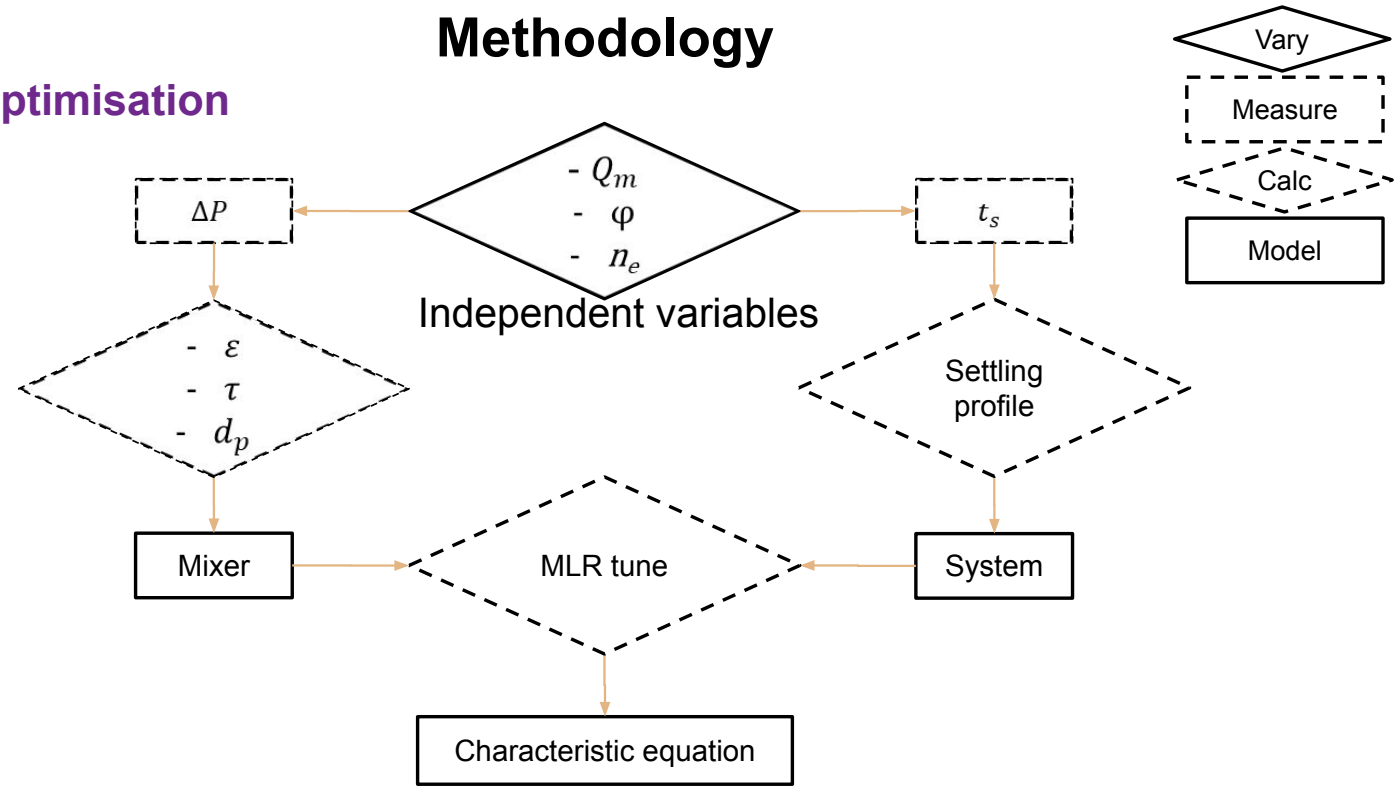

Methodology

Mixing optimisation

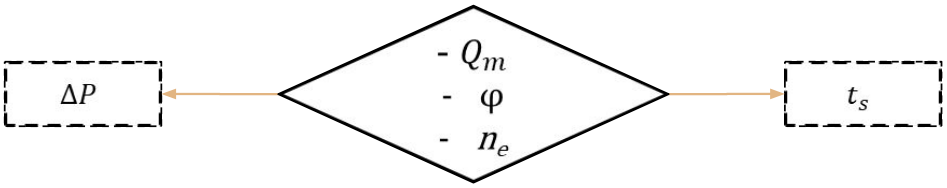

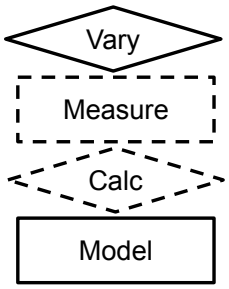

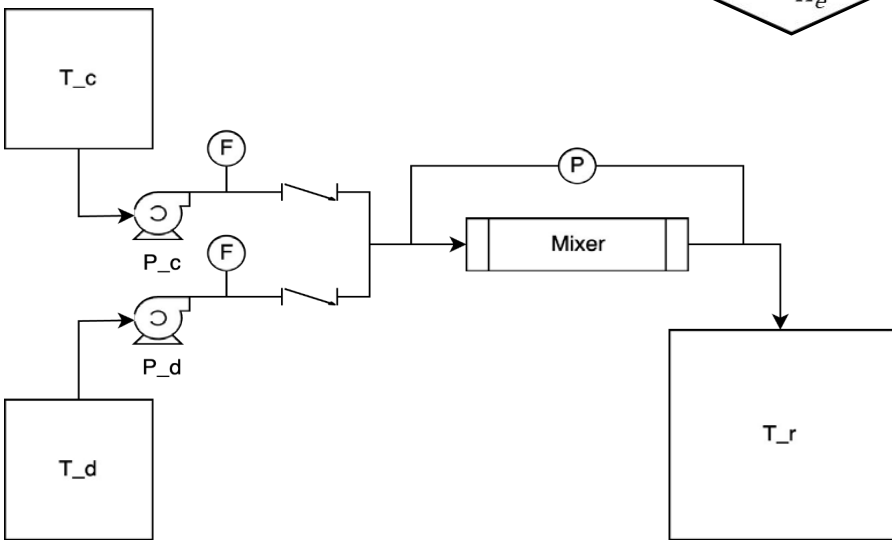

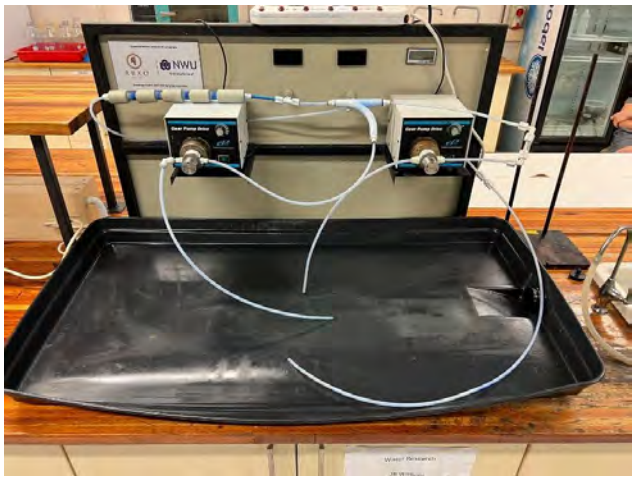

Methodology

Mixing optimisation

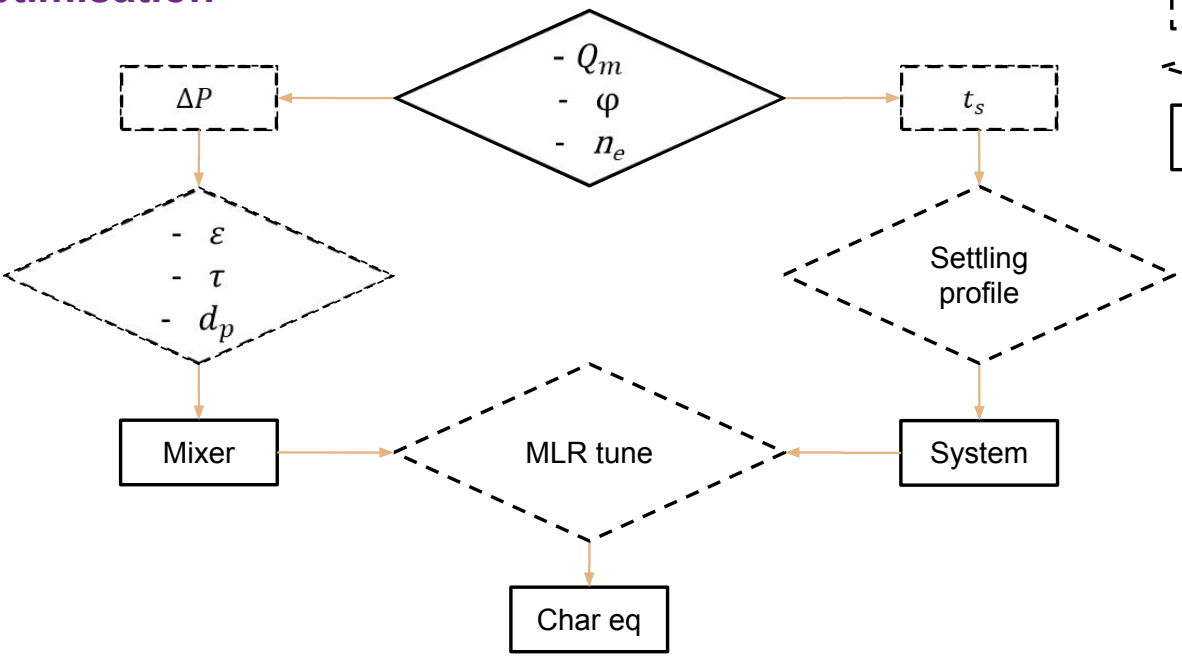

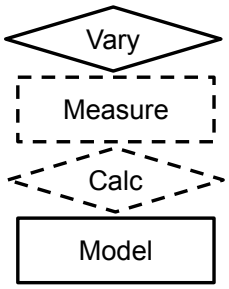

Methodology

Mixing optimisation

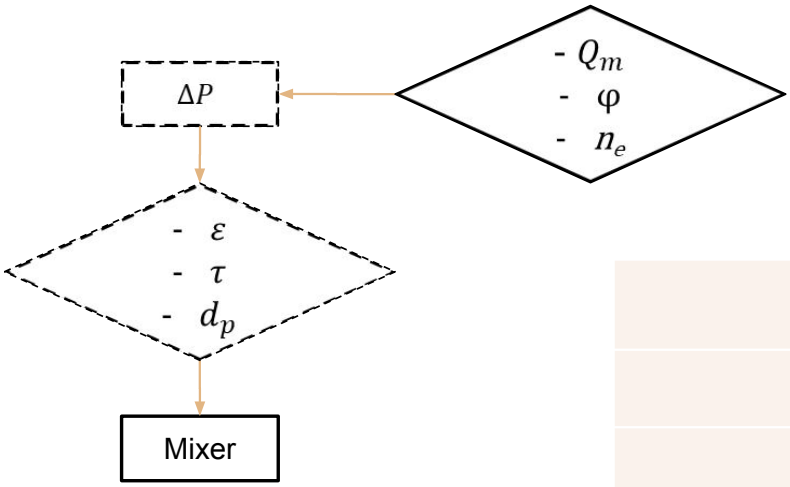

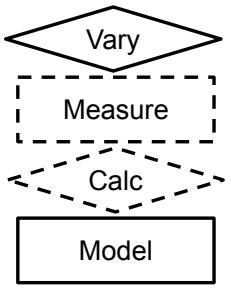

	(1)
	(2)
	(3)
	(4)

Morancais, P., et. al., 1999. Chemical Engineering Communications, 171(1), 77-93.

Methodology

Mixing optimisation

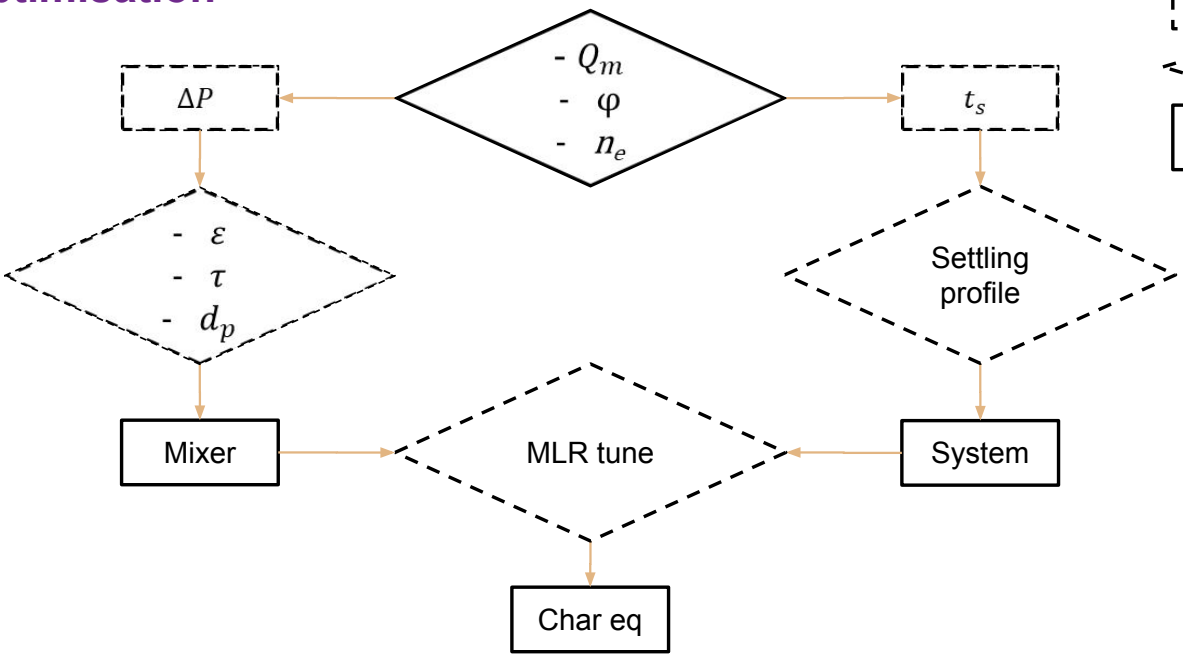

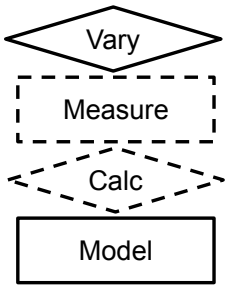

Methodology

Mixing optimisation

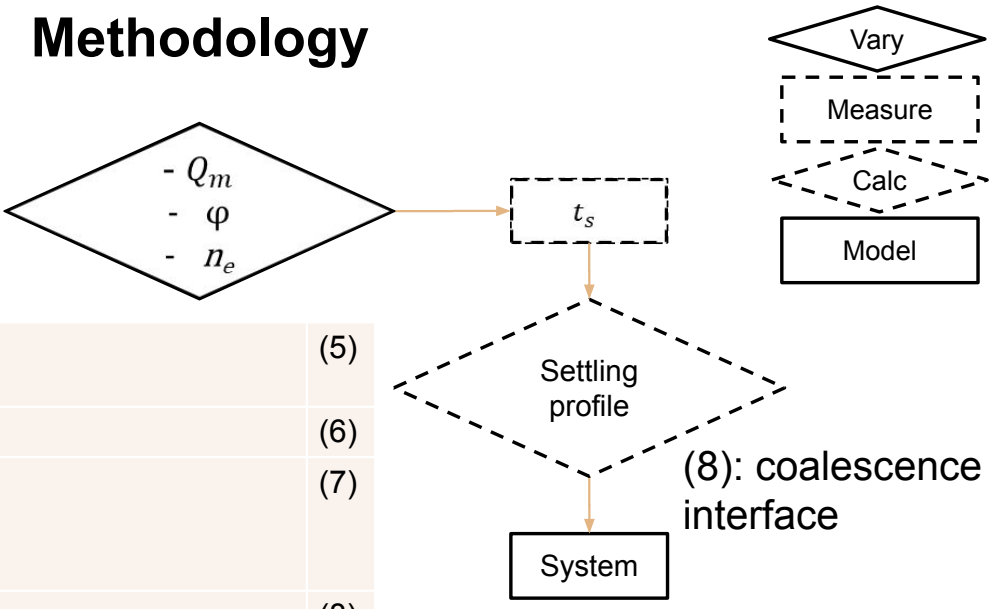

	(5)
	(6)
	(7)
	(8)

(non-linear regression)

Kumar, A. et al.., 1985. The Canadian Journal of Chemical Engineering, 63(3), 368-376.

Yu, G.Z. et al.. 2004. Engineering-Biotechnology, 27(4):407-413.

Methodology

Mixing optimisation

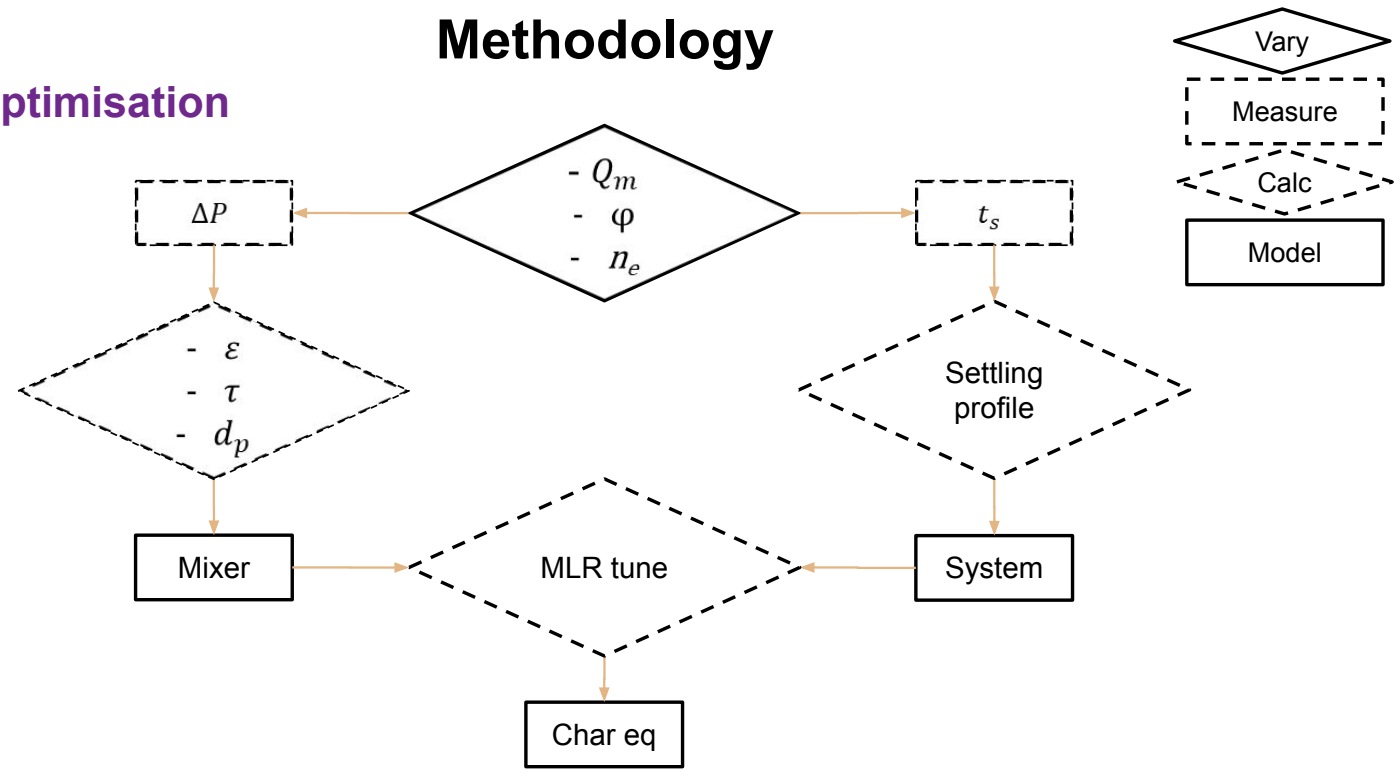

Methodology

Mixing optimisation

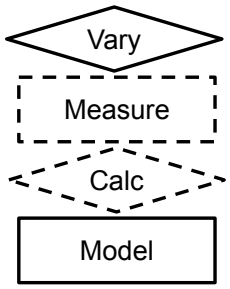

	(9)
	(10)
	(11)

	(12)
	(13)
	(14)

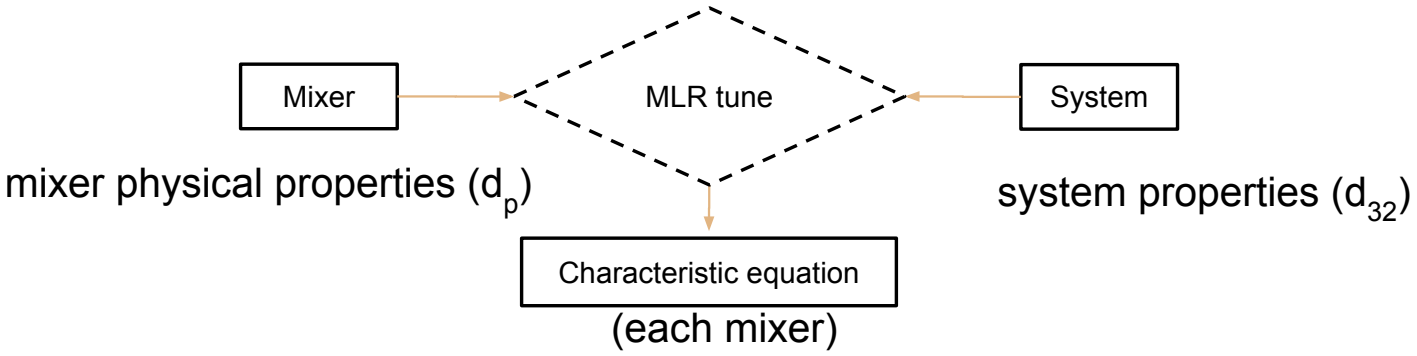

Results and Discussion

Mixing optimisation

ΔP vs d32 empirical

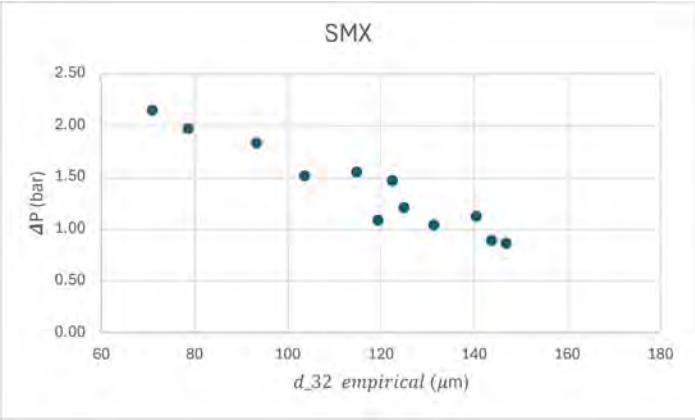

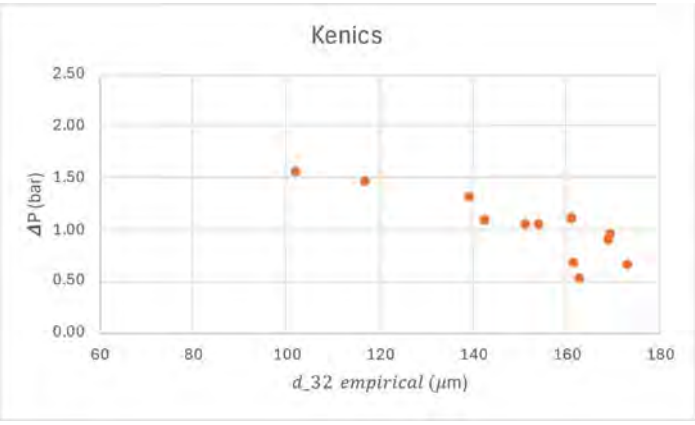

- Kenics: lower pressure drop
- However: increased droplet sizes

Results and Discussion

Mixing optimisation

Settling graph

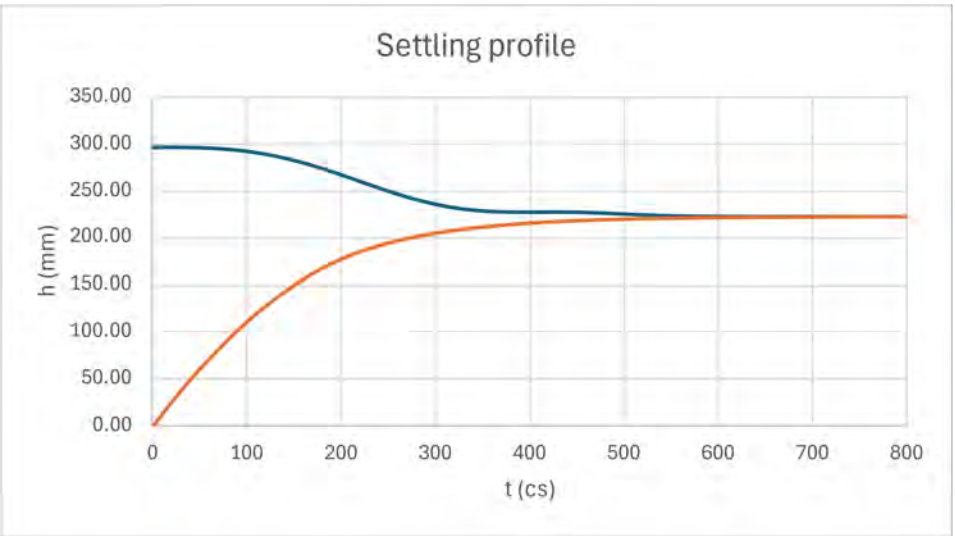

- The data could be fairly well fitted
- The suitable data were used to better approximate j and k
- Used to correlate the empirical Sauter diameter more efficiently

Results and Discussion

Mixing optimisation

Parity plots

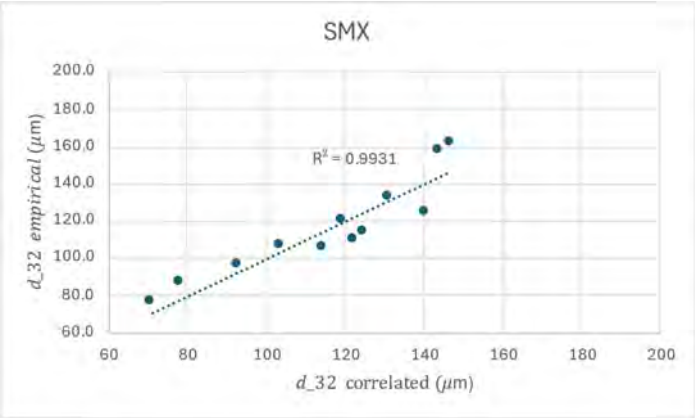

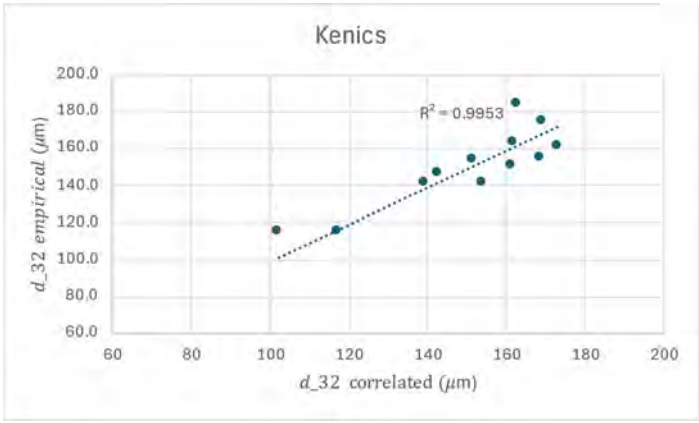

	SMX	Kenics
α	36.42	45.55
β	-4.04	-6.12
γ	1.37	2.83
δ	-0.21	-0.05

- Kenics: Smaller distribution, but better fit

Results and Discussion

Mixing optimisation

%E vs correlated d32

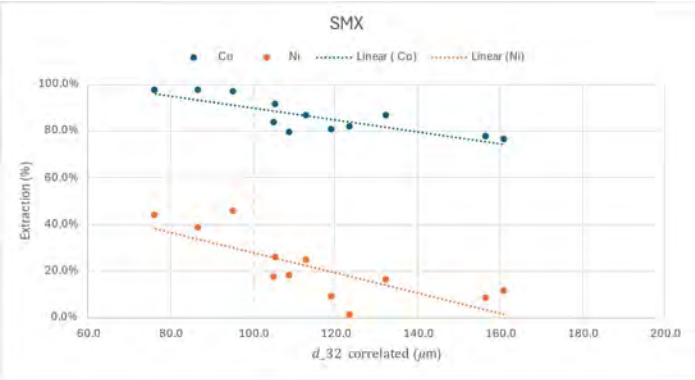

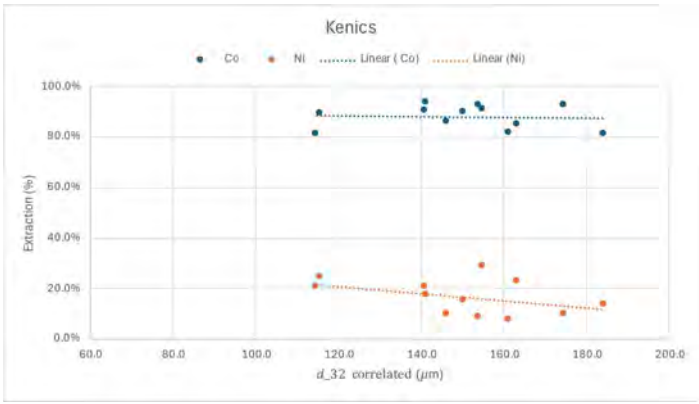

- The smaller droplets in the SMX: higher Co extraction
- Larger droplet size: decreased the extraction rapidly

- Kenics: better contact obtained
- However, a relative higher Ni transfer was also obtained – reduce selectivity

Scope of study

SX contactors: Hybrid Pertraction (HPX)

"Rapid mixing and phase separation"

Hollow fibre membrane contactors

- Feed/Solvent Dispersion is fed into HFM
- Solvent droplets coalesce on fibre inner wall
- Solvent selectively permeates over membrane to module shell-side
- Aqueous Feed retained on lumen-side

van der Westhuizen, D.J., et al., NWU, Co/Ni-HPX Technical Report, 2023

Introduction

SX contactors: Hybrid Pertraction (HPX)

Mixer (dispersion)

Phase separation

van der Westhuizen, D.J., et al., NWU, Co/Ni-HPX Technical Report, 2023

Results and Discussion

Phase separation

Permeate flowrate as a function of retentate back-pressure

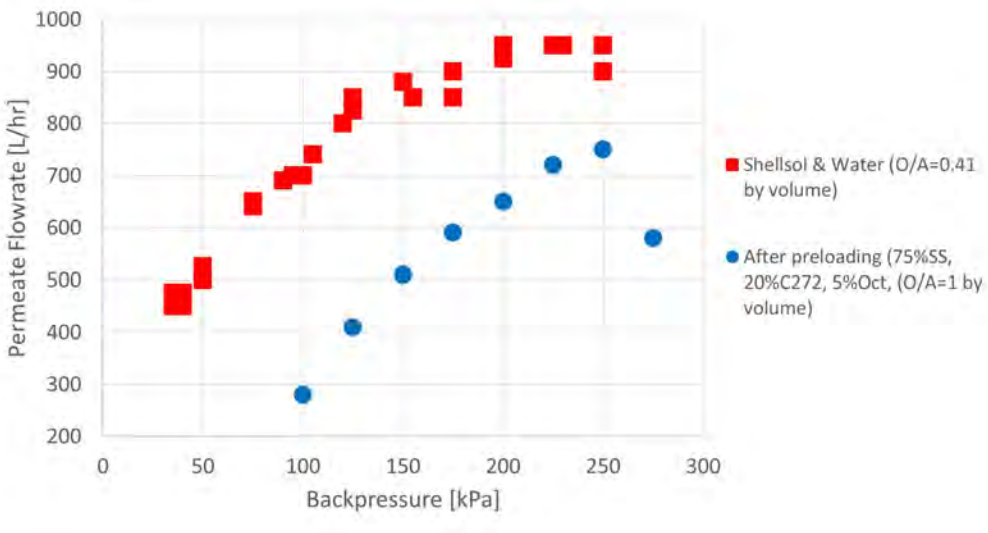

Evident that:

- System can be controlled
- Obtain a clean permeate
- Dispersion Viscosity effects the flow rates directly
- Next step: Co/Ni-system

van der Westhuizen, D.J., et al., NWU, Co/Ni-HPX Technical Report, 2023

Results and Discussion

Phase separation

Clarification of retentate (aqueous raffinate)

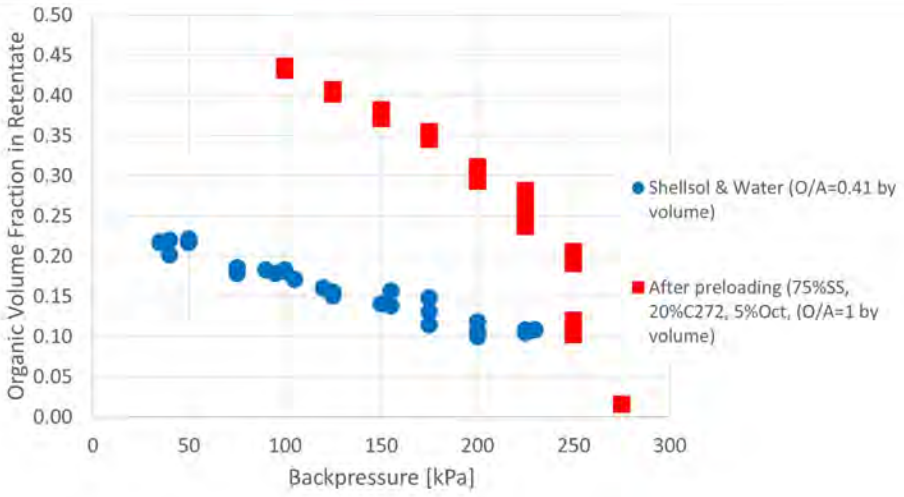

van der Westhuizen, D.J., et al., NWU, Co/Ni-HPX Technical Report, 2023

- At 270kPa < 1% Org in retentate
- Needs to be reduced further to < 10ppm
- At max back-pressure: the org fraction SS-H_2O equals the C272-H_2O

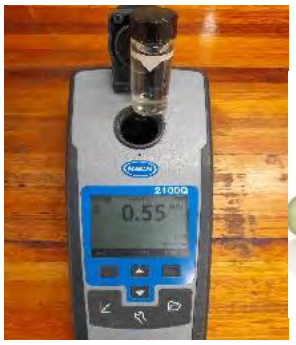

Conclusion and Future work

- Static-mixer connected with an overhead stirrer and homogeniser produces milky dispersion and generates feed pressure to HPX module.
- 8x80 Liqui cell separates aqueous from the organic with a clear organic permeate but does not produce clear aqueous retentate (yet).
- DMF removes fine organic droplets from oil in water dispersion, but it is not effective enough.
- Use PPG hydrophilic membranes as clarifier (<10ppm).
- Procure on-line turbidimeter.
- Repeat and optimise for real feed solution, incl. Ni-scrubbing and Co-stripping

Droplet Size and mass transfer modelling

- GENERAL INFO
- WHY?
- AIM

35

Mass transfer modelling

- Mass transfer occurs between the dispersed and continuous phase and is described by diffusion and reaction parameters.
- Mass transfer is halted when the dispersed and continuous phase are in equilibrium – This occurs at the equilibrium time t_{eq}.
- The equilibrium time, t_{eq}, is dependent on the radius of the droplets in the dispersed phase.

36

Mass Transfer Modelling

- Model Assumptions
  - All dispersed droplets are spherical
  - The concentration of the extractant species is equal at all points within the droplet at $t = 0$.
  - The surface of the droplet is always in equilibrium with the dispersed and continuous phase
  - …

Mass Transfer Modelling

- The rate of extraction can be written as the combined effect of radial diffusion and the reaction rate.

$$\partial_t c_i = D_{ij}\left\{\partial_r^2 c_i + \frac{2}{r}\partial_r c\right\} + R_i$$

- The solution of the reaction-diffusion rate equation can be deduced from the non-reactive diffusion equation considering the following boundary conditions and taking $u = rc_1$.

$$u = 0, \qquad r = 0 \;\forall\; t > 0$$

$$u = rc_0, \qquad t = 0 \;\forall\; r \in (0, r_s)$$

$$u = r_s c_{eq}, \qquad t > 0, \qquad r = r_s$$

- For the purpose of model simplification, we assume that the reaction rate, R_i, is first order and given by

$$R_i = k_1 c_i$$

In this case k_1 becomes a fitting parameter

Mass Transfer Modelling

- Using Danckwert's method (reference) the solution to the reaction-diffusion model is given by:

$$c = k_1 \int_0^t c_1 e^{-k_1 t'} dt' + c_1 e^{-k_1 t}$$

which equates to

$$c = \left(2e^{-k_1 t} - 1\right)\left\{\{c_{eq} - c_0\}\left\{1 + \frac{2r_s}{\pi r}\sum_{n=1}^{\infty}\frac{(-1)^n}{n}\sin\frac{n\pi r}{r_s}\exp(-Dn^2\pi^2 t/r_s^2)\right\} + c_0\right\}$$

- Rewriting the solution in the form $(c - c_0)/(c_{eq} - c_0)$ allows for dimensionless analysis of the equilibrium time needed for the extraction, scrubbing or stripping to occur. This also allows the user to investigate the concentration distribution of a component at any radial position within the droplet as a function of time

39

Mass Transfer Modelling

- MODEL PROS and CONS (TABLE FORMAT)
- The model can be used to estimate equilibrium times based on droplet sizes produced using chosen mixer types or to estimate droplet sizes based on target equilibrium times for a specific system
- The model can be applied to almost any dispersive extraction system – both non-reactive and reactive extraction.
- *The model associates a fitting parameter – Value must be determined experimentally (SOFAR…)*
- *The model does not consider physical interactions in the mixing process*
  - *coalescence, shearing, etc…*

Model Validation – Cobalt Solvent extraction with Cyanex 272

Literature, constants, initial conditions, etc.

Finding Diffusivity and Equilibrium

Shake Flask Tests for equilibrium composition determination

Molecular Dynamics Simulations for Diffusivity determination

- Amorphous cell – Organometallic species, Solvent environment, etc.
- Forcite geometry optimizations, cell annealing cycles and Molecular dynamics simulations
- Mean Square displacement and curve fitting
- Determination of the Diffusivities

Cobalt Mass Transfer model

- Results based on values and constants from literature vs results from MDS
- Equilibrium times are chosen such that all radial positions converge at unity

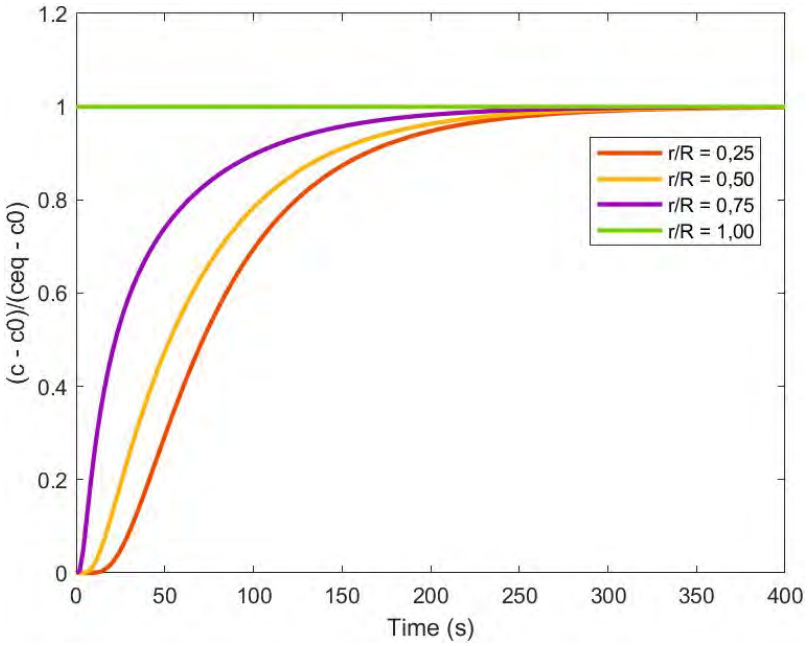

Equilibrium time vs droplet size

- Extrapolated equilibrium times compared to various droplet sizes with curve fitting to suitable function

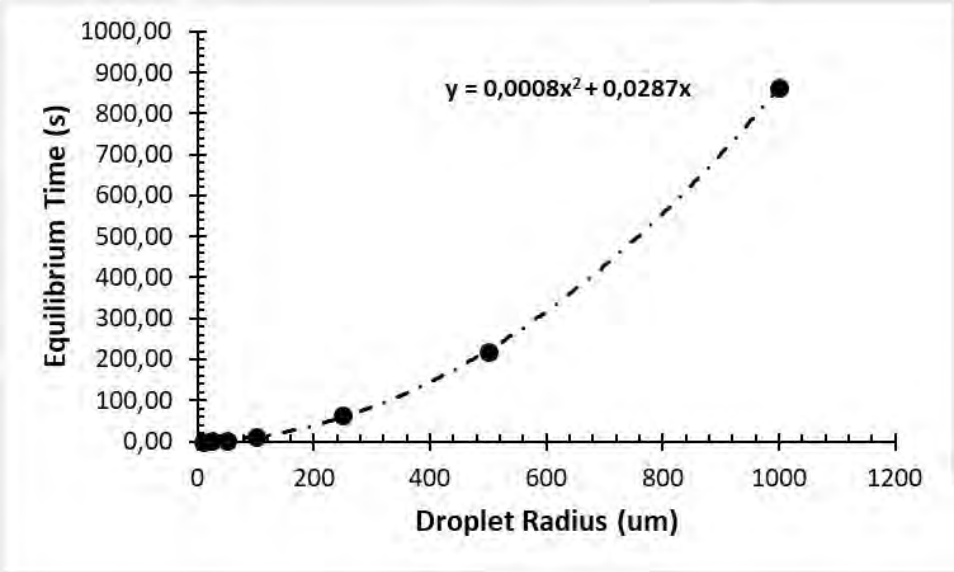

Mixing optimisation

Extraction efficiency $\propto \frac{1}{d_{32}}$

Static mixers

- Static mixers consist of moulded elements, e.g., vanes or baffles, housed in a tube
- These elements are engineered to form tortuous pores
- Turbulent flow is often realised within these narrow pores
- Flow down these pores causes vortices and eddies that promote mixing
- Contact is increased between the solution and solvent

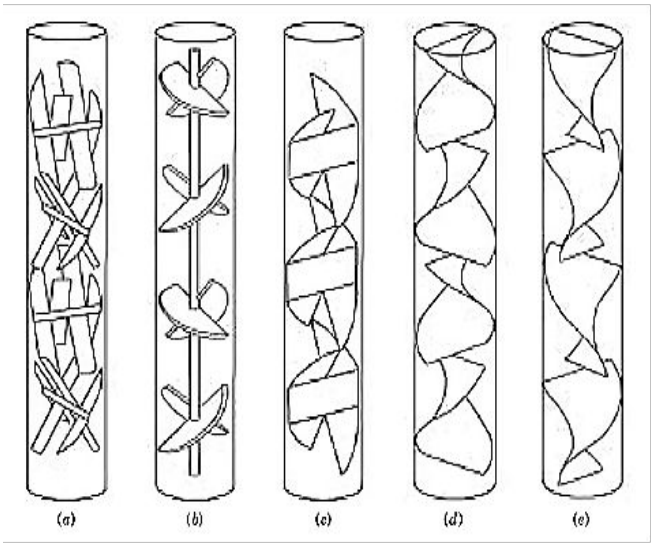

Figure 1: Examples of static mixers
(a) Sulzer SMX (b) Ross LPD (c) Komax (d) Kenics (e) FixMix

Adapted from: Gyenis, J., 2002. Motionless Mixers in Bulk Solids Treatments–A Review. KONA Powder and Particle Journal, 20, pp.9-23.

Experimental regime

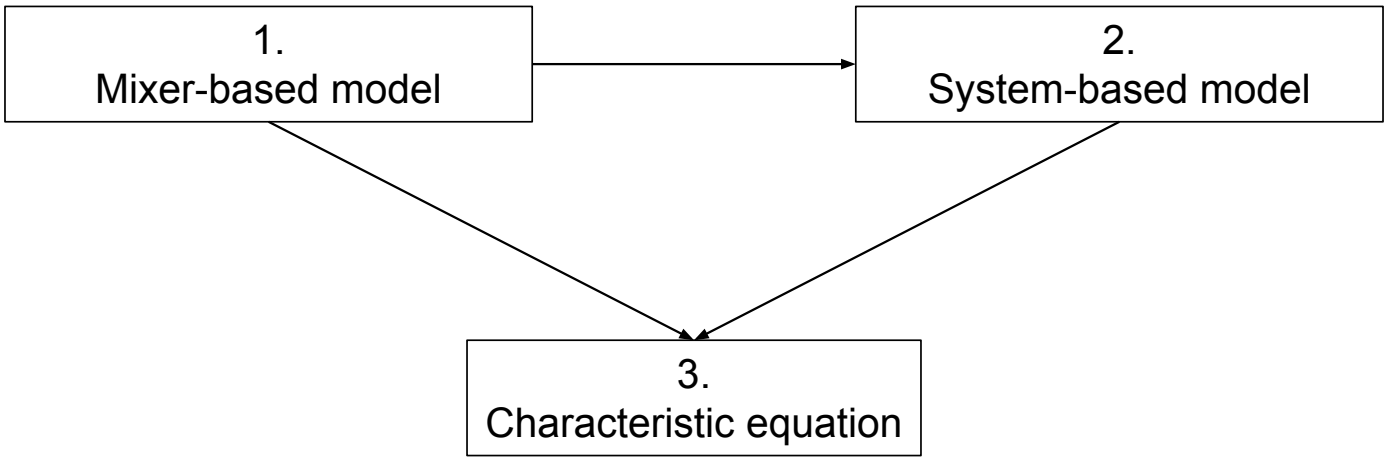

Experimental setup

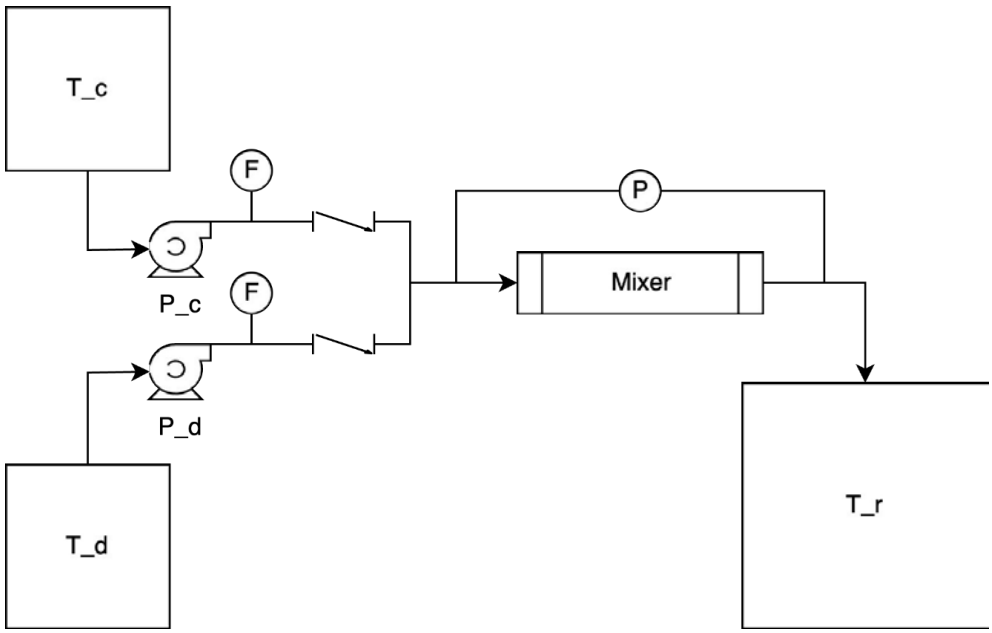

T_c: Continuous phase tank; T_d: Dispersed phase tank; T_r: Residence tank;
P_c: Continuous phase pump; P_d: Dispersed phase pump; F: Flowmeter; P: Pressure meter.

Experimental regime variables

- Independent variables:
  - Mixture flow rate
  - Oil fraction
  - Number of mixing elements
- Dependent variables:
  - Pressure drop over the mixer
  - Settling time of the dispersion

Experimental regime

1.
Mixer-based model

- Measure the pressure drop over the mixer
- Calculate:
  - Porosity
  - Tortuosity
  - Pore diameter

using the method from Morancais *et al. (1998)*.

Mixer-based model

- Porosity:

$$\varepsilon = \frac{v_0}{v}$$

with v_0: void volume (m^3); v: mixer volume (m^3).

- Pore diameter (m):

$$d_p = \left(\frac{32}{K}\right)^{0.75} \left(\frac{J}{0.3872}\right)^{0.5} \varepsilon^{0.25}$$

- Tortuosity:

$$\tau = \left(\frac{32}{K}\right)^{0.25} \left(\frac{J}{0.3872}\right)^{0.5} \varepsilon^{0.75}$$

J, K: slope and intercept of pressure drop equation.

Mixer-based model

- Pressure drop equation [1]:

$$\frac{\Delta P}{L \mu_m U_s} = J \frac{\rho_m U_s}{\mu_e} + K$$

with ΔP: pressure drop over mixer (Pa); L: length of mixer (m);
μ_e: viscosity of mixture $(Pa\,.\,s)$; U_s: superficial velocity $(m\,.\,s^{-1})$;
ρ_m: density of mixture $(kg\,.\,m^{-3})$.

[1]: Morancais, P., Hirech, K., Carnelle, G. and Legrand, J., 1999. Friction factor in static mixer and determination of geometric parameters of SMX Sulzer mixers. *Chemical Engineering Communications*, *171*(1), pp.77-93.

Experimental regime

2.
System-based model

- Measure the settling time in T_r
- Calculate:
  - Experimental settling velocity
  - Calculated settling velocity
  - The Sauter mean drop diameter

using the method from Kumar & Hartland (1985).

System-based model

- Theoretical settling velocity ($m\,.s^{-1}$) [2]:

$$v_{0,calc} = \frac{12\mu_c}{0.53\rho_c d_{\max}}\left[-1+\sqrt{1+\frac{0.53\rho_c\Delta\rho g d_{\max}^3(1-\varphi)}{108\mu_c^2(1+4.56\varphi^{0.73})}}\right]$$

with μ_c: Viscosity of continuous phase ($Pa.s$); ρ_c: Density of continuous phase ($kg.m^{-3}$); $d_{\max}$: Maximum droplet diameter (m); $\Delta\rho$: Density difference ($kg.m^{-3}$); g: Acceleration due to gravity ($m.s^{-2}$); φ: Oil fraction.

[2]: Kumar, A. and Hartland, S., 1985. Gravity settling in liquid/liquid dispersions. *The Canadian Journal of Chemical Engineering*, *63*(3), pp.368-376.

System-based model

- Experimental settling velocity ($m\,.\,s^{-1}$):

$$v_{0,exp} = \frac{h_t - h_\mathrm{d}}{t}$$

with h_t: Total dispersion height (m); h_d: Height of dispersed phase (m); t: Settling time (s).

- $d_{32} = 3\beta d_{\max}$

with d_{32} : Sauter mean diameter (m); β: Size distribution parameter (≈ 0.13).

Experimental regime

3.
Characteristic equation

- Calculate the tuning parameters specific to a static mixer using multiple linear regression.
- Oil fraction:

$$\varphi = \frac{\dot{Q}_d}{\dot{Q}_d + \dot{Q}_c}$$

with $\dot{Q}_c$, $\dot{Q}_d$: Continuous, dispersed phase flow rate ($m^3\,.\,s^{-1}$).

- Mixture flow rate ($m^3\,.\,s^{-1}$):

$$\dot{Q_m} = \dot{Q}_d + \dot{Q}_c$$

Characteristic equation

- Mixture density ($kg\,.m^{-3}$):

$$\rho_m = \varphi\rho_d + (1-\varphi)\rho_c$$

with ρ_c, ρ_d: Continuous, dispersed phase density ($kg\,.m^{-3}$).

- Mixture viscosity ($Pa\,.s$):

$$\mu_m = \mu_c\left[1 + 2.5\varphi\left(\frac{\mu_d + 0.4\mu_c}{\mu_d + \mu_c}\right)\right]$$

with μ_c, μ_d : Continuous, dispersed phase viscosity ($Pa\,.s$).

Characteristic equation

- Superficial velocity ($m\,.s^{-1}$):

$$U_s = \frac{4\dot{Q_m}}{\pi D^2}$$

with D: Pipe diameter (m).

- Pore velocity ($m\,.s^{-1}$):

$$U_p = \frac{U_s\tau}{\varepsilon}$$

Characteristic equation

- Pore Reynold's number:

$$Re_p = \frac{\rho_e U_p d_p}{\mu_e}$$

- Pore Weber number:

$$We_p = \frac{\rho_e U_p^2 d_p}{\sigma}$$

with σ: Interfacial tension ($\mathrm{N}\,.\,m^{-1}$).

Characteristic equation

- Characteristic equation:

$$\frac{d_{32}}{d_p} = \alpha\, Re_p^{\beta}\, We_p^{\gamma}\, n_e^{\delta}$$

with n_e: Number of mixing elements; $\alpha, \beta, \gamma, \delta$: Tuning parameters.

Results: Static mixer 1

#	Q (ml/s)	φ	n_e
1	35	0.3	16
2	50	0.3	16
3	75	0.3	16
4	100	0.3	16
5	125	0.3	16
6	80	0.2	16
7	80	0.25	16
8	80	0.33	16
9	80	0.5	16
10	80	0.3	2
11	80	0.3	6
12	80	0.3	10
13	80	0.3	20
14	80	0.3	40
15	35	0.2	2
16	125	0.5	40

Results: Static mixer 1

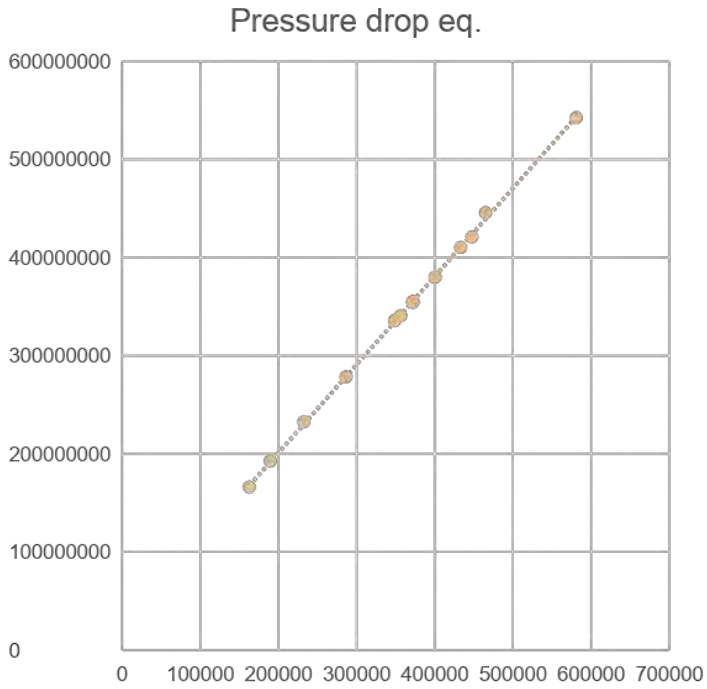

J	898.41
K	21405000
ε	0.77
d_p (mm)	1.93
τ	1.38

Results: Static mixer 1

#	Re	We	d_32 SV (micron)
1	564.44	1.28	134.90
2	806.34	2.62	98.78
3	1209.51	5.90	81.70
4	1612.68	10.49	71.23
5	2015.85	16.39	59.54
6	1502.65	6.83	70.24
7	1389.25	6.77	80.90
8	1236.47	6.68	91.09
9	993.54	6.47	107.47
10	1290.15	6.71	156.99
11	1290.15	6.71	113.00
12	1290.15	6.71	96.00
13	1290.15	6.71	77.00
14	1290.15	6.71	62.00
15	657.41	1.31	179.02
16	1552.41	15.80	61.84

Results: Static mixer 1

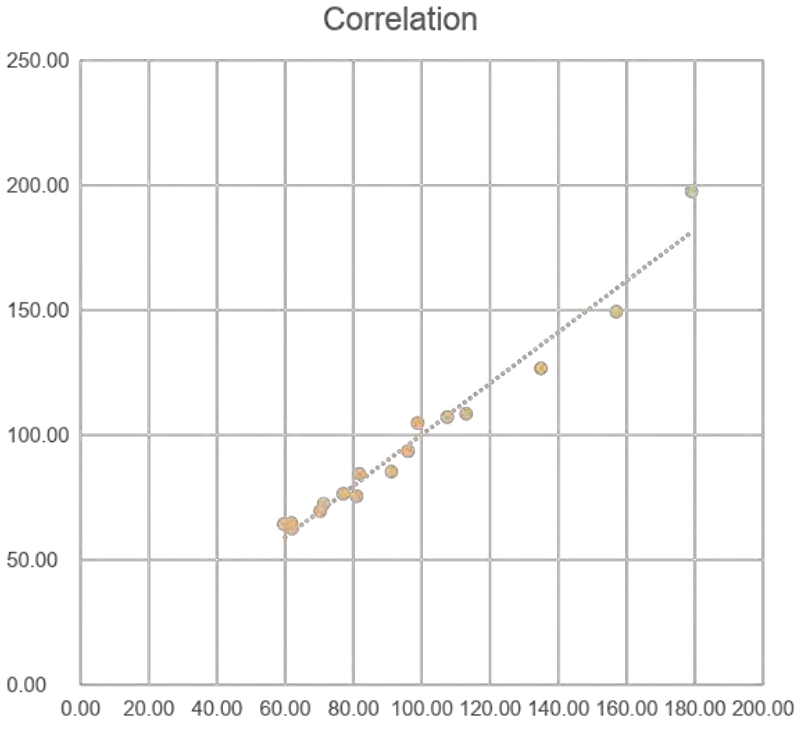

	130.475
	-1.082
	0.275
	-0.291

#	d_32 SV (micron)	d_32 corr (micron)	Error (%)
1	134.90	126.63	6.13
2	98.78	104.74	6.03
3	81.70	84.41	3.33
4	71.23	72.43	1.69
5	59.54	64.33	8.03
6	70.24	69.49	1.07
7	80.90	75.47	6.71
8	91.09	85.28	6.38
9	107.47	107.14	0.31
10	156.99	149.31	4.89
11	113.00	108.48	4.00
12	96.00	93.51	2.59
13	77.00	76.44	0.73
14	62.00	62.49	0.79
15	179.02	197.49	10.32
16	61.84	64.73	4.68

CFD validation

- Which model will be used
- CFD setup
- CFD results

Separation validation

Membranes to the rescue!

Phase separation

- The chemical environment – Solvent and Aqueous composition
- Factors that influence Phase Separation
- Hollow Fiber membrane contactors

Hybrid pertraction

Membranes to the rescue!

PRODUCTION OF BATTERY GRADE NICKEL AND COBALT SULFATE FROM NICKEL LATERITE ORE

By

[1,2]Kaixi Jiang, [3]Haibei Wang [3]Sanping Liu
[1]Fuzhou University, China
[2]Zijing Minning, China
[3]BGRIMM Technology Group, China

Presenter and Corresponding Author

Kaixi Jiang
jiangkaixi@bgrimm.com

ABSTRACT

High-pressure acid leaching process (HPAL) is currently mainly used to treat nickel laterite ore, above 95% of Ni/Co leaching rate can be achieved by it. A two-stage pressure leaching process is developed to treat nickel laterite ore. After HPAL, instead of flash evaporation, the leached slurry is directly sent to the high-pressure neutralization unit, and continue to react with the added saprolite slurry. Utilizing the waste heat of 1st HPAL to neutralize residual sulfuric acid at slightly lower temperatures and pressures, as well as allowing newly generated iron to precipitate and release acid in the form of hematite, while achieving enhanced leaching of saprolite. Meanwhile, it further promotes the hydrolysis of Al^{3+} and reduce the concentration of impurity Al in the neutralized solution. The pressure leached solution is subsequently treated by Fe/Al removal and Ni/Co precipitation. Mixed nickel-cobalt hydroxide (MHP for short) is obtained and used as raw material for refining.

The process for producing battery-grade nickel sulfate and cobalt sulfate from MHP generally includes sulfuric acid leaching, Fe/Al removal, impurities removal by SX, nickel and cobalt separation by SX, etc. At present, Fe/Al removal is mainly conducted by lime milk. This process is widely used, but there exist problems as follows: High Ni loss (~1.5%) due to high residue amount with high Ni content (6-12%); Saturated Ca ions are introduced into the solution. Calcium sulfate crystals will precipitate during P204 impurities removal, which will cause blockage and stoppage. In addition, most factories adopt 2 series of P507 SX to separate Ni/Co/Mg, which will lead to higher CAPEX and OPEX. A new process for Fe/Al removal and Ni/Co/Mg separation by SX is developed. Nickel/cobalt/manganese-based (MHP is preferred) neutralizer is used to remove Fe/Al, followed by L/S separation, the solution is sent for further impurities removal, the residue conducted by acid releaching-Fe/Al removal by lime milk for recovering Ni/Co and Fe/Al open circuit. In P507 SX, Ni saponification is used to control Na from entering to raffinate. After extraction by P507, Co and Mg is completely extracted to organic phase. Raffinate is battery grade Nickel sulfate solution. The loaded organic is scrubbed by many stages of acid solution scrubbing to remove Mg. Finally, the loaded organic is stripped by acid to obtain battery grade cobalt sulfate. In this case, Ni/Co/Mg is separated in one SX series. This new process reduces the dosage of lime milk, the amount of calcium ions introduced into the system and the losses of Ni/Co. The separation of Ni/Co/Mg is simplified as well.

Keywords: Two stage pressure leaching, nickel laterite ore, $NiSO_4$, $CoSO_4$, Battery grade

PRODUCTION OF BATTERY GRADE NICKEL AND COBALT SULFATE FROM NICKEL LATERITE ORE

Kaixi Jiang*, Haibei Wang, Sanping Liu
BGRIMM / Zijin Ming Group / Fuzhou University

May 28th, 2024 Perth, Australia

*Presenter

1. Introduction

Nickel mining production in 2023 (metric tons)

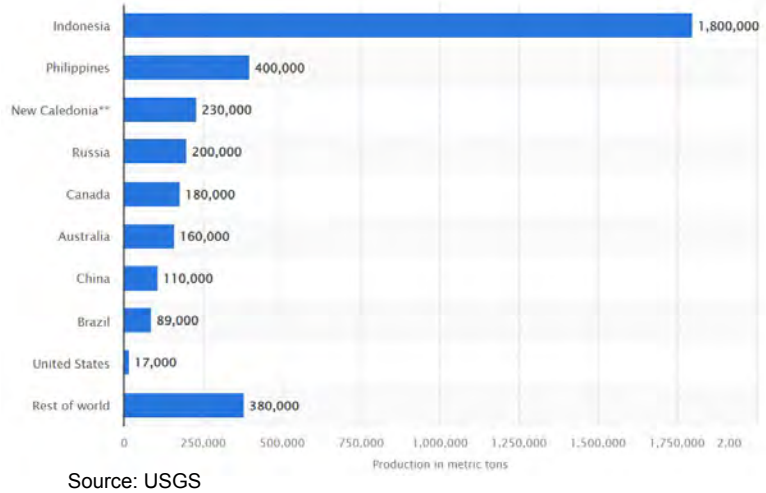

Source: USGS

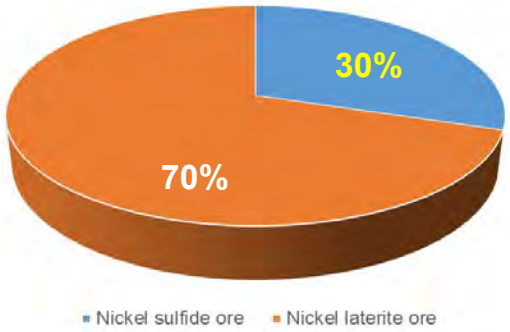

Proportion of ore types in nickel production

- World nickel production: 3.57 Mt in 2023.
- Indonesia nickel production: 1.8 Mt in 2023, accounting for 50.4% of world production.
- Proportion of ore types in nickel production: 30% sulfide ore VS 70% laterite ore.

1. Introduction

◆ Main processes — Nickel laterite ores

Pyrometallurgy

RKEF → ferronickel (Ni>25%)

Blast furnace → pig iron (Ni>5%)

Matte smelting → nickel matte (Ni~70%)

Rotary kiln reduction -- magnetic separation → metallic Ni/Fe powder

Characteristics

- mature and widely used
- high Ni recovery
- high energy consumption
- poor adaptability, suitable for processing high-grade laterite ore
- Co in ferronickel / pig iron devaluated

◆ Main processes — Nickel laterite ores

Hydrometallurgy

High pressure acid leaching (HPAL): a standard technology for limonite laterite ores.

- High nickel extraction (E_{Ni} >95%) ;
- Low acid consumption (iron precipitated as hematite);
- High pressure up to 5.5MPa, high temp. up to 270°C.

Alternative

Atmosphere tank leaching (ATL): LOGIC: Recovery exchanges costs.

Primary leaching: high acid concentration, high Ni and Fe extraction;

Secondary leaching: feed - high magnesium laterite (saprolite), neutralization and iron precipitation with saprolite leaching.

- Low CAPEX and OPEX;
- Lower nickel extraction (E_{Ni} 85~93%) ;
- Higher acid consumption (up to 90% iron precipitated as jarosite or goethite, maybe with lime addition).

◆ Main processes — MHP refining

Pyrometallurgy

Precious nickel matte → refining products

Reduction anode → cathode

Hydrometallurgy

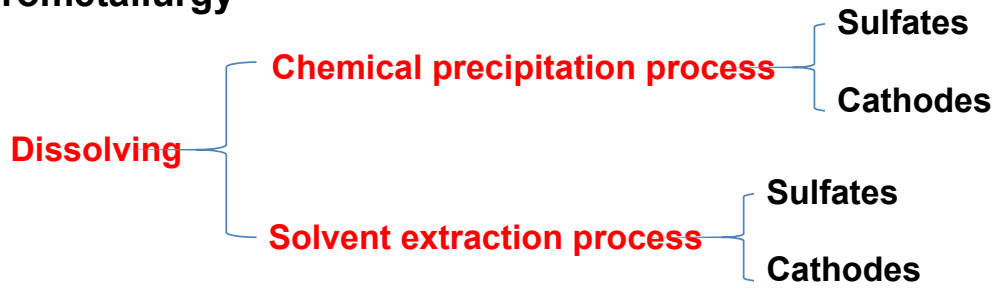

◆ Inverse Leaching* Process

(*ALTA 2013 keynote)

2 types of laterite ores

General process

- Limonite ore → HPAL
- Saprolite ore → AL (Neutralization + Leaching)

Inverse leaching process

- Limonite ore → AL (High acid, ~95 °C)
- Saprolite ore → PAL (150~160°C)

2. Leaching of Nickel Laterite Ores

◆ Inverse Leaching Process

BGRIMM's special flowsheet — an inverse leaching process (patented)

Primary leaching: atmosphere tank leaching

- Feed: limonite portion of laterite ores;
- ~95 °C, input: 100% acid, 97~99% E_{Ni} & E_{Fe};

Secondary leaching: autoclave leaching

- Feed: saprolite portion of laterite ores;
- Around 150~160°C, no acid input, 500~600kPa;
- Total E_{Ni} 93~96%;
- Noacid consumption for 90~95% Fe.

The leaching combination changes the BIG DIFFICULTY of HPAL to "a common routine process"!

Inverse Leaching Process

Pilot plant photos

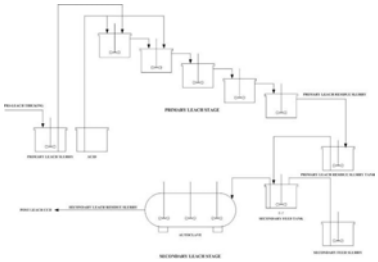

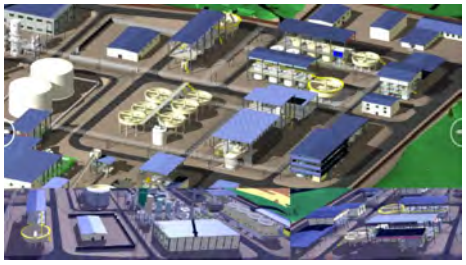

2. Leaching of Nickel Laterite Ores

Inverse Leaching Process

Leaching performance of IL process

	Primary Leach Results			Secondary Leach Results		
	Ni	Fe	Mg	Ni	Fe	Mg
Residue Solids Grade (%)	0.05	8.38	1.32	0.15	21.11	1.57
PLS Concentration (g/L)	5.08	56.70	40.11	5.29	3.40	49.41
Solids-based Metal Extraction (%)	98.40	80.63	94.56	93.44	19.94	92.65
Residue Free Acid (g/L)	18.85	(H_2SO_4)		15.39	(H_2SO_4)	
% Mass Remaining (%)	48.10			64.37		

◆ Two-stage Pressure Leaching Process

HPAL — AL process used in Indonesia

◆ **Limonite ore → HPAL**

- Ni and Co extraction > 95%
- Fe precipitation → acid release

◆ **Saprolite ore → AL**

- HPAL leached slurry is neutralized by SAP to reduce acid consumption
- Ni extraction : 40~60% (low)

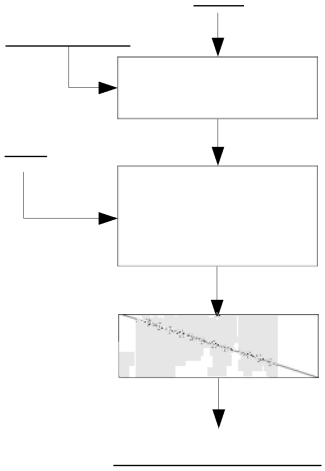

HPAL — AL process

2. Leaching of Nickel Laterite Ores

◆ Two-stage Pressure Leaching Process

HPAL — AL process used in Indonesia

◆ **Disadvantages**

- Ni extraction in AL : 50%.
- More Fe is leached when Ni extraction reaches 65~70% with acid introduction.

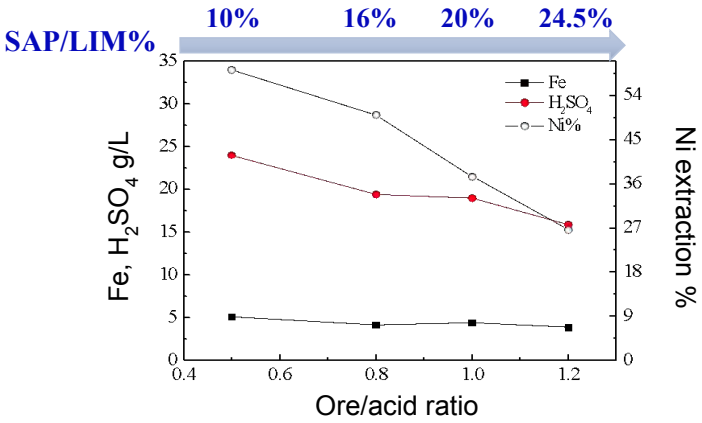

C_{Fe} comparison of HAPL and AL PLS with different SAP additions (AL remaining acid 10g/L)

SAP/LIM%	Fe, g/L	
	HPAL solution	AL solution
8	2.8	4.2
20	1.6	6.2

◆ Two-stage Pressure Leaching Process

In order to improve the inverse leaching process and HPAL – AL process, BGRIMM proposed the combinations of two-stage leaching:

- AL – PAL (95 ℃ / 150~225 ℃, 0.5~2.5 MPa)
- PAL – PAL (150~225 ℃, 0.5~2.5 MPa)
- HPAL – PAL (240~270 ℃, 3.3~5.5 MPa / 150~225 ℃, 0.5~2.5 MPa)

2. Leaching of Nickel Laterite Ores

◆ Two-stage Pressure Leaching Process

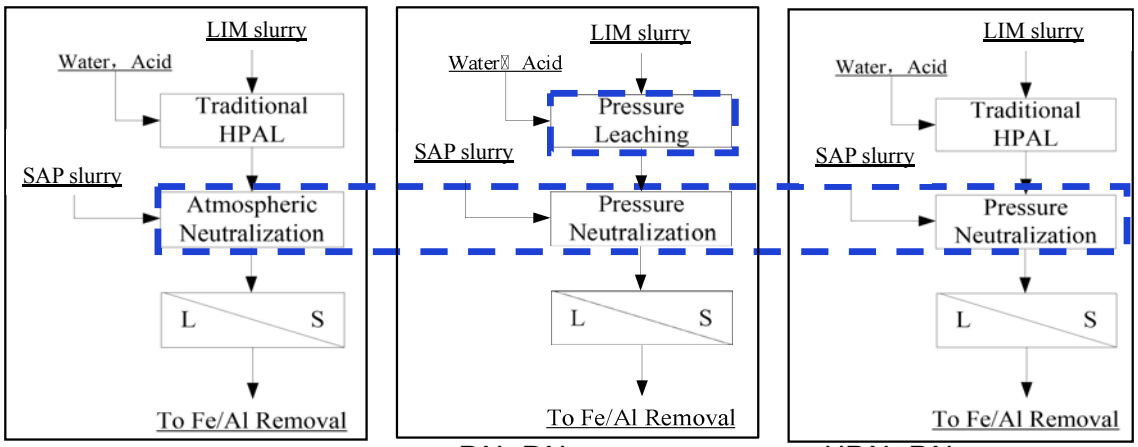

HPAL-AL process　　PAL-PAL process　　HPAL-PAL process

Patented

Two-stage pressure leaching process (PAL-PAL, HPAL-PAL)

- LIM → HPAL
- SAP → PAL: HPAL slurry flows to 2nd autoclave without flashing. SAP slurry is leached by using the heat and remaining acid of HPAL slurry.

◆ Comparison of 3 leaching combinations

Leaching conditions:

- HPAL(250℃) –AL(95℃)
- HPAL(250℃) – PAL (230℃)
- PAL(225℃) -PAL(200℃)

2. Leaching of Nickel Laterite Ores

◆ Comparison 1:

HPAL(250℃) — AL(95℃)

- HPAL: Ni extraction >97%. AL: Ni extraction 47-56%
- Total Ni extraction ~85%.

LIM/SAP		100:25		100:30		100:35	
Leaching stage		HPAL	AL	HPAL	AL	HPAL	AL
Total extraction /%	Ni	96.91	86.80	97.58	85.93	97.58	82.63
Extraction in this stage/%	Ni	96.91	56.06	97.58	55.55	97.58	47.01

◆ Comparison 2:

HPAL(250℃) — PAL (230℃)

- HPAL: Ni extraction >97%. PAL: Ni extraction 80-87.3%.
- Total Ni extraction 92-94%.

LIM/SAP		100:25		100:30		100:35	
Leaching stage		HPAL	PAL	HPAL	PAL	HPAL	PAL
Total extraction /%	Ni	97.73	94.10	97.91	93.45	96.74	92.15
Extraction in this stage/%	Ni	97.73	87.34	97.91	83.84	96.74	80.18

2. Leaching of Nickel Laterite Ores

◆ Comparison 3:

PAL(225℃) — PAL(200℃)

- PAL: Ni extraction >97%. PAL: Ni extraction 73-78.6%.
- Total Ni extraction 87.6-90.6%.

LIM/SAP		100:25		100:30		100:35	
Leaching stage		1	2	1	2	1	2
Total extraction /%	Ni	96.11	90.57	96.91	89.47	93.25	87.64
Extraction in this stage/%	Ni	96.11	78.63	96.91	75.64	93.25	73.00

◆ Comparison of 3 leaching combinations

- ◆ Use heat and remaining acid of HPAL slurry, Ni extraction greatly improved.
  SAP E_{Ni} 56% (AL)→87% (PAL); Total E_{Ni} 86% (AL)→94% (PAL)
- ◆ Under pressure condition and longer retention, more Fe/Al precipitate:
  C_{Fe} 1~2g/L (AL) → 0.75g/L (PAL); C_{Al} 6.5g/L (AL)→0.6g/L (PAL)
  Less limestone consumption and less Ni/Co losses in Fe/Al removal

Leaching stage		HPAL-AL	HPAL-PAL	PAL-PAL
Solution/(g/L)	Fe	1.18	0.68	0.75
	Al	6.53	0.63	1.44
Total extraction /%	Ni	**86.80**	**94.10**	**90.57**
SAP — Extraction/%	Ni	**56.06**	**87.34**	**78.63**

*LIM / SAP = 100 : 25

Disadvantages of current MHP Refining Process

- **Large amount Fe/Al residue results in large Ni/Co losses**
- **$CaSO_4$ crystals scaling**
  - CaO to remove Fe/Al.
  - Ca^{2+} saturated.
  - $CaSO_4$ crystals during P204 scrubbing and stripping.
  - $CaSO_4$ scaling on the wall of tank, pipes, impellers, etc..
- **Complex SX combination to separate Ni, Co and Mg**
  - Ni, Co and Mg separation with C272 and P507, respectively

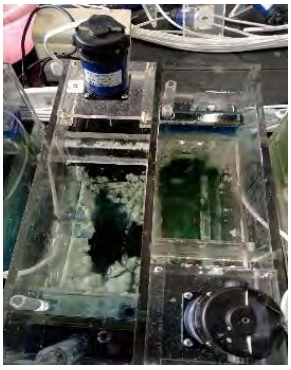

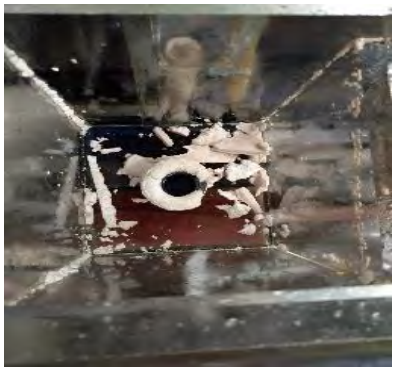

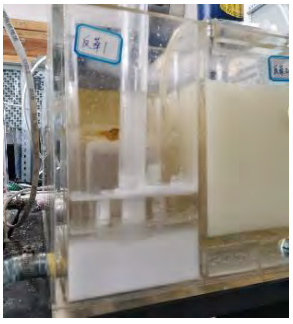

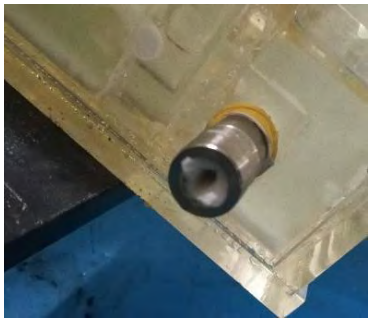

3. MHP Refining

SX isotherm

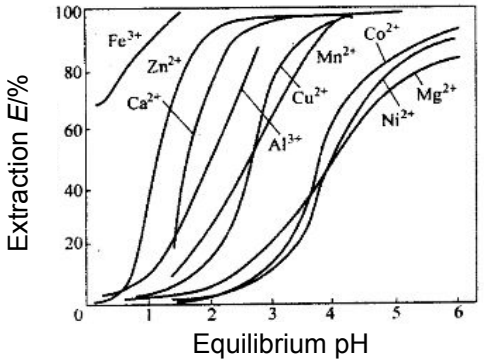

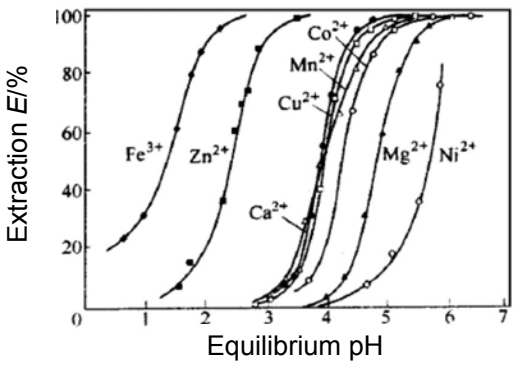

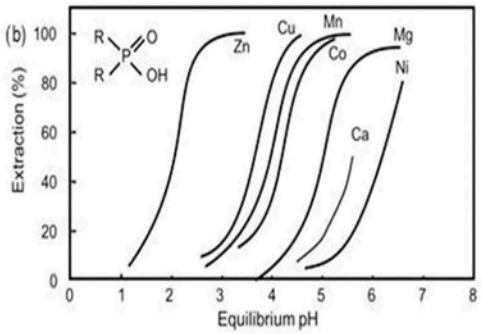

P204 (D2EPHA)

- $Fe^{3+}>Zn^{2+}>Ca^{2+}>Cu^{2+}>Mn^{2+}>Co^{2+}>Mg^{2+}>Ni^{2+}$
- P204: Cu, Zn, Ca, Mn removal

P507 (PC88A)

- $Fe^{3+}>Zn^{2+}>Ca^{2+}\sim Cu^{2+}\sim Mn^{2+}>Co^{2+}>Mg^{2+}>Ni^{2+}$
- P507: Ni, Co, Mg separation

C272

- $Fe^{3+}>Zn^{2+}>Cu^{2+}>Co^{2+}>Mg^{2+}>Ca^{2+}>Ni^{2+}$
- C272: Ni / Co separation (high efficiency)

3. MHP Refining

MHP Composition (Ramu)

Element	Ca	Co	Ni	Cr	Cu	Cd	Fe
Content/%	0.15	3.92	40.85	0.0193	0.10	<0.001	0.076
Element	Li	Mg	Mn	Si	Pb	P	Al
Content/%	<0.001	1.46	5.25	0.14	0.18	0.063	0.24
Element	Ag	Hg	Na	Ti	Zn		
Content/%	<0.001	0.12	0.34	0.014	0.73		

3. MHP Refining

MHP used to remove Fe/Al/Si

- 5~15% MHP is used in neutralization to remove Fe/Al/Si.
- Consume remaining acid.
- 90% CaO consumption is reduced. Thus, the $CaSO_4$ crystallization on scaling is reduced. Meanwhile, Fe/Al residue amount is reduced (less $CaSO_4$), and Ni&Co losses are reduced.

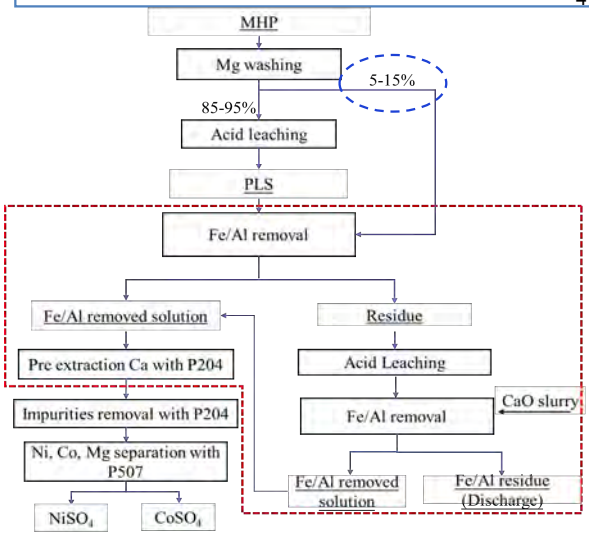

Results

% MHP addition		5.0	11.4	14.7
Final pH		4.19	4.98	5.05
Fe/Al removed solution (g/L)	Fe	<0.001	<0.001	<0.001
	Al	0.099	0.058	0.073
	Cr	0.009	<0.001	0.003
	Si	/	/	0.043

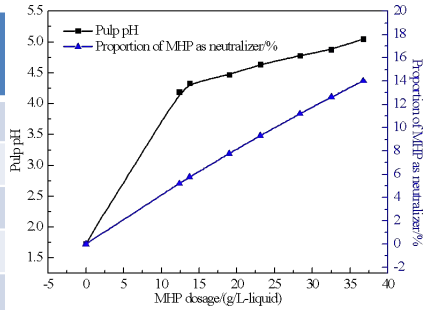

3. MHP Refining

Pre extraction Ca and purification (Cu/Mn/Zn removal) with P204

- Pre extraction Ca with P204.
- 50% Ca is removed.

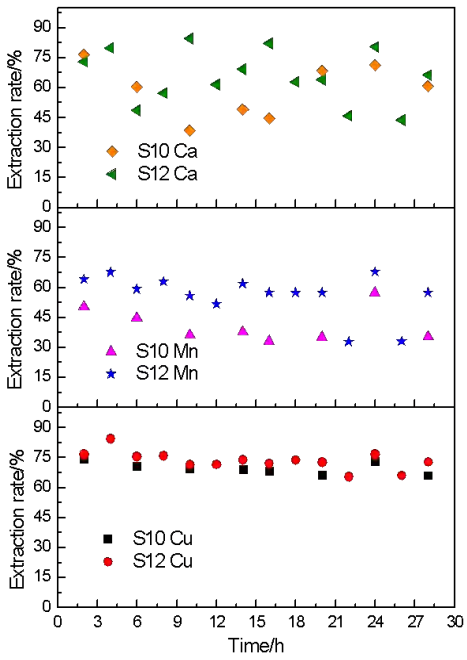

Ni/Co/Mg separation in one SX train

- 6 stages Na and Ni saponification – 8 stages Ni extraction – 10 stages Mg scrubbing – 4 stages Co stripping – 2 stages acid scrubbing.
- Ni in raffinate. Separate Mg by scrubbing. Co by stripping.

Battery grade products

Product	NiSO4.6H2O	CoSO4.7H2O
Ca	5.00	5.00
Co	5.00	
Ni		5.00
Cl	50.00	50.00
Cr	5.00	5.00
Cr6+	5.00	5.00
Cu	2.00	3.00
Cd	2.00	3.00
Fe	4.00	10.00
K	50.00	50.00
Mg	25.00	25.00
Mn	2.00	3.00
Si	50.00	50.00
Sn	5.00	5.00
Pb	2.00	2.00
Al	30.00	30.00
Mo	10.00	10.00
As	2.00	2.00
Hg	2.00	2.00
Na	50.00	50.00
Zn	2.00	3.00
Minimum Content [w%]		
Ni	22	
Co		20.5

3. MHP Refining

◆ Reduction smelting — crude nickel anode electrolysis

Hydro-process problems:

- SX process: large acid and alkali consumption, large $MgSO_4$ open circuit, large amount of waste water, large amount of hazardous wastes
- Mg removal by fluoride: superfluous F^-; F^- has negative impact on Ni electrolysis

Impurities removal by pyrometallurgy process

Reduction smelting — crude nickel anode electrolysis — anode liquid purification process

◆ Reduction smelting — crude nickel anode electrolysis

Test No.	Metal					
	Ni	Co	Mn	Fe	Cu	Zn
1	85.5	4.03	4.2	1.08	0.10	0.31
2	83.4	3.87	4.50	2.13	0.012	0.006
3	84.2	3.92	4.35	2.29	0.012	0.15
4	77.0	3.20	6.10	1.97	0.012	0.006
5	82.8	4.05	4.54	1.77	0.011	0.001
6	85.6	4.08	4.38	1.84	0.011	0.010
7	84.4	4.05	4.22	1.92	0.012	0.025

Crude nickel buttons

- Ni/Co/Cu mainly enter to metal. Crude nickel contains 80-85% nickel and 4% cobalt.
- Almost all CaO, MgO, Al_2O_3, and SiO_2 enter into slag.
- 85~97% zinc enters into dust. Zn is removed.
- 20% Mn enters into metal and 80% enters into slag.

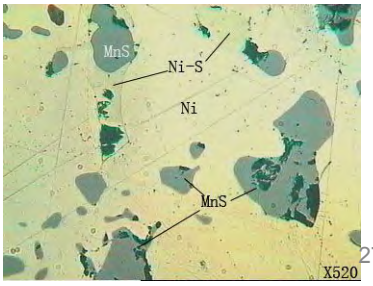

3. MHP Refining

◆ Reduction smelting — crude nickel anode electrolysis

Electrolysis test results

Test No.	Anode current efficiency/%	Cathode current efficiency/%
1	95.8	98.2
2	94.7	99.3
3	94.4	98.9
4	94.7	98.7
5	95.0	98.6
6	95.6	98.9

Nickel cathode composition

Element	Ni+Co	C	S	P	Cu	Pb
Standard*	99.96	0.005	0.001	0.001	0.01	0.001
Test	>99.96	0.0018	0.0004	<0.0001	0.0015	<0.0003
Element	Sn	Sb	Bi	Si	Mn	Mg
Standard*	0.0003	0.0003	0.0003	0.002	-	0.001
Test	<0.0002	0.0002	<0.0005	<0.001	0.0001	<0.001
Element	Zn	Cd	Fe	Al	As	
Standard*	0.0015	0.0003	0.01	-	0.0008	
Test	0.0008	0.0001	0.0021	<0.001	<0.0008	

Standard*: GB/T 6516-2010

- GB/T 6516-2010 electrolytic nickel standard
- Grade: Ni9996

4. Summary

- **Inverse leaching (IL) process is very flexible to treat LIM and SAP (Or transitional laterite ore)**
  - Ni extraction ~ 95%, at least 10% higher than ATL.

- **Two-stage pressure leaching (HPAL — PAL) process is very efficient to treat LIM and SAP**
  - Ni extraction increases greatly. SAP E_{Ni} 50% (AL) → 95% (PAL);
  - PLS: C_{Fe} 1~2g/L (AL) → 0.75g/L (PAL); C_{Al} 6.5g/L (AL) → 0.6g/L (PAL);
  - Less limestone consumption and less Ni/Co losses in Fe/Al removal.

4. Summary

- **MHP refining process -- Dissolving and SX-purification -- High pure Ni/Co - sulfates with battery grade**
  - MHP is used in neutralization, to reduce CaO consumption, thus residues and Ni &Co losses could be reduced;
  - Reduction of $CaSO_4$ crystals during impurities removal with P204 -SX;
  - Ni/Co/Mg separation with P507 in one SX - train;
  - Continous SX purification and separation flow-sheet.

- **Reduction smelting — crude nickel anode electrolysis process**
  - High recovery: Ni >97%, Co > 90%;
  - Easy removal of Ca, Mg, Al, Si, Mn and Zn (into slag / dust);
  - Suitable for low grade MHP (low cost), due to low acid and alkali consumption;
  - Environment friendly (much less wastes).

BREAKTHROUGH IN HALIDE LEACHING

By

Dave Sammut

Loop Hydrometallurgy, Australia

Presenter and Corresponding Author

Dave Sammut
dave@loophydromet.com.au

ABSTRACT

The extraction of minerals using chloride lixiviants has been thoroughly investigated and proven to offer major advantages in low-cost, highly versatile minerals processing, with an extremely low carbon footprint.

Loop Hydrometallurgy continues to innovate in advanced halide-based minerals processing. The Halion Loop™ employs mixed halides to extract copper, nickel, cobalt, lead, zinc, silver, gold, PGMs REEs and other metals from a broad range of concentrates, tailings and industrial waste materials. It operates at atmospheric pressure and less than 100 degrees Celsius, with no noxious gas emissions and no liquid effluents.

In its latest breakthrough, Loop Hydrometallurgy has proposed an entirely new form of leaching that significantly extends the capabilities of economic and efficient processing for refractory materials. This new form of leaching has undergone successful initial trials in the extraction of cobalt from pyrite tailings.

This new technology offers the prospect of near reagent-less leaching for materials that would otherwise be expected to be highly acid- or alkali- consuming by conventional hydrometallurgical processes.

By extending the capabilities of the extraction step, the Halion Loop™ has also been shown to enable significant efficiencies to be captured upstream of the concentrate, at the mine and mill.

This paper will discuss the outcomes of initial studies of the breakthrough technology, as well as some of the broader potential applications in critical and battery minerals, gold processing, the stabilisation of arsenic, and beyond. It will also discuss the outcomes of economic analysis for processing non-traditional concentrate feedstocks, including low grade and polymetallic bulk concentrates, and materials containing high levels of arsenic.

Keywords: Critical minerals, chloride leaching, halide leaching, cobalt process, hydrometallurgy

INTRODUCTION

Halide hydrometallurgy is widely recognised for its versatility[1-4]. It is capable of unlocking value from a very broad range of resources (ores, concentrates, tailings and industrial wastes) at low cost and with minimal environmental impact.

Halides are a significantly stronger lixiviant than sulphate, and significantly safer and cleaner than cyanide. Leaching in halide can be performed swiftly at atmospheric pressure, at less than 100°C, using air as the oxidant, producing no noxious gas emissions and no liquid effluents. By comparison, most sulphate-based processes require high temperatures and pressures, or long leach times to achieve similar levels of extraction.

The Halion Loop™ is based on these thoroughly-established principles of **Hal**ide **Ion** minerals extraction technology. Using a mixed halide liquor, the Halion Loop™ has been proven to achieve >99% copper extraction from a 'conventional' chalcopyrite concentrate in 4-6 hours. For the same feedstock, sulphate-based pressure oxidation would require in excess of 220°C and 35 bar to achieve similar leaching in the same period, also requiring an expensive oxygen plant; bio-oxidation would require 48 hours of leaching; and heap leaching would take up to 200 days to achieve ~60% extraction.

Additionally, halides can dissolve and extract a much broader range of metals than sulphate. Halides form soluble chelates with copper, nickel, cobalt, lead, zinc, gold, silver, PGMs and rare earth elements – plus other metals.

Chloride hydrometallurgy produces environmentally stable residues for safe and low-cost disposal, being primarily composed of hematite, elemental sulphur and (where arsenic is present in the feed) scorodite.

Given these major advantages, multiple technologies have been developed over the last 50 years that use halides exclusively or in combination with sulphate to extract copper from chalcopyrite and other minerals, none of which were ever commercialised. These developments have proven the process engineering, using common and inexpensive materials of construction including fibreglass, HDPE and PVDF, as well as some titanium.

The primary factor keeping multiple chloride technologies from getting to market was the inability of any of the previous technologies to directly recover the copper from the cuprous state in a practical and efficient manner. Maintaining the cuprous state is critical to minimising power consumption on electrowinning, requiring only one electron per atom of copper instead of two.

That problem has been solved by the Halion™ electrowinning cell, presented at ALTA 2023[5]. This novel design is the world's first practical electrowinning cell design for the continuous production and recovery of high purity copper metal from the cuprous chloride state, producing copper as dendritic powder for melting/pressing into product. It is estimated to require 70% less power than conventional sulphate electrowinning, with less than 20% of the tankhouse footprint.

Loop Hydrometallurgy's breakthrough provides the key unit operation that now makes closed-loop metal extraction in a halide lixiviant practical, effective and cost-efficient. It leverages the broad and thoroughly established global knowledge of chloride leaching and purification, then brings to application new developments for the recovery of key co-products and by-products. The company is currently commercialising that technology.

THE HALION™ LOOP

The 2023 ALTA paper[5] described the status of the Halion Loop™ technology and the breakthrough Halion™ electrowinning cell for the continuous production of high purity copper from mixed halide electrolyte.

The Halion™ Loop is a mixed-halide closed-loop hydrometallurgical process for the extraction and recovery of copper, silver, gold, PGMs and REEs from mineral concentrates.

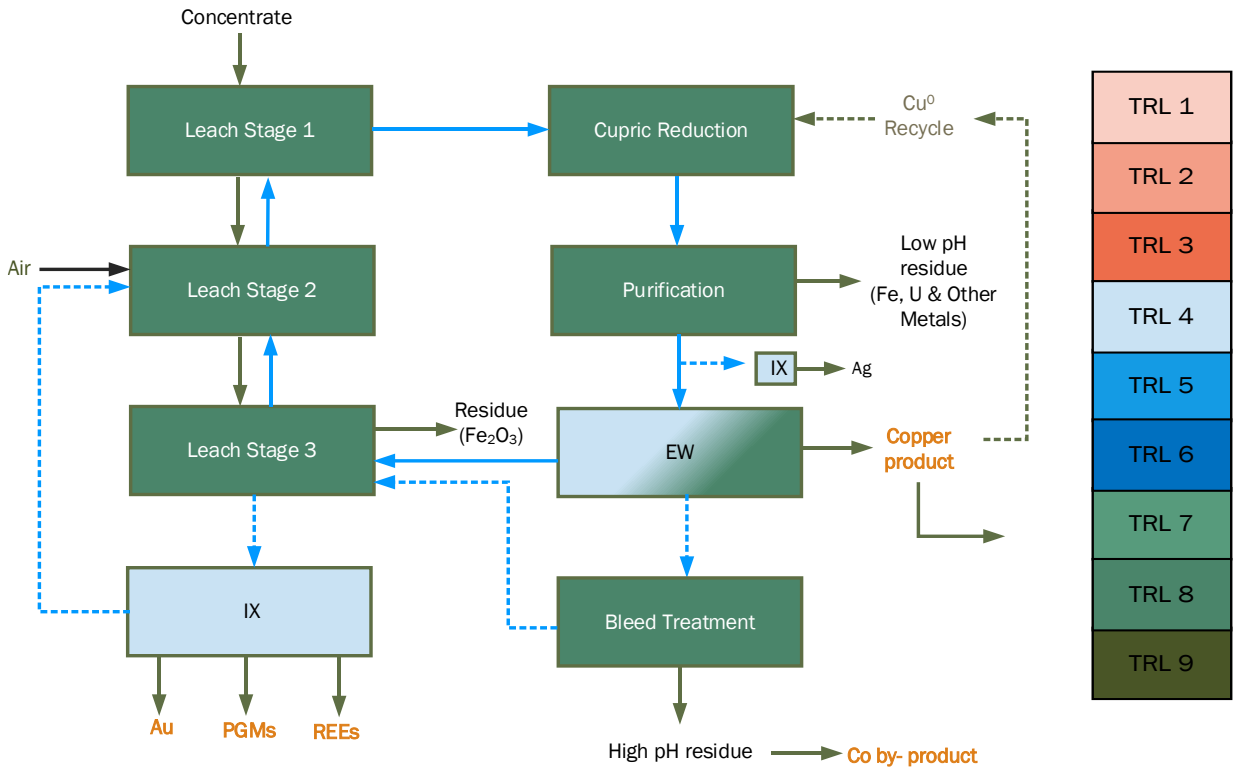

Figure 1: The Halion™ Loop Flowsheet

Table 1: Halion Loop™ Process Parameters

Operating conditions	Atmospheric pressure <100 °C >5M Cl / Br pH~2 4-6 hours leach residence time
Primary reagents	Air Sulphuric acid (if needed) Limestone (if needed)
Residues	Hematite Elemental sulphur Alkaline precipitate

Commercialisation of the Halion Loop™

The overwhelming majority of the Halion Loop™ has already been proven to TRL 7 (Figure 1). The leaching and purification of metals in chloride lixiviants has been widely studied, with pilot and demonstration plants run by multiple companies including Metso, JX Nippon Mining & Metals and Intec.

The invention of the Halion™ electrowinning cell represents the first practical opportunity to close the loop on a full process to leach, purify and electrowin metals in a single co-ordinated process.

This technology is complemented by a range of demonstrated techniques to recover a range of co-product and by-product metals: gold, silver, PGMs, nickel, cobalt, lead, zinc and potentially REEs, uranium and/or thorium.

As a direct application of these multi-element technologies, the existing and proven unit operations are available and ready to be applied at commercial scale. There are a range of immediate project opportunities to produce metal-bearing products (high grade oxide or hydroxide concentrates, sulphates or other intermediates) that could be developed swiftly and relatively inexpensively.

Some of the most immediate opportunities involve the processing of materials that are contaminated with arsenic. As a penalty element in any concentrate or intermediate product, arsenic can have a major adverse effect on operations – not just the economic penalty on sale of the product, but also the negative effect on the operation of the mill, particularly through increased costs and a reduction in total metal recovery while attempting to minimise the arsenic contamination of the concentrate.

This offers a major opportunity for the Halion Loop™ and halide hydrometallurgy more generally. Under oxidising acid conditions and with the right liquor composition, leached arsenic can be swiftly oxidised and reprecipitated as scorodite ($FeAsO_4$), which is stable and safe for disposal to tailings.

This can be leveraged to advantage at the mill by changing the operating principle to maximise metal recovery (over arsenic grade and potentially also metal grade) and minimise mill operating cost. The proven and market-ready unit operations (leaching and purification/recovery) could then be applied for the processing of that material.

In principle, this approach could be applied to unlock value from a range of 'stranded' medium- to high-arsenic resources that are currently uneconomic across the full range of base and precious metals.

Over the last 12 months, studies have continued into the various use cases of the Halion Loop™ process for metals extraction. Two particular use case studies are presented here:

1. (Fast to market) Metal extraction and recovery without electrowinning;
2. Low-grade, polymetallic, arsenic-contaminated concentrate

These studies have demonstrated the ability to unlock value from a 'stranded' copper resource that is low-grade, polymetallic (Pb/Zn) and contaminated with arsenic; and the ability to extract cobalt from low-grade pyritic tailings.

Most particularly, the first case represents a potentially significant extension of halide leaching capabilities to a broader range of low-grade concentrates and tailings, with Loop Hydrometallurgy's second major technology development. This is a new form of leaching apparatus that offers the prospect of significantly reducing the acid/base reagent requirement for the leaching of materials (such as tailings).

CASE STUDY 1: COBALT LEACHING FROM PYRITIC TAILINGS

Case Study Background

Early in 2024, Loop Hydrometallurgy was provided with a sample of cobaltiferous pyrite tailings that is known to be resistant to / uneconomic for conventional processing.

The tailings material graded <0.8% Co and >0.2% As in a 95% pyrite matrix. While no details were provided regarding the specific mineralogy of the cobalt, it can be inferred from available literature such as Holley et al[6] that the cobalt may be present as iron substitution in the pyritic host mineral.

Over the last 10 years, the cobalt price has commonly traded between US$25,000/tonne and US$35,000/tonne. (It peaked twice in excess of US$80,000/tonne). Accordingly, a viable process for these tailings needs to have an operating cost less than the minimum contained metal value (approximately US$200/tonne tailings at a cobalt price of ~US$30,000/tonne), with an allowance for both profit and repayment of capital: say US$100/t opex.

This expense limitation is exacerbated because - in the case of tailings, where the target mineral might typically be <1% of the tailings mass, instead of >40% - most of the reagent consumption will be lost to the leaching of non-value-producing pyrite, rather than extraction of valuable metals.

While it might be feasible for some tailings to roast the pyrite to form hematite – particularly as the sulphuric acid produced from the necessary capture of the resulting SO_2 gas could be reused for the cobalt leaching – this is impractical when the tailings are also contaminated with arsenic.

Understandably, few hydrometallurgical technologies seek to leach highly-refractory pyrite. Generally, leaching of pyrite only represents a cost to a given process via the consumption of oxidant, with no economic return.

Further, even if a given process only oxidises the sulphur to its elemental form rather than sulphate, and thereby only requires two electrons per sulphur atom rather than eight, every tonne of pyrite could equate to a wasted tonne of reagent. For most hydrometallurgical processes, this would require either highly-oxidising reagents or an oxygen plant.

There are many papers which discuss the use of chlorine (Cl_2), hypochlorous acid (HClO) or perchloric acid ($HClO_4$) to leach chalcopyrite, which is among the most refractory forms of copper mineral. Few of these papers mention the ability to leach pyrite.

Halide leaching could potentially provide the solution.

Experimental work – Novel Leach Approach

Loop Hydrometallurgy conducted initial testwork that confirmed that the pyrite would leach in the presence of a mixed halide electrolyte using hypochlorous acid as a reagent. As expected, the reagent consumption rates were excessive, and therefore unlikely to be economic.

This provided an opportunity to consider a new technology concept that Loop Hydrometallurgy had been developing at the time. A prototype was constructed of a novel leaching apparatus.

Scouting leach / extraction tests were conducted at 70°C and using a 'standard' Halion Loop™ lixiviant of ~6M NaCl + NaBr at 70°C, at pH <2 to 10. These tests were conducted from 3 hours to 20 hours with varying slurry densities of tailings.

The tests showed immediate and significant colour-conversion of the tailings from the original greyish colour to a very distinctive rusty brown that is characteristic of the hematite that is formed in conventional Halion Loop™ application from the hydrolysis of leached Fe^{3+}.

$$2Fe^{3+} + 3H_2O \rightarrow Fe_2O_3 + 6H^+ \quad (1)$$

XRD analysis from the early tests barely showed the evolution of the observed hematite phase, most likely because the hematite particle size in short batch tests (3-6 hours) was too small to detect. A detailed study[7] of the precipitation of iron phases from comparable mixed halide systems has previously shown that short batch tests of this system may variously precipitate hematite or goethite, but that the latter is a metastable state.

During routine continuous closed loop halide hydrometallurgical processing, small particles of iron oxide that pass through the leach filter are recycled to the beginning of the leach, and ensure hematite formation via a combination of particle aging and seeding effects. This growth of larger hematite crystals also aids in settling and filtration.

Accordingly, future batch tests may use hematite seeding to better enable hematite particle detection by XRD, with some support to filtration.

All of the successful scouting tests were conducted under highly oxidising conditions, as would be expected to be required for pyrite leaching: typically >800mV (vs Ag/AgCl).

Under these conditions, gold, silver and PGMs would also be expected to leach from any typical copper, nickel or other base metal concentrate. This is 'standard' behaviour for materials being leached in the Halion Loop™. Furthermore, under such conditions, most of the sulphur leached from the minerals would form elemental sulphur, with only a minority (typically <5%) oxidising through to sulphate.

In this application, the data suggests that the sulphur leached from the pyrite was mostly oxidised to sulphate. As example, a 20 hour leach test was conducted on a larger quantity of leach residue, to allow for periodic sampling and analysis. XRF assay of the residues and ICP analysis of filtrate samples show good mass balance closure for sulphur (2.7g difference).

These data suggested that 61% of the sulphur in the original solid (entirely present as pyrite) was leached into solution (presumably as sulphate).

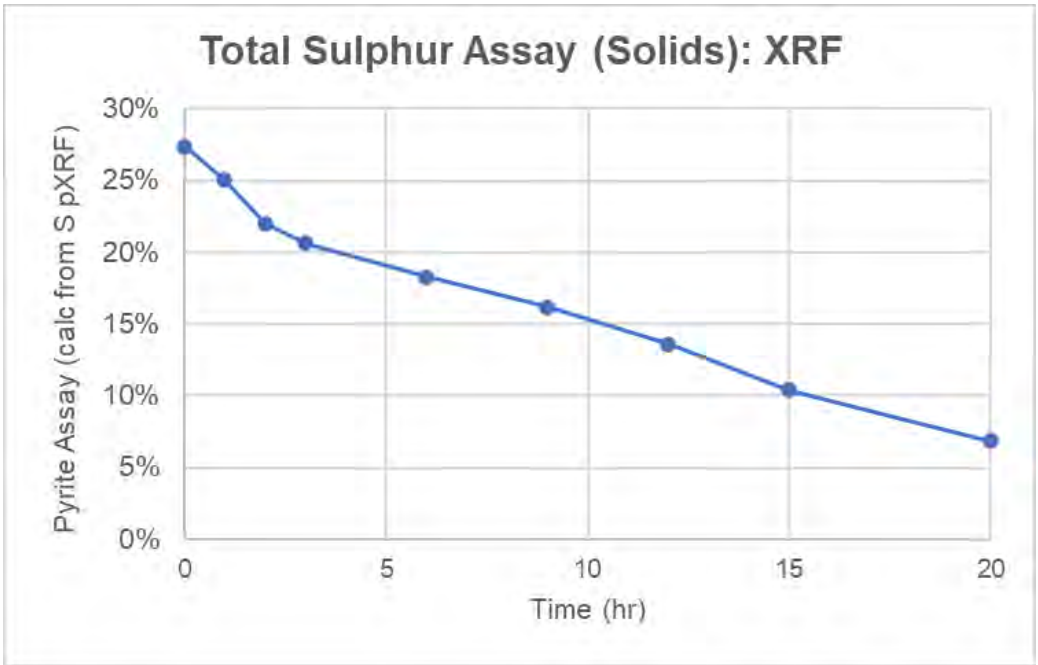

Figure 2: Change in Sulphur Content of Solids/Residues

The mineral / sulphur leaching is based on redox reactions. Indicatively, the leach half-cell reactions may include some combination of:

$$FeS_2 \rightarrow Fe^{3+} + 2S^0 + 3e^- \quad (2)$$

$$Cl_2Br^- + 2e^- \leftrightarrows 2Cl^- + Br^- \quad (3)$$

$$S^0 + 4H_2O + 6e^- \rightarrow SO_4^{2-} + 8H^+ \quad (4)$$

Based on the testing to date, it would appear that the atypically high levels of oxidation of sulphur through to sulphate are an intrinsic property of either the pyrite mineral or the conditions required to achieve pyrite oxidation. While this higher oxidant requirement is not ideal, it does have the advantage that the resulting residues will contain no species that are vulnerable to acid mine drainage. The costs of tailings management should, therefore, be commensurately lower.

For one of the alkaline test residues, a test was then conducted on the leached residue to determine the effect of reducing pH after leaching. In this test, 70% of the mass dissolved in an acid brine matrix, leaving mostly a grey-white residue of needle-like crystals, possibly gypsum or an oxidised aluminosilicate precipitate such as orthoclase or alunite.

In principle, once the pyrite host matrix is broken down, the contained metal should be liberated. Collective extraction of cobalt in this test was 64%, which corresponds to the pyrite destruction noted in the test shown in Figure 2. Similar results were obtained in testing at different pH levels.

Accordingly, it is hypothesised that as the conditions and settings of the prototype are optimised for maximum pyrite leaching, then cobalt extraction should be proportionally increased.

It is notable that throughout the entire test sequence using the prototype equipment, no chemical oxidant addition was required. While these results are not yet definitive, all indications from the scouter testing are that the new Halion™ prototype is prospective for effective and efficient leaching of pyritic tailings without the need for substantial reagent addition.

This, in turn, is prospective for a cost-effective process for cobalt extraction from the tailings. An updated prototype for the novel leaching approach has been designed for further testing.

Cobalt Recovery

The two oxidation states of cobalt (Co^{2+} and Co^{3+}) precipitate at different pH levels, just as the differing Fe^{2+} and Fe^{3+} states do. This might offer an opportunity for separation of the iron and cobalt.

Under the conditions of operation in the Halion™ liquor, gold and platinum are both known to leach, particularly in the presence of excess chloride as shown in reactions (5) to (8). Due to the concentrated salts and complex multi-element chemistry of a typical Halion Loop™ mineral leach, thermodynamic and electrochemical theoretical data has limited application. They can be used as a guide, but not absolute predictors. Using standard reduction potentials, it is not highly likely that cobaltate might form (9) under Halion Loop™ redox conditions. The standard oxidation potential for reaction (9) is more negative than that of gold or platinum:

$Au_{(s)} \leftrightarrows Au^{3+} + 3e^-$ $E^0 = -1.52V$ (5)

$Au_{(s)} + 4Cl^- \leftrightarrows AuCl_4^- + 3e^-$ $E^0 = -1.00V$ (6)

$Pt_{(s)} \leftrightarrows Pt^{2+} + 2e^-$ $E^0 = -1.2V$ (7)

$Pt_{(s)} + 4Cl^- \leftrightarrows PtCl_4^{2-} + 2e^-$ $E^0 = -0.73V$ (8)

$Co^{2+} \leftrightarrows Co^{3+} + e^-$ $E^0 = -1.92V$ (9)

Separation via ion exchange might be an option, and it is conceivable that cobalt metal could be produced using the Halion™ electrowinning cell. Either of these alternatives would be subject to testwork.

Additionally, it is entirely possible that the pyrite matrix could be broken down in such a fashion as to leave the cobalt entirely in the hematite residue. After filtration, the hematite residue might be re-acidified in a sulphuric acid solution to create cobalt sulphate as a product which might be recovered by simple crystallisation. (As noted below, elemental sulphur can be extracted from the residue to make inexpensive acid directly at site, if needed for cobalt sulphate production).

All of these options should be considered during further testwork.

CASE STUDY 2: LOW-GRADE, POLYMETALLIC, ARSENIC-CONTAMINATED CONCENTRATE

Loop Hydrometallurgy's second 2024 study concerned a use-case application of the Halion Loop™ to a stranded polymetallic copper resource.

Previous feasibility studies have found that the processing of this ore to prepare a conventional smelter-grade copper concentrate with silver and gold credits (for export) is uneconomic, because the resources is low-grade, polymetallic and contaminated with arsenic.

The mill capital and operating costs to separate lead, zinc and arsenic from the copper concentrate had proved uneconomic in previous studies. The current study examined two cases of Halion Loop™ concentrate processing:

- a 'base case' processing the smelter-grade copper concentrate (inclusive of by-product zinc, lead, silver and gold, with low penalty arsenic) to copper metal and other products; and
- an 'enhanced case' processing a bulk copper-lead-zinc concentrate (inclusive of by-product silver and gold, with high arsenic) into copper, lead and zinc metal and other products.

Basic parameters of the two study cases are shown in Table 2. Across both cases, the mineralogy was primarily enargite and tennantite, with chalcopyrite, bornite, chalcocite, covellite, sphalerite and galena, with substantial pyrite and non-sulphur gangue phases. Of these, the enargite is known to be a particularly refractory copper mineral, but has been previously proven to be highly amenable to halide leaching.

Table 2: Study Parameters

Parameter	Base Case	Enhanced Case
Concentrate		
- Tonnage	250ktpa	350ktpa
- Cu	~30%	~20
- Pb	~1%	~3%
- Zn	~4%	~11%
- As	~5%	~4%
Products		
- Cu	Metal (99.99%)	Metal (99.99%)
- Ag	Metal	Metal
- Au	Metal	Metal
- Pb	Pb/Zn concentrate	Metal (98%)
- Zn	Pb/Zn concentrate	Metal: (99%) Prime Western Grade
- S	Not recovered / (Optional recovery)	Not recovered / (Optional recovery)
- As	Stabilised for disposal	Stabilised for disposal

Process flowsheets were laid out for both cases, mass and energy balances, equipment lists, capital cost and operating cost estimates. Cost assumptions were based primarily on independent modelling performed on Halion Loop™ copper processing for the Think & Act Differently ('TAD') Ingenious Extraction Challenge in 2021 and data supplied by the project proponent.

The key outcomes of the modelling are shown in Tables 3 and 4.

Table 3: Summary of Comparative Opex Data

	Base Case US$/lb Cu	Enhanced Case US$/lb Cu
Mine & Mill	$1.47	$1.30
Halion Loop™	$0.31	$0.45
Less by-product credit	($0.80)	($1.45)
Total Cost	$0.99	$0.31

Table 4: Profit & Loss Comparison

		Base Case	Enhanced Case
Total revenue	US$M	751	855
Total operating costs	US$M	294	292
EBITDA	US$M	469	577
NPV	US$M	2,900	3,600
IRR	%	76%	77%
Payback	mth	23	23

Existing technology offered no economic solution for the ore. The application of the Halion Loop™ to this stranded resource is transformative to the site economics. Processing just a conventional copper concentrate, the Halion Loop™ offers the production of high purity copper metal on site for a total mine-to-metal production cost of less than US$1 per pound of copper, an IRR of 76% and payback period of less than 2 years.

Leveraging the advantages of the Halion Loop™ for the processing of a low-grade, polymetallic bulk concentrate alternative improves the project revenues by over US$100 million per annum, reducing operating cost to just US$0.31/lb from mine to metal.

There are many equivalent opportunities at projects in Australia and beyond. Loop Hydrometallurgy is actively investigating opportunities to unlock value from such stranded assets.

CONCLUSION

The Halion Loop™ has closed the loop on a clean, versatile and economic approach to the extraction and recovery of copper and a broad range of co-product metals.

The use of halide hydrometallurgy for leaching and purification is thoroughly established, proven and ready for implementation at commercial scale. The Halion™ electrowinning cell provides the final – and critical – unit operation to make the process completely cyclic.

The Halion Loop™ now offers the possibility of creating a paradigm shift in copper metal production, unlocking value from a range of stranded resources and greatly extending the ability to more thoroughly utilise the existing resources – even as global ore grades continue to drop.

This capability can be extended to other critical and strategic metals – notably including cobalt, nickel and REEs – and to tailings and other secondary materials.

ACKNOWLEDGMENTS

The authors would like to thank the staff and management of the Macquarie University DeepTech Incubator for supporting Loop Hydrometallurgy in its technology commercialisation programme, Brisbane Metallurgical Laboratory for its generous collaboration in the first case study, and the teams at Unearthed and BHP for the Think & Act Differently program.

REFERENCES

1. Harris, G.B., 2014, Making Use of Chloride Chemistry for Improved Metals Extraction Processes, Proceedings of the 7th International Symposium on Hydrometallurgy (Hydro 2014), v1. pp.171-184.
2. Watling, H.R., 2014, Chalcopyrite Hydrometallurgy at Atmospheric Pressure: 2. Review of Acidic Chloride Process Options, Hydrometallurgy 146, 96-110.
3. Lu, J. and Dreisinger, D., 2013, Copper Leaching from Chalcopyrite Concentrate in Cu(II)/Fe(III) Chloride System, Minerals Engineering 45, 185-190.
4. Intec Ltd., 2008. The Intec Copper Process.
5. Sammut, D., The Halion Loop: Copper Made Green, 2023, Alta 2023.
6. Holley et al, Cobalt mineralogy at the Iron Creek deposit, Idaho cobalt belt, USA: Implications for domestic critical mineral production, https://doi.org/10.1130/G51160.1
7. Sammut, D. and Welham, N.J., The Intec Copper Process: A Detailed Environmental Analysis, Green Processing Conference 2002, 115-123.

A NEW VORTEX EROSION TEST METHODOLOGY FOR EVALUATING EROSION RESISTANCE

[1]L.J.W.Graham, [2]G.Short, [3]O.Celliers,[4]G. Brown [5]D, Whyte, [6]D. Harris, [7]M. Davoody, B. [8]Nguyen and [9]J. Wu

1. Mechanical Engineer, CSIRO Mineral Resources, Clayton, Australia
2. Senior Technical Officer, CSIRO Mineral Resources, Clayton, Australia
3. Consulting Engineer, Alcoa of Australia, Kwinana, Australia
4. Technology Manager, Alcoa of Australia, Kwinana, Australia
5. Consulting Engineer, Alcoa of Australia, Kwinana, Australia
6. Research Technician, CSIRO Mineral Resources, Clayton, Australia
7. Experimental Scientist, CSIRO Mineral Resources, Clayton, Australia
8. Research Engineer, CSIRO Mineral Resources, Clayton, Australia
9. Senior Principal Research Scientist, CSIRO Mineral Resources, Clayton, Australia.

Corresponding author: Bon Nguyen
Bon.Nguyen@csiro.au

ABSTRACT

Vortices are often generated in industrial slurry flows where flow disturbances exist. These can include bolt heads, weld beads, temperature sensors and other similar flow disturbances. The vortex flow generated typically leads to changed particle impact angles and velocities creating increased localized erosion. Recent work at CSIRO's Fluids Engineering Laboratory has built on previous fundamental erosion studies to develop a standardized methodology for evaluating the erosion performance of different classes of materials under vortex erosion conditions. The fundamental design is a flat plate sample with a cylindrical obstacle protruding from it to provide the vortex generation at the junction of the sample and the cylinder. These samples are then mounted in the large-scale CSIRO slurry erosion test rig and exposed to a sand-water slurry flowing at 3.6 m/s, typical of industrial slurry applications. The erosion on each sample is measured using a coordinate measurement machine (CMM). The relative erosion of mild and alloy steels, a white iron, ceramic materials and polyurethane under vortex erosion conditions was tested using this methodology. The erosion results were then compared with ceramics showing significant resistance to vortex erosion and polyurethane the least erosion of all the materials tested. These results are discussed in terms of the erosion test methodology and improved slurry flow designs to mitigate erosion.

Keywords: Slurry erosion, vortices, fluid dynamics.

INTRODUCTION

Severe erosion attack can occur in mineral processing plants where complex fluid dynamics occurs. Vortex flows are one example of a common flow situation where erosion can be severe and have been discussed in the literature by [1] in the context of a blanked tee in pipe work and [2] who examined the flow around obstacles and the consequent erosion caused by vortices trailing from the obstacle and influencing the flow on the surface adjacent to the obstacle. A summary of the details of vortex flows caused by obstacles is given by [3] as further background on this class of flows.

Erosion testing is commonly undertaken to examine the performance of materials of construction given that selection of appropriate materials is a large part of providing erosion resistant

equipment for mineral processing applications. A recent review of slurry erosion test methods is given in [4]. They point out that erosion testing can have two aspects: i) developing fundamental understanding and material rankings or ii) development of erosion models for use in erosion predictions. Test systems reviewed include slurry pots, jet erosion, Coriolis testers and closed loop pipe tests.

In devising a new test methodology it is desirable that the conditions of the test corresponds as closely as possible to the erosion situation of interest. Given the prevalence of vortex erosion in mineral processing applications, it was desired that a vortex flow system be developed with the following characteristics:

- Consistent vortex action
- Simple geometry – to allow easy sample manufacture
- Able to be readily integrated into a slurry handling system
- Operated at velocities consistent with full scale slurry systems
- Useful for ranking the performance of materials under slurry vortex erosion conditions.

A vortex system which meets these requirements is the horseshoe vortex, well known as a fluid dynamic phenomenon. The horseshoe vortex is generated by an obstacle rising from a surface and the interaction of the oncoming flow with the obstacle. The basic concept of the horseshoe vortex is described in [5]. Fundamentally, the name is due to the shape of the vortex which forms as the obstacle causes the separation of boundary layer which then rolls up to form a vortex upstream of the obstacle. The ends of the vortex system flow either side of the obstacle giving it the characteristic shape. The horseshoe vortex has been studied as a fundamental fluid dynamics example up to recent times, both experimentally and computationally, such as by [6].

The horseshoe vortex has a real-world presence in slurry systems where obstacles are present. These obstacles can include butterfly valve shafts, bolt heads, weld beads, sensors and similar obstacles. Other applications where erosion due to a horseshoe vortex occurs are in the erosion of sediment around bridge piers as described in [7]. The horseshoe vortex is thus considered to be a realistic flow which can be used as a test system for erosion resistance evaluation.

Recently CSIRO and Alcoa have developed a test procedure to use when ranking materials for service in cases where vortex erosion might be expected to occur in slurry flows. The philosophy of the test is to test the materials under a consistent vortex flow with solid particles providing the erodent. This procedure provides a flow similar to the expected service conditions, thus the ranking of material performance should be realistic. The horseshoe vortex as described above is generated in the test rig at CSIRO in such a way that the erosion is applied to flat material samples. The present paper describes the details of the horseshoe vortex test and presents example results of erosion tests of materials of interest in slurry handling.

EXPERIMENTAL FACILITY

A slurry flow loop test facility was developed at the CSIRO Fluids Engineering Laboratory to perform the test program (Figure 1 a). The rig consisted of a 3000L agitated holding tank together with a Warman 4x3 centrifugal pump to provide the flow. The pump was controlled by a Danfoss Variable Frequency Drive. A Rosemount magnetic flow meter was installed in the flow loop to monitor the slurry flow rate. The tank was fitted with cooling coils connected to a chilled water system so that extended runs could be made without the slurry overheating.

Pairs of the vortex erosion samples were installed in square test sections of 53 mm by 53 mm internal dimensions. The square cross-section test sections were 1.89 m in length. Flat material samples were used in these tests with the obstacle being provided by a ceramic covered pin, generating a horseshoe vortex as discussed in the introduction and shown in Figure 1 b. A total of up to12 flat samples can be tested in the rig simultaneously together with up to three cylindrical samples if required [8]. The sample holders are installed vertically in the rig to avoid the effects of stratification of the solids concentration profile.

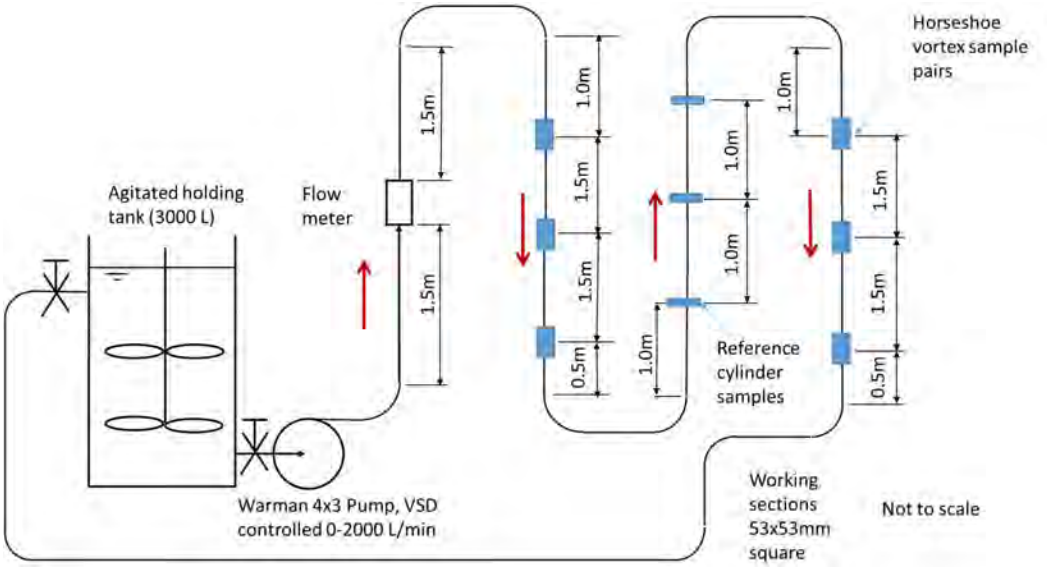

(a)

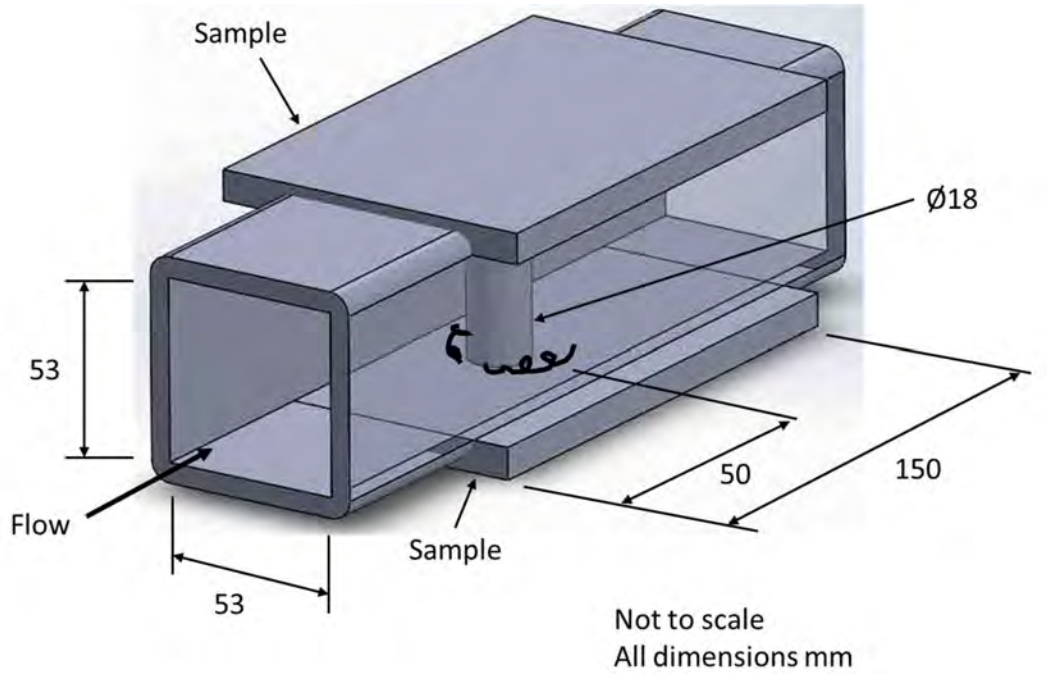

(b)

Figure 1 Erosion Test Rig Set-up schematic. (a) Test rig schematic, (b) test section for vortex erosion samples.

All erosion measurements were made using a Sheffield Discovery II Coordinate Measurement Machine (CMM) as shown in Figure 2. The CMM consists of a computer-controlled touch probe which is used to scan the surface of the object of interest. The repeatability of measurements made using the CMM was of the order of 3 μm as tested by repeat measurements of uneroded samples. The design of the obstacle included a step to leave an uneroded surface in the immediate vicinity of the mounting hole. This feature removed the need to take a CMM scan before

the test as the uneroded surface was able to be used as the reference surface with erosion measurements being taken relative to this surface. This procedure removes one level of uncertainty in the erosion measurements as the erosion measurement is a single measurement rather than two separate measurements taken on separate occasions.

Figure 2. Sheffield Discovery II Coordinate Measurement Machine (CMM) at CSIRO Fluids Engineering laboratory

The slurry used for the test program comprised sand and tap water with sand at a concentration of 12% by volume. All tests used Sibelco Incast 70 sand with a d_{80} of 260 micron as the erodent. The parameters of the test run are given in Table 1. Figure 3 shows a Scanning Electron Microscope micrograph of the particles.

Table 1. CSIRO 2" Slurry Erosion Loop Facility Parameters

Pump description	4x3AH Weir Minerals
Test section pipe ID	53mm
Pipe loop length	~20m
Holding tank volume	~2500 L
Solids concentration	12 %v/v
Particle size d80	~260µm
Flow rate	600 L/min
Velocity	~3.6 m/s

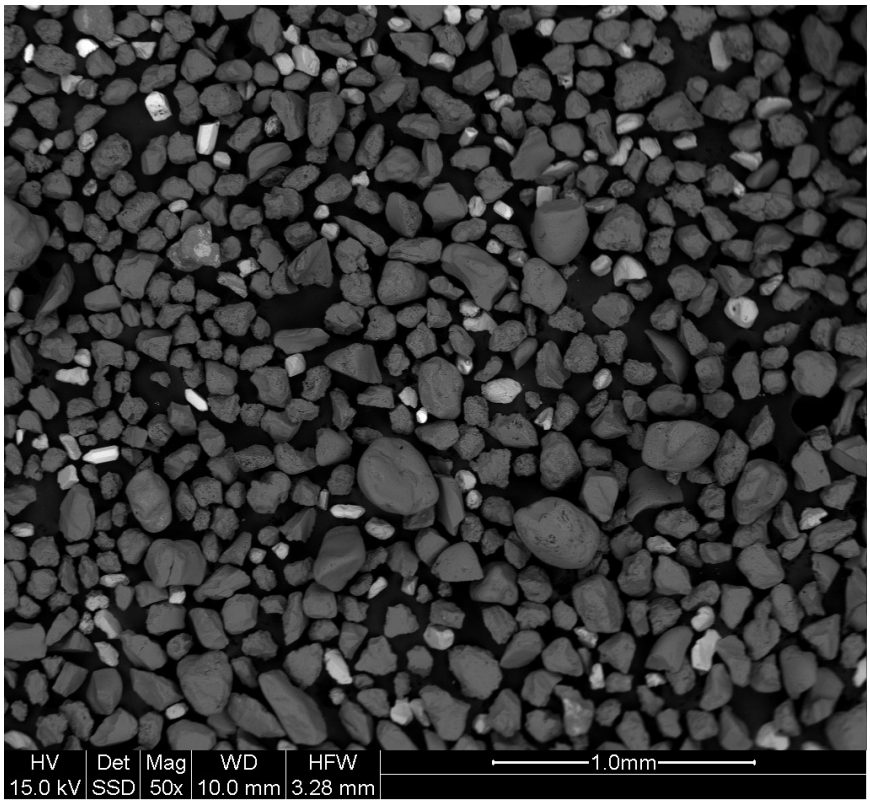

Figure 3. Scanning electron microscope micrograph of Sibelco Incast 70 sand particles.

RESULTS

The experimental duration for the test run reported here was 244 hours after which the samples were removed from the test rig and measured using the CMM. The normalized maximum erosion results relative to the mild steel sample are given in Table 1 for each sample. The highest erosion measured was from the mild steel sample. The polyurethane showed the least erosion of the vortex erosion samples from this series of tests.

Table 2. Erosion test results, after 244 hours of operation, normalized with respect to the mild steel. Test velocity 3.6m/s.

Sample	Normalized Maximum erosion
Mild steel	1.000
Bisalloy	0.754
White iron	0.270
Alumina 99.6%	0.107
Silicon carbide sintered	0.039
Polyurethane	0.013

Photographs of the erosion samples after the test are shown in Figure 4 to Figure 6. The characteristic erosion scar due to the erosion generated by the horseshoe vortex is readily identifiable, at least on the white iron and steel samples. It is less obvious on the ceramic and

polyurethane samples where the erosion is much less, although the shape of the vortex and its trailing ends is clear on the sintered silicon carbide sample. Evidence of vortex driven erosion is also visible on the alumina sample.

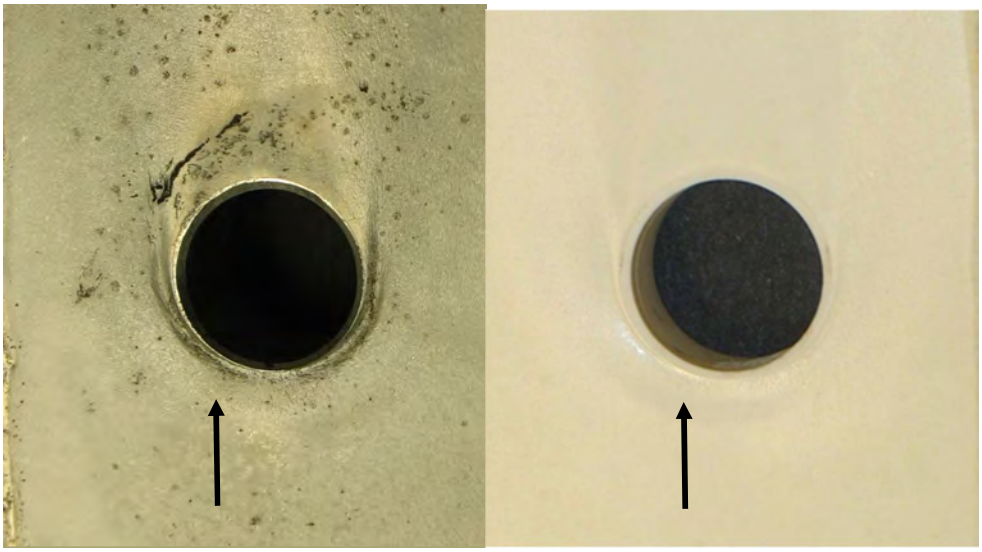

(a) (b)

Figure 4. (a) White iron and (b) 99.6% Alumina after vortex erosion test, 244 hours.

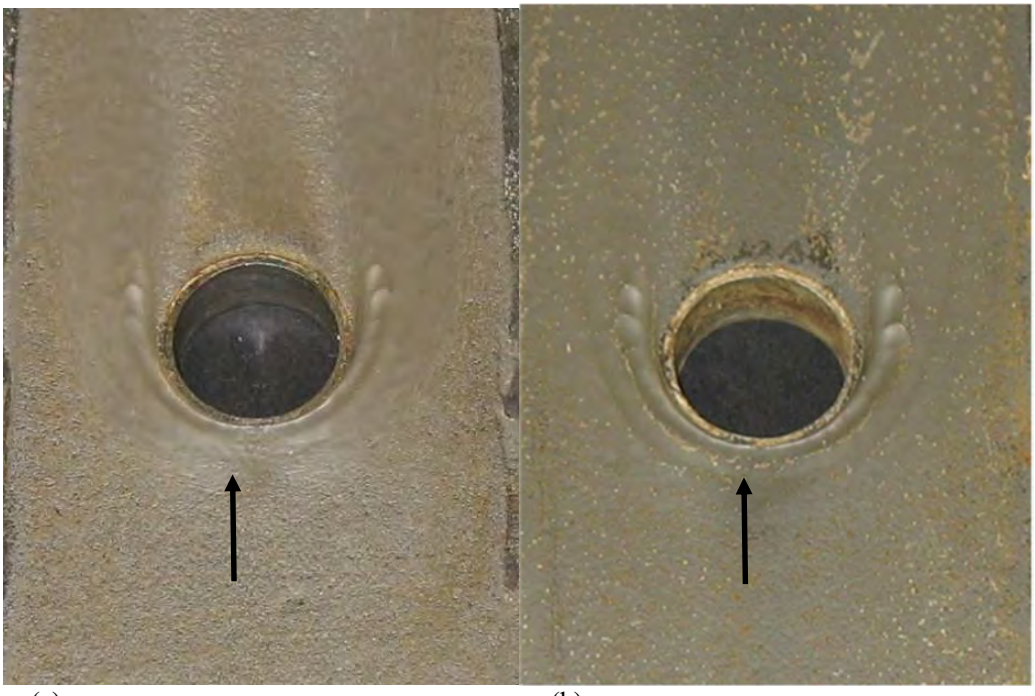

(a) (b)

Figure 5. (a) Bisalloy and (b) Mild steel after vortex erosion test, 244 hours.

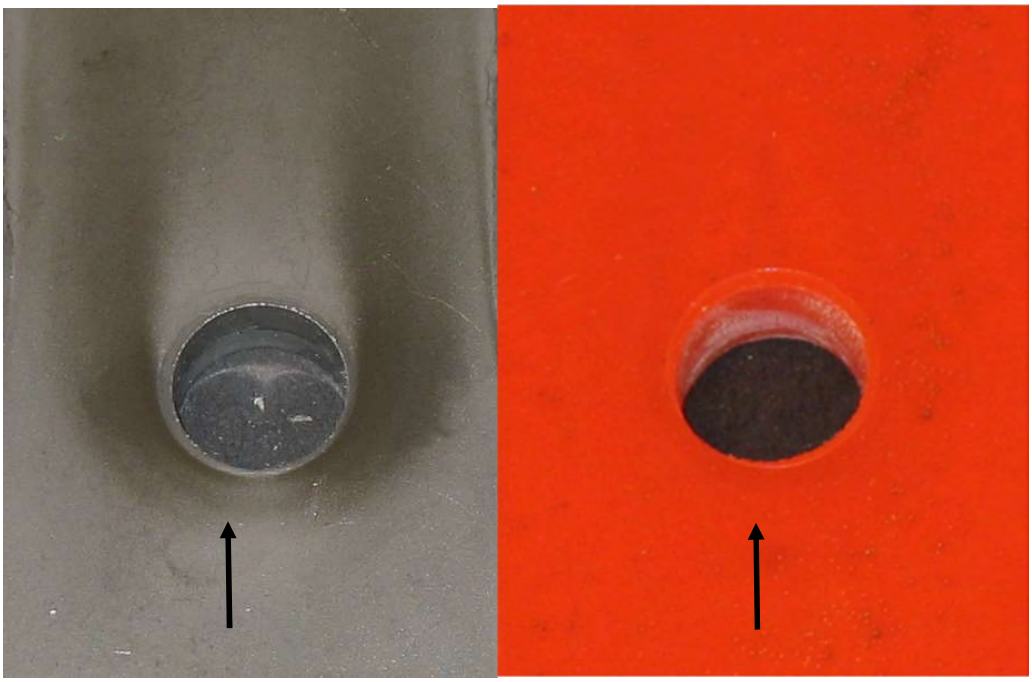

(a) (b)

Figure 6. (a) Sintered Silicon carbide and (b) Polyurethane after vortex erosion test, 244 hours.

RELEVANCE TO MINERAL PROCESSING INDUSTRY

Erosion of mineral processing equipment relevant to the alumina industry has been discussed in [9] including heat exchangers, and a positive displacement pump discharge accumulator, both of which showed vortex erosion damage. Other work by some of the present authors, [10], examined vortex erosion known to occur on the blanked leg of slurry pipeline tee-junctions, building on previous work by [1]. Similar equipment is common in many hydrometallurgical applications with similar erosion issues. Changes to the flow geometry to reduce erosion have been discussed in [9] and is one available approach to reduce erosion severity. Otherwise, the effects of vortex erosion on materials as discussed in the present work can inform material selection in areas vulnerable to vortex erosion.

There is potential in the method described in this paper to explore other aspects of vortex erosion such as the effects on target materials due to changes in:

- Particle size
- Particle shape
- Particle concentration.

It is known that these parameters are of significance to erosion but the effects under vortex conditions are not yet clear. For instance, smaller particles may follow vortices in a different way to larger particles thus leading to different erosion behavior which is not necessarily intuitive. Particle shape can also depend on whether the eroding material is milled and to what degree. Further test work is desirable to explore these issues and their effects on erosion so that full scale erosion can be better modelled and mitigated.

The authors also suggest that equipment vendors consider providing material erosion test data under vortex erosion conditions to potential customers in the mineral processing industry. Given

the prevalence of vortex erosion in hydrometallurgical plants, such data would be valuable to allow for the optimal selection of materials for erosion service.

CONCLUSIONS

An experimental test program was undertaken at the CSIRO Fluids Engineering to measure the vortex erosion on a variety of samples. A new test rig and procedure was developed to provide a vortex flow thus providing a realistic vortex erosion scenario. Sand particles (Sibelco Incast 70) were used as eroding materials. The present tests were 244 hours duration.

For the materials used in the present tests the polyurethane showed the least erosion of the vortex samples with the mild steel sample showing the most erosion.

Erosion due to the presence of vortex generating obstacles in a slurry flow is a relevant and common issue for mineral processing plants. Understanding the response of materials to these conditions can assist in mitigating the effects of erosion especially if used in conjunction with fluid dynamics design changes which can also reduce the severity of the erosion. A standardized test to cover the vortex erosion case such as that described here would be useful for equipment vendors and clients alike to assist the selection process for the most appropriate materials for these erosion conditions. Such a test could be used in addition to the conventional erosion test data already available.

ACKNOWLEDGMENTS

The authors gratefully acknowledge the support of Alcoa of Australia for this work and the CSIRO workshop for manufacturing the test rig.

REFERENCES

1. Brown, G.J., *Erosion prediction in slurry pipeline tee-junctions.* Applied Mathematical Modelling, 2002. **26**(2): p. 155-170.
2. Graham, L.J.W., D.R. Lester, and J. Wu, *Quantification of erosion distributions in complex geometries.* Wear, 2010. **268**(9-10): p. 1066-1071.
3. Simpson, R.L., *Junction flows.* Annual Review of Fluid Mechanics, 2001. **33**: p. 415-443.
4. Javaheri, V., D. Porter, and V.T. Kuokkala, *Slurry erosion of steel - Review of tests, mechanisms and materials.* Wear, 2018. **408**: p. 248-273.
5. Baker, C.J., *THE TURBULENT HORSESHOE VORTEX.* Journal of Wind Engineering and Industrial Aerodynamics, 1980. **6**(1-2): p. 9-23.
6. Kirkil, G. and G. Constantinescu, *Effects of cylinder Reynolds number on the turbulent horseshoe vortex system and near wake of a surface-mounted circular cylinder.* Physics of Fluids, 2015. **27**(7).
7. Guan, D.W., et al., *Characterization of horseshoe vortex in a developing scour hole at a cylindrical bridge pier.* International Journal of Sediment Research, 2019. **34**(2): p. 118-124.
8. Lester, D.R., L.A. Graham, and J. Wu, *High precision suspension erosion modeling.* Wear, 2010. **269**(5-6): p. 449-457.
9. Graham, L., et al., *Reduction of slurry erosion by flow design*, in *11th AQW International Conference* 2018: Gladstone, Australia. p. 308-314.
10. Graham, L.J.W., et al., *Laboratory modelling of erosion damage by vortices in slurry flow.* Hydrometallurgy, 2017. **170**: p. 43-50.

MODULARIZATION OF HPAL AND POX UNITS IN NICKEL & COBALT INDUSTRIES

By

Peng Si, Ming Liu, [2,3]Jim Cainglet, Molly Zhu

Morimatsu Engergy & Materials, China
[2]Morimatsu Singapore, Singapore
[3]Morimatsu-Dialog, Malaysia

Presenter and Corresponding Author

Peng Si
sipeng@mori-matsu.com

ABSTRACT

The application of the pressure leaching process, especially HPAL and POX, in nickel and cobalt industries has seen dramatic growth in recent years, driven by the rapid development of the EV industry. In the past 3 years, more than 20 autoclaves have been delivered to Indonesia for HPAL projects, all of which were successfully ramped up and exceeded the production target in less than one year. Meanwhile, more and more POX projects are being built in China, Indonesia and South Korea, with nickel matte from laterite as the feedstock.

The success of HPAL projects in recent years is based on the lessons learned on engineering, commissioning and ramp up of previous HPAL projects in Australia, Papua New Guinea, Philippines, New Caledonia, Turkey and Madagascar. Although the POX of nickel matte from laterite is newly introduced, the previous POX projects treating nickel matte from nickel sulphide in China and Canada and MS from laterite in Australia, Madagascar and China, provided the engineering templates and commissioning experience.

Different from previous projects, the process and layout of recent HPAL and POX projects were more like templated, with only distinctions on sizing of equipment, pumps, valves and pipes. Modularization of leaching plants are hence quite suitable for HPAL and POX projects in the nickel and cobalt industries, providing schedule certainty, cleaner and safer environment, skilled worker team, reduced site labor and peak, shorter installation time on site, lower environmental/socioeconomic impact and less disturbance by local situation. For those inland projects subjected to transportation limitations of large size modules, a high degree of prefabrication will be an alternative solution.

Keywords: HPAL, POX, Nickel, Cobalt, Module, Modularization, laterite, matte

Modularization of HPAL and POX Units in Nickel & Cobalt Industries

Si Peng
sipeng@mori-matsu.com
Morimatsu Energies & Materials

Solutions by Morimatsu to HPAL and POX Projects:

Autoclaves, Preheaters, and Flash Vessels

Detail design and fabrication, including autoclaves, preheaters, and flash vessels, etc.

Agitators

Detail design and fabrication of Agitating system, including agitator blade, shaft, mechanical seal, flushing system, cooling system, etc.

Modules

Modularization of HPAL and POX system, including module design, fabrication, and pre-assembly. Detail design of piping, pumps, valves, steel structures and E&I.

HPAL-High Pressure Acid Leaching of Laterite

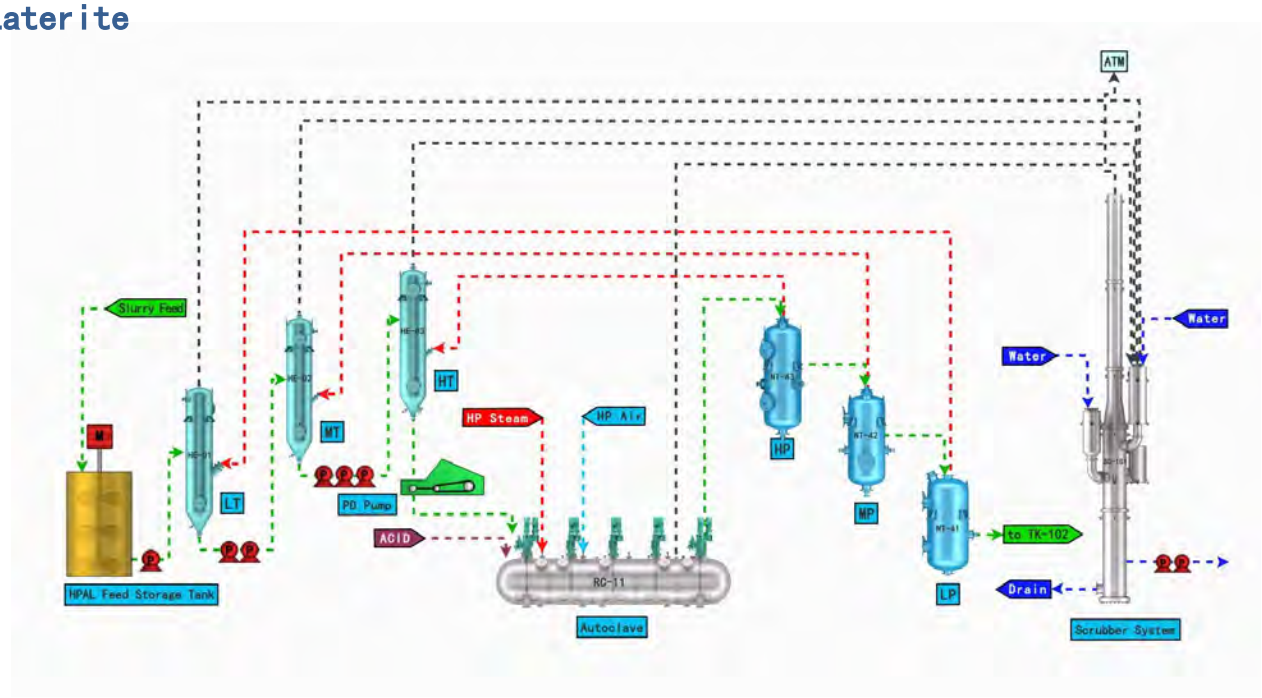

POX - Pressure Oxidation of Ni Matte

MORIMATSU
Your Needs · Our Drive

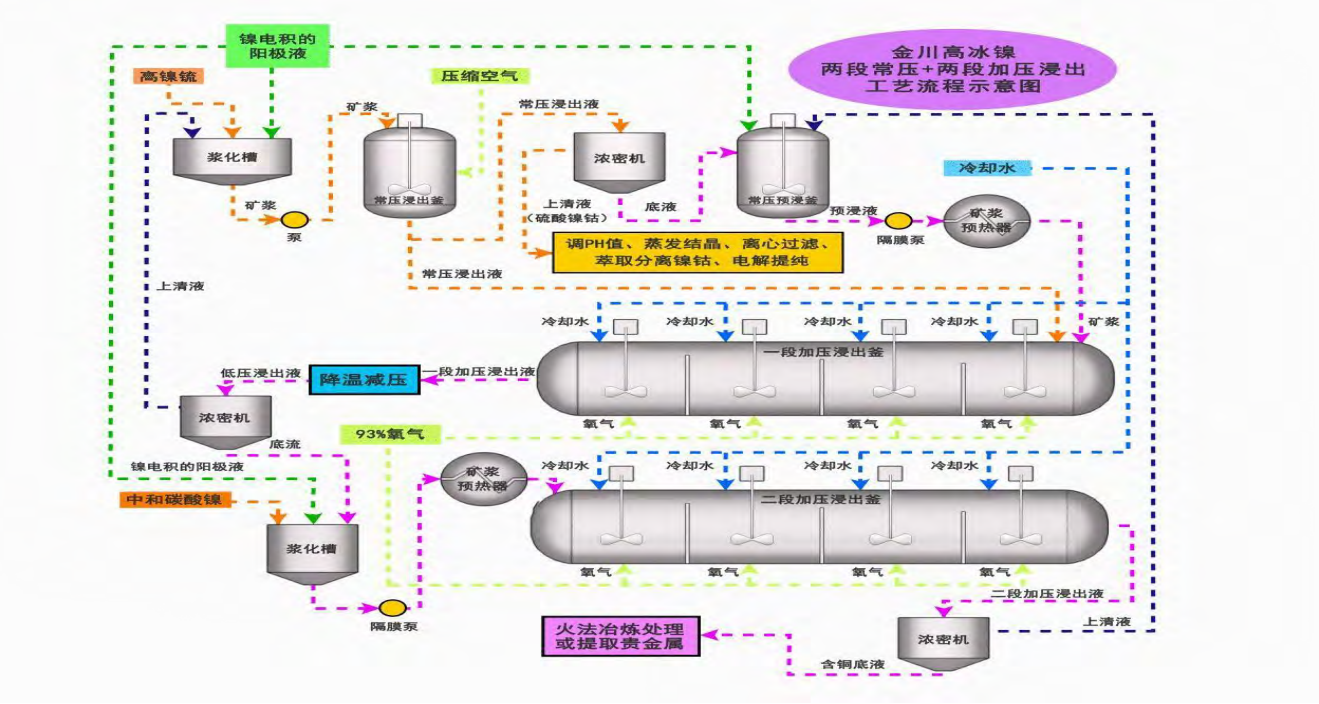

Autocalves for Amabtovy & Ramu HPAL Projects

Size： ID5230xL42400x(118+8)t

Material： SA-516 Gr.70N+SB-265 Gr.17

Delivered in 2008, Madagascar

Size： ID5100xL39300x(118+8)t

Material： SA-516 Gr.70N+SB-265 Gr.17

Delivered in 2009, Papua New Guinea

Autoclave for Meta Gordes HPAL Project

Size: ID5200xL32500x(118+8)t

Material: SA-516 Gr.70N+SB-265 Gr.17

Delivered in 2013, Turkey

Autocalves and Agitators for Lygend HPAL Project

Size: ID5300xL41500x(126+6)t

Material: SA-516 Gr.70N+SB-265 Gr.17

Delivered in 2020, OBI Island, Indonesia

Autoclaves for Huayue and Huafei HPAL Projects

Size: ID5300xL41500x(126+6)t

Material: SA-516 Gr.70N+SB-265 Gr.17

Delivered in 2020, Morowali, Indonesia

Size: ID5900xL44200x(140+8)t

Material: SA-516 Gr.70N+SB-265 Gr.2

Delivered in 2022, Weda Bay, Indonesia

Autoclaves and Agitators for QMB HPAL Projects

Size: ID4800xL33000x(115+6)t

Material: SA-516 Gr.70N+SB-265 Gr.17

Delivered in 2021, Morowali, Indonesia

Size: ID5900xL44900x(138+6)t

Material: SA-516 Gr.70N+SB-265 Gr.17

Delivered in 2023, Morowali, Indonesia

Autocalves and Agitators for Jinchuan Ni/Co POX Projects

Feedstock: Ni matte, MSP, Ni/Cu alloy, Co alloy

Size: ID1800xTT6800 Materials: Q345R+TA1
Size: ID2500xTT8600 Materials : Q345R+TA1
Size: ID3200xTT6500 Materials : Q345R+TA1
Size: ID3800xTT19000 Materials : Q345R+TA1

Autocalves and Agitators for Huayou Ni/Co POX Projects

Feedstock: Ni matte, MSP, Co/Cu Sulphide, Co alloy

Size: ID3900xTT20000 Materials: Q345R+TA2
Size: ID3400xTT13500 Materials: Q345R+TA2
Delivered in 2021 and 2022, China

Size: ID3900xTT24000 Materials: Q345R+Bricks
Size: ID3900xTT18000 Materials: Q345R+Bricks
Delivered in 2014 and 2021, China

Autocalves and Agitators for Nickel Matte POX Projects

Feedstock: Ni matte

Size: ID3900xTT20000Materials: Q345R+TA2
Delivered in 2023, South Korea

Size: ID3900xTT20000 Materials: Q345R+TA2
Delivered in 2023, China

HPAL Modules for QMB Project

Size: 18m(L) ×20m(W)
×30m(H)
Capacity: 2 KTA, Laterite
Location: Indonesia
Delivered: 2020

Morimatsu Scope

Engineering
Feasibility Study
Basic Design
Detail & Shop Design

Procurement
Static & Rotary EQ
E&I, Piping, Valve
Structure Steel

Construction
Fabrication, Assembly
Inspection, FAT
Erec., Com Support

HPAL Modules for Excellen-Silo Project

Size: 24m(L) ×22m(W)
×38m(H)
Capacity: 10 KTA Ni, Laterite
Location: Indonesia
Delivered: 2023

Morimatsu Scope

Engineering
Feasibility Study
Basic Design
Detail & Shop Design

Procurement
Static & Rotary EQ
E&I, Piping, Valve
Structure Steel

Construction
Fabrication, Assembly
Inspection, FAT
Erec., Com Support

Ni Matte POX Modules for GEM Project

Size: 25m(L) ×20m(W) ×24m(H)
Capacity: 20 KTA Ni, Matte
Location: China
Delivery: 2023

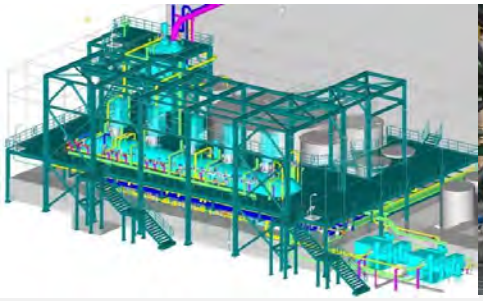

Morimatsu Scope

Engineering
- Feasibility Study
- Basic Design
- Detail & Shop Design

Procurement
- Static & Rotary EQ
- E&I, Piping, Valve
- Structure Steel

Construction
- Fabrication, Assembly
- Inspection, FAT
- Erec., Com Support

Modularization

- ✔ Modularize the building in order to install the process and utilities to one functional unit.
- ✔ Modularize the process into a functional skid.
- ✔ Pre-installation of equipment, piping, electrical and HVAC in the workshop.
- ✔ The numbers of interfaces and installation on site will be minimized.
- ✔ Pre-testing of the modular building with process installations before shipping to final site.
- ✔ Disassembling and re-assembling on site.

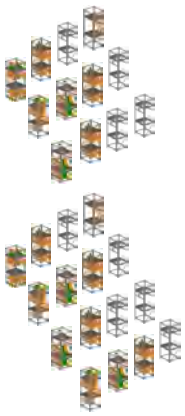

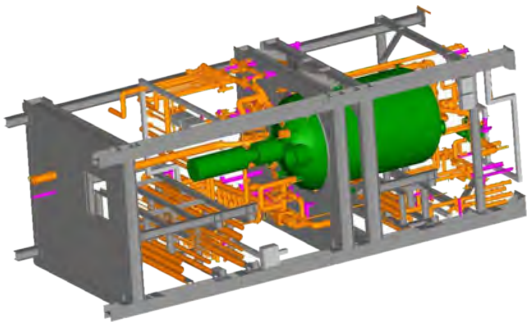

Business Drivers for Modularization

✔ Schedule Certainty

Shorten Schedule through Parallel Activities

80-90% of the fabrication is completed at Morimatsu Workshop

✔ Transplantable & Compatible

Easy for disassembly and reassembly
Facilitate Maintenance & Convenient for renewal

Possible for relocation to meet global market strategy

✔ Competitive Cost

Economic Return for Early Operation

Cost Reduction for Repeated Projects

Business Drivers for Modularization

✔ Benefits of Offsite Construction----Improved Quality & Safety

Cleaner and safer environment

Skilled worker team

Avoid the conflict with other construction teams at client site

Reduced site labor and peak

Shorter installation time on site
Easy to do commissioning at workshop

Lower environmental/socioeconomic impact

Less disturbance by local situation

- Bad Environment
- Poor Infrastructure
- Inefficient / Expensive Local Team
- Unstable Political Environment

Layout and Modularization plan for HPAL Plants

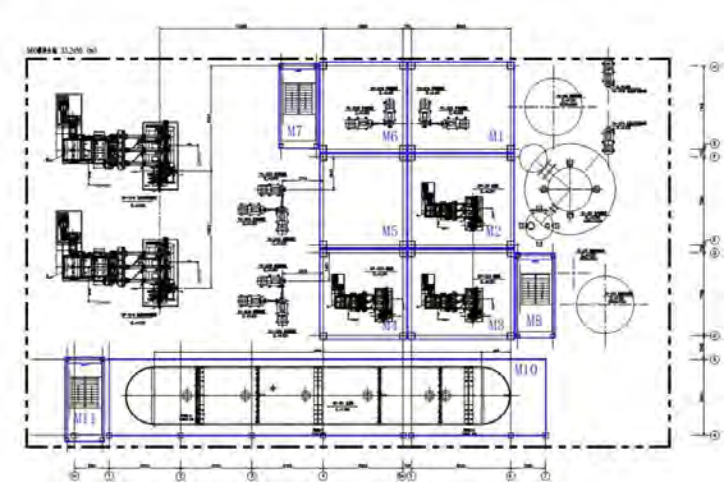

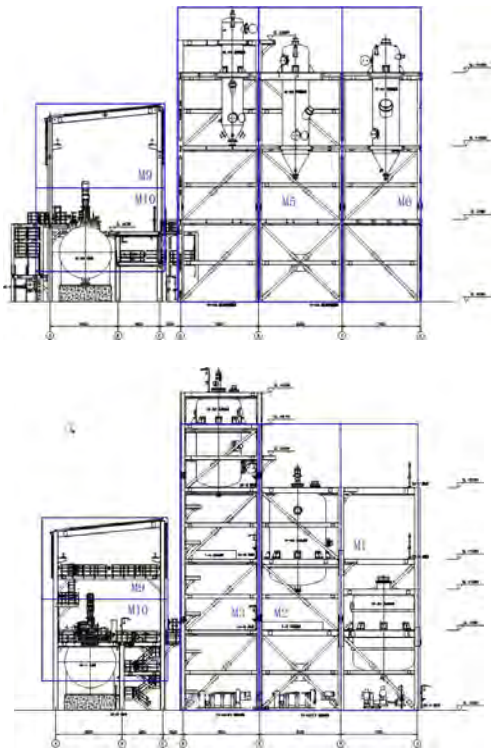

Layout and Modularization plan for HPAL Plants

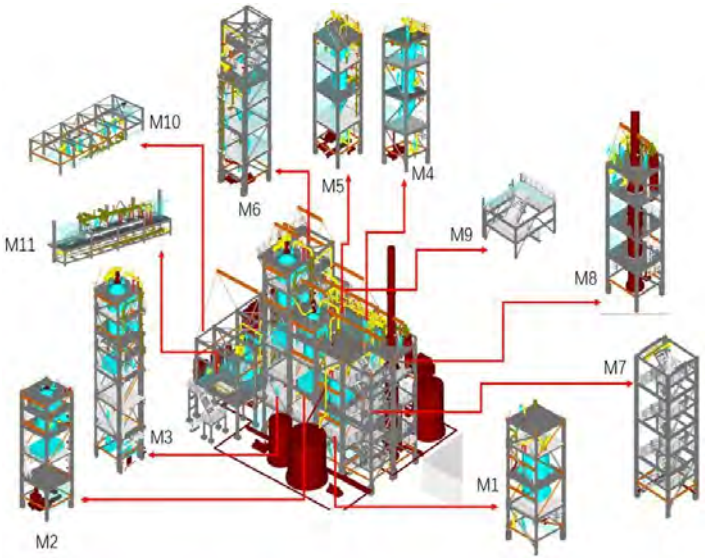

Module List	
M1	LP flash vessel module
M2	MP flash vessel module
M3	HP flash vessel module
M4	LT preheater module
M5	MT preheater module
M6	HT preheater module
M7	High Staircase module
M8	Scrubber module
M9	Reactor staircase module
M10	Reactor roof module
M11	Pipe rack module

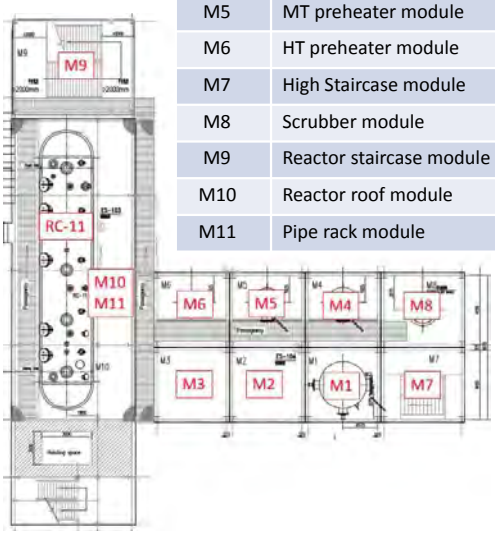

Assembling Plan for HPAL Modules

Step 1: Autoclave	Step 2: M11 Pipe rack module
	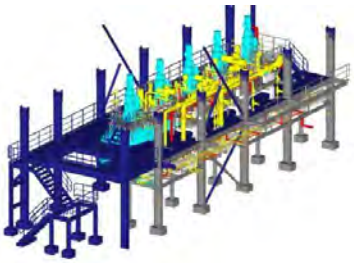
Step 3: M10 Reactor roof module	**Step 4: M9 Reactor staircase module**
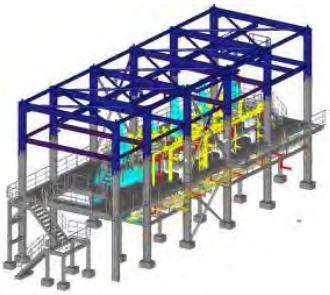	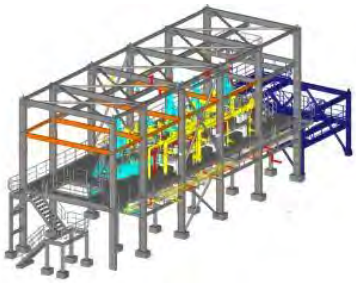

Assembling Plan of HPAL Modules

Step 5: M6 HT preheater module	Step 6: M3 HP flash vessel module
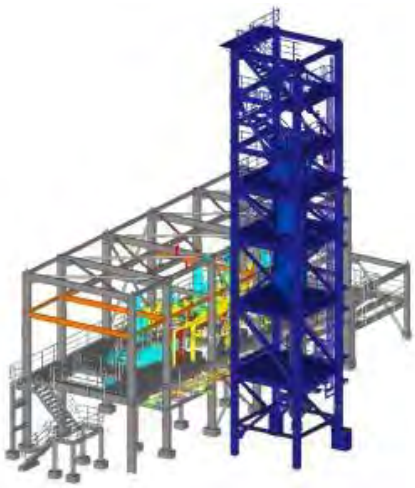	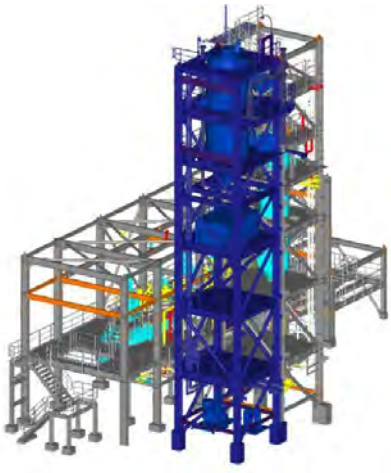

Assembling Plan of HPAL Modules

Step 7: M5 MT preheater module	Step 8: M2 MP flash vessel module

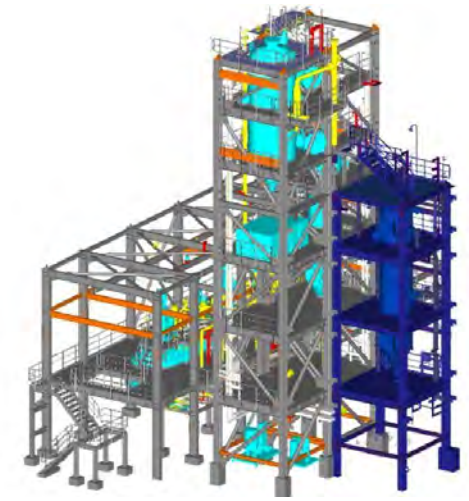

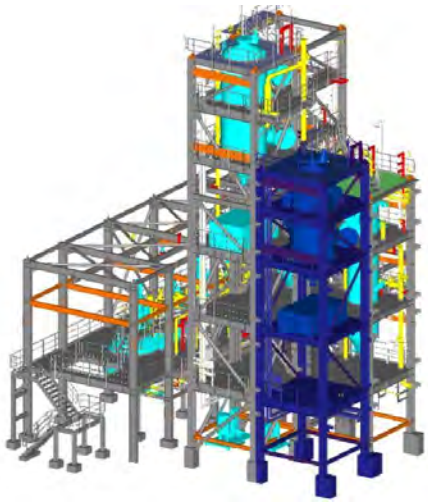

Assembling Plan of HPAL Modules

Step 9: M4 LT preheater module	Step 10: M1 LP flash vessel module

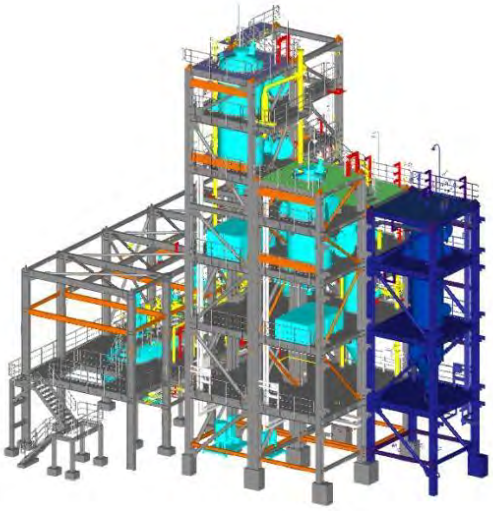

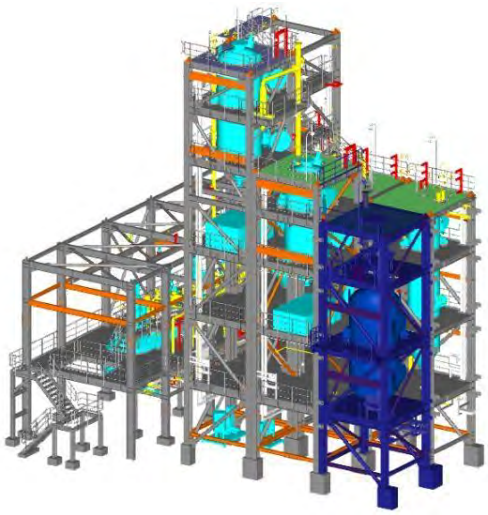

•Assembling and disassembling at Morimatsu workshop


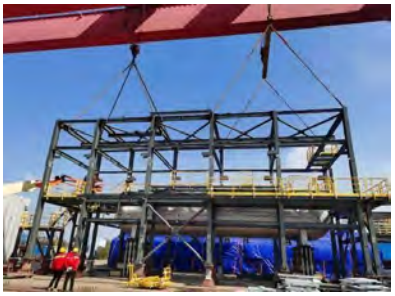


•Re-assembling on site



Modular site installation:
7 days, with 2 units of cranes (100+300) tons.

Installation of miscellaneous:
3 weeks, with two units of 50-ton cranes.

Morimatsu supervision:
4 weeks with 3 Engineers on site

•Commissioning and operation training on site

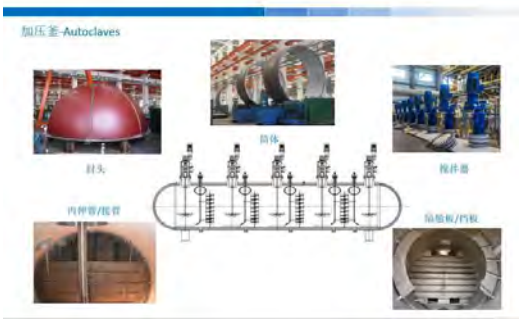

•Commissioning supervision on site

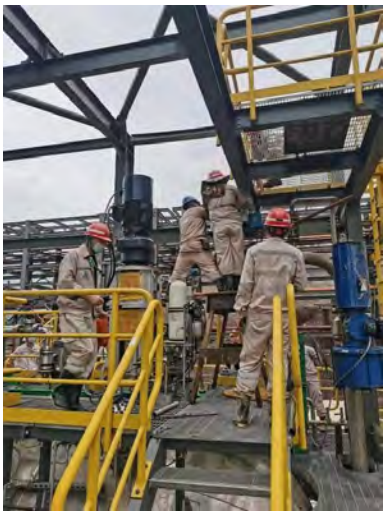

•Commissioning supervision on site

•Successful Commissioning and ramp up

Highly Prefabrication : Alternative solution to modularization of HPAL and POX

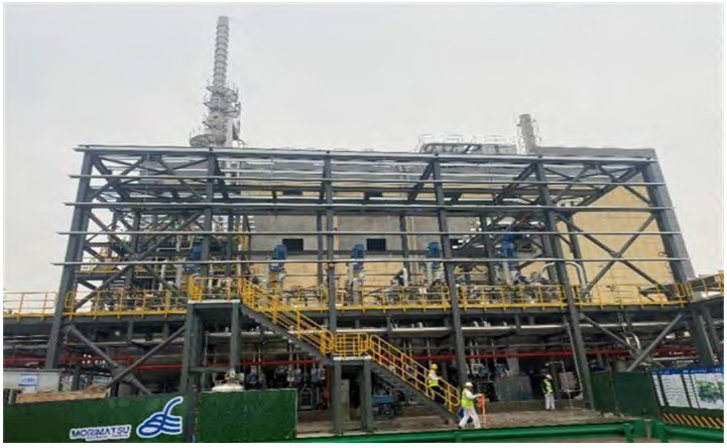

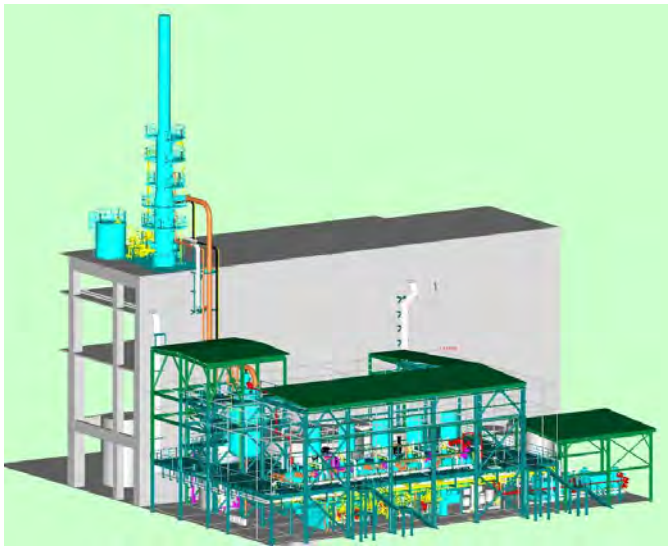

- Successful Commissioning and ramp up

EXTENDING AUTOCLAVE SERVICE LIFE BEYOND THE THIRD DECADE

By

Evelyn Ng

Callidus Group, Australia

Presenter

Evelyn Ng
evelyn.ng@callidusgroup.com.au

ABSTRACT

Autoclaves are critical fixed assets integral to the high-pressure acid leaching (HPAL) process. Traditionally, these vessels are engineered with a thirty-year operational lifespan, aligning with the projected lifespan of mining operations. Throughout this designated lifespan, regular maintenance efforts are directed toward repairing corrosion and erosion damage within the autoclave lining. However, a critical knowledge gap exists regarding the viability of extending the autoclave's service life beyond its designed duration.

Despite the initial design parameters, instances arise where the operational lifespan of an autoclave needs to be prolonged, particularly when the mine's lifespan is extended. Comprising formed carbon steel and explosion-bonded titanium, the autoclave's structure blends mechanical strength with cost-effectiveness. The titanium-clad lining is a vital protective layer, shielding the vessel's interior against high-temperature acidic slurry's corrosive and erosion effects.

Given the considerable size of autoclaves, their construction entails multiple plates of carbon steel and explosion-bonded titanium, meticulously shaped to form the vessel's cylindrical body with hemi-heads at each end. The interior is rendered seamless by strategically welding titanium batten strips, ensuring a tight seal containing the pressurized acidic slurry.

Routine maintenance shutdowns are inevitable to address issues such as leakage, corrosion, and erosion within the autoclave lining. Repair procedures involving the removal and replacement of batten strips and subsequent welding pose concerns regarding the impact of the titanium cladding's material properties. Notably, the potential formation of intermetallic compounds and consequent cracking in the autoclave wall lining remains a looming threat.

This presentation aims to unveil findings regarding the critical threshold of titanium cladding thickness that must not be compromised to mitigate the risk of intermetallic formation and subsequent structural integrity issues. By offering essential insights into long-term maintenance strategies for autoclaves, this research bridges the knowledge gap essential for ensuring the sustained efficiency and safety of HPAL processes.

Keywords: High-Pressure Acid Leach, HPAL, severe service, autoclave, explosion bonded, clad titanium, cladding, carbon steel, sulphuric acid, equipment, corrosion, erosion, performance, high temperature, weld repair, properties, performance, batten strips, cracks, failure, NDT, non-destructive testing, hardness, x-ray fluorescence, intermetallic, microscopy, energy dispersive spectroscopy, SEM, EDS.

Callidus

Extending Autoclave Service Life Beyond the Third Decade

Evelyn Ng
Callidus Group, Australia

The Callidus Group

Specializing in engineered solutions for mining and O&G clients covering all aspects of flow control, in addition to repair and modification of OEM equipment.

Callidus Welding Solutions

A leader in the welding of exotic metals and alloys, fabrication, repair, equipment refurbishment, and innovations in surface modification.


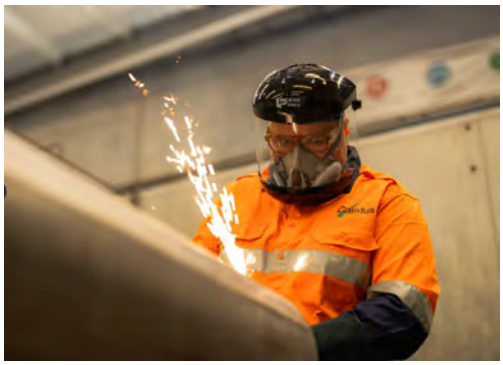


Weld Australia | ISO 9001 2015 CERTIFIED | Materials Australia | ASSDA ACCREDITED | Weld Australia Welding Integrity Assured AS/NZS ISO 3834 Part 2 | iiw Certificate No. 045

Autoclaves require maintenance and repair

Autoclaves are formed from Explosion-Bonded (EB) plates.

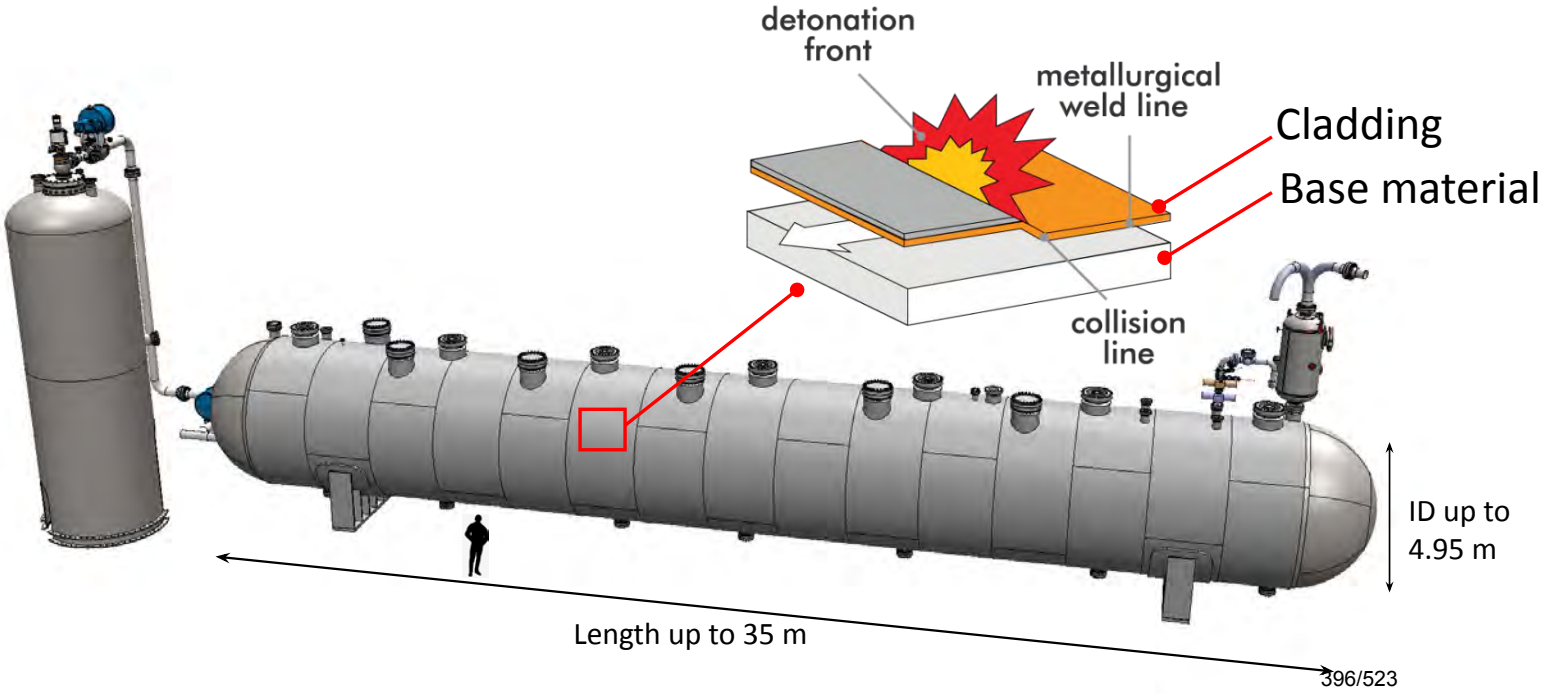

Explosion-Bonded plate material combinations

Carbon steel provides the pressure-containing envelope, while titanium cladding provides the corrosion envelope.

Clad layer
2-8mm thick

Base material
100-170 mm thick

Typical interface profile:
"Cladding wave"

- Fused interface, free of oxide and impurities.
- Typically manufactured in compliance with ASTM B898 to ensure suitability for use.

The challenge of real life versus design

EB plates are connected by up to 2 km of batten strips welded to the Ti cladding.

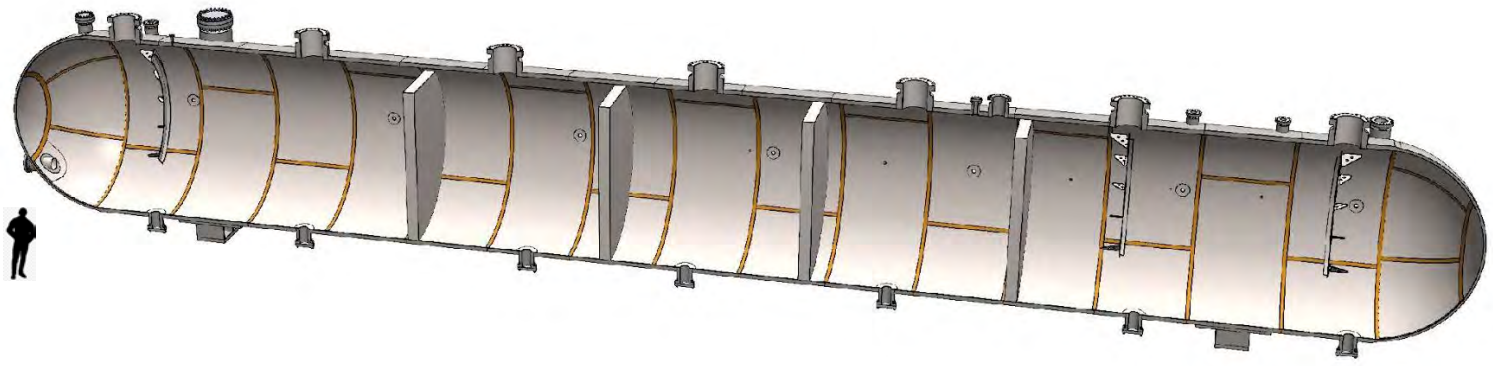

Batten strips create the corrosion envelope

Various batten designs, each present advantages and disadvantages.

Conventional batten design

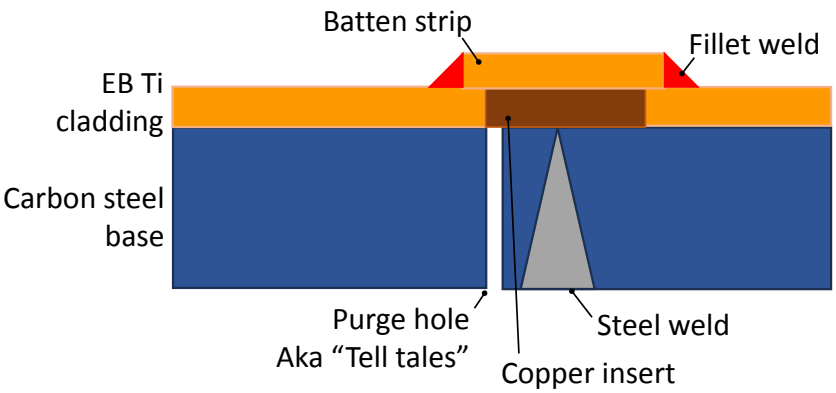

Notable issues:

- Cracking along the centerline of the fillet weld due to thermal expansion
- Stands proud makes it more susceptible to erosion.

Submerged batten design

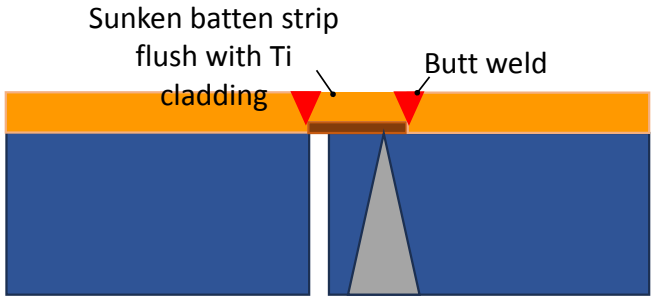

Notable issues:

- Weld repair of batten will compromise the original Ti cladding.
- Lengthier to repair because butt welds require careful excavation.

Design versus the reality of inspection & repair

Repair of autoclave Ti cladding is challenging alongside the absence of an international weld repair standard.

- Confined space
  - Elevated temperature
  - Dim lighting
  - Complex geometry
- Specialized PPE requirements
  - Non-uniform surface profile
- Time constraints

- Absence of an industry standard.
- ASME VIII for vessel design, and ASME IX for qualifying welders and procedures but the Ti cladding is not considered part of the pressure envelope

Autoclave weld repair is up against the clock

Weld repair is limited to a defined window within a typical autoclave shutdown that scheduled for 21 days.

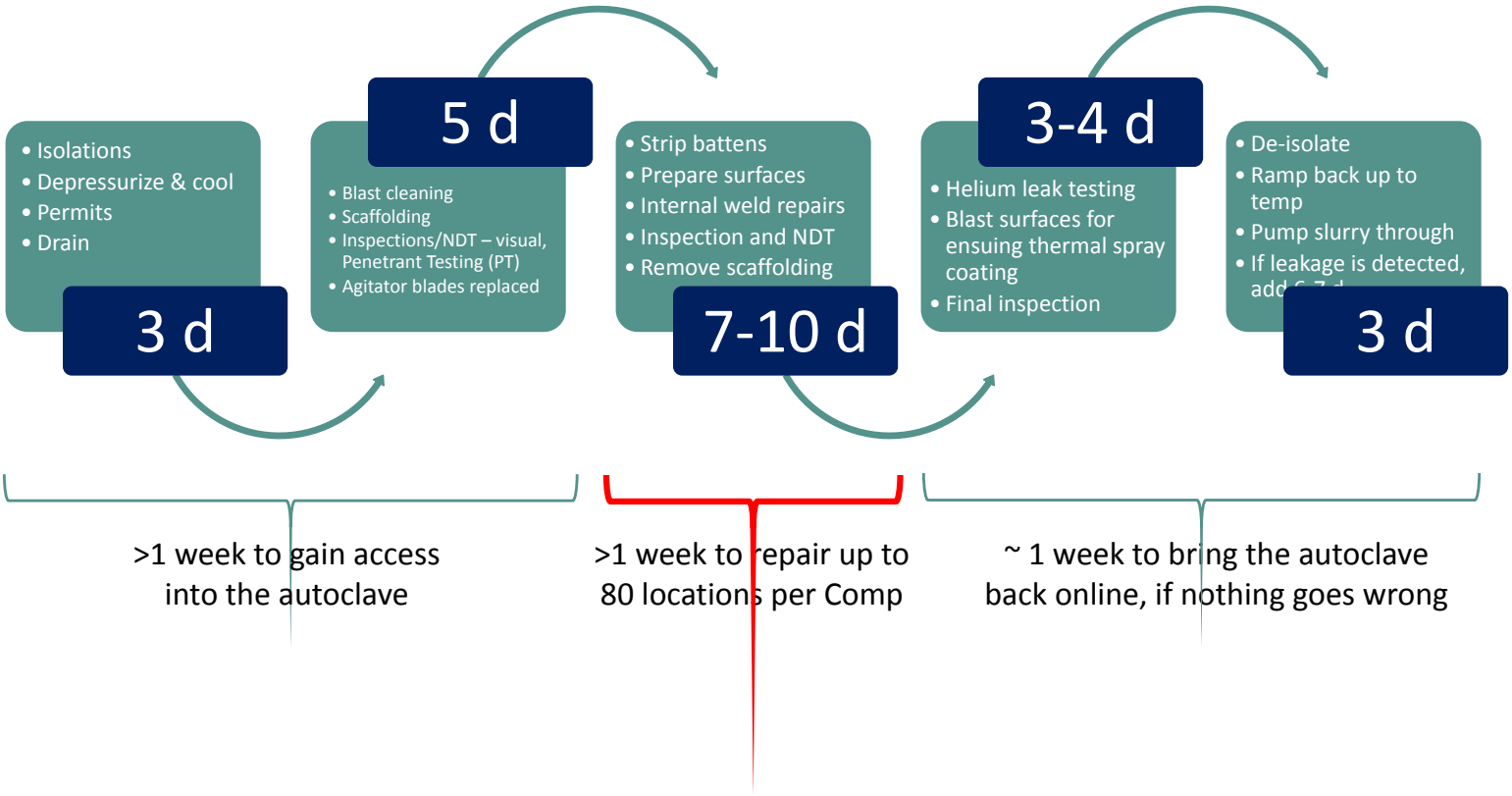

How thin is too thin when welding clad Ti?

The focus of this study: What is the threshold Ti cladding thickness where Fe draw-through occurs?

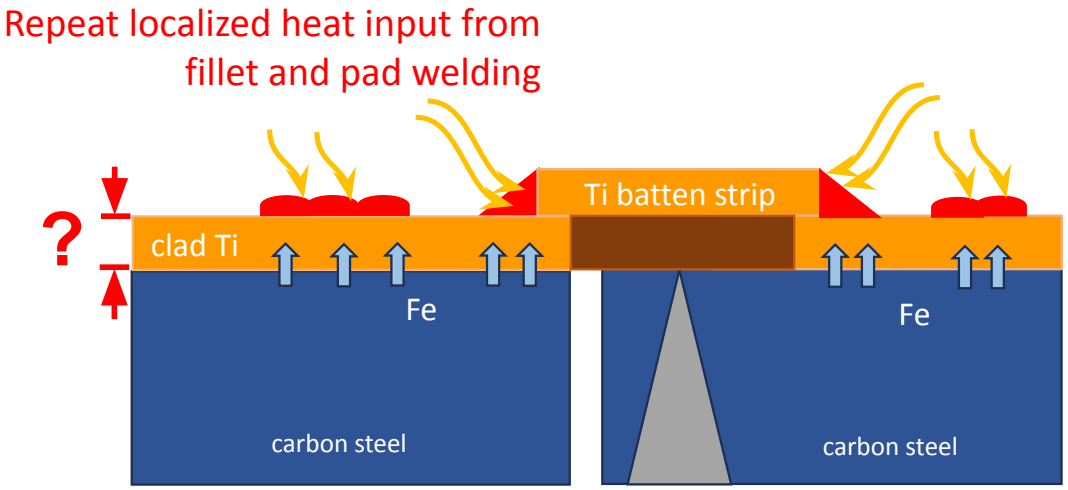

Identifying the gap in knowledge

Defining the starting point for this study based on available data

The starting point says ≥1.98 mm is safe

Limited data is available concerning the risk presented by welding EB clad Ti on carbon steel.

Orr, A. (2019) from Tricor Metals claimed:

- It is risky to weld on anything less than 1.98 mm (0.078”).
- Even a thickness of 2.49 mm (0.098”) could provide too much heat input and contaminate the cladding.

Final Results:

Table 3: Results Comparison

Thickness	Contamination	Intermetallics?	XRF PMI: Iron Detected?	Successful?
0.098"	No	No	No	Yes
0.088"	No	No	No	Yes
0.078"	No	No	No	Yes
0.068"	Possible	Questionable	No	Questionable
0.058"	Yes	Yes	No	Risky
0.048"	Yes	Yes	No	No
0.038"	Yes	Yes	Yes	No
0.028"	Yes	Yes	Yes	No

This is a good starting point, but focusing on autoclave maintenance strategy, what is the risk presented by repair welding? i.e. repeated welding in the same location.

Orr, A. (2019). Clad metal repairs, how thin is too thin? NACE International Corrosion Conference & Expo March 24-28, Nashville, Tennessee. <https://cdn.ymaws.com/titanium.org/resource/resmgr/02_jens_folder/industrial_committee_webpage/map_proceedings/orralex2018_map_presentation.pdf>. Accessed 10 October 2023.

Experiment replicates clad Ti repair & inspection

Fillet and pad welding on a range of Ti cladding thicknesses, from 1 mm to 4 mm thickness.

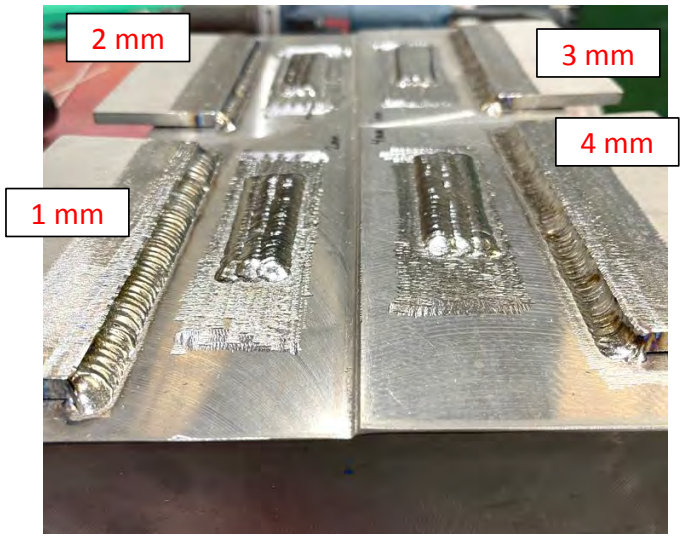

NDT: Penetrant Testing and visual inspection.

Result: NDT of welds showed no indications

Extensive use of Penetrant Testing (PT) and visual inspection in the autoclave to identify local areas for weld repair.

Sequence of actions when performing PT

Surface cleaning ⇨ Cover surface with pink penetrant ⇨ Remove excess penetrant ⇨ Cover with developer and inspect for deviations

But what is occurring below the surface?

Fillet and pad welding on Ti cladding thicknesses, 1 – 4 mm, were characterized in cross-section.

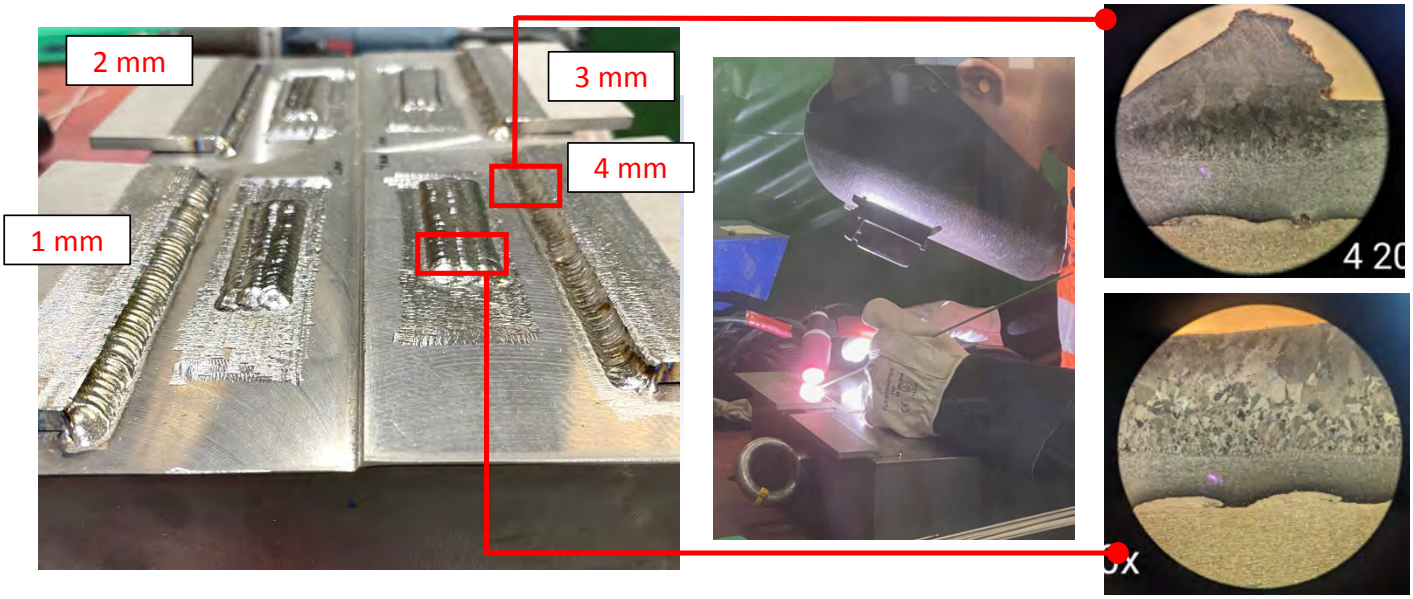

NDT Penetrant Testing and visual inspection

SEM and EDS mapping,
stereo and optical microscopy.

Results clad Ti / carbon steel interface

Visually, the clad Ti Heat Affected Zone (HAZ) appears to contact carbon steel when clad Ti is 2 mm or less.

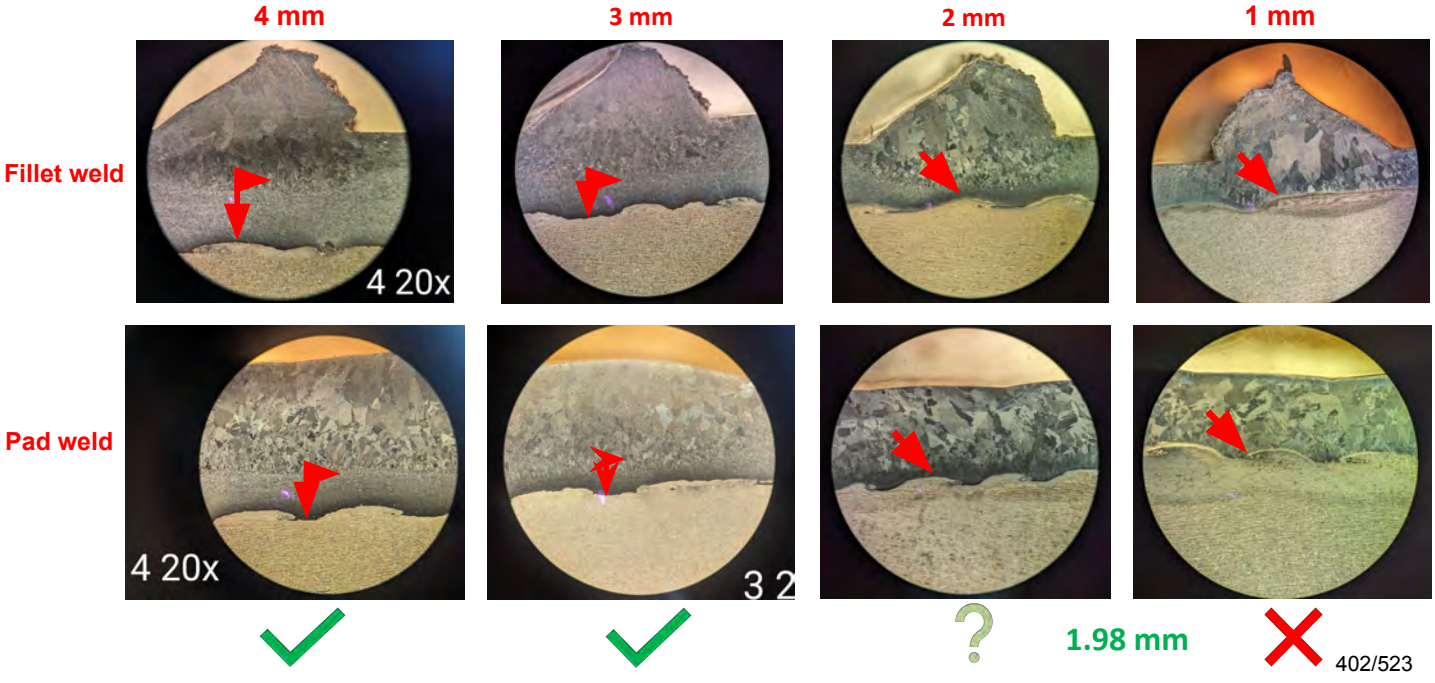

So, 4 mm clad Ti/carbon steel is safe to weld?

SEM/EDS mapping confirms there is no Fe in welded 4 mm clad Ti.

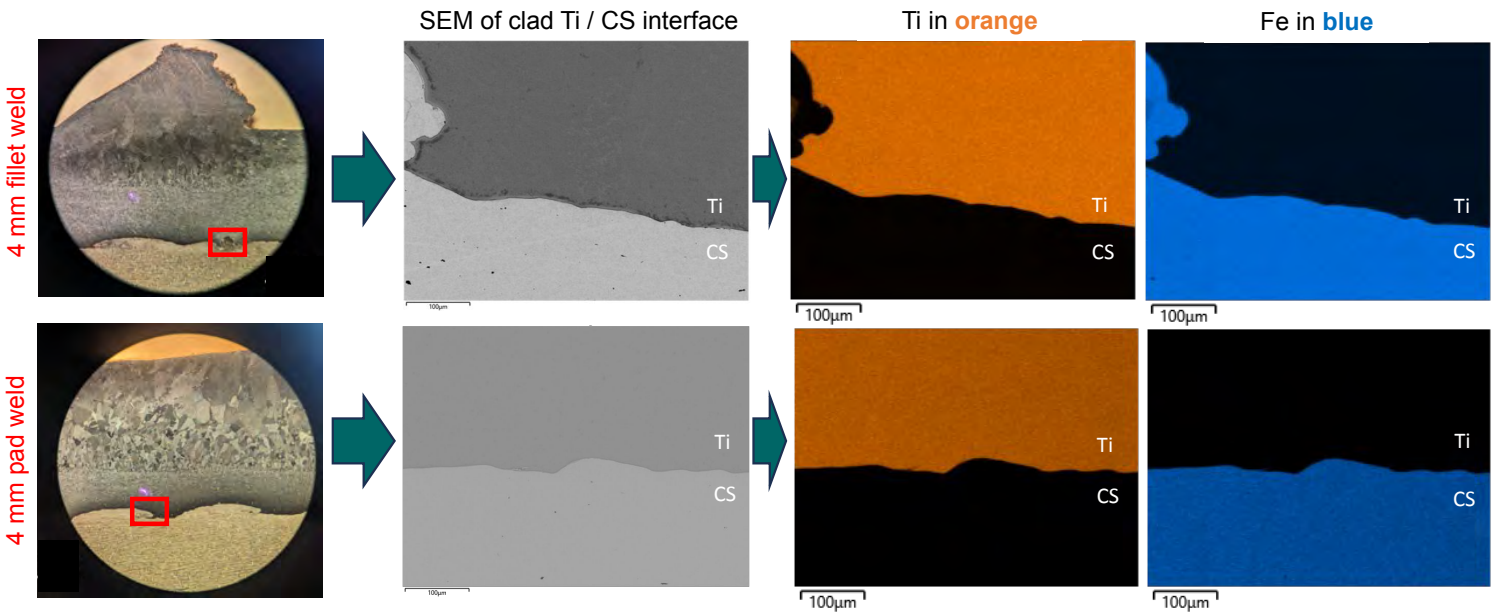

What about 3 mm clad Ti/carbon steel?

Confirmation there *is* Fe migrating into a welded 3 mm clad Ti, both fillet and pad weld. Cracks were also observed.

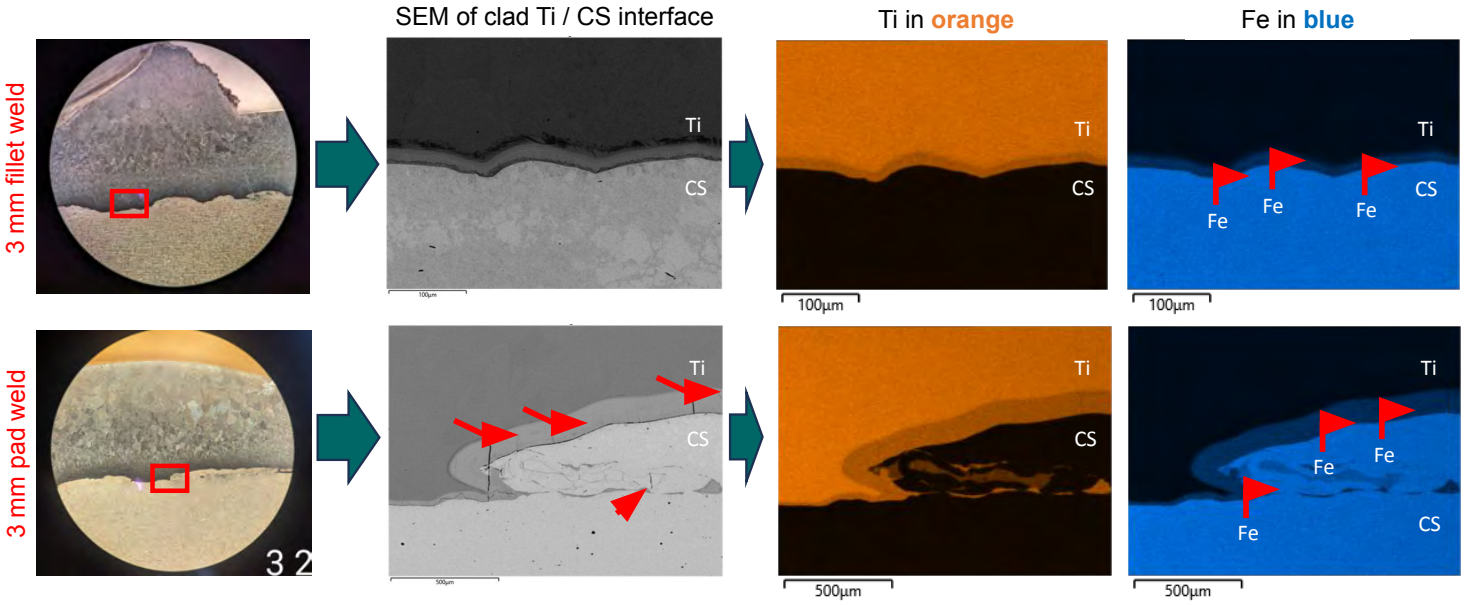

Extensive intermetallics seen at 1 mm clad Ti-CS

In optical micrographs, extensive formation of intermetallics containing cracks was observed at the clad Ti-carbon steel interface.

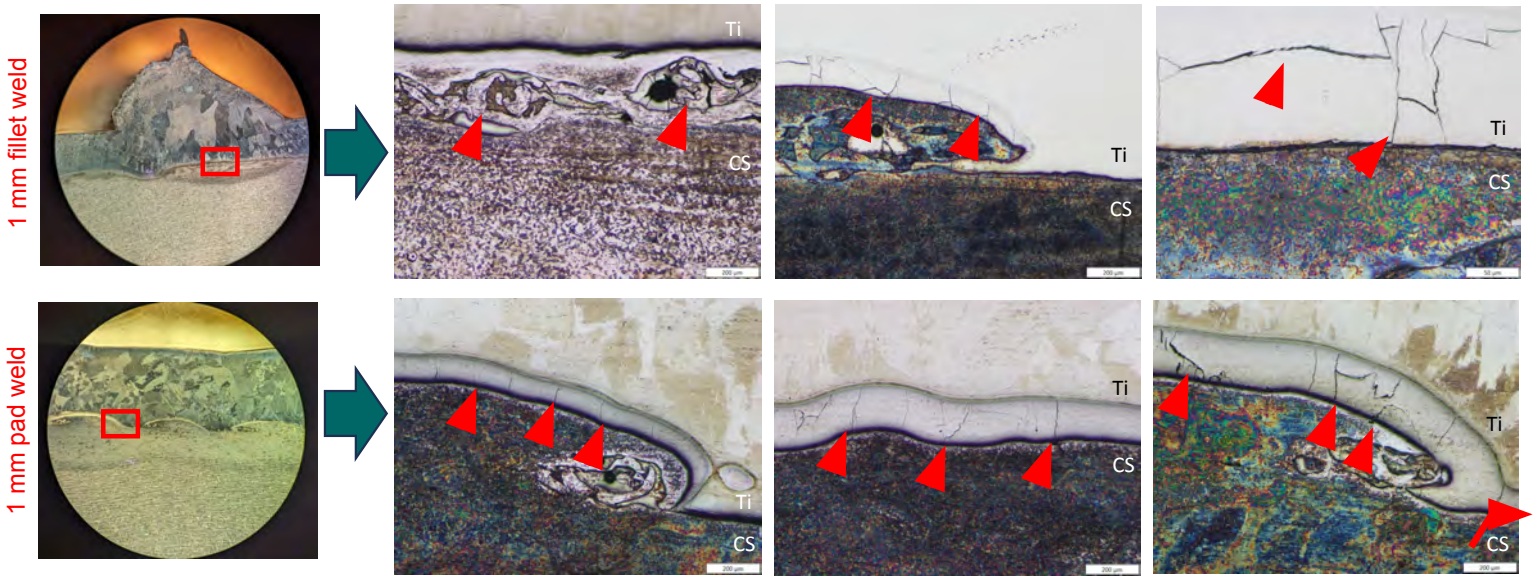

Preliminary conclusions

Defining the go and no-go clad Ti thickness when weld repairing pressure vessels.

NDT, performed on clad Ti per autoclave shutdown activities, does not indicate what is occurring below the surface, i.e. migration of Fe into Ti.

Iron migrating into clad Ti ≤3 mm plate thickness, where intermetallics containing cracks were observed along the clad Ti/carbon steel interface

Even more conservative thickness than what was reported by a previous study by Orr (2019).

Next steps:
Mechanical testing of the interfaces per ASTM shear strength, adhesion, and bend tests.

Repeat the experiment on top of the original

To simulate weld repair on Ti cladding that typically occurs over the same region.

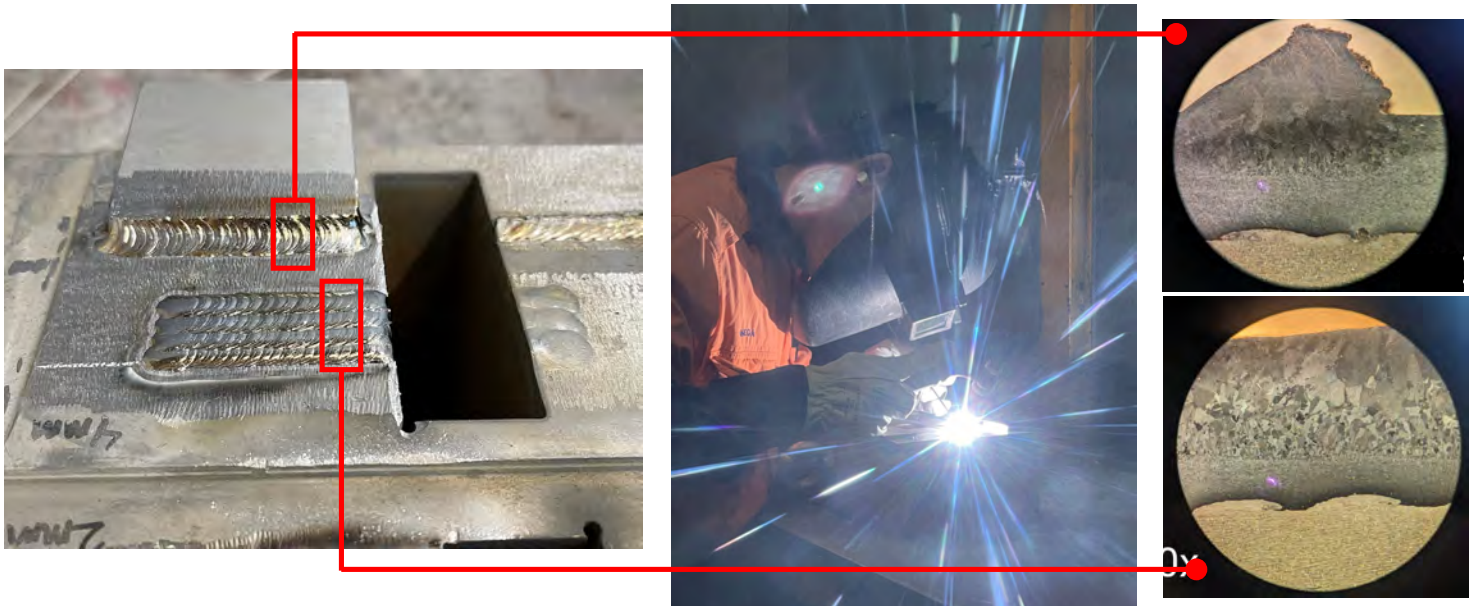

NDT: Penetrant Testing, and visual inspection.

SEM and EDS mapping, stereo and optical microscopy.

Intermetallics seen at 4 mm Ti clad weld repair

Intermetallics containing cracks were observed at 4 mm clad Ti thickness.

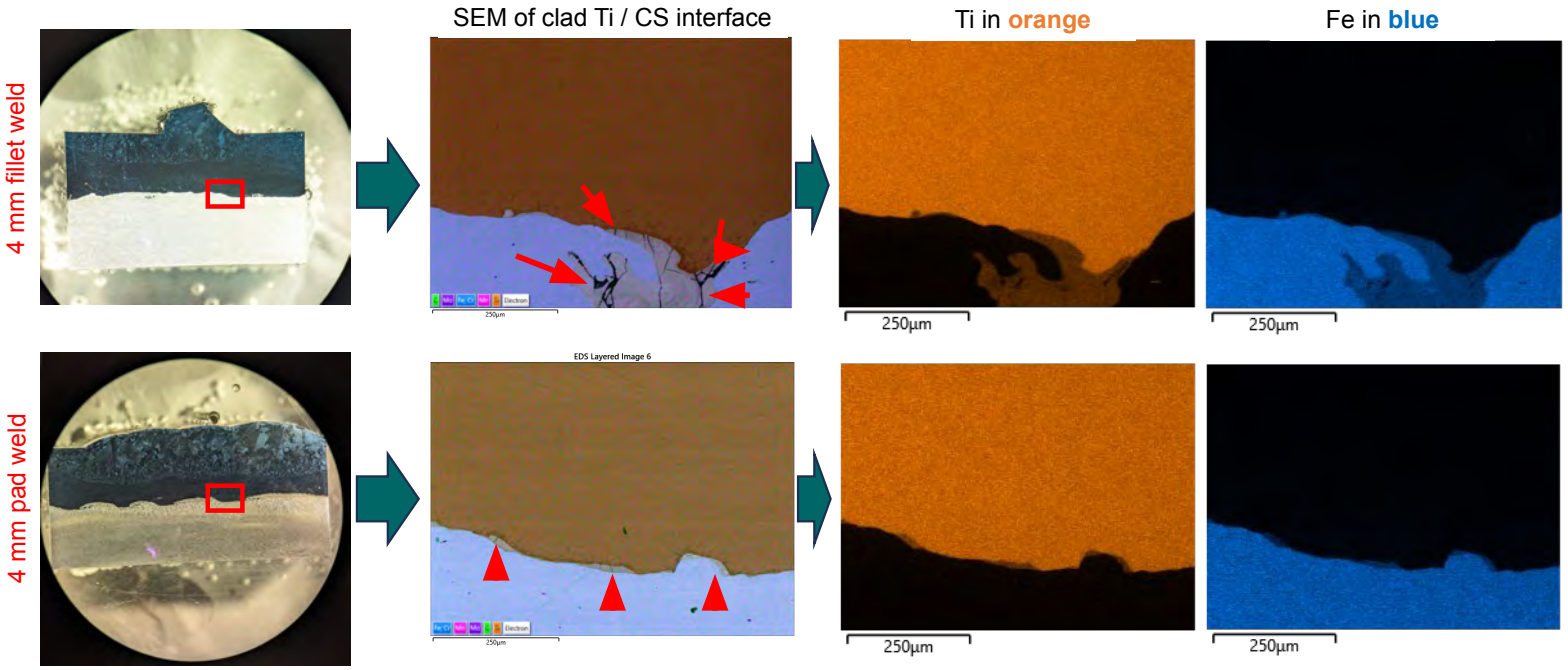

Extensive intermetallics at 2 mm weld repair

Intermetallics, which included cracks, formed continuously along the interface up to 20 mm in length.

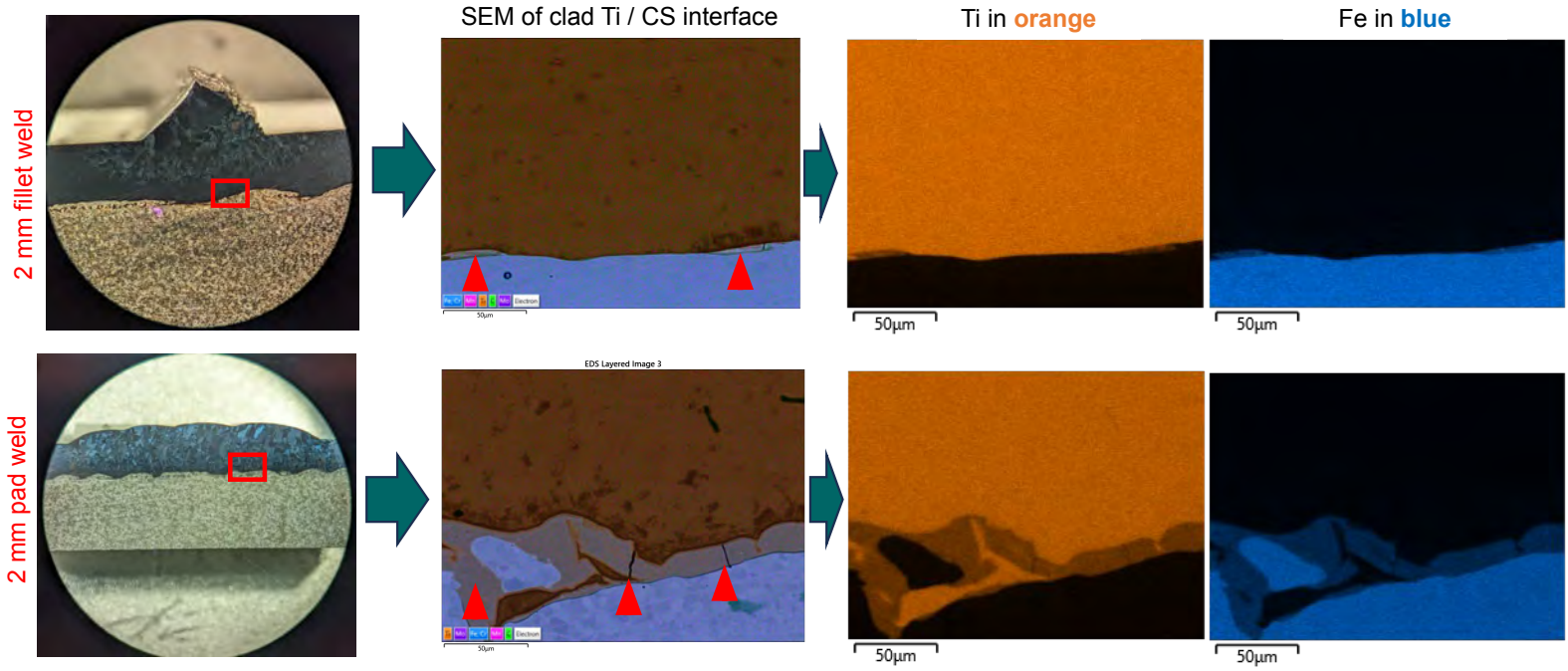

Closing takeaways

Preliminary results are indicative of integrity issues in a repaired Ti clad pressure vessel. Study to continue.

1. Standard NDT is not indicative of the integrity of welded and repaired Ti cladding. Brittle intermetallics form at a 4 mm clad Ti thickness, contrary to a previous study that determined intermetallics formed at 1.98 mm.

2. Options exist to enhance the erosion resistance and service life of cladding, including thermal spray ceramic protective coating, nitriding, and wear plates. Determined on a case-by-case basis guided by experience.

3. Weigh the benefits of a short-term repair versus a long-term strategy because the continued risk of vessel breach is too high.

MODELLING AND SIMULATION OF NICKEL SOLUTION PURIFICATION IN INDUSTRIAL JAROSITE AUTOCLAVES

By

Johann Steyl, Suné Grobbelaar, [2]Karina Beukes and [2]Dirk du Toit

Dynamet Insights (Pty) Ltd, South Africa
[2]Impala Platinum Ltd - Refineries, South Africa

Presenter and Corresponding Author

Johann Steyl
johann.steyl@dynamet.co.za

ABSTRACT

This paper describes how a hybrid first-principles – machine-learning (FP-ML) modelling and simulation platform can help to understand and improve complex industrial processes. Nickel solution purification, predominantly via ammonium jarosite precipitation in a series of autoclave stages, is presented as a case-study example. The case-study is used to demonstrate the model development workflow and benefits of this transient modelling approach to the industry.

Initial modelling identified info gaps in the operational chemical suite, which prompted a short sampling campaign to measure the key species profiles in the autoclaves. Since precipitation mechanisms are complex and difficult to interpret via batch experimentation, only this sampling campaign data was used. The additional model inputs were the logged plant inflow stream flows and upstream block states.

The workflow methodology is discussed in the paper and only relies on basic chemistry, measurement and understanding. The FP modelling construct is based on acausal mass-energy balance equations (macro model), which take care of the dynamic interactions of each inventory block with its neighbouring blocks. Within this FP framework, phenomenological equations were added and ML algorithms trained to capture the observed chemical behaviour (micro model). The advantage of this approach is that the data-science blocks can deal with the microscopic-scale complexities, while the combined model generalises the behaviour so that it becomes predictive.

The end result is a high-fidelity model that is trained on actual plant data, and which is able to predict actual plant behaviour. Moreover, an implementation platform, with a user-friendly front end, is provided where the model, and the associated benefits, can be made accessible to a wider technical team in the operational environment. This compiled application product (APP) digitally captures the key information and becomes a 'living report' of the operation. Validated and predicted trends are presented in the paper, demonstrating that this model qualifies as a true digital twin (DT) that can be used to improve operating strategies and process control, and to help train operators.

Keywords: digital twin, transient modelling, hybrid modelling, simulation, ammonium jarosite, nickel.

INTRODUCTION

Many industrial operations deviate from their design operating points, especially in the case of toll refiners where different feed materials are treated. Furthermore, daily operational challenges often overshadow plant engineers' focus, causing plant sections to underperform metallurgically. Digital twins (DTs) are models that mimic the behaviour of unit blocks in the time domain. As computational power and modelling fidelity improve, DTs will become increasingly important operational and engineering tools to help improve metallurgical performance and process efficiencies. The objective of this paper is to demonstrate the workflow, features and benefits of a hybrid first-principles – machine learning (FP-ML) modelling approach when applied to an actual operating plant.

This case-study focuses on the removal of iron, predominantly as ammonium jarosite, from nickel-rich solutions in an autoclave circuit. Discussing the larger flowsheet configuration is not warranted here since the DT battery limit only covers the two feed tanks – that is, the main feed tank and the weak aqueous ammonia (aqua) tank, and the autoclave vessels (A and B) – see Figure 1. It is however important to note that the main feed tank takes at least three input streams, with varying flows and compositions – these process disturbances are also transferred to the autoclave blocks. Furthermore, weak aqua solution is intermittently dosed via on/off (open/close) valves to the various autoclave compartments, which make the species and chemistry behaviour even more transient. Steady-state (SS) models are incapable of dealing with such complexities. This case-study was therefore the ideal example to demonstrate the hybrid FP-ML transient modelling approach.

A short sampling campaign was undertaken by collecting autoclave profile data to fill some key knowledge gaps. These results are discussed in the paper, emphasising how it helped to close the degrees-of-freedom of the mathematical construct, give confidence in the DT performance during the model validation phase and create insights into the plant operation.

PROCESS MODELLING

Flowsheet

The simplified flowsheet is shown in Figure 1. The logged states refer to the normal plant operation. The feed and aqua tank sections were first modelled so that the simulated results could be reconciled with the logged states. The feed tank states were accurately simulated, as were the feed forward flowrate, composition and temperature to the first autoclave stage (A1). In the case of the aqua tank, the total (integrated) ammonia consumption (over 24 h periods) was logged, as well as the on/off signals of the various aqua valves. The modelled dissolved ammonia concentration approached its saturation point under small positive pressure and slightly elevated temperature variations, varying typically between 22-26 wt% NH_3. These variations had a relatively small impact on the final DT output and was therefore fixed at an average of 24 wt% NH_3, which was close to the average aqua concentration measured on the plant over the sampling campaign period.

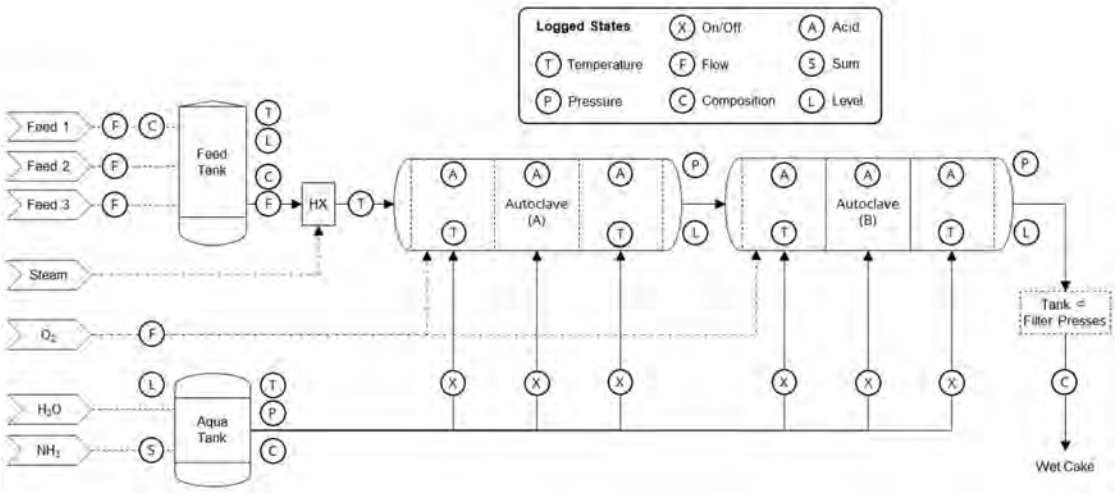

Figure 1: Jarosite Autoclave Section – Simplified Flowsheet.

The weak aqua flow was not measured on the plant and the system had to be constrained by comparing the cumulative ammonia consumption. Figure 2 shows these results for the sampling campaign period, which amounts to an average flow of 15-20 L/min weak aqua per compartment. Since all six on/off valves draw from the same feed pipe, the weak aqua flowrate can vary to any specific compartment when some (or all) of the valves open simultaneously. An additional small flow is also sporadically drawn from the weak aqua tank to a downstream pH adjustment tank, introducing further complexity. Consequently, this is an area where DT model improvement opportunities exist – that is, to measure and record the actual weak aqua mass flows to each compartment on the plant in the future. To simplify the DT model for this initial modelling phase, the flow to each compartment was fixed at an average weak aqua flow of 17.5 L/min.

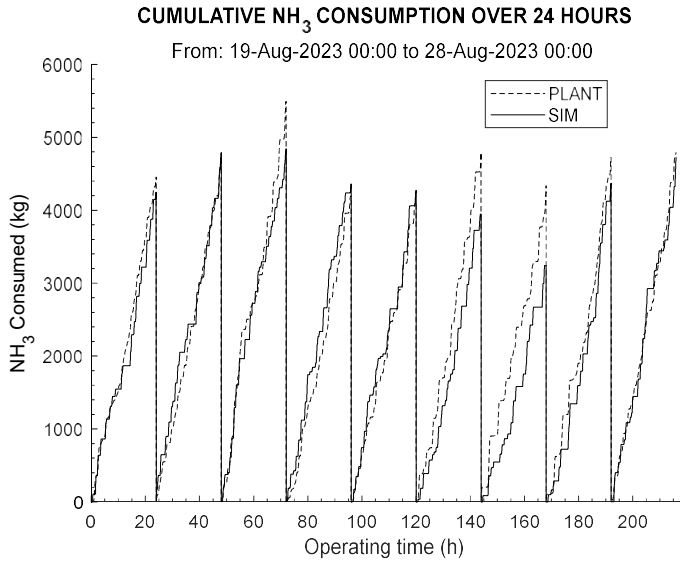

Figure 2: Plant vs simulated ammonia consumption, based on the logged plant on/off signals and an average of 17.5 L/min weak aqua flow to each autoclave compartment.

Macro model

The FP transient mass-energy balance equations of the plant section (Figure 1) represent the macro model. With the feed stream temperatures, flows and compositions accurately mapped, the block states follow directly from the time integration of the system equation set. The detailed DT modelling methodology and FP equation sets have been presented elsewhere[1]. The FP equations construct of each flowsheet unit block have been implemented using the MathWorks®[2] Simscape™ language and a bespoke Metallurgy Domain created by Dynamet[3]. These algorithms can simultaneously deal with particle-, species- and heat-flow in the time domain, including the system causality. Furthermore, since Simscape is implemented in the Simulink® graphical programming environment, the flowsheet model is created by using intuitive drag-and-drop physical-flow connectors between the different unit blocks. Any regulatory and advanced control loops, operating heuristics and event-based aspects, and any derived values, data reconciliations and visualisations are easily dealt with in this single software environment.

Micro model

The micro model describes how the formal species are distributed between the different phases (physico-chemical reactions) and interact chemically with each other (chemical reactions). The first set of equations was used to describe the rapid kinetic changes between the gas species, $H_2O_{(g)}$, $NH_{3(g)}$, $O_{2(g)}$, and their respective liquid-phase states. For example, the oxygen mass-transfer rate, $\dot{m}_{rx,1}$ (kg/s), between the gas and aqueous slurry phase can be described as:

$$O_{2(g)} \leftrightarrow O_{2(a)} \quad (1.1)$$

$$\dot{m}_{rx,1} = k_1\left(m^*_{y,O2} - m_{y,O2}\right) \cdot m_{H2O} \quad (1.2)$$

where k_1 is a lumped parameter that takes care of the physical mixing, temperature variations, and any proportionalities[1]. The mass of inventory water in the control volume m_{H2O} is used to scale the reaction rate $\dot{m}_{rx,1}$ so that the diffusion rate can be expressed as the difference between the

thermodynamic (equilibrium) molality $m^*_{y,O2}$ (mol/kg), and its current state value. All thermodynamic values in the DT were implemented either as lookup tables from reliable data sources or as ML blocks trained on outputs from state-of-the-art software tools, such as OLI Studio[4].

Since the iron(II) concentration entering the autoclave is relatively low (< 3 g/L Fe), the interfacial oxygen mass-transfer rate was never rate limiting – there was therefore no need to include k_1 in the ML training routines. On the other hand, with acid neutralisation being an important driver of the various hydrolysis reactions below, it was included (as formal species) via the following reaction:

$$H_2SO_{4(a)} + 2NH_{3(a)} \rightarrow (NH_4)_2SO_{4(a)} \quad 2.1$$

$$\dot{m}_{rx,2} = k_2 = f(m_{H2SO4}, m_{NH3}) \quad 2.2$$

The neutralisation rate k_2 (kg/s) was trained as a function of the formal species block inventory masses, as shown in Equation 2.2. Since weak aqua is sporadically pumped into the various autoclave compartments, the oxidation of iron(II) was simulated via two parallel pathways – the first being the oxidation to the trivalent state in solution:

$$FeSO_{4(a)} + 0.25O_{2(a)} + 0.5H_2SO_{4(a)} \rightarrow 0.5Fe_2(SO_4)_{3(a)} + 0.5H_2O_{(l)} \quad 3.1$$

$$\dot{m}_{rx,3a} = k_3(1 - x_{Fe}) = f\left(m_{FeSO4}, m_{O2}, \dot{m}_{in,FeSO4}, \dot{m}_{in,H2SO4}\right) \quad 3.2$$

Aside from including the inventory masses, the best training results were obtained by also accounting for the inflow rates $\dot{m}_{in}$ (kg/s) of the indicated species. The fraction of the precipitated iron present as hydrated hematite or goethite phase, $Fe_2O_3.H_2O$, is denoted by x_{Fe}, which was assumed to nucleate rapidly in low-acid environment, via the second parallel pathway:

$$FeSO_{4(a)} + 0.25O_{2(a)} + 1.5H_2O_{(l)} \rightarrow 0.5Fe_2O_3.H_2O_{(s)} + H_2SO_{4(a)} \quad 3.3$$

$$\dot{m}_{rx,3b} = k_3 x_{Fe} = f\left(m_{FeSO4}, m_{O2}, \dot{m}_{in,FeS}\ , \dot{m}_{in,H2SO4}, \dot{m}_{in,NH3}\right) \quad 3.4$$

The particle growth mechanism was assigned exclusively to the formation of ammonium jarosite:

$$3Fe_2(SO_4)_{3(a)} + (NH_4)_2SO_{4(a)} + 12H_2O_{(l)} \rightarrow 2NH_4Fe_3(SO_4)_2(OH)_{6(s)} + 6H_2SO_{4(a)} \quad 4.1$$

$$\dot{m}_{rx,4} = k_4 = f\left(m_{Fe2(SO4)3}, m_{NH3}, \dot{m}_{in,Feed}, \dot{m}_{in,H2SO}\ , \dot{m}_{in,Fe}\right) \quad 4.2$$

The rates of impurities removal, such as arsenic and lead, were not included as part of the ML exercise because they are rapidly removed from solution to below their detection limits in the first autoclave compartment – that is, they were assigned arbitrary fast rate constants:

$$0.5Fe_2(SO_4)_{3(a)} + H_3AsO_{4(a)} \rightarrow FeAsO_{4(s)} + 1.5H_2SO_{4(a)} \quad 5$$

$$3Fe_2(SO_4)_{3(a)} + PbSO_{4(a)} + 12H_2O_{(l)} \rightarrow 2Pb_{0.5}Fe_3(SO_4)_2(OH)_{6(s)} + 6H_2SO_{4(a)} \quad 6$$

During normal plant operation, the compartmental samples are only analysed for FA – that is, to control the addition of weak aqua retrospectively. With the above micro-model framework in place, it became clear that calibration data was needed to better understand the chemical system. Doubt was also created by the variety of different shades of red to brown colours observed in the final autoclave residue (after the filter presses). Furthermore, the residue composition from the normal operational analyses, shown in Figure 3, gave no mechanistic insight into the processes occurring in the autoclave. All these factors prompted a short dedicated sampling campaign.

SAMPLING CAMPAIGN

General

The transient model was fully developed by the time the sampling campaign planning started. In fact, the DT, albeit not yet trained, pinpointed where the knowledge gaps were and how to best leverage the available plant resources to generate this additional information. The campaign ran over the last week of August 2023 and only utilised existing plant operators and laboratory staff.

The first set of analyses were used to confirm whether any iron(II) remained in the autoclave after the first compartment (A1). The iron(II) was below its detection limit, which signified that the A1 block analyses were ideal for regressing the DT micro model. This is because the feed flow and composition were fully defined, while the chemistry was not dominated by slow iron(II) oxidation.

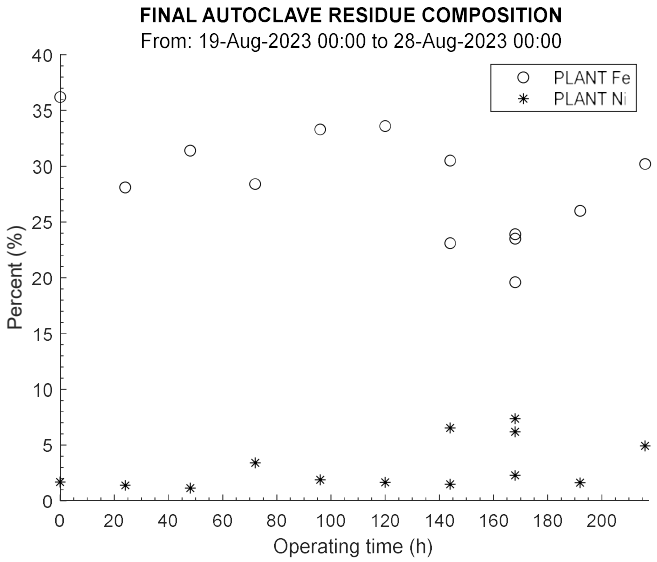

Figure 3: Final residue composition (after filter presses) from normal operational analyses.

Figure 3 shows that nickel was present in varying quantities in the final residue (dropped from the filter presses). At that stage, it was not understood whether the nickel was the remnant of incomplete washing cycles or co-precipitation. The residue samples from the Autoclave A compartments (A1, A2, A3) and Autoclave B compartments (B1, B2, B3) were therefore dried (without washing) in an oven at slightly elevated temperatures and analysed. Figure 4 shows photos of selected A3 residues on different sampling-campaign days. The wide range of different compartment residues were subsequently submitted for X-ray Diffraction (XRD) analyses to help shed some light on the precipitation chemistry.

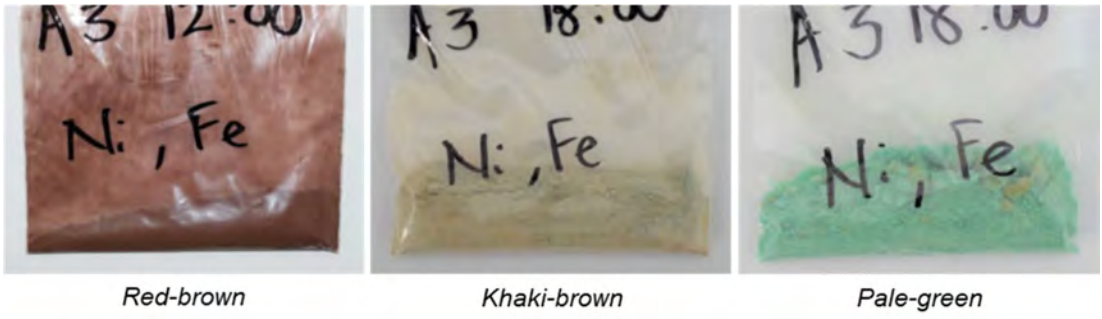

Figure 4: Selected compartment A3 residues on different sampling-campaign days.

The XRD results were definitive (Figure 5) – the major crystalline phase identified in the brown and red-brown samples was ammonium jarosite, $NH_4Fe_3(SO_4)_2(OH)_6$. The khaki-brown and pale-green samples contained increasing to dominant amounts of ammonium nickel sulfate hexahydrate, $(NH_4)_2Ni(SO_4)_2.6H_2O$, respectively. Nickel sulfate hexahydrate, $NiSO_4.6H_2O$, was also present in minor quantities, but assumed to be a remnant of drying the unwashed residues.

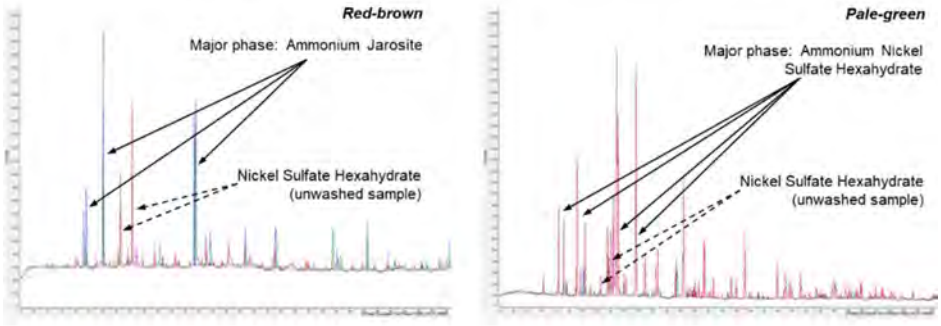

Figure 5: XRD results used to identify the major crystalline phases.

These results prompted the following expansion of the micro model:

$NiSO_{4(a)} + (NH_4)_2SO_{4(a)} + 6H_2O_{(l)} \rightarrow (NH_4)_2Ni(SO_4)_2.6H_2O_{(s)}$ 7.1

$\dot{m}_{rx,7} = k_7 = f\left(m_{NH3}, \dot{m}_{in,Feed}, \dot{m}_{in,H2SO4}, \dot{m}_{in,NH}\right)$ 7.2

Model training

The campaign data was loaded into the model workspace and then used to train the ML algorithms associated with the various reaction rates in A1. The first ML block was set up to vary the neutralisation rate k_2 (Equation 2.2) to mimic the measured FA concentration. Weighting vectors were used to adjust the weak aqua flowrates to each compartment, based on how many valves opened simultaneously at any specific point in time. Figure 6 summarises the outputs of this initial algorithm training exercise.

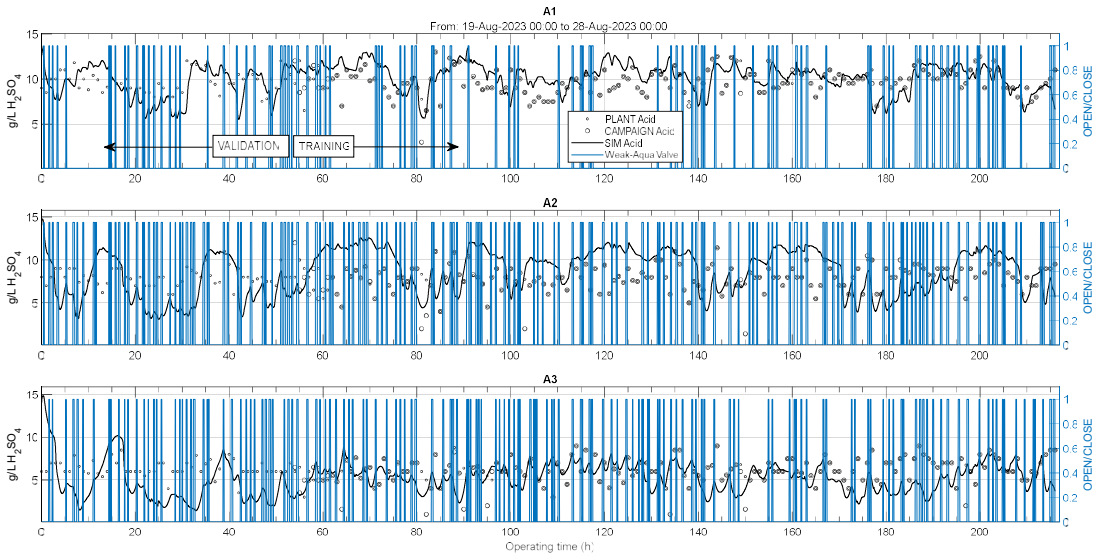

Figure 6: Outputs of the trained ML algorithms used to mimic the FA concentration in A1.

The simulated FA behaviour in the downstream compartments A2 and A3 could be improved in the future by also including those blocks in the training phase, as well as measuring the actual weak aqua flows. It is noteworthy that the system is highly transient due to the infrequent on/off pulses of weak aqua to the various compartments. Figure 7 shows an excerpt of the FA behaviour over a narrower time span – it demonstrates the transient responses to the weak aqua pulses and also serves to put the behavioural model accuracy in context with the typical measurement error.

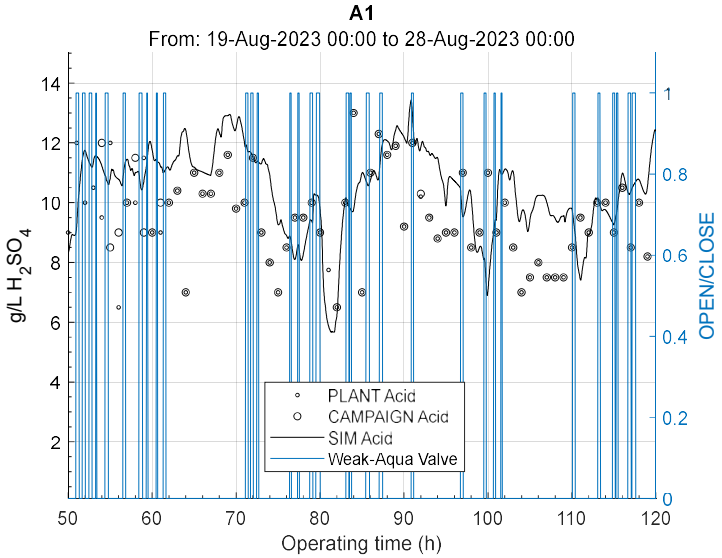

Figure 7: Example of the mimicked FA behaviour in A1 over a narrower time span.

The total oxidation rate k_3, via the two parallel pathways (Equations 3.2 & 3.4), was trained so that the iron(II) concentration fell to below its detection limit in A1 – that is, as confirmed by measurement during the sampling campaign. The fraction of the precipitated iron present as the hydrated hematite (goethite) phase x_{Fe} was trained to match the measured iron content in the A1 residue. Coincidently, this fraction naturally converged to small values (dominant jarosite phase).

The ammonium jarosite precipitation rate k_4 (Equation 4.2) was trained to match the iron(III) concentration remaining in the A1 solution. Figure 8 shows the first-round training output.

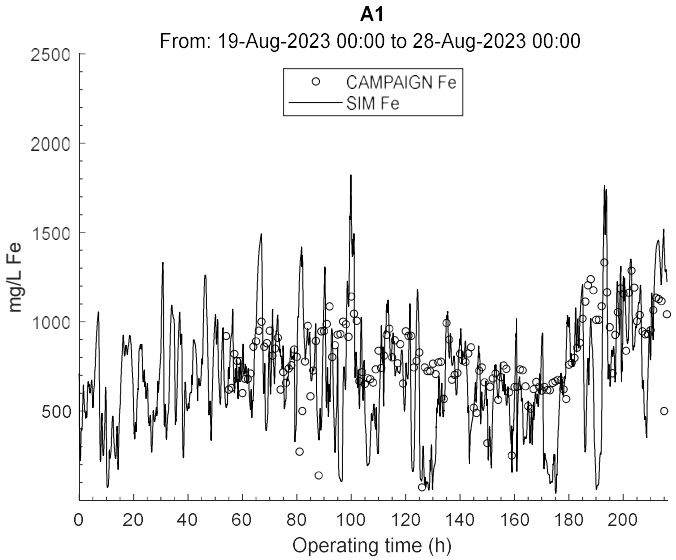

Figure 8: Output of the trained ML algorithms used to mimic the Fe concentration in A1.

The final ML exercise focused on matching the solids phase nickel content in the A1 compartment – that is, training the nickel precipitation rate k_7 (Equation 7.2) via the formation of ammonium nickel sulfate hexahydrate salt. The contribution of nickel sulfate hexahydrate salt, from drying unwashed residues during the campaign analyses, was assumed to be negligible.

SIMULATION RESULTS

Model validation

The ML blocks, trained on the campaign data for A1, were embedded in the hybrid DT model. The DT model was then used to simulate the iron behaviour in A2 and A3 – this is shown in Figure 9.

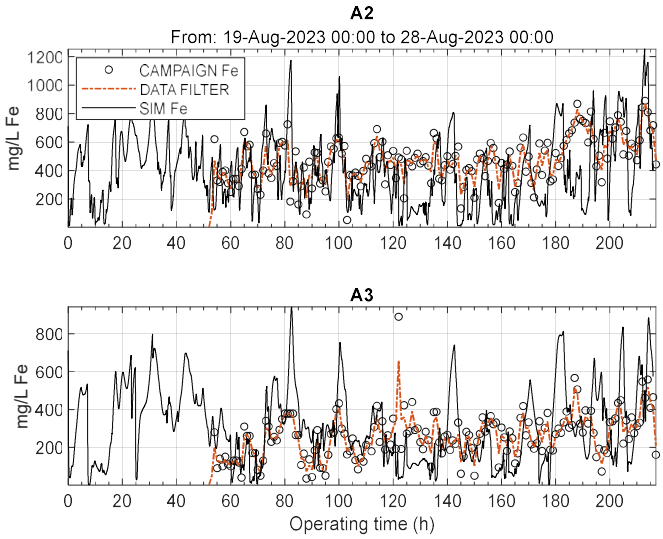

Figure 9: Model validation of the solution Fe concentration in A2 & A3.

Since the campaign data for A2 and A3 were previously unseen by the model, this served as validation of the simulated behaviour. Figure 10 compares the Autoclave A residue compositions to the corresponding model predictions for all three compartments. The FP part of the hybrid DT provides structure to the model and this, in turn, creates a sound generalisation methodology that often surpasses measurement accuracy. The model also corroborates the sampling campaign XRD results, suggesting that ammonium jarosite is the dominant iron-containing phase.

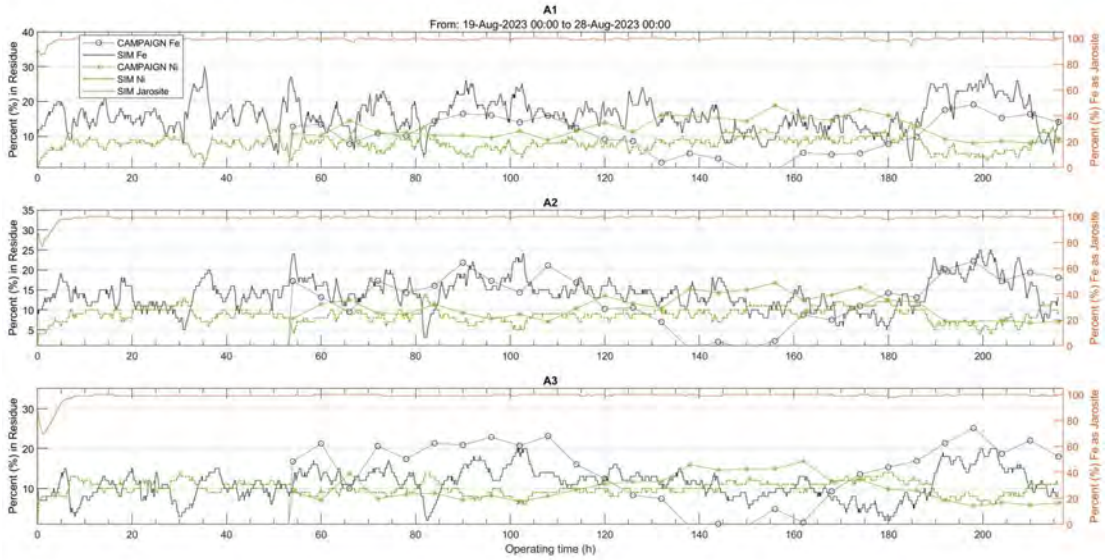

Figure 10: Model validation of the Autoclave A residue composition.

Insights

With the first-round training and validation completed, the DT was used to help explain day-to-day plant issues and observations, and to help make predictions on how the operation could potentially be improved in the future.

Figure 11 repeats the washed filter-press residue data (from the normal operational analyses for the 2nd half of the campaign run) presented in Figure 3, but also superimposes the simulated autoclave residue composition in A3 (albeit not washed). The simulated autoclave residue composition gives insight into the seemingly arbitrary spikes in the final residue nickel content (and the corresponding drops in the iron content) obtained from the plant measurements. Periods of excessive ammonium nickel sulfate hexahydrate salt formation in the autoclave showed up as higher nickel (> 5% Ni) and lower iron (< 25% Fe) in the final residue, likely due to inefficient washing in the filter presses.

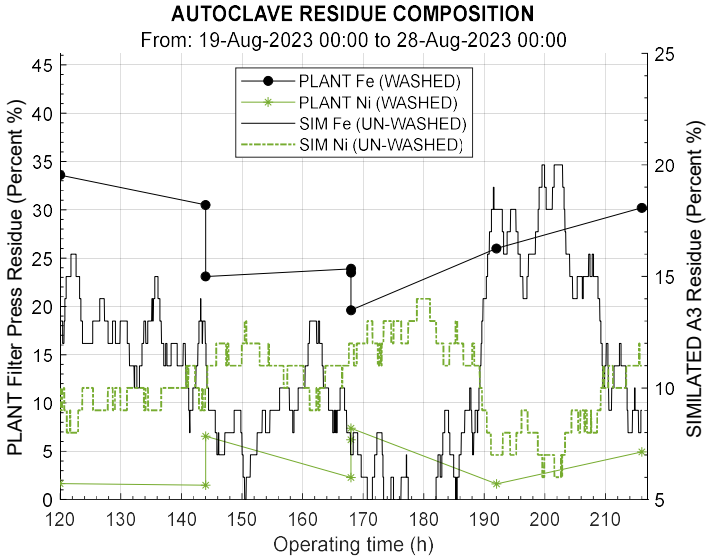

Figure 11: Final residue composition after washing (filter presses) vs the simulated A3 residue composition before washing.

The DT was used to help identify possible reasons behind the observed salt precipitation behaviour. One parameter that featured prominently during training of the rate k_7 (Equation 7.2), and which improved the model performance, is the autoclave feed flowrate, $\dot{m}_{in,Feed}$. Figure 12(a) plots this feed flowrate data, and its moving median. This suggests that prolonged periods of lower feed rates, e.g., between 140-160 h, and hence longer autoclave residence times, could promote ammonium nickel sulfate hexahydrate salt precipitation in the autoclave. A digital experiment was therefore conducted to simulate stabilising the feed flowrate by recycling filtrate back to the feed tank. Only marginally lower nickel content in the simulated autoclave residue was observed. Figure 12(b) shows the A2 aqua valve position, and its Gaussian-weighted moving average. It shows that longer autoclave residence times naturally result in lower weak-aqua flows since the operators set the weak-aqua valve timers based on the FA analyses. Nevertheless, the weak-aqua dosage rates could still have been too high, e.g., between 160-180 h.

In the next digital experiment, the DT was used to predict the outcome if the weak aqua flow to each compartment was varied proportionally to the autoclave feed flowrate and modulated, instead of using on/off valves. Figures 13(a) and 13(b) compare the baseline (on/off), and the scaled modulated cases, respectively. The benefit of the latter case is clearly demonstrated by the lower residue nickel content and the less erratic solution iron predictions. This result suggests that the feed flowrate of iron and acid should ideally be used to control the weak-aqua flows. There is therefore an opportunity to use the autoclave feed flowrate, the feed tank iron and acid tenors, and advanced process control (APC) algorithms to improve the operation. This DT model would be the ideal platform to develop and test such APC algorithms, without any risk to the actual plant operation. These optimised algorithms could then be gradually implemented on the plant for testing, with the ultimate objective of making the operation less reliant on operator interpretation.

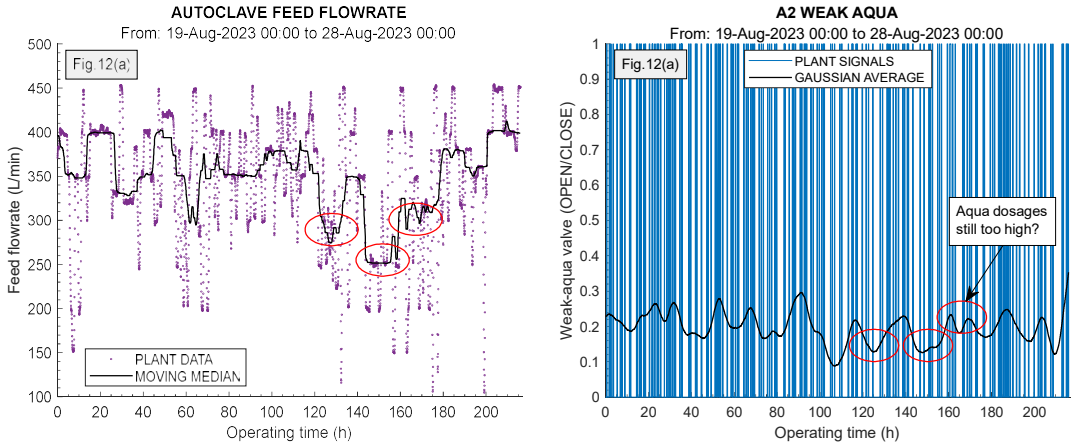

Figure 12: Variation of the (a) Autoclave feed flowrate, and, (b) A2 weak-aqua valve.

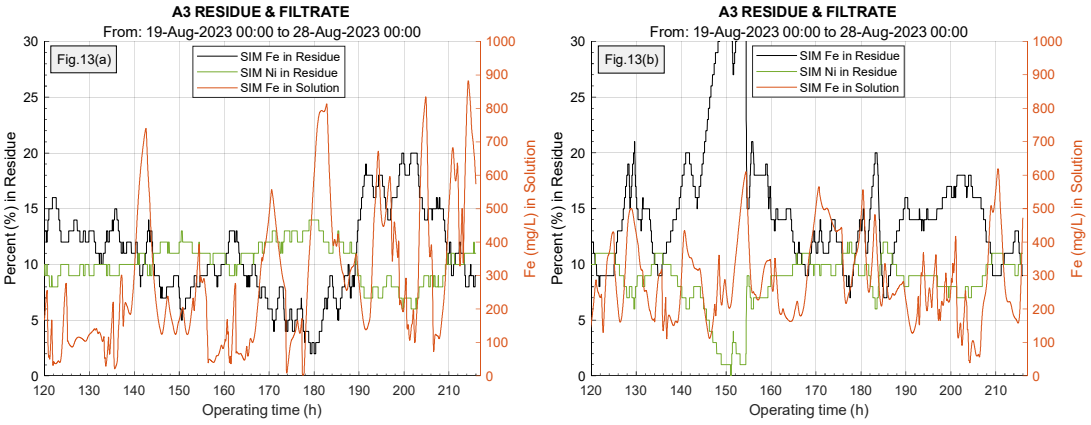

Figure 13: DT simulation of the (a) baseline, and, (b) scaled and modulated weak aqua flows.

Another noteworthy operational issue is the filtration rate through the filter presses. Since the feed pump to the filter presses is controlled by gap control, a persistent drop in the feed flowrate signifies filtration problems. Figure 14 compares the moving median of this flowrate with the simulated A3 pulp density (solids percent).

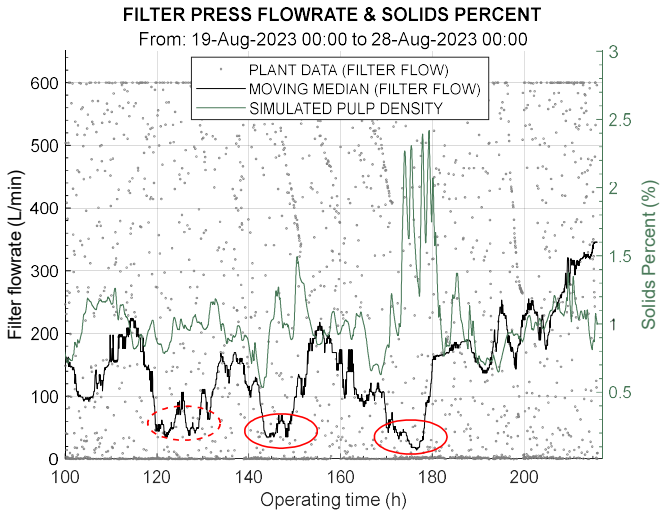

Figure 14: Measured filter feed flowrate vs the simulated A3 pulp density (solids percent). The encircled periods indicate persistent slower filtration rates on the plant.

Periods of slow filtration are encircled, while the predicted spikes in the simulated pulp density are due to the preferential precipitation of ammonium nickel sulfate hexahydrate salt. Despite some anomalies in Figure 14, these results suggest a correlation between the preferential formation of the ammonium nickel sulfate hexahydrate, predicted by the DT, and the slow filtration periods experienced on the plant. Furthermore, nickel losses would depend on the filterability and washing efficiency of the residue, and some of these slow filtration periods align with the elevated nickel levels in the final plant residue from the filter presses (Figure 3).

The above results and insights were gained from evaluating a single simulation period and utilising only an initial ML exercise. Importantly, the DT will be exposed to more datasets in the future and learning will improve – this is the real benefit of implementing a DT on an operational plant. To make the DT available to the operational staff, it has been packaged as an application product (APP) and distributed as a stand-alone executable.

CONCLUSIONS

The jarosite autoclaves at Implats have been in operation since the 1980's[5]. The plant works well, but relatively little new metallurgical information has been generated since its commissioning. Operational issues, like slow filtration, and perceptions of different precipitate phases forming, based on the colour of the final iron residue, have prompted a fresh look at the plant data. Since the operation is dominated by highly transient behaviour, modern state-of-the-art digital tools had to be utilised for this purpose. The results of developing and using a digital twin (DT) to capture the plant data, supplemented by data from a short sampling campaign, are discussed in this paper.

The backbone of the DT is the first-principles (FP) transient mass-energy balance (macro model), which is implemented in a manner that makes extensive use of machine learning (ML) to capture the complicated microscopic-level chemistry (micro model). The FP part of this hybrid DT provides structure to the model, which, in turn, helps to generalise and predict. Albeit exposed to only a single dataset, this powerful digital tool has been validated, and shown to be capable of predicting trends and creating insights into the low-level workings of the plant.

The hydrolysis of iron is driven by the injection of weak aqueous ammonia (aqua) by on/off valves to each autoclave compartment. The DT supports the sampling-campaign X-Ray Diffraction (XRD) analyses, suggesting that ammonium jarosite is the dominant iron hydrolysis product. Furthermore, the results have shown that the precipitation of ammonium nickel sulfate hexahydrate salt was most prominent during long autoclave residence time periods, when the weak-aqua dosage rates may have been too high. What-if scenarios were simulated, showing that valve modulation (instead of on/off timers) has potential. Advanced process control (APC) is also worth considering in the future.

The DT has been implemented as a standalone APP that can be exposed to more datasets in the future. It essentially becomes a 'living' digital report of the process to help improve operating strategies, process control, and operator training.

ACKNOWLEDGMENTS

The authors would like to thank the management of Implats for their vision, collaboration and permission to publish this paper. The authors are also grateful to Dauw Venter for providing the plant data, to Nagitta Kasirye for managing the sampling campaign, to Georg Langenhoven and Alida-Louise Henning for all the campaign analyses, and to Ian Smith for the XRD analyses.

The views of the authors do not necessarily represent those of Implats or its consultants.

REFERENCES

1. Steyl, J.D.T., Grobbelaar, G.B., 2020. Digital twinning in the metallurgical industry: the role of behavioural modelling and simulation. XXX International Mineral Processing Congress (IMPC) Proceedings, Cape Town, South Africa, 18-22 October 2020, 1-12.

2. The MathWorks Inc., Natick, MA, MATLAB, Simulink, Simscape, Release 2024a.

3. Dynamet, 2015. Dynamet Insights (Pty) Ltd., https://dynamet.co.za.
4.
5. OLI Systems Inc., Parsippany, NJ, OLI Studio, Stream Analyzer v11.5.

6. Plasket, R.P., Dunn, G.M., 1986. Iron rejection and impurity removal from nickel leach liquor at Impala Platinum Limited. International Symposium on Iron control in Hydrometallurgy Proceedings, Toronto, Canada, 19-22 October 1986, Ch. 37, 695-718.

ELECTROCHEMICAL SEPARATION OF SULFURIC ACID FROM MAGNESIUM SULFATE SOLUTIONS: APPLICATION FOR NICKEL LATERITE PROCESSING

[1]Mohamed H. Ibrahim, [2]Damien Batstone , [1]James Vaughan and [1]Karen Steel

[1]School of Chemical Engineering, University of Queensland, Australia
[2]Australian Centre for Water and Environmental Biotechnology, University of Queensland, Australia

ABSTRACT

mohamed.ibrahim@uq.edu.au

Nickel is used in various applications, especially in energy storage. To extract nickel from certain ores, a lot of sulfuric acid is needed, mainly because of minerals like magnesium silicates which consume the acid during extraction. This process creates waste solutions containing magnesium sulfate, which is harmful to the environment. However, electrochemical separation can help. It converts these waste solutions into sulfuric acid, which can be reused for nickel extraction, and magnesium hydroxide, which can be used for carbon capture or in the nickel extraction process.

In our recent study, we used a single membrane electrolyser to carry out this conversion. We evaluated its performance by looking at factors like efficiency, energy intensity, current density, and sulfate recovery. We found that starting with low concentrations of magnesium sulfate and applying a specific voltage maintained high efficiency. However, using higher voltages or concentrations had drawbacks like water splitting and excessive precipitation of magnesium hydroxide, which can cause operational issues.

After testing, we found that sulfate recovery ranged from 43-49% after 4 hours, depending on the initial concentration of magnesium sulfate in the solution. The energy required for producing sulfuric acid ranged from 2.94 to 4.44 kWh per kilogram of sulfuric acid produced.

INTRODUCTION

As the demand for nickel rises, particularly for its use in lithium-ion batteries powering electric vehicles and renewable energy systems, there's a pressing need to optimize nickel production and recycling processes. Nickel extraction from ores, especially from laterites, involves the use of sulfuric acid. However, laterite ores, rich in magnesium, present significant challenges during extraction and generate considerable waste. Traditionally, nickel production heavily relied on sulfide ores due to their easier processing compared to laterites. But as sulfide ore reserves dwindle, attention has shifted to laterites, which accounted for half of global nickel production by 2009. Yet, extracting nickel from laterites poses challenges, primarily due to their magnesium-rich composition.

During the extraction process, sulfuric acid leaching is used, resulting in the formation of magnesium sulfate waste streams. These waste streams not only impact the economic feasibility of processing such ores but also pose environmental concerns when disposed of, often into the ocean or stored in evaporation ponds. One promising solution to address the acid consumption in laterite ores, especially due to their high magnesium content, is electrochemical separation. This process involves converting the waste magnesium sulfate into sulfuric acid (H_2SO_4) and magnesium hydroxide ($Mg(OH)_2$) through electrochemical reactions. By doing so, it reduces the need for fresh acid in the leaching process, thus improving efficiency and reducing costs. Moreover, electrochemical separation enables the utilization of the generated magnesium hydroxide for various purposes. For instance, it can be used to precipitate nickel from the solution or in carbon capture processes to produce magnesium carbonates. Additionally, this approach eliminates the need for tailing neutralization, offering both environmental and economic benefits. Hence, electrochemical separation holds immense potential in enhancing the sustainability and efficiency of nickel production. By mitigating acid consumption, reducing waste, and enabling the reuse of by-products, it represents a promising pathway towards a more environmentally friendly and economically viable nickel industry.

The process of separating magnesium sulfate involves splitting sulfate from a neutral solution to create magnesium hydroxide and sulfuric acid. This is typically done in a two-chamber system, where the magnesium sulfate is introduced into the cathodic compartment. This setup helps prevent magnesium scaling on a membrane and reduces internal resistance. During the process, water electrolysis occurs, leading to hydrogen evolution at the cathode and oxygen evolution at the anode. Protons are consumed at the cathode, and hydroxide ions are consumed at the anode, causing ion migration. Sulfate transport from the catholyte to the anolyte is facilitated by an anion exchange membrane (AEM), which prevents magnesium diffusion to the anolyte. As the pH increases in the catholyte and decreases in the anolyte, and sulfate depletes in the catholyte, the faradaic efficiency (FE) decreases due to water splitting (H^+/OH^- migration). However, there's an initial period where high FE (>80%) is achieved before water splitting becomes dominant. This period is crucial for steady-state operation as it maximizes process efficiency and economic viability. Maintaining high FE is important as it ensures that the current passing through the electrolyzer is primarily utilized for sulfate transport. The type of AEM used, along with operational parameters like cell potential and influent concentrations, significantly influences sulfate transport efficiency. While our study focuses on operational parameters to determine sulfate transport efficiency and energy requirements, the choice of membrane properties, particularly a sulfate-specific AEM, plays a crucial role in the process.

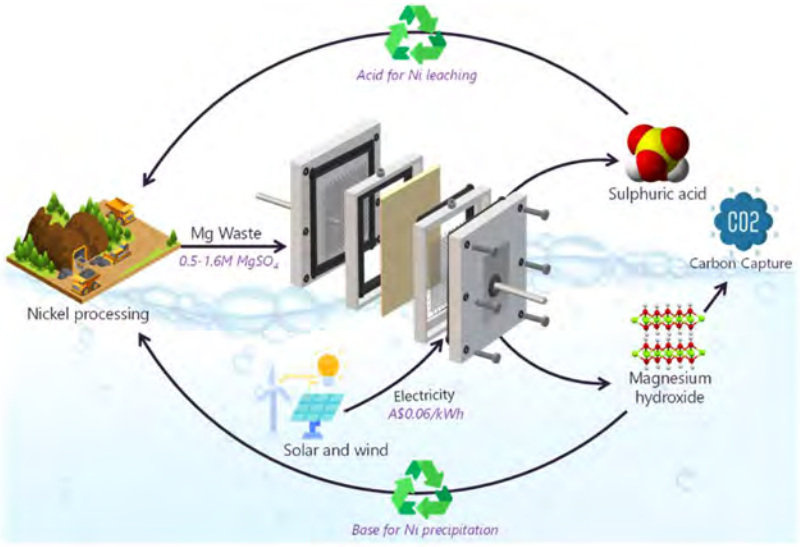

Figure 1. A schematic representation of the proposed magnesium sulfate electrolysis process

RESULTS & DISCUSSION

Effect of electrolyser potential

The study delved into exploring how the voltage applied to an electrolyser affects the transportation of sulfate ions. We conducted experiments using specific concentrations of electrolytes to understand how different voltages impact this process. Sulfate ion transport is influenced by several factors, including the potential gradient (migration), concentration gradient (diffusion), and pressure gradient (convection). Essentially, higher voltage leads to a greater rate of sulfate ion migration. However, there are drawbacks to consider. Higher voltages can reduce the efficiency of the process due to increased transport of non-target ions and greater internal resistance caused by conductivity limitations.

To understand these effects, we examined a range of voltages, from 3V to 5V. We observed that as the voltage increased, sulfate recovery and current density also increased. This suggests that higher voltage promotes more efficient sulfate transportation. However, we also found that FE, which measures how effectively the current is utilized for sulfate transport, decreased over time. This decrease in FE was attributed to membrane leakage, where non-target ions such as hydroxides from the catholyte and protons from the anolyte crossed the membrane. Interestingly, we noted that FE was highest at the beginning of the experiment but declined as the experiment progressed. This decline was more significant at higher voltages, especially beyond 40 minutes of operation. This is because at higher voltages, more water splitting occurs, contributing to the decline in FE.

The study also highlighted the importance of maintaining a low concentration of sulfuric acid in the anolyte to achieve high FE. We found that by keeping the anolyte concentration around 0.16M H2SO4, FE could exceed 80%. However, we noted that differences in temperature and pH between compartments could affect FE. Additionally, we found that energy intensity increased with higher voltage. This means that while higher voltages led to greater sulfate recovery, we also consumed more energy. For example, recovering 24% of sulfate over 1 hour at 5V consumed more energy compared to recovering only 5% at 3V. Finally, while higher voltage can enhance sulfate recovery, it also comes with increased energy consumption. Therefore, it's essential to strike a balance between efficiency and energy cost when optimizing sulfate transport processes.

Effect of initial catholyte concentration

The concentration of the catholyte, or the solution in the cathode compartment, significantly impacts the overall performance of the electrolyser. This concentration affects various aspects of the electrolysis process, including the concentration gradient, conductivity, ion pairing, solubility of reaction products, membrane fouling, and electrode scaling. To comprehensively understand these effects, the

researchers tested three different concentrations of magnesium sulfate (0.5M, 1M, and 1.5M) at two different potentials (4V and 5V).

One crucial finding was that increasing the concentration of the catholyte led to a greater flux of sulfate ions to the anolyte (the solution in the anode compartment). This was primarily due to the larger concentration gradient created by higher catholyte concentrations. Additionally, higher concentrations resulted in greater conductivity, leading to enhanced ion transport. This increase in conductivity was attributed to the availability of more charge carriers (sulfate ions), which reduced the solution's ohmic resistance. However, it was noted that increasing the concentration gradient does not always directly correlate with higher flux. For instance, while a concentration of 1M exhibited approximately 1.7 times higher flux than a concentration of 0.5M at a potential of 5V, the flux was lower for a concentration of 1.5M compared to 1M at all tested potentials. This suggests that there's an optimal concentration range for maximizing sulfate flux. Moreover, it was observed that electrode blockage, or scaling, occurred when the catholyte concentration exceeded 1M. This led to decreased current density, indicating less effective ion movement towards the anode. Significant deposition of magnesium hydroxide on the cathode was also observed at higher concentrations, particularly at 5V and 1.5M concentration. This deposition was attributed to the elevated concentration of magnesium ions (Mg2+) and the high pH of the cathodic compartment. Regarding faradaic efficiency, it was noted that increasing the catholyte concentration resulted in a higher rate of H+/OH- migration, which can decrease FE. This decrease in FE was observed across all tested concentrations when the voltage was increased to 5V. Conversely, energy intensity, which measures energy consumption, followed an opposite trend to FE. Higher FE resulted in lower energy consumption. For example, at 4V, the energy intensity was lower (2.3 kWh/kg) compared to 5V (3.4 kWh/kg). In short, while higher catholyte concentrations can enhance sulfate transport efficiency, they must be carefully controlled to avoid electrode scaling and maintain high FE and low energy consumption. These findings highlight the importance of optimizing catholyte concentration for efficient electrolyzer performance.

Effect of initial anolyte concentration

The concentration of sulfate ions in the anolyte, or the solution in the anode compartment, has both positive and negative effects on the electrolyzer system. This was tested by comparing anolyte solutions with different concentrations of sulfuric acid (H2SO4) - 0M, 0.1M, and 0.2M - at a voltage of 4V.

We found that a 0.1M concentration resulted in more sulfate recovery compared to 0.2M due to a higher concentration gradient. Although the 0.2M solution had slightly higher current density due to increased conductivity, most of this current was used for water splitting rather than transporting sulfate, resulting in lower faradaic efficiency (FE). Consequently, the 0.2M solution required about 45% more energy to transfer sulfate within the same time frame. To determine the minimum anolyte concentration and conductivity needed to maximize sulfate transport, we conducted experiments using 1M MgSO4 catholyte and ultra-pure water anolyte (0M) at 4V. We found that having high initial solution resistance in the anolyte led to lower initial FE. However, over time, conductivity in the anolyte increased, eventually decreasing internal resistance and maximizing sulfate transport.

The experiments showed that a minimum sulfate concentration of 0.05M and a corresponding conductivity of 30 mS/cm were needed to achieve maximum FE. Above 0.15M, FE declined due to sulfate accumulation in the anolyte. Both anolyte concentrations eventually achieved the same current density of approximately 25mA/cm2. After 4 hours, 49% sulfate recovery was achieved at 0M compared to 43% at 0.1M, with the difference primarily due to a larger concentration gradient. The average energy intensity for the 0.1M experiment was 2.94 kWh/kg, while it was 4.44 kWh/kg for the 0M experiment. In essence, maintaining an optimal sulfate concentration and conductivity in the anolyte is crucial for maximizing sulfate transport efficiency and minimizing energy consumption in the electrolyzer system.

Energy intensity analysis

Sulfuric acid holds a pivotal role across various industries worldwide, earning it the status of one of the most indispensable chemicals in industrial processes. However, its conventional production method involves energy-intensive procedures like the oxidation of elemental sulfur, typically sourced as a byproduct of oil and gas extraction. This method is associated with high temperatures, pressure, and sulfur emissions, contributing to its high energy intensity, which is approximately 1.67 kWh/kg H2SO4.

In recent times, there has been growing interest in exploring electrochemical alternatives for sulfuric acid production. These alternatives aim to produce diluted sulfuric acid with lower energy intensity, providing potential downstream benefits such as easier concentration. The thermodynamic limit for energy intensity in such electrochemical processes is around 0.82 kWh/kg H2SO4, significantly lower than conventional methods. However, current electrochemical methods have not yet matched the capacity and purity levels achieved by conventional technologies. The chlor-alkali process serves as a benchmark in the industry, setting standards for current density (often exceeding 100 mA/cm2) and energy intensity (ranging from 2 to 4.5 kWh/kg H2SO4 equivalent). In a comparative analysis, energy intensity associated with electrochemical sulfuric acid production was found to be within the bounds of the chlor-alkali process. Interestingly, higher current densities were linked with lower energy intensity, suggesting potential efficiency gains with improvements in electrochemical processes. To enhance current densities in electrochemical sulfuric acid production, several strategies are being explored. These include modifications to electrode designs, such as increasing surface area and implementing anti-fouling surface treatments. Adjusting the local reaction environment and reducing the gap between electrodes are also promising avenues for improving performance. Additionally, optimizing operating conditions, such as controlling catholyte temperature, can help mitigate issues like magnesium fouling on cathodes by enhancing the solubility of magnesium compounds. Maintaining high faradaic efficiency (FE) is crucial for efficient sulfuric acid production. FE can be optimized by carefully controlling the sulfuric acid concentration in the anolyte, ensuring that electrochemical processes remain efficient and cost-effective. These ongoing advancements in electrochemical sulfuric acid production hold promise for reducing energy consumption and environmental impact in the industrial production of this vital chemical.

Economic analysis

Electrolysis represents a promising avenue for industrial processes, offering energy-efficient operations with significantly lower carbon emissions compared to conventional methods. This advantage becomes even more pronounced when renewable energy sources like solar and wind are employed, which are becoming increasingly affordable, particularly in regions like Australia. As the costs of electricity generation from renewables continue to decline due to advancements in technology and increased market penetration, the overall economics of electrochemical processes, including acid recycling, are expected to improve. The key economic factors influencing electrochemical acid recycling are the capital cost of electrolyzers and electricity expenses. By comparing two electricity scenarios - one based on fossil fuels and the other on renewable sources - it becomes evident that utilizing renewable energy can significantly reduce the cost of acid production. For example, the average cost of generating acid using renewable energy was found to be A$143 per tonne, while the cost using fossil fuels was substantially higher at A$477 per tonne. Even when considering an average acid purchase cost of A$200 per tonne, electrochemical acid generation proves to be a more economically attractive option. Batch experiments were conducted to determine critical operational parameters for industrial applications, such as sulfate flux, faradaic efficiency (FE), power consumption, and the onset of side effects like magnesium hydroxide precipitation. These experiments not only provided insights into the initial costs of acid production but also revealed that the cost decreases over time as the concentration of acid in the anolyte increases. Based on these findings, a basic economic assessment was conducted to evaluate the cost savings associated with producing nickel using sulfuric acid generated through electrolysis with renewable energy. The analysis showed a potential cost reduction of 22% compared to purchasing acid. Furthermore, utilizing magnesium hydroxide generated by the electrolyzer could further decrease costs associated with nickel precipitation. Additionally, carbon capture presents another avenue for cost minimization through potential reductions in carbon taxes.

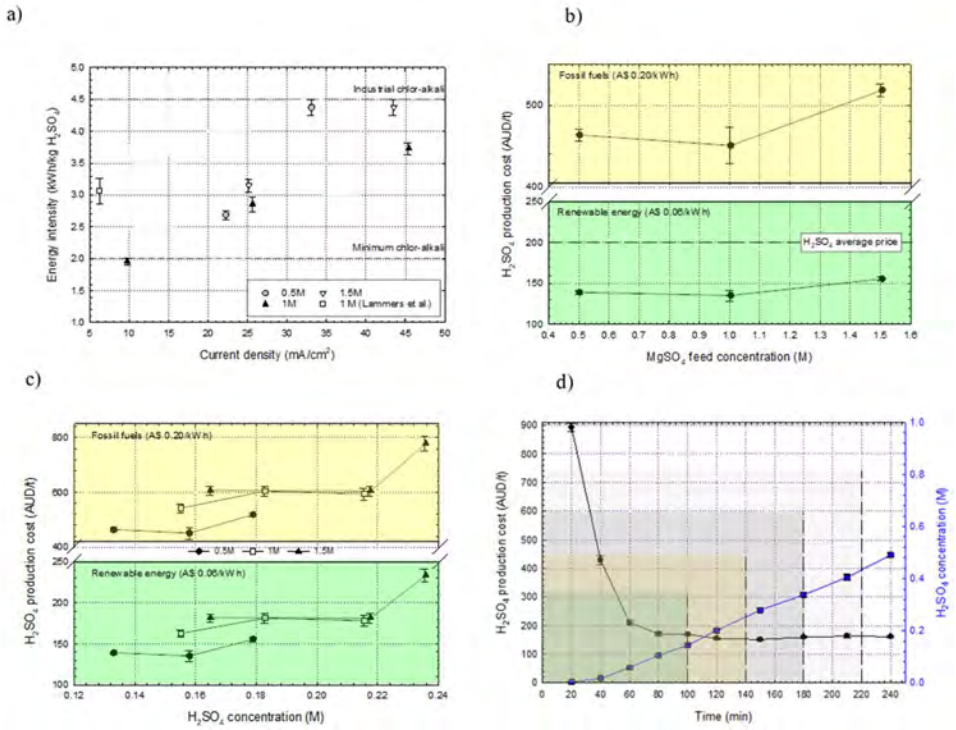

Figure 2. a) sulfuric acid energy intensity as a function of time-average current density at 0.5, 1 and 1.5M MgSO4 and 0.1M H2SO4 compared to data obtained from Lammers et al.[19] using 1M MgSO4 b) sulfuric acid cost using different electricity prices (utilizing the energy intensity data from the first 20 minutes of batch experiments at 4V and 0.1M H2SO4) across a MgSO4 feed range of 0.5 to 1.5M and 0.1M H2SO4 initial anolyte concentration c) sulfuric acid cost using different electricity prices as a function of the recovered acid concentration in the anolyte at 0.5, 1 and 1.5M MgSO4 catholyte concentration and 0.1M H2SO4 initial anolyte concentration d) acid production cost (calculated using average renewable energy price in Australia, A$0.06/kWh) and anolyte concentration as a function of time

CONCLUSIONS

Our study found a strong relationship between faradaic efficiency (FE) and the concentrations of sulfuric acid (H2SO4) in the anolyte and magnesium sulfate (MgSO4) in the catholyte. Lower anolyte concentrations tended to result in higher FE, especially at specific catholyte concentrations and potentials. For example, with a 1M catholyte and 4V potential, FE could exceed 90% until the anolyte concentration reached 0.16M, indicating a good starting point for continuous operation. Increasing the potential difference between the electrodes improved sulfate mass flux per membrane area within a limited range of feed concentrations. However, feed concentrations beyond 1M led to magnesium hydroxide deposition on the electrode, reducing its surface area.

We found that the minimum anolyte concentration required to achieve the highest sulfate FE was 0.05M at a 1M catholyte concentration. In our experiments, operating for 4 hours at 4V with an initial catholyte concentration of 1M resulted in recovering 49% and 43% of sulfate at starting anolyte concentrations of 0M and 0.1M, respectively. The corresponding energy consumption values were 4.44 kWh/kg H2SO4 for 0M and 2.94 kWh/kg H2SO4 for 0.1M. Our study highlights the importance of using renewable energies for the economic viability of acid recycling. However, we also identified that the current density obtained may not be sufficient for seamless integration with renewables, indicating the need for attention to electrolyzer design. Additionally, addressing electrode scaling is crucial to unlocking the full potential of the electrolyzer.

REFERENCES

The information reported in this paper is taken from the following manuscript:

M. H. Ibrahim, D. Batstone, J. Vaughan, and K. Steel, “Electrochemical separation of sulfuric acid from magnesium sulfate solutions: Application for nickel laterite processing,” Sep. Purif. Technol., vol. 336, p. 126291, 2024, doi: https://doi.org/10.1016/j.seppur.2024.126291.

TECHNOLOGY SELECTION AND FLOW SHEET OPTIMISATION FOR NICKEL AND COBALT SULPHATE CRYSTALLISATION PLANTS

By

Nipen M. Shah, Chris Madin, [2]Ivan van Rensburg

JordProxa, Australia
[2]JordProxa, South Africa

Presenter and Corresponding Author

Nipen Shah
nshah@jordproxa.com

ABSTRACT

The safety and performance of lithium-ion batteries are deeply influenced by impurities in their precursors, necessitating the production of the battery materials such as nickel sulphate and cobalt sulphate to the highest purity. The declining prices of battery materials have put pressure on the producers to optimise the capital and operating expenditures to make the projects economically viable.

Crystallisation is the most important final purification step in producing the high purity battery grade products. The optimal design of nickel and cobalt sulphate crystallisation plants hinges on key technological choices and flow sheet optimisations. A properly designed crystalliser producing large, well-formed crystals allows for improved washing to enable the achievement of the highest purities possible. This paper evaluates the efficacy of Forced Circulation (FC) versus Draft Tube Baffle (DTB) crystallisers, evaluating their respective merits in achieving desired purity levels, capital costs, and operational efficiency.

A further technical innovation is the incorporation of mechanical vapour recompression (MVR) technology which results in a significant reduction in the overall energy input per ton of product when compared with steam heated designs. This paper also investigates the trade off between the capital and operating expenditures for both these heat input options.

This paper describes crystalliser design features to produce battery grade nickel sulphate hexahydrate and cobalt sulphate heptahydrate products, and will compare the operating conditions, crystalliser types, preferred energy source, control of product purity, and trade-off between capital and operating costs.

Keywords: nickel sulphate, cobalt sulphate, crystallisation, MVR, purity

Technology Selection and Flow Sheet Optimisation for Nickel and Cobalt Sulphate Crystallisation Plants

by Nipen Shah, Ivan Van Rensberg, Chris Madin

JordProxa

Presented by

Nipen Shah

nshah@jordproxa.com

PURITY - Free from impurities

SUSTAINABILITY - Low carbon footprint

VALUE - High ratio of performance / cost

1

Crystallisation

Simplified crystallisation process

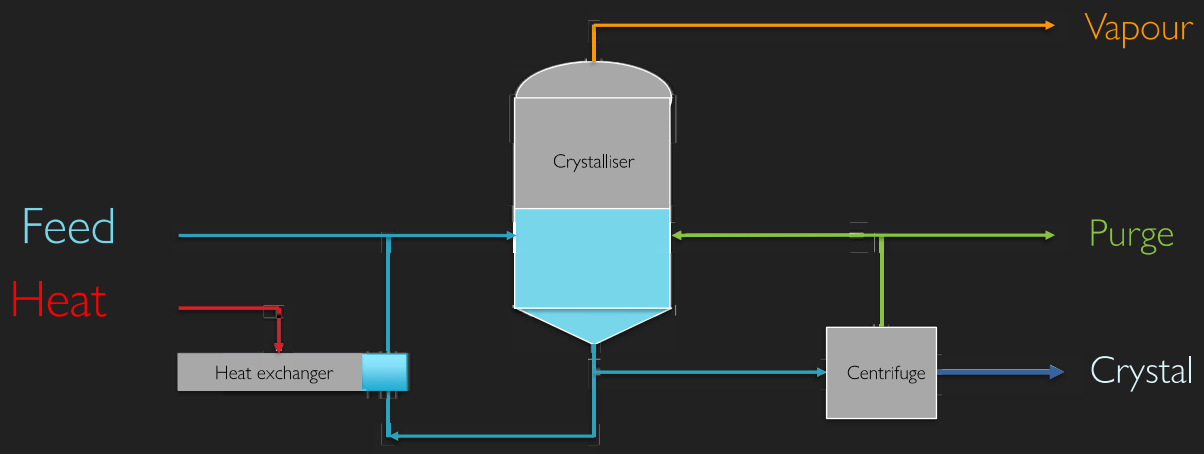

OBJECTIVES

- Product purity
- Large crystal size
- Minimum energy
- Minimum capex
- Ease of operation

Solubility of Cobalt Sulphate

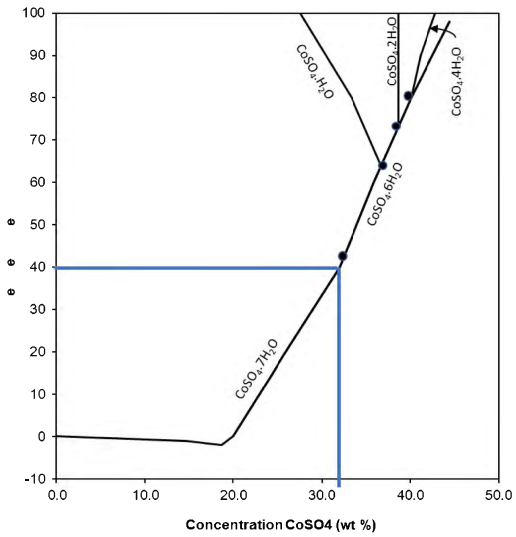

Solubility of Nickel Sulphate

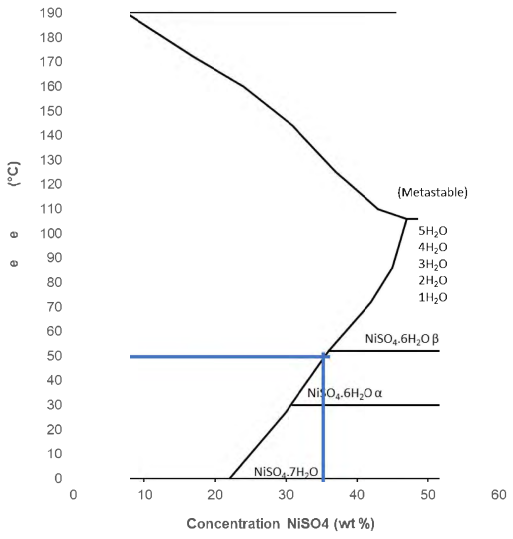

Operating Conditions

	Nickel Sulphate	Cobalt Sulphate
Product form	α-$NiSO_4.6H_2O$	$CoSO_4.7H_2O$
Operating pressure (kPa)	10.9	6.6
Operating temperature (°C)	50	40
Mother liquor concentration (%)	34.5	32.2
Dry product temperature (°C)	50	40

2

Design Considerations to Achieve Product Purity

Boiling Point Elevation

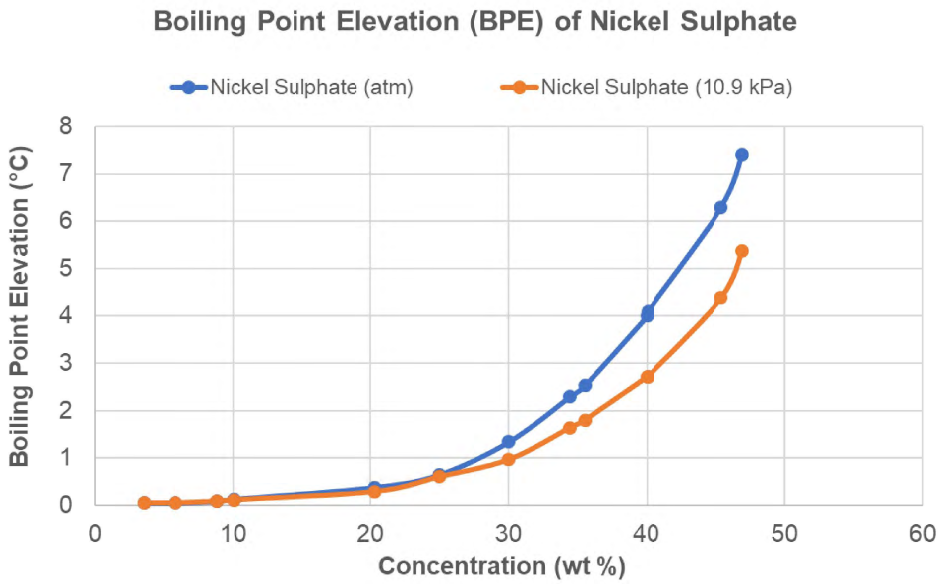

Fines destruction

- By either diluting with water or heating the liquor to increase solubility.
- Addition of water increases thermal load on the crystalliser

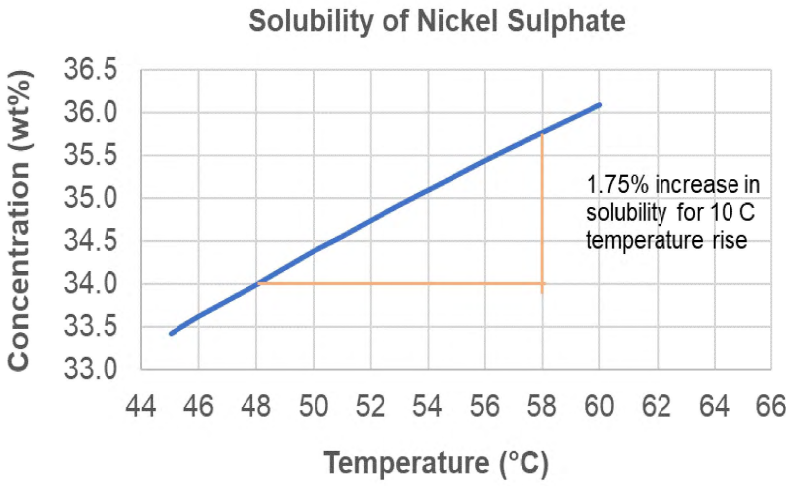

Elutriation leg

- Operates with hindered settling zone i.e. reduced, settling velocity determined by crystal size, liquor and solid properties.
- Thickening / concentration zone to extract a slurry directly to centrifuges

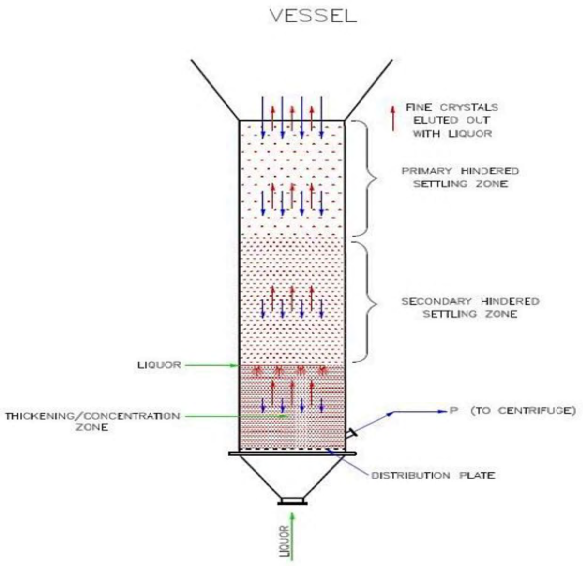

Impurity Entrainment

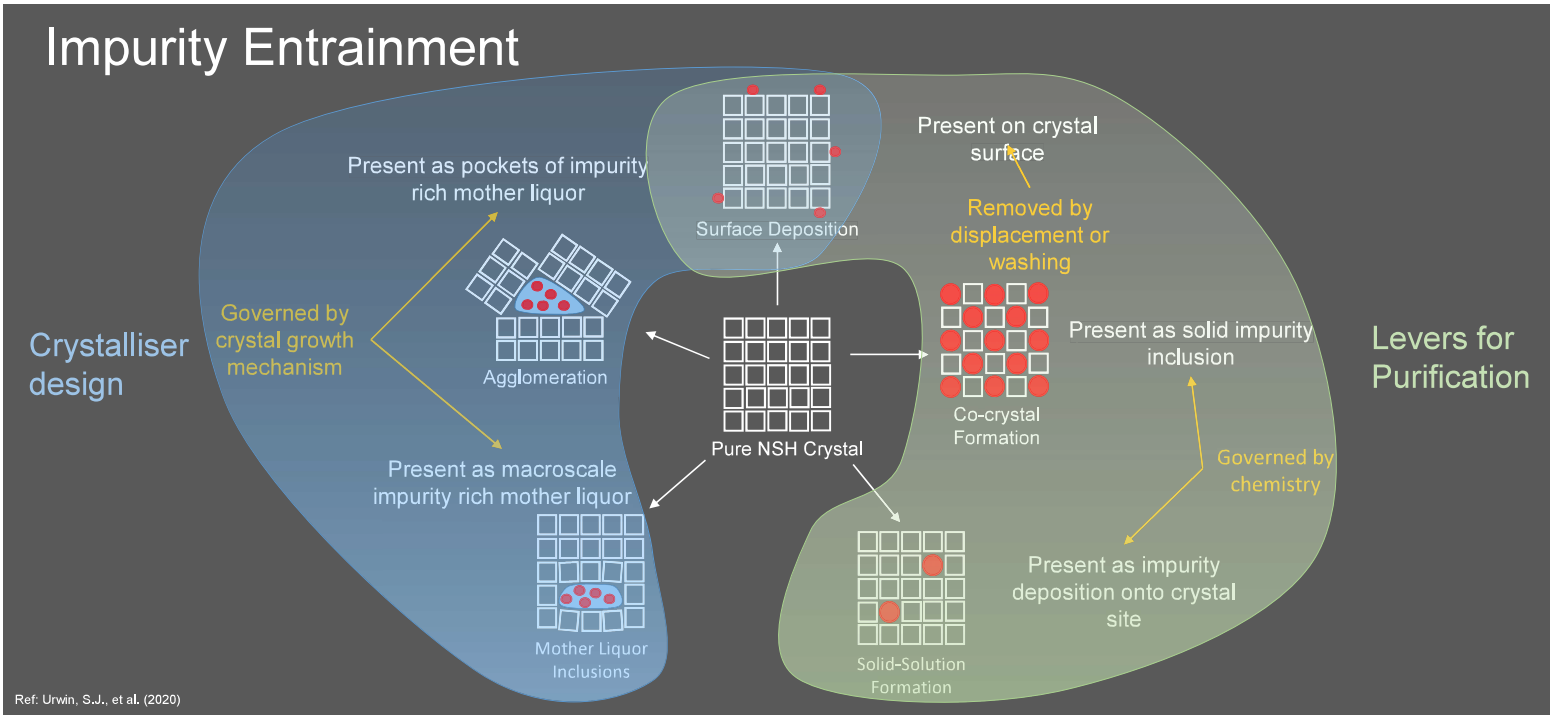

Ref: Urwin, S.J., et al. (2020)

Levers for Purification

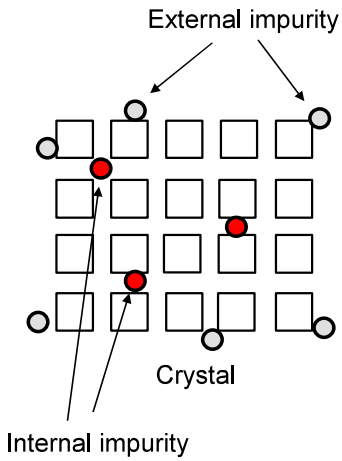

- **Centrifugation** displaces surface depositions by washing and ML removal.
- **Wash legs** reduce surface depositions by partly displacing high impurity ML with feed.

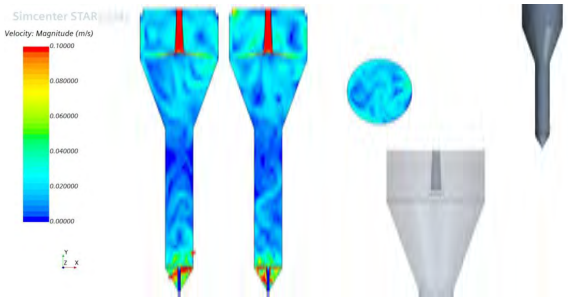

Levers for Purification

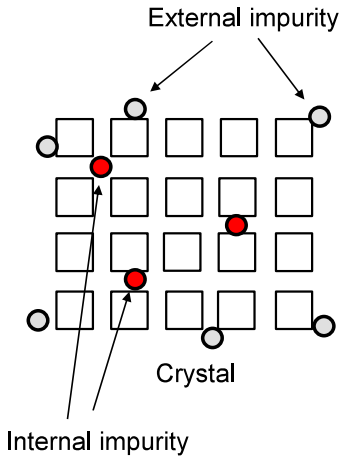

- **Staged crystallisation** reduces ML impurity fingerprint profile.
- **Purge/Recycle rates** reduce ML impurity fingerprint profile.

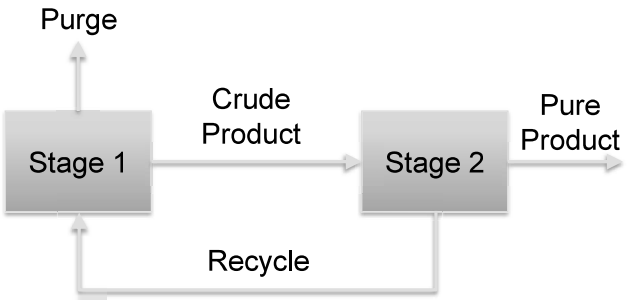

Thermal Considerations

3

Energy Addition

	STEAM	ELECTRICAL POWER
THERMAL	Thermo-vapour recompression (TVR) Multiple Effect	Mechanical-vapour recompression (MVR) fan(s)
COOLING	Flash cooling with steam booster	Surface or flash cooling with chiller

MVR FANS

- Improved fan dynamics
- Better materials, higher speeds
- Higher efficiency, lower power use
- 18 deg temp rise with 2 fans

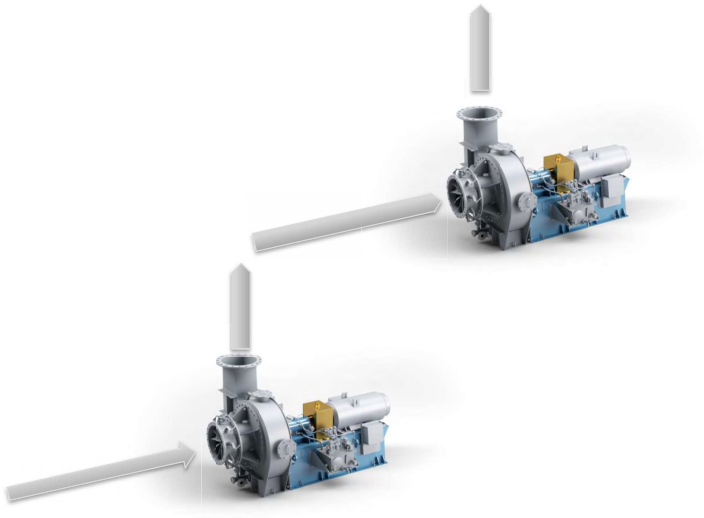

TVR

- Uses steam motive to compress a portion of evaporated vapour
- Reduces steam consumption ~ 2 x
- Balance of evaporated vapour is condensed
- Limit in terms of dT and turn-down

Capex and Opex Trade-off

	MVR	TVR
Steam (kg/h)	Start-up, small makeup	1200 kg/h
MVR Electricity (kW)	60 to 105 kW (depending upon BPE)	N/A
Cooling Water (kg/h)	0 m3/h or small flow for vent	140 m3/h (5deg rise)
Capital Costs	+ 5%	

Basis: 2500 kg/h evaporation

4 Equipment Selection

FC CRYSTALLISER

- High evaporation rates
- Draft tube provides superior mixing and boiling pattern
- Internal baffles provided to control slurry density and fines
- Elutriating legs (optional) provides classified discharge for superior size distribution or slurry density

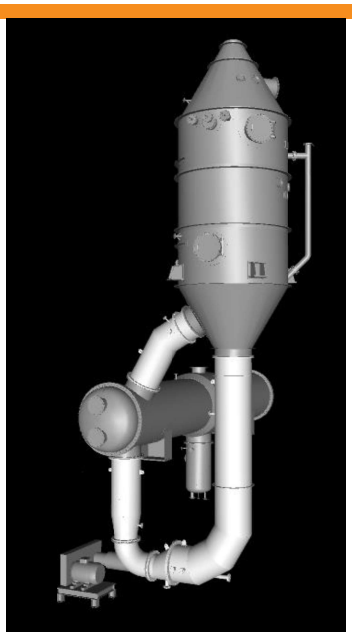

DTB CRYSTALLISER

- Large crystal size
- Internal baffles to enable fines extraction and destruction, resulting in narrow product size distribution
- Internal draft tube with agitator provides high internal circulation
- Elutriating leg (optional) provides classified product size distribution

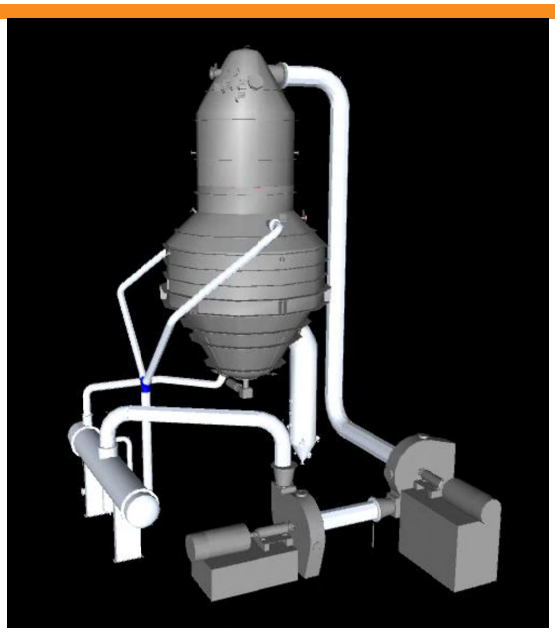

Conclusions

4

CONCLUSIONS

- Crystallisation is a key step in the processing of battery materials such as nickel sulphate to achieve the desired product purity.
- A carefully designed crystalliser can produce crystals large enough for effective dewatering and washing.
- We need to control liquor chemistry & kinetics to prevent lattice substitution; formation of double salts; inclusions and agglomerates.

CONCLUSIONS

- FC and DTB crystallisers can be used for $NiSO_4$ and $CoSO_4$ applications but the trade-off between purity and capital costs must be considered during equipment selection.

- TVR can be a cost effective option when there is waste steam available. Otherwise MVR works out as the most cost effective solution from the operating costs point of view.

- As the demand for the product purity increases, the requirement for optimisation and further enhances in the technology become critical.

THE USE OF ION EXCHANGE RESINS TO PRODUCE HIGH PURITY COBALT AND NICKEL SULPHATE

By

Johanna van Deventer

Purolite

Presenter and Corresponding Author

Johanna van Deventer
Johanna.vandeventer@purolite.com

ABSTRACT

Ion exchange is widely used in hydrometallurgical operations for the recovery and purification of valuable metals, such as nickel and cobalt. The growth of the electric vehicle market has resulted in an increase in demand for metals used in the batteries. Although commonly referred to as lithium batteries, appreciable amounts of cobalt, nickel, manganese and other metals form part of these batteries.

The metal salts used in the manufacturing of EV batteries may be obtained from mining operations. Recycling of used batteries is a growing source of material, with recycling being mandated by law around the world. Regardless of the origin of the metals, there are a number of impurities present in the nickel/cobalt liquor that need to be removed to low levels, to produce precursor materials that are suitable for the production of high-quality batteries. Such impurities typically include iron, uranium, copper, zinc, nickel, cobalt, bismuth and antimony.

Special chelating resins have a high affinity for specific elements, allowing the selective removal of low levels of impurities from a background of highly concentrated valuable metal. Solvent-impregnated resins have been added to this group more recently, expanding the choice of sorbent.

In addition to choosing the right type of resin for the job, manipulation of the operating conditions, such as pH, provides additional selectivity. Choosing the optimum contactor design is critical to ensure consistent quality while at the same time being economically feasible and taking due consideration of incorporation of the ion exchange unit operation in the overall flowsheet.

This article takes a closer look at various applications of ion exchange in the production of high-purity cobalt and nickel sulphate.

Keywords: ion exchange, nickel sulphate, cobalt sulphate, purification, hydrometallurgy

Producing high-purity Nickel and Cobalt

Application of ion exchange resins

Johanna van Deventer

Purolite, South Africa

johanna.vandeventer@purolite.com

Agenda

1. What is the aim of treatment?
2. Matching the target metal with the correct ion exchange resin
3. Design configuration
4. Resin characteristics (mechanical) to suit the design
5. Conclusions

01 What is the aim of the treatment?

Ion exchange resins in hydrometallurgy

Bulk recovery

Ion exchange resins are used to recover the main metal of interest

- Gold
- Uranium

Impurity removal

Ion exchange resins are used to remove low levels of impurities from a high-concentration background

- High purity $CoSO_4$ crystals
- Nickel metal

What do we want from the resin?

- High selectivity for the target metal of interest
- Good rejection of other components
- High capacity
- Low leakage
- Ease of elution
- Robust – to ensure a long life

02 Choosing the best resin for the task

Choosing the right resin (chemistry)

Impurity	Type of resin	Commercial examples
Uranium	Strong base anion exchange	Purolite MTA8000 Dow Ambersep 4400
Copper and Zinc	Amino-methyl phosphonic acid Iminodiacetic acid D2EHPA-impregnated	Purolite MTS9500, Lanxess TP260 Purolite MTS9300, Lanxess TP207 Purolite MTX7010, Lanxess OC1026
Cadmium	Amino-methyl phosphonic acid D2EHPA-impregnated Thiourea	Purolite MTS9500, Lanxess TP260 Purolite MTX7010, Lanxess OC1026 Purolite MTS9140, Lanxess TP214
Nickel	Bis-picolyl amine	Dow M4195 Purolite MTS9600 Lanxess TP220

Chelating resins

Chela:
a latin word for pincers

Iminodiacetic acid (IDA) resin

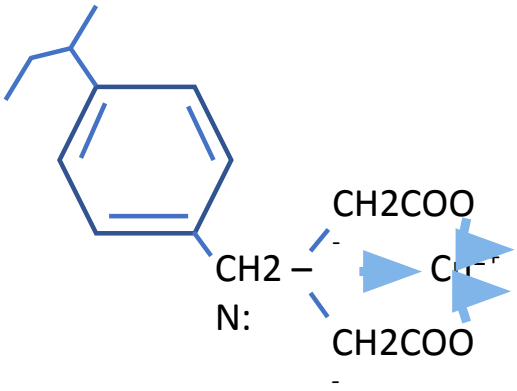

Combination of
- ion exchange
- electron pair sharing

Chelating Resins: Selectivity range

Example: **iminodiacetic acid (IDA) resin**

Selectivity:

$Fe^{3+} > Al^{3+} > Cu^{2+} >> Ni^{2+} > Cd^{2+} > Zn^{2+} > Co^{2+} >> Mn^{2+} > Ca^{2+} > Mg^{2+} > Na^{+} \sim Li^{+}$

- **Iron** should be removed prior to IX
- Good selectivity over alkaline earths (magnesium and calcium)
- Good selectivity over alkali metals (sodium and lithium)

Chelating Resins: Selectivity vs pH

- Resin loading is dependent on the pH of the solution
- pH control is critical

Example: IDA resin

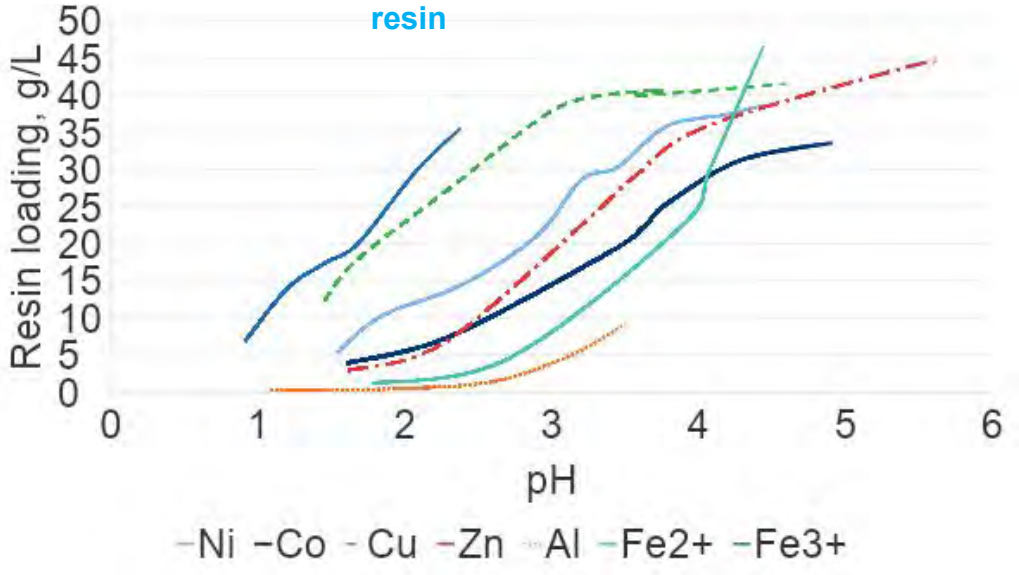

Chelating Resins: split elution

- Additional separation can be achieved during elution
- Less strongly held metal (Co) eluted first with lower concentration acid
- Cu (more strongly held) requires more concentrated acid

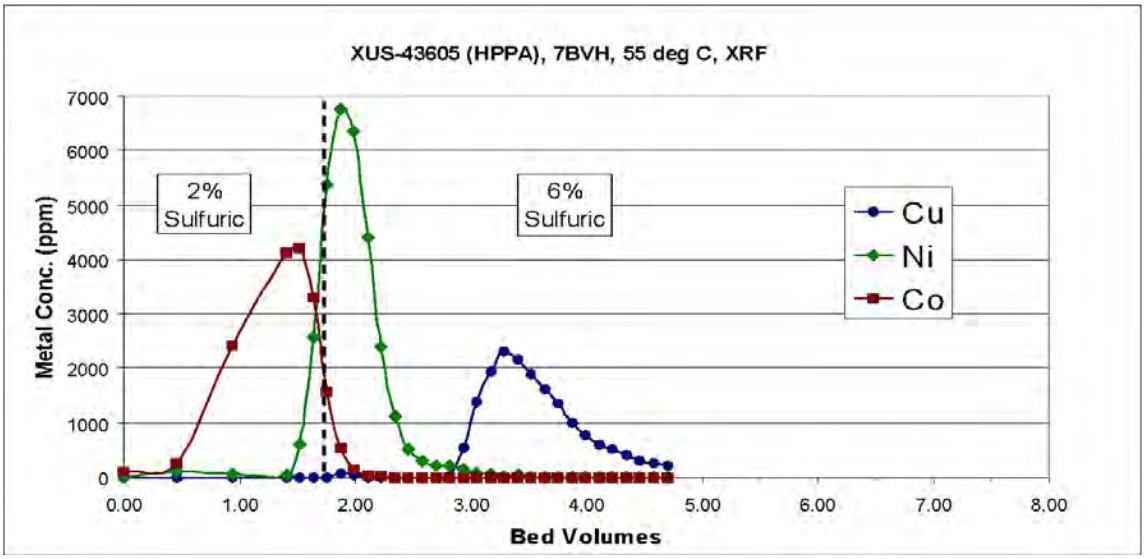

Marston et al, Alta Metallurgical Conference 2010

Marston et al, Alta Metallurgical Conference

Solvent-impregnated resins

- Organic solvent incorporated into ion exchange resin
- Has physical characteristics of an ion exchange resin
  - Reactor design/engineering as for fixed bed ion exchange systems
- Has chemical characteristics of the solvent:
  - selectivity range
  - pH dependence
- Application: production of high-purity liquors

Solvent-impregnated resins

D2EHPA

Removal of Fe, Zn, Ca, Cd from Co and Ni

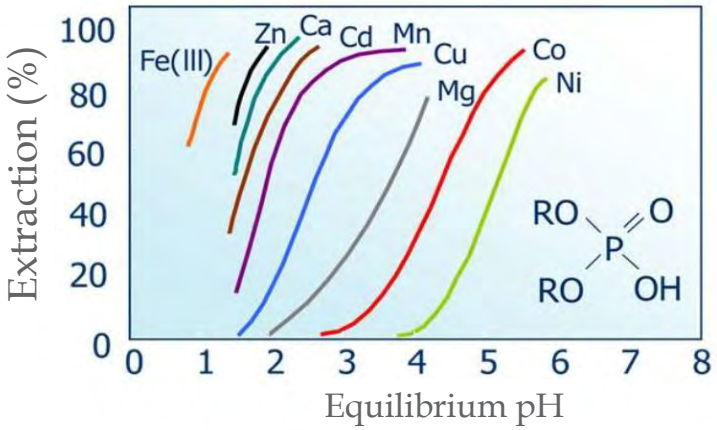

TMPPA

Removal of Zn, Cu, Co from Ni

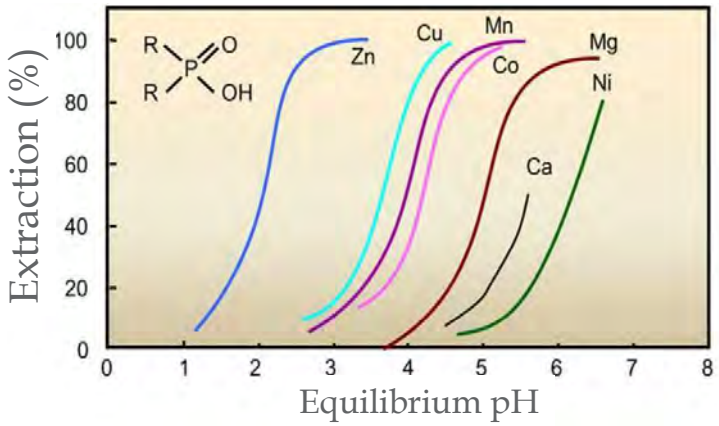

Dr Kathy Sole, Alta 2018, keynote address

A note of caution

- Published graphs are generated with all components in equal concentrations
- Real solutions have vastly varying concentrations

  For example:
  - 50 mg/L Cu and 50 g/L Ni
  - Ni:Cu = 1000

- Both selectivity and pH dependence is affected by the relative concentration of elements
- Test work in the specific matrix is essential to establish relative metal loading

03 Contactor design

Ion exchange reactor design

The choice of IX contactor design is based on the solids content of the feed

Solids content	Ion exchange reactor
Clear liquid, < 1 ppm solids	Fixed bed column
Liquid with some solids, <500 ppm	Fluidised bed column
Pulp, 10 – 50 % solids	Resin-in-pulp (RIP) - agitated vessels

Fixed bed design

- Best for impurity removal tasks
- A fixed or packed bed of resin, i.e. no movement/fluidisation of the resin during forward flow conditions
- Theory: the resin bed is divided into an infinite number of horizontal plates, each having a different concentration than the plate above and below it
- A concentration gradient is established across the vertical of the resin bed
- This ensures very low leakage to the Barren liquor

Resin selectivity at work

Feed liquor:
4 g/L cobalt
0.2 g/L copper
Sulphate salts

Downflow

MTS9500 (AMP resin)

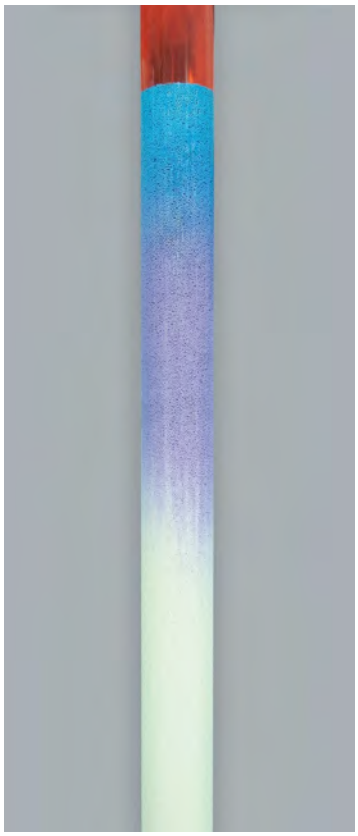

Resin is fully loaded with blue copper

Purple, showing a mixture of blue copper and pink cobalt loaded onto the resin

Beige, similar colour as fresh resin, no metals have loaded onto this portion yet

Fixed bed design: Mass Transfer Zone

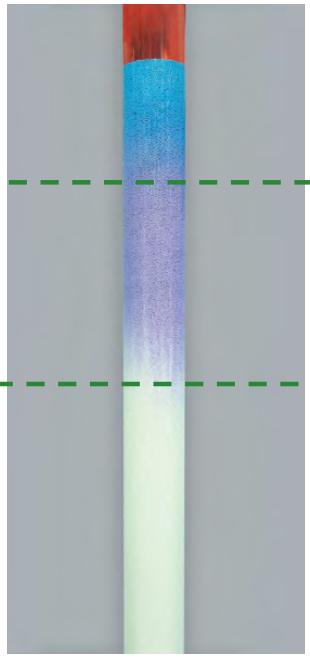

Fixed bed design: options

Continuous operation is most efficient
Ion exchange operates in a batch-continuous manner:

Continuous sorption – stop – continuous elution – stop

Multi-column systems approaches continuous operation
- 20 to 30 columns
- Each receiving a different liquor (Feed solution, washwater, eluant)

Merry-go-round or lead-lag-lag system, 3 columns in series
- Offers flexibility
- Simpler and cheaper

Merry-go-round system

Upon start-up

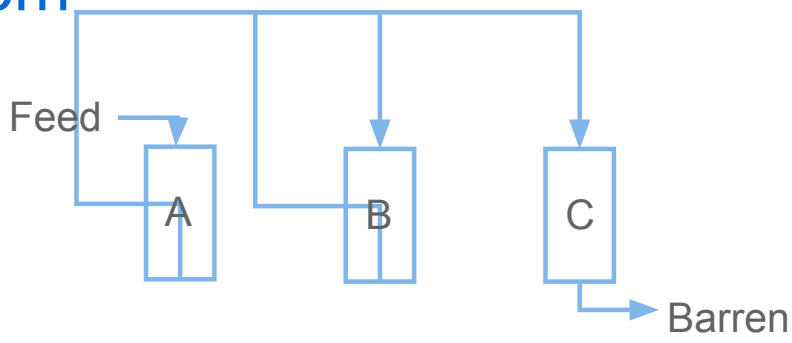

At the end of Cycle 1

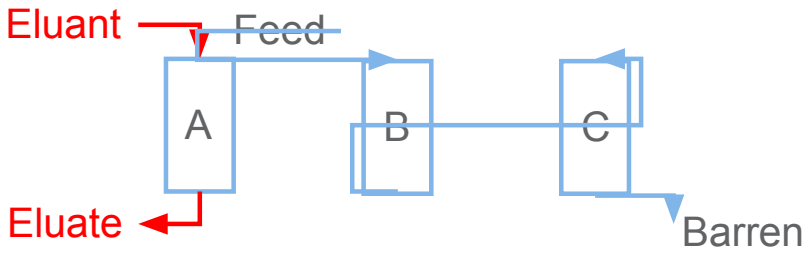

Merry-go-round system

At the end of Cycle 2

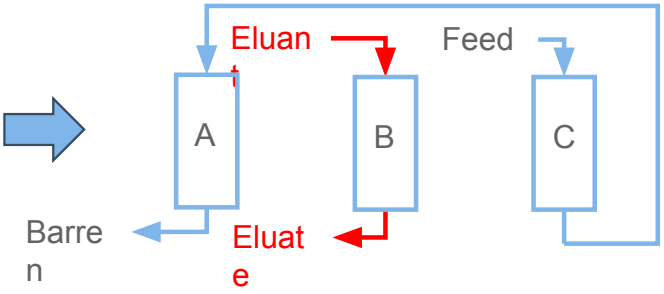

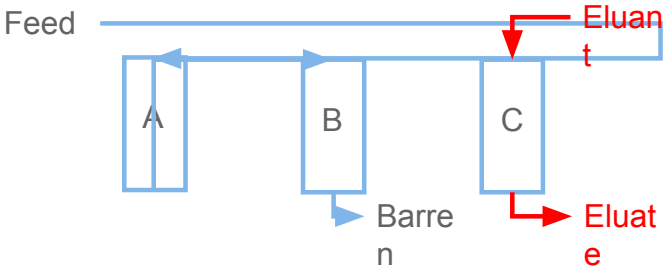

At the end of Cycle 3

At the end of Cycle 4
(similar to configuration at the end of Cycle 1)

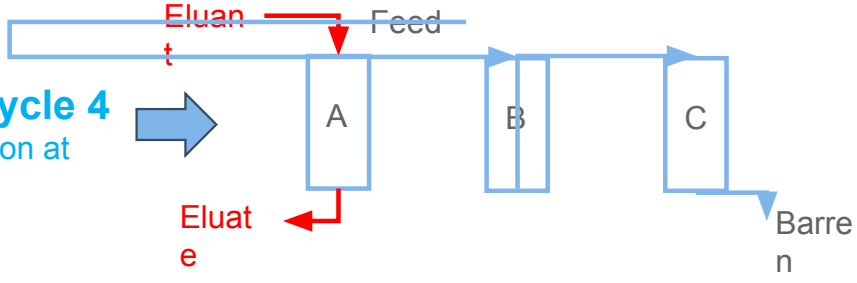

Merry-go-round system: advantages

Ensures maximum resin capacity utilisation on the first column

Ensures low leakage from the last column

Merry-go-round system: advantages

Ensures maximum resin capacity utilisation on the first column

- Low resin volume
- Smaller plant, smaller footprint = low capex
- Reduced reagent consumption = low opex

Ensures low leakage from the last column

- A polishing zone is maintained at the outlet
- Ensure specification of final product is met
  - final product fetches high price
  - Avoid penalties for low quality

04 Resin characteristics to suit the design

Choosing the right resin (mechanical)

- Particle size distribution
- Mechanical strength

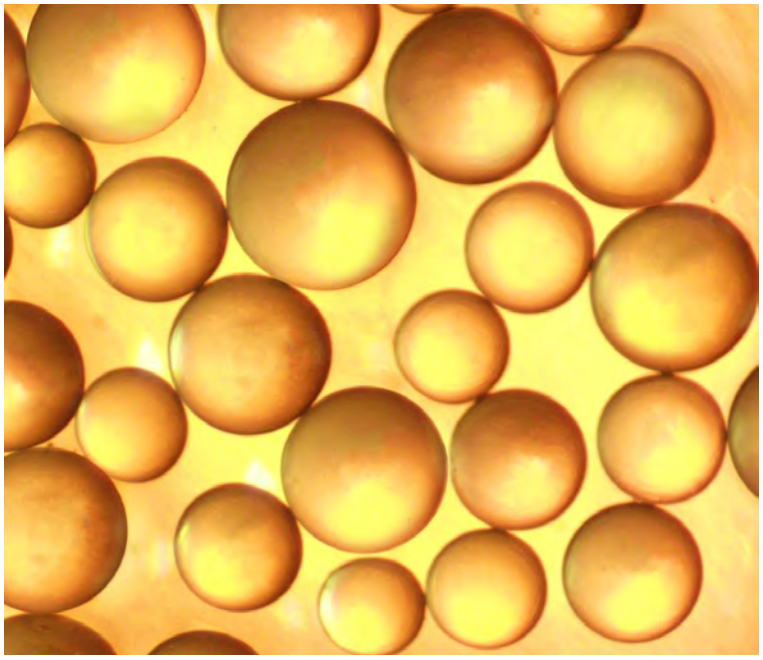

Choosing the right resin: particle size distribution

A small particle size ensures fast kinetics
BUT
also causes high pressure drop across a column

Standard grading: 300 to 1200 micron

Narrow size distribution: 600 to 800 micron

- Uniform kinetics – all resin beads participate equally
- Low pressure drop

Choosing the right resin: physical strength

Causes of resin attrition

- Physical handling
  - pumping,
  - transfer between vessels
- Osmotic shock
  - swelling and shrinking due to exposure to different liquors

Physical strength can be measured in various ways:

- Breaking weight: typically >500 g per bead
- Russian Ball Mill parameter: >92% perfect beads after 6 hours of milling
- Critical in resin-in-pulp (RIP) systems
- Less critical in fixed bed operations

Choosing the right resin: mechanical

IX resins typically last 3 to 5 years
Annual top-up of 5 to 10% required
Complete replacement of the inventory at the end of life

How to take care of the resin:

- Minimise physical handling
- Minimise temperature shock
- Inspect vessel internals regularly to prevent losses

CONCLUSIONS

Conclusions

Ion exchange can be used in a wide range of application

- Bulk recovery of target metals
- Removal of impurities to low ppm, even ppb, levels

Different resins are used to target specific impurities

- selectivity range
- pH dependent
- affected by relative concentrations of elements

Considerations: ion exchange

- What is the target metal(s) or impurity
- Matrix, e.g. acidic (sulphate, chloride, etc) or alkaline (cyanide, sodium carbonate, etc)
- Solution pH
- Recovery from pulp (RIP), clear solution (fixed bed) or ‘dirty’ liquors (fluidised bed)
- Presence of competing ions (which ions, relative concentrations)
- Solution temperature
- Integration with other unit operations, i.e. choice of elution reagent is often dictated by requirements/limitations of downstream processes
- Environmental limitations, e.g. use of sodium

DEVELOPMENT IN BATTERY METALS SOLVENT EXTRACTION PROCESS DESIGN AND SIMULATION

By

Hannu Laitala

Metso Finland Oy, Finland

Presenter and Corresponding Author

Hannu Laitala
hannu.laitala@metso.com

ABSTRACT

During the last decade we have seen a big demand increase for the battery metals like nickel, cobalt, manganese and lithium. At the same time market is demanding higher quality products. Higher quality requirements put pressure on the process design practices. Process design practices must be developed so, that one can not only predict the amount of production, but also the quality of the production.

This means, that modern process design for a solvent extraction plant must be done using a process simulator. A modern SX plant's accurate mass balance can't be calculated manually. Solvent extraction process simulator must be able to calculate not only the main process flows and their compositions, but also calculate the solvent extraction circuit's performance with different feed compositions and amounts. Simulator must also be able to predict how the critical impurities behave in the different circuits. One very important detail is also to model the entrainments in the circuits.

Especially in battery metals solvent extraction processes accepted impurity levels are given in mg/L and this means, that solvent extraction entrainments have big impact how well the SX circuit is performing. Also, SX simulator must be able to predict how the changing process conditions in the different solvent extraction stages changes the chemical equilibrium. Organic phase's metal loading in different stages also affects the chemical equilibrium calculation. Highly loaded organic phase extracts metals differently than a partly or not-loaded organic phase.

Simulator design is also very fast. For a standard SX process, simulator model can be normally done in a few hours. Little bit more complicated cases can be simulated in a few days and even a totally new simulator can be done in less than a week if the base information is readily available. Simulation result accuracies are far better than compared to the process mass balance calculations done without a simulator. Modern simulators can also predict problems in a SX circuit design.

Metso's HSC Sim process simulator is an excellent tool for SX process simulation. HSC Sim is one of the few process simulators, where you can simulate both phases, aqueous and organic, in changing process conditions and given entrainments in every stage and combine the different SX stages to a fully functional SX process. Today HSC Sim models have been used in the process design of several operational SX plants. Several SX plants are being constructed where process simulation has been done by HSC Sim.

Keywords: Solvent extraction, simulation, battery metals, Metso, HSC Sim

INTRODUCTION

Process modelling, especially in the field of hydrometallurgy, has developed very fast during last couple of years. Less than 10 years ago it was quite common to calculate even big process flowsheets using very simple calculation routines. In worst case a whole SX plant's mass balance calculation was done with a couple of main static reactions without any information about the organic phase's features.

Nowadays hydrometallurgical plant's process model contains all unit process equipment separately and different parts of the model can be connected so, that for example SX process is getting the data from the leaching model. SX model in turn can send the calculated results for example to a crystallization or electrowinning process model, where these results can be used as feed data for the simulation.

Most of the models today are static process models. These models can calculate very complicated chemical reactions and equilibriums. Most of the current process models are lacking the dynamical calculation possibility. Current SX models can't usually calculate how temperature changes are affecting the reaction kinetics. Ion cross effects in different process conditions in different phases and between the phases are also missing from the current models. All these features will be added to the simulation models in the future.

SX process models today can already be used for mass balance calculations and operator and metallurgical training. Models can be also used very easily to simulate new process balances. Operator can follow what happens and where if some certain change is made in the feed or the controls.

Metallurgist can calculate SX process balance and verify the simulation result to the data from the actual plant. If more data from the process is achieved later, all these values can be updated easily to the process model.

When a reaction extent closes to 0 %, 100 % or reaction changes direction or reaction happens in conditions where acid or base concentrations are very low, simulator must overcome several difficulties affecting the equilibrium calculations. In these cases, the solution equilibrium and pH calculations are very sensitive.

Very small change in the acid concentration can have a big change in the solution's pH value and thus the metal transfer reaction degree. Acid balance calculation must be very robust, because if simulator's acid concentration goes negative in any of the calculated streams, simulation stops in error. In real life this doesn't happen, because in real SX process acid concentration can go to zero, but not negative.

In this paper a few design examples are presented, where SX simulators have been used to simulate some special SX design cases and these simulated results have had a critical impact on the process design.

ORGANIC PHASE'S TOTAL METAL LOADING EFFECT ON EQUILIBRIUM

When extracted target metal mass flow per time unit is big, but the last extraction stage contains very small amount of the target metal, organic phase can start to extract a different metal because organic phase's activity is high. Usually it is assumed, that solvent extraction equilibrium curves are constant, but in reality, equilibrium curves can change according to the SX process operating point.

This can cause problems in some certain situations. In the example below the target metal was Co and the next metal in the extraction series was calcium. In this case incoming feed solution didn't contain magnesium. In figure 1 below it's shown the base equilibrium curves for a Co SX process using Cyanex 272 (C272) as an extractant. In normal Co SX extraction conditions with Cyanex 272 cobalt is extracted well before calcium.

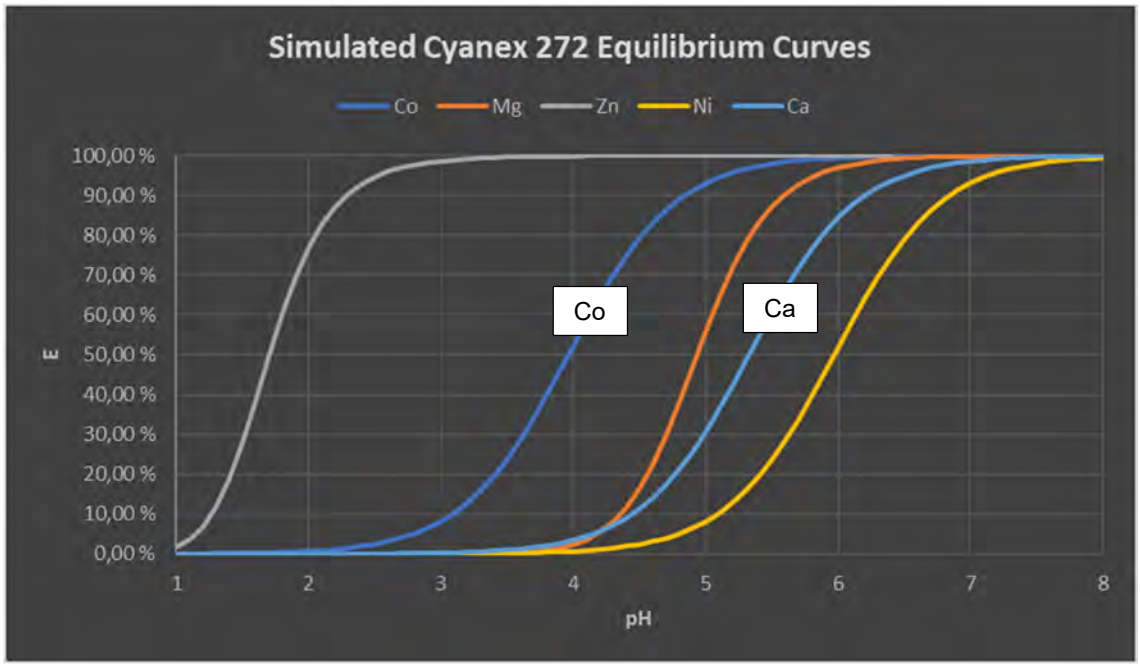

Figure 1: SX Simulator's Cyanex 272 Base Equilibrium Curves

If in the last extraction stage Co concentration in the aqueous phase is low (less than 95 % of the incoming value) and the incoming organic phase's metal concentration is zero, then calcium starts to be extracted if magnesium is not present in the system.

In figure 2 it is shown how calcium's equilibrium curve shifts location in these conditions in the last extraction stage. If organic phase has been preneutralized before organic feeding to the extraction stages, this loading is not calculated as organic phase metal loading.

Calcium starts to be extracted at an aqueous solution pH very close to the Co extraction pH. This can be an operational problem especially when the incoming feed is calcium saturated.

If calcium is extracted excessively in the last extraction stage, calcium concentration increases in the last extraction stage's organic phase much higher than it normally would. When this organic phase flows to the second-last extraction stage, the extra calcium extracted in the last extraction stage will be stripping down from the organic phase to the aqueous phase.

Now there can be a problem if the aqueous phase contains already calcium. Calcium's solubility in sulphate solution is limited and gypsum can start to precipitate easily if the extra calcium stripping down from the organic phase increases calcium concentration in the aqueous phase over calcium's solubility limit.

If water phase's calcium concentration is low or water phase is chloride based, calcium's water phase concentration is not usually a problem. To check if gypsum precipitation will be a problem to a Co SX process different feed and pH profiles can be simulated with a Co SX simulator, which uses the changing extraction equilibrium curves.

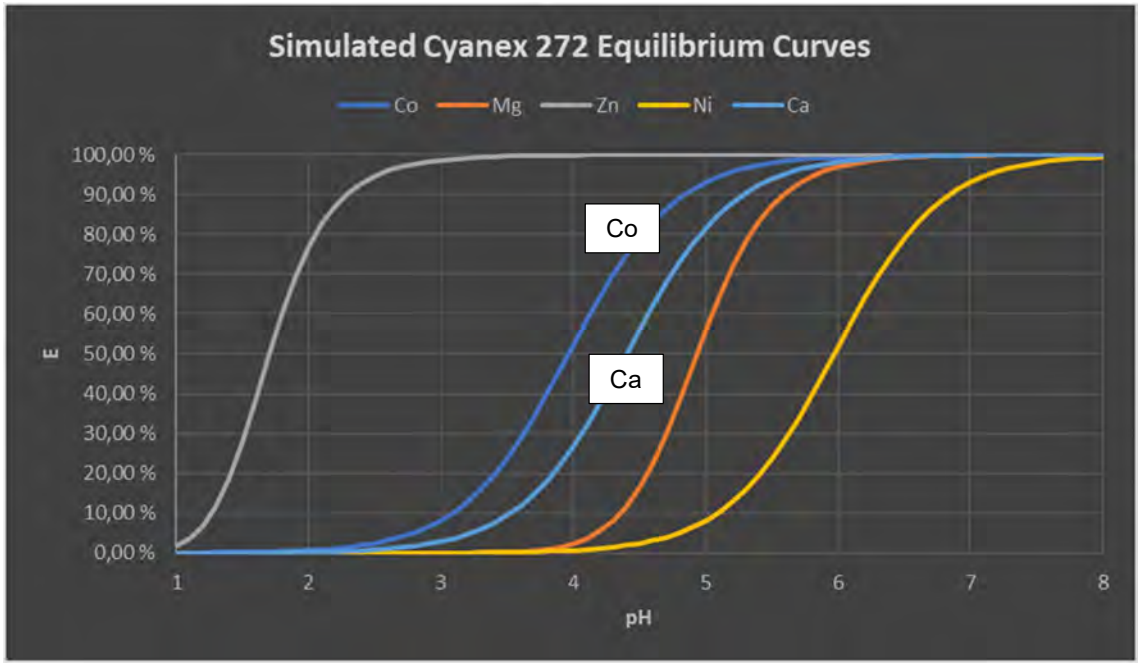

Figure 2: Co SX Simulator's Changed Ca C272 Equilibrium Curve

VERSATIC 10 SOLUBILITY IN Ni SOLVENT EXTRACTION

Versatic 10 (V10) is a carboxylic acid reagent, which is commonly used to extract nickel especially from magnesium and calcium containing solutions. V10's nickel extraction efficiency is excellent, but in the pH range, where Ni extraction happens, V10's solubility to the aqueous phase is high and this can lead in problems at the raffinate treatment plant. V10's high solubility can also affect the operating cost of the SX plant. In figure 3 below some Ni SX simulator's equilibrium base curves are shown.

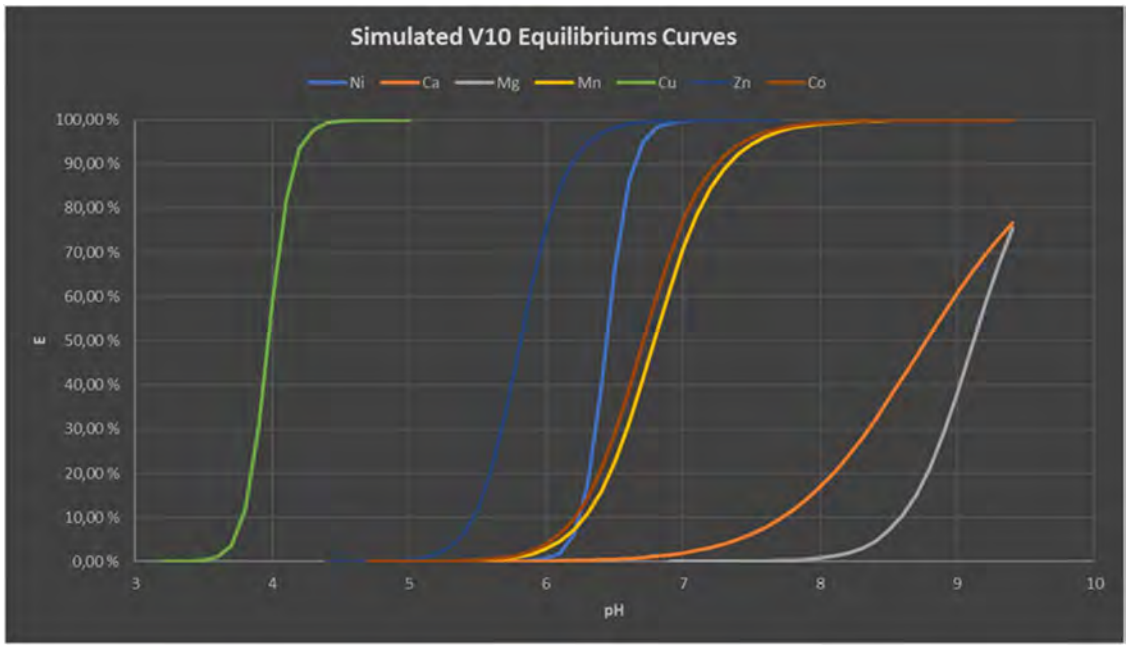

Figure 3: Ni SX Simulator's Versatic 10 (V10) Equilibrium Curves

Aqueous phase pH for a V10 Ni SX extraction stages is 6,0 – 6,5. Equilibrium curves shown in the figure 3 will be adjusted automatically during the simulation based on the organic phase reagent concentration and organic phase's total metal loading degree.

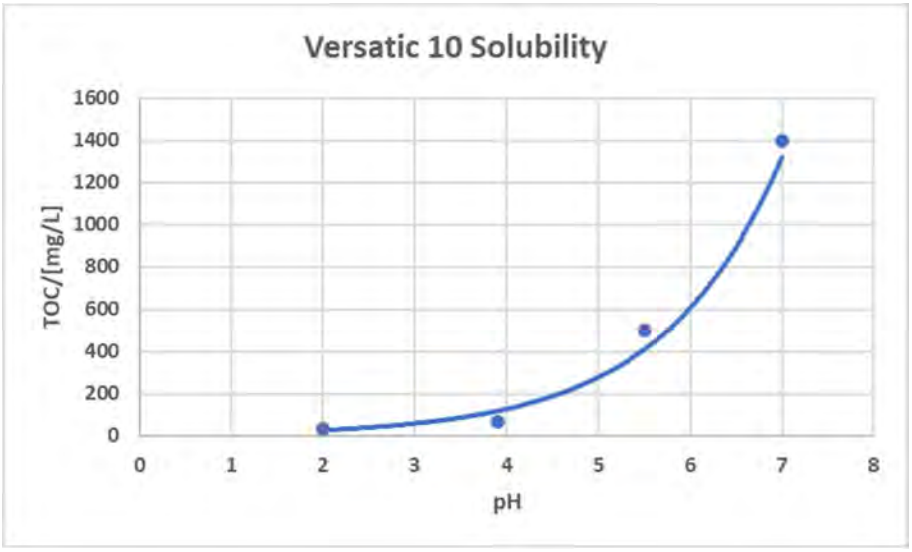

Figure 4: Versatic 10 Solubility

From figure 4 it can be seen, that V10's solubility in the Ni SX operating pH is high. V10's aqueous phase solubility is a function of pH, temperature and ionic strength. At a real SX plant SX process operating temperature and raffinate flow's ion strength can be assumed to be constant with a reasonable confidence, so at the SX plant level V10's aqueous phase solubility is mainly function of aqueous phase pH.

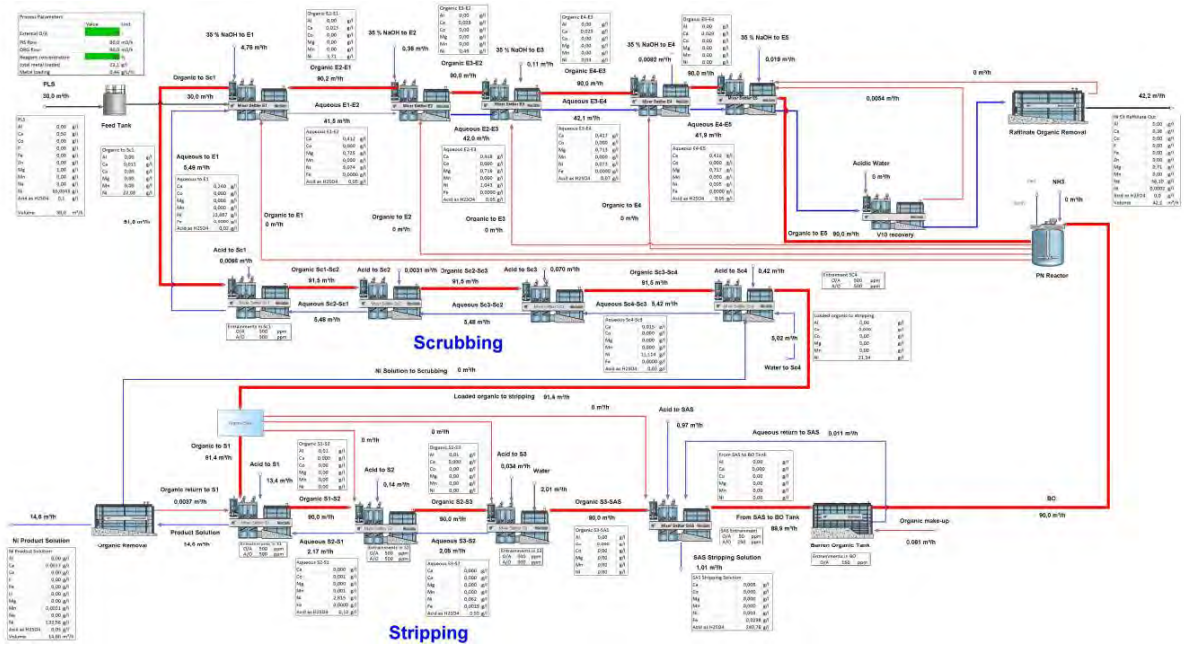

Figure 5: Ni SX Simulator

In this simulation Ni SX feed contained 65 g/L Ni and total PLS flow was 30 m^3/h. Nickel transfer to crystallization was 1 950 kg/h. After the last extraction stage, extraction stage E5 in this simulation, there was an extra mixer settler. In this unit V10's concentration in the aqueous phase was degreased by adjusting the pH of the raffinate. This Versatic solubility reduction stage is usually called a VR stage (VR = Versatic Recovery). First simulation was done without pH adjustment to find out the V10 loss in a case where V10 was not recovered.

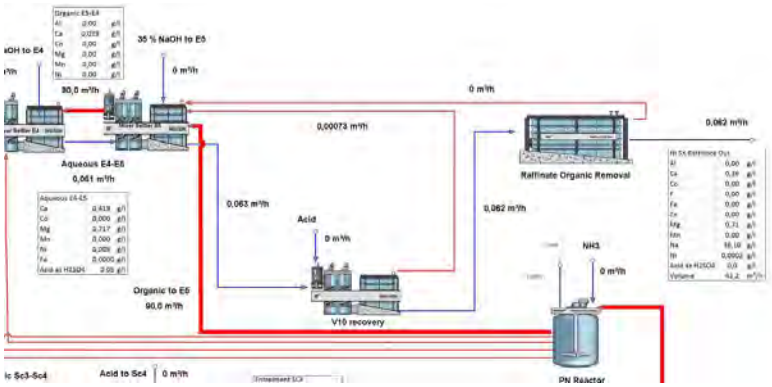

Figure 6: Ni SX without V10 Recovery

According to the simulation organic entrainment in the raffinate stream increases to 1 500 mL/m^3 and V10 loss with raffinate out from the process is over 60 L/h. This V10 loss alone is over 90 % of the total organic loss for the whole simulated system.

Second simulation was done assuming that pH control for the raffinate stream in the VR stage was on. pH of the incoming raffinate was adjusted to 3. No other changes were made in the simulation.

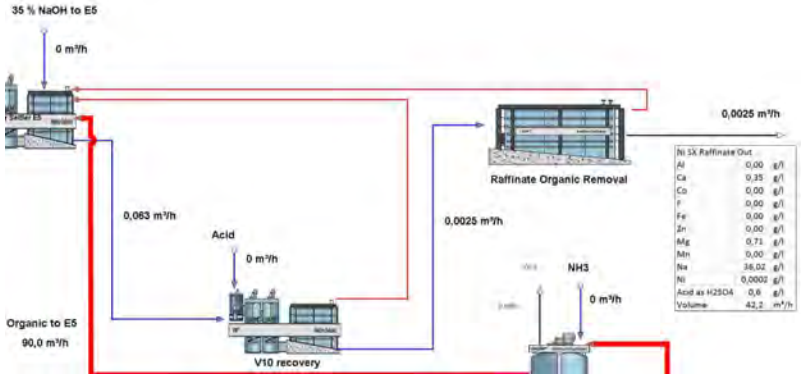

Figure 7: Ni SX with V10 Recovery

When V10 recovery is operational more than 95 % of the soluble V10 can be turned to insoluble organic and returned to the process. Amount of the soluble organic in the raffinate stream drops from 62 L/h to 2,5 L/h. Total organic consumption of the circuit was also reduced more than 90 %.

COPPER REMOVAL SOLVENT EXTRACTION

When producing battery grade manganese, cobalt and nickel salts, one common impurity in the solution coming from the leaching stage is copper. Copper mass flow is usually quite small ranging from 100 to 3 000 t/a Cu. For this kind of case copper production is usually considered to be a by-product production. At a full-size copper production plant plant's main target is to maximize the copper production at the same time when copper unit costs are minimized.

In a Cu removal solvent extraction process copper removal efficiency is maximized so, that battery metals production unit operating costs are minimized. In battery metals production copper solvent extraction's extracted solution (raffinate) is not normally circulated back to the leaching process. In some cases, part of the Cu SX raffinate can be returned to the leaching stage to be used as make-up water and to return part of the acid formed in the SX process back to the leaching stage.

In this example Cu SX is connected to the main process so, that the Co SX process will get its feed solution after the leaching stage's solids removal process. Process block diagram is shown in figure 8.

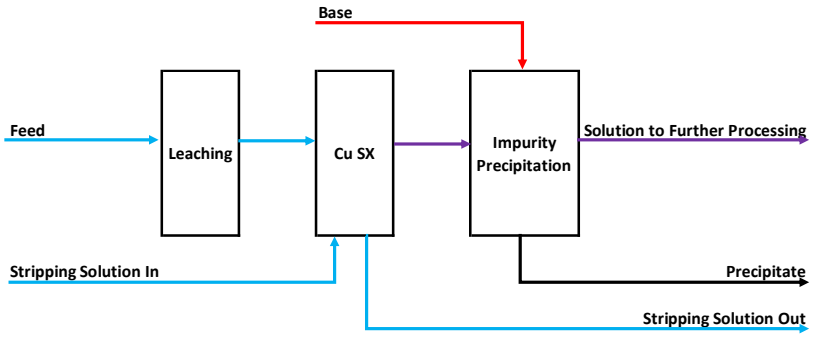

Figure 8: Cu Removal SX Main Process Connection

In this simulation example the main aqueous phase impurities were iron, chloride and manganese. Important feed values for the solution coming from the leaching stage are:

1. Volumetric flow 50 m^3/h and sulphuric acid concentration 5,0 g/L.
2. Minimum temperature +25 °C and maximum temperature +40 °C.
3. Copper concentration 8,0 g/L.
4. Iron concentration 20 g/L
5. Chloride concentration 100 g/L.
6. Manganese concentration 10 g/L.

Cu SX Configuration

Because this Cu SX is cleaning the feed for battery metal salt production, the Cu removal efficiency must be as high as technically and economically possible. Main target of this process is to remove as much copper as possible and produce an easily marketable copper product. Even if in the simulated case copper mass flow is quite small, approximately 320 t/a, copper's economical value is still over two million dollars and worth to recover.

First stage of the simulations is to choose a correct base model for this case. In this case you have high iron, chloride and manganese concentrations and intermediate concentration of copper in the incoming feed. Cu SX simulator was updated to be able to handle high chloride concentration in the feed[1,2].

Cu SX Simulations

Used Cu SX simulator was designed to simulate a Cu SX process with a configuration 3E+LOT+1W+2S in given feed conditions.

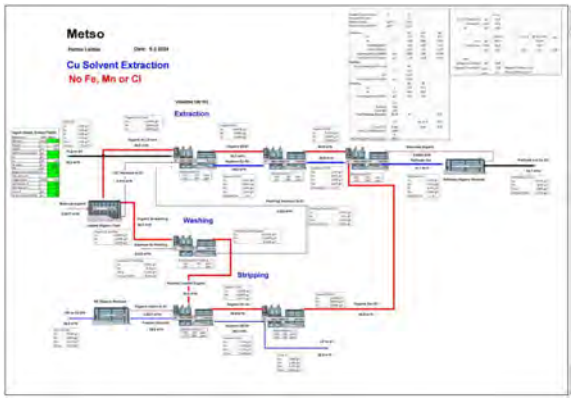

Figure 9: Cu SX HSC Sim Simulator

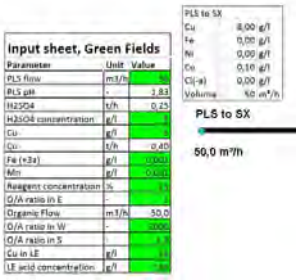

Figure 10: Cu SX Feed Solution's Composition

First simulation was done with two extraction stages connected in series and without any organic phase washing and no chlorides, iron or manganese in the feed. This simulation indicates how high recovery we can get with only two extraction stages.

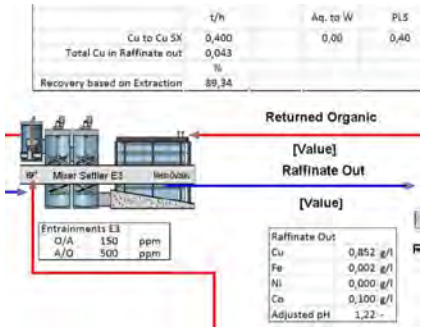

Figure 11: Cu Extraction with 2E+2S Configuration

As it can be seen from the results Cu recovery is below 90 % and the simulated raffinate Cu concentration is 0,85 g/L. This is not acceptable for a Cu removal SX. Second simulation used configuration 3E+2S and simulated copper recovery was 99 % with a raffinate Cu concentration below 0,1 g/L. This was considered as an acceptable result.

For the third simulation all impurity components were added to the feed. Cu recovery was unaffected, but iron and chloride concentrations increased in the product solution. Iron concentration increased 116 mg/L and chloride 86 mg/L. Fourth simulation was done with one washing stage added to the simulator. Addition of the one washing stage decreased the total copper recovery from 99 % down to 95 %, but iron and chloride concentrations in the product solution increased anymore 21 and 14 mg/L. Washing was better, but not good enough.

In the fifth simulation a second washing stage was added to the simulator. According to the simulation copper recovery dropped from 95 % to 94 %, but now iron and chloride concentrations increased in the product solution only 7 and 5 mg/L. Now washing result is acceptable, but we still must compensate the drop in the copper extraction efficiency.

There are three ways how this drop in the copper extraction efficiency can be compensated; Increase reagent concentration, increase organic flow or neutralize acid from the extraction stages. Usually, acid neutralization is not an option for a normal Cu SX process, because acid is circulated back to leaching. However, in this case Cu SX raffinate was the feed solution for battery metal salts production, so acid will be neutralized anyway and thus acid neutralization was an option for this case.

Easiest way to compensate the drop in the copper extraction efficiency is to increase the organic flow if you have the extra pumping capacity available. In the sixth simulation organic flow was increased by 8 % and then copper recovery increased back to 99 %. In the last simulation a base addition was added to the first extraction stage and with this base addition Cu recovery was increased to over 99,7 % and raffinate's Cu concentration dropper down to 0,023 g/L.

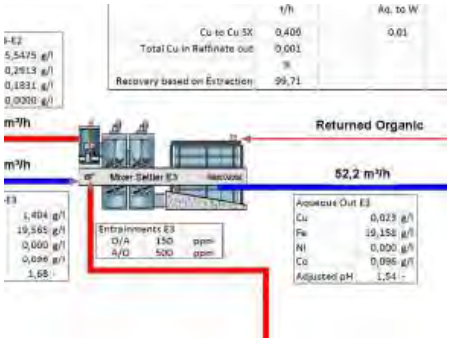

Figure 12: Cu Recovery with pH Control

All different Cu SX simulation main results are shown in the table 1 below.

Table 1: Cu SX Main Simulation Results

	Feed	Cu	Fe	Cl^-	Mn	Cu Rec.	Cu_{raff}	dFe***	dCl^-***	dMn***
Configuration	m^3/h	g/L	g/L	g/L	g/L	%	g/L	mg/L	mg/L	mg/L
2E+2S	50	8,0	0	0	0	89,3	0,85	N/A	N/A	N/A
3E+2S	50	8,0	0	0	0	99,0	0,08	N/A	N/A	N/A
3E+2S	50	8,0	20	100	10	98,6	0,12	116	86	2
3E+1W+2S	50	8,0	20	100	10	95,0	0,40	21	14	0
3E+2W+2S	50	8,0	20	100	10	94,0	0,48	7	5	0
3E+2W+2S*	50	8,0	20	100	10	99,0	0,08	8	6	0
3E+2W+2S**	50	8,0	20	100	10	99,7	0,02	8	5	0

* = Recovery compensation
** = pH control
*** = Concentration change in the stripping solution

Client's conclusion in this case was that the Cu SX plant will use a configuration of 3E+2W+2S. This circuit was equipped also with a base addition to one of the extraction stages to increase the copper recovery before the impurity metals precipitation process. If copper is entering the impurity metals precipitation process, copper will be precipitated with the impurities and all this copper would be lost.

In this case manganese's oxidation stage will be controlled at the leaching plant so, that manganese's oxidation state will be +2. Manganese's higher oxidation states can be a problem for a SX process and especially if manganese is entering an electrowinning process after the Cu SX, where manganese could be oxidized to a level of +7. Permanganate ion (MnO_4^-) is a very strong oxidant and could negatively affect Cu SX's organic phase.

IMPURITY SX PROCESS ORGANIC PRELOADING

Preloading of the organic phase have been used for a long time in certain SX process. In organic phase preloading you extract a metal, which you would normally leave unextracted to the SX raffinate stream. Organic preloading is done in separate SX contactors before you feed the preloaded organic phase to the extraction stages. If preloaded organic phase is used, there are normally no separate pH controls in the extraction stages.

Preloading of the organic phase is different process than organic phase preneutralization. In preneutralization process you neutralize your organic reagent with a base before extraction or preloading stages. In preloading you usually extract a divalent metal to your organic phase.

Organic phase preloading is done for two reasons. First reason is to avoid base cation contamination of the aqueous phase in the extraction stages. Second reason to use the organic phase preloading process is to avoid the aqueous phase dilution in the extraction stages. Aqueous phase dilution can be quite big. This dilution can increase the main aqueous flow in the extraction stages more than 50 % and thus increase the needed equipment size and cost.

In some cases, organic phase preloading is the preferred method, but not always. To use or not to use the organic phase preloading must be considered case by case.

In figure 13 below is shown a process block diagram, which was proposed to be used for a project in China. This block diagram was developed by a local engineering company in China for this particular project.

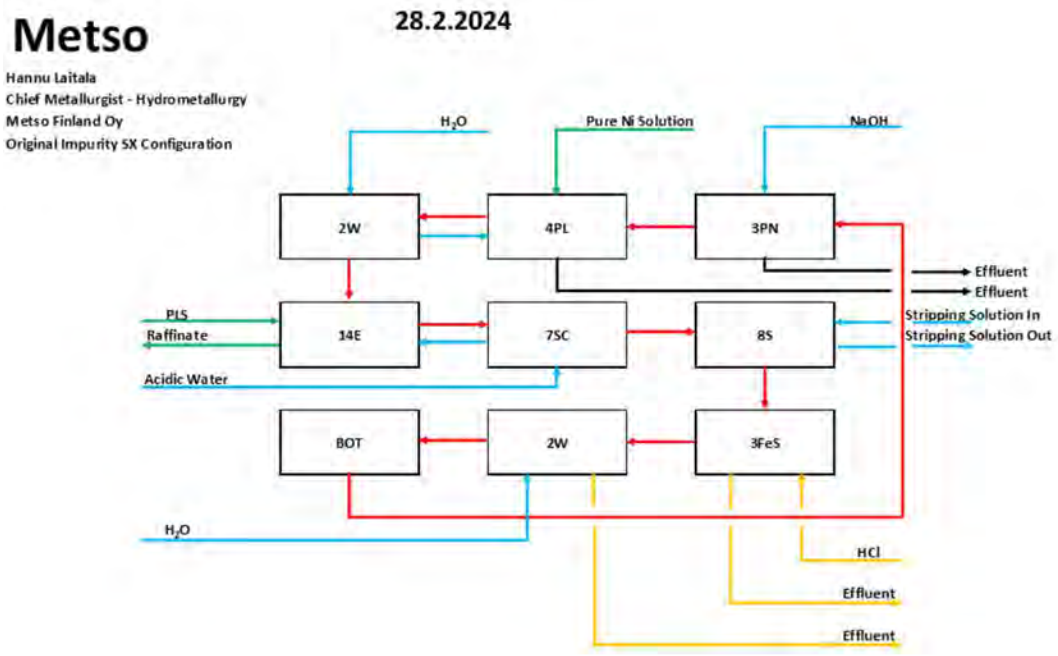

Figure 13: Client's Impurity SX Configuration

Total number of SX contactors was 43 pcs; three preneutralization (PN) stages, four preloading (PL) stages, two base cation washing (W) stages, 14 extraction (E) stages, seven scrubbing (SC) stages, eight stripping (S) stages, three iron stripping (FeS) and two chloride washing (W) stages. This block diagram presents quite standard impurity SX configuration for a manual operated impurity SX circuit.

Manual operation in this case means, that process control is done mainly by controlling the main process flows. In this case manual operation doesn't mean, that client doesn't use DCS. High number of mixer settlers makes this process very robust to operate, but it also makes this plant's investment cost high. Some downsides of this process configuration are discussed below.

Separated Preneutralization and Preloading Stages

Preneutralization and preloading stages are separated increasing the number of the required mixer settlers. In proposed configuration organic phase is first pneneutralized according to the reaction 1. After preneutralization organic phase is fed to the preloading stages, where the organic phase is preloaded with pure Ni solution and any remaining acid in the incoming Ni solution is neutralized with the preneutralized organic phase according to the reactions 2 and 3.

$$HA + NaOH \leftrightarrow NaA + H_2O \quad (1.)$$

$$H^+ + NaA \leftrightarrow Na^+ + HA \quad (2.)$$

$$2NaA + Ni^{2+} \leftrightarrow NiA_2 + 2Na^+ \quad (3.)$$

Caustic soda solution's concentration can't be high because mixing devices used for the mixing are not suitable for this kind of service. Extra water is needed to dilute down the caustic soda. Nickel solution used for the organic phase preloading is pure nickel solution suitable for battery grade nickel sulphate production. Nickel solution's quality is too high for this kind of use.

Preloaded Organic's Washing Stages

Pure water is used in the washing stages to wash the base cation away from the organic phase. Its ionic strength is low and pH is high. Because of these points phase separation is slow and water entrainments are very high in the washing stages. This leads to low washing efficiency in the washing

stages and low washing efficiency in turn means base cation contamination of the incoming aqueous phase in the extraction stages.

Scrubbing Stages

Proposed process configuration uses preloading to avoid the water phase base cation contamination and the aqueous phase dilution in the extraction stages. Used scrubbing water return to the extraction stages doesn't contaminate the extraction stages' aqueous phase with base cation. However, this return causes aqueous phase dilution.

Because of this dilution effect scrubbing stage's external O/A ratio must be high and the number of the scrubbing stages must be increased leading to a higher capital investment cost of the plant.

Stripping Stages

Without properly designed pH control in the stripping stages number of the stripping stages must be increased leading to a higher capital investment cost of the plant. Iron stripping is done with hydrochloric acid leading to usage of very expensive and corrosive chemical. Because of the hydrochloric acid two extra water washing stages must also be installed to remove the entrained chloride from the organic phase before the organic phase is returned to the preneutralization stages.

Modified Impurity SX Configuration

Impurity SX configuration was modified so, that the number of the mixer settlers and consumptions of pure water, sulfuric acid and caustic soda were minimized at the same time while the plant's capacity stayed the same. Modified SX configuration is shown in the figure 14 below. Instead of original amount of 43 mixer settlers, this new configuration will be using only 15 mixer settlers. This new configuration doesn't use hydrochloric acid at all.

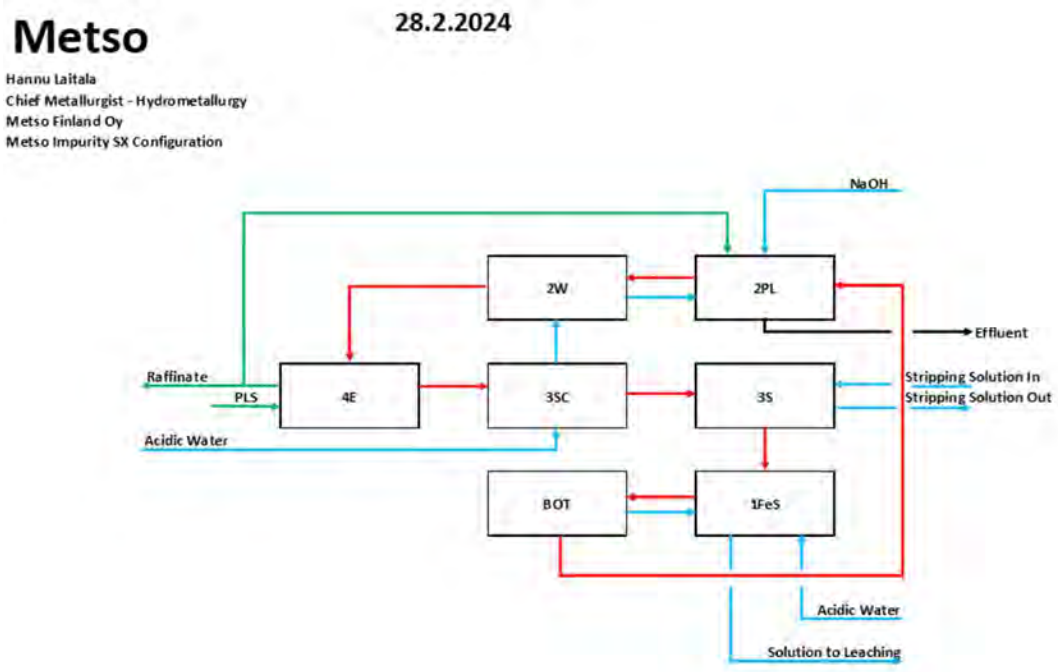

Figure 14: Improved Impurity SX Configuration

This new impurity SX configuration was first simulated with a HSC Sim simulator. After simulations this new configuration was tested in a client pilot plant test run at Metso's research center in Pori, Finland, 2023. This new Metso configuration will be taken into service next year in a project in China.

This new, Chinese plant will use new configurations for their impurity and Co SX circuits. Both configurations were developed by Metso Finland Oy in less than one year.

New Preloading Stages

Because main target is to load the organic phase with the metals from aqueous feed coming in and not to load sodium in the organic phase, preloading process has been changed by combining the preneutralization and preloading stages.

Main reactions happening in the preloading stages are given in the reactions 4 and 5 below. From these reactions it can be seen, that used base cation is not entering the organic phase and this will increase the base cation washing efficiency.

$$H^+ + NaOH \leftrightarrow Na^+ + H_2O \quad (4.)$$

$$2NaOH + 2HA + Ni^{2+} \leftrightarrow NiA_2 + 2Na^+ + 2H_2O \quad (5.)$$

Metal containing feeds are coming from the main process scrubbing and extraction stages. Used scrubbing solution is flowing first through the base cation washing stages, where this solution is washing entrained base cation away from the loaded organic phase.

Metal containing solution can contain any metal, which is not extracted in the SX circuit in question. In this impurity SX case preloading can be made with a solution containing Ni, Co and Mg. Clean Ni solution is not needed for this purpose. In fact, if pure nickel solution would be used for this purpose, it would be a waste of good quality nickel solution.

Caustic soda solution's concentration can be increased because used equipment is specially designed to use base concentration. Currently Metso is using over 10M NaOH solutions for this service. The higher concentration caustic soda can be used, the lower amount of water is needed and because sodium sulphate concentration is also increased in the effluent stream, organic entrainment from the preloading stage will also be lower.

Scrubbing Stages

In this new process configuration used scrubbing solution is used as a base cation wash solution. With the new connection the used scrubbing solution is not diluting the extraction stages' aqueous phase. Because there is no dilution effect, scrubbing stages' external O/A can be increased and the number of scrubbing stages can be reduced.

Scrubbing solution's target in the scrubbing stages is to wash the valuable metals away from the loaded organic phase. In this case the valuable metals are Ni and Co. In base cation washing stages aqueous phase's target is to wash base cation away from the preloaded organic phase. Because used stripping solution doesn't contain base cation and it contains metals, which will be loaded to the organic phase in the preloading stages, used scrubbing solution is a perfect solution to be used as a base cation washing solution after the scrubbing stages.

Stripping Stages

With proper pH control the number of the required stripping stages can be decreased from the original eight to three. Also, iron stripping is done with sulphuric acid in one stage. In the original configuration iron stripping was done with three stripping stages using hydrochloric acid.

Because of the hydrochloric acid two water washing stages were needed for the organic phase. Now iron can be stripped with one sulphuric acid using mixer settler and no extra washing stages are needed. Used iron stripping solution can be easily returned to the leaching plant to be used as a make-up acid for the process. With hydrochloric acid this can not be done and used iron stripping solution must be discarded from the process a waste stream.

REFERENCES

1. Ekman E. (1997). The behaviour of chloride in the extraction of copper from sulphate liquors. Master's Thesis, Lappeenranta University of Technology. Lappeenranta, Finland; 1997.

2. Yanez H, Ardiles L, del Rio C. (2017). High Chloride in PLS and their Impact on Copper Solvent Extraction. In: 9th International Seminar on Process Hydrometallurgy (Hydroprocess) • International Conference on Metal Solvent Extraction (ICMSE). Santiago, Chile; 2017.

IMPURITY REMOVAL PILOTING FOR THE TECH PROJECT: MANGANESE, ZINC AND CALCIUM REMOVAL, GYPSUM MANAGEMENT, AND TRANSFORMATION AND PURIFICATION SX FOR PRODUCTION OF HIGH PURITY COBALT SULFATE

By

Boyd Willis

Boyd Willis Hydromet Consulting, Australia

Presenter and Corresponding Author

Boyd Willis
hydromet@boydwillis.com

ABSTRACT

The Sulfate Refinery in the Queensland Pacific Metals' TECH Project will treat a crude mixed hydroxide precipitate by sulfuric acid leaching, followed by aluminium precipitation, impurity removal, cobalt solvent extraction, nickel solvent extraction, and crystallization of high purity nickel and cobalt sulfate products. All sulfate refinery circuits were piloted sequentially during 2023 at Lakefield, Ontario by SGS Canada.

This paper focusses on the impurity removal circuit which consists of two solvent extraction (SX) circuits that use di (2-ethyl hexyl) phosphoric acid (D2EHPA®), dissolved in a high flashpoint aliphatic diluent. These two circuits are Impurity Solvent Extraction (ISX) and the Transformation and Purification (TSX and PSX) circuit. In ISX, impurity metals, including manganese, zinc and calcium, are preferentially extracted over cobalt and nickel. Extraction is followed by scrubbing with sulfuric acid prior to sequential manganese stripping and zinc stripping, both with sulfuric acid. A bleed of Zn-stripped organic is directed to iron stripping using oxalic acid. The ISX raffinate is forwarded to cobalt solvent extraction (CSX) for cobalt recovery.

In transformation, a bleed of the ISX stripped organic is transformed into cobalt-loaded organic. In purification, cobalt-loaded strip liquor (LSL) from CSX is contacted counter-currently with the cobalt loaded organic. The impurity metals from the cobalt LSL displace cobalt from the organic and the raffinate (purified cobalt LSL) is forwarded to cobalt sulfate heptahydrate crystallisation. The impurity removal pilot plant design, operation and results are presented. The feed to ISX is calcium-saturated, leading to gypsum formation in parts of the circuit. The paper discusses the strategies for gypsum management developed during piloting. Purification increased the Co:Mn ratio from 540:1 to >600,000:1, the Co:Zn ratio from 6,000:1 to >66,000:1, and the Co:Cu ratio from 12,000:1 to >50,000:1, and the maximum Ca and Fe in purified cobalt LSL feed to crystallisation were determined to be 10 mg/L and 1.5 mg/L respectively.

Keywords: Queensland Pacific Metals, TECH Project, nickel, cobalt, battery metals, impurity removal, solvent extraction, D2EHPA, manganese, zinc, calcium, iron, oxalic acid, gypsum, cobalt sulfate, transformation, purification

INTRODUCTION

Queensland Pacific Metals (QPM) is an ASX listed company and is the 100% owner of the Townsville Energy Chemicals Hub (TECH) Project.

The TECH Project will be a modern and sustainable battery metals refinery, 40 km south of Townsville, in northern Queensland. The TECH Project will produce critical metals for the rapidly emerging lithium-ion battery and electric vehicle sector. Processing high grade nickel laterite ore imported from New Caledonia, the TECH Project will produce nickel sulfate, cobalt sulfate, high purity alumina (HPA) and other by-products – leaving, for the first time ever in the world, almost zero waste products..

QPM is currently in the process of finalising a Definitive Feasibility Study (DFS) for the TECH Project. The parameters for the DFS are to design the TECH Project as a 1.6 million wtpa processing plant. The DFS is due to be completed mid 2024.

Queensland Pacific Metals shareholders include global battery manufacturing leader LG Energy Solution, major Korean conglomerate POSCO and American multinational automotive manufacturing company General Motors. Queensland Pacific Metals has secured binding offtake agreements for the sale of nickel and cobalt with LG Energy Solution, POSCO and General Motors.

The QPM TECH Plant is split into three areas: Front End, Extraction Plant and Sulfate Refinery. Non-Process Infrastructure supports the operation of the three main plant areas.

The Front End of the process covers site storage of ore, ore preparation and storage of residue.

The Extraction Plant uses the DNi Process™ which is essentially a closed-loop leaching process whereby the nitric acid reagent is recirculated via regeneration steps to extract valuable metals from the ore. A hydroxide precipitate of nickel, cobalt, aluminium and manganese, and other residual metals including iron, magnesium, zinc and copper, is the main product from the Extraction Plant that feeds the Sulfate Refinery. By-products from the Extraction Plant include hematite and magnesia.

The Sulfate Refinery uses sulfuric acid to leach the hydroxide precipitate produced in the Extraction Plant. The hydroxide leach liquor produced is purified by aluminium precipitation, impurity removal, cobalt solvent extraction and nickel solvent extraction, followed by crystallization of high purity nickel and cobalt sulfate products. Ammonium sulfate is produced as a by-product from the Sulfate Refinery. The solvent extraction configuration is similar to that used at the Terrafame plant in Finland[(1)].

SULFATE REFINERY PROCESS OVERVIEW

A simplified block flow diagram of the Sulfate Refinery (SUR) is shown in Figure 1.

The hydroxide precipitate produced in the Extraction Plant is leached using concentrated sulfuric acid to re-dissolve nickel, cobalt, and other impurity metals, producing a PLS stream. The PLS is then treated with limestone slurry in two stages of aluminium removal to precipitate aluminium, chromium, copper, and iron, with co-precipitation of gypsum. Thickening and filtration are used to separate the solids from the process liquor. The washed filter cake solids are directed to Residue Neutralisation, and the aluminium-depleted solution is forwarded to Impurity Removal.

Impurity Removal consists of Impurity Solvent Extraction (ISX) and Transformation and Purification (TSX and PSX). In ISX, impurity metals are preferentially extracted over cobalt and nickel using D2EHPA® and stripped from the extractant using sulfuric acid. In the commercial flowsheet prior to piloting, a bleed of Zn-stripped organic is sent to iron stripping using oxalic acid, and a separate bleed of Zn-stripped organic is sent to impurity transformation. ISX raffinate is sent to Cobalt SX (CSX) for cobalt recovery.

In CSX, cobalt is selectively extracted over nickel, magnesium and ammonia using Cyanex 272 extractant, then selectively stripped from the extractant using sulfuric acid. The cobalt loaded strip liquor is then sent to Purification (TSX and PSX) to further reduce impurities (mainly manganese, zinc and calcium), before reporting to Cobalt Sulfate Crystallisation. In TSX, the Fe-stripped organic from ISX is transformed into cobalt loaded organic. In PSX, the cobalt loaded strip liquor (LSL) from CSX is contacted counter-currently with the cobalt loaded organic. The impurity metals from the cobalt LSL displace cobalt from the organic and the raffinate (purified cobalt LSL) is forwarded to cobalt sulfate

heptahydrate crystallisation. The cobalt sulfate heptahydrate produced from the crystalliser is centrifuged, washed, dried and packaged before shipping.

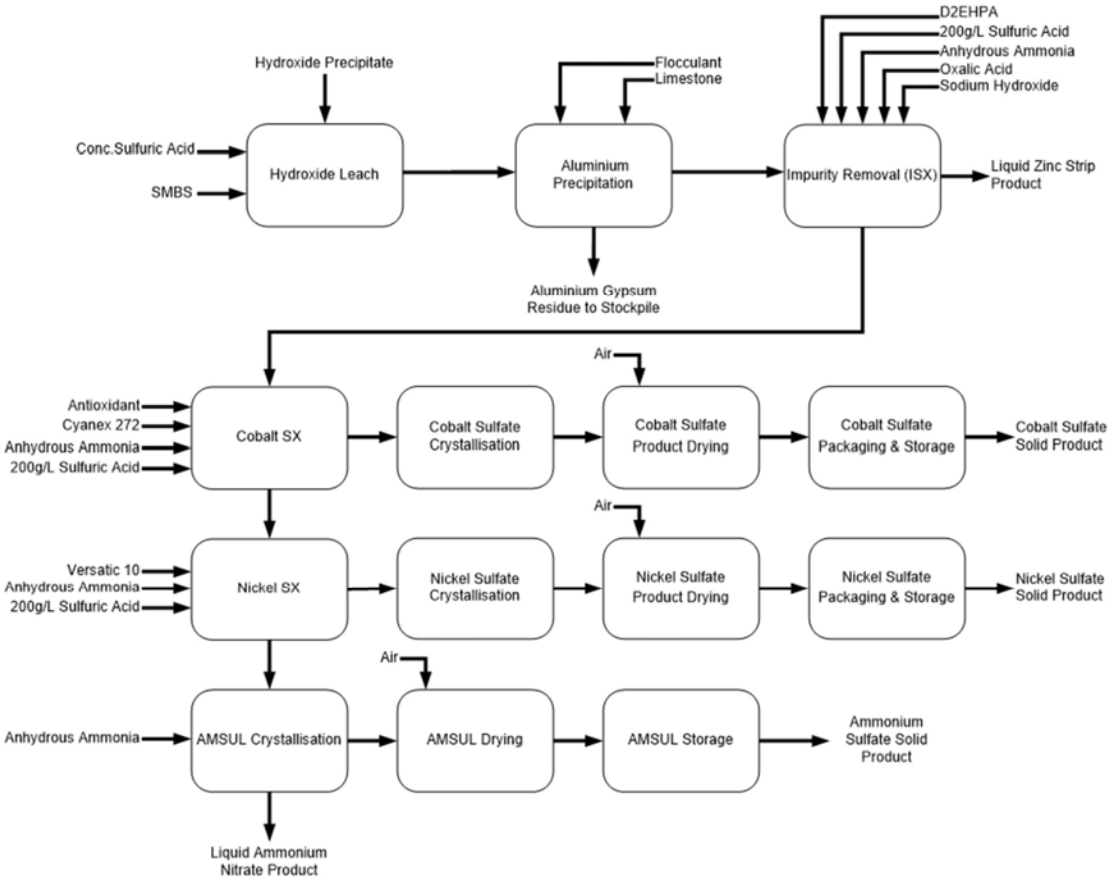

Figure 1: Simplified Sulfate Refinery Block Flow Diagram

The clean raffinate generated from CSX, containing nickel sulfate, magnesium sulfate and ammonium sulfate (AmSul) is forwarded to Nickel Solvent Extraction (NSX). In NSX nickel is selectively extracted over magnesium and ammonium using Versatic 10 extractant, then stripped from the extractant using sulfuric acid. The nickel LSL is filtered and purified before reporting to Nickel Sulfate Crystallisation. The nickel sulfate hexahydrate produced from the crystalliser is then centrifuged, washed, dried and packaged before shipping.

The clean raffinate generated from NSX, containing magnesium sulfate and AmSul, along with ammonium nitrate, is forwarded to AmSul Crystallisation for AmSul and ammonium nitrate production. The AmSul crystals (containing a small amount of magnesium sulfate) produced from the crystalliser are centrifuged, washed and dried before shipping. Ammonium nitrate produced in the crystalliser is sold as a liquid fertiliser.

IMPURITY REMOVAL OVERVIEW

The first part of the impurity removal area is the ISX circuit, for removal of impurity metals (Mn, Zn, Cu, Al, Fe and Ca) from the pregnant leach solution (PLS) to produce a nickel and cobalt enriched solution for the downstream process. The second part of the impurity removal area, Purification, comprises the transformation and purification SX circuits (TSX and PSX), for the removal of residual impurities from the cobalt loaded strip liquor prior to crystallisation.

The extractant is di (2-ethyl hexyl) phosphoric acid, or D2EHPA®, dissolved in a high flashpoint aliphatic diluent. At the design pH, D2EHPA® preferentially extracts key impurity metals over Ni and Co, as well as Mg, in the following extraction order: $Fe^{3+} > Fe^{2+} > Zn^{2+} > Ca^{2+} > Mn^{2+} > Cu^{2+} > Co^{2+} > Mg^{2+} > Ni^{2+}$.

Transformation and purification are considered to be part of the ISX area because these circuits share the same extractant. The D2EHPA® equilibrium pH curve for extraction of various metals is shown in Figure 2. At the design pH, impurity metals displace cobalt from cobalt loaded D2EHPA®.

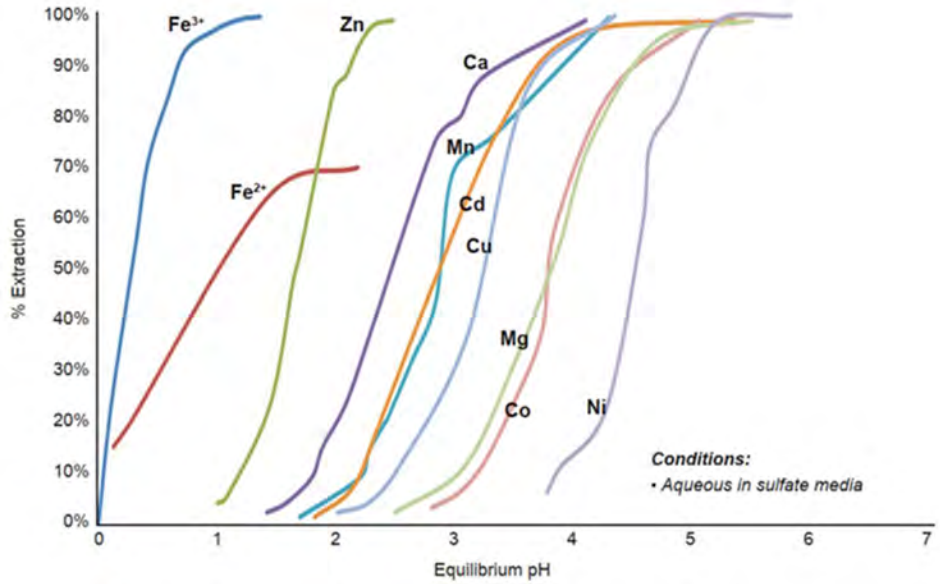

Figure 2: D2EHPA® Selectivity in Sulfate Solutions

ISX Process Description

In ISX, impurity metals are preferentially extracted over cobalt and nickel using D2EHPA® and stripped from the extractant using sulfuric acid. ISX raffinate is sent to CSX for cobalt recovery. A bleed of the stripped organic is directed to Iron Stripping, using oxalic acid, and the Fe-stripped organic is forwarded to TSX. The ISX flowsheet incorporates the following process steps:

Saponification

To ensure efficient impurity transfer from the aqueous to the organic, it is important to maintain an optimum pH during extraction. This is achieved by pre-loading the organic with ammonium ions via contact with gaseous ammonia. The pre-loading reaction is as follows:

$$NH_3\ (g) + H\text{-}D2EHPA(o) = NH_4\text{-}D2EHPA(o)$$

Extraction

In extraction, the PLS is contacted with the organic, which contains a maximum active D2EHPA® concentration of 372 g/L. Increasing the extractant concentration further would increase the organic viscosity which would impact phase disengagement performance in the settlers.

The feed solids content is reduced to 5 mg/L using dual media filters, prior to being contacted counter-currently in four stages with saponified organic. Most of the impurity metals, especially Mn, Zn and Ca, and a small amount of Co, Mg and Ni, are extracted onto the organic at the optimum pH. The raffinate, containing Ni, Co, Mg and ammonium, is filtered and treated before advancing to CSX, whilst the loaded organic exiting the first stage of extraction advances to scrubbing.

The extraction reaction produces AmSul as shown in the following equation for di-valent metal sulfates:

$$MSO_4(a) + 2\ NH_4\text{-}D2EHPA(o) = (NH_4)_2SO_4(a) + M\text{-}(D2EHPA)_2(o)$$
(where M = divalent cation)

Magnesium is not separated in ISX because its equilibrium pH curve is close to that of cobalt (see Figure 2).

Raffinate Wash

The raffinate exiting the last stage of extraction is sent to a raffinate wash mixer-settler, where it is contacted counter-currently with diluent. Due to higher solubility of the extractant in the diluent than in aqueous, entrained extractant is transferred from the aqueous into the organic phase. The aqueous is filtered via two dual media filters to further reduce the organic entrainment, further limiting D2EHPA® cross contamination into CSX.

Scrubbing

The loaded organic exiting from the first stage of ISX is scrubbed with acidified process condensate to remove co-extracted Mg, Co and Ni from the organic as well as washing out any entrained AmSul solution. The sulfuric acid concentration of the scrub solution is controlled to achieve the target equilibrium pH exiting the last scrub stage (nominally pH 2). To minimise the Co and Ni loss, the aqueous is recycled back to the ISX extraction stages. The scrubbed organic with reduced Co and Ni content is sent to stripping.

Some gypsum precipitation is anticipated in the latter stages of scrubbing due to the transfer of calcium from the organic into a small aqueous stream.

Manganese Stripping

During manganese stripping, the scrubbed organic is counter-currently contacted with a sulfuric acid solution, which is added to maintain a pre-determined sulfuric acid concentration in the product liquor. At a suitable pH most of the Mn and other metals including Ca, Cu, Mg, Co and Ni are transferred from the organic to the aqueous. The Mn-stripped organic advances to zinc stripping. Gypsum precipitation is expected in manganese stripping due to the transfer of Ca into a small aqueous stream.

Zinc Stripping

During zinc stripping, the organic is counter-currently contacted with a sulfuric acid solution, which is added to maintain a pre-determined sulfuric acid concentration in the product liquor. At the desired acidity, Zn and the remaining metals (except for Fe and Al) are transferred from the organic to the aqueous. In the commercial flowsheet prior to piloting, the stripped organic is split and fed to impurity extraction, iron stripping and impurity transformation. The zinc strip product is a saleable product.

Some gypsum precipitation is anticipated in zinc stripping due to the transfer of Ca into a small aqueous stream.

Iron Stripping

Iron is not quantitatively removed from the organic by sulfuric acid during stripping, potentially leading to iron accumulation in the organic and subsequently inhibiting the extraction of the other metals when the stripped organic is recycled back to extraction. To prevent the accumulation of iron on the organic, a bleed stream of the Zn-stripped organic (less than 10%) is fed to iron stripping. Oxalic acid is used as the stripping agent to remove Fe and the remaining metals from the organic.

This step is conventionally performed using hydrochloric acid, but the extraction plant in the TECH Project is sensitive to chlorides hence the switch to oxalic acid.

Iron Wash

The organic with reduced levels of Fe is washed using process condensate.

Gypsum and crud treatment is performed by a tricanter centrifuge, with the recovered aqueous and recovered organic streams recycled back to the process.

A schematic of the commercial ISX flowsheet as proposed prior to piloting is shown in Figure 3.

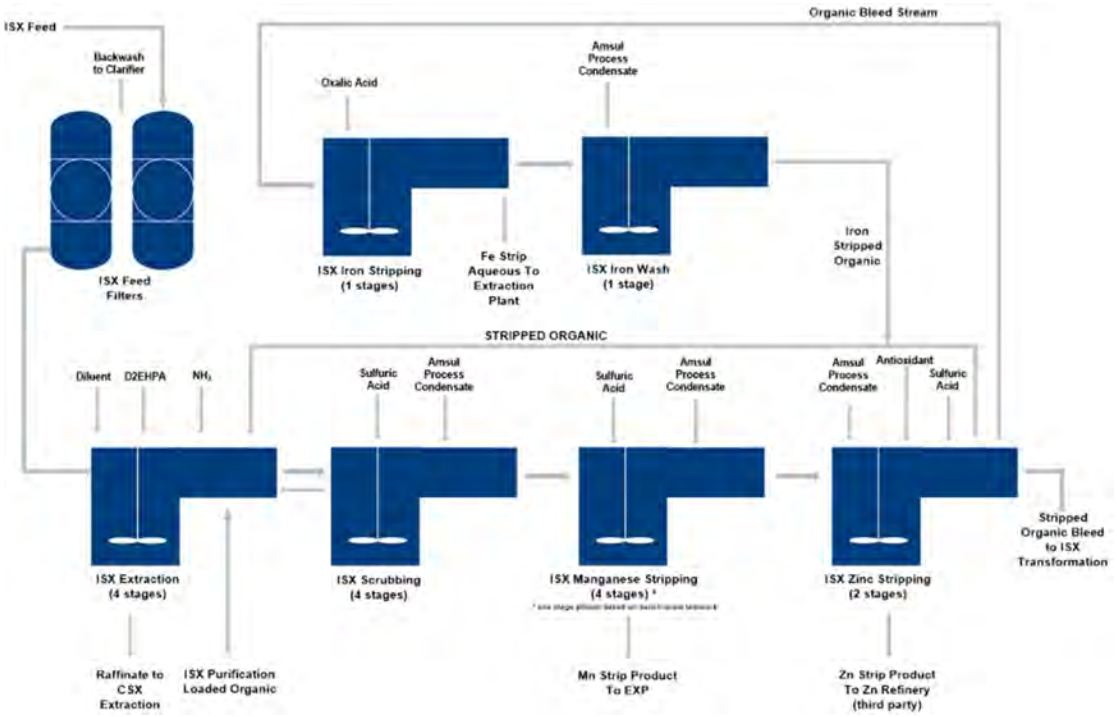

Figure 3: Schematic of the Proposed Commercial ISX Circuit (pre-piloting)

Transformation and Purification Process Description

TSX and PSX utilise the D2EHPA® organic to further purify CSX cobalt LSL ahead of cobalt crystallisation. In TSX, a portion of the ISX stripped organic stream (containing minimal amounts of Zn and Mn) is first preloaded with sodium ions in a saponification stage before contacting a bleed of the purified cobalt LSL. Cobalt displaces sodium to transform the organic into cobalt loaded organic before feeding to PSX.

The PSX step is essential to ensure that there are minimal impurities and organic entrained in the cobalt sulfate crystallisation feed. The cobalt LSL from CSX is contacted with the cobalt loaded organic from TSX. The impurity metals from the cobalt LSL displace cobalt from the organic into the aqueous, thus impurities are removed from the cobalt LSL and replaced by additional cobalt.

The purified cobalt LSL is passed through dual media filters and carbon columns to remove entrained organic before cobalt crystallisation.

The TSX/PSX flowsheet incorporates the following process steps:

Saponification

A portion of the ISX stripped organic is sent to the transformation area, where it is preloaded with sodium ions to maintain the required pH in the system. The preloading reaction is as follows:

$$NaOH(a) + H\text{-}D2EHPA(o) = H_2O(a) + Na\text{-}D2EHPA(o)$$

Transformation

The feed solution, purified cobalt LSL (approx. 120 g/L Co), is contacted counter-currently in four stages with the sodium preloaded organic. At the optimum pH, cobalt displaces sodium and loads onto the organic. The primary objective is the transfer of cobalt from the aqueous to the organic phase. The advance O/A is optimised to achieve this objective.

The transformation reaction is as follows:

$$2\ \text{Na-D2EHPA(o)} + \text{CoSO}_4\text{(a)} = \text{Na}_2\text{SO}_4\text{(a)} + \text{Co-(D2EHPA)}_2\text{(o)}$$

The cobalt loaded organic exiting from the first stage of transformation is forwarded to the purification circuit, whilst the aqueous, containing sodium sulfate, discharges from the last stage of transformation and is combined with the ISX manganese strip liquor.

Purification

The cobalt LSL from CSX contains cobalt sulfate and minor amounts of impurities such as Mn, Zn, Cu and Ca sulfates. The impurity content is further reduced before the cobalt sulfate enriched solution is fed to cobalt crystallisation for cobalt sulfate heptahydrate production. The purification step is necessary to ensure minimal impurity and organic entrainment in the crystalliser feed solution, in order that the cobalt product meets the required specification.

The cobalt LSL is contacted counter-currently in eight stages with the cobalt loaded organic from TSX. At the optimum pH the impurity metals displace cobalt and load onto the organic. The PSX raffinate (purified cobalt LSL), with reduced impurity levels, becomes the feed to cobalt crystallisation.

The key purification reactions are as follows:

$$\text{Co-D2EHPA(o)} + \text{MnSO}_4\text{(a)} = \text{CoSO}_4\text{(a)} + \text{Mn-(D2EHPA)}_2\text{(o)}$$
$$\text{Co-D2EHPA(o)} + \text{ZnSO}_4\text{(a)} = \text{CoSO}_4\text{(a)} + \text{Zn-(D2EHPA)}_2\text{(o)}$$
$$\text{Co-D2EHPA(o)} + \text{CaSO}_4\text{(a)} = \text{CoSO}_4\text{(a)} + \text{Ca-(D2EHPA)}_2\text{(o)}$$
$$\text{Co-D2EHPA(o)} + \text{CuSO}_4\text{(a)} = \text{CoSO}_4\text{(a)} + \text{Cu-(D2EHPA)}_2\text{(o)}$$

Stripping (pilot plant circuit only)

In the commercial plant the PSX loaded organic returns to the ISX loaded organic tank, combining with the ISX loaded organic feed to scrubbing. In the TSX/PSX pilot plant the organic was recycled within the circuit, with two stages of stripping contacting the impurity loaded organic with a sulfuric acid strip solution. Co, Mn, Ca, Zn and the remaining metal impurities except Fe and Al were transferred from the organic to the aqueous. The stripped organic was returned to saponification.

A schematic of the commercial Purification (TSX and PSX) flowsheet as proposed prior to piloting is shown in Figure 4.

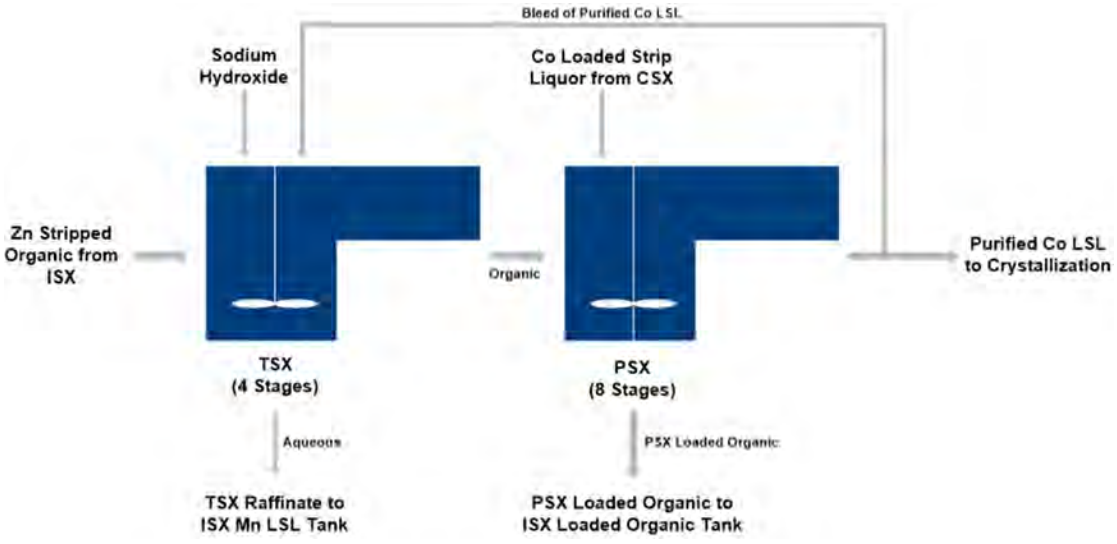

Figure 4: Schematic of the Proposed Commercial TSX and PSX Circuit

PILOTING STRATEGY

The Sulfate Refinery was piloted in 4 stages at SGS, as follows:

- Aluminium Removal (PP1)
- ISX (PP2)
- CSX and NSX (PP3)
- Purification (TSX and PSX) (PP4)

and the product liquor from each pilot plant was stored to feed the subsequent pilot plant.

Since the ISX raffinate is the feed to CSX, and the feed to TSX/PSX is cobalt LSL, the impurity removal pilot plant was run across two campaigns. ISX was run first, to generate feed for the CSX pilot plant, and the TSX and PSX pilot plant was run after the CSX pilot plant had been completed.

PILOT PLANT DESIGN

The results of a comprehensive bench-scale testwork program and the outputs from the SysCAD process model, along with complementary modelling by Syensqo (formerly Solvay), the D2EHPA® manufacturer, were inputs to the pilot plant design.

The ISX pilot plant flowsheet consisted of seven stages: Saponification, Extraction, Scrubbing, Mn Strip, Zn Strip, Fe Strip and Fe Wash. SGS provided a schematic flowsheet for the pilot plant, complete with initial flowrates and initial operating conditions, presented in Figure 5. SGS uses an internal convention of numbering the mixer-settlers in the direction of the organic flow. Notably, the four extraction mixer-settlers are numbered in the reverse order to the project PFD's, with organic feeding E1 and aqueous feeding E4.

The ISX pilot plant was constructed using jacketed cylindrical glass mixers and settlers of the Hazen-Quinn type, with a nominal volume of 437 mL for the mixers and 2,036 mL for the settlers. The mixers and settlers were mounted at a suitable working height on a frame. The mixers and settlers were interconnected using plastic tubing with plastic compression tube fittings. Settler interface height control was by height adjustment of an external inverted-Y connector on the aqueous advance. The design organic feed rate to Fe Strip was 10% of the primary circulating organic rate. Two smaller mixer-settlers with a nominal volume of 199 mL for the mixers and 823 mL for the settlers were used for Fe Strip and Fe Wash.

The process temperature was maintained at approximately 60°C by recirculating hot water via a distribution manifold through each jacketed mixer and settler. Peristaltic and positive displacement pumps were used for the aqueous and organic flows, and aqueous recycles were pumped using multi-head pumps. Pumps and controllers were generally located above the cells.

One mixing compartment was installed in each stage. The mixing compartment was baffled by four equally spaced indentations moulded into the inside glass wall. Each mixer was fitted with a 51 mm diameter low shear six-blade pump-mix impeller (Figure 6) driven by a variable speed motor. The design mixer speed was 800 rpm and the design tip speed was 2.1 m/sec. Mixer speeds were adjusted during the campaign as required, to maintain pumping and mixing. The two smaller mixer-settlers used for Fe Strip and Fe Wash were fitted with 32 mm diameter impellers. The impellers were of polypropylene construction, and the stainless steel agitator shafts were sheathed in polypropylene tubing welded to the agitator heads.

Loose covers were fitted on all mixers and settlers. The mixer covers were slotted to accommodate removal of the covers without removing the agitator shaft. Each mixer and settler cover was mechanically ventilated via plastic tubing (Figure 7) to a manifold and a central scrubber. A pH electrode and a thermocouple were installed in each mixer via openings in the lids (Figure 7).

In order to prevent transfer of entrained organic with the exiting diluent wash aqueous raffinate stream, a coalescer was installed. The unheated glass coalescer was filled with granular anthracite and was operated not flooded in downflow mode to minimise the risk of cooling and precipitation of metal ammonium sulfate double salts within the coalescer. The feed gravitated onto the top of the carbon and the solution was discharged from the bottom of the column.

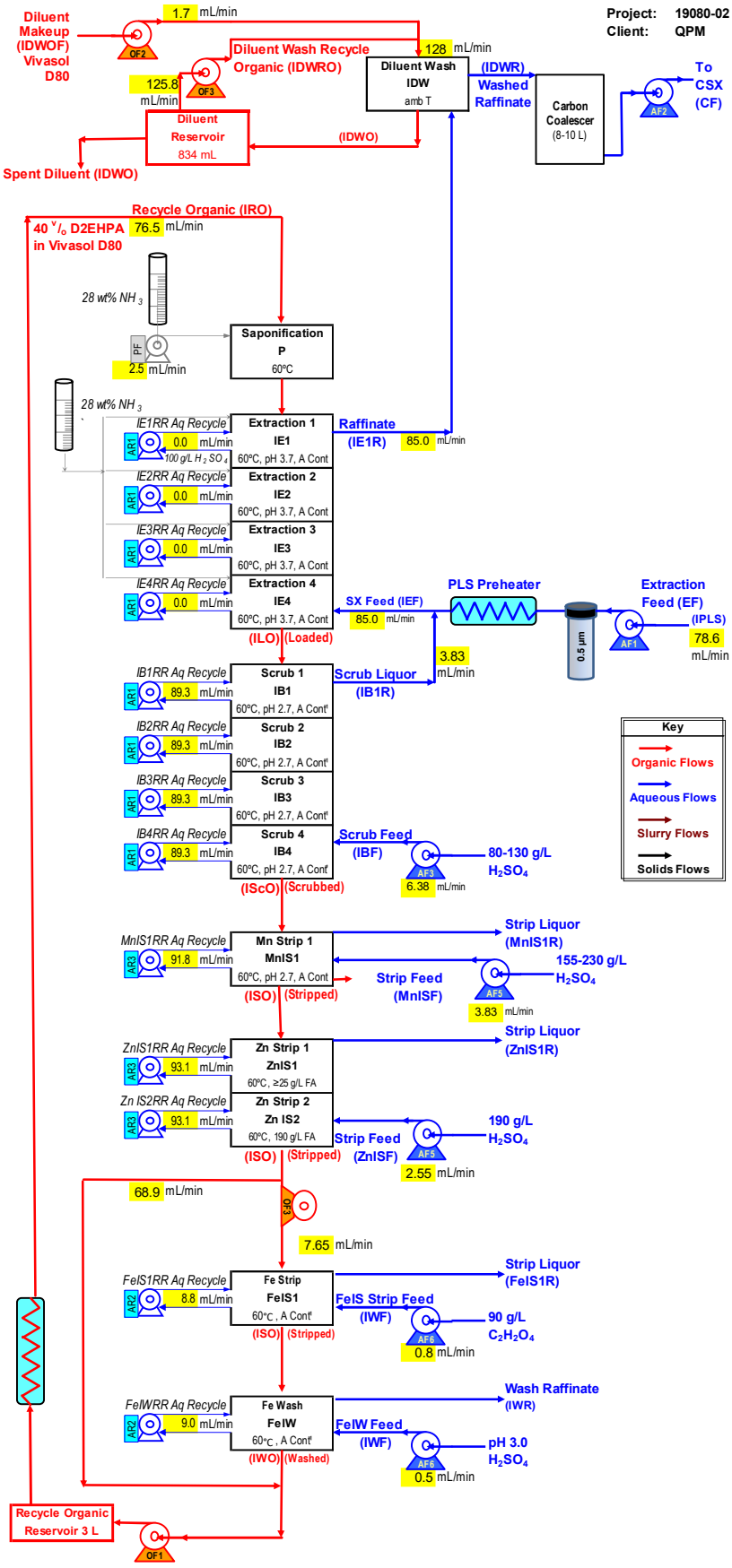

Figure 5: ISX Pilot Plant Schematic (source: SGS)

Figure 6: Photograph of 51 mm Six-Blade Low Shear Pump-Mix Impeller

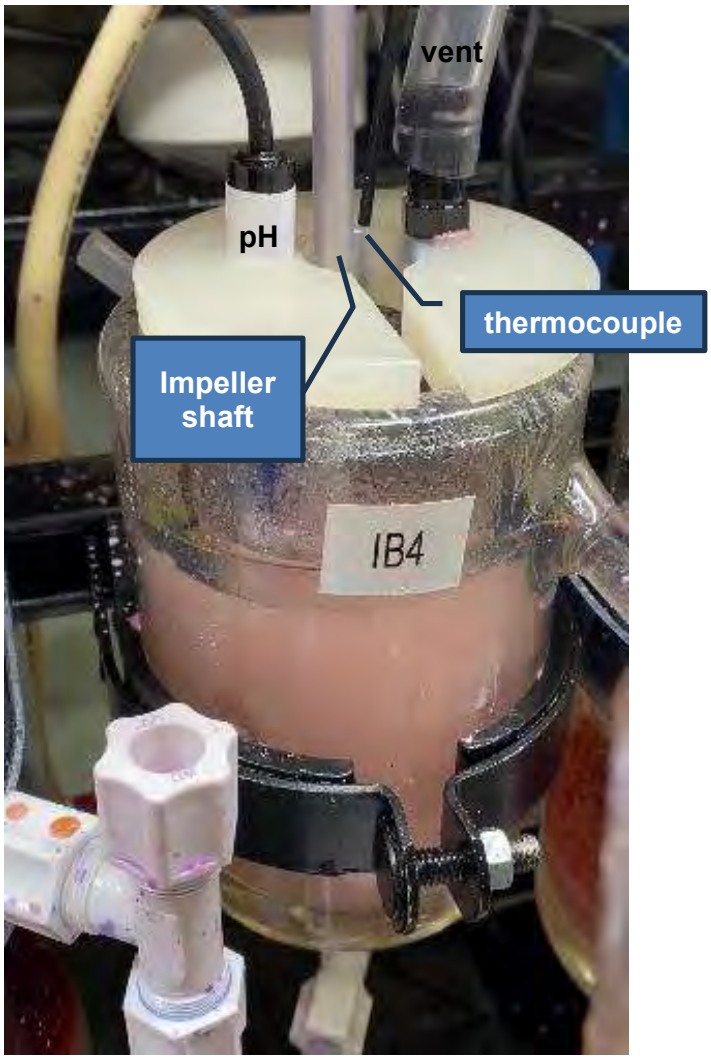

Figure 7: ISX Scrub 4 Mixer, showing clear plastic vent tubing connected to the slotted cover

A photo of the ISX pilot plant at SGS is shown in Figure 8.

Figure 8: Photograph of the ISX Pilot Plant at SGS Canada

The TSX and PSX pilot plant flowsheet consisted of a saponification stage, four stages of Transformation (TSX) to preload the organic extractant with cobalt, followed by eight stages of Purification (PSX), and two stages of stripping using sulphuric acid. Stripping is not a feature of the commercial TSX/PSX process, since commercially the PSX loaded organic returns to the ISX loaded organic tank. SGS provided a schematic flowsheet for the pilot plant, complete with initial flowrates and operating conditions, presented in Figure 9. SGS use an internal convention of numbering each mixer-settler in the direction of the organic flow. Notably, the four Transformation mixer-settlers are numbered in the reverse order to the project PFD's.

Equipment of sufficient size for metallurgical validation of the flowsheet, and with materials of construction suitable for the solution matrices, was used for the TSX and PSX pilot plant. The SGS pilot plant was constructed using jacketed cylindrical glass mixers and settlers of the Hazen-Quinn type, with a nominal volume of 199 mL for the mixers and 823 mL for the settlers. The mixers and settlers were interconnected using plastic tubing with plastic compression tube fittings. Settler interface height control was by height adjustment of an external inverted-Y connector on the aqueous advance. The organic saponification mixer was a jacketed glass cylindrical mixer with a nominal volume of 562 mL

The process temperature was maintained at approximately 60°C by recirculating hot water via a distribution manifold through each jacketed mixer and settler. Peristaltic and positive displacement pumps were used for the aqueous and organic flows, and aqueous recycles were pumped using multi-head pumps. Pumps and controllers were generally located above the cells.

One mixing compartment was installed in each stage. The mixing compartment was baffled by four equally spaced indentations moulded into the inside glass wall. Each mixer was fitted with a 32 mm diameter low shear six-blade pump-mix impeller (similar to the 51 mm impeller shown in Figure 6) driven by a variable speed motor. Mixer speeds were adjusted during the campaign as required to maintain pumping and mixing, typically between 800 and 1,200 rpm. The impellers were of polypropylene construction, and the stainless steel agitator shafts were sheathed in polypropylene tubing welded to the agitator heads.

Loose covers were fitted on all mixers and settlers. The mixer covers were slotted to accommodate removal of the covers without removing the agitator shaft. Each mixer and settler cover was mechanically ventilated via plastic tubing to a manifold and a central scrubber.

To prevent transfer of entrained organic with the exiting Purification aqueous product stream, a coalescer was installed. The coalescer was filled with granular anthracite and was operated flooded, in up-flow mode.

A photo of the Purification (TSX/PSX) pilot plant at SGS is shown in Figure 10.

The raffinate from TSX and the strip liquor (S1R) was collected in pails while the PSX raffinate (P1R) was passed through a heated carbon coalescer and then collected in pails, as shown in the pilot plant schematic (Figure 9). As with ISX, the stages were numbered according to the flow of organic throughout the circuit.

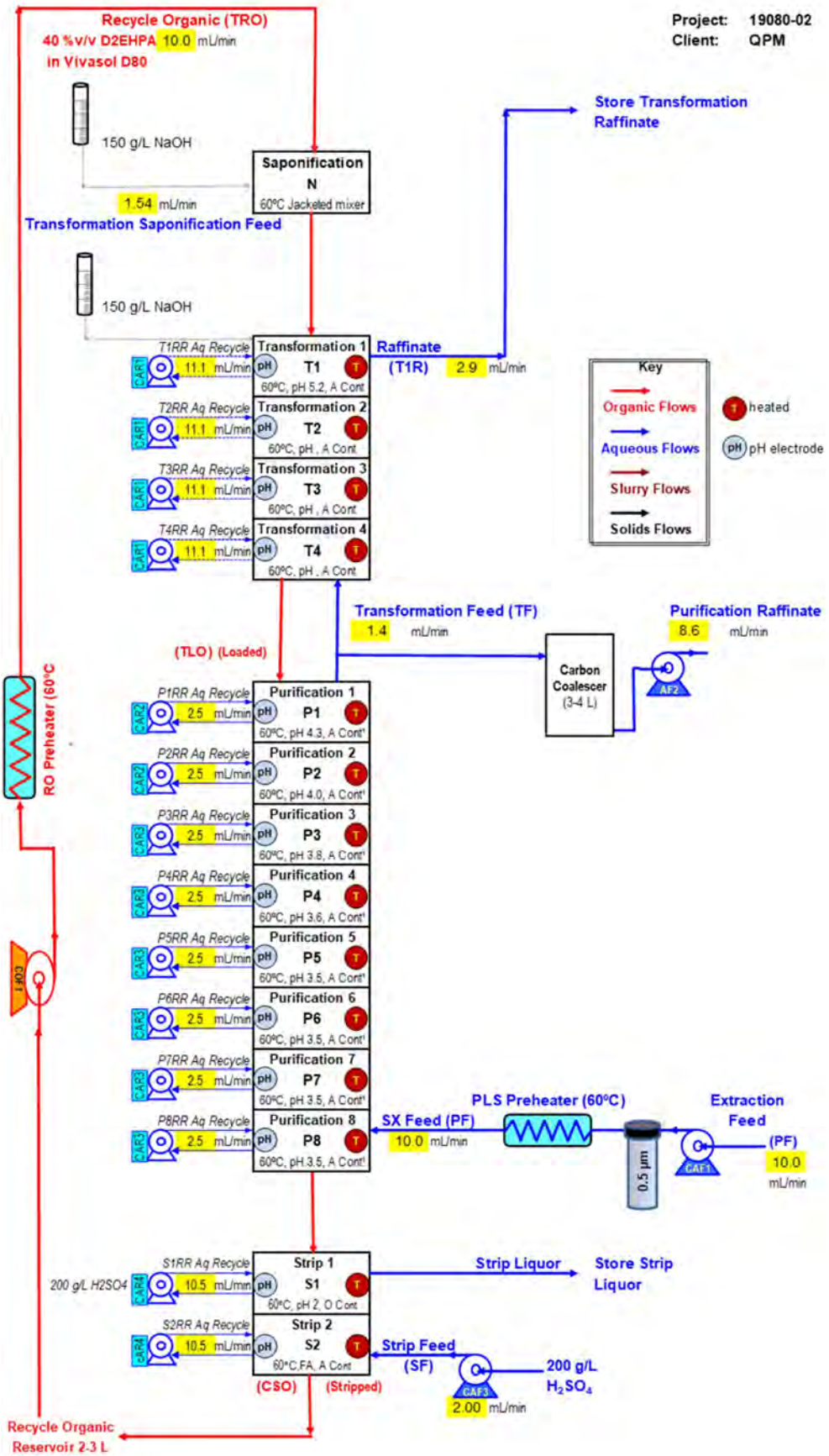

Figure 9: Transformation and Purification Pilot Plant Schematic (source: SGS)

Figure 10: Photograph of the Purification (TSX and PSX) Pilot Plant at SGS Canada

CONTINUOUS PILOT PLANT OPERATIONS

The key objective of the ISX and TSX/PSX continuous pilot plants was the metallurgical confirmation of the commercial plant design. The ISX pilot (PP2) plant was operated for 24 hours per day, for ~231 hours, over the period May 23 to June 2, 2023. Following the subsequent CSX and NSX pilot plant, the TSX/PSX pilot plant (PP4) was operated for 24 hours per day, for ~183 hours, over the period July 12 to 20, 2023.

ISX Pilot Plant Operation and Results

Feed Preparation

The feed for the ISX pilot plant was the product liquor from the preceding Aluminium Removal pilot plant. There were two feed solutions prepared, Extraction Feed 1 (EF-1) was fed from startup on May 23 and then Extraction Feed 2 (EF-2) was introduced after 74 hours on May 26.

EF-1
1200 L of feed solution (sufficient for 10 days operation) was prepared by the addition of metal sulfate salts (Al, Ni, Fe, Zn, Cu) to Aluminium Removal product liquor as required. Fe was added as Fe(II) sulfate. EF-1 was homogenised and stored at ambient temperature in 2 x 600 L IBCs. EF-1 was used as feed during the initial 74 hours of operation. The chemical composition of EF-1 which was unavailable prior to startup of the ISX continuous pilot plant was found to be significantly above target for Ca (37%) and Zn (10%), and below target for Mg (15%).

EF-2
800 L of feed solution (sufficient for 7 days operation) was prepared by blending 600 L of EF-1 with 200 L of ISX raffinate product and adding metal sulfate salts as required to achieve a feed composition closer to the targets. EF-2 was homogenised and stored at room temperature in one IBC.

Initially the feed solution (EF-1) was not diluted as the concentrations of nickel and cobalt post aluminium removal were lower than expected in ISX feed. However, the solution was calcium saturated, with a calcium concentration 37% higher than expected for ISX. The high calcium tenor resulted in significant gypsum precipitation throughout the scrub, manganese strip and zinc strip stages, causing frequent blockages and very unstable operation. The commercial plant design employs a 10% dilution via a calcium-free aqueous recycle stream from the downstream plant. It was therefore decided on day 3 to dilute the ISX feed by 10% using raffinate from the first few days of operation, the composition of which closely resembled the modelled recycle stream. Concentrations of manganese and zinc in the adjusted feed were then spiked to reflect the values expected in ISX feed. The compositions of the solutions are listed in Table 1.

Table 1: ISX Continuous Pilot Plant Aqueous Feed Compositions

	Concentration g/L		
Component	**EF-1**	**EF-2**	**Target**
Al	0.005	0.003	0.005
Ca	0.706	0.477	0.491
Co	6.274	5.874	6.286
Cu	0.031	0.022	0.035
Fe	0.005	0.003	0.005
Mg	7.080	6.631	8.349
Mn	4.522	4.307	4.339
N	not available	6.15	7.27
NO_3	tba	26.2	tba
Na	0.516	0.508	0.596
Ni	60.40	58.35	57.34
S	41.70	41.95	41.37
Zn	1.106	0.983	0.991

The feed solution composition used for the continuous pilot plant simulated a maximum Mg impurity case rather than the nominal Mg case (4.51 g/L Mg). Precipitative Ca stripping was anticipated in Scrubbing (minor), Mn strip (majority) and Zn strip (minor).

Piloting

The organic was saponified using ammonia and fed to the first of 4 extraction stages (IE1). In Saponification the design advance O/A was 31:1 and the design flow rate targets of 76.5 mL/min ISX recycle organic (IRO) and 2.47 mL/min saponification feed (PF) were intentionally not changed during the pilot plant campaign. The saponification results summarised in Figure 11 show the target advance O/A was not attained consistently. Steady state operation of saponification was not achieved during the first nine operating days due primarily to uncontrolled variability in the PF flow rate. During each day the ambient air temperature at the ammonia solution drum increased due to solar heating of the adjacent exterior wall of the building. The ammonia solution began to gasify inside the plastic tubing, affecting the solution flow rate. Gasification of the ammonia solution was not an issue overnight when the ambient air temperature was cooler.

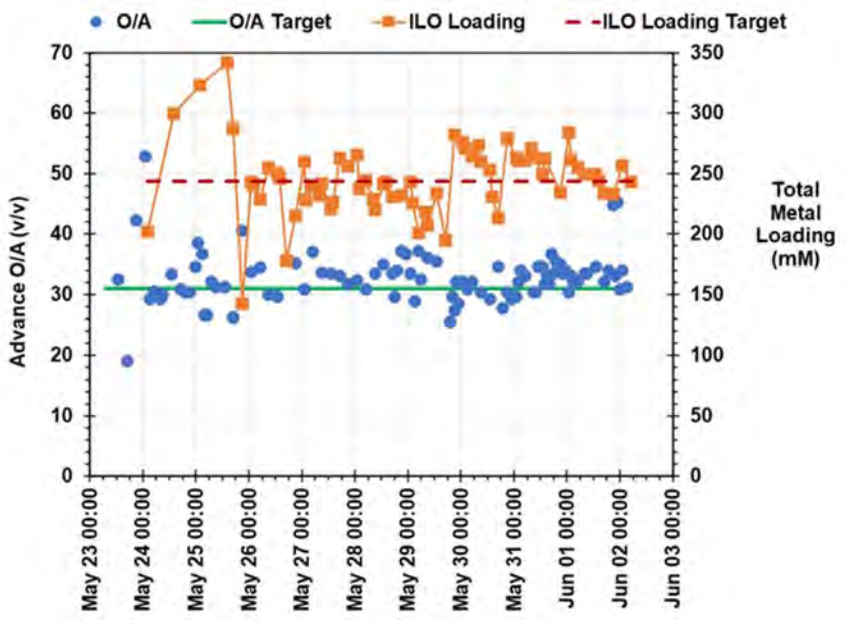

Figure 11: ISX Organic Saponification Advance O/A and Total Metal Loading in Impurity Loaded Organic

A short-term upset during May 25 was caused by third phase formation in the saponification settler. Total metal loading in ISX loaded organic (ILO) was calculated using the results of four-hourly back-stripped assays. The total metal loading trend shown in Figure 11 is not consistent. The total metal loading in ILO was also affected by initial high levels of Zn and Mn in recycle organic. In particular, Zn in IRO increased to almost 6 g/L during May 24-25 (Figure 12).

Figure 13 shows the measured advance O/A in extraction, which was adjusted by changes to the extraction feed flowrate in an effort to control the circuit. The setpoint target is identified by the orange line. Assay trends for the extraction raffinate (CSX feed) are plotted in Figure 14. Mn in the extraction raffinate ranged from 1.7 to 190 mg/L. There were periods when Mn was consistently less than 10 mg/L, and it was less than 5 mg/L about 20% of the time. Periods of high Mn (and Zn) in the recycle organic contributed to high Mn in the raffinate, particularly early in the campaign. Ca ranged from 1.7 to 18.4 mg/L and averaged 3.9 mg/L for the campaign. Cu ranged from <0.1 to 7.5 mg/L and averaged less than 1.5 mg/L overall. Zn was generally below detection limit (2 or 4 mg/L) and only those samples above detection limit are included in the figure below.

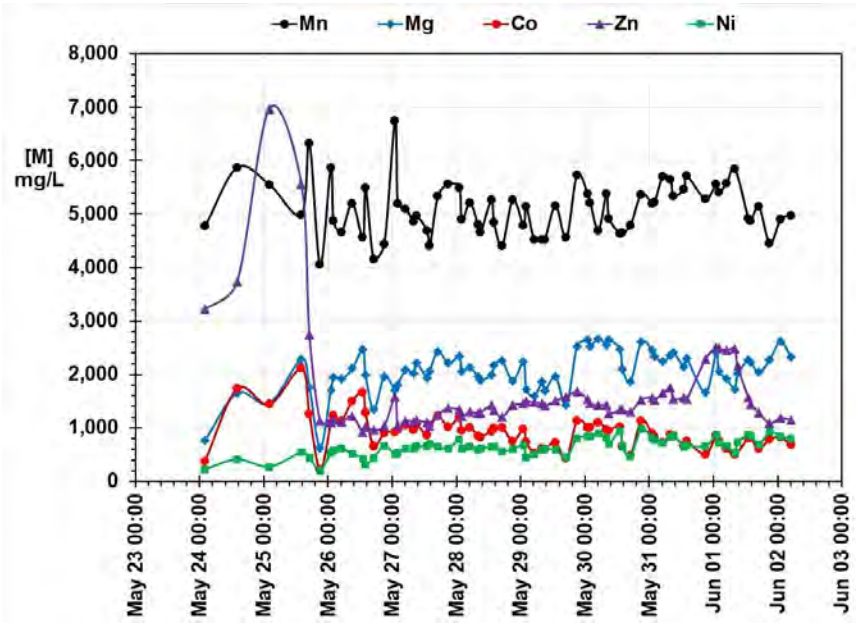

Figure 12: ISX Loaded Organic (ILO) Composition

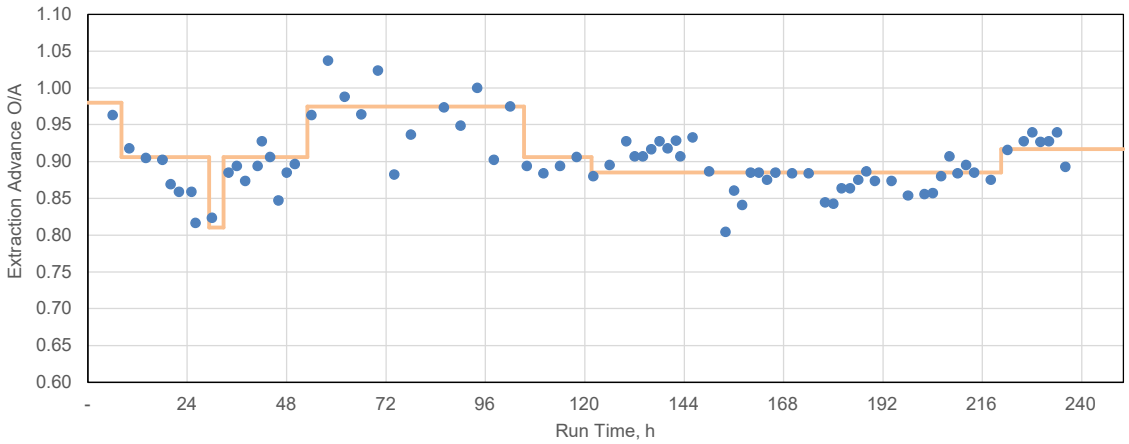

Figure 13: ISX Extraction Measured Advance O/A

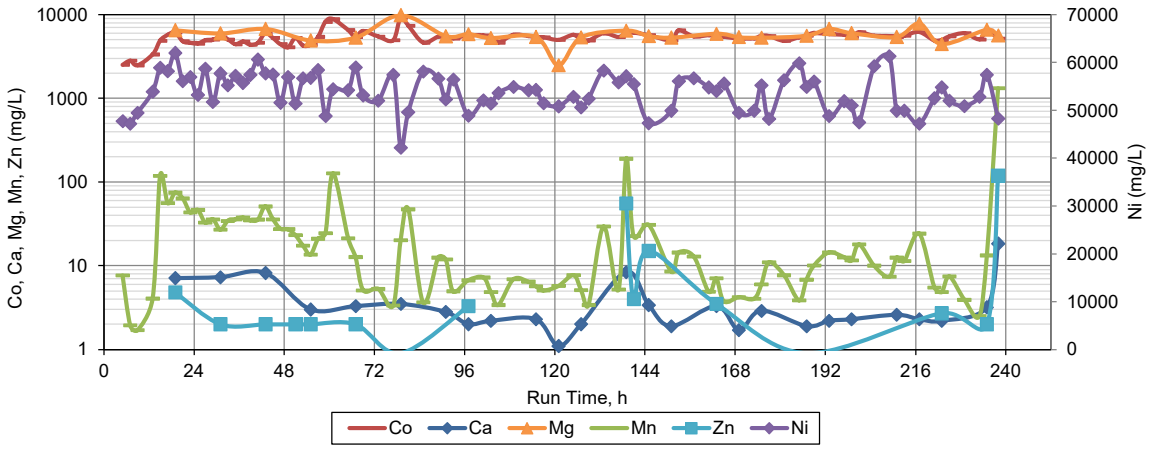

Figure 14: ISX Extraction Raffinate (IE1R) Assay Trends

ISX loaded organic (IE4O) assays are plotted in Figure 15, including both organic analysis by back-stripping (hollow symbols with line) as well as direct organic assays (filled symbols and no line). The data illustrate that the back-strip analyses generally aligned well with the direct organic assays.

Total metal loading ranged from 214 g/L to 271 mmol/L from hour 72 onwards and averaged 243 mmol/L during that period with minor variation. Mg loading increased at around hour 154, which aligns generally with a decrease in the advance O/A, and Ni loading also increased around this time. Zn loading increased around hour 200, corresponding to an increase in Zn in the recycle stripped organic.

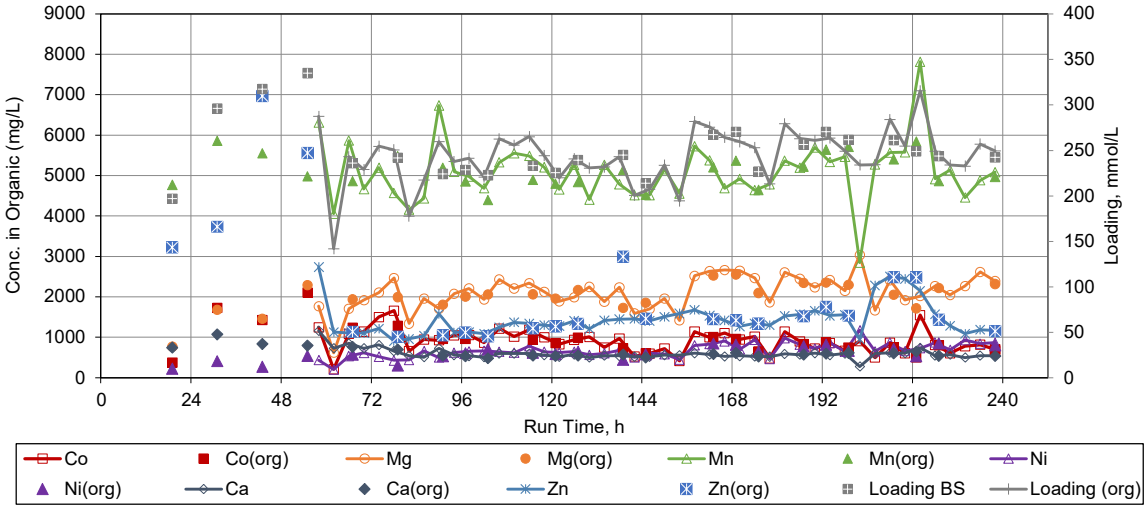

Figure 15: ISX Loaded Organic (IE4O) Assay Trends

Recorded pH measurements for IE mixers are shown in Figure 16. The measured IE1 mixer pH (blue dots) is observed to be close to the value of 2.75 indicated by Syensqo's predictive modelling.

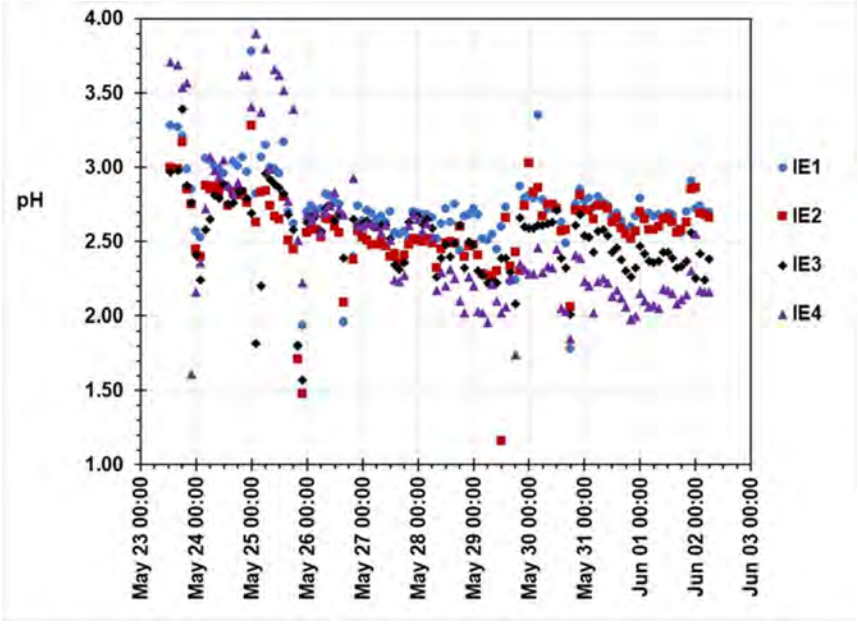

Figure 16: pH Measurements in ISX Extraction Mixers

The loaded organic advanced to 4 stages of scrubbing. In the early stages of the campaign precipitative Ca stripping by the sulfuric acid scrub solution took place in the 3rd and 4th scrubbing stages (IB3 and IB4) (see Figure 17 and Figure 18). IB4 was the stage with the lowest mixer pH. Vacuum filtration of the IB4 aqueous recycle stream (IB4RR) stream (IB4 is the fourth scrubbing stage with the lowest mixer pH and the greatest risk of precipitative Ca stripping by the sulfuric acid scrub

solution) was implemented on May 27 to minimise gypsum crud accumulation in the IB4 settler (Figure 19). The equipment readily facilitated this as the aqueous discharge is from the bottom of the settler.

Figure 17: Gypsum from Scrub 3 Settler, May 25

Figure 18: Gypsum from Scrub 4 Settler, May 25

Figure 19: Gypsum Crud in ISX Scrub 4 Settler

The scrub feed sulfuric acid concentration was intentionally varied during the campaign as shown in Figure 20. In the first instance, acid concentration was increased to increase Ni and Co scrubbing efficiencies and later decreased to decrease Ca scrubbing efficiency sufficiently to prevent gypsum precipitation in IB4.

Figure 20: Molarities of ISX Scrub Feed Acid and Total Metals in IB1R

Starting at hour 158 the pH in IB4 was directly controlled by the addition of 200 g/L sulfuric acid and at hour 178 the Scrub Feed (IBF) was stopped with all scrub solution (as 80 g/L H_2SO_4) added via pH control in IB4. The pH trends in scrubbing are plotted in Figure 21.

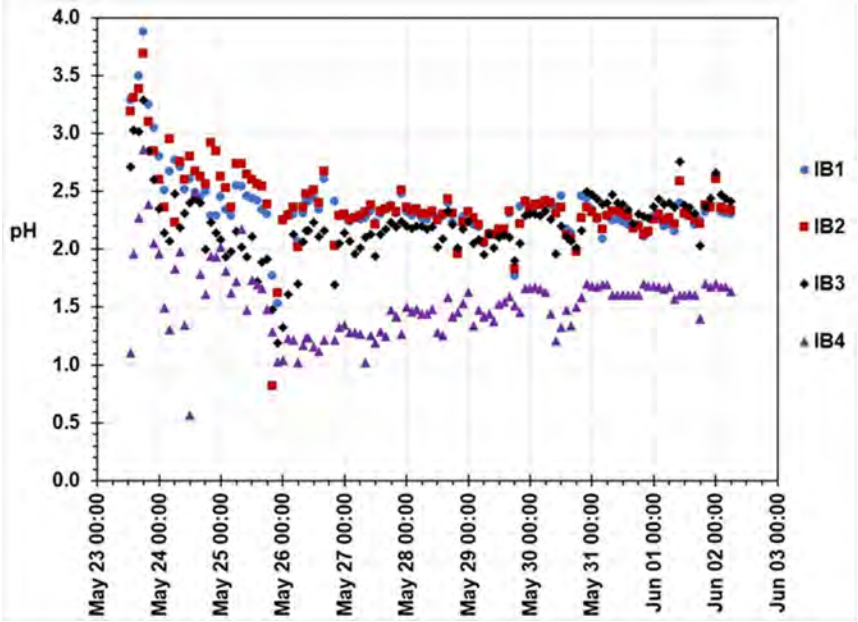

Figure 21: pH Measurements in ISX Scrub Mixers

No further gypsum precipitation was observed in IB4 after the implementation of pH control. Figure 22 shows the filter paper on the IB4 aqueous recycle filter on June 1, completely free of solids 48 hours after last being replaced. Ca tenors in IB4 recycle aqueous before and after the implementation of pH control are shown in Figure 23. Figure 24 shows the Scrub 2 and 3 settlers on May 28.

Figure 22: Scrub 4 (IB4) Settler Gypsum Filter after 48 hours, May 31

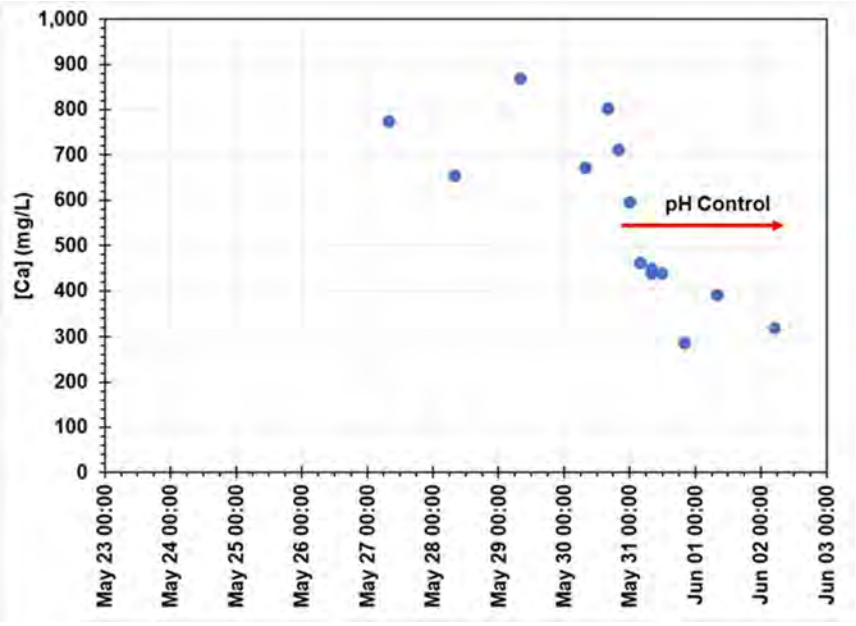

Figure 23: Ca in ISX Scrub Stage 4 Aqueous Recycle (IB4R)

Figure 24: ISX Scrub 2 and 3 Settlers, May 28

The primary objectives of scrubbing were to achieve high scrub efficiencies for Ni and Co, while minimising Zn, Ca, Mn and Cu scrubbing and avoiding gypsum precipitation in the scrubbing mixers. The trends for Ni, Co, Mg, Ca, Cu and Mn scrubbing efficiencies are shown in Figure 25. Ni scrubbing efficiency >99.5% and Co scrubbing efficiency >90% were achieved consistently. From May 27 onwards, Mn scrubbing efficiency was <5% and Cu scrubbing efficiency was <20%. Ca scrubbing efficiency at 30 to 70% was too high following start up, largely due to the loaded organic variability. The change to pH control for scrub feed acid addition on May 30 resolved this issue and Ca scrubbing efficiency was reduced to <10%. In general, the scrubbing section achieved the process objectives quite well, and confirmed the Syensqo predictive modelling.

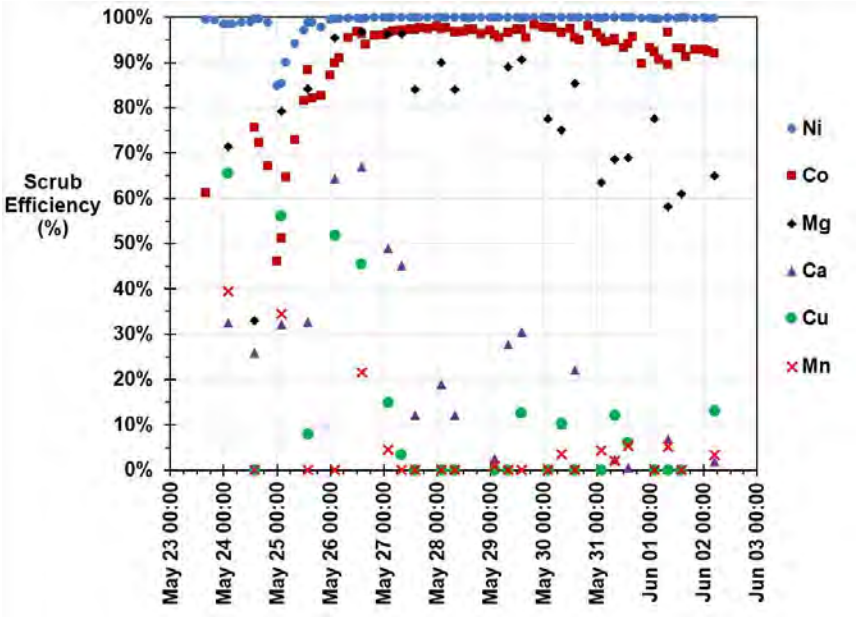

Figure 25: ISX Scrubbing Efficiency

The scrubbed organic advanced to a single stage of Mn Stripping. The Mn Strip objectives were to strip approximately 80% Mn and 10% Zn from the organic, and to achieve precipitative stripping of the majority of the Ca. At the design advance O/A of 20:1, the solubility of Ca in the sulfuric acid strip solution is significantly exceeded (maximum 20 x 600 = 12,000 mg/L); gypsum precipitates in the mixer and largely settles to the floor of the settler. Filtration of the Mn strip (MnIS1) aqueous recycle was implemented on May 25 to minimise accumulation of gypsum crud in the settler (Figure 26 and Figure 27). Gypsum collected from Mn strip on May 29 is shown in Figure 28.

Figure 26: ISX Manganese Strip Gypsum, May 25

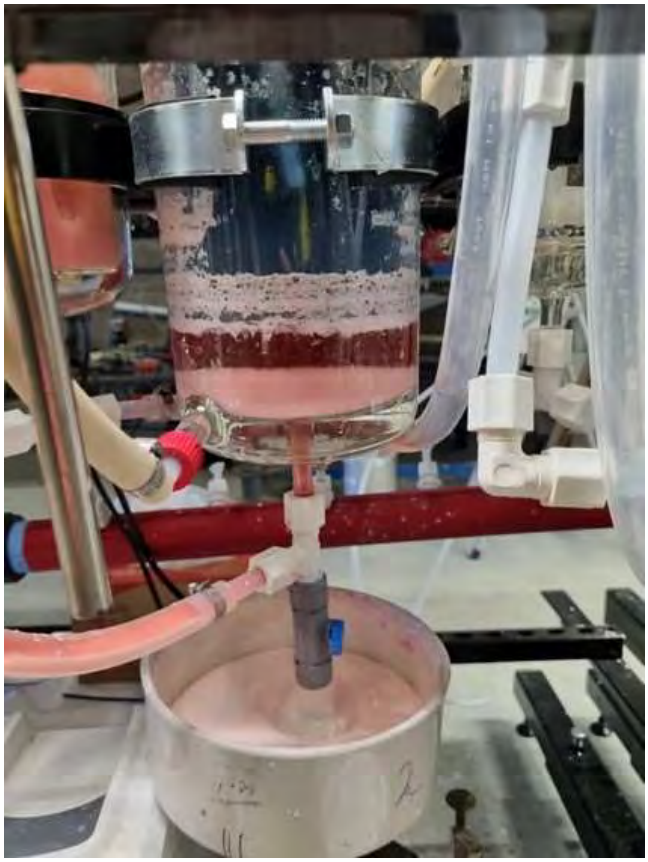

Figure 27: ISX Mn Strip Gypsum Filter

The Mn strip feed acid concentration was increased from 155 g/L to 200 g/L and then 230 g/L to target higher Mn tenor and decreased water content of Mn strip product (MnIS1R) solution (Figure 29).

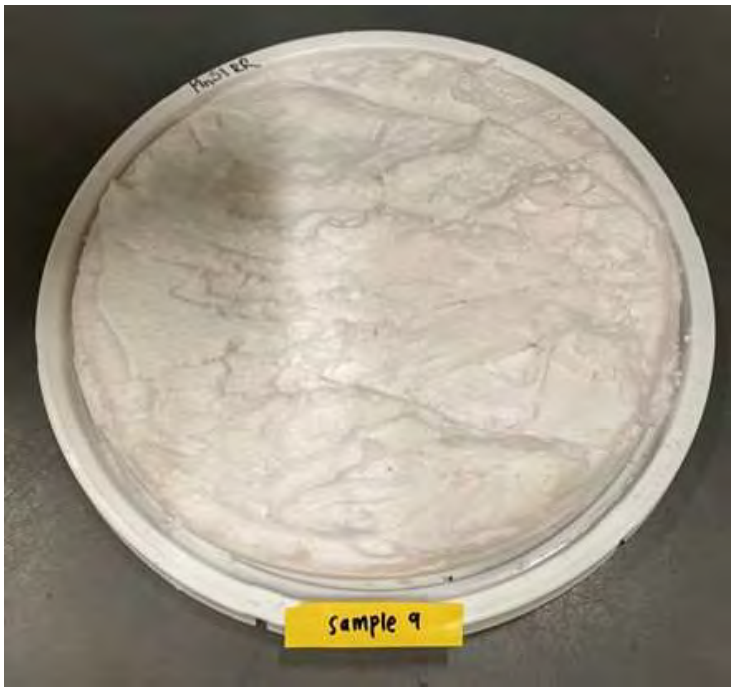

Figure 28: Partially Air-dried ISX Mn Strip Gypsum, May 29

Commencing on May 31, 4-hourly rush analysis of back-stripped Mn-stripped organic (MnIS1O) commenced to improve process control, and 30 mg/L Ca in Mn-stripped organic was targeted in order to avoid gypsum precipitation in Zn strip (Figure 30).

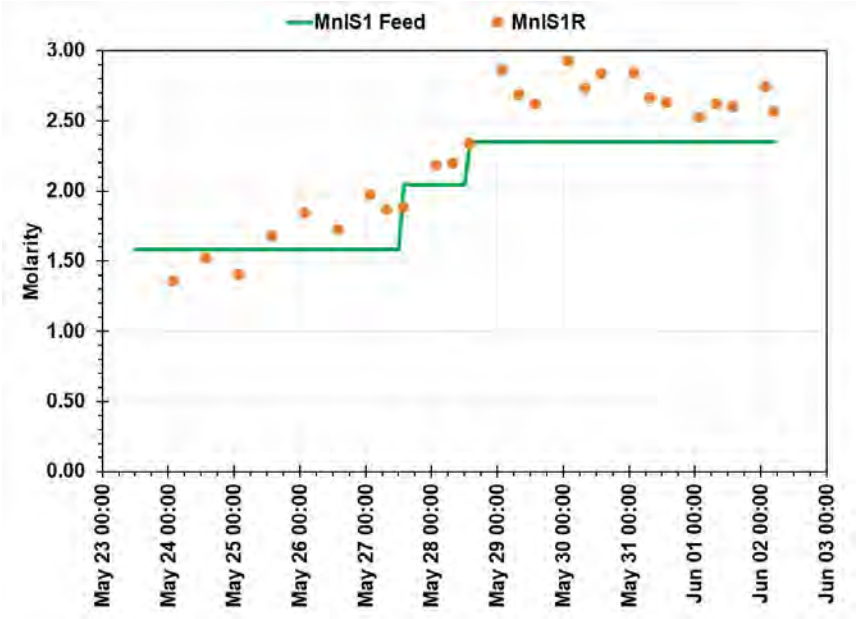

Figure 29: Molarities of ISX Mn Strip Feed Acid and Total Metals in Mn Strip Aqueous

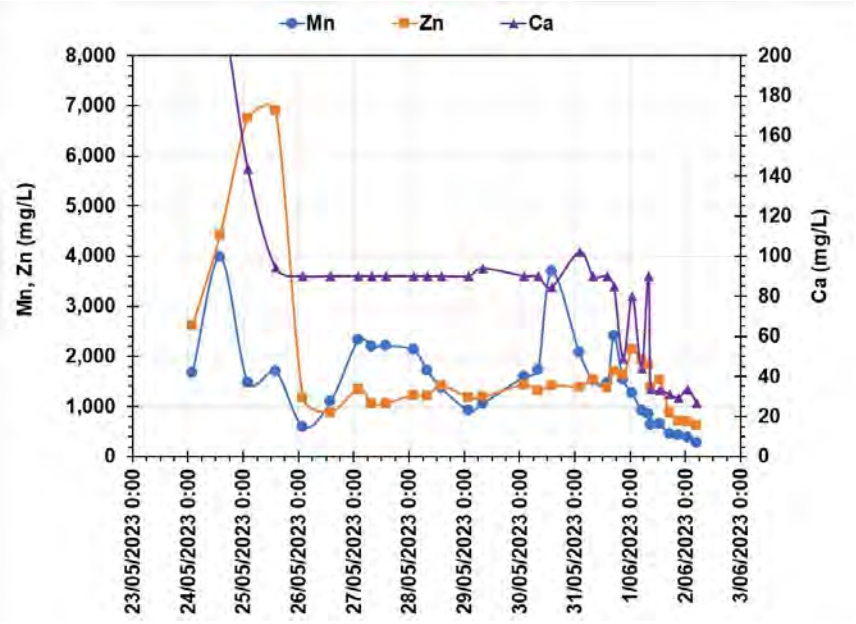

Figure 30: ISX Manganese-Stripped Organic (MnIS1O) Composition

Gypsum scale was observed to adhere to wetted stainless steel and polypropylene surfaces. Scale was not observed to adhere to any wetted surfaces (walls, floor) in the glass settler. The scale growth rate on the polypropylene pump-mix impellers in MnIS1 mixer (and IB4 mixer) was such that the impeller stopped pumping and required removal and cleaning each two days. The appearance of the scale accumulation on a 51 mm diameter pump-mix impeller is shown in Figure 31.

The scale growth rate on wetted stainless steel in MnIS1 mixer was investigated over the period May 27 to June 2. A stainless steel coupon was prepared by bending 6.4 mm tubing. The appearance of scale accumulation on the stainless steel coupon is shown in Figure 32. The coupon was inserted in MnIS1 mixer for up to a day at a time, to quantify the scale growth rate.

Figure 31: Gypsum Scale on an ISX Pump-Mix Impeller

Figure 32: Gypsum Scaling on 316SS Tube Coupon in Mn Strip

As might be expected, scale growth was shown to be proportional to the free acid concentration (Figure 33). At higher acidity, Ca is stripped into a smaller volume of strip feed aqueous resulting in higher Ca tenors.

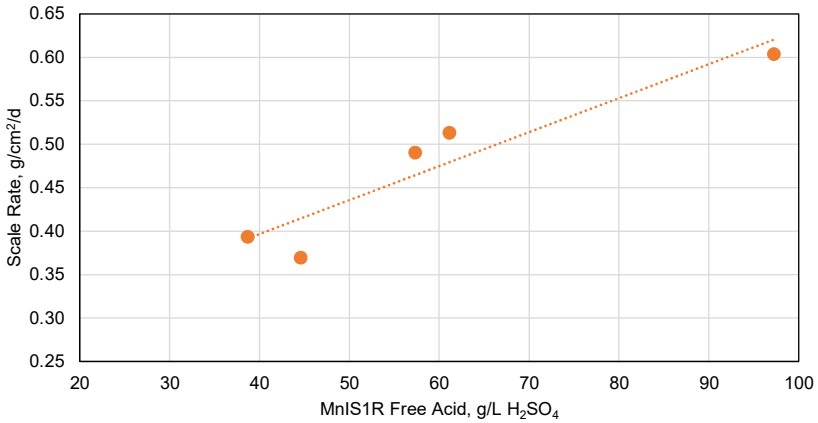

Figure 33: Effect of Free Acid on Scaling Rate in MnIS1

The trends for the Mn content of the key organic streams exiting each stage in the ISX circuit are shown in Figure 34. The Mn content of scrubbed loaded organic was around 5,000 mg/L and the design target was 80% Mn stripping efficiency in Mn Strip, equivalent to 1,000 mg/L Mn in Mn-stripped organic (MnIS1O). This target was achieved only occasionally between May 23 and June 1. While the design target of 80 g/L Mn in Mn strip aqueous product was exceeded, this was at the cost of under-stripping Mn. The sampling schedule included direct analyses of MnIS1O samples each 12 hours but the turnaround time for these assays was several days. It was not possible to consistently achieve the 80% Mn stripping efficiency target without timely MnIS1O assay results. Following the implementation of additional 4 hourly RUSH assays of back-stripped MnIS1O at 17:00 on May 31, the Mn and Zn contents of MnIS1O were controlled to <1,000 mg/L during the final 24-hour period of the campaign.

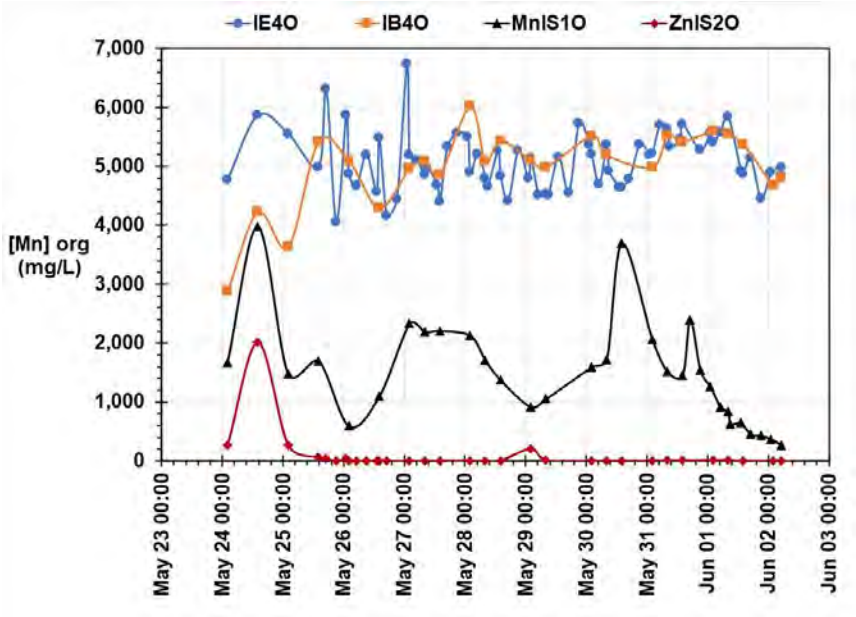

Figure 34: Mn Contents of Key Organic Streams Exiting Each Stage in ISX

In Zn strip, the Mn-stripped organic was contacted in two counter-current stages with sulfuric acid solution. The key objective was to strip 100% of the remaining Zn, Ca, Mn, Cu, Mg, Co and Ni from the organic to the aqueous phase.

During the initial part of the campaign significant gypsum precipitation was experienced in the first stage of Zn stripping (ZnIS1) as shown in Figure 35 and Figure 36. It was demonstrated over several days that it is possible to avoid gypsum precipitation in Zn strip by ensuring the Ca content of Mn-stripped organic is sufficiently low to avoid Ca saturation in the ZnIS1 mixer.

Figure 35: Gypsum Scaling on ZnIS1 Impeller

The results of the bench scale Zn stripping isotherm test were not available until after completion of the ISX pilot plant campaign. The pilot plant identified that the nominal advance O/A in Zn stripping was 6:1. Previously this was expected to be 20 to 30:1. The organic flow rate target was fixed for the duration of the campaign and the Zn strip feed (ZnISF) flow rate target was adjusted on multiple occasions during the campaign in response to process results. The advance O/A based on manually measured organic and ZnISF flow rates is shown in Figure 37.

Figure 36: Zinc Strip Gypsum, May 25

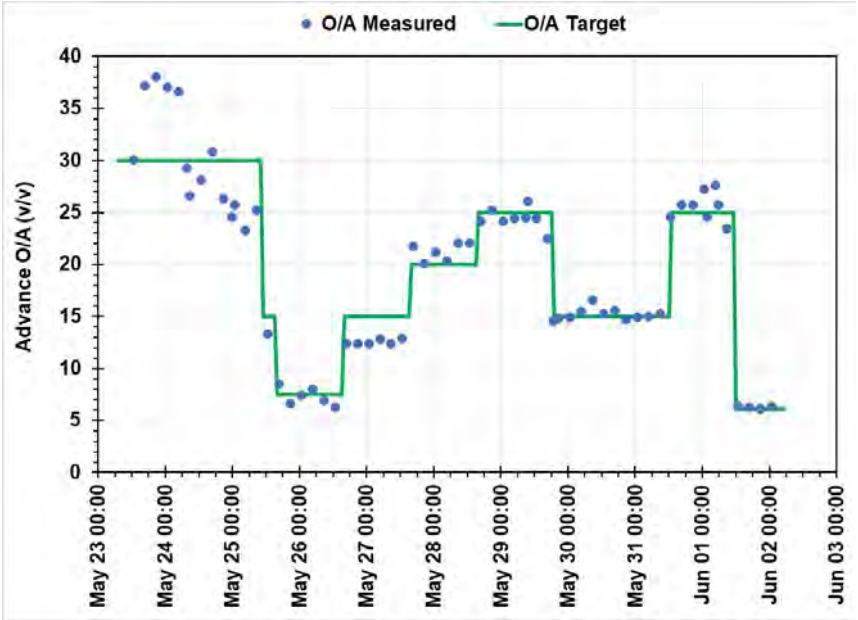

Figure 37: ISX Zn Strip Advance O/A

The design Zn stripping target was 100% stripping of Zn (and Mn). The trends for the Mn and Zn contents of ZnIS2 organic are shown in Figure 38. For much of the campaign the design target was not met.

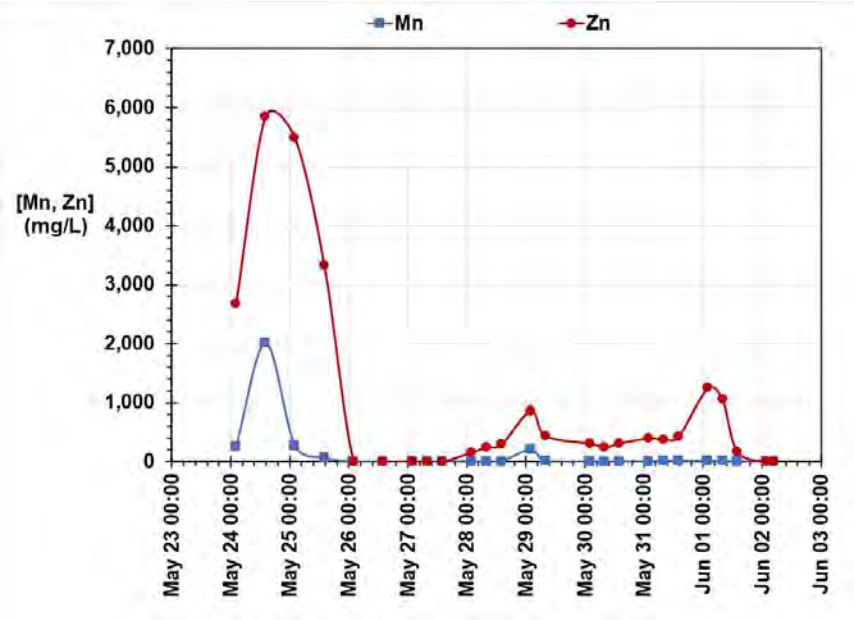

Figure 38: ISX Zn Stripped Organic Composition

A 10% bleed of the Zn-stripped organic was directed to two counter-current stages of Fe stripping (FeIS1 and FeIS2), using a 90 g/L oxalic acid strip feed solution. It is more commonplace for an Fe strip of D2EHPA® to be performed using hydrochloric acid, however the upstream Extraction Plant is sensitive to chlorides, hence the selection of oxalic acid. The key objective of Fe stripping was to strip sufficient Fe from the organic to prevent build-up in the ISX circuit.

The trend for the Fe content of the organic feed stream to Fe stripping is shown in Figure 39. The Fe content increases to 80 mg/L during the first few days of the campaign and then declines to a steady state range of 50 to 60 mg/L. This indicates that the rate of Fe stripping was equal to the Fe loading rate in extraction.

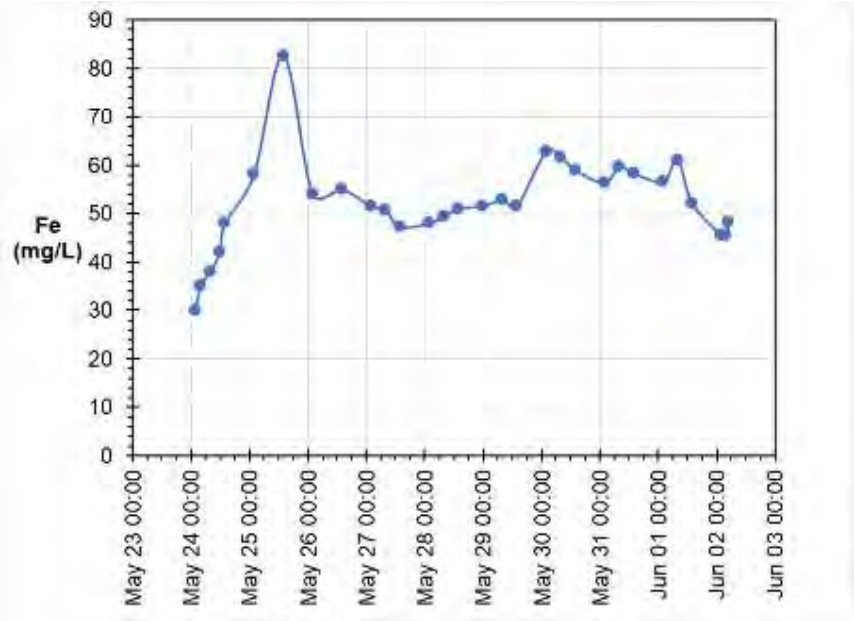

Figure 39: Fe Content of Zinc-Stripped Organic

The trends for Fe stripping efficiency and free oxalic acid in Fe strip raffinate (FeIS1R) are shown in Figure 40. A good correlation between Fe stripping efficiency and the free oxalic acid concentration is evident.

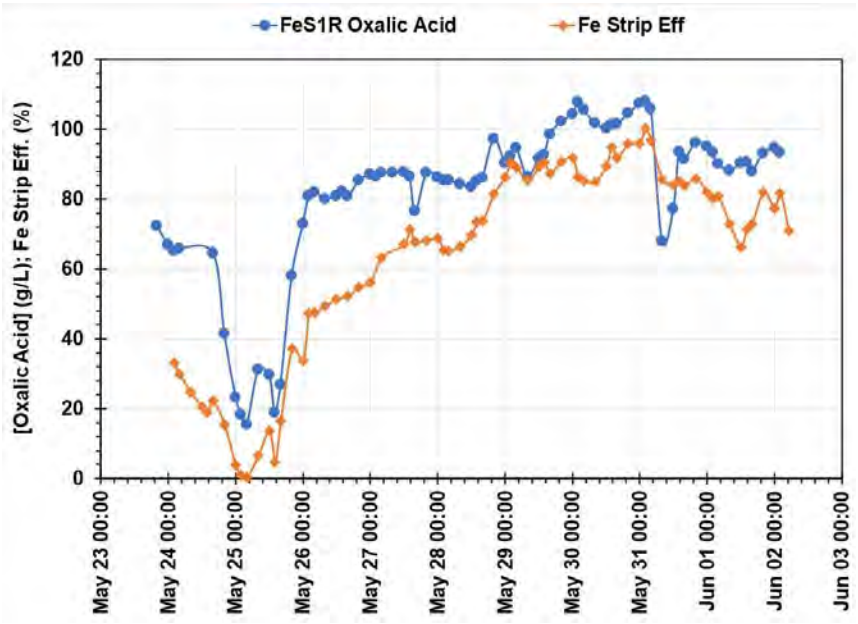

Figure 40: ISX Fe Stripping Efficiency & FeIS1R Free Oxalic Acid

The ISX continuous pilot plant experienced precipitation of mixed metal oxalate solids (Zn/Mn) in the Fe strip mixer and settler due to under-stripping of divalent metals in the Zn strip (Figure 41). Chemical analysis confirmed the solids were Zn and Mn oxalates (both insoluble) formed when the Zn-stripped organic contained slightly elevated levels of unstripped Zn and Mn.

Figure 41: Solids Removed from ISX Fe Strip Settler, May 27

It was subsequently decided to add a third Zn strip stage to the commercial flowsheet, on the Zn-stripped organic bleed stream to Fe strip, with the full Zn strip acid feed flow contacting that 10% bleed stream to ensure quantitative stripping. Two bench-scale acid strip contacts were conducted on separate samples of pilot plant Zn-stripped organic to confirm the design.

The continuous pilot plant campaign proved the technical feasibility of Fe stripping using oxalic acid. An Fe stripping efficiency of 90% could be achieved in a single stage using 90 g/L oxalic acid strip solution and an advance O/A of 10:1.

Purification (TSX and PSX) Pilot Plant Operation and Results

Feed Preparation

For TSX and PSX, a synthetic Transformation aqueous feed solution was prepared from reagent grade cobalt sulphate salt for use during start up, until Purification raffinate was available. The composition is listed in Table 2. The organic feed was a fresh solution of 40% v/v D2EHPA® in VivaSol D80, to replicate ISX stripped organic.

The available quantity of cobalt LSL from the CSX continuous pilot plant was 16 L, sufficient for ~24 hours feed to PSX. Enough synthetic cobalt LSL solution was prepared to feed Purification for the remainder of the planned eight days test duration. The synthetic feed solution composition was intended to replicate the expected CSX cobalt LSL composition arising from the maximum design concentrations of Zn, Ca, Mn, Cu and Fe in ISX raffinate (CSX feed), as shown in Table 3. The composition of both purification feed streams (synthetic and CSX cobalt LSL) are listed in Table 2. The CSX pilot plant cobalt LSL contained significantly elevated concentrations of Ni and Mg that would not be expected in the commercial purification feed stream, but which persisted due to upsets experienced during CSX pilot plant operations.

Table 2: TSX & PSX Pilot Plant Aqueous Feed Composition

Component	Concentration (mg/L)			
	Synthetic Transformation Feed	Purification Feed		
		Synthetic	CSX Co LSL	Design
Al	< 0.4	< 0.3	1.5	0
Ca	3.9	44	12	39
Co	122,000	124,308	132,667	117,499
Cu	< 0.1	37	11	0.7
Fe(III)	< 4	6.0	2.5	24
Mg	2.79	27	3,533	8
Mn	0.98	202	246	98
Na	< 3	<2	16	0
Ni	20.4	39	1,530	12
S	75,700	69,854	77,667	64,821
Zn	< 2	32	22	39

Table 3: Maximum Impurity Design Basis for Purification Feed

ISX Raffinate					Purification Feed (Co LSL)		
Co	6,000	mg/L			Co	120,000	mg/L
Zn	2.0	mg/L	Co/Zn w/w	3,000	Zn	40	mg/L
Ca	2.0	mg/L	Co/Ca w/w	3,000	Ca	40	mg/L
Mn	10.0	mg/L	Co/Mn w/w	600	Mn	200	mg/L
Cu	2.0	mg/L	Co/Cu w/w	3,000	Cu	40	mg/L
Fe	0.3	mg/L	Co/Fe w/w	20,000	Fe	6	mg/L

Piloting

In TSX organic saponification, the feed organic (TRO) was contacted with an aqueous NaOH solution to pre-neutralise the target fraction of the organic extractant (initially 50% n/n). The advance O/A was controlled to a target of 6.5:1 to achieve this. The saponification target was reduced from the design value of 50% to 40% n/n Na loading when third phase formation occurred at startup on July 12.

NaOH solution addition was split between the saponification (N) and transformation stage 1 (T1) mixers after 16:00 on July 16 to eliminate third phase formation, as follows:

- 150 g/L NaOH solution addition to the saponification mixer at 35% n/n Na loading in saponified organic (NO) (40% v/v D2EHPA® basis)
- 100 g/L NaOH solution addition to T1 mixer under pH control at setpoint 4.0.

Figure 42 shows the organic saponification advance O/A based on manually measured organic and NaOH flowrates. The advance O/A was intentionally varied to achieve process targets, either Na loading in saponified organic (NO) or operating pH in the T1 mixer.

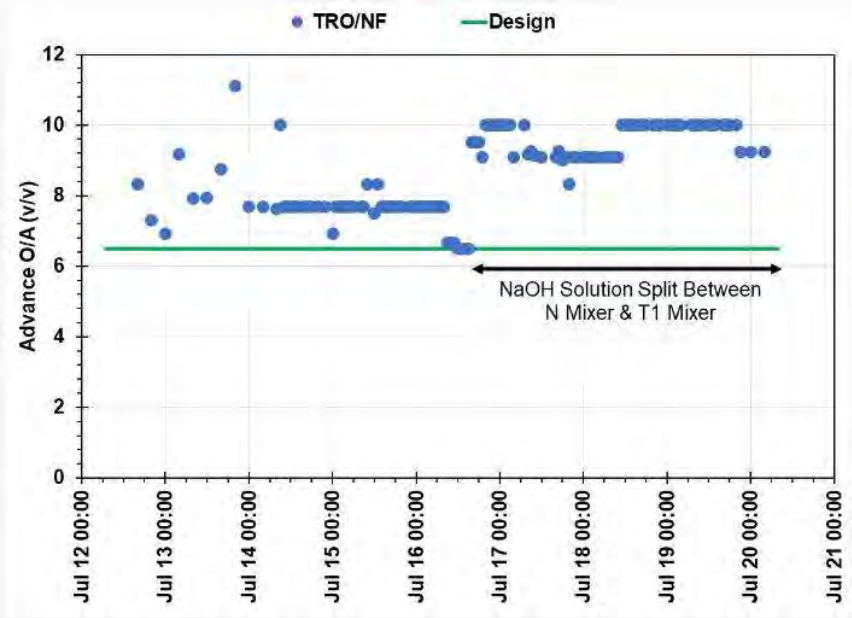

Figure 42: TSX Organic Saponification Advance O/A (40% v/v D2EHPA® Basis)

Trends for Na loading in NO and Co loading in transformation loaded organic (TLO) are shown in **Error! Reference source not found.**. The Na content of NO was under-reported during July 12 to 15 due to third phase formation. From July 16 onwards, 35% n/n Na loading was targeted in NO.

In Transformation, the feed solution (synthetic purification raffinate at 120 g/L Co) was contacted in four counter-current stages with saponified organic. The key objective was to maximise transfer of Co from the aqueous to the organic phase. The advance O/A was optimised to achieve this objective. Transformation feed was changed from the synthetic Co solution used for startup to Purification raffinate (P1R) early on July 13.

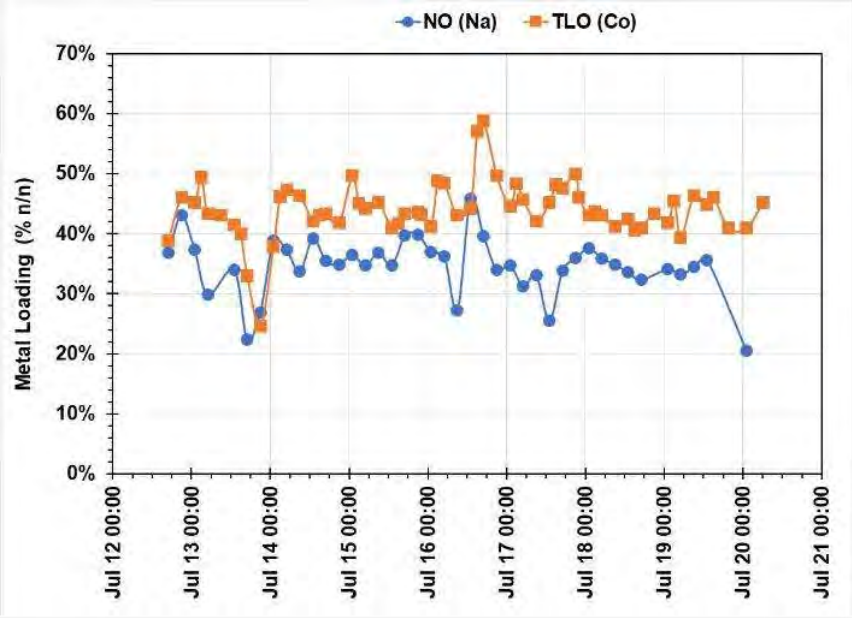

Figure 43: TSX Metals Loading in NO and TLO (40% v/v D2EHPA® Basis)

Advance O/A was used as the primary control tool in Transformation. TRO and transformation feed (TF) flow rates were varied to increase/decrease Co loading in TLO. Figure 44 shows the TSX advance O/A based on manually measured TRO and TF flow rates.

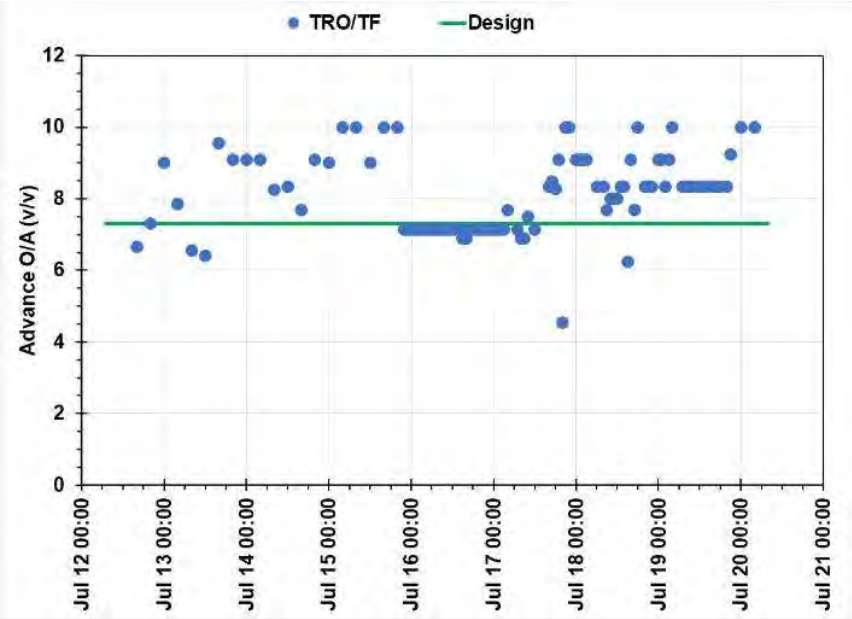

Figure 44: TSX Transformation Advance O/A

During July 15 the Co content of transformation raffinate (T1R) was near the design target of 300 mg/L and trending lower, and T1 mixer pH was between 4.0 and 4.2. These process results indicated that pH 4.0 could be a suitable setpoint for T1 mixer pH control. As discussed above, NaOH solution was added to T1 mixer under pH control (setpoint 4.0) from July 16 onwards.

Figure 45 shows the T1R Co trend. Upsets corresponding with each full profile (FP) sampling were observed, as the sample volumes of organic and aqueous abstracted from each TSX settler (~30 mL) were significant relative to the TSX feed rates (~10 mL/min organic and ~1.2 mL/min aqueous), resulting in temporary loss of interstage advance flows.

Each TSX mixer-settler was prefilled prior to startup using synthetic TF (120,000 mg/L Co). Due to the long aqueous transit time in TSX of ~ 48 hours, 72 hours of continuous operation was required to displace the prefill Co inventory through the circuit. The Co content is maintained at or below the design value of <300 mg/L from July 16 onwards.

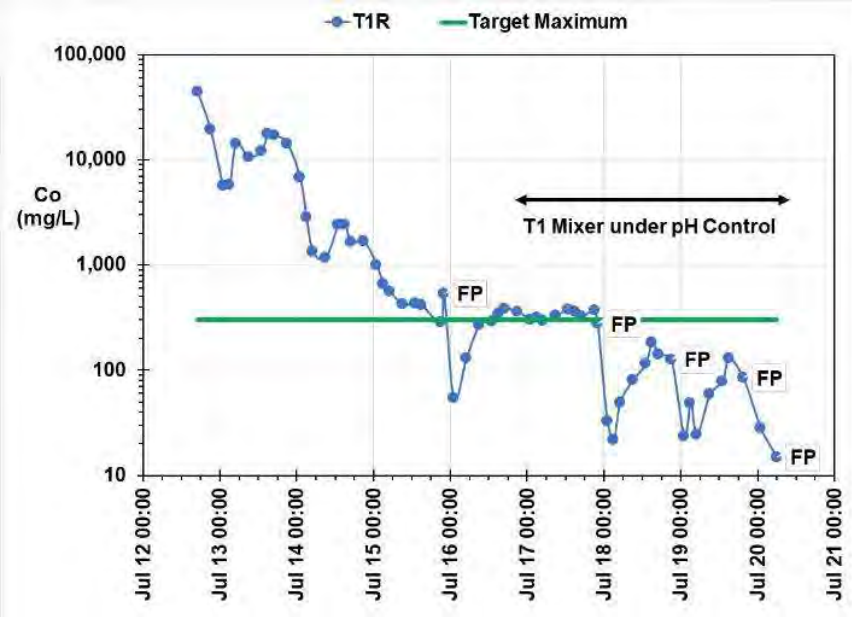

Figure 45: TSX Transformation Raffinate Cobalt Content

TLO Co loading is shown in Figure 46. The design Co loading value of 16,500 mg/L (50% n/n, 40% v/v D2EHPA® basis) was not consistently attained. Referring to the Co loading operating isotherm in Figure 47, it is apparent that the Co loading is limited to a maximum of about 14,500 mg/L when using the saponification approach with TF containing 120,000 to 140,000 mg/L Co.

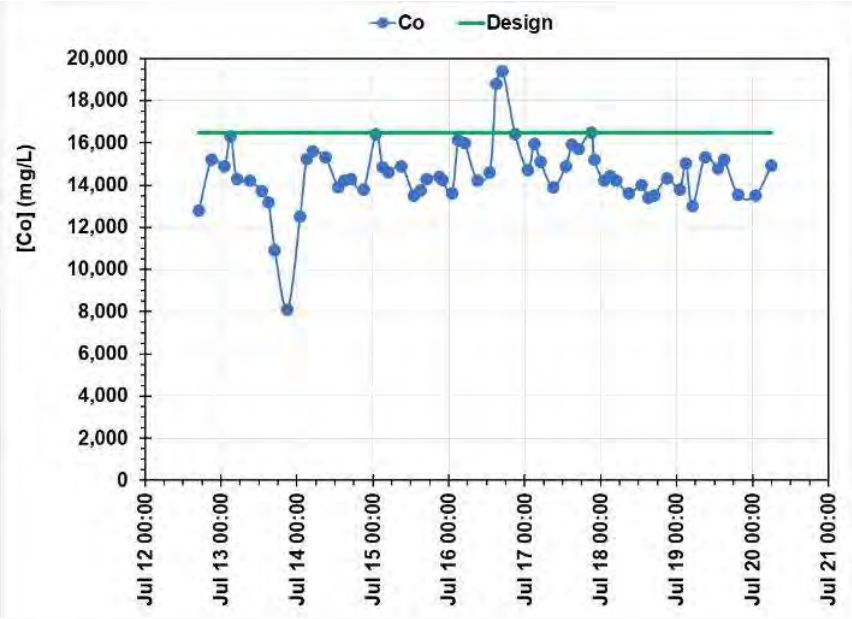

Figure 46: Co Content of TSX Transformation Loaded Organic

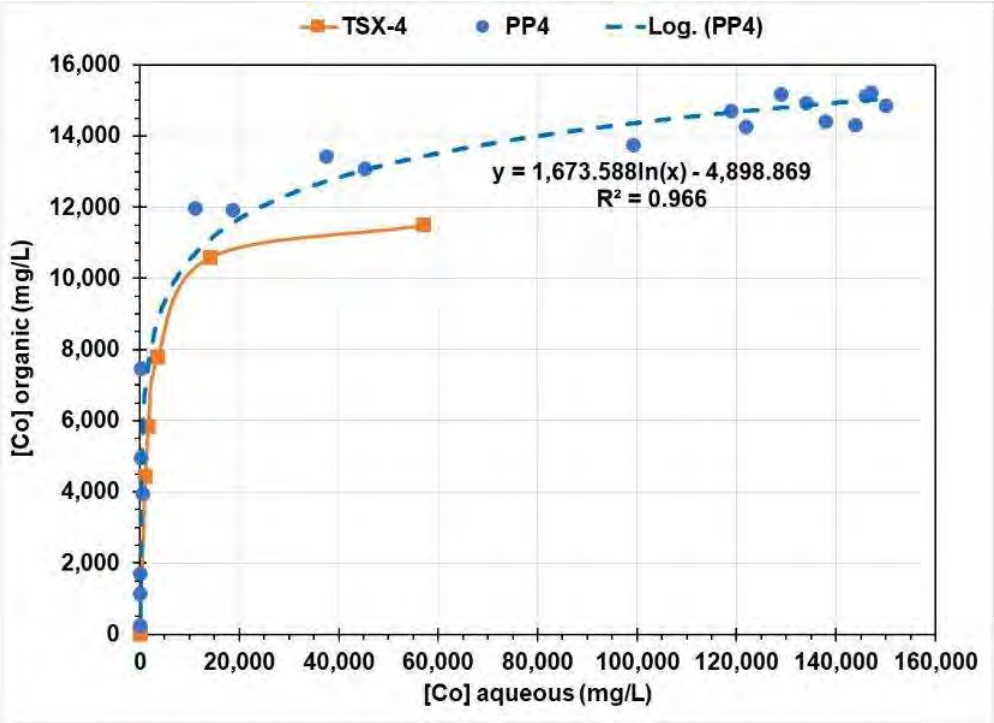

Figure 47: TSX Transformation Cobalt Loading Operating Isotherm

In Purification, the feed solution is contacted with Co pre-loaded organic in eight counter-current stages. The key objective was to maximise the transfer of Fe, Al, Zn, Ca, Mn and Cu impurities from the aqueous to the organic phase. The advance O/A was optimised to achieve this objective.

Synthetic feed solution was used for most of the campaign. CSX cobalt LSL was added over a 24-hour period, followed by a final 9-hour period, again using the synthetic feed solution, during which the aqueous inventory in the eight PSX mixer-settlers corresponding to CSX cobalt LSL was displaced.

The results of the bench-scale purification isotherm tests indicated that Cu extraction was the limiting criterion. The McCabe-Thiele diagram showed that Cu could be reduced from 40 mg/L to 2.2 mg/L with 8 stages using an advance O/A of 0.8:1. The PSX pilot plant was intentionally started with an advance O/A target of 1:1, to be conservative. Once process results confirmed the Purification stage was working well, the advance O/A target was reduced from 1:1 to 0.8:1 on July 16. Most Cu assays were below the lower reporting limit during the operating period at 1:1 PSX advance O/A target, however Cu in purification raffinate (P1R) was greater than the product maximum limit for about 36 hours during the operating period at 0.8:1 PSX advance O/A target.

It was subsequently established that the advance O/A calculated using the measured TRO feed rate to Saponification was misleading. In a typical 24-hour period, there were 21 organic samples withdrawn from the circuit between Saponification and P8, which effectively decreased the PSX advance O/A. In comparison only three samples of PF solution were collected each 24 hours. The ratio of the Cu contents of purification feed (PF) and purification loaded organic (P8O) were compared. The average Cu content of the synthetic PF solution was 37 mg/L so at an advance O/A of 1:1 and <1 mg/L Cu in P1R the expected Cu content of P8O would be expected to be close to 37 mg/L. However the P8O Cu trend showed a gradual increase to >50 mg/L Cu. The PSX effective O/A (calculated from the PSX Cu metallurgical balance) averaged 0.77:1 during the latter 48-hour period when the PSX O/A target was 1:1, and averaged 0.66:1 in the following 48-hour period when the PSX O/A target was 0.8:1.

This explains why the Cu impurity concentration was above the P1R product maximum limit. The PSX advance O/A was effectively ~0.8:1 during the period when the PSX advance O/A target was 1:1, and the PSX O/A was effectively <0.7:1 during the period when the PSX advance O/A target was 0.8:1. It has therefore been concluded that Cu Purification was successfully achieved at the design PSX O/A of 0.8:1 (Figure 48).

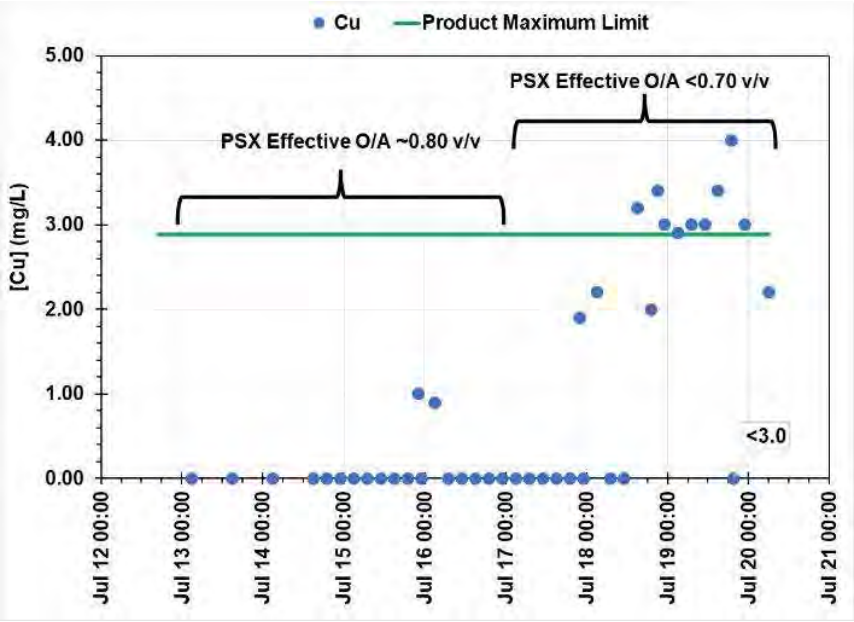

Figure 48: PSX Purification Raffinate Cu Content

Other impurities such as Mn and Ca were reduced to well below the target values for the duration of the Purification pilot campaign (Figure 49 and Figure 50). Na Purification was successful, with all P1R assay results below the product maximum limit. The majority of Zn, Fe and Al assays (for P1R progress samples) were below the reporting limits for those elements, demonstrating successful Zn, Fe and Al Purification.

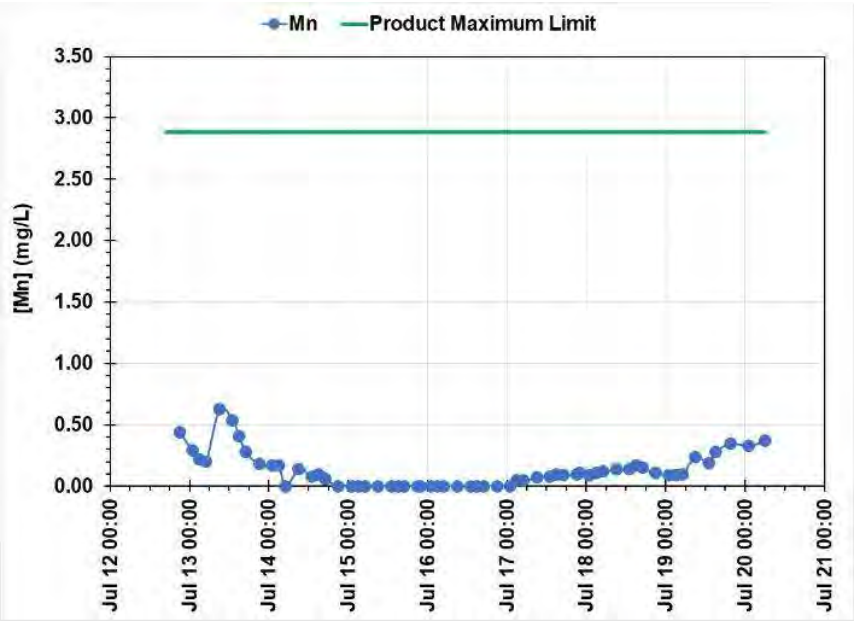

Figure 49: PSX Purification Raffinate Mn Content

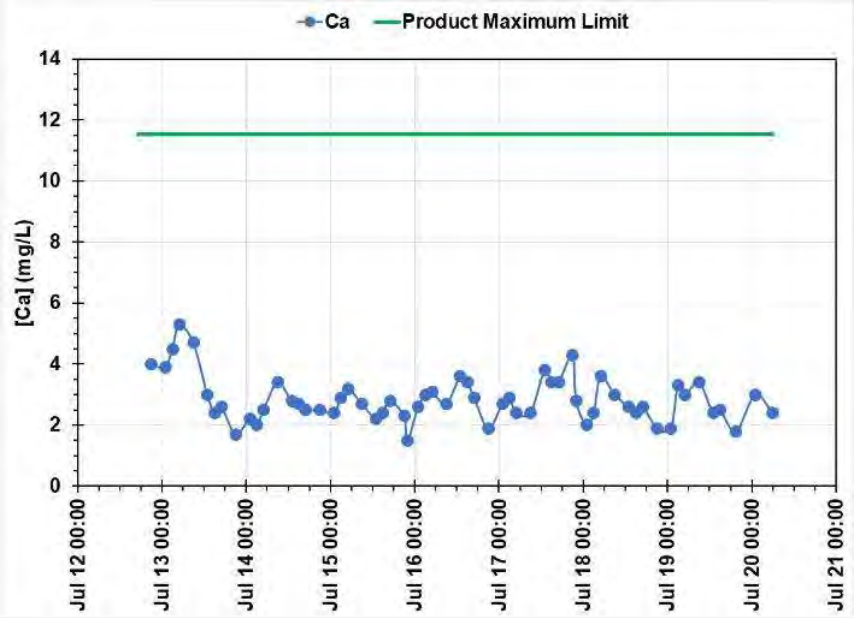

Figure 50: PSX Purification Raffinate Ca Content

The composition of each Purification raffinate pail (purified Co LSL) is shown in Table 4. Pails 1 to 5 are produced from synthetic PF and Pail 6 is produced from CSX cobalt LSL. The maximum limits shown in Table 4 are derived from QPM's maximum impurity specification for the cobalt sulfate heptahydrate product. Ni and Mg are not able to be separated from the feed solution by PSX, and the P1R results that are above the product maximum limits for those elements arise from operational issues during the preceding CSX continuous pilot plant.

Table 4: Composition of PSX Purification Raffinate Pails

Pail #	1	2	3	4	5	6	Product Maximum Limit
Component (mg/L)	Jul 14 16:13	Jul 15 20:12	Jul 17 05:05	Jul 18 07:09	Jul 19 07:57	Jul 20 06:28	
Al	< 0.2	< 0.2	< 0.2	< 0.2	< 0.2	< 0.2	2.9
Ca	3.8	< 0.9	< 0.9	1.6	2.2	< 0.9	11.4
Co	129,000	133,000	138,000	133,000	129,000	132,000	119,077
Cu	< 2	< 2	< 1	< 2	2.6	2.6	2.9
Fe	< 0.3	< 0.4	< 0.6	< 0.4	1.4	1.3	2.9
Mg	9.6	9.5	9.1	9.9	10.2	1 580	11.4
Mn	0.21	< 0.04	< 0.04	0.08	< 0.20	0.21	2.9
Na	< 2	< 2	< 2	2	< 5	20	57
Ni	16	18	18	18	18	857	229
Zn	< 2	< 2	< 2	< 2	< 2	< 2	2.9

As it was operated separately from the ISX pilot plant, the TSX/PSX pilot plant also included a stripping stage so that the organic could be recirculated. In the commercial plant the organic returns to the ISX Loaded Organic Tank for treatment in the ISX scrubbing and stripping circuits.

CONCLUSIONS

The ISX pilot plant outcomes validated many aspects of the design and identified opportunities for improvements to the process design criteria in several facets of the circuit. Key findings included the following:

- Confirmed four extraction and four scrubbing stages.
- Confirmed that only a single manganese stripping stage is required (reduction from four stages previously).
- Gypsum precipitation can be isolated to the manganese stripping area by pH control in scrubbing and management of the acidity in manganese and zinc stripping.
- Target raffinate quality was achieved for extended periods of time, producing a raffinate (CSX feed) with <10 mg/L Mn and <2 mg/L of Zn, Ca and Cu.
- Reduction of magnesium was achieved, effectively increasing the Co:Mg ratio in raffinate compared to feed, positively impacting downstream CSX operation.
- The preliminary commercial plant design included separate organic feed streams from the ISX Zn-stripped organic tank to Fe stripping and TSX. It is now proposed to configure Fe strip and TSX in series so that the feed organic to TSX is Fe-stripped organic with a very low Fe content.
- A sulfuric acid strip of the organic bleed to Fe Strip has been added ahead of Fe Strip. This would be effectively a third zinc stripping stage, utilising the total incoming Zn Strip acid feed flow to quantitatively strip any residual Zn and Mn from the small organic bleed flow advancing to Fe Strip, to prevent metal oxalate precipitation.
- The number of Fe stripping stages has been increased to two in series. This is expected to provide 99% Fe stripping efficiency and improved oxalic acid reagent efficiency.

The updated ISX schematic for the commercial plant is shown in Figure 51.

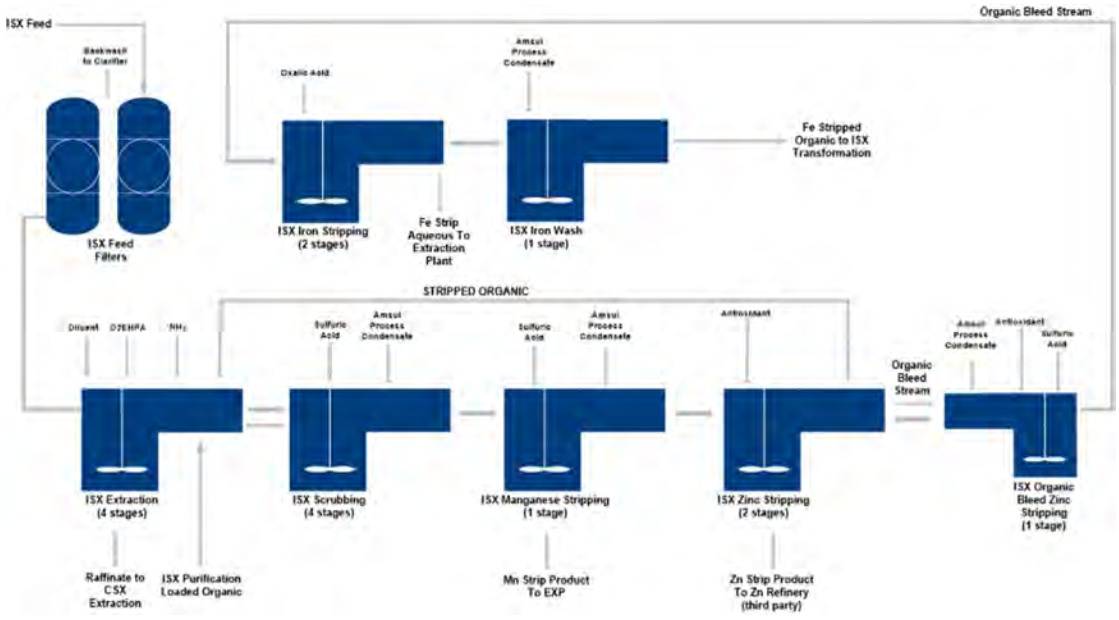

Figure 51: Schematic of the Proposed Commercial ISX Circuit after Piloting

The Purification pilot plant was successful in confirming design values for achieving a purified cobalt LSL feed to crystallisation in the commercial plant, and flagged improvements to the process design criteria in several facets of the circuit. Key findings included the following:

- Purification substantially reduces the impurity content of the cobalt LSL feed to crystallisation. The Cobalt LSL Co:Mn ratio was improved from 540:1 to 600,000:1. the Co:Zn ratio from 6,000:1 to >66,000:1, and the Co:Cu ratio from 12,000:1 to >50,000:1.

- Maximum Ca and Fe in PSX raffinate (Cobalt LSL feed to crystallisation) were determined to be 10 mg/L and 1.5 mg/L respectively.
- Confirmed 4 transformation and 8 purification stages.
- The organic loading in saponification was revised from 45-50% n/n Na loading to 35% n/n.
- The maximum achievable Co loading is about 13.5 g/L (41% n/n) using the saponification approach and 120 g/L Co in Transformation feed. This is equivalent to an advance O/A of ~9:1.
- Control to pH 4.0 using 100 g/L NaOH is required on the last stage of transformation. An equilibrium pH value of approximately 4.0 is required to achieve the raffinate target of <300 mg/L Co.
- The organic stoichiometric load in TSX is increased from 20% n/n to 40% n/n (max 45%).
- The equilibrium pH in P8 is revised from 3.5 to 2.0-2.4.

Overall, the ISX and Purification pilot plant achieved their objectives.

ACKNOWLEDGMENTS

The author would like to express thanks to John Fittock for his invaluable contributions to the planning and operation of the pilot plants and interpretation of the data, and the management of Queensland Pacific Metals for permission to prepare and present this paper. The author acknowledges the contributions of the SGS Canada pilot plant team.

The views of the author do not necessarily represent those of Queensland Pacific Metals.

REFERENCES

1. Arpalahti, A. (2023). “2023 Update on The Terrafame Nickel Operation”. Proceedings of the ALTA Nickel-Cobalt-Copper Conference, Perth, Australia, May 1-3, 2023.

SELECTIVE CO-EXTRACTION OF Ni&Co FROM HIGH Ca/Mg SOLUTIONS

By

[1,2] Guiqing Zhang, [1,2] Qinggang Li, [1,2] Zuoying Cao, [1,2] Mingyu Wang, [1,2] Wenjuan Guan, [1,2] Xinsheng Wu, [1,2] Shengxi Wu,

[1]School of Metallurgy and Environment, Central South University, China
[2]Laboratory of Metallurgical Separation Science and Engineering, Central South University, China

Presenter and Corresponding Author

Shengxi Wu
csuwushengxi@126.com

ABSTRACT

Ni&Co extraction and purification is a critical operation for the preparation of high purity Ni&Co salts from various raw materials, especially in the NCM battery industry. However, due to the insufficient separation coefficient of industrial classic extractants, traditional Ni(Co) recovery and separation process has to go through operations of impurities removal extraction (Ca, Mg, Cu, Zn, Fe, Al, etc.) with D2EHPA, Co extraction with HEHEHP, Mg extraction with Cyanex 272, Ni extraction with HEHEHP in the case of spent LIBs, suffering issues of process redundancy, large reagent consumption and high cost. Even worse, loaded organic phase in procedures of Co extraction, Mg extraction require more than 8-stage acid scrubbing and produces considerable $MgSO_4$ wastewater containing small amount of Ni(Co). In current industry, most plants adopt Na_2S precipitation method to remove and solidified Ni(Co) into sulfides which releases toxic H_2S gas and generates Ni(Co)-Mg sulphide solid waste. Then, preferential extraction of Ni(Co) from Ca(Mg) concentrated solutions would be an ideal solution for these issues, based on what a synergistic extraction organic solvent consisted of acid and esters (HBL-116) was proposed. In single stage tests, high separation coefficient of $\beta_{Ni/Mg}$>500 was obtained under optimal conditions, moreover, excellent separation performance was also achieved in industrial application. For example, selectively and completely extracted 1.0~5.0g/L Ni(Co) from 40~60g/L Mg contained scrubbing solution was achieved by HBL-116 extraction production line in Guangdong Fangyuan New Materials Group Co., Ltd., leaving <1mg/L Ni(Co) in raffinate and produced 35~50g/L Ni(Co) stripping solution with Mg<0.1g/L. In addition, the acid and alkali consumption is about 105~110% of stoichiometric ratio for Ni(Co) cation exchange depends on the concentration of Ni(Co) in feed solutions. According to the feedback from applied plants that HBL-116 shown excellent separation performance for Ni(Co) to Mg.

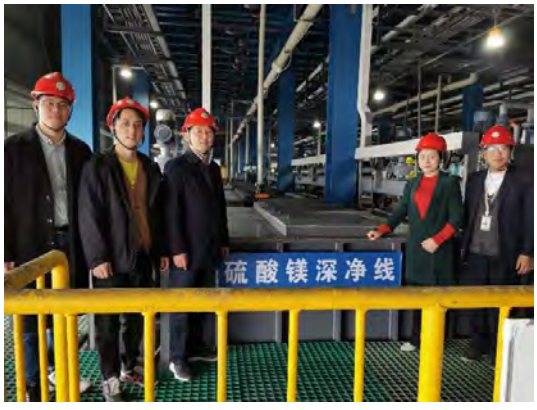

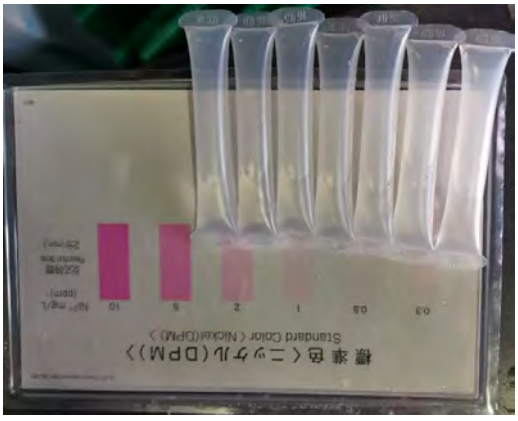

Keywords: Nickel, cobalt, Co-extraction, separation, magnesium, calcium.

Selective co-extraction of Ni&Co from high Ca/Mg solutions

Associate Prof./Dr. Shengxi Wu

E-mail: shengxiwu@hydrometaltech.com/csuwushengxi@126.com

Key Laboratory of Metallurgical Separation Science and Engineering, Chinese Non-Ferrous Industry Association, Institute of Rare Metal Metallurgy research, School of Metallurgy and Environment， Central South University

Self introduction of Shengxi Wu/ Dr. Wu or Shengxi

Shengxi Wu, born in February 1991, from Fujian China, Ph. D. in engineering, now as a associate professor in Central South University (personal page: https://faculty.csu.edu.cn/wushengxi/zh_CN/index.htm)

In the past about four years, published 41 papers, 20 patents and built up 12 leaching and extraction production lines and finished 10 pilot scale line tests (treating >500L solution per day)

Selective co-extraction of Ni&Co from high Ca/Mg solutions

1. Research Background

2. Technological solution for Ni&Co co-extraction

3. Experimental and industrial progress

4. Summary of Ni&Co co-extraction technology

1. Research Background

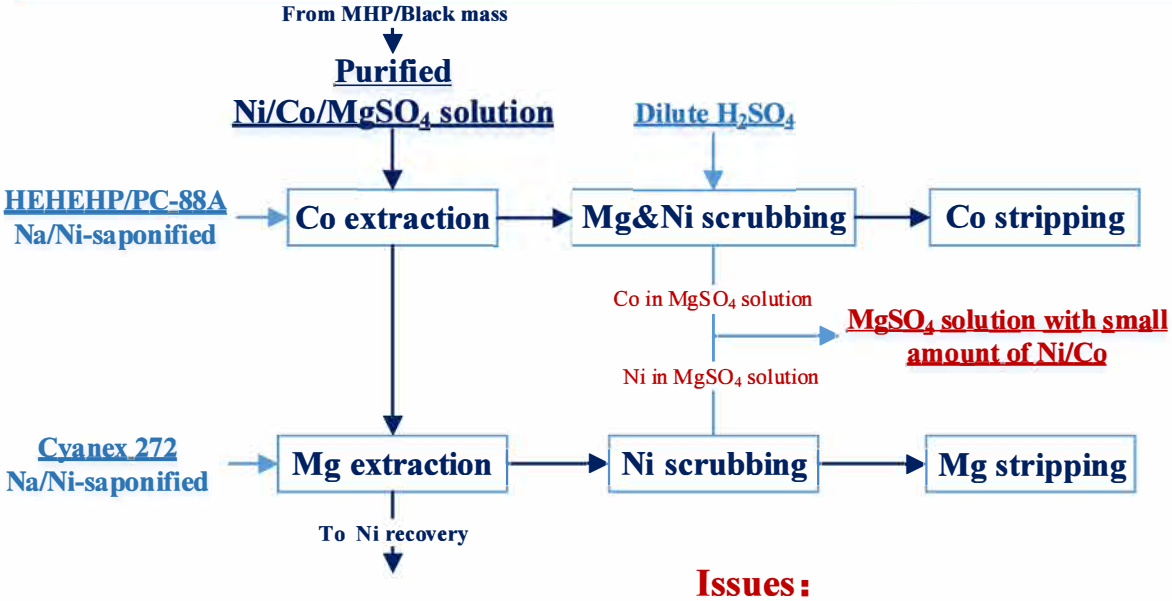

Issues:

- Difficult in Ni/Co separation from massive Mg; High cost of sulfide precipitation, [Ni] unable to 1mg/L, Toxic gas emission; Extra pressure oxidation leaching is needed;

plus: Basic conceptions and principles in solvent extraction

Reagent Cost Structure for metal recovery from spent LIBs

- **Alkali for saponification;**
- **Acid for stripping and scrubbing**
- **CaO/Na_2S for trace heavy metal and As/P/F precipitation in wastewater**
- **NaOH for pH adjusting (neutralization)**

Seponification: $2NaOH+2\overline{(HL)_2} \leftrightarrow \overline{Na(L{\cdot}HL)_2} + H_2O$

Extraction: $Me^{2+} +2\overline{Na(L.HL)_2} \leftrightarrow \overline{Me(L{\cdot}HL)_2} + 2Na^{+}$

Scrubbing: $\overline{Me(L{\cdot}HL)_2} + 2H^{+} \leftrightarrow Me^{2+} +2\overline{(HL)_2}$

Stripping: $\overline{Me(L{\cdot}HL)_2} + 2H^{+} \leftrightarrow Me^{2+} +2\overline{(HL)_2}$

Principle 1st: Extracting small amount of elements from huge body element is economic

1. Extraction basis for Ni/Co from high Ca/Mg concentration solutions

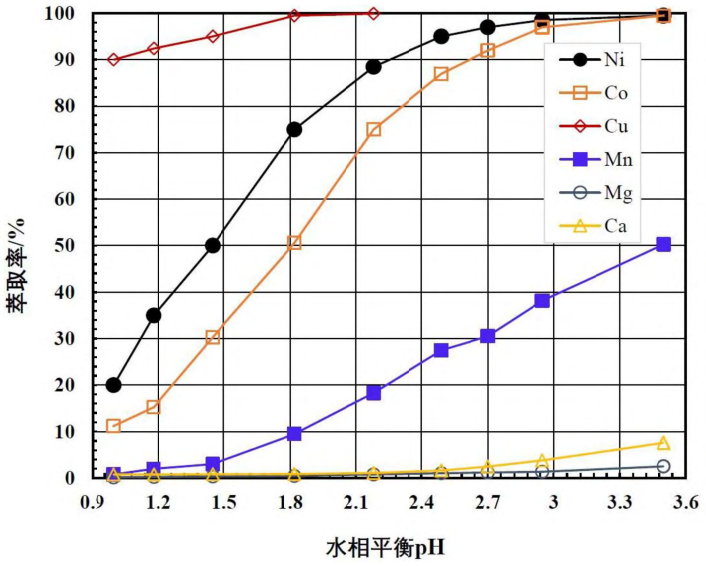

Effect of pH on extraction efficiency of metal caions

20% HBL116； Feed（g/L）： 1.71 Ni^{2+}, 0.12 Co^{2+}, 15.7 Mg^{2+}, 0.11 Ca^{2+}, A/O 1:1； 30°C

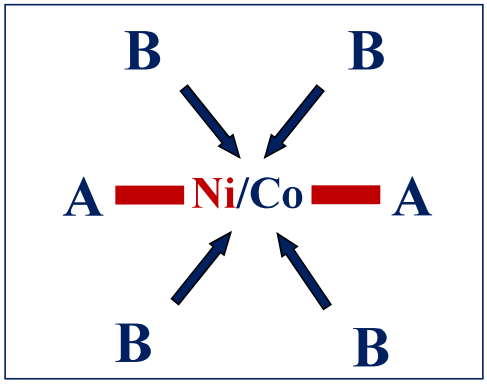

A: Cation exchanger; B: Steric hindrance provider

Ni and Co can be selectively extracted by HBL-116 (HT-059) from high Ca/Mg concentration solutions

1. Extraction basis for Ni/Co from high Ca/Mg concentration solutions

1.1 batch extraction experiments

Five-stage countcurrent extraction of Ni/Co from high Ca/Mg concentration solutions

Elements	Co	Ni	Mg	Ca
Feed（g/L）	0.115	1.68	15.7	0.112
Raffinate（g/L）	0.0009	0.0038	16.1	0.127
Loaded organic（g/L）	0.141	4.36	0.0364	0.0041
Extraction efficiency（%）	99.8	99.8	0.093	1.47

Stripping efficiency of Ni/Co from loaded organic by 0.75mol H_2SO_4 via 5 stages

Elements	Co	Ni	Mg	Ca
Scrubbed organic（g/L）	0.140	4.35	0.0067	0.0011
Stripping solutions（g/L）	1.41	42.2	0.0801	0.0203
Regenerated organic（g/L）	0.0001	0.0131	---	---
Stripping efficiency（%）	99.5	99.9		
Impurity removal efficiency（%）	---	---	99.97	99.26

Organic： 20% HBL116 + 80% diluent；Feed（g/L）：0.115 Co^{2+}，1.68 Ni^{2+}，15.7 Mg^{2+}，0.112 Ca^{2+}，O/A =1:2.5；
30°C；saponification ratio：50%；stripping O/A 10:1

1. Extraction basis for Ni/Co from high Ca/Mg concentration solutions

Five-stage countcurrent extraction of Ni/Co from high Ca/Mg concentration solutions

Rows	Co in raffinate (g/L)	Ni in raffinate (g/L)	Mg in raffinate (g/L)	Equibrium pH
1	1.723	0.903	13.17	3.48
2	0.007	0.003	13.10	4.43
3	0.005	0.001	13.12	4.33
4	0.0008	0.0005	13.15	4.32
5	ND	ND	13.11	4.36
6	ND	ND	13.15	4.29
7	0.0009	0.0004	13.18	4.31
8	0.0012	0.0006	13.35	4.28
9	0.0014	0.0008	13.40	4.23
10	ND	0.0005	13.19	4.26
11	0.0011	0.001	13.12	4.31
12	0.001	0.0004	13.15	4.35
13	0.0009	0.0008	13.11	4.32

E_{Ni}>99.99%， E_{Co}>99.99%

Feed：Co 8.50 g/L；Ni 9.70 g/L；Mg 14.2 g/L；pH 5.0
20%（v/v）HBL116 , O/A=2.8:1，225 rpm，t=10 min，T=25°C

1. Extraction basis for Ni/Co from high Ca/Mg concentration solutions

Phase segregation performance

Photos of phase segregation row 13 (50s after stop mixing), stage 1st to stage 5th, excellent phase segregation excellent

2. Pilot test and industrial application of Ni/Co extraction from high Ca/Mg solutions

2.1 Guangdong Fangyuan New Material Group Co., LTD

廣東芳源新材料集團股份有限公司
Guangdong Fangyuan New Materials Group Co., Ltd.

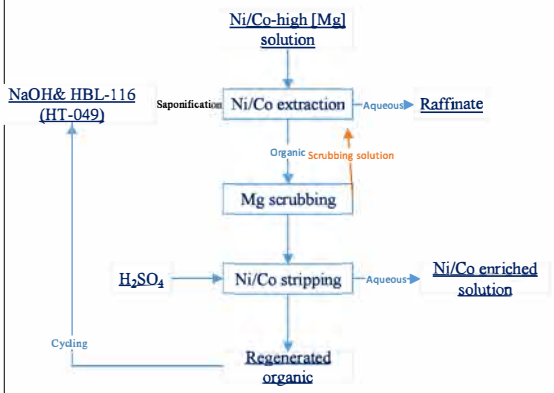

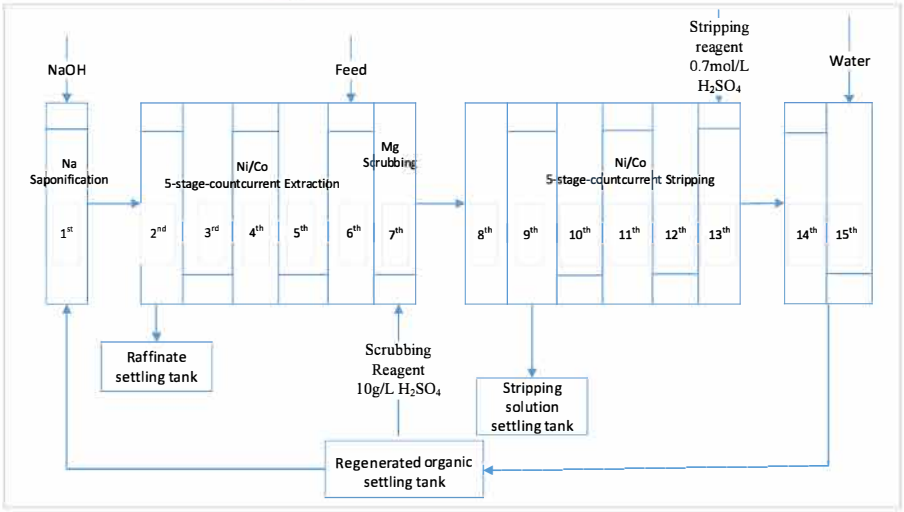

Production Lines: Selectively extraction of Ni/Co from $MgSO_4$ solutions by HBL-116(HT-059). (launched in June 2020)

2. Pilot test and industrial application of Ni/Co extraction from high Ca/Mg solutions

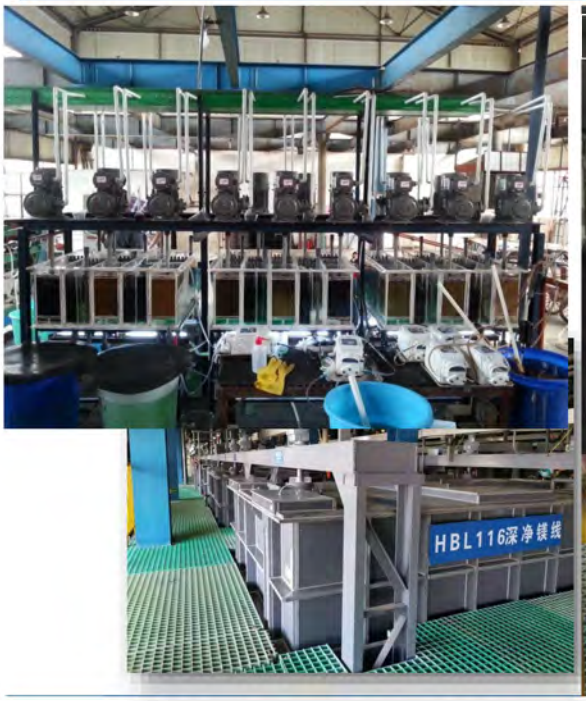

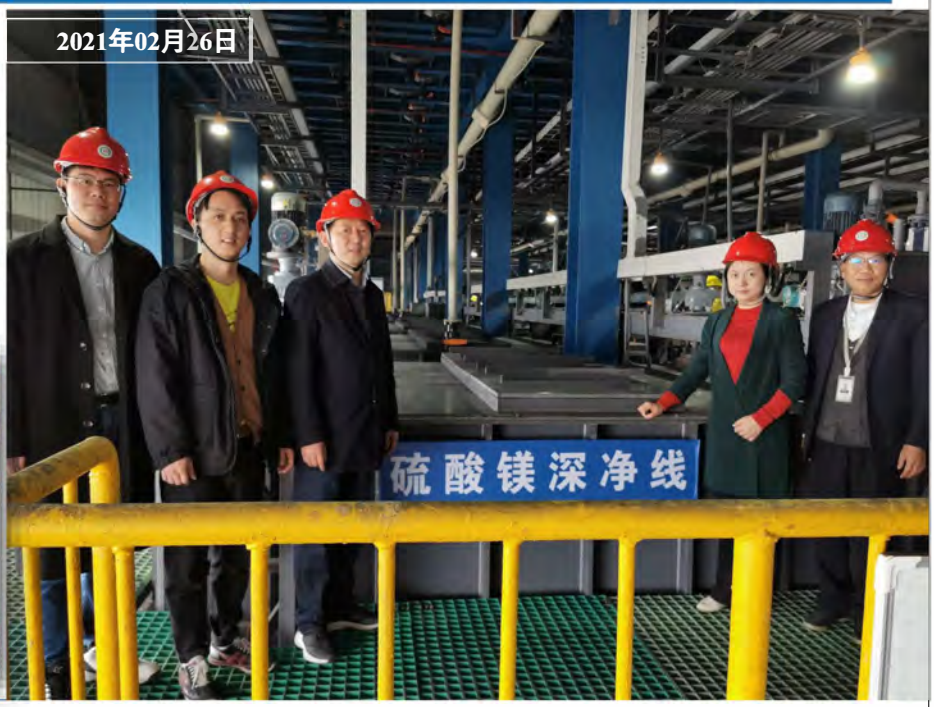

Pilot test & Production Lines: Selectively extraction of Ni/Co from $MgSO_4$ solutions by HBL-116(HT-059).
Feed solution treating Scale: 400m³/day（launched in June 2020 ）

2. Pilot test and industrial application of Ni/Co extraction from high Ca/Mg solutions

2.2 Continuous Running Data

表 3 HB116 镁水深净线皂化-萃取-萃洗-反萃-反洗连续稳定运行试验结果

时间	萃取			萃洗		反萃		反洗		皂化		萃余液				反萃液					
												Ni		Co		Ni		Co		Mg	
	有机 L/h	水相 L/h	萃余 pH	流量 L/h	出口 pH	流量 L/h	反萃 pH	流量 L/h	出口 pH	皂化率/%	碱量 L/h	mg/L	萃取率/%	mg/L	萃取率/%	g/L	反萃率/%	g/L	反萃率/%	g/L	除去率
01-09:00	3600	2800	6.76	150	5.15	750	1.1	530	1.55	70	63	未测出	99.99	0.8	99.94	3.81	99.95	11.55	99.99	0.023	>99.99%
01-11:00	3600	2800	6.64	150	5.2	800	0.93	560	1.77	70	63	未测出	99.99	0.1	99.99	3.98	99.97	10.33	99.99	0.014	>99.99%
01-13:00	3300	3300	6.98	150	5.47	800	0.93	560	1.82	73	60	0.4	99.99	0.3	99.97	3.12	99.98	10.15	99.99	0.007	>99.99%
02-09:10	3500	3500	7.55	150	5.68	800	0.99	560	1.92	71	62	0.07	99.97	0.8	99.94	3.19	99.97	10.76	99.95	0.010	>99.99%
02-11:00	3500	3500	6.98	150	5.61	800	1.01	560	1.91	70	65	未测出	>99.99	未测出	99.99	2.8	99.52	9.26	99.96	0.008	>99.99%
02-13:00	3700	3500	6.74	150	5.66	800	1.01	560	1.81	70	65	未测出	>99.99	未测出	99.99	4.14	99.52	11.88	99.96	0.012	>99.99%
03-09:00	3900	3500	6.29	150	5.22	800	0.96	560	2.13	70	68	0.06	99.98	0.27	99.98	4.29	99.89	14.5	99.97	0.012	>99.99%
03-11:00	3900	3500	6.27	150	5.25	800	1.02	560	1.97	70	68	0.74	99.72	0.19	99.99	3.84	99.87	15.74	99.97	0.013	>99.99%
03-13:00	3900	3500	6.57	150	5.49	800	1.17	560	2.09	70	68	0.42	99.85	0.13	99.99	3.24	99.86	15.19	99.97	0.006	>99.99%
04-09:00	3900	3500	6.31	150	4.85	750	1	530	2.02	70	68	0.43	99.84	0.35	99.97	4.29	99.86	14.5	99.97	0.012	>99.99%
04-11:00	4200	3500	6.27	150	4.9	750	1	530	1.82	70	73	0.74	99.03	0.19	99.88	3.84	99.87	15.74	99.97	0.013	>99.99%

The content of Ni/Co in raffinate was kept less than 1mg/L after 4 days of test running

2. Pilot test and industrial application of Ni/Co extraction from high Ca/Mg solutions

2.2 Continuous Running Data

时间	萃取			萃洗		反萃		反洗		皂化		萃余液				反萃液					
												Ni		Co		Ni		Co		Mg	
	有机 L/h	水相 L/h	萃余 pH	流量 L/h	出口 pH	流量 L/h	反萃 pH	流量 L/h	出口 pH	皂化率/%	碱量 L/h	mg/L	萃取率/%	mg/L	萃取率/%	g/L	反萃率/%	g/L	反萃率/%	g/L	除去率
25-09:00	6500	2000	5.05	130	368	900	1.24	630	1.89	70	113	未测出	100	0.48	99.89	25.1	99.95	7.56	99.83	0.008	>99.59%
25-13:00	6200	2200	5.31	130	384	950	1.12	660	1.76	70	105	0.68	99.85	0.58	99.87	23.77	99.96	7.77	99.89	0.005	>99.59%
26-17:00	5600	2200	5.53	130	377	920	0.73	660	1.75	70	98	未测出	100	未测出	99.99	17.8	99.97	5.34	99.92	0.015	>99.59%
26-19:00	5300	2200	5.46	120	398	900	0.7:	630	1.82	70	92	未测出	100	未测出	99.99	17.78	99.97	6.23	99.92	0.015	>99.59%
26-21:00	4700	2200	5.21	130	397	870	0.6:	609	1.79	70	81	0.79	99.88	0.26	99.97	15.37	99.97	4.86	99.92	0.012	>99.59%
27-09:00	4700	2500	7.78	150	427	810	0.7:	560	1.91	70	81	0.26	99.99	0.35	99.95	20.99	99.97	6.15	99.92	0.009	>99.59%
27-11:00	4700	2700	5.86	150	444	810	0.82	560	1.89	70	81	0.28	99.99	0.36	99.95	21.53	99.96	7.98	99.92	0.02	>99.59%
28-13:00	4700	3000	-	170	415	810	1.0:	560	1.81	70	81	0.88	99.86	0.31	99.98	23.91	99.96	10.79	99.92	0.012	>99.59%
30-09:00	4800	2500	5.97	170	421	810	0.88	810	1.83	70	83	未测出	100	0.73	99.96	16.9	99.95	10.89	99.92	0.014	>99.59%
30-11:00	5100	2700	5.46	170	433	780	0.73	780	1.76	69	88	未测出	100	0.59	99.96	15.39	99.95	10.71	99.94	0.005	>99.59%
30-13:00	5100	2700	5.43	170	431	750	0.72	750	1.7	69	88	未测出	100	未测出	99.99	16.61	99.95	12.56	99.94	0.016	>99.59%
平均	4671	2935	6.09	177	434	774	0.98	556	1.80	69	81	0.40	100	0.49	99.96	12.89	99.92	14.36	99.94	0.081	>99.59%

The content of Ni/Co in raffinate was still kept less than 1mg/L after 45 days of production running

2. Pilot test and industrial application of Ni/Co extraction from high Ca/Mg solutions

2.2 Continuous Running Data

Elements	Ni	Co	Mg
Feed（g/L）	0.1~3	1~5	25~60
Stripping（g/L）	1~4.5	10~15	1.07
Raffinate（mg/L）	<1	<1	>32
Extraction efficiency/%	99.9	99.9	---
Mg removal efficiency/%	---	---	99.7

Oil content in raffinate：8.14-16.06ppm，COD：59.43-96.68ppm

Oil content in stripping：4.19-10.97ppm，COD：28.04-40.67ppm

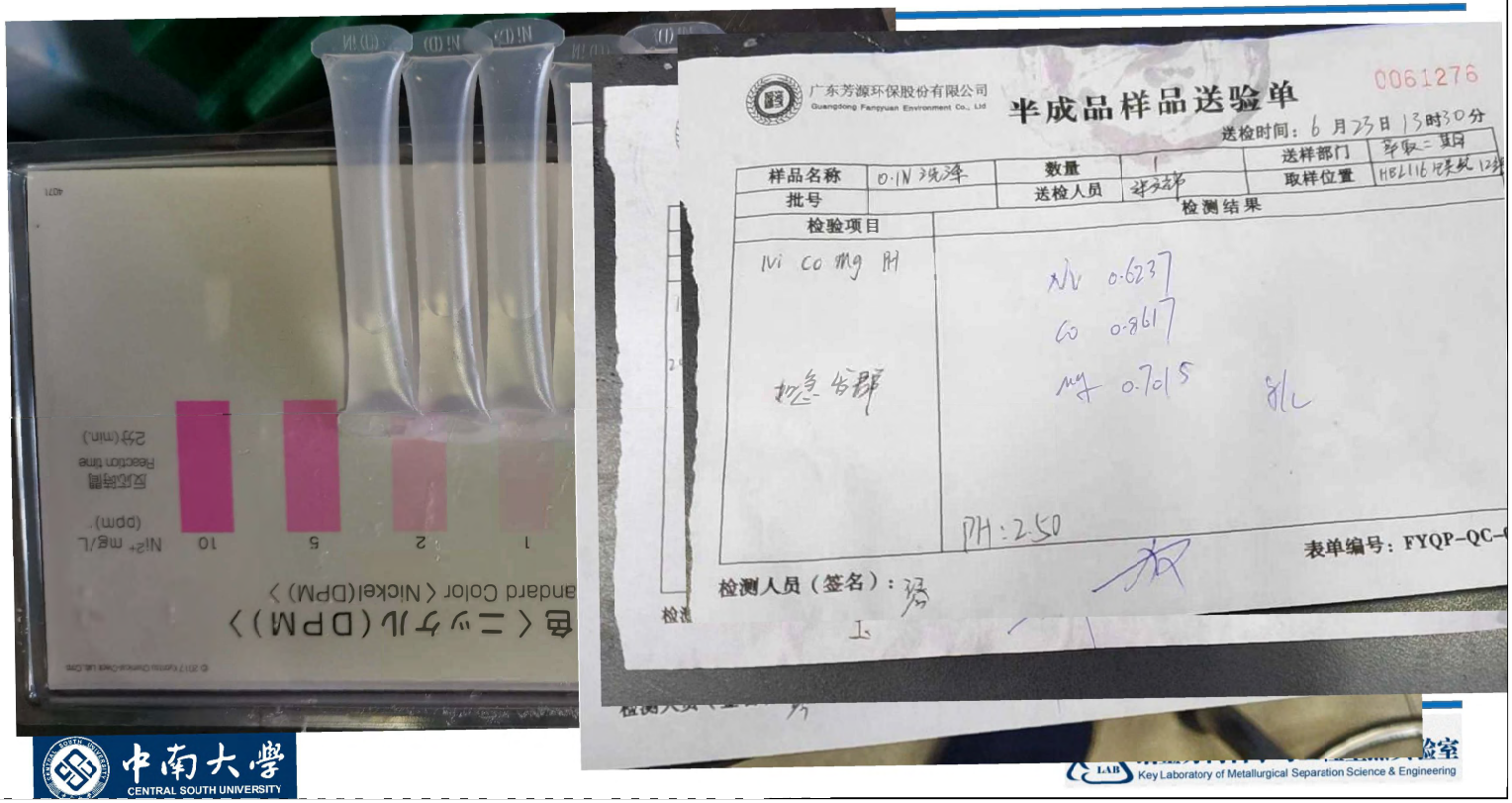

Segregation in 1st stage

Loaded organic

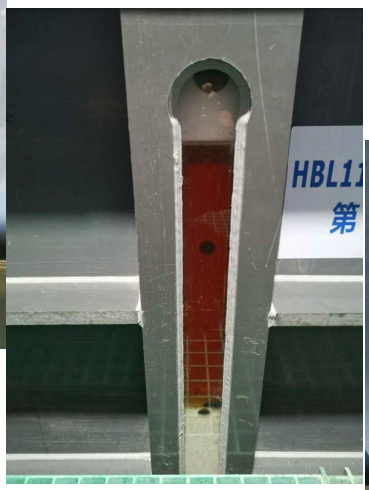

Stripping segregation

Regenerated organic

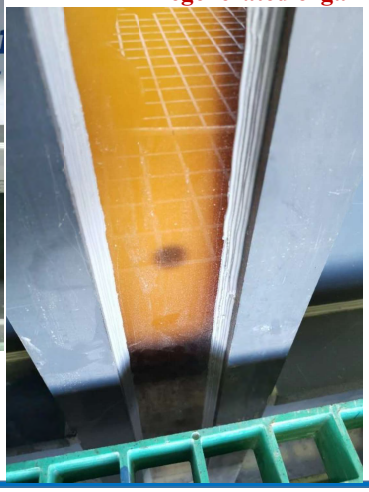

3 month after test running

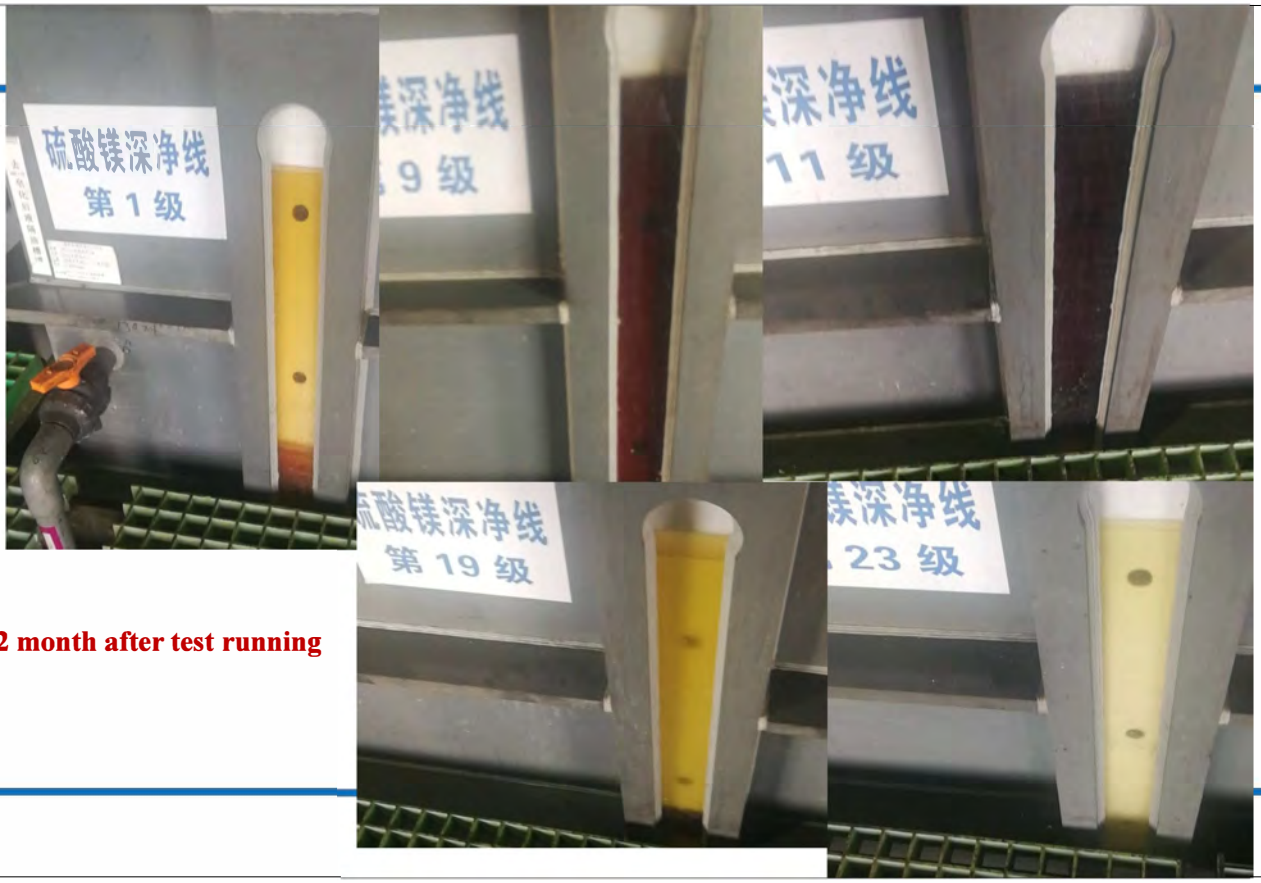

12 month after test running

2. Pilot test and industrial application of Ni/Co extraction from high Ca/Mg solutions

廣東芳源新材料集團股份有限公司
Guangdong Fangyuan New Materials Group Co., Ltd.

Reagent consumption for Ni/Co extraction from high Ca/Mg solutions

Reagent	Sulfuric acid consumption (98%H_2SO_4)			Alkali （100%NaOH）	
	Scrubbing Acid	Stripping Acid	Acid in total	Saponified alkali	**Total**
Theoretical consumption （t/t Ni&Co）			1.66		**1.36**
Dosage (kg/m³) feed solution	0.59	19.41	20.01	10.04	**10.04**
Dosage (t/t) Ni/Co metal	**0.09**	**2.92**	**3.01**	**1.66**	**1.66**

2. Pilot test and industrial application of Ni/Co extraction from high Ca/Mg solutions

2.2 Huayou Cobalt Group Co., LTD ---pilot test

Goal: Ni+Co in raffinate <20ppm; Stripping solution Ni>80g/L, Mg<10ppm Ammonia<100ppm;

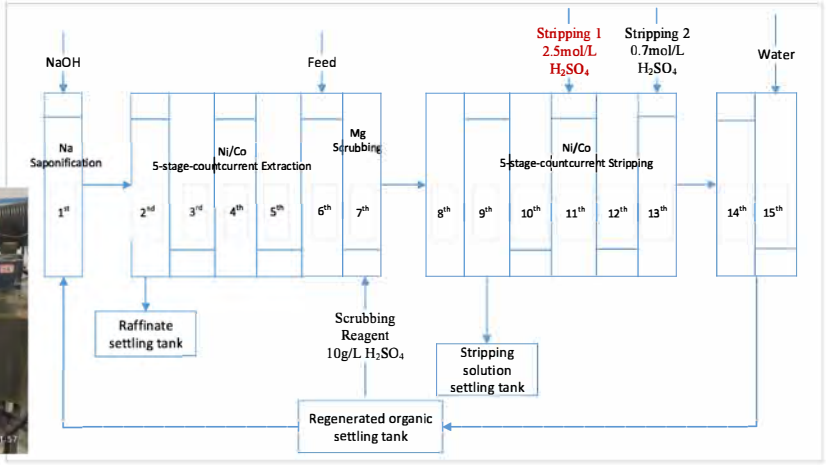

	Saponification	extraction	Scrubbing		Stripping		scrubbing
Flow rate(L/h)	Organic	Alkali	Feed	0.3N acid	5N acid	1.5N acid	Water
	18	0.72	48	6	1.5	0.96	3

	Raffinate				Stripping solution					
Element	Ni	Co	pH	TOC	Ni	Co	Mg	pH	NH_3-N	TOC
g/L	0.009	0.02	4.25	0.025	87.52	0.75	0.0032	1.31	0.046	0.036

2. Pilot test and industrial application of Ni/Co extraction from high Ca/Mg solutions

	Aqueous					Oragnic		
	Co	Mg	Ni	pH	NH_3-N	Co	Mg	Ni
萃取一	**0.017**	**15.39**	**0.0062**	**4.26**		0.31	4.66	0.49
萃取二	0.13	17.14	0.07	4		3.55	1.25	3.56
萃取三	1.73	16.08	1.74	3.33		2.65	0.14	6.35
萃取四	1.43	15.34	3.58	3.15		1.07	0.048	8.13
萃取五	0.87	14.91	4.66	3.18		0.44	0.046	9.83
洗涤一	1.51	0.89	10.51	2.82	0.36	**0.42**	**0.0087**	**8.77**
洗涤二	1.34	0.017	12.28	2.7	0.064	0.35	0.0026	9.00
洗涤三	0.99	0.0034	11	2.65	0.054	0.24	0.00086	9.11
洗涤四	0.58	0.0011	12.25	2.58	0.049	0.17	0.0022	9.04
洗涤五	0.27	0.0017	7.92	2.15	0.032	0.1	0.00084	7.70
反萃一	**0.78**	**0.00098**	**83.23**	**1.34**	0.055	0.047	0.00051	6.98
反萃二	0.32	0.00085	79	0.85	/	0.026	0.00041	5.46
反萃三	0.1	0.00062	51.05	0.2	/	0.029	0.00037	1.48
反萃四	0.07	0.00097	27.06	0.2	/	0.069	0.00043	1.4
反萃五	0.031	0.00073	12.97	0.1	/	0.047	0.00069	1.3

- **Ni Raffinate is less than 50ppm (meet the low limit concentration requirement);**
- **2-stage-scrubbing for loaded organic， NH_3-N was reduced to less than 64ppm;**
- **Ni concentration in stripping solution is about 80g/L with Mg <10ppm**

2. Pilot test and industrial application of Ni/Co extraction from high Ca/Mg solutions

华友钴业 HUAYOU COBALT

Reagent consumption for Ni/Co extraction from high Ca/Mg solutions

	Liquid alkali (32% NaOH)/kg	5N H_2SO_4 /m^3	Feed/m^3	Solvent loss /kg	Diluent loss /kg
Reagent t/t Ni	5297	9.89	32.17	2.81	4.22

2. Pilot test and industrial application of Ni/Co extraction from high Ca/Mg solutions

HBL-116 (HT-059) extraction production line for Ni selective extraction from Co extraction raffinate produced for the Cu-Co ore, will be launched June 2024, Brunp, Yichang, Hubei, Chine (1462m^3/d)

ATL 新能源科技 Ampere Technology Limited

BRUNP 邦普循环 BRUNP RECYCLING

Ni(g/L)	Co(g/L)	Mg(g/L)	NH_4^+(g/L)	SO_4^{2-}(g/L)	油分(mg/L)	Cod(g/L)	pH
1.12	0.10	3.38	27.48	93.04	40-60	1.2	5.0-5.5

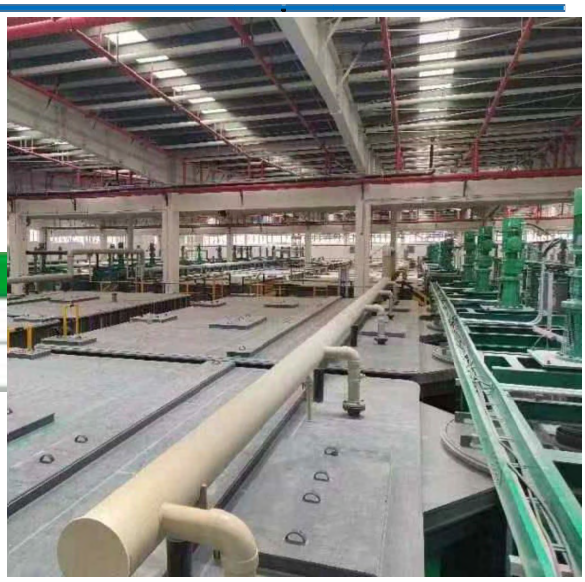

HBL 116 (25%) 萃镍线出口水相金属浓度

物料 / 元素	Ni(g/L)	Co(g/L)	Mg(g/L)	油分(mg/L)	Cod(g/L)	pH
萃余液	<0.005	<0.005	3.26	40-60	1.20	3.5-4.5
反镍液	40.42	3.61	1.22	50-60	0.60	0.5-1.5

HBL 116 (25%) 萃镍线级数

萃取功能	皂化	萃余液澄清	萃取	洗铵镁	有机澄清	反萃	洗酸	有机澄清	总级数
级数	1	2	5	3	1	6	3	1	22
萃取槽混合室规格	φ1.8×2.65m	/	φ1.8×2.65m					/	/
萃取槽澄清室规格	7*2.1*1.3	7*4.0*1.3	7*4.0*1.3	7*2.1*1.3				7*2.1*1.3	/

2. Pilot test and industrial application of Ni/Co extraction from high Ca/Mg solutions

Lanzhou Jintong Energy Storage Power New Materials Co., LTD、Austin Elements (USA) pilot test for Ni&Co coextraction from Li/Ni/Co/Mg mixed solutions、Guizhou Daong Huicheng Co., LTD using HBL-110 (HT-059-2nd) to selectively co-extract Ni/Co/Mn from Ca/Mg/Fe/Al/Ni/Co/Mn mixed solutions

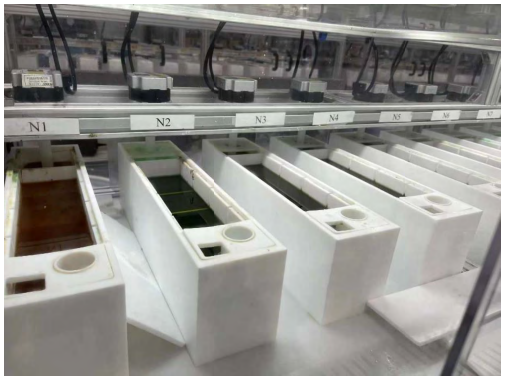

2.2 Industrial application of Ni extraction from leaching solution of electroplating

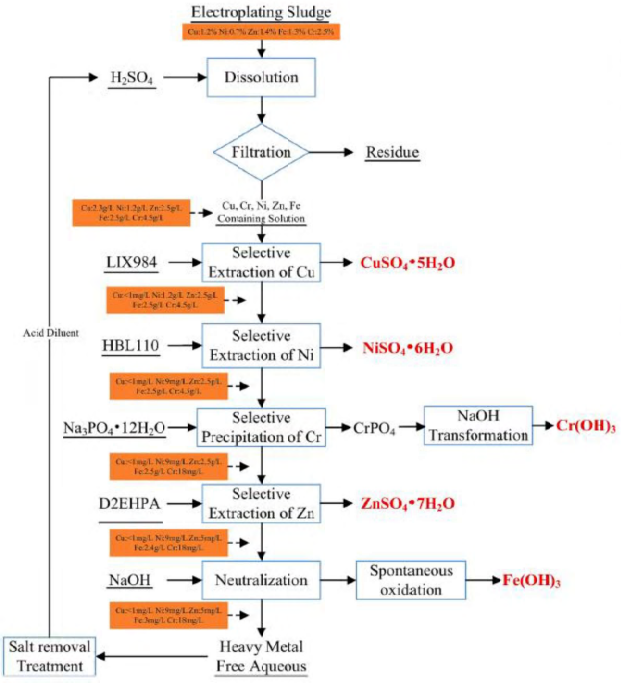

Chemical Engineering Journal 467 (2023) 143484

Contents lists available at ScienceDirect

Chemical Engineering Journal

journal homepage: www.elsevier.com/locate/cej

Complete recycling of valuable metals from electroplating sludge: Green and selective recovery of chromium

Jiawei Du [a,b], Li Zeng [a,b,c], Shuanglong Zhang [a,b], Chao Xiao [a,b], Guiqing Zhang [a,b], Zuoying Cao [a,b], Qinggang Li [a,b], Mingyu Wang [a,b], Wenjuan Guan [a,b], Shengxi Wu [a,b,*]

[a] School of Metallurgy and Environment, Central South University, Changsha 410083, China
[b] Key Laboratory of Metallurgical Separation Science and Engineering, China Nonferrous Metals Industry, Changsha 410083, China
[c] CSIRO Minerals Resource National Research Flagship, Australia

The composition of the EPS.

Composition	Fe	Ni	Cu	Zn	Cr
Content (wt%)	1.3	0.7	1.2	1.4	2.5

Recovery and reagent consumption:

Ni left in raffinate: less than 5mg/L, >99% Ni recovery;

NaOH: 1.45t/t Ni; H_2SO_4:1.72t/t Ni;

3. Industrial application of Ni/Co extraction from Ca/Mg/Fe/Al mixed solutions




Direct selectively extraction of Ni from acid leach solutions of stainless steel sludge, Jiuli Co. Ltd. , Zhejiang Province

$NiSO_4$: 800 ton/a， put into production in Feb, 2018

3. Industrial application of Ni/Co extraction from Ca/Mg/Fe/Al mixed solutions

Electroplating sludge contains massive various impurities with a high concentration

Element	Zn	Ni	Ca	Mg	Al	Fe
Con.	~20g/L	5~6g/L	~0.5	~0.3g/L	~0.1g/L	<0.1g/L

production line5: Direct extraction of Ni from the leaching solution of EPS in Ruijin Shengyuan Environmental Protection Technology Co., LTD.

From Oct. 2019

Using HBL110 as the extractant for Ni


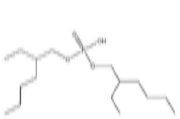
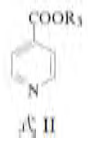

Components in stripping solutions: Ni 98g/L

Zn，Ca，Mg<10ppm； Al，Fe <30ppm

3. Industrial application of Ni/Co extraction from Ca/Mg/Fe/Al mixed solutions

Electroplating sludge contains massive various impurities with a high concentration

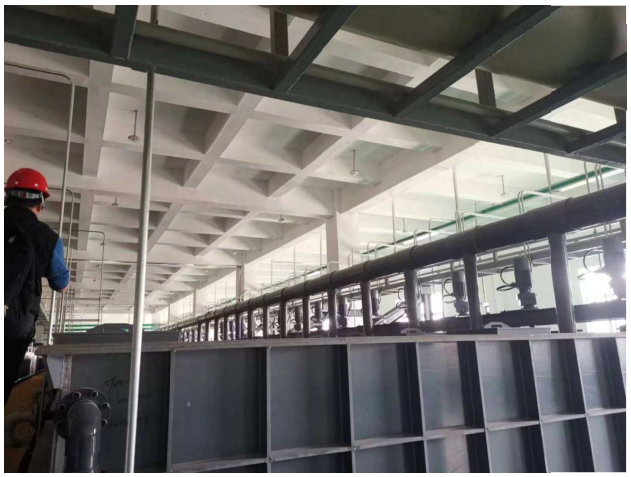

Using HBL110 (HT-059-2nd) extraction followed by Ni electrowinning to produce >99% Ni metal

Production capacity:

10000 ton of Ni metal

Jiangxi Barton Environmental Protection Technology Co., LTD launch in Sep. 2023.

3. Industrial application of Ni/Co extraction from Ca/Mg/Fe/Al mixed solutions

$NiSO_4$: 800 tonne/a
Mixer: 0.42m³;
Put into production on Aug. 2014

DSX of Ni from acid leach solutions of electroplating sludge using HBL110 (HT-059-2nd) Shuangneng, Ningbo, Zhejiang Province

3. Industrial application of Ni/Co extraction from Ca/Mg/Fe/Al mixed solutions

Guizhou DalongHuicheng Co. Ltd. Acid leaching solution of heavy metal sulfide precipitate that contains high Ca/Mg/Mn and considerable Ni/Co

Feed solution					
Element	Mn	Co	Ni	Ca	Mg
Con. (g/L)	50~80	4~5	2~3	0.1~0.2	0.1

Using HBL110 (HT-059-2nd) directly prepare pure NCM mixed solution

Stripping solution					
Element	Mn	Co	Ni	Ca	Mg
Con. (g/L)	~17	~25	~10	<5ppm	<5ppm

The first and the only plant that recover NCM without separation in China

4. Summary and Thanks

Summary for direct solvent of Ni/Co from high Ca/Mg solutions:

- **Short process** – omit of sulfide precipitation and pressure oxidation leaching operations
- **Excellent Ni/Co recovery - >99%,** illustrating a **>10%** increase in Ni/Co recovery;
- **Significantly reduce scrubbing solution (20~60g/L Mg, 0.5~10g/L Ni/Co);**
- **Low Cost recovery method for Ni/Co from high Ca/Mg (even with Fe/Al solutions)**
  HBL116 (HT-059) for Ni/Co separation from Ca/Mg, HBL-110 (HT-059-2nd) from Ca/Mg/Fe/Al
- **Environmental friendly, Ni/Co in raffinate was reduced to <1mg/L**

4、Summary

- **Core conception:** "separation as the key method、application is the final goal、achieve resource sustainable development via green and high efficient utilization"

Fundamental research

Technology development

Engineering transformation and application

4、Summary- International project solution provider in hydrometallurgy

Hydrometal Tech: International website for our group project

Pioneering Sustainable Solutions provider in Battery Recycling

Hydrometal Tech was founded from a vision to revolutionize the battery recycling technologies in industry. With over 50 years of combined experience in hydrometallurgy, our founders, a group of esteemed professors and engineers, saw the potential to make a substantial impact on the environment and the economy. Our journey began with a commitment to excellence, innovation, and sustainability, which continues to be the bedrock of our operations today.

Website: https://hydrometaltech.com/

E-mail: shengxiwu@hydrometaltech.com